DOTTORATO DI RICERCA IN CHIMICA

Convenzione tra
UNIVERSITÀ DEGLI STUDI DI TRIESTE
e
UNIVERSITÀ CA' FOSCARI DI VENEZIA

In cotutela con
THE UNIVERSITY OF SYDNEY

THE UNIVERSITY OF SYDNEY

School of Chemistry, PhD in Science

CICLO XXX

GREEN REACTIONS AND TECHNOLOGIES FOR BIOMASS VALORISATION

Settore scientifico-disciplinare: **CHIM/06**

DOTTORANDA
LISA CATTELAN

COORDINATORE
PROF. MAURO STENER

SUPERVISORE DI TESI
PROF. Maurizio Selva, Università Ca' Foscari
PROF. Thomas Maschmeyer, The University of Sydney

ANNO ACCADEMICO 2016/2017

Green Reactions and Technologies for Biomass Valorisation

A thesis submitted in fulfilment of the requirements for the degree of

Doctor of Philosophy (Cotutelle)

by

Lisa Cattelan

The University of Sydney

Università Ca' Foscari di Venezia

Università degli Studi di Trieste

Ciclo XXX

November 2017

PREFACE

This thesis is a report of original research undertaken by the PhD Candidate and it is submitted for admission to the degree of Doctor of Philosophy (Cotutelle) at the Università Ca' Foscari Venezia, Università degli Studi di Trieste and the University of Sydney. The work and results presented in this thesis are those of the PhD Candidate, unless otherwise acknowledged.

The work presented in this thesis has been published or is in preparation for publication:

–Chapter 1: Introduction–

- M. Selva, A. Perosa, S. Guidi, L. Cattelan, Ionic liquids as transesterification catalysts: applications for the synthesis of linear and cyclic organic carbonates. *Beilstein Journal of Organic Chemistry* **2016**, 12, 1911–1924;
- M. Selva, A. Perosa, S. Guidi, L. Cattelan. Dimethylcarbonate for the Catalytic Upgrading of Amines and Bio-Based Derivatives. In Encyclopedia of Inorganic and Bioinorganic Chemistry, John Wiley & Sons, L., Ed. 2016; pp 1–11.

–Chapter 2: O-Alkylation of bio-based derivatives with dialkyl carbonates & hydrotalcites–

- L. Cattelan, A. Perosa, P. Riello, T. Maschmeyer, M. Selva, Continuous-Flow O-Alkylation of Biobased Derivatives with Dialkyl Carbonates in the Presence of Magnesium–Aluminium Hydrotalcites as Catalyst Precursors. *ChemSusChem* **2017**, 10 (7), 1571–1583.

–Chapter 3: CF-Synthesis of symmetrical dialkyl organic carbonates–

- L. Cattelan, A. Perosa, M. Selva, Continuous-Flow Disproportionation of Methyl Alkyl Organic Carbonates to Symmetric Dialkyl Carbonates in the Presence of Magnesium–Aluminium Hydrotalcites. *Manuscript in preparation*.

–Chapter 4: Renewable Aromatics from Kraft Lignin with Molybdenum-Based Catalysts–

- L. Cattelan, A. K. L. Yuen, M. Y. Lui, A. F. Masters, M. Selva, A. Perosa, T. Maschmeyer, Renewable Aromatics from Kraft Lignin with Molybdenum-Based Catalysts. *ChemCatChem*, **2017**, 9 (14), 2717–2726.

–Chapter 5: Extractive denitrogenation of fuel oils with ionic liquids: a systematic study–

- M. Y. Lui, L. Cattelan, L. C. Player, A. F. Masters, A. Perosa, M. Selva, T. Maschmeyer, Extractive Denitrogenation of Fuel Oils with Ionic Liquids: A Systematic Study. *Energy & Fuels* **2016**, 31 (3), 2183–2189.

Sections of this work have been presented by the PhD Candidate at scientific conferences and seminars:

- L. Cattelan, M. Noe', P. Riello, A. Perosa, A. F. Masters, T. Maschmeyer, M. Selva, Continuous-Flow O-alkylation of Bio-Based Derivatives with Dialkyl Carbonates in the presence of Mg–Al hydrotalcites as Catalyst Precursors. 9th ICEC Conference, Newcastle (Australia) 10-13th July 2016 (*Oral and Poster Communication*);
- L. Cattelan, M. Noè, M. Selva, A. Perosa, Methylphosphonium methylcarbonate, ylide precursor for halyde- and base-free Wittig reactions. European Winter School on Physical Organic Chemistry, Bressanone 1-6 febbraio 2015. (*Poster Communication*);
- L. Cattelan, M. Selva, Selective catalytic etherification of bio-based derivatives with dialkyl carbonates. Green Chemistry School, Verbania 27-29th September 2015 (*Oral Communication*);
- L. Cattelan, S. Guidi, M. Selva, Dimethylcarbonate for the catalytic upgrading of bio-based derivatives. Sigma Aldrich Young Chemists Symposium (SAYCS), Rimini 27-29th October 2015 (*Oral and Poster Communication*);
- L. Cattelan, Green reactions and technologies for biomass valorisation: upgrading of glycerol derivatives and furans. I workshop dottorato interateneo Venezia-Trieste, 2-3/07/2015;
- L. Cattelan, Extractive denitrogenation of fuel oils with ionic liquids: a systematic study. PhD progress review at the University of Sydney, 12/12/2016;

- L. Cattelan, Green reactions and technologies for biomass valorisation. III workshop dottorato interateneo Venezia-Trieste, 15-16/06/2017.

ABSTRACT

This research project has focussed on the upgrading of biomass derivatives, particularly glycerol derivatives and lignin, to higher added-value chemicals by means of green and sustainable technologies.

The fundamental principle of sustainability is that waste is not an *old* useless substance that needs to be disposed of, but is rather an important and multicomponent feedstock that can be exploited to produce *new* chemicals, materials and energy sources, thus re-entering the material cycle. Furthermore, the valorisation of waste must be done in a sustainable way, *i.e.* using environmental friendly technologies. These concepts have been the guidelines by which methods and chemical transformations have been conceived in this Thesis work.

The experimental work was divided into three main areas, which were all commonly aimed at combining green technologies and biobased compounds for the development of sustainable protocols.

i) Development of new methodologies for the upgrading of glycerol and furan bio-based derivatives.

1. Continuous-flow alkylation reactions. OH-bearing bio-based compounds (O-BBs), as glycerol acetals/carbonates and furfuryl alcohol derivatives, are suitable for a number of derivatisation processes. Of particular note, alkylation protocols allow the potential of O-BBs to be expanded through the synthesis of added-value products, including intermediates, solvents and biologically active molecules as glycerol ethers and carbonates, and additives for biodiesel blends based on furanyl ethers. In this context, an innovative alkylation protocol was implemented in this Thesis using dialkyl carbonates, which are green and safe compounds, as alkylating agents under continuous-flow (CF) conditions (Scheme 1). Different classes of catalysts were compared: Na-exchanged Y- and X-faujasites and Mg-Al hydrotalcites.

Calcined hydrotalcites (c-HTs), particularly c-HT30 (Mg:Al ratio=30), proved to be the most effective system for highly chemoselective transformations: functionalised bio-based alcohols and dialkyl carbonates were activated preferentially towards *O*-alkylations over the competitive transesterifications and other side-reactions. *O*-alkylation selectivities as high as 99% were achieved at complete conversion.

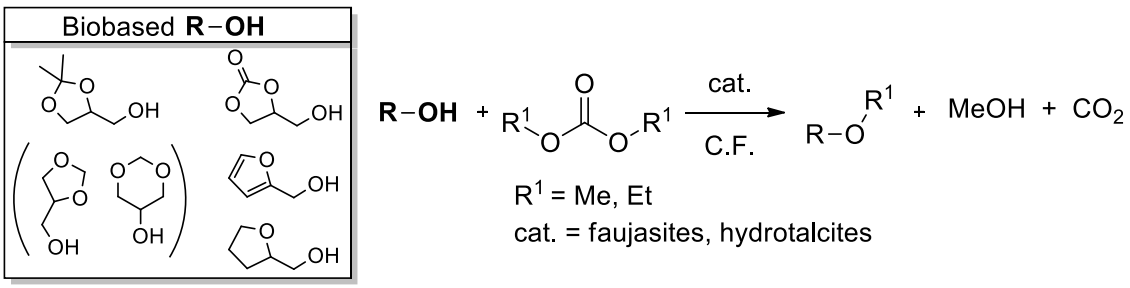

Scheme 1. CF-alkylation of OH-bearing biobased derivatives with dialkyl carbonates and c-HT30.

Characterisation studies proved that the hydrotalcites act as catalyst precursors: during the thermal activation pre-treatments of such solids, the lamellar structure typical of hydrotalcites was broken down gradually into a magnesia-alumina solid solution, which was the active catalytic phase.

2. Synthesis of symmetrical dialkyl carbonates (DAlCs). The synthesis of symmetrical dialkyl carbonates is a highly desirable target since symmetrical DAlCs are of great interest as eco-friendly solvents and intermediates. Symmetrical DAlCs of renewable origin can be synthesised *via* catalytic transesterification/disproportionation reactions starting, for example, from methyl alkyl organic carbonates. These products in turn, can be obtained *via* a transesterification of OH-bearing bio-based derivatives with the non-toxic dimethyl carbonate (DMC). In this Thesis, carbonate interchange reaction (CIR) strategies have been investigated and a continuous-flow protocol for the disproportionation of four different methyl alkyl carbonates was optimised, using a calcined hydrotalcite (c-HT30) as a heterogeneous catalyst (Scheme 2).

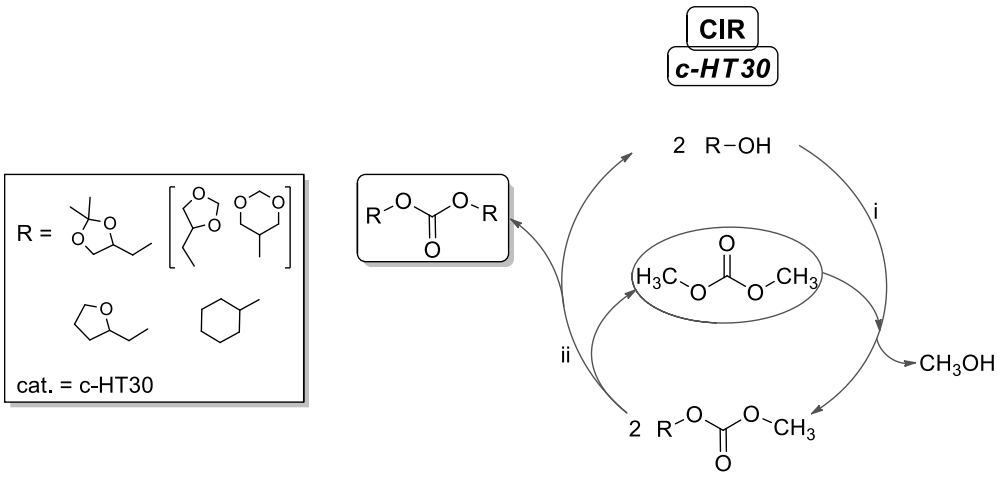

Scheme 2. Synthesis of s-DAlCs catalysed by c-HT30: i) batch CIR for the production of methyl alkyl carbonate and ii) CF-disproportionation of methyl alkyl carbonates to the corresponding s-DAlCs.

ii) Catalytic depolymerisation of Kraft lignin into renewable aromatic compounds. Lignocellulosic biomass has been proposed as one renewable feedstock to supplement dwindling fossil reserves. This is ideal when the use of biomass can be integrated into existing supply chains to avoid detrimental land use changes or when combined with waste treatment and recycling. Lignin constitutes around 25-30% of lignocellulosic biomass and it is the most abundant source of renewable aromatic compounds in the terrestrial biosphere. Of the many target compounds that can be produced from the conversion of lignin, phenol(s) and BTX-type arenes are economically attractive due to their large market volumes. In this Thesis, the catalytic depolymerisation of Kraft lignin in supercritical ethanol (which acted as both the solvent and the H-donor) was explored in the presence of eight different Mo_2C- and MoS_2-based catalysts, affording aromatic yields as high as 506 mg/g lignin, amongst the highest yields reported to date (Scheme 3).

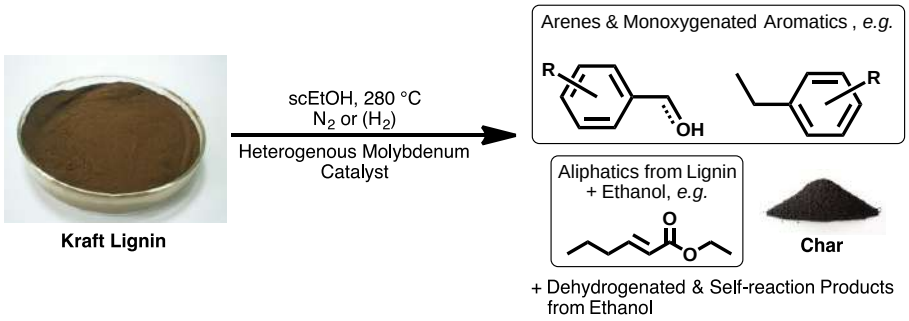

Scheme 3. Overview of Kraft lignin depolymerisation under supercritical reaction conditions in the presence of Mo-based heterogeneous catalysts.

iii) Cleaning up fuels: removing pollutants from renewable feedstock with ionic liquids. Nitrogen-based compounds are commonly found in biocrude oils when they are generated from biomass containing some residual protein, *e.g*. algae, seaweed or municipal green waste. These N-containing residues interfere with traditional refining methods and need to be removed prior to their integration into the supply chain. Ionic liquids (ILs) have previously been suggested as useful and green extractants of aromatic N-containing compounds from fuel oils. In this thesis, twelve ILs based on common cations and anions were synthesised and used for the selective extraction of two archetypical N-compounds, pyridine and indole, from a model oil, consisting of *n*-decane and toluene. The performance of these ILs as extractants of N-compounds was compared and rationalised, demonstrating that the cation and anion

sizes and the hydrogen bond donor/acceptor abilities are the major factors determining the effectiveness of the extraction of N-compounds.

ABSTRACT

Il progetto di ricerca è stato focalizzato sulla valorizzazione di derivati da biomassa, in particolare derivati di glicerolo e lignina, a sostanze aventi più alto valore aggiunto, per mezzo di tecnologie green e sostenibili.

La sostenibilità si basa sul principio fondamentale che i rifiuti non debbano essere considerati scarti privi di valore, ma piuttosto una materia prima da valorizzare in nuovi prodotti o composti chimici, rientrando così in un virtuale ciclo della materia.

Tale valorizzazione del rifiuto, inoltre, deve essere effettuata in modo sostenibile, sfruttando tecnologie compatibili con l'ambiente.

In questo lavo di tesi, tali concetti ci hanno guidato verso lo sviluppo di nuove metodologie e trasformazioni chimiche, di seguito riportate.

i) Composti bioderivati contenenti gruppi –OH (O-BBDs), quali acetali/carbonati del glicerolo e derivati dell'alcol furfurilico, vengono derivatizzati tramite una serie di processi chimici. Tra questi, le reazioni di alchilazione permettono di valorizzare tali O-BBDs in composti a più elevato valore aggiunto impiegabili come solventi e additivi nelle benzine.

Un innovativo protocollo di alchilazione è stato sviluppato nella presente Tesi (cfr. Chapter 2) attraverso l'uso di carbonati alchilici, composti green e non tossici, come reagenti alchilanti in condizioni di flusso continuo. Diverse classi di catalizzatori sono state studiate: faujasiti di tipo Y e X, e idrotalciti di Mg e Al.

In particolare, l'idrotalcite calcinata c-HT30 ha esibito le migliori performance catalitiche verso trasformazioni altamente chemoselettive: O-BBDs e carbonati alchilici vengono selettivamente attivati verso reazioni di O-alchilazione a discapito di altre reazioni secondarie.

ii) Recentemente, carbonati organici simmetrici stanno ricevendo grande interesse in quanto utilizzabili come solventi o reagenti a basso impatto ambientale. Carbonati simmetrici possono essere sintetizzati via reazioni catalitiche di transesterificazione/disproporzione a partire da carbonati misti di origine rinnovabile. Quest'ultimi possono essere ottenuti attraverso reazioni di transesterificazione tra i suddetti alcoli di origine rinnovabile (O-BBDs) e il dimetil carbonato. In questa Tesi (cfr. Chapter 3), questa strategia di sintesi è stata ottimizzata per quattro diversi metil alchil carbonati in condizioni di reazione di flusso continuo catalizzate da c-HT30.

iii) La lignina, presente nel 20-30% nella biomassa lignocellulosica, è considerata la principale sorgente di composti aromatici rinnovabili. Tra le molteplici classi di composti ottenibili dalla depolimerizzazione di tale biopolimero, i fenoli e i BTX riscuotono un importante interesse economico. In questo capitolo di tesi (cfr. Chapter 4), la decomposizione riduttiva della lignina Kraft è stata investigata in etanolo supercritico (come solvente e sorgente di H) utilizzando otto differenti catalizzatori a base di Mo.

iv) Composti contenenti azoto sono comunemente presenti nei bio-carburanti, in particolare quando generati da rifiuti organici o da alghe. Tali composti interferiscono con i tradizionali metodi di raffinazione e necessitano pertanto di essere rimossi. I liquidi ionici sono stati impiegati come possibili estraenti selettivi di tali composti contenenti azoto. Nel presente lavoro di tesi (cfr. Chapter 5), dodici liquidi ionici sono stati sintetizzati e impiegati nell'estrazione selettiva di composti modello quali piridina e indolo, da miscele di n-decano e toluene. Le performance di tali liquidi ionici sono state comparate e razionalizzate.

CONTENTS

LIST OF ABBREVIATIONS

AC	Activated carbon
ACS	American Chemical Society
AE	Atom economy
AFEX	Ammonia Fiber Explosion
AFRL	U.S. Air Force Research Laboratory
APR	Aqueous Phase Reforming
BDO	1,4-butanediol
BET	Brunauer-Emmett-Teller
BPR	Back pressure regulator
BTX	Benzene-toluene-xylene
CC	Catechol carbonate
CE	Carbon efficiency
CE	Circular Economy
CF	Continuous flow
CFPP	Cold filter plugging point
CHR	Carbothermal hydrogen reduction
CI	Cost index
COSY	Correlation Spectroscopy
CSTR	Continuous stirred tank reactors
DA	US Department of Agriculture
DABCO	1,4-diazabicyclo[2.2.2]octane
DAlC	Dialkyl carbonate
DBnC	Dibenzyl carbonate
DBU	Diazabicycloundecene
DES	Deep eutectic solvents
DMAP	4-Dimethylaminopyridine
DMS	Dimethyl sulphate
DPC	Diphenyl carbonate
DVLO	Derjaugin–Landau–Verwey–Overbeek
E	Environmental factor
EAN	Ethyl ammonium nitrate
EC	Ethylene carbonate
ECL	ε-Caprolactone
EG	Ethylene glycol
ESI	Electrospray ionization
EU	European Union

EWG	Electron withdrawing group
FAME	Fatty acid methyl ester
FAU	Faujasites
FCC	Flash column chromatography
FDCA	furan-2,5-dicarboxylic acid
FPR	Flow photochemical reactors
GAs	Glycerol acetals
GBL	γ-Butyrolactone
GC	Gaschromatography
GCI	Green Chemistry Institute
GFR	Gas flow reactors
GHSV	Gas hourly space velocity
GOST	Green Organic Syntheses Team
GVL	γ-Valerolactone
HER	Hydrogen evolution reaction
HMBC	Heteronuclear Multiple Bond Correlation
HMF	5-Hydroxy methylfurfural
HMPA	Hexamethylphosphoramide
HMQC	Heteronuclear Multiple Quantum Coherence
HPLC	High pressure liquid chromatography
HR	HYDRANAL®-reagent
ICP	Inductively coupled plasma
IEA	International Energy Agency
IL	Ionic liquid
LA	Levulinic acid
LA	Linoleic acid
LCB	Lignocellulosic Biomass
LD	Lethal dose
LDA	Lithium diisopropylamide
LG	Leaving group
LHSV	Liquid hourly space velocity
LHW	Liquid hot water
Lim	Limonene
LLE	Liquid-liquid extractions
LO	Limonene oxide
Mo_2C_2	Molybdenum hemicarbide
MoS_2	Molybdenum disulfide
MOF	Metal-organic framework
MP	Multiphase systems
MR	Micro-reactor
MRP	Material Recovery Parameter

MS	Mass spectrometry
NAcS	Nucleophilic acyl substitution
NBA	N-bromoacetamide
NBM	N-butylmaleimide
NMR	Nuclear Magnetic Resonance
NPs	Nanoparticles
NREL	US National Renewable Energy Laboratory
PNNL	Pacific Northwest National Laboratory
NPM	N-Phenylmaleimide
NPrM	N-propylmaleimide
OPL	Organosolv poplar lignin
P2Bs	Phase II biorefineries
PBR	Packed-Bed Reactor
PC	Polycarbonate
PEF	Polyethylene furanoate
PET	Polyethylene terephthalate
PFR	Tubular plug-flow reactors
PLimC	poly(limonene carbonate)
PMO	Porous metal oxide
RME	Reaction mass efficiency
RT	Room temperature
S^{-1}	Mass index
sc-CO_2	Supercritical-CO_2
SCF	Supercritical fluid
SF	Stoichiometric factor
SV	Space velocity
TG/DTG	Thermogravimetry and differential thermogravimetry
TMS	Teramethylsilane
TPS	Thermoplastic starch
US DOE	United States Departments of Energy
WE	Water equivalent
WHSV	Weight hourly space velocity

The noblest pleasure is the joy of understanding

Leonardo da Vinci

1. INTRODUCTION

1.1. Our common future: the need for a change

Roughly 200 years into the fossil fuel era, we find ourselves at the epicentre of a global economic crisis, which may have unprecedented and dramatic implications for the environment and life on our Planet. This criticality has come to the point where it needs not only to be discussed but also faced and resolved.

The depletion of fossil fuel reserves is increasing rapidly, with the two main causes being:

- the consistent global population growth,
- the race for economic development.

From 1800 to 2016, the global population grew from 0.9 to 7.4 billion people, and this is forecast to rise by 33% to 9.9 billion people by 2050.[1] This growth is primarily caused by the soaring populations in the developing Countries. As shown in Figure 1.1 for example, the Africa population is expected to double over the next 35 years, from the actual 1.2 billion to more than 2.5 billion by 2050. This is expected to correspond to a massive increase in the energy demand, which nowadays is mostly provided by fossil fuels.

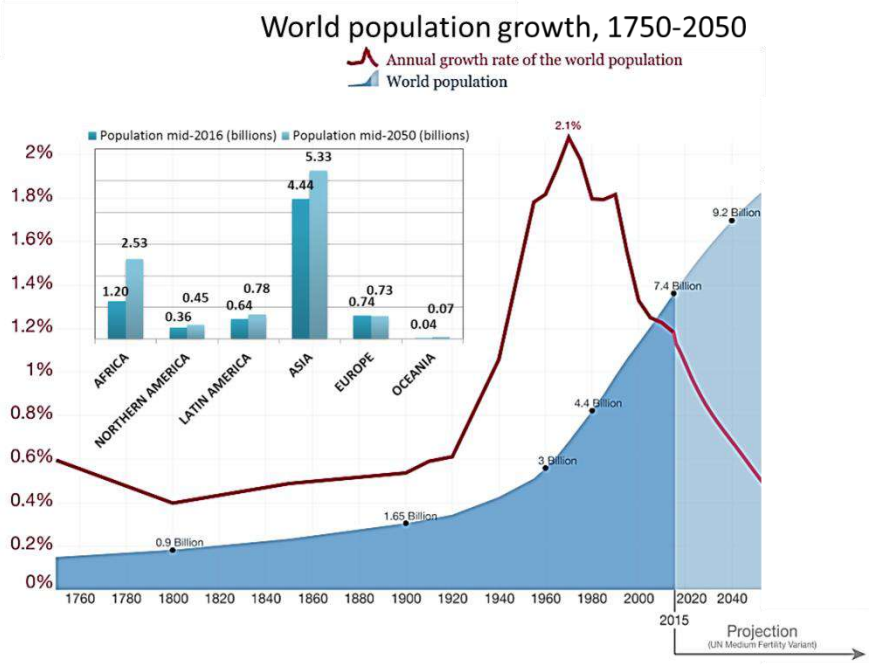

Figure 1.1. Growth of the world population from 1750 to 2050, detail of the population growth by continents.[1]

This aspect, particularly the consumption of fossil fuels, has been largely debated in the last four decades with several possible scenarios. According to the analysis proposed by the US Environmental Protection Agency, the current and forecast global consumption of the conventional fuels is summarised in Figure 1.2. A massive exploitation of oil, coal and natural gas has occurred over the last 80 to 100 years and it is expected to peak in the next 5 to 10 years. After this, the forecasts suggest that a dramatic depletion of these resources will follow.

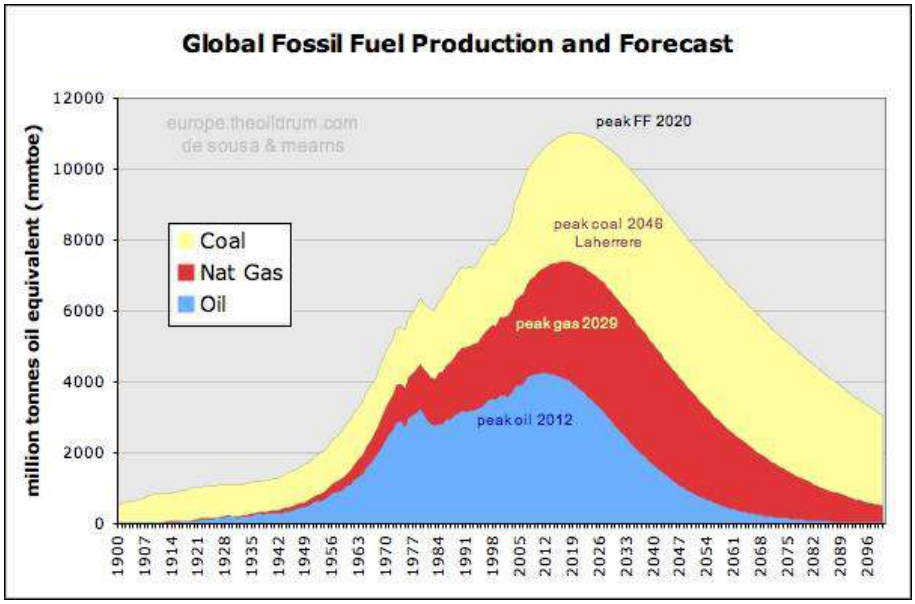

Figure 1.2. Global fossil fuel production and forecast.[2]

In addition to the depletion of non-renewable resources, a major consequence of the persistent increase in fossil fuel consumption has been the alarming rise of gaseous and particulate emissions in the atmosphere. Just to cite the most known case of CO_2, the atmospheric concentration of this gas has grown from 280 to 393 ppm between the first industrial revolution in 1750 and 2012. A further increase is expected due to the tremendous development that far-eastern Countries, mainly China and the Indian subcontinent, are currently experiencing. The effect of CO_2, along with other greenhouse gases (GHG) originating from anthropogenic activities, is recognised to be among the most significant drivers of climate change, which is producing devastating events like unusually hot summers, unprecedented coral bleaching, stronger tropical storms, increased rates of melting of polar ice and glaciers, etc.[3] Pollution is another issue which is exemplified by several situations, one of the most representative is that of Beijing. In 2011, this city hosted 20.2 million people within an area of 16,800 km^2, making it one of the largest and most densely populated megalopolis worldwide.[4] This impressive number has resulted in a consumption of coal and other fossil

fuels that in only 25 years, from 1986 to 2011, corresponded to a 2.5-fold increase in the total energy usage, from 27.1 Mton to 70.0 Mton (standard coal equivalent).[5] Perhaps, the more direct evidence of this trend on a macroscopic scale of this trend, is the dramatic change of the Beijing skyline due to smog (Figure 1.3). However, a much more worrying consequence is the recent increase of mortality from cardiovascular diseases and malignant tumours in the city area.[5]

Figure 1.3. Disappearance of the Beijing skyline with the recent increase of smog.

Analysts and Governments - unfortunately, with a few recent, but notable exceptions[6] - recognise that the situation the whole Planet is living with, has been largely determined by the development model adopted by the Society after the industrial revolution, which was (and is still) grounded on a linear economy focused around fossil fuel resources. The concept by which the growth of the economy and the job market is driven by a 'bigger-better-faster-safer' syndrome and where the main target is to please the consumers by selling high volumes of cheap materials,[7] has been one of the dominating principles of the last fifty years. However, the weakness of this vision becomes clearer every day, as it is no longer conceivable that precious raw materials such as natural gas, crude oil and coal continue to be converted at the current (too high) rate into energy and goods, and sold without considering their life cycle or disposal. This brings about unacceptable overconsumption and production inefficiency: shortly, but more precisely speaking, this is not sustainable.

1.2. Circular economy

The notion of sustainability can be expressed through several paradigms which however, all provide a common basis aimed at assigning more value to the available resources, either fossil fuels or renewables, and replacing the "make, use, dispose" system. In 1989, the environmental economists David W. Pearce and R. Kerry Turner were the first to propose an alternative model to the conventional linear economy. This has been done by addressing the theme of sustainable economic development and the importance of recyclable waste, which would not just end the material chain, but re-enter the cycle and provide "old" substrates for "new" materials.[8] This concept was further developed by Walter R. Stahel and his "Cradle to Cradle" theory, as opposed to the old "Cradle to Grave" one, which led to the development of the larger concept of Circular Economy (CE, Figure 1.4).[7]

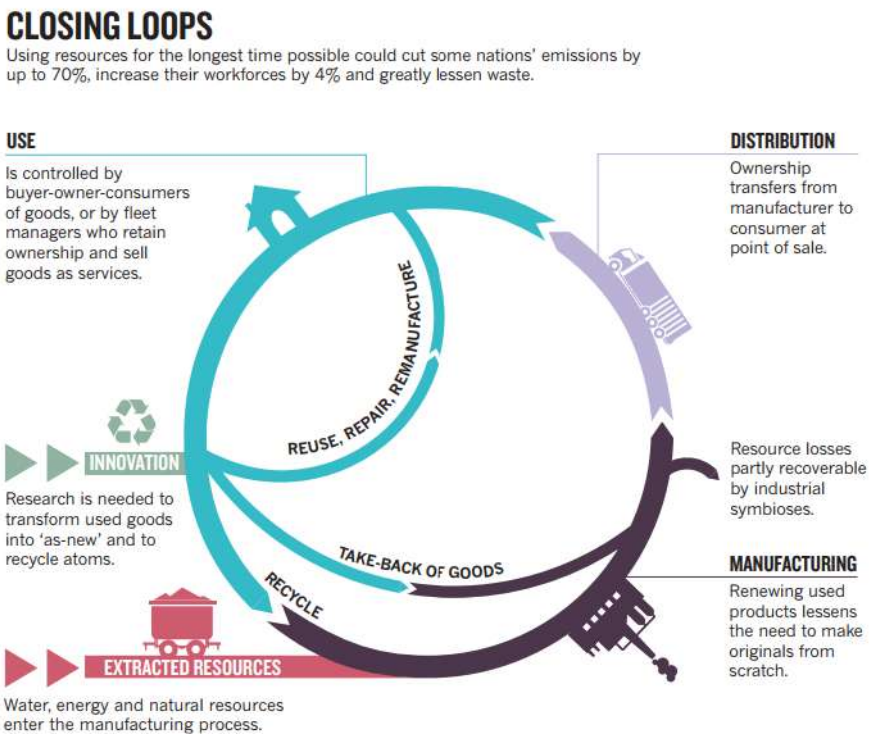

Figure 1.4. Schematic representation of the circular economy philosophy: closing loops.[7]

In his work about the circular economy, Stahel pointed out how our Society is still looking at old things as undesirable, while what is usually called waste should be treated as a resource.[9] In other words, when goods are at the end of their life and appear worthless, they should be repaired or recycled and turned back into valuable products.[7] This means closing the loop by re-introducing materials into the industrial ecosystem, which could potentially solve the

problems regarding both the depletion of fossil fuels and the pollution caused by their exploitation.[10]

The circular economy proposed by Stahel obviously requires a radical change to the foundation of our Society. People must be educated to see the value of waste and everyone, irrespective of their status and job, should cooperate at sustainability by embracing the CE model, where both starting materials and the derived goods acquire a higher value than in the linear system. In particular, in this model not only the lifetime of the products, but also their reusability or remanufacture into new items or commodities, are extended/practiced. Some analyses have estimated that the circular economy will increase the workforce by 4%, as it will require more labour and time, but fewer primary resources, to restore an old object than to produce a new one.[7]

The other milestone of the circular economy is the elimination of waste. By closing the loop of Figure 1.4, humankind would be able to make today's waste tomorrow's resource, with potentially no residues released into the environment and a significant reduction of pollution. Again, projections estimate that the adoption of the CE model would decrease the GHG emissions by around 70%.[11] To make the most of this system, the feedstocks at the beginning of the cycle need to be taken from renewable sources, which, by definition, have the ability to replenish themselves in a relative short period and therefore can be used indefinitely. Contrary to fossil resources (*i.e.* coal, crude oil and natural gas), which were formed through CO_2 fixation over millions of years and are being depleted much faster than their re-generation,[12] biomass supplies genuine renewable materials and compounds. As a logical outcome, the exploitation of biomass has become one of the pillars of the CE model, particularly aimed at the development of biorefineries. These are the facilities that allow for the upgrading of biomass into added-value compounds for energy, chemicals, and materials.

1.3. The biorefinery concept. Definitions

1.3.1. The Lignocellulosic biomass

Biomass is a very general term that is used today to encompass a variety of feedstocks, including forest and mill residues, agricultural crops and wastes, wood and wood wastes,

animal wastes, livestock operation residues, aquatic plants, fast growing trees, and municipal and industrial wastes.

However, several more detailed descriptions have been proposed. To cite only a few, the British Biomass Energy Centre has defined biomass as: *"The biological material derived from living or recently living organisms",*[13] while one of the most recent and widely accepted classification of biomass is that of Cavalier-Smith, which is based on the eukaryote domain. In this domain, the majority of biomass derives from plants (kingdom *Plantae*) and is more precisely defined as "lignocellulosic biomass" (Figure 1.5).

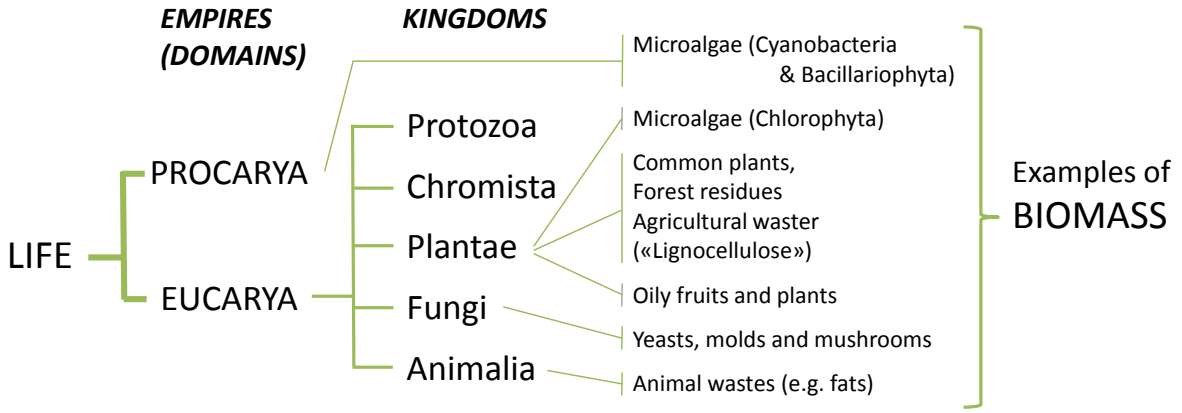

Figure 1.5. Life domains and kingdoms, with examples of biomass sources.

Within this kingdom, aquatic plants are also included, among which microalgae are becoming more and more attractive for biodiesel and bioenergy production.[14] Although animal wastes and even fungi represent bio-feedstocks that can be valorised, the lignocellulosic biomass (LCB) is currently the most abundant, the most easily available, and the most versatile source. Lignocellulosic biomass is widely contained in common agricultural residues, herbaceous crops, hardwood and softwood trees and municipal solid wastes. Its composition varies according to the parent biomass (Table 1.1) but, as the name suggests, LCB is mainly composed of the two carbohydrate polymers cellulose and hemicellulose. In addition, LCB also contains lignin and, to a lesser extent, other compounds such as proteins and extractives (*e.g.* triglycerides and terpenes, acids, salts and minerals).

Table 1.1. Cellulose, hemicellulose and lignin content in common agricultural residues and waste.[15]

Lignocellulosic material	Cellulose (%)	Hemicellulose (%)	Lignin (%)
Hardwood stems	40-55	24-40	18-25
Softwood stems	45-50	25-35	25-35
Nut shells	25-30	25-30	30-40
Corn cobs	45	35	15
Grasses	25-40	35-50	10-30
Paper	85-99	0	0-15
Wheat straw	30	50	15
Sorted refuse	60	20	20
Leaves	15-20	80-85	0
Cotton seed hairs	80-95	2-20	0
Newspaper	40-55	25-40	18-30
Waste papers from chemical pulps	60-70	10-20	5-10
Primary wastewater solids	8-15	n.a.	n.a.
Solid cattle manure	1.6-4.7	1.1-3.3	2.7-5.7
Coastal bermudagrass	25	35.7	6.4
Switchgrass	45	31.4	12
Swine waste	6.0	28	n.a.

Cellulose, hemicellulose and lignin are the substances that vegetal cell walls are made of, where each of the three components plays a distinct function to contribute to the shape, the robustness, and the mechanical properties of the cells (Figure 1.6).[16] Specifically: *i)* cellulose is the main component of cell walls. It is a linear cellobiose polymer (artificially is a double molecule of glucose) whose rigid and crystalline structure is due to the orientation of the chains and the occurrence of hydrogen bonds between them (Figure 1.7, a). This feature also confers a high chemical resistance to the polymer; *ii)* hemicellulose consists of different saccharide heteropolymers of five carbon (mainly xylose, arabinose) and six carbon molecules (galactose, glucose and mannose). While cellulose possesses a crystalline and strong scaffold, hemicellulose has a random and amorphous structure, which is relatively easy to hydrolyse with dilute acids or bases as well as by numerous hemicellulase enzymes (Figure 1.7, b).[17]
iii) Lignin (Figure 1.8) is a phenolic polymer (monomeric units are called monolignols) located in the secondary cell wall. It provides strength and rigidity to the plant walls together with resistance to diseases, insects, cold temperatures, and other stresses. Lignin plays also a crucial part in conducting water in plant stems.

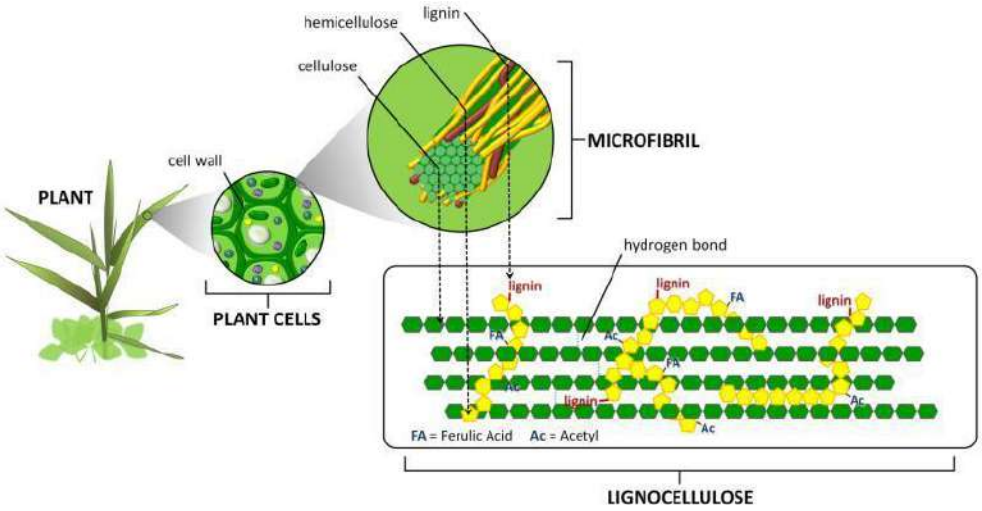

Figure 1.6. Lignocellulosic plant cell wall.

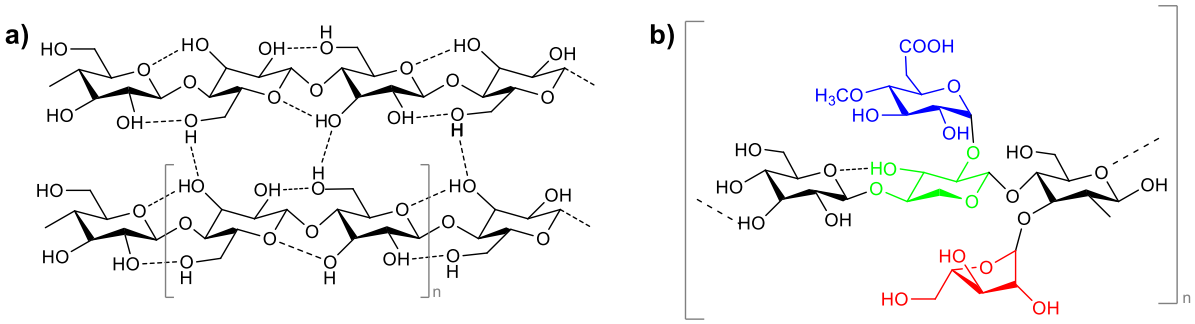

Figure 1.7. (a) Structure of cellulose. (b) Structure of hemicellulose showing L-arabinose (red), D-xylose (green), D-glucose (black) and D-galactose (blue).

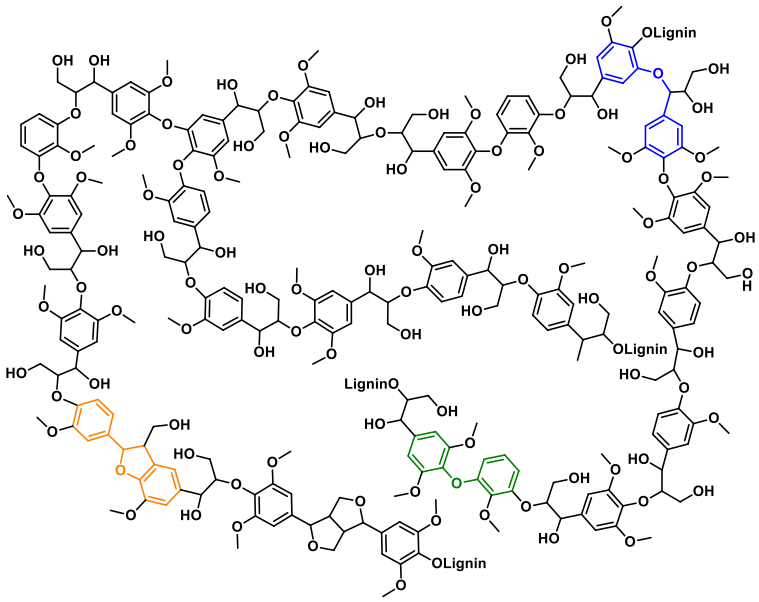

Figure 1.8. Structure of lignin.

The chemical diversity and richness of components of LCB, clearly indicates the potential of this source for supplying a variety of sustainable and bio-based chemicals and fuels. According to the analysis by US Departments of Energy (DOE) and Agriculture (DA), if the content of LCB

was fully exploited, it could replace one third of the current petroleum consumption of North America.[18]

However, the handling and valorisation of LCB are not trivial issues. Cellulose is an exemplifying case: both the bio-polymer (as such or in its crystalline nano-structure) and the sugar monomers, are extremely attractive as building blocks for new biomaterials and as synthons for chemicals and energy products.[19] However, the achievement of pure (nano) crystals of cellulose and the so-called saccarification of cellulose (breakdown into sugar molecules) require hydrolytic conditions with strong acids, these reactions being complicated to run and control. Similarly, the heterogeneity and the lack of a defined primary structure in lignin make its transformation into lignols even more complex and less selective than the degradation of cellulose. Not to mention the importance of the choice of feedstocks to avoid the competition for land and water between renewable fuels/chemicals and food/feed.

In the past fifteen years, several approaches and solutions to these challenging tasks have been made possible and cost-effective by the development of the concept of integrated operations for the biomass treatment within biorefinery plants.

1.3.2. Biorefinery

A biorefinery has been defined by the International Energy Agency (IEA) Bioenergy Task 42 as the co-production of fuels, chemicals, power and material from *biomass*.[20] It is a facility where renewable feedstocks are upgraded to bioenergy, biochemicals, biomaterials, food and feed by maximising the value of the biomass, including waste, while reducing the waste itself. Analogous to a petrorefinery, where chemicals, energy and materials are produced from fossil resources, a biorefinery is capable of generating a range of products. These vary from large-volume low-value fuels (*e.g.* biodiesel and bioethanol), to high-value low-volume chemicals, which are important to the pharma, cosmetics, nutraceutical, advanced materials, and other sectors.

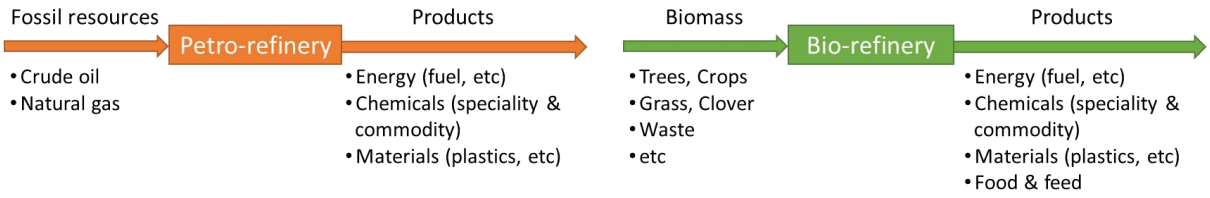

Figure 1.9. Comparison between the petro-refinery and the biorefinery processes.

As shown in Figure 1.9, the main difference between the two refineries is in the feedstock. In the petro-refinery, crude oil as a mixture of hydrocarbons, is transformed into different products through numerous processes. In the biorefinery, biomass as a mixture of carbohydrates and biopolymers is transformed into a range of higher value targets. The upgrading of biomass and fossil resources can also lead to similar products. However, because of the significant differences between the starting feedstocks, the concepts and technologies applied in the petro-refinery are often useless for the biorefinery processes or at best, they must be drastically modified to be adjusted for uses in the biorefinery.

1.3.3. Biorefinery classifications

Despite initial difficulties, biorefineries are becoming more sophisticated with time. Some biorefineries are already competitive in the market and more are growing and developing. Forecasts from the Joint European Biorefinery Vision for 2030 announced that an increasing proportion of energy, chemicals and materials would be derived from biomass by 2030. In particular, by this date it is expected that:

- 30% of the overall chemical production (and up to 50% of high added-value chemicals and polymers) will be derived from biomass;
- 25% of Europe's transport energy needs will be supplied by clean and CO_2-efficient biofuels, with advanced fuels (especially for jet aircrafts) having an increasing share of the total fuel market;
- 30% of heating and power generated in Europe will be of bio-origin.

The growth not only in the number of biorefineries, but also of the different types of biorefineries, has prompted the development of a classification system.[21,22,23] Although this is not univocal and is still under debate, the most accepted categorisation separates the biorefineries into three major Phases, based on the flexibility of feedstocks, processing capability and product generation:[24]

- Phase I biorefinery (single feedstock, single process and single major product);
- Phase II biorefinery (single feedstock, multiple processes and multiple major products);
- Phase III biorefinery (or developed biorefinery, multiple feedstocks, multiple processes and multiple major products).

1.3.3.1. Phase I biorefinery

A Phase I biorefinery is characterised by a fixed processing capability and produces a fixed amount of a specific product. It has almost no flexibility in processing. Common examples of Phase I biorefineries are the facilities for the manufacture of pulp and paper and for the production of biodiesel. Figure 1.10 shows a schematic flowchart of a Phase I biorefinery producing biodiesel from rapeseed.

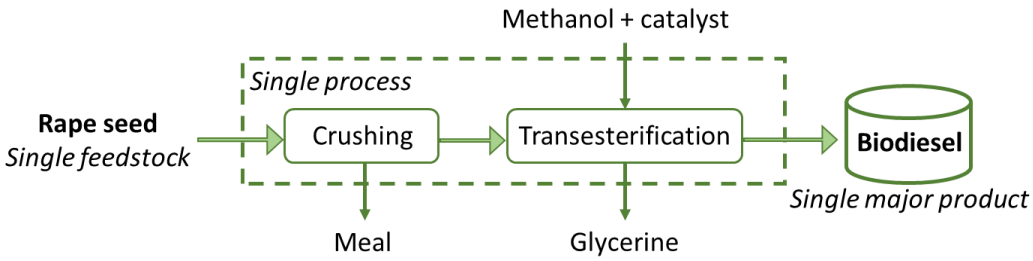

Figure 1.10. The biodiesel process: an example of a Phase I biorefinery process.

Another recent model of first generation biorefinery is the Eni Green Refinery in Porto Marghera, Venice (Italy). This also represents a remarkable case of industrial reconversion in an area where conventional petrorefinery plants were no longer sustainable. The former refinery establishment was first built in 1926 and converted into a Mineral Oil Refinery Industry in 1947. Due to damages caused during the Second World War, the plant was subsequently rebuilt, and acquired by Eni in 1978. In the late 2014, the same company accomplished one of the world's first ever conversion of a conventional mineral oil refinery into a biorefinery, which is currently operating on the hydrogenation of triglycerides contained in vegetable (first generation biofuels) and cooking oils (second generation biofuels) to Green Diesel. This fuel can be mixed with a fossil-based diesel up to 15%, and the so achieved blend, named "Diesel+", is already available in more than 3500 Italian petrol stations.[25]

Despite the notable results of Phase I biorefineries, these plants have almost no versatility and, at present, they are no longer representing a perspective for innovation in the field of biomass conversion.

1.3.3.2. Phase II biorefinery

One step further in the evolution of biorefineries has been achieved by implementing Phase II biorefineries, where a single substrate/feedstock is transformed into a range of end-

products (energy, chemicals and materials). Due to a higher flexibility than the former Phase I plants, Phase II biorefineries answer much more efficiently to market demand and prices.

Among modern Phase II biorefineries, some significant examples are located in Italy and managed by the Novamont Company, which was born in 1990 from the older Montedison chemical industry.[26] Originally aimed at promoting innovative chemistry more compatible with the environment and agriculture, Novamont is now a modern corporation focused on the production of bioplastics and biochemicals from renewable sources. The concept followed by Novamont is based on the development of biorefineries integrated into the local areas, where local raw materials (low-input crops, waste, etc.) produced by the local agricultural industries, are exploited with respect to the specific characteristics of each region. Novamont is known worldwide for three major products, which include Mater-Bi®, Matrol-Bi® and Celus-Bi®, which are biodegradable bioplastics, biodegradable biolubricants and bio-based ingredients for the cosmetic sector, respectively.[27] In all cases, the production of these materials has been conceived through the same bioeconomy model, where a dismissed or non-competitive industrial site was revitalised by its conversion into an innovative biorefinery. For example, the Mater-Bi® trademark sells four classes of thermoplastic starch (TPS): A, Z, V, and Y.[28] These are biodegradable and compostable bioplastics made of non-genetically modified corn starch, which comes in nature in a crystalline form composed of amylose (a linear alpha-D-(l-4)-glucan) and amylopectin (a branched alpha-D-(l-4)-glucan with alpha-D-(1-6) linkages at the branch point) and vegetable oils cultivated in Europe using conventional agricultural practices. Mater-Bi TPSs are realised by an initial destructurisation of starch, followed by its complexation with vegetable biodegradable derived polyesters (*e.g*. poly(ε-caprolactone) for Mater-Bi class Z).

Another noteworthy example of a biorefinery developed by Novamont into a local area is that designated to the production of bio-based 1,4-butanediol (BDO). BDO is an important commodity chemical used for the synthesis of 2.5 million tonnes of plastics, polyesters, and spandex fibres, annually. Although BDO is still majorly produced from petroleum-based feedstocks such as acetylene, butadiene, and propylene oxide (Figure 1.11, pathways **a**, **b**, and **c**, respectively),[29] recent researches have demonstrated that an effective microbial fermentation of sugars can be exploited for the synthesis of BDO (Figure 1.12).[30]

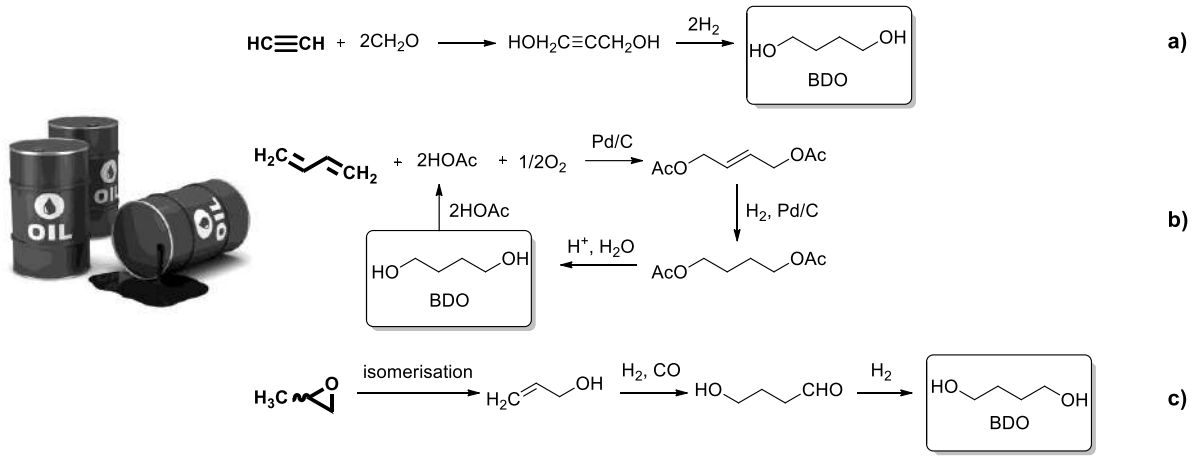

Figure 1.11. Synthesis of BDO from acetylene, butadiene and propylene oxide (a, b and c, respectively).

Starting from a modified strain of *Escherichia Choli* engineered by Genomatica,[31] Novamont was able to scale up the process from 2000 to 30000 tonnes/year in a fully refurbished industrial site operating in Bottrighe (Rovigo, Italy). This plant is fed by wastes from local rural activities and is expected to reach its full capacity by the end of 2017. Novamont has estimated that this new technology will save over 50% of CO_2 emissions with respect to conventional BDO productions.[27]

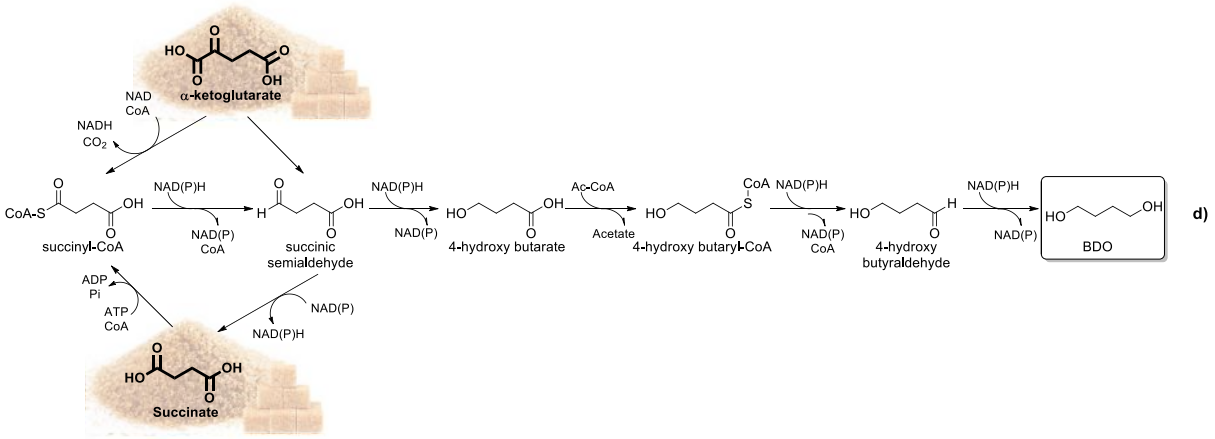

Figure 1.12. A sequence of the metabolic pathway for the production of BDO (d).

This example adds to the list of virtuous cases that confirm how the development of investment and infrastructure, in the context of the circular economy, may strongly contribute to the growth, employment and capital of innovation of a Nation by reconnecting the economy and society.

1.3.3.3. Phase III biorefinery

Phase III biorefineries are the most developed/advanced type of biorefinery, in which different processing technologies are used to process different feedstocks for the production of different chemical products and energy. It should be noted first that biorefineries of such a complexity still do not exist on an industrial scale; however, according to the Biofuels Research Advisory Council, they are expected to become established in Europe around 2020.[32] These biorefineries will bring the highest degree of versatility, affording conversions of different sources, including wastes. Hence, they will be capable of efficiently meeting the market demand by selecting the most profitable combination of raw materials for that specific time period.

Phase III biorefineries have been divided into five major groups depending on the feedstock and the number of products achievable:

- lignocellulosic feedstock biorefinery;
- whole-crop biorefinery;
- green biorefinery;
- two-platform biorefinery;
- marine biorefinery.

Due to the size and the complexity of the subject, an in-depth analysis of model Phase III biorefineries has been considered beyond the scope of this Thesis work. However, to focus the discussion on some critical aspects, the following Sections 1.3.4, 1.3.5 and 1.3.6 offer a survey on major technologies used to approach the treatment of several types of biomass feedstocks.

1.3.4. Biorefinery feedstocks and their pre-treatments

A biorefining process starts with the choice of the raw materials. Among other issues, two points deserve a special consideration in this context: *i)* feedstocks destined for chemicals and fuels must in no case compromise the ability to produce food and feed;[33] *ii)* biomass is not an unlimited resource, the availability and quality of which may depend on seasonality and geographic locations of areas of harvests. The significance of these points should never be underestimated, especially in the perspective of implementing large scale processes, where the requisite of having physically and chemically consistent starting materials with a constant supply over the year is a stringent requirement.

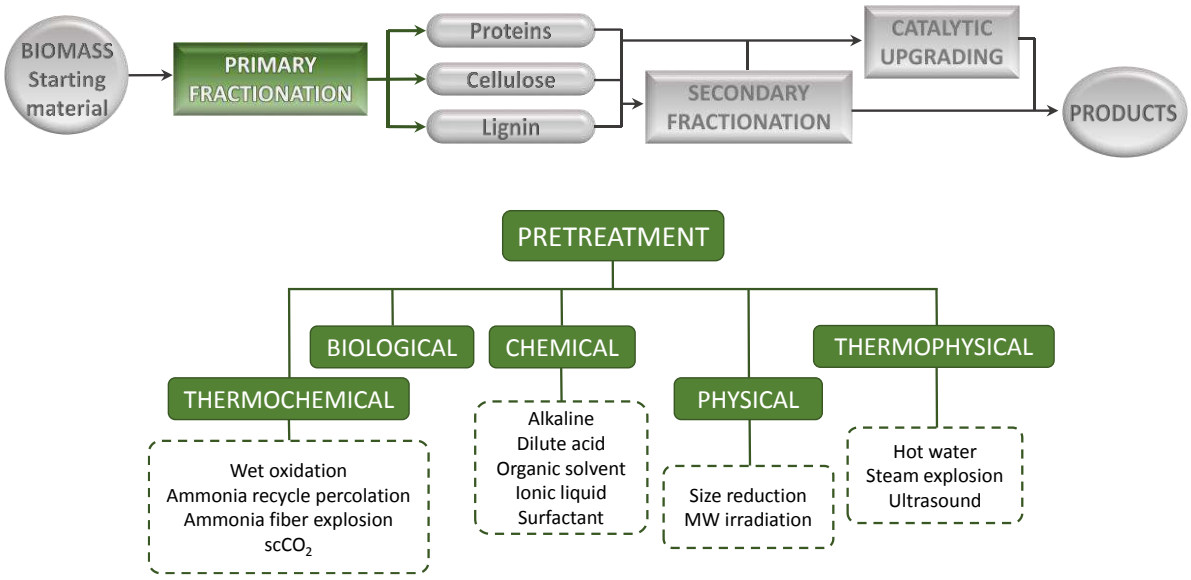

Figure 1.13. Top: Flowchart of an advanced biorefinery highlighting the primary fractionation of biomass; Bottom: pre-treatments commonly used for fractionating lignocellulosic biomass.

As mentioned in Section 1.3.1, biomass is composed of a mixture of very different constituents including polysaccharides (starch, cellulose, hemicellulose, chitin, etc.), lignin, proteins and other organics (triglycerides, terpenes, pigments, waxes, etc.). Moreover, variable amounts of inorganics and ash may also be present. The latter could represent a concern when producing pure chemicals and materials, but also represents an opportunity to prepare new bio-based catalysts, *e.g.* aluminosilicates, for applications in the biorefinery.

Therefore, initial treatments of the feedstock of a biorefinery clearly depend on the nature/type of the chosen biomass. These operations are necessary to break down lignin, cellulose and hemicellulose, which are organised together with acetyl groups, minerals and phenolic substituents.[15,34] Pre-treatments are generally classified into physical, chemical, thermophysical, thermochemical and biological processes.[35] These are highlighted for the fractionation of lignocellulosic biomass in Figure 1.13.

The choice of a pre-treatment must be done by not only evaluating the potential products that can be achieved, but also other parameters such as the economic feasibility and the environmental impact.[36]

Physical pre-treatments usually consist of: *i)* size reduction performed to disrupt biomass crystallinity and thus increasing its specific surface area to a suitable biomass particle size; *ii)* microwave irradiation, which has proven to break down lignin-hemicellulose complexes, to partially remove silicon and lignin, and to increase the accessible surface area of cellulose.[37]

Chemical pre-treatments are focussed on the removal of hemicellulose and lignin from cellulose. Depending on the desired target/results, several procedures/reactions can be used. A list of the most common chemicals and the corresponding effect on biomass is summarised in Table 1.2.

Thermo-physical and thermo-chemical pre-treatments are also widely used to improve the fractionation of lignocellulosic materials. One of the most promising procedures is the so called liquid hot water (LHW) method which uses water at elevated temperature and pressure. Besides the low environmental impact, this technology is effective in hydrolysing the lignocellulosic biomass and, as an added advantage, it does not require any washing of the residues after the treatment. Supercritical-CO_2 (sc-CO_2) is also used as a nonpolar, low-viscosity solvent for thermal fractionation of biomass. In this case, the breakdown of lignocellulose structures is favoured by the high diffusivity of sc-CO_2, which can deeply penetrate within the solid material. Another solution is offered by ultrasound based methods, which utilise cavitation to enhance heat and mass transfer during biomass breakdown.

Table 1.2. Effect and chemical substances of lignocellulosic biomass pretreatment.[33]

Chemical Pretreatment	Chemicals	Effect
Alkaline	H_2O_2, NaOH, Na_2SO_3,Na_2S, lime ($CaOH_2$), Na_2CO_3,NH_4OH	High lignin removal, enrichment of holocellulose, increase the porosity of biomass and cellulose swelling
Acid	H_2SO_4, peracetic acid, HCl	Remove hemicellulose fraction and increase biomass crystallinity
Ionic liquids	[bmim][OAc], [bmim][Cl], [emim][OAc], [emim][CH_3COOH], [emim][$DEPO_4$], [dmim][$MeSO_4$], [amim][Cl], [DMSO/LiCl], [Bmpy][Cl]	Weaken the van der Walls interaction between cell walls polymers, disrupt arabinoxylan–lignin linkages, alter the fibrillar structure of cell wall, decrease cellulose crystallinity, increasing cellulose surface accessibility
Organic solvent	Ethyl acetate, ethanol, acetic acid, formic acid	Break down internal lignin and hemicellulose bonds, increasing pore-volume and surface area of biomass
Surfactant	Polyethylene glycol, Tween 80, Tween 20, sodium dodecyl sulfate (SDS), dodecyltrimethylammonium bromide (DoTAB), Triton X-100, Triton X-114, Agrimul NRE 1205, HM-EOPO, amphoteric Anhitole 20BS, Neopelex F-25	Alter biomass structure, stabilise enzyme, increase interaction between holocellulose and enzyme, reduce adsorption of enzyme on lignin

Finally, biological pre-treatments are extensively studied for thermally labile bio-based derivatives, since they afford low energy requirements and mild operation conditions. Nonetheless, due to their cost, these (biological) methods are still far from being industrially applicable.[38]

1.3.5. Biomass secondary treatment

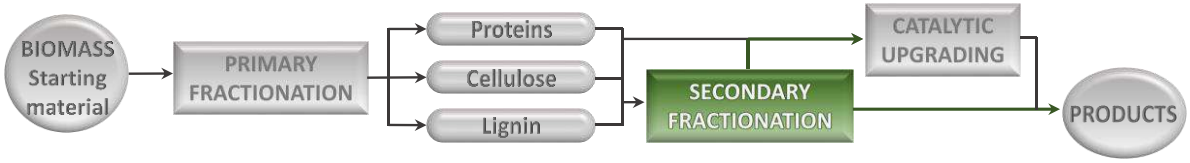

Figure 1.14. Biorefinery flow scheme: secondary treatment.

The second step in the processing of biomass in a biorefinery is the secondary treatment, which is aimed at further simplifying the components derived from the primary fractionation. Cellulose and hemicellulose are converted into small oligomers and sugars, together with furans, through the partial or total cleavage of the glycosidic bonds. Cellulose is a robust polymer where strong hydrogen bond interactions, van der Waals forces and resistance of the anomeric oxygen to protonation contribute to preserve the cellulose structure. This means that its conversion to processable sugars is not trivial and it generally involves depolymerisation/hydrolysis reactions at high temperatures. These processes include steam explosion at high temperatures and pressures (*e.g*. the Proesa™ process commercialised by Beta Renewables in Crescentino, Italy[39]) and supercritical solvolysis in water or polar aprotic solvents.[40] A promising route for the depolymerisation of cellulose involves its solubilisation in biomass-derived solvents such as γ-valerolactone (GVL, which is obtained from biomass-derived carbohydrates *via* levulinic acid),[41] and subsequent acid hydrolysis. In particular, J. S. Luterbacher *et al*. demonstrated how mixtures of GVL/water solutions (containing ~0.05 wt% H_2SO_4) afford soluble carbohydrates from corn stover, hardwood and softwood (Figure 1.15). The process was carried out using a stainless steel flow-through reactor packed with the lignocellulosic biomass. The solvent mixture was passed through the reactor at 157–217 °C, allowing for the recovery of 90 to 95% of the soluble polysaccharides. Finally, the aqueous phase was separated along with 75–91% of the carbohydrates from GVL/water solvent systems by either the addition of NaCl or liquid CO_2, which allowed for the recovery and recycling of GVL.[42]

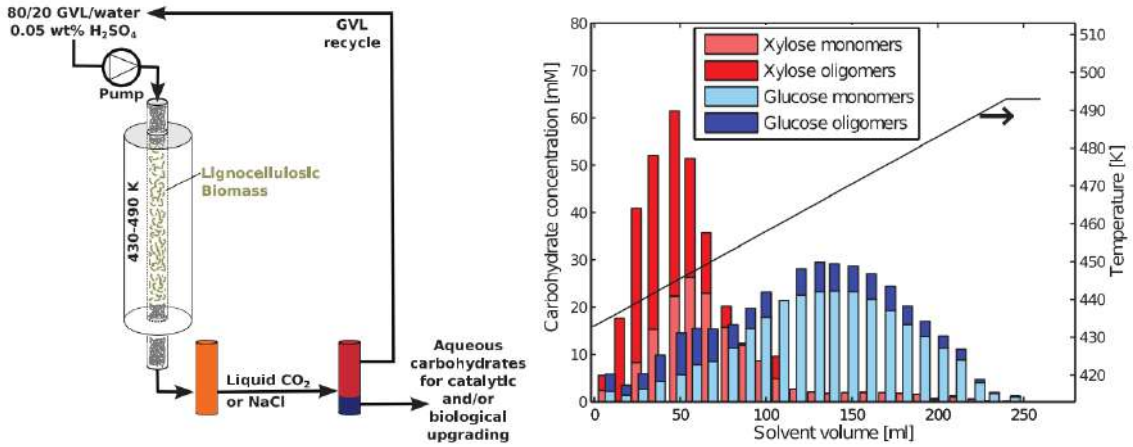

Figure 1.15. Overview of the aqueous-phase soluble-sugar production using GVL as the solvent (left). Soluble carbohydrates produced by the progressive heating of corn stover in a packed-bed flow-through reactor using 5 mM H_2SO_4 in 80 wt% GVL and 20 wt% water (right).[42]

Recently, non-thermal technologies have been reported for the selective break down of cellulose to low molecular weight glucans, with notable advantages in terms of selectivity and downstream processing.[43] These include ionic liquids[44] and mechanocatalysis, which is based on a synergistic effect between mechanical forces and acid catalysts (*e.g*. solid layered mineral kaolinite[45] or impregnation of cellulose with a catalytic amount of a strong acid such as H_2SO_4 or HCl and subsequent grinding of the mixture[46]).

On the other hand, lignin is first separated from the cellulose and hemicellulose and then treated with dedicated processes, which are specifically designed for the production of either monomeric aromatic compounds or energy. One of the most important technology for the upgrading of cellulose and lignin is the Kraft process of wood.[47] This allows for the selective removal of lignin and the parallel production of fibres with high strength properties. In Kraft pulping, wood chips are impregnated with the so called white liquor, which consists of a mixture of hot water, NaOH and Na_2S. The suspension is then cooked at 140–170 °C for 1.5–4 hours until the lignin is extensively degraded by the action of the sulfide and bisulfide anions, and the degradation products are dissolved. Heating temperatures and time, together with amount of alkali and sulfide ion concentration (sulfidity), are properly tuned depending on the type of raw material used. In particular, softwoods usually require harsher pulping parameters compared to hardwoods (*i.e*. higher cooking temperatures, higher content of alkali, 18–23% compared to 16–20%, and higher sulfidity, 25–40% instead of 20–30%).[47] The cooking step takes advantage of the fact that the activation energy for the bulk delignification of both softwood and hardwood is in the range of 119–127 kJ/mol and it is much lower than the activation energy of 180 kJ/mol necessary for the degradation of cellulose.[47] After the liquid

removal, the left solid pulp, the brown stock, is washed and collected. At this point, cellulose and the residual hemicellulose can be efficiently depolymerised by other reactions including those described above. On the other hand, the combined liquid, known as black liquor, is made of 10–18 wt.% of dry solids *i.e*. lignin fragments, residual carbohydrates and inorganic chemicals as Na_2CO_3, Na_2SO_4 and other (these last ones accounting for the 40–50 wt.% of the dry solids, Figure 1.16).

Figure 1.16. The Kraft process main steps.

At this point, the black liquor can be treated in different ways, which involve either the precipitation and isolation of the lignin, to be used as a process chemical, or burning it for the production of energy to be used inside the pulp plant.

Unfortunately, nowadays the black liquor is mainly used for this last purpose, and the potential of lignin as aromatic chemical source is not fully exploited. In this case, the black liquor is therefore sent to the evaporation plant, where it is concentrated to 60–80% of dry solids thus forming a thick black liquid. This one undergoes a combustion treatment in the recovery boiler, which is a special combustion furnace that functions both as a steam boiler and as a chemical reactor, yielding heat energy, steam (H_2O and CO_2) and the cooking chemicals (Na_2CO_3 and Na_2S). These are then dissolved in water, thus forming the green liquor (the greenish colour is due to small amounts of iron sulfides). The last step of the Kraft pulp mill is the recausticising step, where pulping chemicals are recovered by converting the Na_2CO_3 back to NaOH. This is performed by reacting Na_2CO_3 with slaked lime (CaO), thus giving NaOH and $CaCO_3$, which is separated from the mixture (Eq. 1.1). The NaOH and Na_2S (white liquor) can therefore re-enter the pulp cycle and be reused (Figure 1.17).

$$Na_2CO_3 + CaO + H_2O \rightarrow 2NaOH + CaCO_3 \qquad \text{(Eq. 1.1)}$$

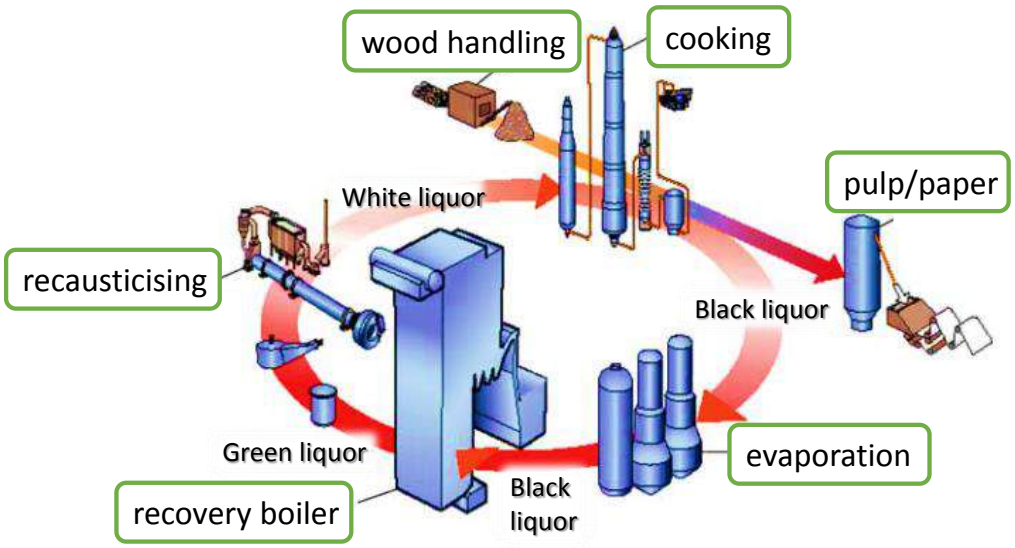

Figure 1.17. Recovery system for a Kraft pulp mill.

Recently, studies for the development of new technologies for the upgrading of lignin into useful chemicals and materials have attracted high interest from the scientific community. Lignin is one of the most important renewable sources of aromatic compounds but, despite the fact that achieving the single monomers is challenging due to the complicated structure of lignin, it is still a very attractive source of phenolic compounds.

1.3.6. Platform chemicals: the biorefineries output

The biorefinery chain can produce an output comprising of several intermediate products with an exceptional chemical diversity. This richness may certainly represent a value, but it also poses a non trivial issue in the identification of the most promising molecules, or families of compounds, to which the research and investments should be directed. Of the many analyses carried out to cope with this challenging scenario, the extensive work reported in 2004 by the US National Renewable Energy Laboratory (NREL) and the Pacific Northwest National Laboratory (PNNL) and its revision in 2010 probably offer the best guidelines in this field.[48,49] These studies proposed a systematic classification of bio-based chemicals by adopting concepts and selection conditions employed in traditional petrochemical industry flow-charts. In 2004, screening criteria included the type of raw material, the estimated processing costs and selling price, the chemical functionality, the potential use and development in the market, etc. The 2010 revision was even more market-addressed, considering for each of the examined bio-based derivative: the attention in the literature, the occurrence of flexible technologies suitable for high-volume production, the potentiality for the substitution of

existing petrochemicals and the use as starting materials for other derivatives, the engineering scale-up or the existence of demo plants, the occurrence as an already existing commercial intermediate or commodity, the role as a primary building block and the occurrence of a manufacturing process already recognised within the industry. Overall, these investigations allowed for the identification of a rather restricted list of compounds, which were named ***top platform chemicals***. Table 1.3 shows the results for the "***revisited top 10s***": each entry (compound) is classified according to the mark received for any of the reported selection criteria. Of note, only three compounds earned full marks (triple star) with respect to all the selection criteria: ethanol, sorbitol and glycerol.

Although Authors stated that results could include a degree of subjectivity due to the rapid change and expansion of the biorefining industry, a recent re-visitation of these studies indicates that most of the original Top 10s still represent the current platform compounds from biomass. These include ethanol, some furan derivatives, mono- and di-carboxylic functionalised acids, 3-hydroxy butyrolactone, biohydrocarbons derived from isoprene, glycerol and derivatives, and few other sugars as sorbitol and xylitol.[50]

This picture helps to clarify the further content of this Section.

The intermediates products (outputs) of the biorefinery process can be grouped after the raw feedstock where they come from.

Table 1.3. Revisited top 10 chemicals from ref. 50.

Compound	Extensive recent literature	Multiple product applicability	Direct substitute	High volume product	Platform potential	Industrial scale-up	Existing commercial product	Primary building block	Commercial biobased product
Ethanol	+++	+++	+++	+++	+++	+++	+++	+++	+++
Furfural	++++	++	+	++	+	+	+++	++	+++
HMF[a]	+++	++	+	+	++	+	+	++	+
FDCA[a]	+++	+	+	+++	++	+	+	+	+
Glycerol	+++	+++	+++	+++	+++	+++	+++	+++	+++
Isoprene	+++	++	+++	+++	+	+++	+++	+	+
BHC[a]	++++	++	+++	+	+	+	+	++	+
Lactic acid	+++	+++	+	+++	++	+	++	+	+
Succinic acid	+++	+++	+	+	+++	+++	+	+	+
HPA[a]	+++	+	+++	+++	++	+	+	+	+
Levulinic acid	+++	++	+++	++	+++	+++	+	+++	+
Sorbitol	+++	+++	+++	+++	+++	+++	+++	+++	+++
Xylitol	+++	+++	+	+	+++	+	++	+++	++

a)HMF = Hydroxymethylfurfural; FDCA = Furan-2,5-dicarboxylic acid; BHC = Biohydrocarbons; HPA = 3-hydroxypropionaldehyde. +++: high; +:low.

Saccharides

Saccharides constitute the most dominant fraction of biomass and they are likely to become the major source for platform molecules in the long term. Beside mono-and di-saccharides, which can be directly upgraded through either fermentation, chemical or thermal processes, polysaccharides need a previous saccharification treatment, where they are hydrolysed into the single monomer sugars (*e.g.* xylose, glucose and fructose).

Table 1.4 summarises some of the relevant platform chemicals that can be achieved from monosaccharide processing. The most promising compounds are highlighted in bold.

Table 1.4. Platform chemicals obtainable from saccharides.

C2-C6 acids and alcohols		
C2		***C5***
Acetic acid		Itaconic acid
Ethanol		**Levulinic acid**
Oxalic acid	***C4***	**Xylonic acid**
	1,4-butanediol	**Furfural**
C3	**3-hydroxybutyrolactone**	
1,2-propanediol	**Aspartic acid**	***C6***
1,3-propanediol	**Butanol**	**2,5 Furandicarboxylic acid**
1,3-hydroxypropionic acid	**Fumaric acid**	**5-Hydroxymethylfurfural**
Lactic acid	**Malic acid**	**Citric acid**
Propionic acid	Succinic acid	**Gluconic acid**
Acetone		**Sorbitol**

Lighter molecules, such as ethanol and butanol, can be efficiently produced from hemicellulose.

After saccharification of cellulose, pentose (C5) sugars are mainly upgraded to furfural, which is one of the major platform feedstock (Table 1.3 and Scheme 1.2, top). Of note, furfural has already been produced on an industrial scale for almost 100 years from non-edible biomass, such as corncobs, oat hulls, almond husks, bagasse, residues of olive extraction, and other biomasses rich in pentose biopolymers, and it can be further upgraded by means of many successful processes. In the Sylvan process, for example, pentose biopolymers are converted into premium diesel *via* furfural.[51] First, the pentosan containing biomass (mainly xylose) is dehydrated to furfural in an aqueous acidic process and then hydrogenated to 2-methylfuran (or Sylvan). In a recent optimisation reported by Corma *et al.*, three molecules of 2-methylfuran are then reacted under acidic (H_2SO_4, or solid acids such as the Amberlyst 15 resin and *p*-toluenesulfonic acid) conditions, yielding a C_{15} oxygenated intermediate molecule

(hydroxyalkylation/alkylation step). This step is performed using water as the solvent and so, as soon as the organic product forms, it spontaneously separates from the aqueous phase. Beside the easy separation of the product, this step allows for the recovery and reuse of the catalyst dissolved in the aqueous media. Finally, this intermediate is converted to the corresponding 6-butylundecane *via* a hydrodeoxygenation step with a final overall yield of 87% (Scheme 1.1).[51] This product is suitable for mixing with high quality diesel fuel.

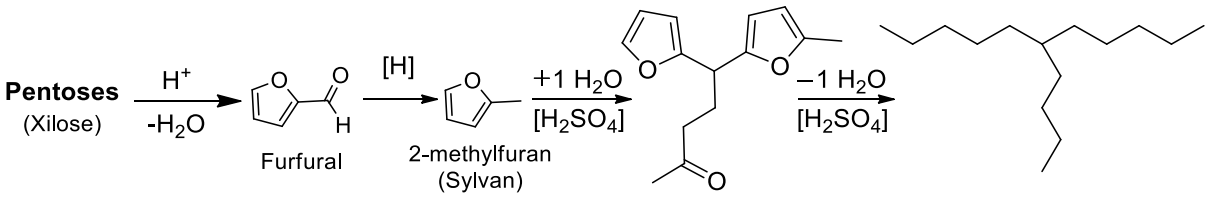

Scheme 1.1. The Sylvan process for the production of 6-butylundecane.[51]

Furfural can also be stepwise hydrogenated to furfuryl alcohol, which is another platform chemical of the furan family, and to 2-methyltetrahydrofuran (2-MeTHF), which is widely used as a bio-based solvent. Otherwise, other popular strategies also include the oxidation of furfural to furoic acid and ring opening reactions aimed at the production of ethyl levulinate.

On the other hand, hexoses (C6) sugars are the major source for other platform chemicals such as 5-hydroxy methylfurfural (HMF), levulinic acid and sorbitol (Scheme 1.2, bottom). Of these compounds, HMF has received the most attention as it is a precursor of furan-2,5-dicarboxylic acid (FDCA).[52]

HMF derives from C6 sugars *via* a two-steps dehydration process,[53] and it can subsequently lead to FDCA through three oxidative steps. This is usually performed at temperatures in the range of 90–150 °C, under an oxygen atmosphere and in the presence of a basic catalyst (*e.g.* Mg-Al hydrotalcite, sodium carbonate, sodium hydroxide).[54] The interest for FDCA relies on its use as a bio-based monomer for the synthesis of polyethylene furanoate (PEF) (Scheme 1.2, bottom). The Avantium's YXY technology for example, aims at replacing the petroleum-based polyethylene terephthalate (PET) with 100% renewable PEF in the near future.[55]

Other higher-value platform molecules can also be readily derived from the sugars, including xylitol, levulinic acid and itaconic acid.

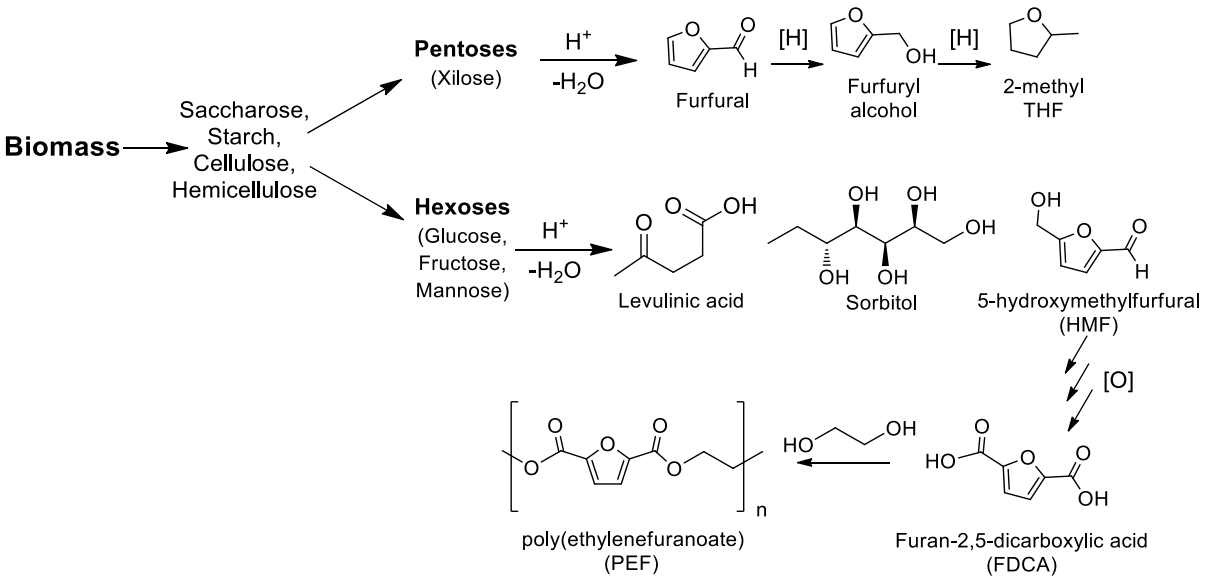

Scheme 1.2. Acid dehydration of hexoses and pentoses.[17]

In recent years, also chitin has been widely studied as another sugar-bearing bio-polymer and it is generally composed of N-acetyl-D-glucosamine and D-glucosamine monomers bound by beta-1,4 linkages (Scheme 1.3). Chitin is abundant in nature since it constitutes the major component of the exoskeletons of crustaceans, and it is becoming a sizeable by-product of the seafood industry. Chitin can be used as such or processed to form the more soluble deacetylated polymer (chitosan), for the synthesis of new functional biomaterial of high potential in various fields, such as in the textiles, in membranes and medical aids, in catalysis, etc..[56] Otherwise, it can be hydrolysed under acidic conditions or pyrolysed to the glucosamine monomer or 3-acetamido-5-acetyl furan, respectively (Scheme 1.3).

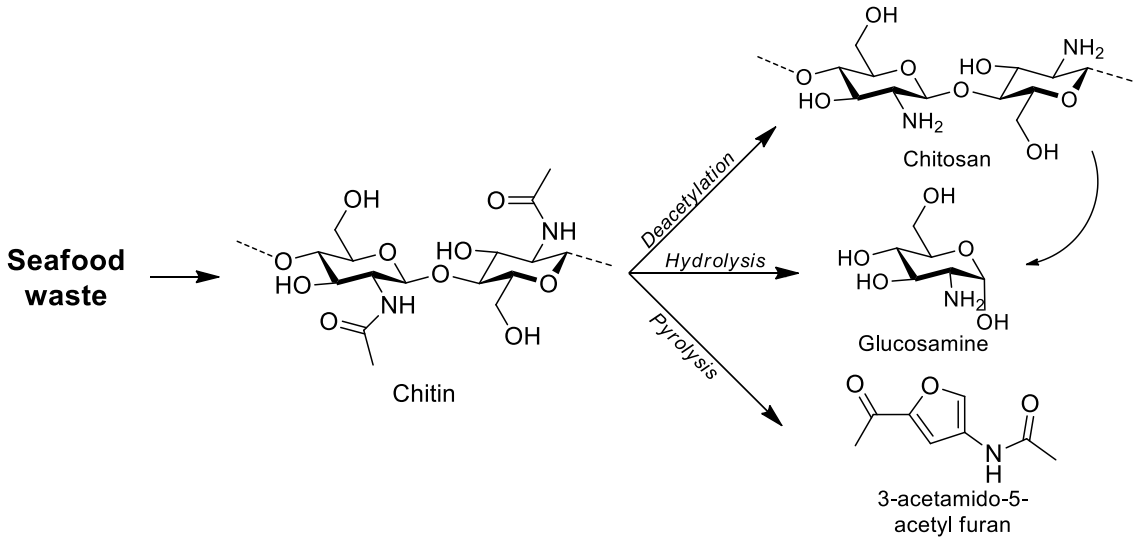

Scheme 1.3. Potential platform chemicals from chitin.

Lignin

Lignin is the most important source of renewable aromatic compounds and different technologies have been recently studied for its depolymerisation. Although an estimated 130 million tons of lignin are generated annually by industry, it remains the least valorised fraction of woody biomass. The main technical difficulties for the processing of lignin are attributed to its complex, irregular structure and its propensity for repolymerisation during thermochemical depolymerisation (*e.g.* pyrolysis and solvothermal liquefaction). This is also the reason why lignin (mostly recovered from the Kraft pulping, see Section 1.3.5), continues to be used mainly as a boiler fuel for energy recovery.

To date, research efforts to produce platform chemicals from lignin are focused on either the pyrolysis or chemical depolymerisation (including hydrothermal hydrolysis and hydrogenolysis) techniques. Fast pyrolysis is often preferred, by which lignin is rapidly heated at high temperatures (>500°C) to afford a mixture of gases, char and bio-oil as a complex mixture of organic compounds.[57] Hydrothermal hydrolysis is instead carried out in the presence of steam, generally at a lower temperature (<400 °C) than pyrolysis. However, higher pressures of 220–250 bar are needed to increase the efficiency of this process.[58] The hydrogenolysis of lignin usually occurs under milder conditions, where H_2 or an H_2 source such as ethanol or formic acid, are used to avoid repolymerisation processes. The hydrogenolysis of lignin has been part of the research program developed in this Thesis work. This subject will be further described in Chapter 4.

Extracts

A variety of natural oils and resins, generally termed as extracts, can be obtained by the straightforward extraction of biomass through the use of solvents or the pressing of seeds. These operations are more often carried out by conventional solvents, however, green solvents and green extraction technologies have been studied in order to improve the characteristics of energy reduction, eco-friendliness, non-toxicity and more efficient extractions. Among these, bio-derived solvents, supercritical fluid (SCF) technology, ionic liquids (ILs) and deep eutectic solvents (DES) represent the existing and emerging green solvents. On the other hand, accelerated solvent extraction, sonication- and microwave-assisted extractions are among the process intensification technologies recently applied.[59]

Extracts in turn, are an excellent source of several families of bio-based compounds; the four major ones are listed in Figure 1.19. These include terpenes, reduced sugars, and hydroxy acids, and derivatives of triglycerides, respectively.

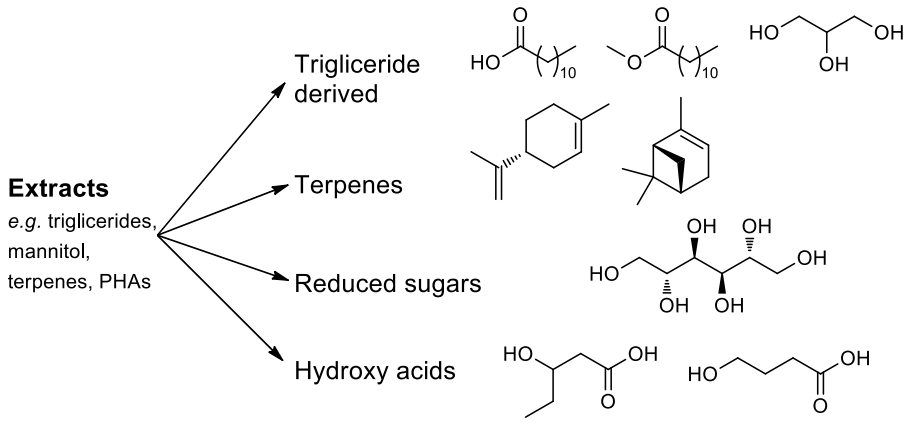

Figure 1.18. Examples of platform molecules obtained *via* direct extraction or derived from biomass extracts.

The isolation of terpenes from biomass has been extensively investigated since these derivatives find many applications as solvents, monomers, fragrances and flavours. Additionally, these compounds can readily be upgraded *via* oxidation, isomerisation, reduction and hydration reactions. An exemplary case is the epoxidation of limonene to 1,2-limonene epoxide (LO), a bio-based monomer for the production of 100% sustainable polycarbonates. The alicyclic terpene limonene (Lim), is a renewable non-food resource, obtained by extraction from citrus oil in 70,000 tons per year (in 2013)[60] and it can be efficiently oxidised to 1,2-limonene epoxide *via* both homogeneous (*e.g.* by mean of molybdenum or rhenium complexes) and heterogeneous (*e.g.* supported titania) catalysis. Completely bio-based poly(limonene carbonate) (PLimC) can then be achieved by coupling LO and carbon dioxide using zinc-based catalysts (Scheme 1.4). The reported PLimCs possess attractive thermal (glass transition temperature, Tg = 130 °C) and optical properties (transmission 94%, haze 0.75%), a thermal stability as high as 240 °C and they are characterised by excellent transparency and hardness.[61]

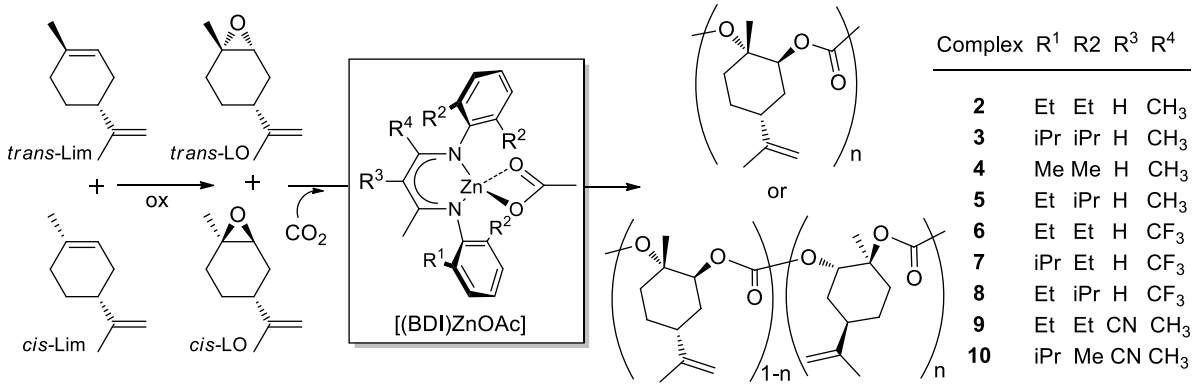

Complex	R^1	R2	R^3	R^4
2	Et	Et	H	CH_3
3	iPr	iPr	H	CH_3
4	Me	Me	H	CH_3
5	Et	iPr	H	CH_3
6	Et	Et	H	CF_3
7	iPr	Et	H	CF_3
8	Et	iPr	H	CF_3
9	Et	Et	CN	CH_3
10	iPr	Me	CN	CH_3

Scheme 1.4. Epoxidation of *trans*- and *cis*-Lim to *trans*- and *cis*-LO and subsequent copolymerisation of *cis*/*trans*-LO and CO_2 in the presence of a Zn complex.[61]

Natural polymers, such as polyhydroxyalkanoates (PHAs), which form as intracellular granules during microbial metabolism,[62] allow for the production of simple molecules such as reduced sugars (*e.g.* D-mannitol) and hydroxyl acids. Both these classes of compounds are derived from the controlled hydrolysis of PHAs and are of interest in the field of bio-based thermoplastics and bio-materials.[63]

Derivatives of triglycerides (TGs) represent the largest source of platform molecules that are directly or indirectly achieved from extracts. The most relevant example is glycerol, which is mainly produced as a by-product of the biodiesel manufacture (Scheme 1.5).[64,65]

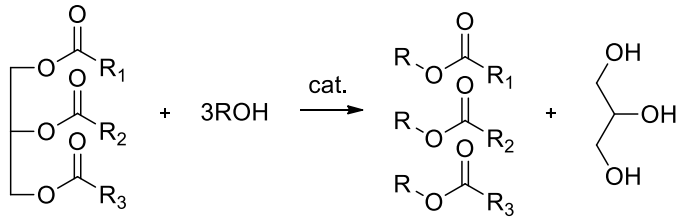

R=CH_3; CH_2CH_3
cat.=NaOH; KOH; $NaOCH_3$; $KOCH_3$

Scheme 1.5. Biodiesel and glycerol production *via* catalytic transesterification of TGs.

The stoichiometry of Scheme 1.5 shows that the transesterification of TGs (mostly from colza, soybean and palm oils) with light alcohols produces a sizeable amount of glycerol, which is approximately 10 wt.% of the total biodiesel. Therefore, the steady growth of the biodiesel production in the past fifteen years has resulted in an unprecedented interest from both the Academia and the Industry for programs aimed at the conversion of the co-product glycerol into energy and high-added value chemicals. This aspect largely contributed to the ranking of glycerol on the Top 10 platform chemicals list (Table 1.3).

The upgrading of glycerol and some of its derivatives *via* alkylation and transesterification reactions has been also part of the program developed in this Thesis work. This subject will be further detailed in Chapters 2–3.

1.4. If Sustainability is the goal, Green Chemistry will show the way!

The use of renewable carbon sources is a necessary, but not sufficient, requisite to move towards a sustainable manufacturing industry. In the modern biorefinery practice, technologies and protocols for both the primary fractionation of biomass and the further conversion of bio-based platform molecules must be designed to make any process the least detrimental for the environment and the least harmful to human health. Shortly speaking, transformations of biomass derivatives have to be chosen to fulfil the general principles of Green Chemistry and of Green Engineering, which are summarised in Table 1.5.[66]

Table 1.5. The 12 principles of Green Chemistry and the 12 principles of Green Engineering.[66]

	Principles of Green Chemistry		Principles of Green Engineering
P-	Prevent wastes	**I-**	Inherently non-hazardous and safe
R-	Renewable materials	**M-**	Minimise material diversity
O-	Omit derivatisation steps	**P-**	Prevention instead of treatment
D-	Degradable chemical products	**R-**	Renewable material and energy inputs
U-	Use safe synthetic methods	**O-**	Output-led design
C-	Catalytic reagents	**V-**	Very simple
T-	Temperature, Pressure ambient	**E-**	Efficient use of mass, energy space & time
I-	In-Process monitoring	**M-**	Meet the need
V-	Very few auxiliary substances	**E-**	Easy to separate by design
E-	E-factor, minimise feed in product	**N-**	Networks for exchange of local mass&energy
L-	Low toxicity of chemical products	**T-**	Test the life cycle of the design
Y-	Yes it's safe	**S-**	Sustainability throughout product life cycle

The two acronyms "IMPROVEMENTS" and "PRODUCTIVELY" have been coined as simple mnemonic rules to recall the meaning behind the most important guidelines for the design of eco-friendly chemical reactions and processes.

The Green Chemistry/Engineering principles are no longer perceived like a collection of single elements, but rather as a cohesive system aimed at generating innovation through new performance, function, and efficiencies. Several mathematical tools have been introduced to put these principles into practice and to assess the "*greenness"* of a reaction/process. Table 1.6 shows some of the more used metrics in Green Chemistry.[67,68,69]

Table 1.6. Most common green chemistry metrics.

Metric		Formula
Atom economy	**AE**	$\mathrm{AE} = \frac{\mathrm{M.W.\,product}}{\sum \mathrm{M.W.\,reagents}} \cdot 100$
Reaction mass efficiency	**RME**	$\mathrm{RME} = \frac{\mathrm{mass\ of\ product\ [kg]}}{\sum \mathrm{mass\ reagents\ [kg]}} \cdot 100$
Carbon efficiency	**CE**	$\mathrm{CE} = \frac{\mathrm{carbon\ mass\ in\ product\ [kg]}}{\sum \mathrm{carbon\ masses\ in\ reagents\ [kg]}} \cdot 100$
Mass index	**S^{-1}**	$\mathrm{S}^{-1} = \frac{\sum \mathrm{reagents + solvents + catalysts\ [kg]}}{\mathrm{product\ [kg]}}$
Environmental factor	**E**	$\mathrm{E} = \frac{\mathrm{total\ waste\ [kg]}}{\mathrm{product\ [kg]}}$
Cost index	**CI**	$\mathrm{CI} = \frac{€}{\mathrm{kg}}\ \mathrm{of\ product}$

These metrics are already so frequently cited in the literature that comments on their definitions would sound redundant. It should however be noted that this subject has been largely investigated in recent years, and among the several proposed elaborations, an inventive approach was the one implemented by John Andraos, who introduced the graphical analysis of the "*greenness"* of a transformation.[70] Through the use of new additional metrics, including the stoichiometric factor (SF) and the Material Recovery Parameter (MRP) (Eq. 1.2 and Eq. 1.3), Andraos was able to merge the meaning of several conventional and green metrics such as the chemical yield, AE, RME, etc. The final goal was to provide the so-called radial polygons, by which one may visually (and readily) appreciate pros and cons of any chemical transformation in term of its impact on the environment (generated wastes, excess reagents), costs (yield, recycle of solvents) and so on.

For a given reaction A + B $\rightarrow$ P + Q where P is the desired product, it is assumed that A is the limiting reagent. If "x" and "z" are the moles of A and B, respectively, (z-x) is the molar excess of B. The stoichiometric factor (SF) is then defined as:

$$SF = 1 + \frac{[(MW_B(z-x)]}{(MW_A x + MW_B x)]} \qquad \text{(Eq. 1.2)}$$

where [MW_B (z-x)] is the mass excess of reagent B, while [(MW_A x) + (MW_B x)] is the stoichiometric mass of reagents (based on the moles "x" of the limiting reagents.

The material recovery parameter (MRP) is defined as:

$$MRP = \frac{1}{1+\frac{(\varepsilon)(AE)(c+s+\omega)}{m_p(SF)}} \quad \text{(Eq. 1.3)}$$

c, s, and ω are the mass of catalyst, solvent, and all other post-reaction materials, while m_p is the mass of the desired product.

For now, it is pointed out that one of the key aspects of the integration of the green chemistry/engineering principles in the chain for the upgrading of bio-based derivatives is based on the use of clean and selective reagents that may not only replace harmful chemicals, but also minimise side-reactions and wastes. Dialkyl carbonates (DAlCs) nicely exemplify this category, at least where alkylation and transesterification reactions are concerned. Due to the interest for such compounds in this Thesis work, the following Section will describe properties and reactivities of DAlCs.

1.4.1. Dialkyl carbonates (DAlCs)

For years, alkyl halides (RX, X = I, Br, Cl; R = Me, Et, Bu, Allyl, etc.) and dialkyl sulfates ($ROSO_3R$) have been used as alkylating agents,[71] while alkyl chloroformates ($ClCO_2R$) and phosgene ($COCl_2$) have been widely used in carboxylation reactions.[72] Despite their high reactivity and selectivity towards the desired alkylated/carboxylated products, these compounds exhibit a number of drawbacks as they: *i)* are corrosive and highly toxic; *ii)* require stoichiometric amounts of bases to neutralise acidic by-products, this implying the disposal of co-produced salts; *iii)* more often undergo exothermic reactions, which ask for an accurate control of the reaction parameters; *iv)* require additional organic solvents to homogenise the reactant mixture and the temperature throughout the reaction vessel. Safer and eco-friendly alternatives for the replacement of these noxious compounds are dialkyl carbonates (DAlCs, Figure 1.19).

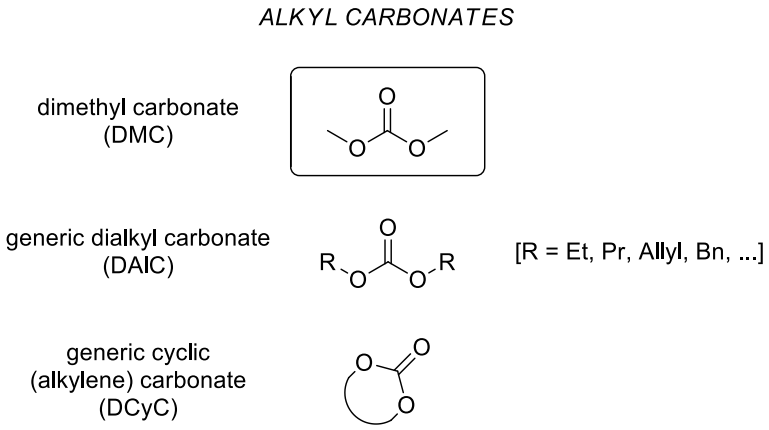

Figure 1.19. DMC and examples of commonly used alkyl organic carbonates.

Dimethyl carbonate (DMC), as the lightest term of the series, is a very good model of DAlC to introduce aspects related to the safety and the toxicological properties, the tuneable reactivity and the performance as solvents.

The production of DMC. Over the last 30 years, the industrial production of DMC has been remarkably improved in terms of environmental impact, safety and economics.

Before the 80's, the synthesis of DMC was based on phosgenation of methanol (Scheme 1.6, path a). Soon after, two main phosgene-free large-capacity processes were optimised and they became operative by the end of the 90's. Both processes were based on catalytic reactions of carbon monoxide with methanol. The first one was patented by EniChem in the early 80's and it was operative in Ravenna (Italy): the reaction involved the oxidative carbonylation of methanol with air catalysed by copper chloride (Scheme 1.6, path b).[73] The second protocol was optimised by the Ube industries in 1993 and it used methyl nitrite as the oxidant and a palladium-based catalyst (Scheme 1.6, path c).[74] These large-scale pathways were by far safer and greener than that starting from phosgene, because not only were reactants less toxic, but also reactions were catalytic and no inorganic salts were generated as by-products that needed to be disposed of. Nonetheless, the use of carbon monoxide, methyl nitrite and chlorine-based catalysts was still a concern. A breakthrough in the synthesis of DMC was achieved in the early 2000s, when a synthesis employing carbon dioxide as the building block was implemented. Carbon dioxide is the natural green candidate as a source for carbonyl groups, though its thermodynamic stability often poses severe challenges for applications. This limitation was overcome by the Asahi Kasei Corp., which industrialised a process where the catalytic preparation of DMC was integrated in the chain of production of polycarbonate from bis-phenol A.[75] Scheme 1.6 and Scheme 1.7 report the overall sequence. The first

reaction involves the insertion of CO_2 into ethylene oxide to give ethylene carbonate (Scheme 1.6, path d: cat. 1). The typical catalyst is a quaternary onium salt. In the second step, ethylene carbonate undergoes a carbonate interchange reaction with methanol (transcarbonation) to yield pure dimethyl carbonate. This process is also catalysed by a quaternary ammonium anion exchange resin in the presence of alkali hydroxides (Scheme 1.6, path d: cat. 2).

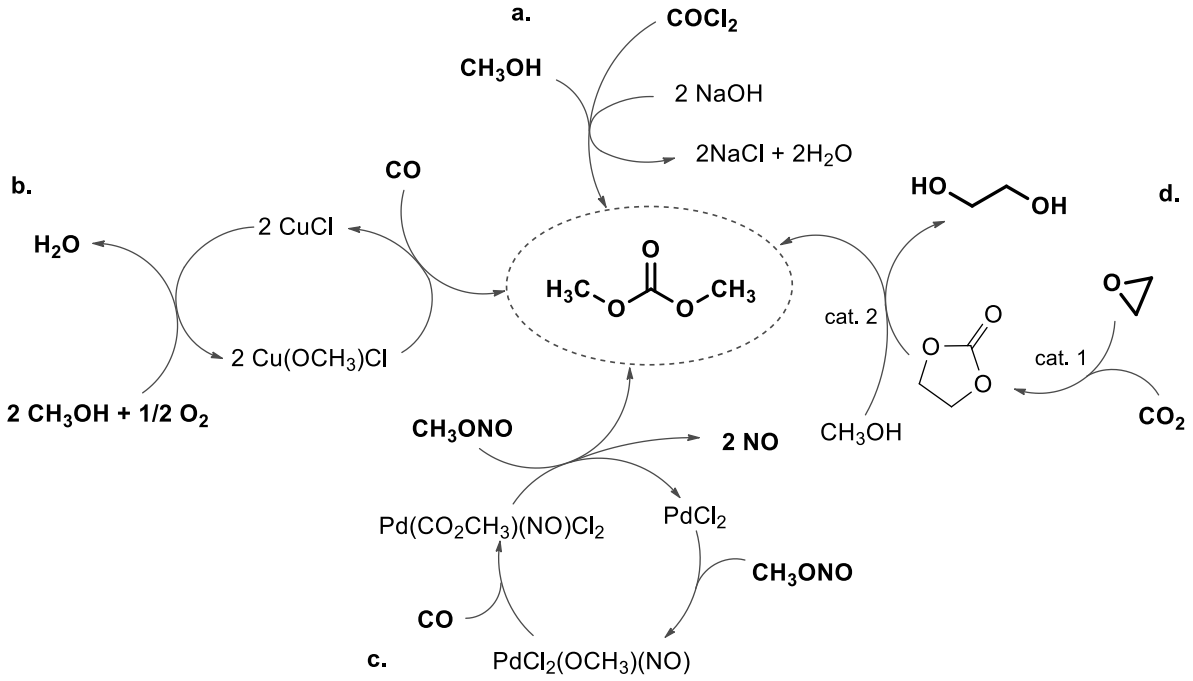

Scheme 1.6. The methods for the synthesis of dimethyl carbonate.

DMC is then reacted with phenol for the synthesis of diphenyl carbonate (DPC) which in turn, is used for the final reaction with bis-phenol A to produce polycarbonate (PC) (Scheme 1.7). Both of these processes are base-catalysed transesterification reactions, which take advantage of specific technological solutions: the preparation of DPC makes use of a reactive distillation column, patented by the manufacturer (Asahi Kasei Corp.), while PC is obtained in a thin-film in a non-agitated reactor, where gravity is used to control the polymerisation rate.

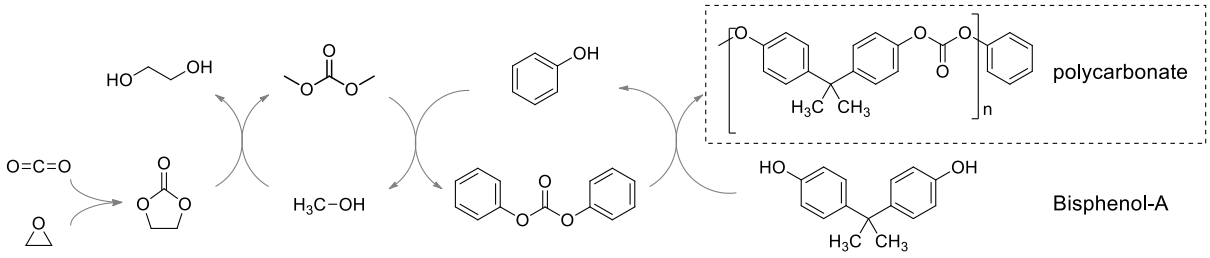

Scheme 1.7. Asahi Kasei's non-phosgene polycarbonate process.

Scheme 1.7 highlights how the Asahi protocol represents one of the best examples of green and sustainable chemical processes available today for industrial productions, where harmful chemicals are avoided and pollution is prevented at the source.

As a result of the catalytic phosgene-free methods discussed so far, the product dimethyl carbonate is classified as a nontoxic compound.[76] Table 1.7 compares some of the toxicological and eco-toxicological properties of DMC to those of phosgene and dimethyl sulfate (DMS), of which DMC can be considered the *green* replacement. Few doubts remain about the substantial benefits of DMC: conversely to phosgene and DMS, it has no irritating or mutagenic effects and it can be handled safely without special precautions.

Table 1.7. Comparison between Toxicological and Eco-Toxicological Properties of DMC, Phosgene and DMS.

Property	DMC	phosgene	DMS
oral acute toxicity (rats)	LD50 13.8 g/kg		LD50 440 mg/kg
acute toxicity per contact (cavy)	LD50 > 2.5 g/kg		
acute toxicity per inhalation (rats)	LC50 140 mg/L; (4 h)	LC50 16 mg/m^3; (75 min)	LC50 1.5 mg/L (4 h)
mutagenic properties	None		mutagenic
irritating properties (rabbits, eyes, skin)	None	Corrosive	
biodegradability (OECD 301 C)	> 90% (28 days)	Rapid hydrolysis	Rapid hydrolysis
acute toxicity (fish) (OECD 203)	NOEC 1000 mg/L		LC50 10-100 mg/L (96 h)
acute toxicity on aerobial bacteria of wastewaters (OECD 209)	EC50 > 1000 mg/L		

The general reactivity of DMC. DMC is an ambident electrophile. Depending on the reaction conditions, it can afford both methylation and carboxymethylation processes.[77] In the presence of a generic nucleophile (NuH) and a base (B), the two possible pathways are shown in Scheme 1.8. The nucleophile is initially activated by the base to produce an anionic species (Nu^-, eq. a), which in turn, may undergo two reactions:

i) at a moderate temperature (below or at the reflux temperature of DMC, 90 °C), an acyl nucleophilic substitution occurs at the carbonyl carbon of DMC, *via* a $B_{Ac}2$ mechanism (eq. i). A carboxymethyl derivative ($NuCO_2CH_3$) forms.

ii) at a higher temperature (usually above 120 °C), a $B_{Al}2$ mechanism predominates where the activated nucleophile (Nu^-) attacks the alkyl carbon of DMC to give a methyl derivative ($NuCH_3$, eq. c).

Due to the poorer electrophilic character of the methyl *vs* the carbonyl carbon of DMC,[78] the activation barrier of methylations are always higher than the corresponding carboxymethylations. Moreover, the methylcarbonate anion ($CH_3OCO_2^-$) generated as a

leaving group, is unstable and it spontaneously decomposed into CH_3O^- and CO_2. This makes the methylation process irreversible.

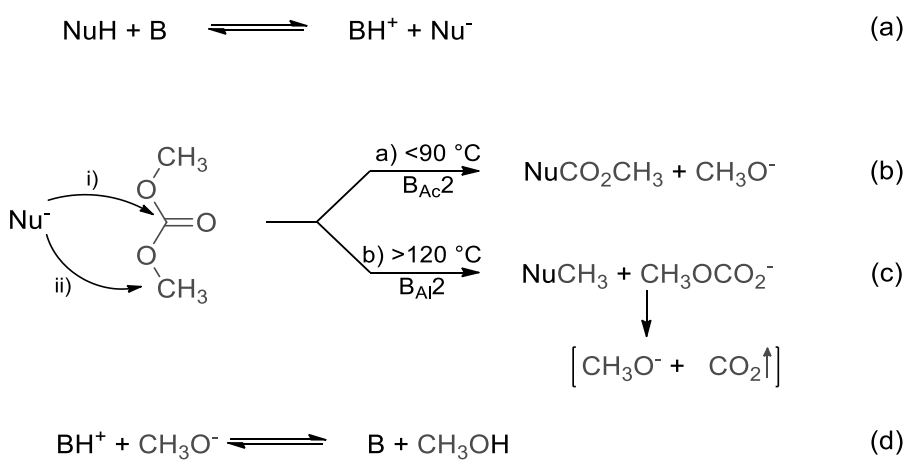

Scheme 1.8. The dual reactivity of dimethyl carbonate.

At the end of both pathways b) and c), the methoxide species CH_3O^- is neutralised by the protonated base BH^+ (eq. d): methanol forms, while the base is restored, thereby closing the catalytic cycle.

Overall, through eqn. b) and c), DMC acts as a safe replacement of phosgene and methyl halides or dimethyl sulfate, respectively. The two reaction co-products, CH_3OH and CO_2 (the latter formed only in the case of methylations), can be directly or indirectly recycled for the synthesis of DMC itself (Scheme 1.6), or easily conveyed for other uses. Additional solvents are usually not required since DMC may serve both as a reactant and a reaction medium.

Scheme 1.8 has been validated by many O-, N-, C-, and S-nucleophiles. Over the past 20 years, the reactivity and the use of organic carbonates, with emphasis on dimethyl carbonate, have been extensively investigated by the group (GOST*: Green of Organic Syntheses Team* @ Ca' Foscari University) where most of this Thesis work has been carried out. Most of these studies have been reviewed in recent papers.[79] It should be noted that although a neat cut-off between paths b) and c) is not always possible, the tuning of some reaction parameters, especially the temperature and the nature of the catalyst, often allows for the reaction to be tuned selectively towards the alkylation or the carboxymethylation process.

A brief overview will now follow, aimed at further clarifying the reactivity of organic carbonates (both DMC and others) by describing model examples, some of them also closely relevant for the upgrading of bio-based derivatives.

Reactivity of Organic carbonates: model examples. The properties of DMC also reflect favourably on its higher carbonate homologues, many of which can be achieved by the catalytic transcarbonation of DMC with both alcohols, phenols, and diols. Both linear and alkylene carbonates can be so prepared (Scheme 1.9).

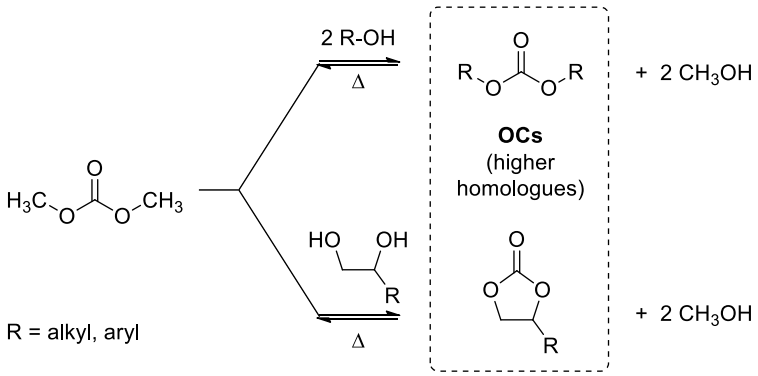

Scheme 1.9. Transesterification of DMC with alcohols to yield higher dialkyl and alkylene carbonates.

The most common catalysts for this reaction are both heterogeneous and homogeneous acids and bases such as carbonates, hydroxides, and alcoholates of alkali and alkali-earth metals, sulfonic acids, metal-based Lewis acid salts ($ZnCl_2$, $YbCl_3$, etc.),[80] but also several organocatalysts have recently been proposed. For example, at atmospheric pressure and in the proximity of the reflux temperature of DMC, the quantitative conversions and selectivity towards the synthesis of symmetric dialkyl carbonates were achieved by using as 1,5,7-triazabicyclo[4.4.0]dec-5-ene,[81] and ionic liquids (ILs) based on tetraethylammonium amino acids ($[N_{2222}][AA]$). Quantum-mechanical calculations combined with experimental data, proved that tetraethylammonium prolinate ($[N_{2222}][Pro]$) could activate BuOH and DMC to afford dibutyl carbonate in very high yields.[82]

Bernini and co-workers also reported the selective carboxymethylation of the alcoholic chain of a series of phenols [2-(2'-hydrophenyl)ethanol, tyrosol, and hydroxytyrosol] with dimethyl carbonate in the presence of either a strong homogeneous base, 1,8-diazabicyclo[5.4.0]undec-7-ene (DBU), or sulfuric acid as the catalysts.[83] The corresponding products were isolated in yields up to 98% after 1.2–12 h at 90 °C. In a similar context, the selective mono-transcarbonation of DMC and diethyl carbonate (DEC) with a number of different alcohols was described with a class of IL catalysts derived from methyl trioctylphosphonium methyl carbonate ($[P_{8881}]^+X^-$; X = CH_3OCO_2; $HOCO_2$; AcO; PhO).[84] At 90–240 °C, selectivities up to 99% and isolated yields >90% were achieved with catalyst loadings as low as 1 mol% (Scheme 1.10).[85]

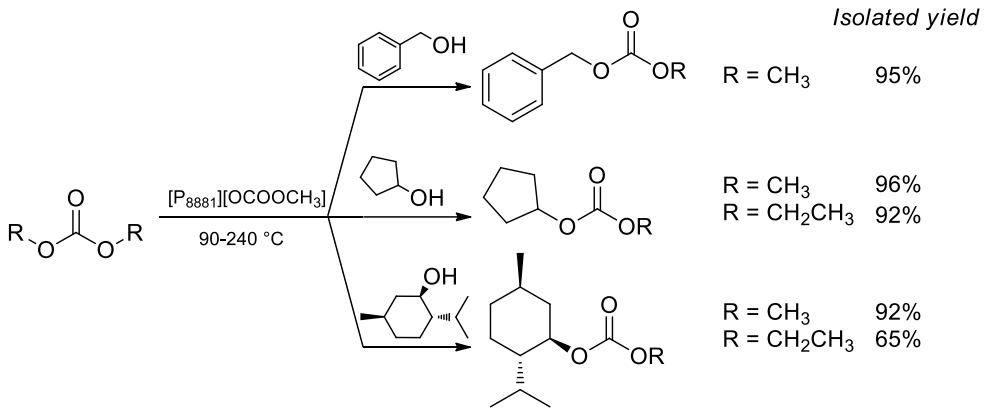

Scheme 1.10. Unsymmetrical carbonates obtained by transcarbonation reactions using phosphonium salts as the catalysts.

Compared to conventional heterogeneous and homogeneous bases (K_2CO_3, DBU, DMAP), these IL-based catalysts proved to be far more active. It was also noted that the reactions of DMC were always faster than those of DEC. This difference was plausibly due to steric reasons, and it was in analogy to the trend of the relative reactivity observed in many comparative tests of the two dialkyl carbonates.[58,86]

The activity of $[P_{8881}][X]$ (X = HCO_2 and CH_3OCO_2) was also tested on the carbonate interchange reactions of DMC and DEC with (1,*n*)-diols possessing both primary and secondary OH groups. Organocatalysts proved effective for highly selective reactions: for example, 1,2-diols yielded exclusively the corresponding cyclic carbonates, while 1,3-diols, depending on their structures, yielded either cyclic or acyclic carbonates as shown in Scheme 1.11.[87] The performance of IL-catalysts was explained by a cooperative ambiphilic (nucleophilic–electrophilic) mechanism in which the anion and the cation of the IL act synergistically for the activation of both the nucleophilic and electrophilic reactants, respectively (Scheme 1.12).

IL-catalysts were efficient catalysts also for the transcarbonation of DMC with (bio-based) glycerol. This is a useful reaction for the synthesis of glycerol carbonate (GC), a compound of interest as a renewable synthon, a green solvent and an additive to biofuels.[88] The structures of most active ILs are shown in Scheme 1.13: for example, at 74 °C with 5 mol% of BMIM-2-CO_2, GC was isolated in yields of 100% and 93% after 30 min and 5 h, by using pure and crude glycerol (with up to 41% of water), respectively.[89]

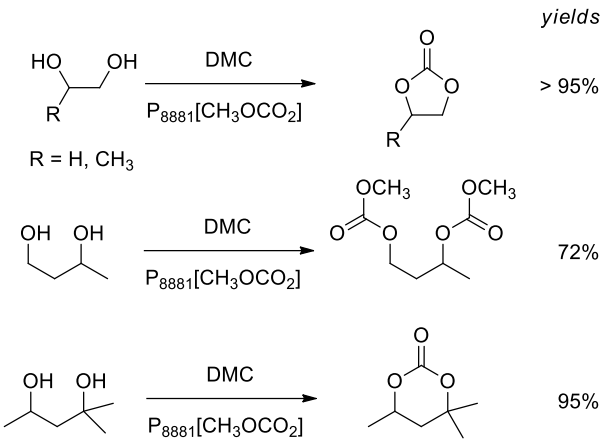

Scheme 1.11. Examples of carbonates obtained from different diols using $[P_{8881}][CH_3OCO_2]$ as the catalyst.

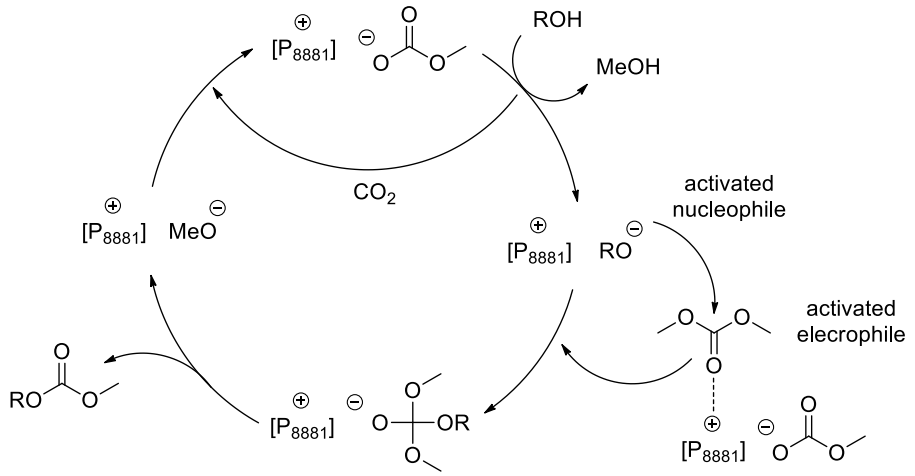

Scheme 1.12. Ambiphilic catalysis for model transcarbonation reactions of DMC in the presence of $[P_{8881}][CH_3OCO_2]$.

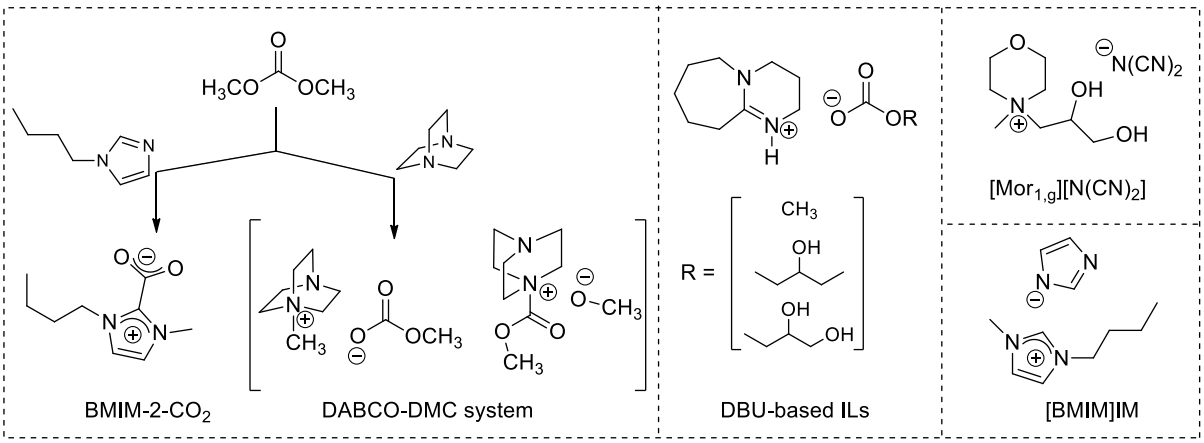

Scheme 1.13. Most reported ILs for the transesterification of DMC with glycerol.

At 70–120 °C and variable reaction times (90 to 780 min), other types of ILs including $[Mor_{1,g}][N(CN)_2]$, [BMIM][IM], DABCO-DMC systems, and 1-n-alkyl-3-methylimidazolium-2-

carboxylates as such or supported on siliceous mesostructured cellular foam (MCF), also allowed for substantially quantitative yields of GC.[61c,90]

In the field of aromatic carbonates, it is worth mentioning a recent paper of the group in which this Thesis work has been carried out. The work describes a selective transcarbonation of DMC with catechol in the presence of $NaOCH_3$ as the catalyst.[91] The reaction was optimised through a reactive distillation system and it occurred to be one of the most efficient ever reported for the synthesis of catechol carbonate (CC: benzo-1,3-dioxolan-2-one). This compound was achieved in substantially quantitative yields under mild conditions (90 °C, 1 bar: Scheme 1.14, eq. a).

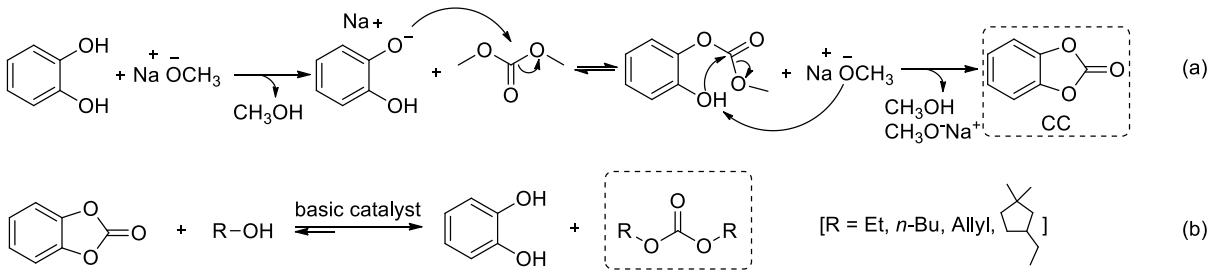

Scheme 1.14. Transcarbonation of: (a) DMC with catechol for the synthesis of CC; (b) CC with primary alcohols to give symmetric dialkyl carbonates.

The properties and reactivity of CC are still rather unknown. In this respect, the above quoted paper[91] also demonstrated that either $NaOCH_3$ or MgO were effective catalysts to activate carbonate interchange reactions between CC and primary and secondary alcohols, diols and polyols including glycerol (Scheme 1.14, eq. b). The investigation not only proved the potential of CC for the synthesis of symmetric dialkyl carbonates, but a comparative analysis of the same process carried out with DMC and ethylene carbonate (EC) confirmed that reactions of CC were by far faster and more selective than those of both DMC and EC. This was plausibly explained looking at the involved leaving groups (LGs): the catecholate-like anion released during the reaction of CC was remarkably more stable than the methoxide and glycolate-like species formed as LGs from DMC and EC, respectively. As it was mentioned above for DMC (Scheme 1.8), dialkyl and alkylene carbonates exhibit a dual reactivity as carboxyalkylating and alkylating agents, and alkylation reactions are usually more energy demanding than carboxyalkylations. These processes may take place at 120 °C, but they more often require temperatures above 160 °C, preferably between 180 and 220 °C. Scheme 1.15 reports major reaction conditions for the alkylation of phenols, thiophenols and CH_2-active compounds with DMC, DEC and dibenzyl carbonate (DBnC), respectively.[58,59,92]

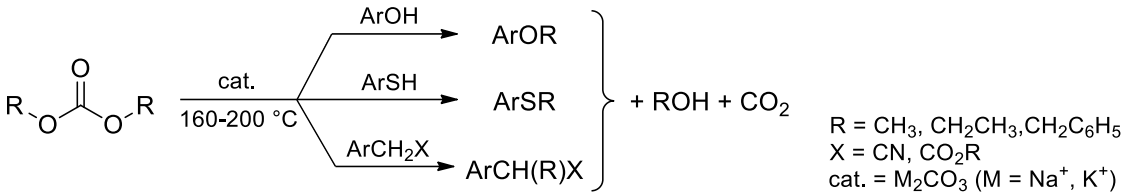

Scheme 1.15. Selective alkylation reactions of different nucleophiles with dialkyl carbonates.

Conventional inorganic bases such as alkali metal carbonates are probably the most used catalysts for these reactions. Notwithstanding the high temperature, *O*-, *S*-, and *C*-alkylations often proceed with selectivity up to 99% at complete substrate conversion. One of the key reason for this result stands on the nature of alkylations mediated by DAlCs. According to Scheme 1.8, once the high temperature allows for the activation barrier of the alkylation process to be overcome, the reaction takes place irreversibly with the release of CO_2. Therefore, even if the competitive carboxyalkylation occurs, this (equilibrium) reaction is forced to backtrack because of its reversibility.

Alkylations of a series of phenols, indoles, and benzimidazoles (8 examples, Yields = 91–99 %) by DMC were also described by using homogeneous bases such as DBU as the catalyst.[93]

Examples of alkylations of bio-based derivatives with DAlCs were also reported. Under conditions similar to those of Scheme 1.12, acetal derivatives of glycerol, typically solketal and glycerol formal, were selectively transformed into the corresponding *O*-alkyl ethers.

At T ≥ 200 °C, in the presence of K_2CO_3 as the basic catalyst, reactions proceeded with excellent selectivity and yields up to 99% and 86–99%, respectively.[86b] Using thiocarbamide as the catalyst and microwave irradiation, a method for the reaction of cassava starches with DMC afforded a moderate degree of *O*-methylation within minutes.[94] Another recent investigation explored the reaction of dilignol model compounds with DMC: at 180 °C and in the presence of Cs_2CO_3 as the base catalyst, reactants underwent the cleavage of the β-O-4 linkage and the simultaneous *O*-methylation of phenolic groups to produce veratrole and 1,2,3-tri methoxybenzene in 61 and 62% isolated yields, respectively.[95] The reactivity of organosolv poplar lignin (OPL) with a MeOH/DMC co-solvent system was studied at 300 °C by using a Cu-doped porous metal oxide (Cu/PMO) as the catalyst. It was demonstrated that Cu/PMO was simultaneously active for: *i*) MeOH reforming and water gas shift reactions with H_2 generation; *ii*) CO hydrogenolysis of ether bonds which cleaved β-O-4 and α-O-4 linkages of OPL and generated phenolic intermediates; *iii*) the *O*-methylation of phenolic intermediates.[96]

To conclude this analysis, it should be noted that by changing the nucleophile, specifically using amines rather than alcohols, phenols or thiols, can result in a dramatic change in the product distribution. This has been clearly recognised in the studies of the reaction of anilines with DAlCs for which several examples have been reported for either base- or acid- catalysed processes. Primary aromatic amines react with DAlCs to generate highly stable products of carboxyalkylation, *i.e.* carbamates ($RNHCO_2R'$). Contrarily to the corresponding derivatives of *O*-, *C*-, and *S*-nucleophiles (Scheme 1.15), such compounds (carbamates) persist even at very high temperatures (≥180 °C). Some results are described in Table 1.8 for the model reaction of aniline and DMC.

Table 1.8. Synthesis of methyl phenyl carbamate (MPC) from aniline and DMC.

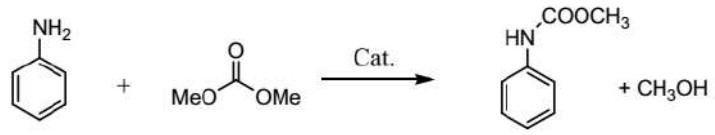

Entry	Catalyst	T, t (°C, h)	Conv.'n (%)	Product: MPC (Sel., %)	Ref.
1	$Pb(OAc)_2$/ $Pb(OH)_2$	180, 1	97	97	97
2	$Zn(CO_3)_2$	200[b]	97	95	98
3	$Zn(OAc)_2$	140, 6	>99	>99	99
	$Zn(OAc)_2$/AC[a]	150, 4	72	98	100
4	ZnO-TiO_2	170, 7	97	67	101
5	γ-Al_2O_3	90, 48	>99	95	102
6	K_2CO_3	180[b]	46	11	103

a) AC: activated carbon; b) continuous-flow conditions.

However, selective alkylations of anilines by DAlCs become possible by using different catalysts possessing ampotheric (acid/base) properties such as alkali metal-exchanged Y and X faujasites (FAUs: MY or MX, M = Li, Na, K), a particular class of zeolites.[104] In the presence of these solids, primary aromatic amines not only undergo alkylation reactions, but even more interestingly, they yield the corresponding derivatives of mono-*N*-alkylation (ArNHR) with an unprecedented high selectivity (93–98%) at conversions up to 95%. Only traces of bis(N,N)-dialkylated compounds are observed. This behaviour is also observed for anilines deactivated by steric and/or electronic effects and it finds even more notable applications for ambident substrates such as aminophenols, or aminobenzylalcohols bearing functional groups susceptible themselves to undergoing alkylations or carboxyalkylations with DAlCs.[105]

Scheme 1.16 exemplifies the model case of DMC-mediated methylation reactions. In the case of aminophenols, conventional catalysts (*e.g.* K_2CO_3, $[Pb(AcO)_2]$) promote competitive *O*-and *N*-methylation, and carboxymethylation processes, while the NaY faujasite allows the exclusive mono-methylation at the *N*-atom, while OH groups are fully preserved from any functionalisation. The corresponding derivatives are isolated in yields of 91–99%, respectively. Of note, due to the strong nucleophilic character of aminophenols, their *N*-methylations are low-energy demanding, these processes taking place at 90 °C.

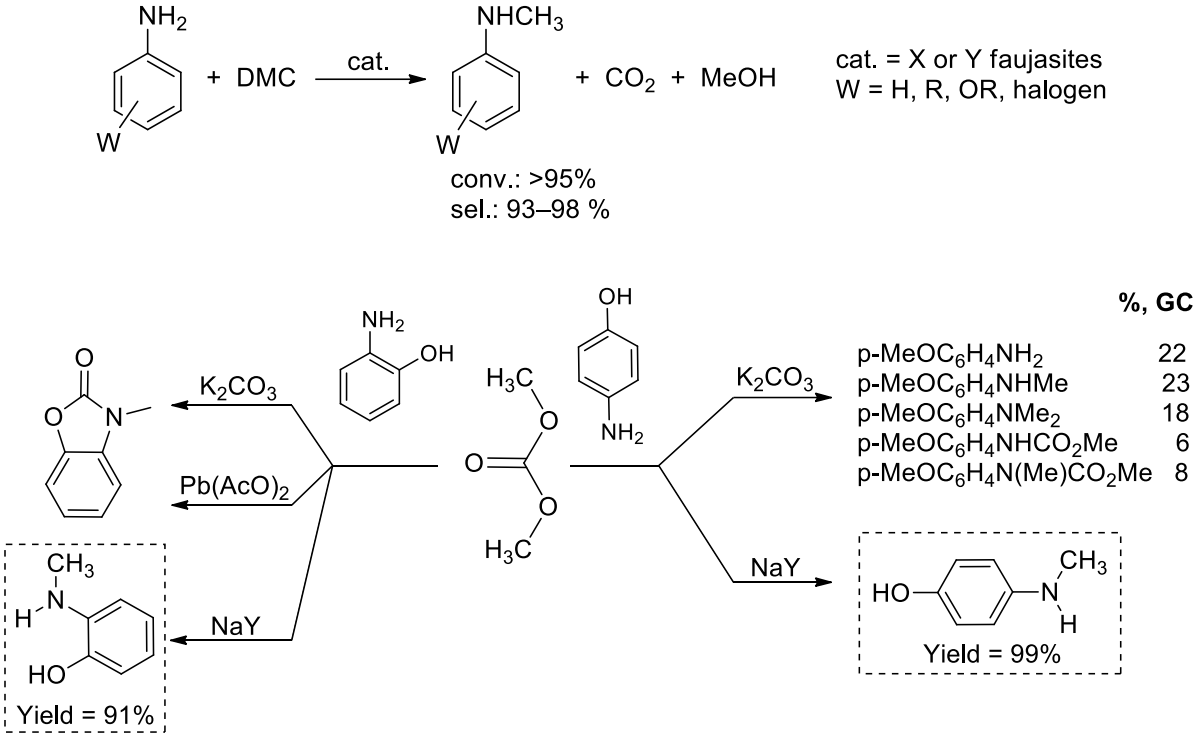

Scheme 1.16. DMC-mediated *N*-methylation of anilines catalysed by faujasites. Top: both activated and deactivated anilines. Bottom: ambident anilines (aminophenols).

To explain the unusually high selectivity observed in these processes, adsorption phenomena of aniline and DMC within the supercavities of FAU catalysts have been investigated by diffraction and IR techniques.[106] Results were consistent with a mechanism in which both reactants (aniline and DMC) diffuse into the cavities of the FAU and are coordinated by the surface of the catalyst through H-bonding and the formation of π-complexes and acid–base adducts. Then, reagents approach each other only according to the steric requisites of their adsorption patterns, and the final selectivity is the result of both the morphology (shape-selectivity) and the acid-base properties of the catalyst.

Our group also used FAU catalysts for several other chemoselective reactions, in which DAlCs acted as alkylating agents of different nucleophiles, including mercaptophenols,

mercaptobenzoic acids, carboxylic acids bearing OH substituents, indolyl acids, and benzyl alcohols.[107] FAUs have also been used in this Thesis work for the upgrading of some bio-based derivatives with dialkyl carbonates. The results will be described in Chapter 2.

1.4.2. Ionic liquids

Another remarkable approach to contribute to the integration of the green chemistry/engineering principles in the chain for the upgrading of bio-based derivatives, is based on the use of innovative solvents, which may not only replace conventional liquid media, but also create reaction environments with new and unique properties. Ionic liquids may serve this purpose. In the previous paragraphs, several ILs have been already described as organocatalysts. In this section, other features of ILs will be examined, particularly their ability to form multiphasic systems (MPs) suitable for extractions or for the separation of products and catalysts during chemical reactions. Such MPs have been used in this Thesis work.

The most accepted definition of ionic liquids is "*liquids composed entirely of ions that are liquid at or below 100 °C*".[108,109] Only in recent years have these compounds attracted great interest for many diverse applications in chemistry, physics, biology, and engineering; though, they have a rather long history. The first ionic liquid was attributed to Walden who, in 1914, prepared ethylammonium nitrate by neutralising ethylamine with concentrated HNO_3.[110] Thereafter, a second generation of ionic liquids was reported in 1951, by mixing alkylpyridinium chlorides with $AlCl_3$. These ILs were intended to be used primarily as electrolytes, but they were unstable to moisture.[111] This drawback was overcome by Wilkes and Zaworotko who, in 1992, synthesised a family of imidazolium salts exchanged with $[BF4]^-$ $[NO3]^-$ and acetate $[OAc]^-$ anions.[112] These ILs proved to be moisture and air-stable compounds and received wide attention from both the academia and industry. However, it was only a few years later when the first class of air-stable and hydrophobic ILs (starting from the 1-ethyl-3-methylimidazolium hexafluorophosphate, $[C_2mim][PF_6]$) were introduced: these compounds were able to form biphasic systems with water, thereby providing an innovative liquid-liquid system for extraction or other applications (Figure 1.20).[113]

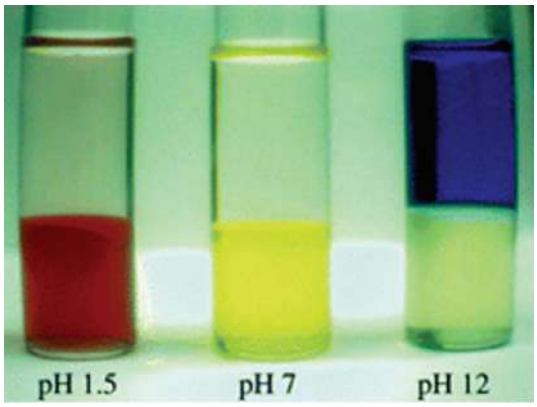

Figure 1.20. The phase preference of three forms of an indicator dye, thymol blue, at varying pH conditions in $[C_2mim][PF_6]$ (bottom layer)/water (top layer) biphasic systems.[113b]

Since then, ILs have been named "designer solvents", a definition which implies that they could be applied to clean technologies in an almost limitless range of potential applications. At the beginning of their explosive growth however, too much confidence was given to this class of compounds. ILs were considered as a group of non-volatile and water stable compounds, inherently safe and *green*. The generalisation used to describe ILs is now considered a common mistake. With the potential for ~10^{18} ion combinations, ILs can be either toxic or benign, safe or explosive, non-volatile or distillable.[114] As it was demonstrated for one of the most used and studied model of IL, the well-known $[C_4mim][PF_6]$ may undergo hydrolysis, forming $[C_4mim]F{\cdot}H_2O$ together with HF.[115] The occurrence of this side-reaction off-sets most of the benefits associated with $[C_4mim][PF_6]$. Therefore, today, the understanding of the chemical and physical properties of each ion combination in ILs goes well beyond considerations on vapour pressure and non-volatility, but rather it evaluates every other property based on observation and quantifiable data.

1.4.2.1. Applications of ILs in multiphasic systems

ILs can be used in a broad range of applications since their properties can be adjusted systematically by varying the anion and cation. Just to name a few fields of use of ILs, these include catalysis, CO_2 capture, gas detection, electrodeposition studies and electrochemical application as in batteries, solar cells and capacitors. In most of these applications, ILs allow for the set-up of multiphasic systems (IL-MPs), the establishment of which becomes a key advantage for the process itself or for the following workup procedure, and it often also ensures the recyclability of the ionic liquid. IL-MPs employing binary or ternary mixtures of immiscible aqueous, organic and IL phases represent a widely used arrangement for different

purposes; though, the intimate reasons for the occurrence of such MPs mediated by ILs are still far from being fully understood. It is known that the molecular forces and interactions in ILs are more complex than those present in classical salts. In fact, ions in ILs are poorly symmetric, which impairs crystal packing and very often leads to the occurrence of mixtures of hydrogen bonded ionic structures and free ions. The presence of both strong (Coulombic) and weak directional interactions, including hydrogen bonding, cation-π, and van der Waals inductive and dispersion forces, induces the formation of different domains characterised by polar/non-polar regions/behaviours, which impose a microphase separation similar to the liquid crystal structures.[116] These regions have also been described as nano-scale structures.[117]

Catalysis

Reactions catalysed by either homogeneous or heterogeneous systems may take advantage of IL-MPs: the catalyst itself can be confined and stabilised in the ionic liquid, while the reaction substrates and products are usually segregated in another aqueous or organic phase.[118] When applicable, these arrangements provide both built-in methods for the catalyst separation/recycle and product recovery, thereby improving not only the synthetic operations and work-up, but also the environmental compatibility of the process.

Of the possible configurations, simple biphasic liquid systems (L-L) are recognised only for homogeneous catalysts,[119] while more complex MPs such as liquid-liquid-solid (L-L-S), liquid-liquid-liquid (L-L-L), and liquid-liquid-liquid-solid (L-L-L-S) systems can be involved for both homogeneous and heterogeneous catalysts.[120] Figure 1.21 offers a pictorial view of these arrangements.

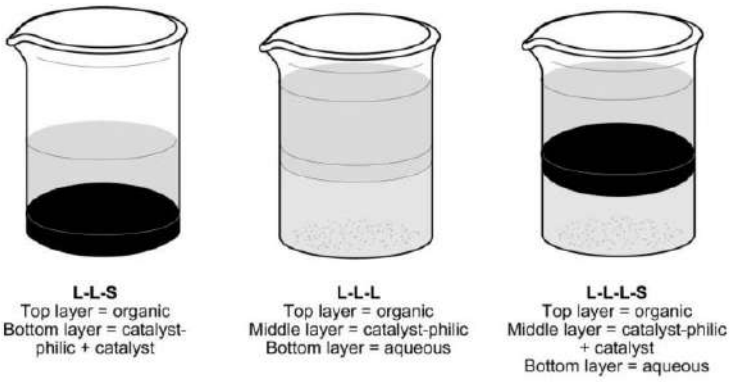

Figure 1.21. Schematic representation of L-L-S, L-L-L and L-L-L-S systems.[120]

In simple biphasic systems (LL) (not shown in the figure), ionic liquids usually constitute the bottom phase (given their –high- density), in which the homogeneous catalyst is soluble. On

the other hand, reactants and products are confined in the lower density upper phase. When an heterogeneous catalyst is used, the MPs can be comprised of a catalyst suspended in the IL phase (at the bottom) and an upper organic (or aqueous) phase which dissolves reagents and products (Figure 1.21: LLS, left). A further evolution of this latter case is the triphasic LLLS system, which consists of an aqueous, an organic and an IL layer. In these systems the heterogeneous catalyst, typically a C-supported noble metal (Ru, Pd, Pt), is confined within the ionic liquid phase, which is usually located between the other two layers (Figure 1.21: LLLS, right). This configuration has been reported in several examples: Figure 1.22 (left) describes a case reported by our group, in which a suspension of Pd supported on carbon is perfectly confined in $[N_{8881}][Cl]$ (Aliquat 336) as the ionic liquid (middle phase), and the bottom and the top phases are an alkali aqueous solution and *i*-octane, respectively.

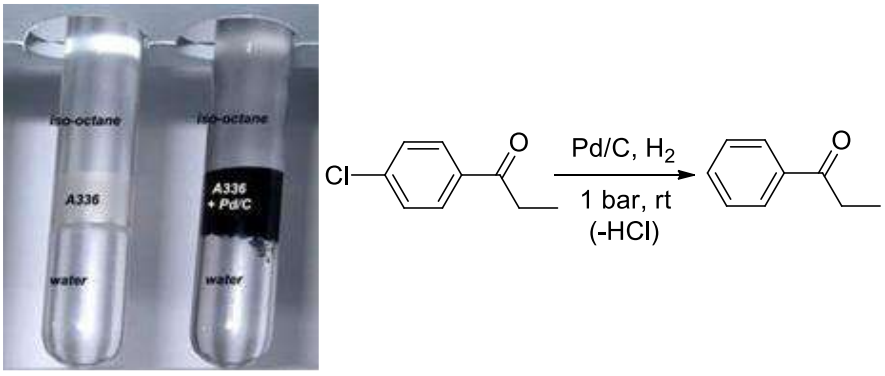

Figure 1.22. Left: multiphasic system: *i*-octane (top layer), trioctyl methyl ammonium chloride ($[N_{8881}][Cl]$) with suspended Pd/C (middle layer), and alkaline aqueous solution of KOH (20%, bottom layer). Right: multiphasic hydrodechlorination of 4-chloroprorpiophenone.

This LLLS system was tested for catalysis in many reactions, of which the hydrodehalogenation of 4-chloropropiophenone exemplifies a simple model process (Figure 1.22, right).[121] At room temperature and under H_2 pressure (1 bar), a quantitative and highly chemoselective removal of chlorine was achieved with not even traces of carbonyl reduction. When the stirring was stopped, the multiphasic mixture settled down: *i*) the organic product (PhCOEt) was isolated into the *i*-octane top layer; *ii*) the Pd catalyst remained segregated in the middle IL phase, and it could be recycled, and *iii*) the inorganic by-product HCl was scavenged by neutralisation in the alkaline aqueous solution (bottom).

An even more peculiar situation is represented by LLL systems in which the catalytic phase is confined in the form of metal nanoparticles (NPs) stabilised by the IL. The literature is extremely abundant on this subject.[122] For brevity, one case reported some years ago by our group is described and illustrated in Scheme 1.17, which shows a LLL stabilising Ru-NPs.[123]

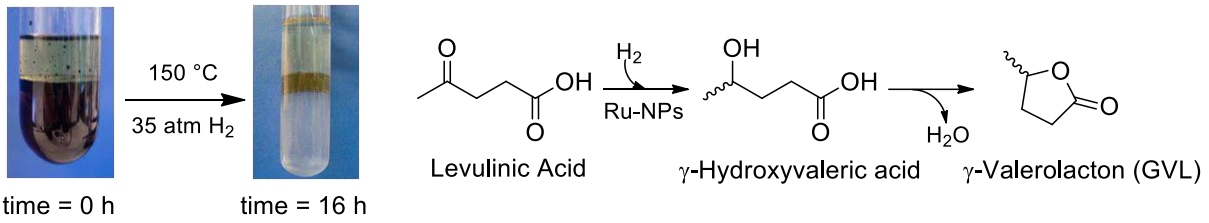

Scheme 1.17. A model triphasic system for the stabilisation of Ru-NPS.

Starting from a LLS system composed of a top layer of *i*-octane and a bottom layer of methyl trioctyl phosphonium chloride ($[P_{8881}][Cl]$) as the ionic liquid, water, and $RuCl_3$ (Scheme 1.17, left), after reduction with H_2, a well separated triphasic system was achieved (left). Ru-NPs of 2–3 nm were confined and stabilised in the IL medium, placed in between the organic and aqueous phases. This LLL arrangement was successfully applied for the conversion of levulinic acid into GVL: the reaction occurred in the aqueous phase, where the product GVL was isolated in a substantially quantitative yield (Scheme 1.17, right).

The peculiarity of ILs to stabilise metal nanoparticles (NPs) has been extensively investigated in similar LLL systems.[124] The results of these studies are briefly summarised in the remaining part of this section. One of the prevalent models to explain this effect proposes that ILs may act as supramolecular media in which a hydrogen bond network undergoes a self-organisation in non-polar and charged regions (Figure 1.23), the latter (polar) domains being capable of entrapping positively charged nanoparticles.

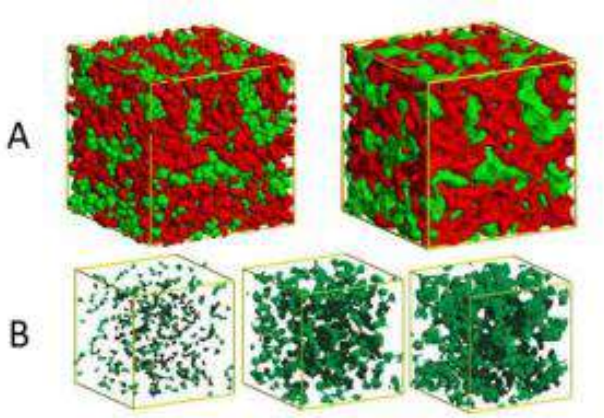

Figure 1.23. Snapshots simulation boxes containing 700 ions of $[C_n mim][PF_6]$. A: charged (red) and non-polar (green), domains in $[C_8 mim][PF_6]$; B: Topology of the non-polar domains: (left) $[C_2 mim][PF_6]$; (middle) $[C_4 mim][PF_6]$; (right)$[C_6 mim][PF_6]$.[126]

More specifically, three major effects have been accounted for the protection/stabilisation activity of ILs on NPs: *i*) the *electrostatic stabilisation,* which hypothesises that ILs form a double ionic layer surrounding the NPs surface.[125] A different standpoint has been introduced by the DVLO (Derjaugin–Landau–Verwey–Overbeek) theory: this assumes that ions of ILs act

as punctual charges of a network, where extra hydrophobic and steric interactions (*i.e.* DVLO forces) operate in the stabilisation of NPs.[126] *ii*) The *steric stabilisation,* by which the simultaneous action of van der Waals forces between alkyl chains and cation-anion attractions in ILs, inhibits the dissociation of ILs. The IL works like a polymer, where ions place themselves near the growing nanoparticles, while the alkyl chains of cations point towards the bulk, thereby forming a hydrophobic layer which prevents the diffusion of NPs through the medium (IL).[127] *iii*) The *stabilisation by solvation* that comes from the supramolecular nature of the ILs. Van der Waals forces and hydrogen bonding operating within ILs, may provide layers of different thickness, which induce different packing effect around the nanostructures. For example, the relatively small size of ions in ethyl ammonium nitrate (EAN) offers an efficient packing effect, while bulkier imidazolium based ILs provide less effective protective shells.[128]

Extraction and separation processes

Of the many strategies devised to perform selective liquid-liquid extractions (LLE),[129] one direction includes the use of ionic liquids. Physicochemical properties of ILs, particularly their low vapour pressure and high thermal stability, mostly account for this choice,[130] particularly for the implementation of novel methods of solute recovery through evaporative-pervaporative techniques for volatile substrates.[113a]

ILs have confirmed their role as novel media for liquid–liquid extraction not only of organic compounds, but also of inorganic species such as metal salts (of Hg^{2+}, Cd^{2+}, Co^{2+}, Ni^{2+}, Fe^{3+}, Na^{+}, Cs^{+}, and Sr^{2+}) in aqueous solutions. In this respect, ILs allowed for some important difficulties to be overcome, which were related to the low affinity of hydrated metal ions for common hydrophobic organic solvents,[131] as well as for the extraction of rare earth elements[132] and in the treatment of dye wastewater.[133] Notable results have been achieved for the extraction of (complex) organic compounds, such as the selective separation of a typical natural phenolic product, α-tocopherol, from its mixture with methyl linoleate,[134] the extraction of the excess glycerol from biodiesel,[135] the complete extraction of alkaloids such as caffeine and nicotine from both aqueous phases and more complex matrixes, such as human urine-type samples[136] and the extraction of free fatty acids from soybean oil.[137]

More recent applications of ILs have been reviewed in the selective extraction of bio-based components, specifically lignin from lignocellulosic materials.[138] Table 1.9 summarises these results.

Table 1.9. Ionic liquids used to extract lignin from some wood and non-wood materials.[138]

Ionic liquid abbreviation	Raw material	Conditions	Lignin removed (%)
[EMIM][OAc]	Maple wood	130 °C, 1.5 h	52
[EMIM][OAc]	Oak	100 °C, 16 h	35
[EMIM][OAc]	Corn stover	125°C, 1 h	44
[EMIM][OAc]	Switchgrass	160 °C, 3 h	69
[EMIM][OAc]	Triticale straw	150 °C, 1.5 h	64
[BMIM][HSO_4] (20% water)	Miscanthus	120 °C, 22 h	93
[BMIM][HSO_4] (20% water)	Willow	120 °C, 22 h	85
[EMIM][OAc]	Rice hull	110 °C, 4 h	46
[EMIM][OAc] (50% water)	Triticale straw	150 °C, 1.5 h	29
[BMIM][SO_3][HSO_4] (ethanol/water)	Sugarcane bagasse	200 °C, 30 min	100

Multiphasic systems assisted by ILs have been widely used for the clean-up of fuels, *i.e.* for the selective extraction of nitrogen and sulfur compounds. This method has shown its potential to replace or to become a supplementary technique to the conventional hydrodesulfurisation and hydrodenitrogenation procedures.[139] In this respect, a perspective is also the use of IL-MPs for the cleaning of biofuels. This topic has been part of the program developed in this Thesis work and it will be further discussed in Chapter 5.

1.4.3. Continuous-flow techniques: a greener perspective

The last part of this chapter is devoted to continuous-flow (CF) techniques. In the past two decades, a massive effort has been focused on the development of 'green' techniques aimed at minimising the environmental impact of chemical syntheses, not only by using clean reagents, solvents and catalysts, but also through the choice of reaction conditions. To mention an event acting as a driver in this field, in 2007, the Green Chemistry Institute (GCI) as a part of the American Chemical Society (ACS), promoted a round table in conjunction with a series of global pharmaceutical key areas to facilitate the identification and development of sustainable manufacturing.[140] The importance of CF-processing was recognised and ranked as one the pillar technologies for the research in the Green Chemistry sector. Consequently, many 'big pharma' looked towards new CF-techniques for green research and production with a renewed interest. This trend has certainly continued and it has expanded over the years until today.[141]

The same philosophy has also inspired a consistent part of this PhD Thesis, in which CF-based procedures have been used as a tool to conceive and implement new green processes for the upgrading of bio-based derivatives.

"Flow chemistry" encompasses a wide range of chemical processes taking place in a continuous mode by allowing a reactants stream to flow through a reactor in which a catalyst is often, but not always, placed. A simplified scheme of a CF-system for chemical reactions is shown in Figure 1.24.

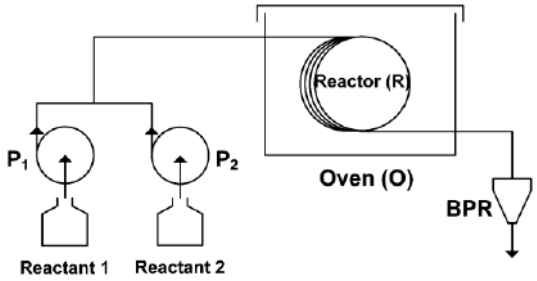

Figure 1.24. A general scheme for a CF-apparatus. P1 and P2: pumps for the delivery of reactants 1 and 2; Oven and BPR (back-pressure regulator) for the control of the temperature and the pressure.

The core of the system, where the reaction takes place, is the reactor. Reactors for continuous-flow apparatus fall into three major categories: *i*) *Continuous stirred tank reactors (CSTR)* in which the mixing of a liquid mixture and the control of the temperature are calibrated to have an identical concentration of reactants/products in every point inside the reactor. This configuration is primarily used for liquid phase reactions.[142] *ii*) *Tubular plug-flow reactors* (PFR). These are usually cylindrical pipes operating under conditions by which reactants are continually consumed as they flow down the length of the reactor with the concentration that varies continuously in the axial direction through the length of the reactor.[143] *iii*) *Packed-bed reactor* (PBR). This kind of flow reactors has also been used in this PhD Thesis. For this reason, they are described more in details than the two previous systems. A PBR is a hollow tube, pipe, or other vessel filled with a packing material. The packing more often consists of small objects like raschig rings or other designed solids (spheres, etc.), which serve to improve the contact between reactants. For catalytic reactions, packed beds can also be made of catalyst particles or adsorbents such as zeolite pellets, granular activated carbon, etc. In a PBR, fluid-solid heterogeneous reactions occur at the surface of the catalyst, if used. Consequently, the reaction rate is based on the mass of the solid catalyst, rather than on the simple reactor volume, and it may be sensitive to the solid-liquid mass transport phenomena. Several examples can be found in the literature.[144] The efficiency of a continuous-flow process is usually described by the space velocity (SV), which is the quotient of the entering volumetric flow rate of the reactants divided by the amount of the reactor catalyst (or the volume, if no catalyst is used). The SV indicates how many reactor volumes of feed can be treated in a time

unit.[145] Depending on the physical nature of the reactants, the SV can be calculated by considering the reactant liquid, gas or mass flow rate using Liquid-, Gas- or Weight hourly space velocity (LHSV, GHSV and WHSV respectively). For instance, WHSV is calculated with the following equation,[146]

$$WHSV\ (h^{-1}) = FA\ (g \cdot h^{-1})/Wcat\ (g) \qquad \text{(Eq. 1.4)}$$

where F_A is the flow of the reactant A and W_{cat} is the amount of catalyst loaded in the reactor. Beside liquid flow reactors, several types of gas flow reactors (GFR) have been designed to deal with continuous processes in the presence of gaseous reagents.[147] For instance, trickle bed reactors have been developed for continuous triphasic processes, in which various gas and liquid feeds are delivered to a fixed bed packed with a solid catalyst.[148] Of note is also the so-called tube-in-tube system which uses a semi-permeable membrane able to control the solubilisation of gaseous reagents into a reactant liquid stream.[149]

Flow photochemical reactors (FPR) have revolutionised procedures for either small- or large-scale reactions promoted by light. FPRs benefit from improved yields, decreased reaction time-scales, and reduced catalyst loadings, due to the efficient irradiation that results from short path lengths.[150]

Finally, the use of micro-reactors for CF-reactions has been considerably expanded in recent years. Micro-reactors (MRs) are generally comprised of channels having volumes from 10 to 1000 µL,[151] which become very effective in gathering large amounts of data with small amounts of material. Moreover, investigations of chemical reactions on a small scale usually minimise issues with mixing and heat transfer. Unlike the macro scale equipment, fluid behaviour is dominated by non-convective laminar flow, wherein only diffusion affects the mixing.

1.4.3.1. Flow advantages

With respect to batch reactions, CF-processes offer significant improvements in mixing and heat management, scalability, energy efficiency, waste generation, safety, access to a wider range of reaction conditions and unique opportunities in heterogeneous catalysis, multistep synthesis, and more.[152]

Efficient Mixing and Heat Transfer. Both micro- and meso- reactors possess a high surface to volume ratio, which allows for a more efficient heat absorption compared to any batch

reactor. Moreover, the high quality and precision of the mixing regime is achieved over a short distance (a few cm).

Figure 1.25 shows the profiles of the heating and mixing distribution for the model exothermic neutralisation reaction between HCl and NaOH are described.[153] In a batch reactor the exothermic reaction brings about a strong temperature gradient, since the cooling takes place only at the surface of the reactor (Figure 1.25, left, top). A much flatter gradient – almost at the detection limit – is noted for a microreactor (Figure 1.25, left, bottom). A similar behaviour is also observed for the reagent mixing.

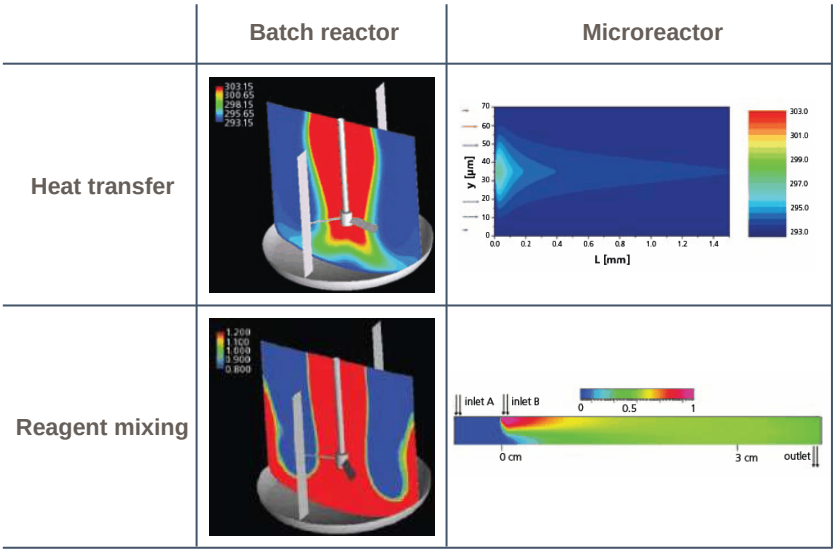

Figure 1.25. Exothermic neutralisation reaction of HCl with NaOH: heath distribution in a batch reactor (top-left) and in a microreactor (top-right); mixing efficiency in a batch reactor (bottom-left) and in a microreactor (bottom-right).[153]

Reaction efficiency and product intensification.

The atmospheric boiling point of solvents and reagents often limits the batch reaction conditions. By contrast, flow reactors allow for the safe manipulation of both the pressure and the temperature far beyond atmospheric conditions, resulting in improved energy, time, and space efficiency.[154] The use of smaller reactor volumes in flow also reduces the risks associated with reactor failure and facilitates reactor containment. Moreover, although more energy may be required to reach elevated temperatures, the CF-system is well suited to insulation to prevent heat loss, and to the recycling of the energy given off from exothermic reactions. These aspects greatly contribute to improve the efficiency on a commercial scale.[155]

In batch reactors, rapid and exothermic reactions are tricky and the corresponding quenching operations are scale dependent.[156] As mentioned above, the effective heat transfer of flow

reactors allows for the reactions to be run at higher concentrations than in batch systems with a major benefit in term of product intensification. The material production may often increase by a factor of 200-250 at identical reactor volumes.

Handling of poorly stable intermediates.

Flow chemistry techniques allow for an easier manipulation of unstable intermediates without the loss of yields and side-reaction runaways. A model example is the Moffat-Swern CF-oxidation of alcohols carried out in a MR (Scheme 1.18).[157]

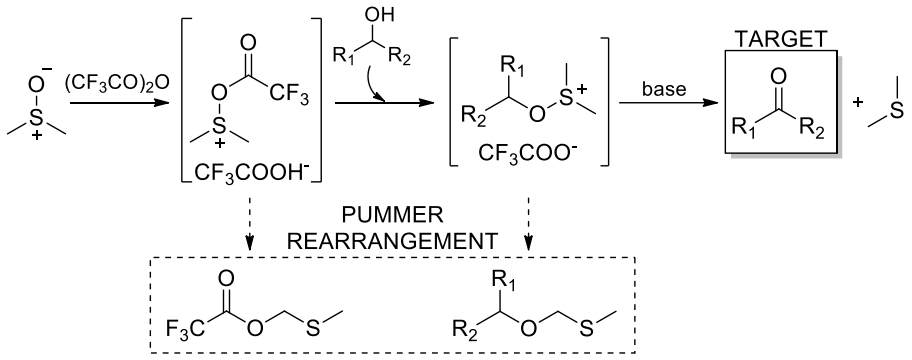

Scheme 1.18. Moffat-Swern alcohols oxidation (top); undesired Pummerer rearrangements (bottom).[157]

This flow reaction operates with a short residence time, which ensures a double advantage: *i*) the minimisation of undesired side-reactions such as Pummerer rearrangements (Scheme 1.18, bottom). Unstable sulfonium intermediates proceed straight to the target ketone; *ii*) the use of remarkably higher temperatures (0-20 °C) in comparison to the batch reactions that require cryogenic temperatures (-70 °C). In this case, the MR provides a narrow temperature profiles (closer to the ideal one) limiting the access to multiple reaction pathways.[158]

H*eterogeneous catalysis and recycling*. In a continuous process, the (heterogeneous) catalyst is usually confined inside the reactor, while the reagent mixture is allowed to flow over it. This is the best configuration to combine reaction and product separation in a single step and, at the same time, to reactivate and recycle the catalyst. Moreover, the decreased exposure of the catalyst to the environment may improve its lifetime.[159]

Telescoping multistep reactions. The synthesis of fine chemicals sometimes requires multistep sequences involving extractions, additions of several agents (quenching, drying etc.), filtration, evaporation, purification, distillation and/or recrystallization. These procedures require significant input of energy and materials that ultimately results in the production of large

amounts of waste. Continuous processing is particularly suitable for 'telescoping' reaction sequences by integrating several operations into one (or a few) continuous process.[160]

Scale-up.

Continuous techniques allow for the scale-up of reactions from grams to kilograms, without variations in yields, purities or safety. This can be achieved in three different ways (Figure 1.26): *i*) by using a single flow reactor for an extended time; *ii*) with multichannel parallel reactors (numbering-up process), or *iii*) with a larger flow reactor by which an increase of the total flow rate is allowed.

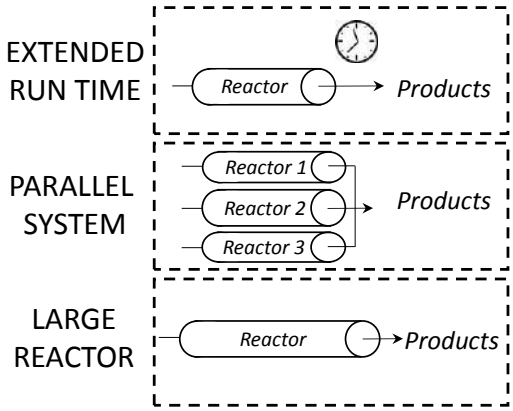

Figure 1.26. The reaction scale-up under flow conditions: three possible configurations.

Continuous processing has demonstrated a great flexibility for both laboratory and pilot-plant scale-up of pharmaceuticals and fine chemicals.[161] Particularly, the MR approach has proved efficient for the scale-up of chemical reactions.[162] Probably one of the most important features that distinguishes a continuous flow apparatus from a batch reactor is that the amount of product generated is determined by the length of time the entire flow regime is operated. In batch reactors, on the other hand, the maximum quantity of product produced per reaction is predetermined by the amount of starting material.

Albeit higher initial investments are required, the MR plant saves scaling efforts, requires fewer operating personnel, increases yields and reduces (moderately) the consumption of solvent. In addition, since MR-based technologies operate with very small volumes, they minimise safety concerns when performing dangerous reactions involving explosive or toxic reagents.[163]

CF-systems have also been applied in combination with renewable reagents for the setup of greener synthesis, as well as in the upgrading of bio-based derivatives. In a first example, the CF-synthesis of cyclic organic carbonates from epoxides and CO_2, has been considered (Figure

1.27). Compared to previously reported batch reactions,[164] the CF-protocol afforded the same yields of desired products, but using much milder reaction conditions (120 °C, 6.9 bar).[165]

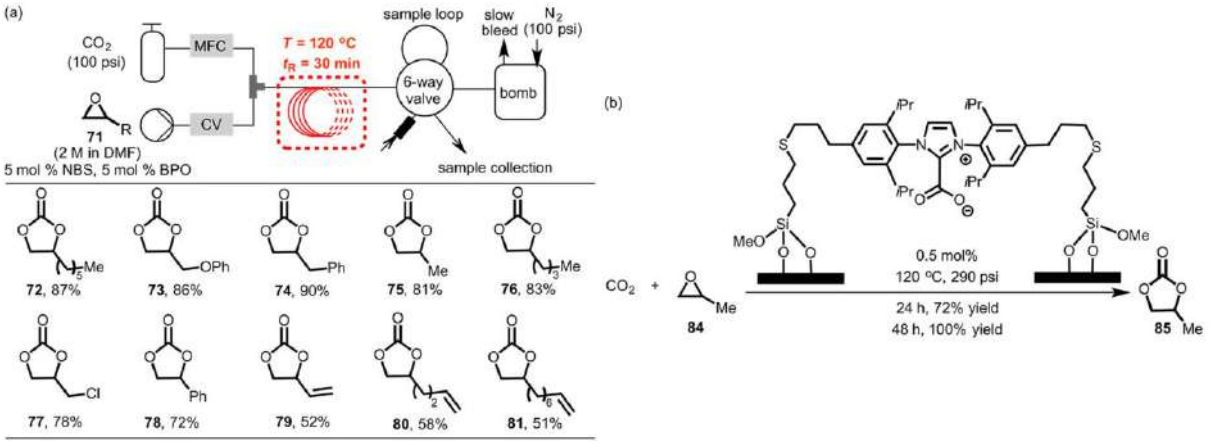

Figure 1.27. (a) Synthesis of cyclic carbonates from epoxides and carbon dioxide in flow. (b) Representative batch reactor synthesis of cyclic carbonates from epoxides and carbon dioxide.[166]

CF-systems were also explored for the conversion of glycerol and its derivatives by a number of reactions including deoxydehydrations,[167] hydrogenolysis,[168] acetalysations,[169] carbonations and transesterifications.[170,171] Several biomass reforming CF-processes, involving different feedstocks, were also developed.[172]

In the present PhD Thesis, CF-reactions have been successfully carried out for the implementation of both the etherification of some OH-bearing platform molecules and the synthesis of symmetric organic carbonates. The results will be described in Chapters 2–3.

1.5. Aim and overview of the Thesis

The present research project has been developed as part of a PhD cotutelle agreement between the Università Ca' Foscari Venezia and The University of Sydney. The activity research was carried out by the Green Organic Synthesis Team laboratory (GOST; Venice) and by the Laboratory of Advanced Catalysis for Sustainability (Sydney). Both these research groups have a long standing interest in the area of green and sustainable chemistry. One of the primary objectives of GOST is the design of organic syntheses with reduced environmental impact. This includes using biomass derived building blocks, safe chemicals like dialkyl carbonates, sustainable solvents such as ILs and sc-CO_2, and green/safe catalysts including solid heterogeneous systems (K_2CO_3, zeolites, hydrotalcites) and homogeneous systems (ionic liquids). In the Laboratory of Advanced Catalysis for Sustainability, studies are focused on the

design and development of new catalysts and methods for renewable feedstock processing. The transfer and integration of expertise and knowledge between the two groups has been essential to the discovery of new scientific breakthroughs and has not only prompted the collaboration for the present PhD project, but also for other research projects over the past years.

In line with objectives/focus outlined above, the aim of this PhD project was the development of novel green chemical technologies, generally based on the upgrading of platform chemicals derived from renewable feedstocks. Specifically, reactants chosen for this purpose were glycerol derivatives and furans (Venice, Chapter 2–3) and lignin (Sydney, Chapter 4), while reactions were developed according to the expertise of the two research groups at Ca' Foscari and Sydney: in Venice, new protocols were implemented by the use of dialkyl organic carbonates as green reagents and solvents in the continuous-flow mode; in Sydney, new catalytic systems were prepared. Also, some ionic liquids were synthesised for their application as extractants (Sydney, Chapter 5).

The description of the work has been articulated into five main chapters, each one focused on a platform chemical (or class of platform chemicals) and a particular transformation or green process.

- **Chapter 2: Upgrading of glycerol and furan bio-based derivatives with DMC as solvent/reagent**

Solketal was chosen as a model for OH-bearing bio-based derivatives. The continuous-flow *O*-methylation of solketal with dimethyl carbonate was first investigated in the presence of heterogeneous catalysts (Scheme 1.19).

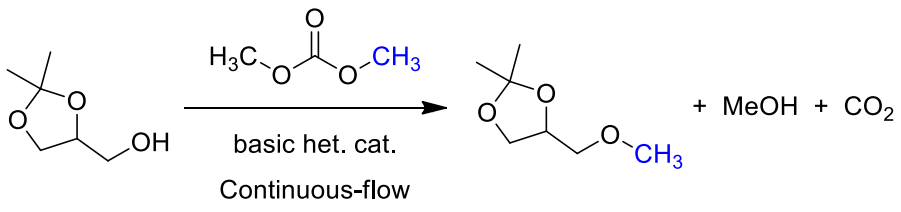

Scheme 1.19. Basic catalysed O-methylation of solketal.

The transformation was then extended to the selective preparation of a range of different bio-based ethers, derived from glycerol formal, glycerol carbonate, and tetrahydrofurfuryl alcohol.

The chapter is divided into two main parts: in the first one, different catalysts (mostly faujasites and hydrotalcites) and reaction conditions were investigated to achieve complete conversion of solketal and selectivity up to 98% towards the desired O-methyl ether. In the second part, the protocol was further elaborated for the selective *O*-alkylation of other bio-based reactants by using both DMC and DEC (Scheme 1.20).

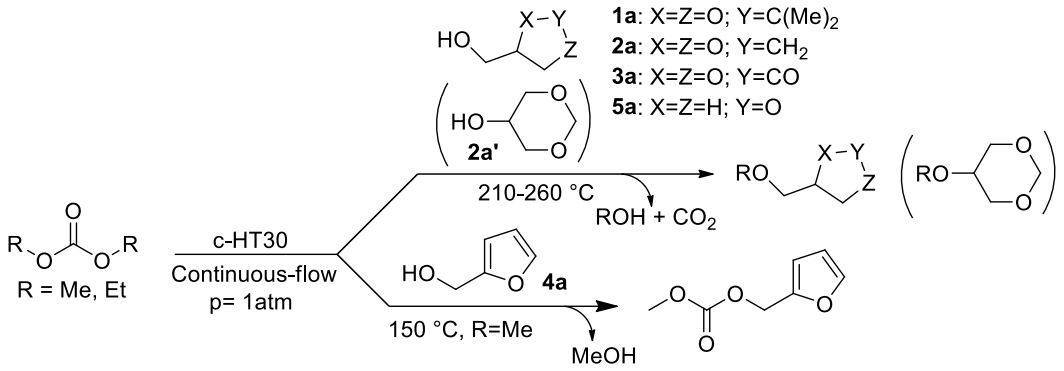

Scheme 1.20. The etherification of OH-bearing bio-based derivatives **1a**-**3a** and **5a** (top). The transesterification of furfuryl alcohol by DMC (bottom).

- **Chapter 3: Synthesis of symmetrical organic dialkyl carbonates**

In this chapter, a continuous-flow protocol for the disproportion reaction of methyl alkyl carbonates is reported. The reaction was optimised for the synthesis of symmetrical dialkyl carbonates. Hydrotalcites were used as heterogeneous basic catalysts (Scheme 1.21).

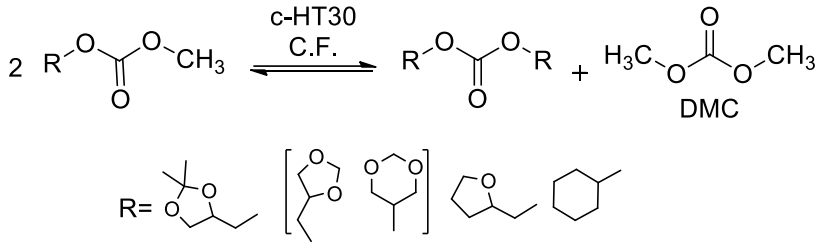

Scheme 1.21. CF-synthesis of symmetric dialkyl carbonates catalysed by different hydrotalcites.

At 210 °C and 1 bar, symmetrical carbonates were achieved with conversions and selectivities as high as 90% and 92%, respectively, with an average productivity in the range of 90.2–163.5 $mg_{prod}/(g_{cat}$ min).

Reactants (methyl alkyl organic carbonates) were easily produced *via* the transesterification of DMC with OH-bearing derivatives, *via* a reactive azeotropic distillation catalysed by c-HT30.

- **Chapter 4: Synthesis of renewable aromatics from Kraft lignin**

Morphology-controlled molybdenum disulfide (MoS_2) in supercritical ethanol (sc-EtOH) is known to be a highly effective catalyst for the depolymerisation of Kraft lignin. Under similar conditions, molybdenum hemicarbide (Mo_2C) is suited for the upgrading of Kraft lignin to aromatic chemicals. In this chapter, the catalytic depolymerisation of Kraft lignin in sc-EtOH is described. Both Mo_2C- and MoS_2-based catalysts were used for this purpose. The chapter is divided into three sections: in the first one, the synthesis and characterisation of a series of different Mo_2C- and MoS_2-based catalysts is reported; these systems are then used in the second part, for the investigation of the depolymerisation of Kraft lignin for the production of aromatic compounds (Scheme 1.22). Finally, based on the catalytic results and on inductively coupled plasma (ICP) analysis of the reaction mixtures, a possible reaction mechanism will be discussed.

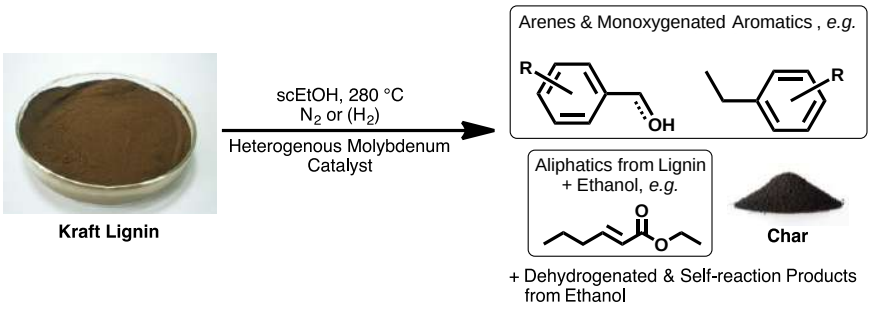

Scheme 1.22. Overview of Kraft lignin depolymerisation under supercritical reaction conditions in the presence of Mo-based heterogeneous catalysts.

- **Chapter 5: Cleaning up fuels: removing pollutants from renewable feedstock with ionic liquids**

Biocrude oils, when generated from biomass that contained some residual protein, *e.g.* algae, seaweed or municipal green waste, usually contain nitrogen-based compounds. These nitrogen-containing residues interfere with traditional refining methods and need to be removed prior to their integration into the supply chain. Ionic liquids have previously been suggested as useful extractants of aromatic nitrogen-containing compounds (N-compounds) from fuel oils. In this chapter, a series of ILs are compared for the selective extraction of the archetypical N-compounds, pyridine and indole, from a model oil consisting of decane and toluene.

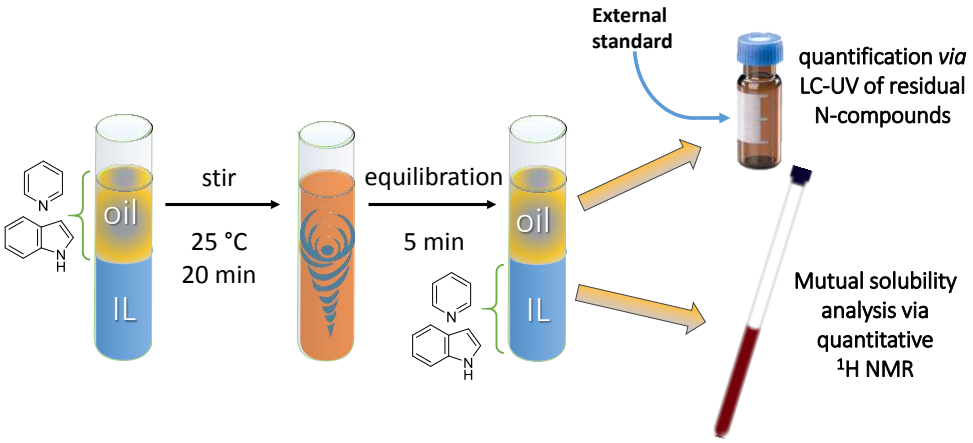

Scheme 1.23. Extraction procedure for the removal of pyridine or indole (5.00×10^{-3} M) from a model oil (n-decane and toluene in 85:15 wt.%).

1.6. Bibliography

[1] Population Reference Bureau. http://www.prb.org/Publications/Datasheets/2017/2017-world-population-data-sheet.aspx (accessed 01/09/2017).

[2] United States Environmental Protection Agency. https://www.epa.gov/climate-indicators#explore & http://shrinkthatfootprint.com/carbon-emissions-and-sinks (accessed 23/07/2017).

[3] Intergovernmental panel on climate change. www.ipcc.ch/report/ar5/wg1 (accessed 01/09/2017).

[4] Beijing Municipal Bureau of Statistics, http://www.stats.gov.cn/english/Statisticaldata/AnnualData (accessed 01/09/2017).

[5] G. Tang, P. Zhao, Y. Wang, W. Gao, M. Cheng, J. Xin, X. Li, Y. Wang, *Atmospheric Environment*, 2017, **150**, 238–243.

[6] http://edition.cnn.com/2017/08/21/politics/white-house-climate-change-committee-dismantled/index.html (last access, September 08, 2017)

[7] W. R. Stahel, *Nature*, 2016, **531**, 435–438.

[8] D. W. Pearce, R. K. Turner, Economics of Natural Resources and the Environment, London: Harvester Wheatsheaf, 1989.

[9] J. H. Clark, *Current Opinion in Green and Sustainable Chemistry*, 2017, **8**, 10–13.

[10] P. Ghisellini, C. Cialani, S. Ulgiati, *J. Clean. Prod.*, 2016, **114**, 11–32.

[11] J. H. Clark, *Nat. Chem.*, 2009, **1**, 12–13.

[12] C. Okkerse, H. van Bekkum, *Green Chem.*, 1999, **1**, 107–114.

[13] Biomass Energy Centre (UK), https://www.forestry.gov.uk/fr/beeh-9uhlqv (accessed 23/08/2017).

[14] F. Fernand, A. Israel, J. Skjermo, T. Wichard, K. R. Timmermans, A. Golberg, *Renew. Sust. Energ. Rev.*, 2017, **75**, 35–45.

[15] P. Kumar, D. M. Barrett, M. J. Delwiche, P. Stroeve, *Ind. Eng. Chem. Res.*, 2009, **48**, 3713–3729.

[16] J. B. Reece, L. A. Urry, M. L. Cain, S. A. Wasserman, P. V. Minorsky, R. B. Jackson, *Campbell Biology*. 9th ed.; Benjamin Cummings, Pearson Education: San Francisco (US), 2010.

[17] A. Corma, S. Iborra, A. Velty, *Chem. Rev.* 2007, **107**, 2411–2502.

[18] U.S. Department of Energy. 2011. U.S. Billion-Ton Update: Biomass Supply for a Bioenergy and Bioproducts Industry. R.D. Perlack and B.J. Stokes (Leads), ORNL/TM-2011/224. Oak Ridge National Laboratory, Oak Ridge, TN. 227p.

[19] Y. Habibi, *Chem. Soc. Rev*., 2014, **43**, 1519–1542.

[20] E. de Jong, A. Higson, P. Walsh, M. Wellisch, Bio-based chemicals value added products from biorefineries. IEA Bioenergy, Task42 Biorefinery, 2012.

[21] B. Kamm, M. Kamm, *Appl. Microbiol. Biotechnol.*, 2005, **64**, 137–145.

[22] R. van Ree, B. Annevelink, Status report biorefinery 2007. No. 847. Agrotechnology & Food Sciences Group, 2007.

[23] F. Cherubini, G. Jungmeier, M. Wellisch, T. Willke, I. Skiadas, R. Van Ree, E. de Jong, *Biofuel. Bioprod. Bior.*, 2009, **3**, 534–546.

[24] Dyne, D. L. V.; Blase, M. G.; Clements, L. D. A strategy for returning agriculture and rural America to long-term full employment using biomass refineries. In PerspectiVes on New Crops and New Uses; Janick, J., Ed.; ASHS Press: Alexandria, VA, 1999.

[25] Eni Green Refinery https://www.eni.com/en_IT/innovation/technological-platforms/green-refinery.page (accessed 01/09/2017).

[26] Sistema Informativo Unificato per le Soprintendenze Artistiche. http://siusa.archivi.beniculturali.it/cgi-bin/pagina.pl?TipoPag=prodente&Chiave=51606 (accessed 01/09/2017).

[27] The Novamont Model. http://www.novamont.com/eng/the-novamont-model (accessed 01/09/2017).

[28] C. Bastioli, *Polym. Deg.Stab.*, 1998, **59**, 263–272.

[29] J.I. Kroschwitz, M. Howe-Grant, Encyclopedia of Chemical Technology, John Wiley and Sons, New York, 1993.

[30] H. Yim, R. Haselbeck, W. Niu, C. Pujol-Baxley, A. Burgard, et al., *Nat. Chem. Biol.*, 2011, **7**, 445–452.

[31] https://www.genomatica.com/ (last access 14/09/2017).

[32] Biofuels in the European Union, a vision for 2030 and beyond. Available at: https://ec.europa.eu/research/energy/pdf/draft_vision_report_en.pdf (accessed 01/09/2017).

[33] BSI (2013) Bio-based products: Guide to standards and claims. Bio-based and Renewable Industries for Development and Growth in Europe, Strategic Innovation and Research Agenda. Available at https://shop.bsigroup.com/ProductDetail/?pid=000000000030262005.

[34] J. N. Putro, F. E. Soetaredjo, S.-Y. Lin, Y.-H. Ju, S. Ismadji, *RSC Adv.*, 2016, **6**, 46834-46852.

[35] W. C. Lam, T. H. Kwan, V. L. Budarin, E. B. Mubofu, J. Fan, C. S. K. Lin, Pretreatment and Thermochemical and Biological Processing of Biomass, in Introduction to Chemicals from Biomass, Second Edition (eds J. Clark and F. Deswarte), John Wiley & Sons, Ltd, Chichester, UK, 2015.

[36] P. F. H. Harmsen, W. Huijgen, L. Bermudez, R. Bakker *Literature review of physical and chemical pretreatment processes for lignocellulosic biomass*; Wageningen UR - Food & Bio-based Research: Wageningen, 2010.

[37] H. Ma, W. W. Liu, X. Chen, Y. J. Wu, Z. L. Yu, *Bioresour. Technol*., 2009, **100**, 1279–1284.

[38] L. D. Gottumukkala, K. Haigh, J. Görgens, *Renew. Sust. Energ. Rev.*, 2017, **76**, 963–973.

[39]Proesa™process:https://www.bio.org/sites/default/files/files/beta%20renewables%20proesa%20technology%20june%202013_bio_michele_rubino.pdf (accessed 29/09/2017).

[40] (a) D. A. Cantero, M. D. Bermejo, M. J. Cocero, *ChemSusChem*, 2015, **8**, 1026–1033; (b) A. Ghosh, R. C. Brown, X. Bai, *Green Chem*., 2016, **18**, 1023–1031.

[41] J. Q. Bond, D. M. Alonso, D. Wang, R. M. West, J. A. Dumesic, *Science*, 2010, **327**, 1110–1114.

[42] J. S. Luterbacher, J. M. Rand, D. M. Alonso, J. Han, J. T. Youngquist, C. T. Maravelias, B. F. Pfleger, J. A. Dumesic, *Science*, 2014, **343**, 277–280.

[43] F. Jérôme, G. Chatel, K. De Oliveira Vigier, *Green Chem.*, 2016, **18**, 3903–3913.

[44] (a) J. B. Binder, R. T. Raines, *Proc. Natl. Acad. Sci. U.S.A.*, 2010, **107**, 4516–4521; (b) C. G. Yoo, Y. Pu, A. J. Ragauskas, *Current Opinion in Green and Sustainable Chemistry*, 2017, **5**, 5–11.

[45] R. G. Blair, K. Chagoya, S. Biltek, S. Jackson, A. Sinclair, A. Taraboletti, D. Restrepo, *Faraday Discuss*., 2014, **170**, 223–233.

[46] N. Meine, R. Rinaldi, F. Schüth, *ChemSusChem*, 2012, **5**, 1449–1454.

[47] M. Ragnar, G. Henriksson, M. E. Lindström, M. Wimby, J. Blechschmidt, S. Heinemann, Pulp. In *Ullmann's Encyclopedia of Industrial Chemistry*, 2014; pp 1–92.

[48] US DOE, T. Werpy, G. R. Petersen, *Top Value Added Chemicals From Biomass*; Volume I: Results of Screening for Potential Candidates from Sugars and Synthesis Gas, 08/2004.

[49] J. J. Bozell, G. R. Petersen, *Green Chem.,* 2010, **12**, 539–554.

[50] T. J. Farmer, M. Mascal, In *Introduction to Chemicals from Biomass*, 2nd Ed., J. Clark and F. Deswarte, Eds., John Wiley & Sons, Ltd, Chichester, 2015, UK.

[51] (a) A. Corma, O. de la Torre, M. Renz, N. Villandier, *Angew. Chem. Int. Ed.*, 2011, **50**, 2375-2378; (b) A. Corma, O. de la Torre, M. Renz, *Energ. Environ. Sci.*, 2012, **5**, 6328–6344.

[52] W. P. Dijkman, D. E. Groothuis, M. W. Fraaije, *Angew. Chem. Int. Ed.*, 2014, **53**, 6515–6518.

[53] (a) I. K. M. Yu., D. C. W. Tsang, *Bioresour. Technol.*, 2017, **238**, 716–732; (b) M. Bicker, J. Hirth, H. Vogel, *Green Chem.*, 2003, **5**, 280–284.

[54] (a) Y. Y. Gorbanev, S. Kegnæs, A. Riisager, *Catal. Lett.*, 2011, **141**, 1752–1760; (b) M. Besson, E. Nadine, A. I. T. Hicham. "Method for preparing 2, 5-furandicarboxylic acid." U.S. Patent No. 9,499,506. 22 Nov. 2016; (c) H. Y. Hsu, Y.C. Liu, J. D. Wu. "Method for preparing 2, 5-furan dicarboxylic acid." U.S. Patent No. 9,321,744. 26 Apr. 2016.

[55] Avantium YXY technology: Groundbreaking technology for a biobased future https://www.avantium.com/yxy (accessed 28/09/2017).

[56] (a) C. Choi, J. P. Nam, J. W. Nah, *J. Ind. Eng. Chem.*, 2016, **33**, 1–10; (b) M. Rinaudo, *Prog. Polym. Sc*i., 2006, **31**, 603–632; (c) M. N. V. Ravi Kumar, *React. Funct. Polym.*, 2000, **46**, 1–27.

[57] (a) W. J. Liu, W. W. Li, H. Jiang, H. Q. Yu, *Chem Rev*, 2017, **117**, 6367–6398; (b) L. Fan, Y. Zhang, S. Liu, N. Zhou, P. Chen, Y. Cheng, M. Addy, Q. Lu, M. M. Omar, Y. Liu, Y. Wang, L. Dai, E. Anderson, P. Peng, H. Lei, R. Ruan, *Bioresour. Technol.,* 2017, **241**, 1118–1126.

[58] S. Kang, X. Li, J. Fan, J. Chang, *Renew. Sust. Energ. Rev.*, 2013, **27**, 546–558.

[59] (a) S. P. Jeevan Kumar, G. Vijay Kumar, A. Dash, P. Scholz, R. Banerjee, *Algal Research*, 2017, **21**, 138–147; (b) M. Arshadi, T. M. Attard, R. M. Lukasik, M. Brncic, A. M. da Costa Lopes, M. Finell, P. Geladi, L. N. Gerschenson, F. Gogus, M. Herrero, A. J. Hunt, E. Ibáñez, B. Kamm, I. Mateos-Aparicio, A. Matias, N. E. Mavroudis, E. Montoneri, A. R. C. Morais, C. Nilsson, E. H. Papaioannou, A. Richel, P. Rupérez, B. Škrbić, M. Bodroža Solarov, J. Švarc-Gajić, K. W. Waldron, F. J. Yuste-Córdoba, *Green Chem.*, 2016, **18**, 6160–6204.

[60] R. Ciriminna, M. Lomeli-Rodriguez, P. Demma Cara, J.A. Lopez-Sanchez, M. Pagliaro, *Chem. Commun*., 2014, **50**, 15288–15296.

[61] (a) C. M. Byrne, S. D. Allen, E. B. Lobkovsky, G. W. Coates, *J. Am. Chem. Soc*., 2004, **126**, 11404–11405; (b) O. Hauenstein, M. Reiter, S. Agarwal, B. Rieger, A. Greiner, *Green Chem*., 2016, **18**, 760–770.

[62] C. S. K. Reddy, R. Ghai, Rashmi, V. C. Kalia, *Bioresour. Technol*., 2003, **87**, 137–146.

[63] B. S.T. Gadgil, K. Naresh, V. N. R. Gundloori, *Med. Chem. Commun.*, 2017, 8, 1774–1787.

[64] D. Y. C. Leung, X. Wu M. K. H. Leung, A review on biodiesel production using catalyzed transesterification, *Appl. Energy*, **2010**, 87, 1083–1095.

[65] E. Lotero, Y. Liu, D. E. Lopez, et al., Synthesis of Biodiesel *via* Acid Catalysis, *Ind. Eng. Chem. Res.*, **2005**, 44, 5353–5363.

[66] P. T. Anastas, J. C. Warner, Green Chemistry Theory and Practice, Oxford University Press, New York, 1998.

[67] (a) B. Trost, *Science,* 1991**, 254** (5037), 1471–1477; (b) B. Trost, *Handbook of Green Chemistry*, Wiley, 2010.

[68] A. Curzons et al. *Green Chem.*, 2001, **3**, 1–6.

[69] R. Sheldon, *Green Chem.,* 2017**, 19**, 18–43.

[70] (a) J. Andraos J*. Chem. Educ*., 2015, **92**, 1820−1830; (b) J. Andraos in The Algebra of Organic Synthesis: Green Metrics, Design Strategy, Route Selection, and optimization, CRC Press, 2016.

[71] (a) G. S. Hiers, F. D. Hager in *Organic Syntheses*, Vol. Coll. 1, ed. H. Gilman, A. H. Blatt, Wiley 1941, 2nd Ed., pp. 58-60; (b) J. March in *Advanced Organic Chemistry*, Wiley: New York, 4th Ed., 1991.

[72] M. Matzner, R. P. Kurkjy, R. J. Cotter, *Chem. Rev*., 1964, **64**, 645–687.

[73] Romano, U.; Rivetti, F.; Di Muzio, N. US Pat. 4,318,862,1981.

[74] T. Matsuzaki, A. Nakamura, *Catal. Surv. Jpn*., 1997, **1**, 77.

[75] S. S. Fukuoka, I. Fukawa, M. Tojo, K. Oonishi, H. Hachiya, M. Aminaka, K. Hasegawa, K. Komiya, *Catalysis Surveys from Asia*, 2010, **14**, 146–63.

[76] P. Tundo, M. Selva, *Acc. Chem. Res.*, 2002, **35**, 706–716.

[77] M. Selva, *Pure Appl. Chem.,* 2007, **79**, 1855–1867.

[78] P. Tundo, L. Rossi, A. Loris, *J. Org. Chem.*, 2005, **70**, 2219–2224.

[79] (a) M. Selva, A. Perosa, S. Guidi, L. Cattelan, Dimethylcarbonate for the Catalytic Upgrading of Amines and Bio-Based Derivatives. In *Encyclopedia of Inorganic and Bioinorganic Chemistry*, John Wiley & Sons, L., Ed. 2016; pp 1–11; (b) M. Selva, A. Perosa, S. Guidi, L. Cattelan, *Beilstein J. Org. Chem.*, 2016, **12**, 1911–1924; (c) G. Fiorani, A. Perosa, M. Selva, *Green Chem.,* 2017, DOI: 10.1039/C7GC02118F.

[80] A.-A. G. Shaikh, S. Sivaram, *Chem. Rev.*, 1996, **96**, 951–976.

[81] H. Mutlu, J. Ruiz, S. C. Solleder, M. A. R. Meier, *Green Chem.,* **2012,** *14*, 1728.

[82] F. Ouyang, Z. Z. Wang, Y. Zhou, Z. Cheng, Z. H. Lu, Z. Yang, D. J. Tao, *Appl. Catal. A: Gen.,* **2015,** *492*, 177–183.

[83] R. Bernini, E. Mincione, F. Crisante, M. Barontini, G. Fabrizi, P. Gentili, *Tetrahedron Lett.*, 2007, **48**, 7000–7003.

[84] M. Fabris, V. Lucchini, M. Noè, A. Perosa, M. Selva, *Chem. Eur. J.* 2009, 15, 12273–12282.

[85] M. Selva, M. Noe, A. Perosa, M. Gottardo, *Org. Biomol. Chem.*, 2012, **10**, 6569–6578.

[86] (a) M. Selva, M. Fabris, A. Perosa *Green Chem*., 2011, 13, 863–872; (b) M. Selva, V. Benedet, M. Fabris *Green Chem*., 2012, 14, 188–200.

[87] M. Selva, A. Caretto, M. Noè, A. Perosa, *Org. Biomol. Chem*., 2014, **12**, 4143–4155.

[88] J. R. OchoaGomez, O. Gomez-Jimenez-Aberasturi, C. Ramirez-Lopez, M. Belsue, *Org. Process Res. Dev.,* 2012, **16**, 389–399; (c) M. O. Sonnati, S. Amigoni, E. P. Taffin de Givenchy, T. Darmanin, O. Choulet, F. Guittard, *Green Chem.,* 2013, **15**, 283–306.

[89] P. U. Naik, L. Petitjean, K. Refes, M. Picquet, L. Plasseraud, *Adv. Synth. Catal*., 2009, **351**, 1753–1756.

[90] (a) C. Chiappe, S. Rajamani, *Pure Appl. Chem*., 2012, **84**, 755–762; (b) J. A. Stewart, R. Drexel, B. Arstad, E. Reubsaet, B. M. Weckhuysen, P. C. A. Bruijnincx, *Green Chem*., 2016, **18**, 1605–1618.

[91] T. Tabanelli, E. Monti, F. Cavani, M. Selva, *Green Chem.,* 2017**, 19**, 1519–1528.

[92] (a) M. Selva, C. A. Marques, P. Tundo, *J. Chem. Soc., Perkin Trans. I,* 1994, 1323–1328; (b) A. Bomben, M. Selva, P. Tundo, L. Valli *Ind. Eng. Chem. Res.*, 1999, **38**, 2075–2079.

[93] W.-C. Shieh, S. Dell, O. Repič, *Org. Lett.*, 2001, **3**, 4279–4281.

[94] C. Hou, Y. Chen, W. Chen, W. Li, *Carbohydrate Res.*, 2011, **346**, 1178–1181.

[95] S. Dabral, J. Mottweiler, T. Rinesch, C. Bolm, *Green Chem*., 2015, **17**, 4908–4912.

[96] J. A. Barrett, Y. Gao, C. M. Bernt, M. Chui, A. T. Tran, M. B. Foston, P. C. Ford, *ACS Sustain. Chem. Eng.*, 2016, **4**, 6877–6886.

[97] Zi-H. Fu, Y. Ono, *J. Mol. Catal*., 1994, **91**, 399–405.

[98] S. Grego, F. Aricò, P. Tundo *Org. Process Res. Dev.*, 2013, **17** (4), 679–683.

[99] A.E. Gurgiolo, The Dow Chemical Company, USP 4,268,683 (May 19, 1981).

[100] X. Zhao, Y. Wang, S. Wang, H. Yang, J. Zhang *Ind. Eng. Chem. Res.* **2002,** *41,* 5139–5144.

[101] F. Li, Y. Wang, W. Xue, X. Zhao, *J. Chem. Technol. Biotechnol.*, 2009, **84**, 48–53.

[102] I. Vauthey, F. Valot, C. Gozzi, F. Fache, M. Lemaire, *Tetrahedron Letters,* 2000, **41**, 6347–6350.

[103] F. Trotta, P. Tundo, G. Moraglio. *J. Org. Chem.*, 1987, **52**, 1300.

[104] F. Schwochow, L. Puppe. *Angew. Chem., Int. Ed.,* 1975, **14**, 620.

[105] (a) M. Selva, A. Bomben, P. Tundo. *J. Chem. Soc., Perkin Trans.*, 1997, **1**, 1041; (b) M. Selva, P. Tundo, A. Perosa. *J. Org. Chem.*, 2003, **68**, 7374.

[106] (a) M. Czjiek, T. Vogt, H. Fuess. *Zeolites,* 1991, **11**, 832; (b) F. Bonino, A. Damin, S. Bordiga, M. Selva, P. Tundo, A. Zecchina. *Angew. Chem., Int. Ed.,* 2005, **44**, 4774.

[107] (a) M. Selva, E. Militello, M. Fabris, *Green Chem*., 2008, **10**, 73–79; (b) M. Selva, P. Tundo, D. Brunelli, A. Perosa, *Green Chem*., 2007, **9**, 463–468; (c) M. Selva, P. Tundo *J. Org. Chem.,* 2006, ***71***, 1464–1470.

[108] R. D. Rogers, K. R. Seddon, *Science*, 2003, **302**, 792–793.

[109] J. S. Wilkes, *Green Chem.*, 2002, **4**, 73–80.

[110] P. Walden, *Bull. Acad. Imp. Sci. St.Petersbourg, Ser.*, 1914, **8**, 405–422.

[111] F. H. Hurley, T. P. Wier, *J. Electrochem. Soc.*, 1951, **98**, 207–212.

[112] J. S. Wilkes, M. J. Zaworotko, *J. Chem. Soc. Chem. Commun.*, 1992, 965–967.

[113] (a) J. G. Huddleston, H. D. Willauer, R. P. Swatloski, A. E. Visser, R. D. Rogers, *Chem. Commun.*, 1998, 1765–1766; (b) A. E. Visser, R. P. Swatloski, W. M. Reichert, J. H. Davis Jr, R. D. Rogers, R. Mayton, S. Sheff, A. Wierzbicki, *Chem Commun*, 2001, 135–136; (c) M. Freemantle, *Chem Eng News*, 1998, **76**, 12–12.

[114] P. D. McCrary, R. D. Rogers, *Chem. Commun.*, 2013, **49**, 6011–6014.

[115] R. P. Swatloski, J. D. Holbrey, R. D. Rogers, *Green Chem.*, 2003, **5**, 361–363.

[116] M. Selva**,** A. Perosa, P. Canton, *Curr. Org. Chem.*, 2017**, 20**, doi: 10.2174/1385272820666161009222123.

[117] (a) S. Chen, S. Zhang, X. Liu, J. Wang, J. Wang, K. Dong, J. Sun, B. Xu, *Phys. Chem. Chem. Phys.*, 2014, **16**, 5893–5906; (b) T. Ueki, *Macromolecules*, 2008, **41**, 3739–3749; (c) J. Luczak, *Adv. Colloid Interface Sci*., 2016, **230**, 13–28.

[118] R.V. Chaudhari, P.L. Mills, *Chem. Eng. Sci.* 2004, **59**, 5337–5344.

[119] B. Cornils, W. A. Herrmann, I. T. Horvath, W. Leitner, S. Mecking, H. Olivier-Bourbigou, D. Vogt, Multiphase Homogeneous Catalysis, Wiley-VCH, Weinheim, 2005.

[120] P. Tundo, A. Perosa, *Chem. Soc. Rev.*, 2007, **36**, 532–550.

[121] C. A. Marques, M. Selva, P. Tundo *J. Org. Chem.,* 1995, **60**, 2430–2435.

[122] (a) C. Chiappe, D. Pieraccini, D. Zhao, Z. Fei, P. J. Dyson, *Adv. Synth. Catal.,* 2006, **348**, 68-74; (b) X. Yang, N. Yan, Z. Fei, R. M. Crespo-Quesada, G. Laurenczy, L. Kiwi-Minsker, Y. Kou, Y. Li, P. J. Dyson, *Inorg. Chem.,* 2008, **47**, 7444–7446; (c) C. Zhao, H.-z. Wang, N. Yan, C.-x. Xiao, X.-d. Mu, P. J. Dyson, Y. Kou, *J. Catal.,* 2007, **250**, 33–40.

[123] M. Selva, M. Gottardo, A. Perosa, *ACS Sustain. Chem. Eng.*, 2012, **1**, 180–189.

[124] (a) J. Dupont, J. D. Scholten, *Chem. Soc. Rev*., **2010**, *39*, 1780-1804; (b) J. N. Canongia Lopes, A. A. Padua, *J. Phys. Chem. B,* 2006, **110**, 3330–3335.

[125] H. S. Schrekker, M. A. Gelesky, M. P. Stracke, C. M. Schrekker, G. Machado, S. R. Teixeira, J. C. Rubim, J. Dupont, *J. Colloid Interface Sci.*, 2007, **316**, 189–195

[126] E. Redel, M. Walter, R. Thomann, C. Vollmer, L. Hussein, H. Scherer, M. Kruger, C. Janiak, *Chem. Eur. J.,* 2009, **15**, 10047–10059.

[127] P. S. Campbell, C. C. Santini, D. Bouchu, B. Fenet, K. Philippot, B. Chaudret, A. A. Padua, Y. Chauvin, *Phys. Chem. Chem. Phys.*, 2010, **12**, 4217–4223.

[128] R. Atkin, G. G. Warr, *J. Phys. Chem. C,* 2007, **111**, 5162–5168.

[129] T. C. Lo, in Handbook of Separations Techniques for Chemical Engineers, ed. P. A. Schwietzer, McGraw-Hill, New York, 1996, pp.1-450–1-529.

[130] J. Płotka-Wasylka, M. Rutkowska, K. Owczarek, M. Tobiszewski, J. Namieśnik, *TrAC Trends in Analytical Chemistry*, 2017, **91**, 12–25.

[131] (a) A. E. Visser, R. P. Swatloski, S. T. Griffin, D. H. Hartman, R. D. Rogers, *Sep. Sci. Technol.*, 2001, **36**, 785–804; (b) A. E. Visser, R. P. Swatloski, W. M. Reichert, S. T. Griffin, R. D. Rogers, *Ind. Eng. Chem. Res.*, 2000, **39**, 3596-3604; (c) A. E. Visser, W. M. Reichert, R. P. Swatloski, H. D. Willauer, J. G. Huddleston, R. D. Rogers, 2002, **818**, 289–308.

[132] N. N. Hidayah, S. Z. Abidin, *Miner. Eng.*, 2017, **112**, 103–113.

[133] (a) J. Liu, L. Wang, W. Zhu, C. Jia, Q. Deng, S. Yao, *Sep. Sci. Technol.*, 2013, **49**, 146–153; (b) X. Chen, F. Li, C. Asumana, G. Yu, *Sep. Purif. Technol.*, 2013, **106**, 105–109.

[134] X. Ni, H. Xing, Q. Yang, J. Wang, B. Su, Z. Bao, Y. Yang, Q. Ren, *Ind. Eng. Chem. Res.*, 2012, **51**, 6480–6488.

[135] A. P. Abbott, P. M. Cullis, M. J. Gibson, R. C. Harris, E. Raven, *Green Chem.*, 2007, **9**, 868.

[136] M. G. Freire, C. M. S. S. Neves, I. M. Marrucho, J. N. Canongia Lopes, L. P. N. Rebelo, J. A. P. Coutinho, *Green Chem.*, 2010, **12**, 1715.

[137] M. S. Manic, V. Najdanovic-Visak, M. N. da Ponte, Z. P. Visak, *Aiche J.*, 2011, **57**, 1344–1355.

[138] J. L. Espinoza-Acosta, P. I. Torres-Chávez, E. Carvajal-Millán, B. Ramírez-Wong, L. A. Bello-Pérez, B. Montaño-Leyva, *BioResources*, 2014, **9**, 3660–3687.

[139] (a) R. Abro, M. Abro, S. Gao, A. W. Bhutto, Z. M. Ali, A. Shah, X. Chen, G. Yu, *RSC Adv.*, 2016, **6**, 93932–93946; (b) M. H. Ibrahim, M. Hayyan, M. A. Hashim, A. Hayyan, *Renew. Sust. Energ. Rev.*, 2017, **76**, 1534–1549.

[140] C. Jiménez-González, P. Poechlauer, Q. B. Broxterman, B.-S. Yang, D. am Ende, J. Baird, C. Bertsch, R. E. Hannah, P. Dell'Orco, H. Noorman, S. Yee, R. Reintjens, A. Wells, V. Massonneau, J. Manley, *Org. Proc. Res. Dev.*, 2011, **15**, 900–911.

[141] K. S. Elvira, X. Casadevall i Solvas, R. C. Wootton, A. J. deMello, *Nat. Chem.*, 2013, **5**, 905–915.

[142] Picture of a continuous stirred-tank reactor. https://en.wikipedia.org/wiki/Continuous_stirred-tank_reactor (accessed 22/08/2017).

[143] (a) D. Ghislieri, K. Gilmore, P. H. Seeberger, *Angew. Chem. Int. Ed. Engl.*, 2015, **54**, 678–682; (b) S. H. Lau, A. Galvan, R. R. Merchant, C. Battilocchio, J. A. Souto, M. B. Berry, S. V. Ley, *Org. Lett.*, 2015, **17**, 3218–3221.

[144] (a) C. Battilocchio, F. Feist, A. Hafner, et al., *Nat. Chem.*, 2016, **8**, 360-367; (b) M. Chen, S. Ichikawa, S. L. Buchwald, *Angew. Chem., Int. Ed.*, 2015, **54**, 263–266.

[145] For instance, a reactor with a space velocity of 7 h^{-1} is able to process feed equivalent to seven times the reactor volume per hour.

[146] P. Harriott, Ideal Reactors, in *Chemical Reactor Design*, chap. 3, Marcel Dekker, Inc. New York, USA, 2003.

[147] (a) F. Levesque, P. H. Seeberger, *Angew. Chem., Int. Ed.*, 2012, **51**, 1706–1709; (b) F. Mastronardi, B. Gutmann, C. O. Kappe, *Org. Lett.*, 2013, **15**, 5590–5593.

[148] (a) T. Ouchi, C. Battilocchio, J. M. Hawkins, et al., *Org. Proc. Res. Dev.*, 2014, **18**, 1560–1566; (b) T. Ouchi, R. J. Mutton, V. Rojas, et al., *ACS Sustain. Chem. Eng.*, 2016, **4**, 1912–1916.

[149] M. Brzozowski, M. O'Brien, S. V. Ley, et al., *Acc. Chem. Res.*, 2015, **48**, 349–362.

[150] (a) J. P. Knowles, L. D. Elliott, K. I. Booker-Milburn, *Beilstein J. Org. Chem.*, 2012, **8**, 2025–2052; (b) J. F. B. Hall, R. A. Bourne, X. Han, et al., *Green Chem*, 2013, **15**, 177–180; (c) K. G. Maskill, J. P. Knowles, L. D. Elliott, et al., *Angew. Chem. Int. Ed.*, 2013, **52**, 1499–1502; (d) K. Gilmore, P. H. Seeberger, *Chemical Record,* 2014, **14**, 410–418; (e) Z. J. Garlets, J. D. Nguyen, C. R. J. Stephenson, *Isr. J. Chem.*, 2014, **54**, 351–360.

[151] K. Geyer, J. D. Codee, P. H. Seeberger, *Chem. Eur. J.*, 2006, **12**, 8434–8442.

[152] (a) S. G. Newman, K. F. Jensen, *Green Chem.*, 2013,**15**, 1456–1472; (b) C. Wiles, P. Watts, *Green Chem.*, 2012, 14, 38–54; (c) J. Yoshida, H. Kim, A. Nagaki, *ChemSusChem*, 2011, **4**, 331–340.

[153] Continuous Flow Synthesis in Microstructured Reactors — A New Way of Thinking Chemical Synthesis http://www.sigmaaldrich.com/technical-documents/articles/chemfiles/microreactor-technology.html#ref (access 22/08/2017).

[154] T. Razzaq, C. O. Kappe, *Chem. Asian J.*, 2010, **5**, 1274–1289.

[155] S. Huebschmann, D. Kralisch, V. Hessel, et al., *Chem. Eng. Technol.*, 2009, **32**, 1757–1765.

[156] R. L. Hartman, J. P. McMullen, K. F. Jensen, *Angew. Chem. Int. Ed.*, 2011, **50**, 7502–7519.

[157] J. J. M. v. d. Linden, P. W. Hilberink, C. M. P. Kronenburg, et al., *Org. Proc. Res. Dev.*, 2008, **12**, 911–920.

[158] D. Ferenc, H. Volker, D. György, in *Flow chemistry Volume 1: Fundamentals*, De Gruyter, 2014.

[159] C. G. Frost, L. Mutton, *Green Chem.*, 2010, **12**, 1687–1703.

[160] D. Webb, T. F. Jamison, *Chem. Sci.*, 2010, **1**, 675–680.

[161] N. G. Anderson, *Org. Proc. Res. Dev.*, 2001, **5**, 613–621.

[162] L. Ducry, D. M. Roberge, *Org. Proc. Res. Dev.*, 2008, **12**, 163–167.

[163] X. Zhang, S. Stefanick, F. J. Villani, *Org. Proc. Res. Dev.*, 2004, **8**, 455–460.

[164] H. Zhou, Y.-M. Wang, W.-Z. Zhang, J.-P. Qu, X.-B. Lu, *Green Chem.,* 2011, **13**, 644–650.

[165] J. A. Kozak, J. Wu, X. Su, F. Simeon, T. A. Hatton, T. F. Jamison, *Journal of the American Chemical Society*, 2013, **135**, 18497–18501.

[166] J. A. M. Lummiss, P. D. Morse, R. L. Beingessner, T. F. Jamison, *Chemical Record*, 2017, **17**, 667–680.

[167] N. N. Tshibalonza, J.-C. M. Monbaliu, *Green Chem.*, 2017, **19**, 3006–3013.

[168] J. Humberto Sepulveda Flores, D. Manuale, L. Santiago, N. Carrara, G. Torres, C. Vera, M. Gonçalves, W. A. Carvalho, D. Mandelli, *Quim Nova*, 2017, **40**, 371–377.

[169] S. Guidi, M. Noè, P. Riello, A. Perosa, M. Selva, *Molecules*, 2016, **21**, 657–676.

[170] M. Selva, S. Guidi, M. Noè, *Green Chem.*, 2015, **17**, 1008–1023.

[171] (a) N. Galy, R. Nguyen, H. Yalgin, N. Thiebault, D. Luart, C. Len, *Journal of Chemical Technology & Biotechnology*, 2017, **92**, 14-26; (b) V. O. Samoilov, M. O. Onishchenko, D. N. Ramazanov, A. L. Maximov, *ChemCatChem*, 2017, **9**, 2839–2849.

[172] A. A. Peterson, F. Vogel, R. P. Lachance, M. Fröling, J. M. J. Antal, J. W. Tester, *Energ. Environ. Sci*, 2008, **1**, 32–65.

2. *O*-ALKYLATION OF BIO-BASED DERIVATIVES WITH DIALKYL CARBONATES & HYDROTALCITES

2.1. Introduction

As was mentioned in Chapter 1, the leitmotif of this PhD project was the search for genuine sustainable protocols by the integration of catalytic procedures using clean reagents and solvents in the biorefinery chain for the valorisation of bio-based derivatives (BBDs). Part of this research has focused specifically on upgrading OH-bearing BBDs with non-toxic dialkyl carbonates ($ROCO_2R$, DAlCs).[1] The structures of the five model BBDs used in this work are shown in Figure 2.1.

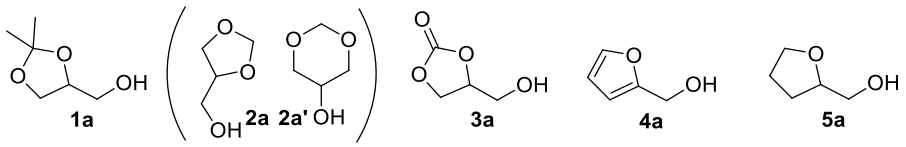

Figure 2.1. Model OH-bearing BBDs.

Of these, solketal (**1a**), glycerol formal (**2a**/**2a'**), and glycerol carbonate (**3a**) are among the most celebrated derivatives of glycerol, with applications spanning across multiple sectors: from fine chemicals, cosmetics and pharmaceuticals to bio-based solvents, bio-fuels, lubricants and polymers.[2] Additionally, the availability of glycerol in the market is mostly fuelled by plant-oil-based biodiesel manufacture and this currently greatly exceeds demand (see Chapter 1).[3]

The other two model compounds in Figure 2.1, furfuryl alcohol (**4a**) and its hydrogenated homologue tetrahydrofurfuryl alcohol (**5a**), are derived from furfural, which, in turn, is generated by the dehydration of sugar components (glucose and xylose) from lignocellulosic biomass (see Chapter 1, section 1.3.6).[4] Both **4a** and **5a** find uses as modifiers and templates for polymers, as fibres and nanocomposites,[5] and as sources of polyols.[6]

The presence of an OH-capped tether (hydroxymethylene group) in all five compounds (**1a**–**5a**), provides an excellent avenue for their derivatisation by both esterification and alkylation protocols. These reactions allow the potential of OH-BBDs to be expanded through the synthesis of high-added value products, including intermediates, solvents and biologically

active molecules from the glycerol ethers, esters and carbonates,[7] and additives for biodiesel blends based on the furanyl ether derivatives. In this context, our group previously reported a batch procedure for the etherification of glycerol acetals (GAs) with dialkyl carbonates (DAlCs) (Scheme 2.1).[8]

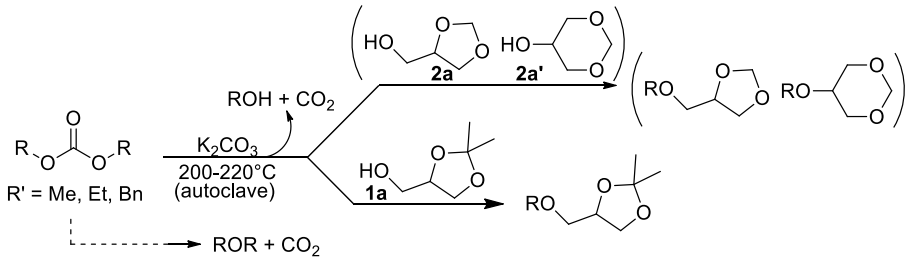

Scheme 2.1. The etherification of glycerol acetals with dialkyl carbonates in the presence of K_2CO_3 catalyst (top). The dashed path shows a concurrent decarboxylation reaction of dialkyl carbonates.

The process combined the effect of high reaction temperatures (200–220 °C) and a base catalyst (K_2CO_3) to facilitate the, almost exclusive, O-alkylation of GAs. The reaction showed excellent features from both synthetic and environmental standpoints, as it afforded etherification selectivities and yields as high as 99% and >80%, respectively. Moreover, this protocol coupled the use of renewable and/or non-toxic reactants, such as glycerol acetals and DAlCs, in a catalytic process, producing CO_2 and alcohols as the only co-products, which could be directly or indirectly recycled for the synthesis of DAlCs (See chapter 1) or easily conveyed for other uses. Only trace amounts of by-products from the competitive transesterification processes were detected.

However, under the explored conditions, the system suffered from two major drawbacks:

i) slow alkylation kinetics, *i.e.* reactions could require up to 80 h for completion;

ii) extensive competitive decarboxylations of dialkyl carbonates with the formation of the corresponding dialkyl ethers, (dashed path, Scheme 2.1). The decarboxylation of DAlCs was previously described by our group and by others in the presence of different heterogeneous catalysts such as alkaline carbonates and faujasites.[9]

These issues could be resolved through the use of an excess of the alkylating agents but, importantly, resulted in autogenous pressure ≥ 60 bar, both of which largely hinder the scale-up of this process. Both the benefits and the disadvantages of this procedure were an incentive to devise a new protocol aimed at expanding the alkylating capabilities of dialkyl carbonates towards different OH-bearing BBDs and, at the same time, minimising the

limitations described above. The implementation of a continuous-flow (CF) procedure was an attractive option with which to reach the conversion targets, because it offered the best possible control of the reaction parameters (T, p, and reactant molar ratios) to improve process kinetics, productivity and safety (see Chapter 1). Under CF-conditions, however, alkaline carbonates needed anion activators (*e.g.* polyethylene glycols) and/or specifically shaped reactors (*e.g.* continuous-stirred-tank-reactors, CSTR) or both to perform as catalysts.[10] Due to both the low basicity and the partial solubility of the alkaline carbonates in the reactant DAlCs and the co-produced alcohols (Scheme 2.1),[11] alternative solid base systems had to be considered. Candidates were chosen from among the families of faujasites (FAU) and Mg-Al hydrotalcites (HT), whose general structures are shown in Figure 2.2.

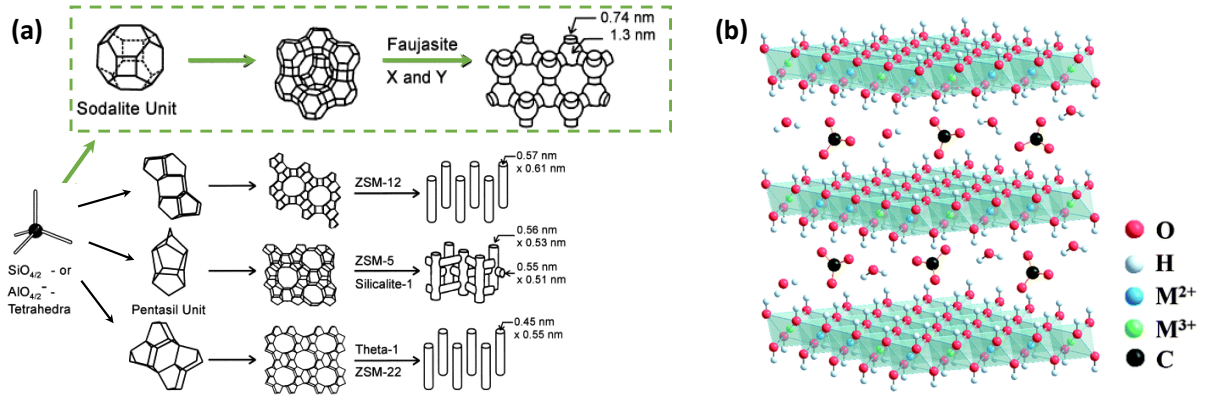

Figure 2.2. The structures of faujasites (a) and hydrotalcites (b).

Both Y- and X-type FAU have been extensively reported by our group as catalysts for DAlCs-promoted N-, O-, and S-alkylations of a large variety of nucleophiles, including anilines, benzyl alcohols, aminophenols, aminobenzyl alcohols, mercaptophenols, mercaptobenzoic acids, hydroxybenzoic acids, and functionalised phenols of the lignin scaffold.[12] On the other hand, HTs have been widely investigated as catalysts for the transesterification of dialkyl carbonates,[13] but there are only few reports describing the methylation of benzyl alcohol and some phenols by dimethyl carbonate over either Mg-Al HTs or other modified HT systems.[14] Due to the interest for this Thesis work, the following paragraph will survey properties and applications of HT-based catalysts.

2.2. Hydrotalcites

2.2.1. Structural features of hydrotalcites

The structure of hydrotalcite was first described in 1842, when it was discovered in Sweden in an ore with serpentine. The name hydrotalcite was assigned due to both its resemblance to talc and its high water content.[39a] HTs were also later referred to as layered double hydroxides (LDHs) or "Feitknecht compounds", named after the scientist who first synthesised them.[15] Since 1920, HTs have been prepared as hydroxyl carbonates of magnesium and aluminium, belonging to a large class of anionic and basic clays.

HTs display the lamellar structure of brucite ($Mg(OH)_2$) in which each Mg^{2+} ion is surrounded by six OH^- ions in an octahedral coordination, with shared edges forming continuous sheets (Figure 2.3).[16]

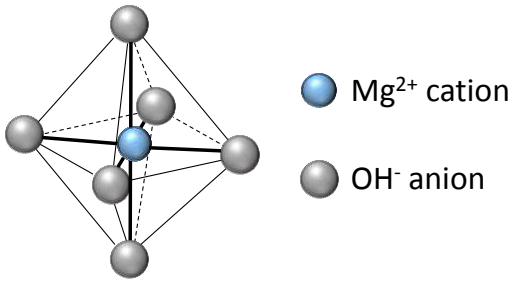

Figure 2.3. The octahedral unit of brucite, $Mg(OH)_2$.

However, since Mg^{2+} and Al^{3+} have similar ionic radii (0.65 and 0.50 Å, respectively), some of the divalent magnesium cations of the structure undergo isomorphic substitution with trivalent aluminium cations. HTs therefore consist of octahedral units in which a divalent or trivalent cation is located at the centre, with six OH^- groups positioned at the vertices (Figure 2.4, left).[16] These (octahedral) units are linked by their edges, thus forming the parallel layers of hydrotalcite (Figure 2.4, right). The substitution of Mg^{2+} by Al^{3+} leads to the generation of an excess positive charge across the brucite-like layers of HT, which is balanced by gallery anions located in the interlayer spaces. The remaining voids between the layers are filled by water molecules, which form strong hydrogen bonds with the structural hydroxide species and/or the interlayer anions.

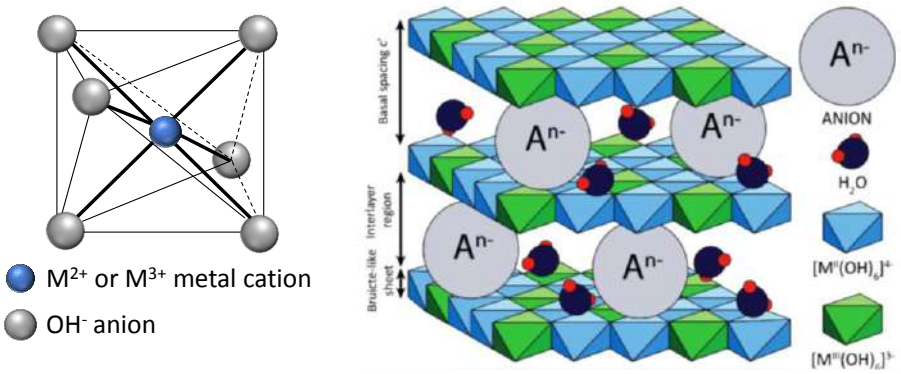

Figure 2.4. Brucite-like octahedral unit in the HT structure (left). Schematic representation of the HT structure (right).

The general formula for HTs can be written as:

$$[M^{2+}_{1-x}M^{3+}_{x}(OH)_2][(A^{n-}_{x/n})\cdot mH_2O],$$

where M^{2+} and M^{3+} are di- and tri-valent cations, the most common being Mg^{2+} and Al^{3+}. However, other cations (*e.g.* Ni^{2+}, Co^{2+}, Zn^{2+} and Cr^{3+}, Fe^{3+}, In^{3+}) have been reported. A^{n-} are interlayer anions, for example CO_3^{2-}, NO_3^-, OH^-, and SO_4^{2-}; x is the mole fraction of trivalent cations, namely $x = M^{3+}/(M^{3+}M^{2+})$, normally ranging between 0.17 and 0.33,[17] and m is the degree of hydration. Therefore, $[M^{2+}_{1-x}M^{3+}_{x}(OH)]_2$ refers to the composition of the brucite-like layers while $[(A^{n-}_{x/n})\cdot mH_2O]$ describes the composition of the interlayer spaces.

The variation of the ratio between the divalent (M^{2+}) and trivalent (M^{3+}) cations can be used to tune the basicity, the charge density and the anion-exchange capacity of the HTs. Moreover, the anions and water molecules, which are randomly located between the layers, possess a high degree of mobility and they are easily exchangeable. Both of these features allow for the synthesis of a wide range of complex intercalation materials.

2.2.2. Mg/Al hydrotalcite-like LDH preparation

The most common synthesis of HTs is based on co-precipitation methods and urea hydrolysis, but other procedures include ion-exchange, microwave irradiation, sol-gel, hydrothermal, steam activation, and solvothermal methods.[18]

The most important factors in determining the surface properties of the HTs are the nature of both the di- and tri-valent cations and the interlayer species, as well as the calcination temperature. Therefore, the basicity and structural changes of HTs can be readily adjusted by varying the Mg/Al ratio during the synthesis.[18a]

The co-precipitation of inorganic salts dissolved in an aqueous solution is carried out at either constant or increasing pH, within the range of 8–10. The pH must be carefully monitored: at too low a pH, the different metal ions may not all precipitate; while, at too high a pH the re-dissolution of some metal ions may occur. The procedure can also be performed at low or high supersaturation: *i*) in the first case, co-precipitation is achieved at constant pH by the simultaneous addition of a mixed solution of M^{2+} and M^{3+}, and a second alkaline solution, to a reactor containing the desired interlayer anions. The pH is essential to control the Mg/Al ratio. *ii*) In the second case (high supersaturation), the co-precipitation is similarly performed, but higher concentrations of the solutes and/or faster addition rates are used. Both procedures require a careful washing step to remove residual alkali from the solid products, followed by a thermal treatment. Of the two methods, the first yields more crystalline materials than the second one.

In the urea hydrolysis method, where urea is utilised as the precipitating agent, the crystallinity and uniformity of the particle size can be tuned through the reaction temperature. At low temperatures (100 °C), the nucleation rate is relatively low and particles of ~3 μm are obtained, while at higher temperatures (150 °C), the average particle size is reduced to 2 nm.[19] Compared to the co-precipitation procedures, products achieved by this method are more readily purified.[18a]

The hydrothermal synthesis is carried out by heating the reactants up to *ca* 200 °C in a pressurised aqueous media. In general, the hydrothermal method or a combined co-precipitation and hydrothermal synthesis, can be employed to improve the crystallinity of the final product.

Finally, sol-gel preparations are implemented by hydrolysing the metal precursors in an aqueous solution or in a liquid-organic solvent to produce a polymeric or particulate sol. A gelation and drying steps follow, affording highly pure materials that are suitable for drug-delivery.[20]

2.2.2.1. Hydrotalcites: Thermal treatment and applications

The calcination of hydrotalcites at 300–600 °C, remarkably increases the surface area of the final solids. This behaviour is opposite to the one usually induced by the thermal treatment of inorganic materials, the reason is ascribed to the loss of both adsorbed water from the surface, as well as the loss of anionic interlayer molecules, hydroxyl groups and interlayer water. This

leads to a breakdown of the lamellar hydrotalcite structure and the formation of a homogeneous mixture of bulk metal oxides. Details on this process will be discussed later in this chapter. It should be noted here that the decomposition of HTs can be achieved not only through calcination at high temperatures,[21] but also *via* other techniques such as cold plasma.[22] The so-produced solid mixture of basic oxides exhibit excellent characteristics such as smaller crystal size, stronger basic character, higher dispersion and larger specific surface areas that can be exploited for different applications. These include in catalysis and as ion exchangers, decontaminants and filters for water, industrial adsorbents of CO_2,[23] surfactants,[24] polymer stabilisers, as decolourising agents, optical hosts and ceramic precursors.[18a]

In catalysis, HTs have been used either as such, keeping their lamellar structure unaltered, or after their decomposition into a homogenised mixed oxide solid. Remarkable advantages have been obtained through the tuning of the basic/acidic strength of HTs (or mixed oxides) by which the selectivity of several fundamental reactions such as transesterifications,[25] aldol condensation of carbonyl compounds,[26] and other similar processes including the Knoevenagel and Claisen-Schmidt reactions,[27] have been enhanced. HTs have also been used as catalysts for the selective reduction of unsaturated ketones/aldehydes by hydrogen transfer from alcohols.[28]

Other applications include the catalysis of the Fischer-Tropsh reaction, the oxidative steam reforming of methanol for the selective production of hydrogen and other reactions involving the conversion of biomass derived molecules such as selective oxidation of HMF to 2,5-furandicarboxylic acid, oxidation of glycerol, hydrogenation of furfural and isomerisation of levulinic acid. These processes and many other applications for the conversion of biomass-derived molecules have been recently reviewed by Yan *et al.*.[29]

Significantly, if exposed to an aqueous anion solution, calcined solids derived from HTs exhibit an unusual capability to restore (at least in part) the double layered structures of the original precursors (Figure 2.5). This property is known as the memory effect and it distinguishes HT materials from all the other solid anionic clays.[30] Two important parameters must be controlled during this process: *i*) the choice of the starting HT-material - *i.e*. thermally labile anions - and, *ii*) the calcination temperature. The latter (T) is particularly critical, as thermal treatments of HTs at T above 650 °C can lead to the formation of spinel structures, which are resistant to rehydration.[21]

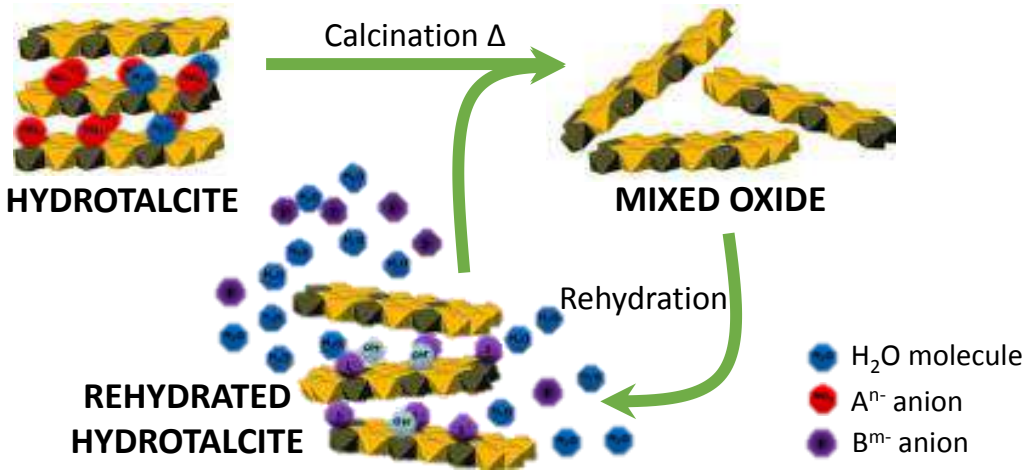

Figure 2.5. Calcination-rehydration-calcination process of hydrotalcites.

The memory effect expands the potentials of HTs to the synthesis of a wide range of tailor-made materials, with the intercalation of different anions used to tune the chemical, electronic, optical, and magnetic properties of the lattice, which can then be applied for multiple purposes.

2.3. Results and discussions

As mentioned in section 2.1, the reaction of dialkyl carbonates, specifically dimethyl and diethyl carbonate, with model OH-bearing bio-based derivatives, shown in Figure 2.1, was explored under continuous-flow conditions in the presence of both faujasites and hydrotalcites as catalysts. The results are described and discussed in the following sections.

2.3.1. The CF-apparatus

The schematic chart of the experimental set-up used for the continuous-flow (CF) reactions is depicted in Figure 2.6. The major components of the apparatus included an HPLC pump (P1) for the delivery of liquid reactants, a thermostat oven (O) equipped with additional thermocouples for temperature control, a tubular reactor (R) made of an 1/4" steel tube (L = 12 cm; V = 1.16 mL) filled with the catalyst and placed in the upright position, a 7725i-Rheodyne injector fitted with a 10 µL sample loop for the withdrawal of samples, and a back-pressure regulator (BPR, Swagelok K-series) for pressure control.

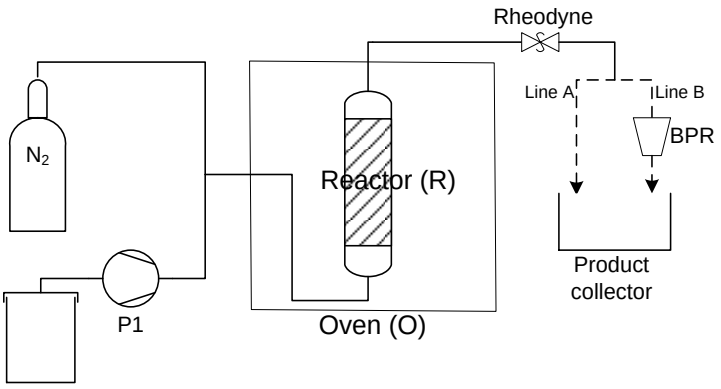

Figure 2.6. Experimental set-up used for the continuous-flow reactions.

2.3.2. Catalysts

Three alkali metal exchanged X- and Y-type faujasites, including two commercially available NaX and NaY solids (from Aldrich) and a CsY zeolite, were used. The latter was prepared as described in the experimental section (Section 2.5.1.1).

Four commercially available hydrotalcites were also used. Three of them were labelled as HT30, HT63 and HT70: these were from Sasol (Italy).

A fourth sample was labelled as KW2000 and was sourced from Kyowa Kagaku Kogyo Company Limited. Some features of these HT solids including the $MgO:Al_2O_3$ ratio and the surface areas are summarised in Table 2.1.

Table 2.1. Hydrotalcites used in this project.

Entry	Label of sample	MgO/Al_2O_3 (%)	Surface area (m^2/g)[a]	Source	Post-Synthesis residues (%)
1	HT30	30:70[b]	250	Pural® MG30, Sasol	Na: 1.5 x 10^{-3} [a]
2	HT63	63:37[b]	230	Pural® MG63, Sasol	K: 1.7 x 10^{-3} [a]
3	HT70	70:30[b]	180	Pural® MG70, Sasol	Na: 2.5 x 10^{-2} [c]
4	KW2000	64:36[b] (65:35)[c]	190	Kyowa Kagaku Kogyo Co. Ltd	K: 1.1 x 10^{-2} [c]

a) Data specified by the supplier; b) ratio [wt%] specified by the supplier; c) determined by ICP/MS measurements.

In the case of KW2000, ICP analysis was used to determine the post-synthesis residues of Na and K (see experimental). MgO as such and a 30:70 physical mixture of MgO (Aldrich, particle size: 325 mesh; surface area: 114 m^2/g; average pore diameter: 9.4 nm) and basic γ-Al_2O_3 (Macherey-Nagel, pH 9,5 ± 0,3; particle size: 50–200 µm; surface area: 130 m^2/g) were also used as additional catalysts for two comparative tests.

The reaction of solketal (**1a**) with DMC (Scheme 2.2) was chosen as a model in order to investigate the activity of different catalysts and the effect of four major reaction parameters, *i.e.* temperature, pressure, time, and reactants molar ratio.

2.3.3. CF-tests over different catalysts

The performance of the FAU and HT catalysts were compared using the CF-apparatus described above. The temperature and pressure for initial tests were selected according to previous results obtained for both batch alkylation and CF-transesterification reactions of glycerol acetals with dialkyl carbonates:[8,38a] experiments were carried out at T and p in the range of 200–275 °C, and 5–50 bar, respectively. Other conditions were defined by the apparent density of the catalysts and the geometry/inner volume of the CF-reactor. Each of the investigated catalyst was used to fill the inner volume of the CF-reactor as uniformly and completely as possible.[31] Therefore, the amounts of solid samples were adjusted according to their apparent density: NaY, NaX, CsY, KW2000, HT30, HT63, and HT70 were therefore used at slightly different amounts of 0.68, 0.54, 0.86, 0.52, 0.73, 0.51, and 0.85 g, respectively. Each solid sample was dehydrated under vacuum (70 °C, 18 mmHg, overnight) before use. In all tests, the same 1.83 M solution of solketal in DMC [DMC:solketal molar ratio (*W*) = 5] was fed into the reactor at a total volumetric flow rate (*F*) of 0.1 mL min^{-1}, corresponding to a contact time of about 10 min. The excess DMC served both as a reagent and as a carrier/solvent.

During the CF-experiments, periodic GC/MS analyses of the mixtures collected by the Rheodyne valve at the reactor outlet, allowed for the evaluation of both the reaction conversion (measured with respect to solketal as the limiting reagent) and the product distribution. Each test was duplicated to verify the reproducibility; in each reaction, fresh samples of the same batch of catalysts were used.[32]

Several reactions took place under the conditions explored. The double electrophilic reactivity of dimethyl carbonate accounted for the formation of *O*-methyl and transesterification derivatives **1b** and **1c**, respectively (Scheme 2.2: paths i and ii).

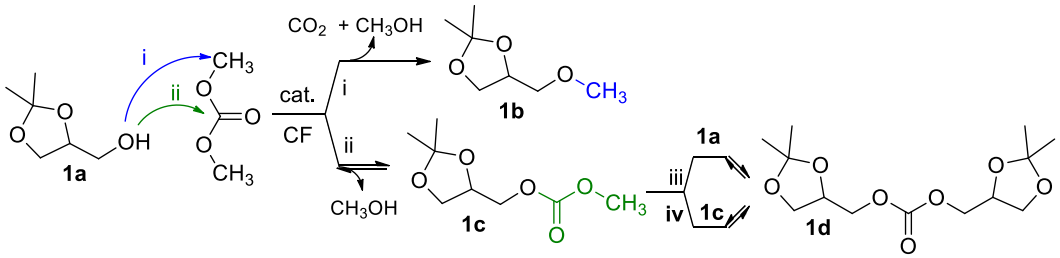

Scheme 2.2. Major products of the CF-catalytic reaction of solketal with DMC.

Subsequently, compound **1c** could undergo a further transesterification with solketal or a disproportionation reaction to afford the symmetric carbonate product **1d** (Scheme 2.2: paths

iii and iv). The structures of **1b**, **1c**, and **1d** were assigned by GC/MS and NMR spectroscopy analysis and by comparison to previously synthesised authentic samples. Moreover, some unidentified side-products were also observed. These compounds are referred to as "others" and their GC/MS data are consistent with a ring-opening reaction of the acetal ring, followed by methylation and transesterification of the corresponding (linear) derivatives.

2.3.3.1. Faujasites as catalysts

Figure 2.7a-b shows some representative results obtained in the presence of FAU catalysts. The trends of the solketal conversion and the selectivity for the different products are reported for CF-tests carried out for 3 h at 10 bar and 250–275 °C.

FAUs were clearly unsuitable catalysts for the reaction investigated. At best, the conversion of solketal was moderate (60–70%, Figure 2.7, dashed line) with *O*-methylation selectivity even poorer. The more basic NaX and CsY systems were slightly more active than NaY, but they favoured the transesterification product **1c** with a selectivity of 60–70% (Figure 2.7, green bars).[33] NaY improved the formation of the *O*-methyl derivative **1b** (40%, Figure 2.7, blue bar); on the other hand, NaY also induced side-reactions leading to a sizeable amount of unidentified by-products (Figure 2.7, red bars). In all cases, both the conversion and the selectivity remained largely steady after 180 min. Other experiments demonstrated that the outcome of the FAU-catalysed reactions were unaltered even when the CF-tests were prolonged from 3 to 18 h (Table 2.2).

Plausible reasons for this observed behaviour are discussed below.

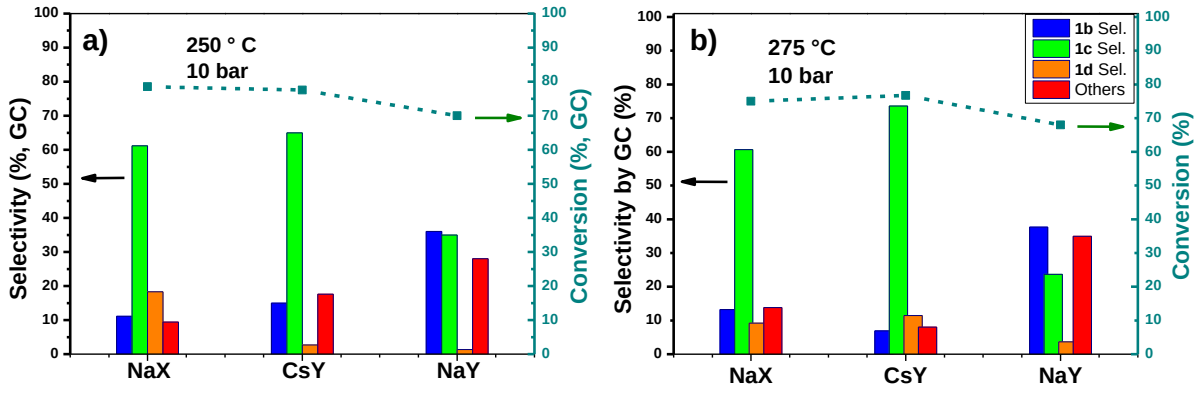

Figure 2.7. Trends of soketal conversion (dashed line) and product distribution (column bars) for the CF-reaction of **1a** with DMC carried out at 250 and 275 °C, in the presence of NaX, NaY and Cs, catalysts. The selectivity towards the *O*-methyl product (**1b**, ●), the transesterification and/or dismutation derivatives (**1c**, ●, and **1d**, ●, respectively), and unidentified compounds (others, ●) is shown. DMC and solketal were used in a 5:1 molar ratio (*W*), respectively, and the total flow rate was 0.1 mL min^{-1}.

Table 2.2. Prolonged tests for FAU-catalysed CF-reactions of solketal with DMC

Entry	FAU (g)	T, °C (P, bar)	t (h)	Conv. (%)	Products distribution (%, GC)			
					1b	1c	1d	Others
1	NaX (0.86)	275 (10)	18	73	20	55	6	19
2	NaY (0.68)	275 (10)	18	18	38	28	2	32

Other conditions: DMC:solketal in a 5:1 molar ratio; F = 0.1 mL min^{-1}

Alkali metal exchanged FAU zeolites are often described as amphoteric solids where the acidity and basicity come from the metal cations (mostly Na^+ and K^+) and the oxygen atoms of the aluminosilicate structure, respectively. This can be used to explain the high selectivity of FAU-catalysed alkylation of anilines, phenols, and thiols with dialkyl carbonates, with the acid-base character of the catalyst accounting for the simultaneous adsorption and activation of both the electrophilic and nucleophilic partners of the reaction.[15,34] Particularly, spectroscopic investigations have proven that aromatic nucleophiles (RC_6H_4QH, Q = O, S, NH) undergo both H-bonding and π-bonding at the catalyst surface (dashed red lines; Figure 2.8), while dialkyl carbonates are activated via acid–base adducts between the basic oxygens of the carbonate moiety and the Lewis acidic sites (Na^+) of the aluminosilicate framework (dashed blue lines; Figure 2.8).[35]

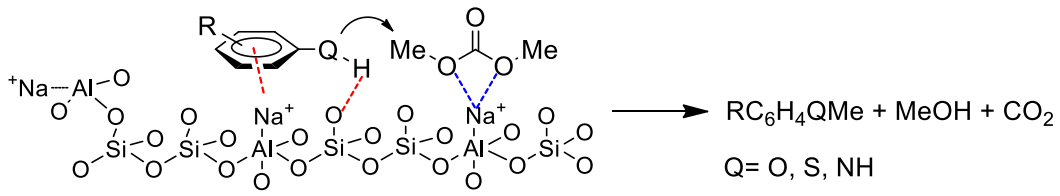

Figure 2.8. The alkylation of a generic aromatic nucleophile (ArQH, Q =, O, S and NH) with a dialkyl carbonate (the model case of DMC is shown) catalysed by a FAU. Pictorial view of the adsorption and activation modes of reactants at the FAU surface.[35]

Benzyl-type alcohols also react with DMC to produce the corresponding *O*-methyl ethers in the presence of NaX and NaY catalysts.[36] However, the results of Figure 2.7 clearly demonstrate that FAUs predominantly promote the transesterification of DMC with solketal, and the more basic the zeolite, the higher the extent of transesterification. Unlike aromatic or benzyl substrates, it is plausible that the cycloaliphatic structure of solketal is more weakly coordinated by the FAU surface, thereby altering the modes by which reactants (**1a** and DMC) approach each other over the catalyst. According to the HSAB principle, it has been proposed

that hard nucleophiles, such as aliphatic alcohols, prefer the hard electrophilic site of DMC (*i.e*. the carboxyl carbon), rather than the softer methyl groups.[37]

2.3.3.2. Hydrotalcites as catalysts

This scenario was found to be reversed in the presence of HTs. In particular, the use of KW2000 improved the conversion and, even more remarkably, the methylation selectivity. The reactions using HTs were performed under the same conditions as for FAUs (275 °C, 10 bar, W = 5; F = 0.1 mL min^{-1}), but were run for longer periods of time (18–20 h). The results are summarised in Figure 2.9.

While all the HTs investigated were found to be better catalysts than the FAUs, KW2000 afforded a performance far superior to those of the other HTs (HT30, HT63, and HT70; Figure 2.9). The KW2000-catalysed reaction proceeded with a very high conversion and an excellent selectivity towards *O*-methylation of 99% and 89%, respectively (dashed green line and blue bar). Of note, the ring of the reactant acetal was substantially preserved, and further transformations were avoided; only traces of the transesterification product **1c** were observed. The second best HT (*i.e.* HT30) still allowed for a substantially quantitative process (conversion 96%), although the methyl derivative **1b** did not exceed 60% of the total observed products (second group of bars, from left).

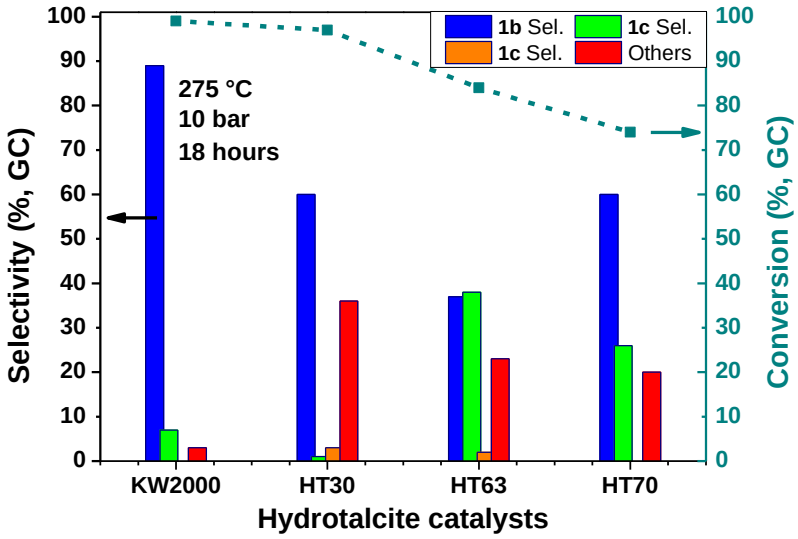

Figure 2.9. Trends of conversion and product distribution for the CF-reaction of solketal with DMC: comparison of different HT catalysts at 275 °C and 10 bar. The conversion (dashed line) and selectivity towards the *O*-methyl product (**1b**, ●), the transesterification and/or dismutation derivatives (**1c**, ●, and **1d**, ●, respectively), and unidentified compounds (others, ●) are shown. DMC and **1a** were used in a 5:1 molar ratio (W), respectively, and the total flow rate was 0.1 mL min^{-1}.

The reactions catalysed by KW2000 and HT30 were explored in greater depth by analysing samples of the mixture collected at the CF-reactor every 60 min for up to 20 h (Figure 2.10).

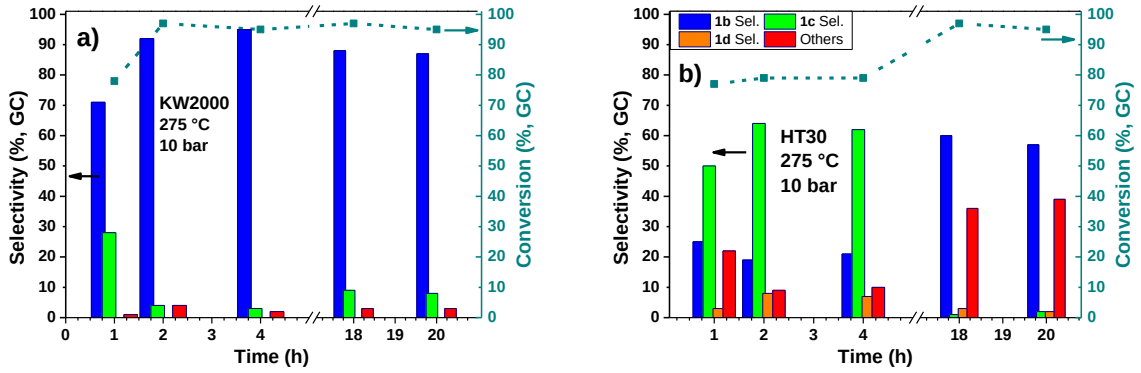

Figure 2.10. Effect of reaction time on conversion and products distribution for the CF-reaction of **1a** with DMC in the presence of: a) KW2000 and b) HT30 as catalysts. The reactions were completed at 275 °C and 10 bar; DMC and solketal were used in a 5:1 molar ratio (*W*), respectively, and the total flow rate was 0.1 mL min^{-1}. The conversion (dashed line) and selectivity towards the *O*-methyl product (**1b**, ●), the transesterification and/or dismutation derivatives (**1c**, ●, and **1d**, ●, respectively), and unidentified compounds (others, ●) are shown.

In the presence of KW2000, a steady and nearly complete conversion was obtained after just one hour, while the *O*-methylation selectivity reached a maximum of 95% after 4 h and it had decreased only slight to 87–89% by the end of the test (18–20 h) (Figure 2.9). By contrast, the HT-30-catalysed process showed a conversion of below 80% after the first 4 h, with the transesterification compound **1c** as the dominant product (Figure 2.9). After 18–20 h, the residual solketal was present in trace amounts (2–5%), and the steady formation of both **1b** and unidentified products was observed (≈60 and 40%, respectively). Albeit with different product distributions, both reactions displayed an initial (induction) period during which mixtures of products formed. The conversion and selectivity then stabilised, with the almost exclusive formation of the ether **1b** observed for KW2000. This catalyst was then further tested by performing additional experiments (4 h each) aimed at examining the effect of the temperature, the pressure, and the *W* (DMC:solketal) molar ratio in the ranges of 200–275 °C, 5–60 bars, and 1.1–5, respectively. The total flow rate (*F*) was constant at 0.1 mL min^{-1} in all tests. Results are reported in Figure 2.11.

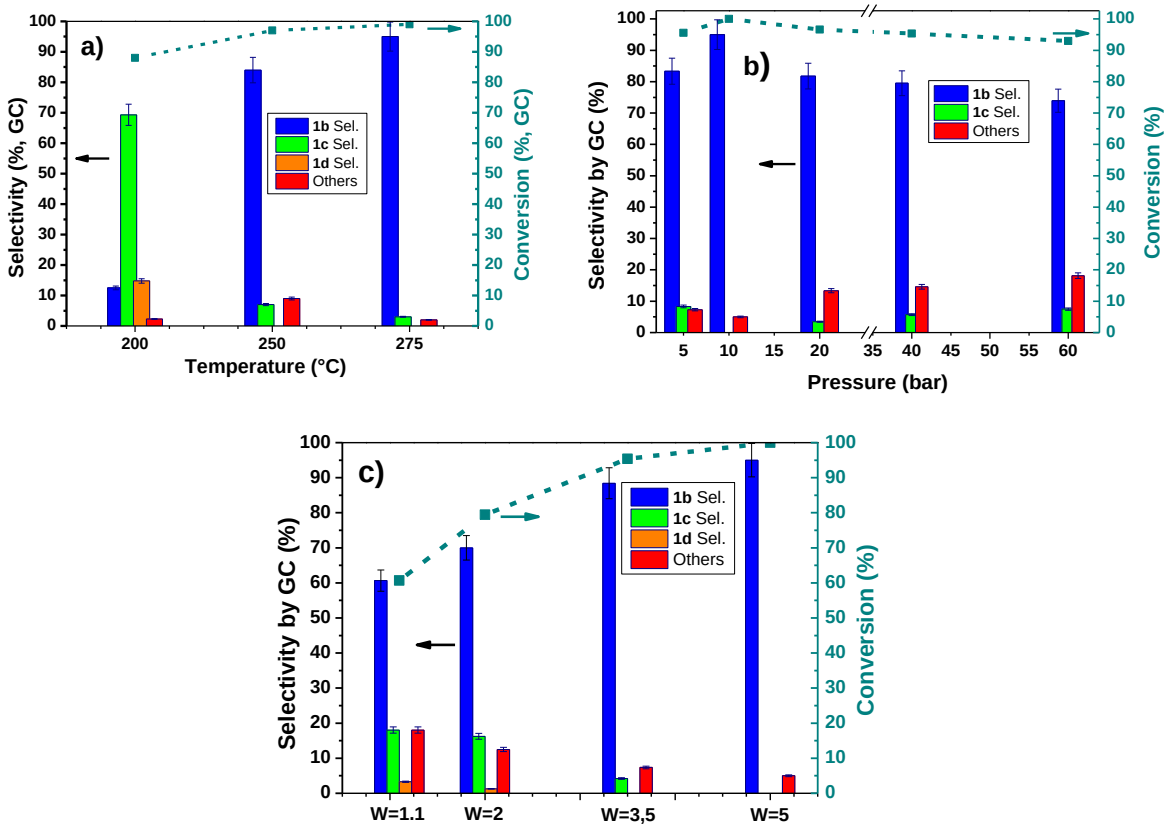

Figure 2.11. Effect of the reaction temperature (a; 10 bar, *W* = 5, 4 h), pressure (b; 275 °C, *W* = 5, 4 h), and *W* (DMC:solketal) molar ratio (c; 275 °C, 10 bar, 4 h) on the conversion and product distribution, for the CF-reaction of solketal with DMC, catalysed by KW2000. The conversion (dashed line) and selectivity towards the *O*-methyl product (**1b**, ●), the transesterification and/or dismutation derivatives (**1c**, ●, and **1d**, ●, respectively), and unidentified compounds (others, ●) are shown.

At 200 °C, the transesterification and disproportionation reactions were the major transformations; while the *O*-methylation process was clearly triggered by a temperature increase and was progressively favoured above 250 °C (Figure 2.11a). The result was consistent with the features of DMC-mediated reactions, *i.e.* the higher activation barrier and the non-reversible nature of methylations with respect to carboxymethylations (see introduction, Section 1.4.1.).

At 275 °C (*W* = 5, *F* = 0.1 mL min^{-1}, 4 h), if the pressure was either decreased or increased to 5 or 60 bar, respectively, the conversion was diminished slightly (from 99 to ~95%), but the selectivity towards methylation dropped from 95 to 75–80%, due to the onset of transesterification and unidentified side-reactions (Figure 2.11b). Pressure could potentially affect the partition of reactants between the liquid and the vapour phases and, consequently, affect the contact of solketal and DMC with the catalyst surface. A similar behaviour was

previously noted during investigations by our group on the thermal (catalyst-free) transesterification of glycerol acetals and glycerol with DMC.[38]

Finally, at 275 °C and 10 bar (*F*=0.1 mL min^{-1}, 4 h), if *W* is decreased from 5 to 1.1, both the conversion and the *O*-methylation selectivity decreased to 58 and 62%, respectively, with a sizeable formation of products **1c**, **1d** and "others" (Figure 2.11c). Two effects could potentially account for these results, at a constant *F*: *i*) the higher the DMC concentration (*W*=5) the higher the rate (and conversion) of DMC-mediated reactions. Under these conditions, even though (reversible) transesterifications occurred, the corresponding products (**1c** and **1d**) were observed only as minor products. This is because these compounds were consumed by the onset of the parallel and irreversible *O*-alkylation reaction, which proceeded almost to completion (Scheme 2.2, Figure 2.9–2.12). However, for *W*<5 and particularly at *W*=1.1, lower-energy-demanding reaction pathways, that is, transesterification processes, became more evident; therefore, the quantities of derivatives **1c** and **1d** increased. *ii*) Low DMC/solketal molar ratio (*W* = 1.1–2) not only disfavoured the solvation of the acetal by DMC and the mutual interactions between reactants, but it also facilitated the occurrence of intramolecular side-processes including, for example, the ring opening of solketal ("others" as by-products) adsorbed over the catalyst surface.

2.3.3.2.1. CF-tests with calcined HTs.

As described in section 2.2.2.1, if hydrotalcites are heated at approximately 200 °C, they release water; however, in the proximity of 300 °C (near the temperature used in Figure 2.9) and above, a collapse of the typical layered structure of HTs occurs, and Mg/Al mixed oxides form.[39] These facts prompted us to explore the catalytic activity of calcined hydrotalcites (c-HTs) in the reaction of solketal with DMC. The c-HTs were prepared by heating the Pural® (HT30, HT63, HT70) and KW2000 solids at 450 °C in a dried air-flow for 16 h.[40] The c-HTs showed similar apparent densities to each other and so the same amount (0.5 g) of each catalyst was used for the experiments. In all cases, a 1.83 M solution of solketal in DMC [DMC:solketal molar ratio (*W*) = 5] was fed into the reactor at *F* = 0.1 mL min^{-1}. Tests proved that c-HTs, particularly c-HT30, improved the reaction outcome dramatically: not only in terms of increasing the solketal conversion and the *O*-methylation selectivity, but also significantly decreasing the temperatures and pressures at which these catalysts are most efficient.

Maintaining the other reaction conditions (W = 5, F = 0.1 mL min^{-1}), the reactions could be run at temperatures and pressures as low as 210 °C and 1 bar.

The performance of c-HT30 during 20 h on-stream is detailed in Figure 2.12, and the activities and *O*-methylation selectivities of different c-HTs are compared in Table 2.3. Each test was duplicated in order to confirm the reproducibility of the results.

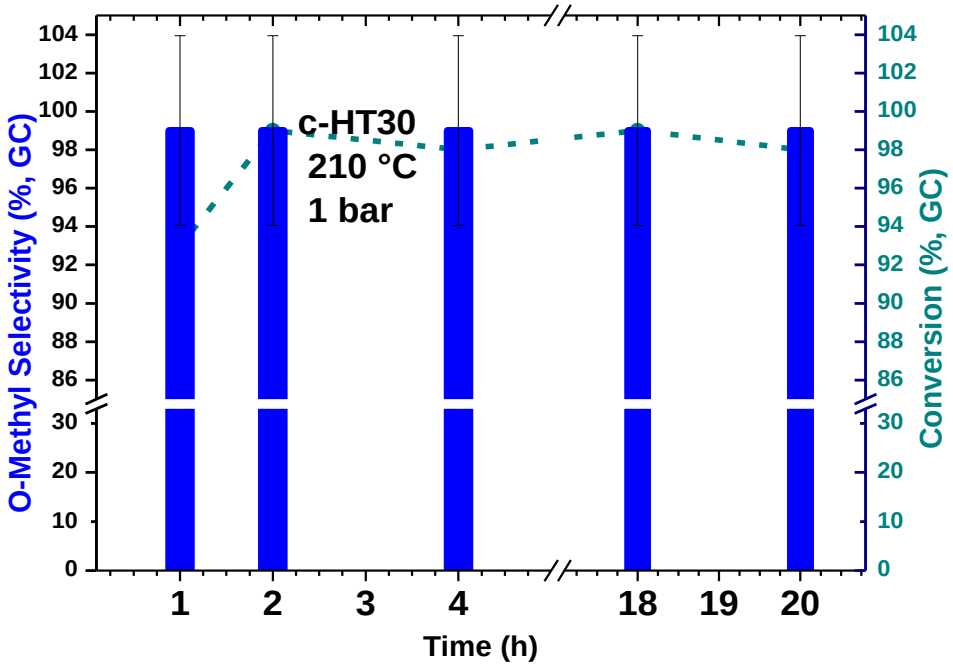

Figure 2.12. Effect of time on the CF-reaction of solketal with DMC in the presence of c-HT30 at 210 °C and ambient pressure. The conversion (dashed line) and selectivity towards the *O*-methyl product (**1b**, ●) are shown. Other conditions: W = 5, F = 0.1 mL min^{-1}.

Table 2.3. Comparison of c-HTs for the reaction of solketal with DMC

			Reaction temperature 210 °C				Reaction temperature 225 °C			
Entry	Catalyst	p/t (bar/h)	Conversion (%)[a]	Selectivity (%)[a]			Conversion (%)[a]	Selectivity (%)[a]		
				1b	1c	Others		1b	1c	others
1	c-HT30	10/18	99	99	-	-	99	99	-	-
2	c-HT70		88	27	49	24	95	40	42	18
3	c-KW2000		85	15	61	24	93	20	68	12
4	c-HT63		78	2	68	30	87	8	61	31

a) Conversion of solketal and selectivity towards the *O*-methyl derivative **1b**, the transesterification compound **1c**, and other products (including the disproportionation derivative **1d** and unidentified by-products). Other conditions: W = 5, F = 0.1 mL min^{-1}.

The outcome of the reaction catalysed by c-HT30 exemplifies one of the best reported *O*-methylation reactions of an alcohol-like function mediated by DMC. Solketal was transformed quantitatively into the methyl ether **1b**, and a steady efficiency was ensured for at least 20 h. The comparison of Figure 2.9–2.15 also indicated that the catalytic properties of both HT30 and KW2000 were considerably modified not only by the calcination of the HTs, but also by the thermal treatment during high-temperature (275 °C) reactions.

At the same reaction temperature (210 °C) used for c-HT30, the other c-HT catalysts resulted in conversions and *O*-methylation selectivities which did not exceed 88 and 27%, respectively, even operating at 10 bar (Table 2.3: compare c-HT70, c-KW2000 and c-HT63 in entries 2–4, columns 4–7). Minor improvements were achieved at 225 °C (entries 2–4, columns 8–11). Only at 275 °C (10 bar, W = 5, F = 0.1 mL min^{-1}) did the reaction proceeded with the complete conversion of solketal to the methyl derivative **1b** over all c-HTs catalysts.

The ability of c-HTs to promote the investigated reaction was contrasted with other CF experiments, in which c-HT catalysts were replaced by either MgO (0.85 g of a mixture of MgO in 60 wt% with ground Rashig rings) or a physical mixture of MgO and basic γ-Al_2O_3 in 30:70 molar ratio, respectively (0.85 g), which mimicked the formal composition of HT30. Both these solids were calcined at 450 °C for 6 h before use. Under the conditions described above (275 °C, 10 bar, W = 5, F = 0.1 mL min^{-1}), the two catalysts gave modest results: the best being MgO, for which the reaction proceeded with a conversion and a *O*-selectivity of only 80% and 48%, respectively. Although MgO and γ-Al_2O_3 were reported recently to catalyse both *O*- and *N*-alkylations mediated by DMC,[41,42] these solids were clearly inadequate for the reaction investigated.

The study has so far demonstrated that KW2000 and HT30 are the most promising catalysts. To continue exploring the potential of such materials, in particular of the calcined system c-HT30, this investigation next focused on the scope and limitations of the CF-etherification of other OH-bearing bio-based derivatives with both dimethyl and diethyl carbonates.

2.3.4. Scope of the reaction*:* different reactants, productivity, and on-stream stability of the catalyst.

Different reactants and Productivity. The substrates shown in Figure 2.1, including glycerol formal (**2a**/**2a'**), glycerol carbonate (**3a**), furfuryl and tetrahydrofurfuryl alcohols (**4a** and **5a**), were set to react with DMC or diethyl carbonate (DEC) under CF-conditions. Accordingly, a

homogeneous solution of dialkyl carbonate and the substrate was delivered to the CF-reactor filled with c-HT30 (0.5 g) as a catalyst for 6 h with a total flow rate of 0.1 mL min^{-1}. All CF-tests were repeated twice to confirm reproducibility.

The reaction conditions, isolated yields (*Y*) and productivities (*P*: g products obtained in 1 h per g of catalyst) for each of the studied processes are listed in Table 2.4, which, for completeness, also includes the above-described results for the *O*-methylation of solketal with DMC. The reactions and the structures of the products are summarised in Scheme 2.3.

Reactions could be performed at atmospheric pressure, but the operating temperature and the molar ratio of the reactants needed to be optimised, on case-by-case basis, in the ranges of 210–275 °C and 5–20, respectively. Except for compound **4a**, quantitative conversions were reached for all the substrates, with *O*-alkylation selectivity in the range of 65–99%. All the products were isolated and characterised by NMR spectroscopy and GC/MS (see Appendix for details).

Solketal (**1a**) and glycerol formal (**2a**/**2a'**) could be converted quantitatively into the corresponding methyl and ethyl ethers (**1b** and **2b**/**2b'**) by using DMC and DEC as the *O*-alkylating agents. From the results of Table 2.4, two facts emerged:

i) regardless of the dialkyl carbonate, the etherification of glycerol formal was more energy-demanding than that of solketal. Methyl and ethyl ethers **2b**/**2b'** and **2e**/**2e'** were obtained at 220 and 275 °C, respectively, while compounds **1b** and **1e** formed at lower temperatures of 210 and 250 °C (Table 2.4, entries 1 & 2 and 6 & 7). The same trend was observed by our group in the transesterification reaction of glycerol acetals with DAlCs, and similar findings were recently reported by others:[43] in general, the application/implementation of the Hansen approach and the COSMO-RS model, indicated that glycerol formal not only had a stronger structuration in the liquid state than solketal, but formaldehyde-based acetals were less reactive under acidic (hydrolytic) conditions than ketal acetone-based homologues. Additionally, the higher density of glycerol formal (1.21 g mL^{-1}) with respect to that of solketal (1.07 g mL^{-1}) may also play a role under the CF-conditions explored in this Thesis work. Although these aspects offer an interesting basis for discussion, the interpretation of experimental and modelling results is still unable to explain the different behaviours of GAs at a molecular level. Further investigations will be necessary to clarify such aspects.

ii) The synthesis of ethyl ethers required considerably higher reaction temperatures (250–275 °C) than those for methyl ethers (210–220 °C, Table 2.4, entries 1 & 6 and 2 & 7). This result

was in line with the trend noticed for several processes mediated by DAlCs, including transesterifications, decarboxylations, etherifications and alkylations.[9] Steric reasons most probably account for the lower electrophilic reactivity of DEC compared to DMC.

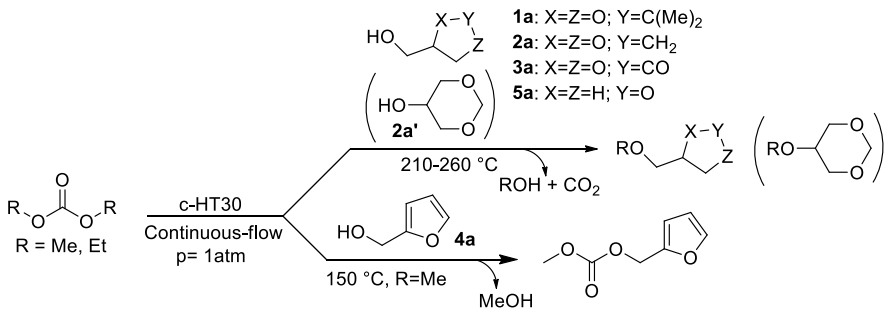

Scheme 2.3. The etherification of OH-bearing BBDs **1a–3a** and **5a** (top) and the transesterification of **4a** with DMC (bottom).

The products were recovered in good-to-excellent isolated yields (81–92%); however, the more volatile derivatives of glycerol formal gave slightly poorer results because of some technical difficulties in their separation from DMC or DEC (**2b**/**2b'**: 81%; **2e**/**2e'**: 84%; entries 2 and 7).[44] The isomeric ethers **2b**/**2b'** and **2e**/**2e'** were obtained in the same (3:2) relative ratio as that of the starting acetals **2a** and **2a'**.

Table 2.4. The CF-reactions of substrates 1a–5a with DMC and DEC in the presence of c-HT30.[a]

Entry	Substrate	DAlC	W[b] ratio	T (°C)	Conv.'n (%)[c]	Sel. (%)[d]	Products		
							Structure	Y[e] (%)	P[f] [$g_{prod}/(g_{cat}$ h)]
1	**1a**	DMC	5	210	99	99	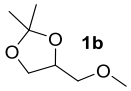 **1b**	92	2.64
2	**2a/2a'**	DMC	5	220	99	99	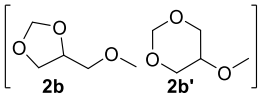 **2b** **2b'**	81	1.92
3	**3a**	DMC	20	210	98	65	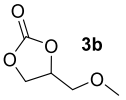 **3b**	55	0.42
4	**4a**	DMC	10	150	88	91	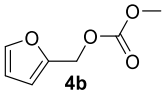 **4b**	80	1.26
5	**5a**	DMC	5	260	99	92	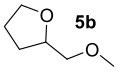 **5b**	82	1.94
6	**1a**	DEC	5	250	99	99	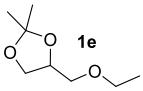 **1e**	92	2.04
7	**2a/2a'**	DEC	5	275	99	99	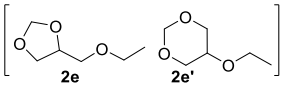 **2e** **2e'**	84	1.62

a) Reactions were carried out for 6 h (20 h only for **1a**, entry 1) at ambient pressure and at F = 0.1 mL min^{-1}; b) dialkyl carbonate:substrate molar ratio; c) conversion determined by GC); d) selectivity towards the shown product (determined by GC); e) isolated yield was evaluated by the work-up of the mixture collected at the reactor outlet for 6 h (15 h for **1a**, entry 1); f) reaction productivity was calculated from isolated yields.

The reaction productivity, calculated from the isolated yield, allowed further remarkable considerations: if compared to the batchwise (autoclave) method previously reported by our group,[9] which allowed *P* values of 0.01–0.02 $g_{prod}/(g_{cat}$ h) for the synthesis of compounds **1b** and **2b**/**2b'**, the CF-procedure boosted the productivity by a factor of 100–200 [to ~ 2 $g_{prod}/(g_{cat}$ h); Table 2.4, entries 1 & 2], thereby substantiating the synthetic potential of such a protocol. The overall mass balance for the alkylation of glycerol acetals was also validated by NMR spectroscopy of the crude mixtures collected at the reactor outlet and gravimetric analyses of the catalytic bed before and after the CF-tests. Both these checks indicated that neither heavy products nor noticeable coke formation (on the catalyst) occurred even after prolonged experiments (up to 20 h, Table 2.4, entry 1).

A similar outcome was also observed for the CF-reaction of tetrahydrofurfuryl alcohol (**5a**) with DMC, in which the corresponding *O*-methyl ether (**5b**) was obtained with 92% and 80% selectivity and isolated yield, respectively (Table 2.4, entry 5). However, a higher operating temperature of 250 °C was necessary.

The control of the chemoselectivity was significantly more difficult for the reactions of glycerol carbonate (**3a**) and furfuryl alcohol (**4a**). Glycerol carbonate was sensitive to competitive transesterification[38] and decarboxylation[45] reactions producing higher carbonate homologues and glycidol, respectively. In this case, *O*-methylation selectivity of 65% could be achieved at 210 °C in the presence of a large excess of the alkylating agent (Table 2.4, entry 3 and Scheme 2.4).

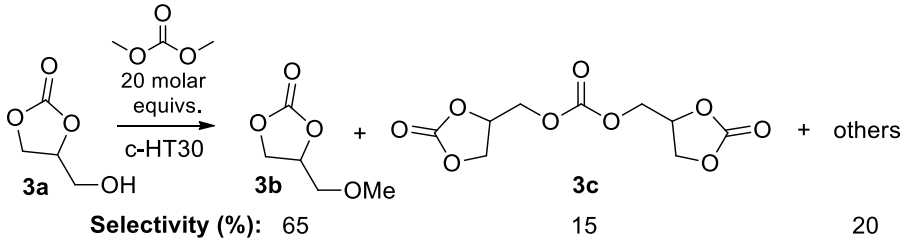

Scheme 2.4. The CF-reaction of glycerol carbonate with DMC in the presence of c-HT30 (the structure of **3c** was assigned by GC/MS; others were unidentified by-products).

Owing to dilution or solvation effects, these conditions contribute to minimise the contact between the glycerol carbonate and the catalytic surface, thereby limiting undesired decarboxylation reactions. Of note, the methylation productivity (P = 0.42 $g_{prod}/(g_{cat}$ h)) of the process was twice as high as the best previously reported value (P = 0.21 $g_{prod}/(g_{cat}$ h)) obtained in a batch reaction of glycerol carbonate with DMC catalysed by Al_2O_3.[46]

Furfuryl alcohol (**4a**) was too reactive to allow for the formation of the corresponding alkyl ether. At T≥180 °C, the reaction of **4a** with DMC gave polymeric by-products, which clogged the catalytic bed rapidly. However, at a lower temperature (150 °C), a highly selective transesterification reaction provided (furan-2-yl)methyl methyl carbonate (**4b**) in 80% isolated yield (Table 2.4, entry 4). This equilibrium reaction was favoured by a large excess of DMC (10 molar equiv. with respect to **4a**). Of note, all previously reported syntheses of **4b** are based on the reaction of furfuryl alcohol with a harmful phosgene derivative such as methyl chloroformate;[47] the process described here was the first successful example of the same preparation using DMC, a non-toxic reagent.

On-stream stability of the catalyst. The results listed in Table 2.4 proved that c-HT30 was an efficient catalyst and that it could be recycled without any loss of performance. For example, once the CF-alkylation of solketal was run for 20 h (Table 2.4, entry 1), a simple cleaning cycle of the catalytic bed with methanol (50 mL at 1 mL min^{-1}, 50 °C, atmospheric pressure) restored the system to its initial conditions. No differences in activity were observed when a used sample of c-HT30 was compared to a freshly calcined HT30 sample, thereby confirming the robustness of the CF-procedure. This was further substantiated by ICP/MS measurements carried out to evaluate the Al and Mg concentrations in the stream recovered at the outlet of the reactor. After the reaction of entry 1 (Table 2.4), such (ICP/MS) analyses demonstrated that the Al and Mg contents in the final mixture were 40 and 85 ppb, respectively. (Details on these measures are provided in the experimental section). The estimated mass loss of the catalytic bed corresponded to 38 μg per 20 working hours. Very low levels of metal leaching were previously observed for other reactions catalysed by HT-derived Mg/Al mixed oxides: two examples being the transesterification of natural fats and liquid-phase Michael additions.[48]

After the vacuum distillation of the mixtures collected at the reactor outlet, it was also estimated that up to 80% of the unreacted DMC (and its azeotrope with MeOH)[49] and DEC could be recovered and recycled with minimal waste generation.

Overall, the CF procedure proved versatile and suitable for both carbonates and alcohols. In particular, c-HT30 provided a rational long-term stability and selectivity (with no appreciable leaching or poisoning) as well as a productivity that could be orders of magnitude higher than that achieved by batch alkylation methods. To the best of our knowledge, a result comparable

to that of c-HT30 was reported only for the continuous-flow *O*-methylation of primary alcohols with DMC catalysed by γ-Al_2O_3 (Scheme 2.5, top).[42]

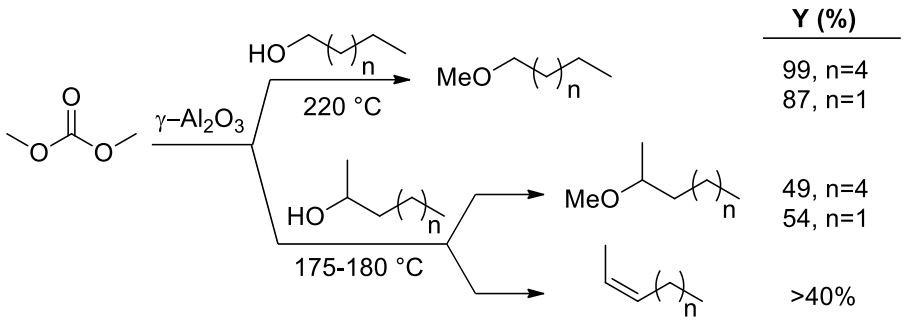

Scheme 2.5. The reaction of DMC and alcohols over γ-Al_2O_3 (from ref. 42). *Y*: % GC yields. Other conditions: Alcohol and DMC in a 1:1 molar ratio, *P* = 1 atm.

However, this protocol does have some non negligible drawbacks: *i*) it could not be extended to *sec* alcohols. These substrates gave substantial side-reactions of eliminations to alkenes due to the acidity of the catalyst (Scheme 2.5, bottom);[50] *ii*) even at 150 °C, it was demonstrated that γ-Al_2O_3 promoted an almost quantitative decarboxylation (>98%) of DMC to dimethyl ether;[51] *iii*) for functionalised alcohols used in this study, γ-Al_2O_3 would have also posed a chemoselectivity concern. In fact, glycerol acetals (solketal and glycerol formal) and furfuryl alcohol are extremely sensitive to ring aperture and polymerisation reactions catalysed by acids, while glycerol carbonate would release CO_2 rapidly.

Finally, it should be noted that the decarboxylation of dialkyl carbonates may be catalysed not only by γ-Al_2O_3, but also by FAUs[9] or hydrotalcites as such.[52] However, under the CF conditions explored here, we observed that calcined HTs were far less efficient for the same process. This was corroborated by an additional test in which solketal methyl carbonate (**1c**) was set to react at 210 °C and ambient pressure over a catalytic bed of c-HT30. At a conversion of 75%, **1c** underwent a predominant disproportion reaction towards bis[(2,2-dimethyl-1,3-dioxolan-4-yl)methyl] carbonate (**1d**, 80%) rather than the decarboxylation to derivative **1b** (10%, Scheme 2.6). Product **1d** was isolated in a 58% yield and characterised by GC/MS and NMR spectroscopy. Albeit indirectly, this test confirmed that c-HT30 could also improve the efficiency of the alkylation reactions desired here. This subject was further investigated and results are discussed in Chapter 3.

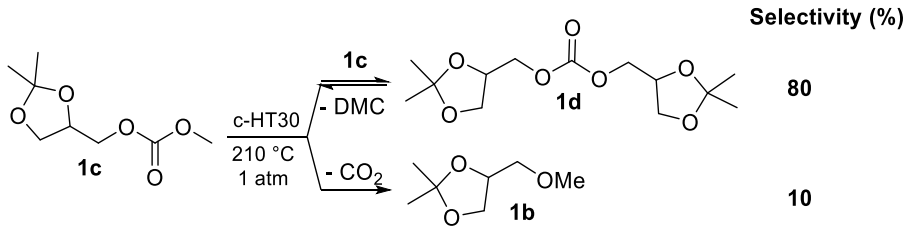

Scheme 2.6. The CF reaction of **1c** over c-HT30 at 210 °C and ambient pressure. Cyclohexane was used as a solvent (5 equiv. with respect to **1c**). Total flow rate: 0.1 mL min^{-1}.

2.3.5. Characterisation and role of the catalyst

HT-catalysts were characterised by both XRD and BET techniques.

A total of eight samples were examined for XRD analysis (Table 2.3). Four of them (f-KW2000, f-HT30, f-HT63 and f-HT70) were fresh solids that had never been used for catalytic tests, while the other four specimens (c-KW2000, c-HT30, c-HT63 and c-HT70) were calcined solids that were used for reactions carried out under the conditions reported in Table 2.5.

Table 2.5. Samples of KW2000 and HT30 for XRD analyses

Entry	Sample	Label	Pretreatment (70 °C, 18 mm, overnight)	Calcination (450 °C, air, 16 h)	Conditions of use[a]
1	fresh KW2000	f-KW2000	yes	none	none
2	fresh HT30	f-HT30			
3	fresh HT63	f-HT63			
4	fresh HT70	f-HT70			
5	calcined KW2000	c-KW2000	yes	yes	18 h at 210 °C, 1 bar
6	calcined HT30	c-HT30			
7	calcined HT63	c-HT63			
8	calcined HT70	c-HT70			

a) The fresh (f-) solids were not used for catalytic tests. Calcined (c-) samples were used for catalytic CF-tests run at 210 °C and ambient pressure, for 18 h.

Fresh samples. Figure 2.13 reports both the XRD patterns for all the fresh materials (left) and the Rietveld fit carried out for f-HT30 and f-KW2000 samples (right). The analyses showed that fresh solid samples of HT63 and HT70 were clearly single-phase hydrotalcites: structures were confirmed by comparison to data available at the Inorganic Crystal Structure Database (ICSD) # 81963. (Figure 2.13b and c). By contrast, both f-KW2000 and f-HT30 were constituted by at least two identifiable phases in which the hydrotalcite structure (ICSD 81963) was present along with large fractions of: i) periclase [MgO, ICSD 9863; (60±1) wt%] in f-KW2000 and boehmite [aluminum oxide hydroxide, ICSD 36340; (53±1) wt%] in f-HT30, respectively. The quantitative relationships between the components of these solid materials were obtained by

Rietveld analysis, shown in Figure 2.13e and Figure 2.13f (right). (Further details are given in the experimental section).

Calcined samples. The XRD patterns of c-KW2000, c-HT63, and c-HT70 were very similar to each other and were consistent with those already reported in the literature for calcined samples of HTs.[53] The results are shown in Figure 2.14 (top). In all cases, the presence of cubic MgO (periclase) along with an extremely dispersed or amorphous phase responsible for a broad peak at 2ϑ = 35° were observed. This composition was typical of c-HT systems characterised by an Al/(Al + Mg) molar fraction of up to approximately 50% (~55 wt% of Al_2O_3).[45,54]

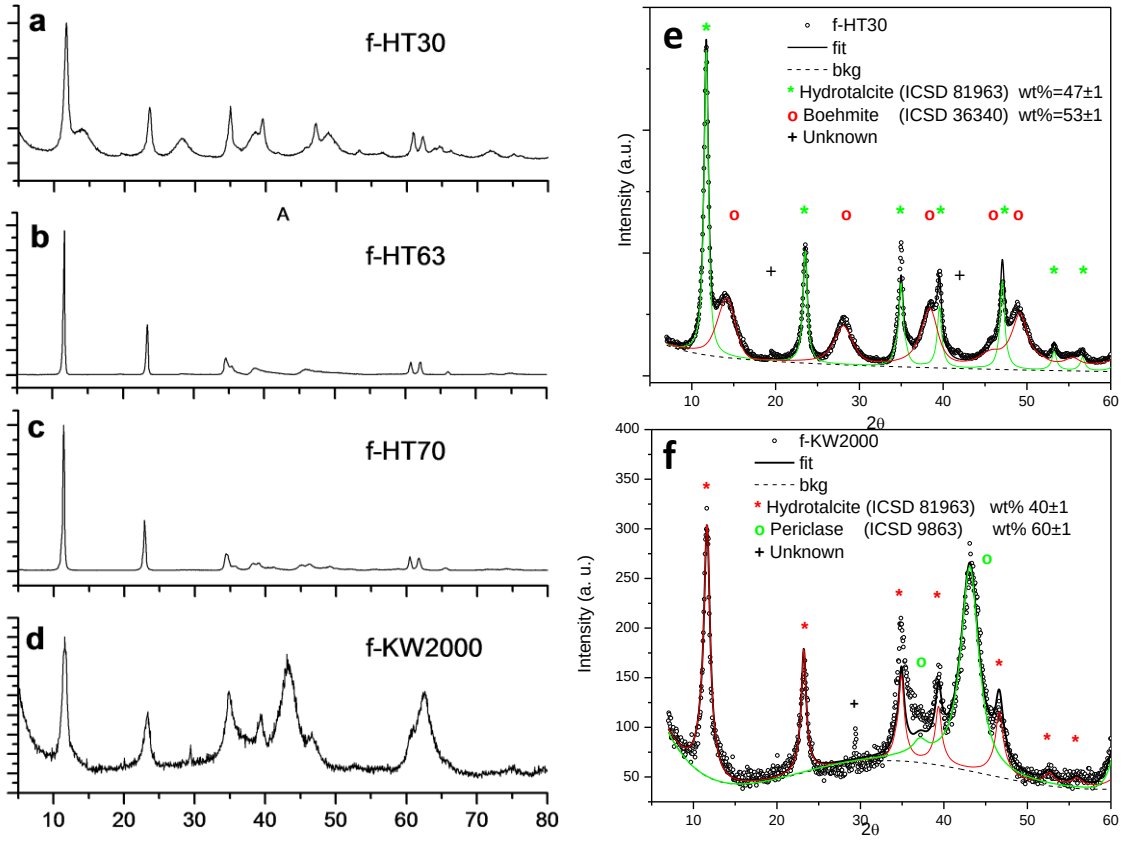

Figure 2.13. XRD patterns of fresh HT samples (a-d) and Rietveld fits of f-HT30 (e) and f-KW2000 (f).

A Rietveld analysis was then performed on the model sample of c-KW2000. Two aspects were considered for this investigation:

i. In addition to MgO, both Al_2O_3 and the spinel Al_2MgO_4 were the most probable components of the c-KW2000 system. This was inferred by the analysis of the phase diagram of Al_2O_3/MgO system.[55]

ii. If the thermal degradation of a hydrotalcite occurred at 300–500 °C, metastable phases of MgO and finely dispersed Al_2O_3 or solid solutions of Al_2MgO_4/Al_2O_3, MgO/Al_2O_3 or both could form.[56]

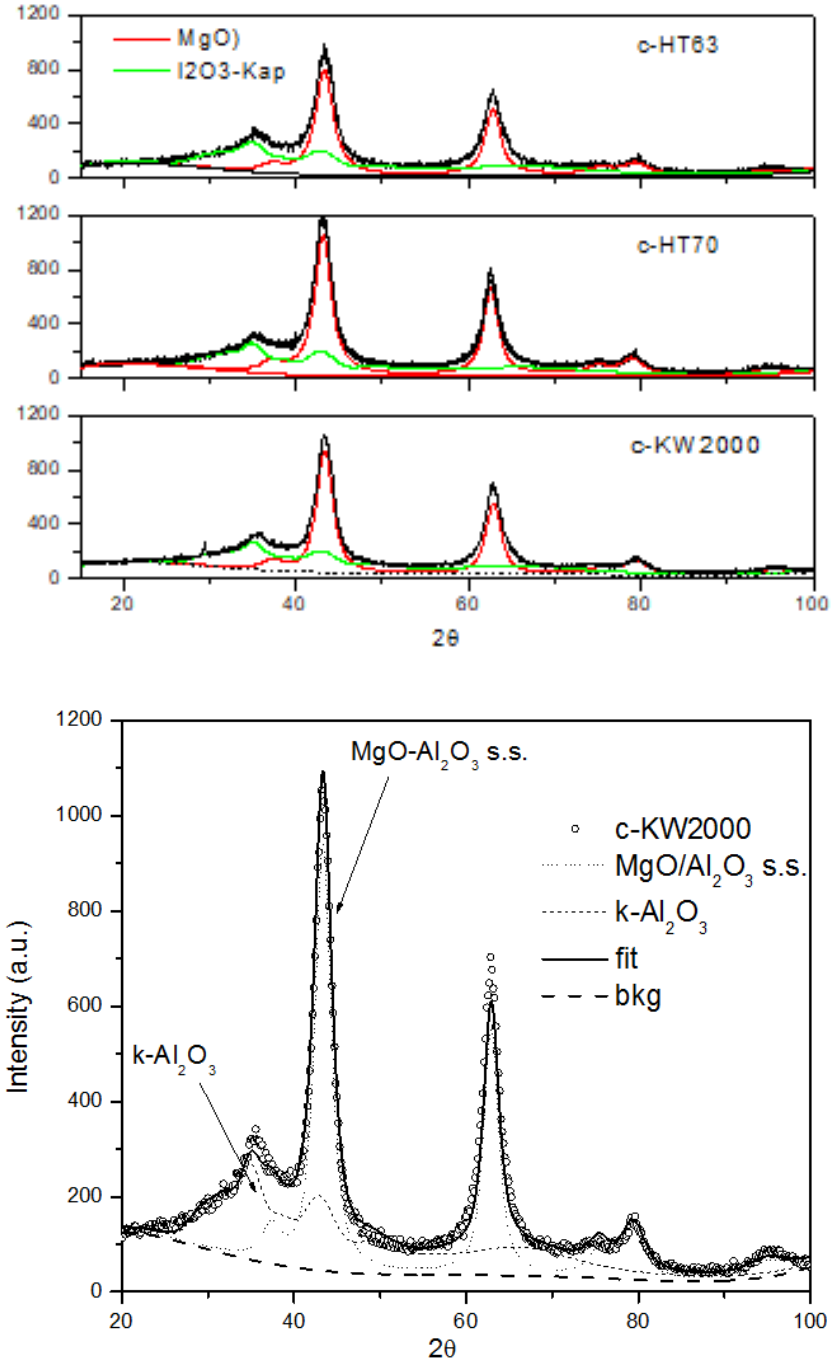

Figure 2.14. Top: XRD patterns of c-KW2000, c-HT63, and c-HT70 (black profiles). Bottom: Rietveld fit of c-KW2000 (R_{wp} = 9.5%).

Of the hypothesised crystal structures, Al_2MgO_4 did not provide an acceptable result, while among possible aluminas, k-Al_2O_3 (ICSD 94485) gave the best fit of the XRD pattern (Figure 2.14, bottom). It was also noticed that the refined cell for MgO was smaller [(4.190±0.001) Å]

than that of pure MgO (4.2112 Å), thereby indicating the formation of a solid solution (ss) of alumina in magnesia in which the Al atoms occupied 15% of the cationic sites.[56] By assuming that the ss dissolved the Al_2O_3 phase, the quantitative Rietveld analysis of Figure 2.14 allowed us to estimate proportions of Al_2O_3 (39 wt%) and MgO (61 wt%) that were very close to the nominal composition of the sample. This indirectly supported the presence of almost pure Al_2O_3 as the amorphous phase. Finally, the ss was completely absent in the fresh sample of KW2000 (Figure 3b), in which periclase showed a unit-cell parameter of (4.213±0.002) Å.

The diffraction pattern of c-HT30, which contained a higher fraction of Al, was remarkably different from those previously shown for other c-HTs (Figure 2.15).

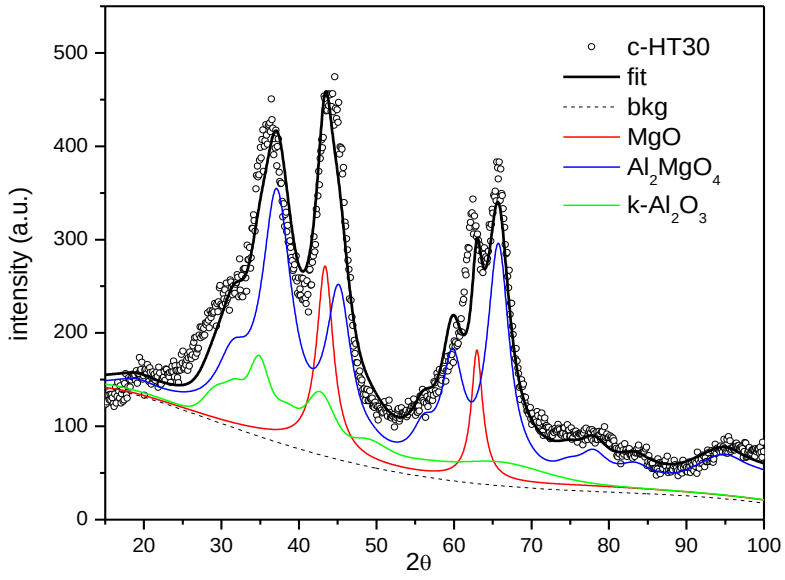

Figure 2.15. XRD pattern and Rietveld fit of c-HT30 (R_{wp} = 11.6%).

In this case, the Rietveld analysis allowed us to identify the presence of a ss of MgO/Al_2O_3, the spinel Al_2MgO_4 and k-Al_2O_3. The corresponding amounts of these three phases were estimated at 15, 63 and 22 wt%, respectively. Although the obtained fit was not as good as the previous one (cfr. the R_{wp} indices of Figure 2.14 and Figure 2.15), the calculated proportions of Al_2O_3 (69 wt%) and MgO (31 wt%) were very close to those of the nominal composition of the sample.

Table 2.6. BET analysis of the KW2000 and HT30 samples.

Entry	Label	Calcination (450 °C, air, 16 h)	Surface area (m^2/g)	Pore Volume (cm^3/g)[a]	Conditions of use
1	f-KW2000	none	108	0.79	None[b]
2	c-KW2000	yes	199	0.72	18 h at 210 °C, 10 bar[e]
3	f-HT30	none	138	0.33	None[b]
4	c-HT30	yes	247	0.48	18 h at 210 °C, 10 bar[e]

Surface area and pore volume were determined by BET analyses. a) determined from the nitrogen adsorbed volume at p/p0 = 0.977; b) the fresh (f-) solids were not used for catalytic tests; e) calcined (c-) samples were used for catalytic tests under the conditions in Table 2.3. BET analyses were carried out before the use of c-solids as catalysts.

The BET characterization was carried out only for the KW2000 and HT30 catalysts. Results are reported in Table 2.6.

A substantial increase in the surface area (S_{BET}) was observed once both solids were calcined at 450 °C: specifically, this rose from 108 to 199 $m^2\ g^{-1}$ for f- and c-KW2000, and from 138 to 247 m^2g^{-1} for f- and c-HT30, respectively. Although fresh samples of KW2000 and HT30 were not pure hydrotalcite phases, the S_{BET} data matched the trend of surface area that is usually observed for fresh and calcined HTs.[39a,57] The thermal collapse of the ordered layered structures of HTs and the subsequent formation of crystalline Mg/Al mixed oxides could account for this behaviour.

Overall, the performance of the investigated catalysts was consistent with structural modifications induced by calcination and, potentially, during the reaction itself. More specifically, the characterisation of the two most active systems indicated that both KW2000 and HT30 acted as precursors of active phases, which were composed of solid solutions of Mg/Al oxides along with amorphous alumina. These phases formed during the thermal treatment of HTs according to the reactions summarised in Scheme 2.7.[39,41,54]

$$Mg_{1-x}Al_x(OH)_2(CO_3)_{x/2}\cdot mH_2O \xrightarrow{25\text{-}200\ ^\circ C} Mg_{1-x}Al_x(OH)_2(CO_3)_{x/2}$$

$$x/2\ MgAl_2O_4 + (1\text{-}3x/2)\ MgO \xleftarrow{250\text{-}500\ ^\circ C}$$

Scheme 2.7. The thermal decomposition mechanism of Mg-Al hydrotalcites.

Above 250 °C, HTs decompose due to the release of interlayer water and the extensive dehydroxylation and decarbonation reactions of the intralayer OH^- and CO_3^{2-} anions (Scheme 2.7 and Figure 2.5). However, as the produced phases ($MgAl_2O_4$, Al_2O_3 or Al-doped MgO) often have small nuclei, they are hard to distinguishable from each other.[58] This is the main reason

why the outcome of the thermal process and the precise nature of the mixed oxides have not been completely resolved.

In the light of this behaviour, a hypothesis was formulated to explain why KW2000 could be used as such in the investigated *O*-alkylation reactions (Figure 2.9: f-KW2000), while HT30 was active only upon calcination (Figure 2.9 and Table 2.3). The two starting (fresh) solid materials showed quite different chemical compositions in which the layered HT structure coexisted with large proportions of periclase in f-KW2000 or boehmite in f-HT30 (Figure 2.13a and d, respectively). It was therefore plausible that the breakdown in Scheme 2.7 occurred under different conditions for the two solids: in the case of f-KW2000, the process could be completed during the CF alkylation reactions with heating to 275 °C, whereas the collapse of f-HT30 is a more energy-demanding transformation, which could be achieved only during a high-temperature calcination at 450 °C.

Another question was why there was such a large difference in the performances of the investigated c-HT systems. Mixed Mg/Al oxides obtained through the calcination of HTs are often defined as amphoteric solids.[41,59] As mentioned in section 2.2.2.1, this dual (acid/base) activity has been used as an explanation to account for the nucleophilic and electrophilic activation of organic substrates promoted by c-HTs in several model reactions, including transfer hydrogenations and aldol condensations of ketones,[26,41] transesterification and carbonylation processes[25] as well as eliminations and condensations of alcohols.[57,60]

The basicity of c-HT systems has been the subject of many fundamental investigations. It is generally agreed that the basic sites of HTs can be classified according to their relative strength: weak, medium, and strong as determined by the functional groups present; OH groups, Mg–O or Al–O pairs, and low-coordinated O^{2-} anions, respectively.[39,54,61] In this respect, although direct measures of surface basicity (and acidity) were not carried out in this Thesis work, some data were available from the suppliers of HT solids, which reported that the densities of total basic sites determined by CO^{2-} TPD (temperature programmed desorption) profiles of c-HT30 and c-HT70 were 1.35 and 3.00 μmol m^{-2}, respectively.[62] Both these solids were obtained by the calcination of the corresponding fresh HTs at 450 °C. This finding was consistent with the Mg/Al ratios of the samples: the higher the Al content (the more electronegative metal cation), the higher the nucleation of Al-rich phases, and the lower the average basicity of the solid.[41,54] In particular, the segregation of a large amount of a spinel phase in c-HT30 (Al_2MgO_4: 63 wt%; see XRD of Figure 2.15) probably led to the partial coverage

of the sites on the surface of MgO, thereby decreasing the basicity with respect to c-HT70 (composed mostly of a solid solution of alumina in magnesia: Figure 2.14, top). An extensive analysis of these aspects was performed by Cavani *et al.*,[39,61,63] who concluded that for c-HTs, the Al/Mg ratio induced a variability of the surface properties, but in the range 2.0<Mg/Al<3.5, all materials were less basic than MgO as they possessed basic sites mostly of medium strength, while Lewis-acid sites were manifest at low Mg/Al ratios in the form of coordinatively unsaturated Al^{3+} species. The same Authors then proposed that in the presence of c-HTs of Mg/Al = 2 a cooperative mechanism, through a synergetic effect of the basic and Lewis-acidic sites, could explain the selective *O*-methylation of phenol with methanol in the gas phase.[60]
A similar formulation would appear consistent with the behaviour of the c-HTs observed in Figure 2.12, Table 2.3 and Table 2.4. The results were obviously not due to a purely basic mechanism since the best-performing catalyst c-HT30 was less basic than c-HT70 and far less basic than pure MgO. On the other hand, among the tested c-HTs, c-HT30 not only had a different bulk structure (Figure 2.15) but also a lower Mg/Al ratio, which possibly favoured the occurrence of Lewis-acid sites. Therefore, it would appear that c-HT30 displayed the best compromise between the acid and base properties, of the HTs studied, for a plausible mechanism hypothesised in Scheme 2.8.

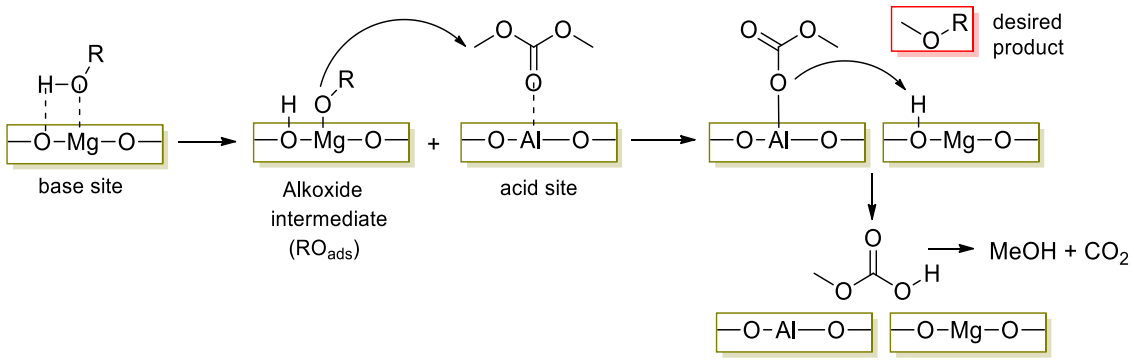

Scheme 2.8. Proposed mechanism for the reaction of OH-bearing BBDs (ROH) and DMC at the HT surface.

This mechanism suggests that both nucleophilic and electrophilic partners need to be activated by the catalyst. After the adsorption of an OH-bearing BBD (ROH: Figure 2.1) on a Brønsted basic site (*e.g.*, Mg–O pairs), a deprotonation reaction follows to form the alkoxide intermediate RO_{ads}, while at the same time, the dialkyl carbonate (DMC in Scheme 2.8) is activated by Al^{3+} cations acting as Lewis-acid sites in the HT framework. A similar electrophilic activation of DAlCs by metal cations has already been described by our groups in FAU catalysts.[35] Then, RO_{ads} undergoes a $B_{Al}2$-type reaction with the adsorbed DMC to produce the

desired methyl ether (ROMe) and methyl hydrogen carbonate ($MeOCO_2H$). The latter is an unstable derivative which spontaneously decomposes into MeOH and CO_2. In this mechanism the RO_{ads} could also attack the carboxyl carbon atom of DMC to form the corresponding transesterification product ($ROCO_2Me$; $B_{Ac}2$ mechanism, see Scheme 2.2). However, the equilibrium of the reversible transesterification reaction shifts towards the re-formation of the starting material as it is consumed by the irreversible *O*-methylation reaction. The product distribution was also directed by the temperature. In line with previously reported results,[1,8,9,13,47] alkylation and transesterification processes involving DAlCs were discriminated based on their different activation energies, with methylations occuring only at relatively high temperatures, usually above 150 °C.

A different situation was identified for the four fresh HT solids investigated here, of which f-KW2000 was the best catalytic system (Figure 2.9). As mentioned above, the composition of f-KW2000 with a large excess of periclase (Figure 2.13d) may facilitate the decomposition of the solid towards a catalytically active phase (MgO/Al_2O_3 ss) even at the much lower temperature of 275 °C that was used for the CF tests. However, KW2000 showed remarkable resemblances to the HT63 and HT70 samples since all these solids had comparable Mg/Al ratios of (Table 2.1) and similar bulk structure after calcination (see Figure 2.14). This was further substantiated by the similar catalytic performances of the three calcined solids (c-KW2000, c-HT63 and c-HT70) in the *O*-methylation of solketal (Table 2.3). Therefore, although f-KW2000 could be converted into the active catalyst at 275 °C (and 10 bar), the corresponding active phase of Mg/Al oxide needed to be more basic to effectively catalyse the reaction, and consequently, it was less efficient than c-HT30.

Finally, the effect of post-synthetic alkaline impurities on the catalytic activities of c-HTs was considered. Although it is well known in literature that the doping of HTs with alkali-metal carbonates and hydroxides increases the basicity and the activity of these systems, it has also been reported that the necessary quantity of alkaline dopants must corresponded to an alkali-metal (Na, K) content of 0.5–10 wt%.[64] These levels were at least 250- and 20-fold higher than those determined by ICP in HT30 and KW2000, respectively (Table 2.1). Reasonably, any alkalinity due to residual Na or K salts in the investigated catalysts is expected to have had a negligible, if any, role in the catalysis of the *O*-alkylation reactions with DAlCs.

2.4. Conclusions

This investigation integrates an archetypical green reaction, involving non-toxic and renewable reactants, with an efficient continuous-flow (CF) procedure for the synthesis of alkyl ethers of one class of bio-based derivatives. Calcined HTs, particularly c-HT30, have proved effective for highly chemoselective transformations: functionalised bio-based alcohols and dialkyl carbonates are activated towards *O*-alkylations with respect to the competitive transesterifications and other side-reactions including the ring opening of acetal functions, decarboxylations of dialkyl carbonates and oligo- or polymerisations. It was found to be possible to achieve *O*-alkylation selectivities as high as 99% with complete conversion using this method. To the best of our knowledge, this result has no precedent in the class of biomass-derived compounds investigated. The analyses of the bulk structures of the fresh and calcined hydrotalcites investigated here are consistent with the formation of catalytically active phases constituted by mixed Al/Mg oxides. These originated either upon calcination or by simply heating at the reaction temperature, and their composition varies between the different HTs. The activity of the best catalyst (c-HT30) is consistent with both a lower density of basic sites and a more pronounced acidic character than those of the other solids of the family. Overall, the CF protocol provides the multiple advantages described in Chapter 1, of which the most relevant ones include the high process safety, the recyclability of (excess) unconverted DAlCs, which serve as solvents and reagents, the reuse of the catalysts and the simplification of downstream operations for the isolation and purification of products to improve the productivity (greater by orders of magnitude) with respect to those of batch methods.

2.5. Experimental Section

2.5.1. General

Solketal (**1a**), glycerol formal (GlyF, **2a**/**2a'**), furfuryl alcohol (**4a**), tetrahydrofurfuryl alcohol (**5a**), dimethyl carbonate (DMC), diethyl carbonate (DEC) and MgO were ACS grade from Aldrich. If not otherwise specified, they were employed without further purification. Glycerol carbonate (**3a**) was from JEFFSOL® and used as received. Solketal methylcarbonate (**1c**) was

prepared via the transesterification reaction of solketal with DMC, by adjusting a method developed by us.[10]

GC/MS (EI, 70 eV) analyses were run using a HP5-MS capillary column (L = 30 m, Ø = 0.32 mm, film = 0.25 μm). The following conditions were used: carrier gas: He; flow rate: 1.2 mL·min^{-1}; split ratio: 10:1; initial T: 50 °C (3 min), ramp rate: 10 °C/min; final T: 250 °C (3 min).

CG/FID analyses were run using an Elite-624 capillary column (L = 30 m, Ø=0.32 mm, film = 1.8 μm). The following conditions were used. Carrier gas: N_2; flow rate: 5.0 mL·min^{-1}; split ratio: 1:1; initial T: 100 °C (0 min), ramp rate: 15 °C/min; final T: 220 °C (5 min).

^{1}H NMR spectra were recorded at 400 or 300 MHz, ^{13}C NMR spectra at 100 MHz, and chemical shifts were reported in δ values downfield from TMS; $CDCl_3$ was used as the solvent.

2.5.1.1. Catalysts

FAUs of formula $M_z[(AlO_2)_z(SiO_2)_w]\cdot mH_2O$ (M = Na, Cs; X- and Y-type: z = 86 and 56, w = 104 and 136, m = 264 and 250, respectively) included NaX and NaY faujasites from Aldrich and a CsY zeolite synthesised by a conventional ionic exchange reaction of NaY with aq. CsCl.[17] The percentage of ionic exchange ($Na^+ \rightarrow Cs^+$) was 58%: it was evaluated through atomic emission according to a procedure already reported by our group.[65]

Before their use, they were dehydrated under vacuum (70 °C, 18 mmHg, overnight).

Hydrotalcites (HTs) were aluminium magnesium hydroxyl carbonate hydrates of formula $Mg_{2x}Al_2(OH)_{4x+4}(CO_3)\cdot nH_2O$ (x = 0.5-2.3). Four commercial HTs were used (their Mg/Al molar ratio is given in parentheses): KW2000 (1.8); PURAL® MG30 (0.5), MG63 (1.9) and MG70 (2.3). KW2000 was from Kyowa Chemical Industry Co., Ltd., while PURAL® MG solids were from CONDEA/Sasol Germany GmbH, Inorganic Specialty Chemicals. According to the manufacturer specifications, these materials are aluminium magnesium hydroxycarbonate hydrates $Mg_{2x}Al_2(OH)_{4x}+4(CO_3)\cdot nH_2O$ with x varying between 0.5 and 2.3. Carbonate content is about 10 wt% and the maximum loss on ignition (3 h, 1000 °C) is between 40–45%. Due to its high Al content, HT30 contains a significant amount of boehmite (γ-AlO(OH)). All HTs were used both as-received and after calcination. If used as received, solids were dehydrated under vacuum (70 °C, 18 mmHg, overnight) before being loaded in the CF-reactor. Otherwise, the calcination treatment was carried out according to a procedure already reported for HTs:[34] solid samples (5 g) were heated in a quartz reactor (in the upright position) under a flow of dry air at 450 °C for 16 h. The heating rate was 30 °C/min.

Catalyst characterisation

Adsorption–desorption isotherms of nitrogen were obtained at the liquid nitrogen temperature using a Micromeritics ASAP 2010 system. Each sample has been degassed at 130 °C overnight before measuring the N_2 physisorption isotherm. From the data, the Brunauer-Emmett-Teller (BET) equation and the Barrett-Joyner-Halenda (BJH) model were used to calculate the specifc surface areas and the pore size distributions, respectively. X-ray powder diffraction (XRD) analyses were recorded with a Philips X'Pert powder diffractometer (Bragg-Brentano parafocusing geometry). A nickel-filtered Cu Ka1 radiation (l ¼ 0.15406 nm) and a voltage of 40 kV were employed. XRD were carried out for all the non-calcined (as-received) hydrotalcite solids and the two most catalytically relevant samples of calcined KW2000 and calcined HT30.

ICP analyses

ICP analyses were carried out to evaluate both the composition of the KW2000 including the Mg:Al ratio and the post-synthesis amounts of Na and K, and the leaching of Mg and Al from the catalytic bed of c-HT30 used in this investigation. Analyses were run on a Perkin Elmer Nexion 300XX Inductively Coupled Plasma Mass Spectrometer (ICP/MS). Calibration curves were obtained by using three aqueous solutions containing 50, 100 and 200 ppb of Na, K, Al and Mg respectively. These solutions were prepared by dilution of a 200 mg/L multi element commercially prepared standard solution.

Mg:Al ratio and post-synthesis amounts of Na and K in KW2000. KW2000 (0.1 g) was dissolved in concentrated HCl and subsequently diluted with Milli-Q H_2O in a 100 mL volumetric flask.[66]

Leaching of Mg and Al from the catalytic bed of c-HT30. Once the CF-reaction of solketal with DMC was carried out under the conditions of Figure 2 (20 h), the mixture sampled at the reactor outlet was rotary evaporated (50 °C, 5 mbar). The residue was digested with concentrated HNO_3, and diluted with Milli-Q H_2O in a 10 mL volumetric flask.

Table 2.7. ICP analyses of the Na, K, Mg and Al contents.

Entry	Sample	Metal content (µg/L)			
		Na	K	Mg	Al
1	f-KW2000 (0.1 g/100 mL)	265	117	246842	130660
2	Effluent from c-HT30[a]	-	-	40	85

a) Liquid solution recovered after the reaction of solketal with DMC: conditions of Figure 2.12 (20 h).

2.5.1.2. CF-Apparatus

The apparatus used for the investigation was assembled in house according to the chart in Figure 2.6. An HPLC pump (P1) was used to deliver liquid reactants to a stainless-steel tubular reactor (L = 12 cm, Ø = 1/4", 1.16 cm^3 inner volume) containing the catalyst. The reactor was placed in the upright position in a gas chromatographic oven (GC oven), and heated to the desired temperature. A Swagelok back pressure regulator (BPR), placed at the outlet of the reactor, was used to keep the pressure constant over the whole system throughout the reaction (line B). When experiments were carried at ambient pressure, the BPR was bypassed (line A). A Rheodyne Model 7725i injector, equipped with a 10 µL sample loop, was placed before the BPR and used for sampling. All components are connected by 1/16 inch stainless-steel (AISI 316) tubing.

SAFETY WARNING. Operators of high pressure equipment should take proper precautions to minimise the risk of personal injury.[67] The individual components that we describe work well, but they are not necessarily the only equipment of this type available.

2.5.2. General CF-methylation reactions procedure

A typical CF *O*-methylation reaction was carried out according to the following procedure.

The oven was set at a temperature of 150 °C and N_2 was flushed for one hour throughout the CF-apparatus. Then, the reacting mixture (DAlC and the bio-based alcohol) was allow to flow for 10 min at 1 mL min^{-1}, while the BPR and the oven were set to the operating pressure and temperature (5–60 bar, and 150–300 °C, respectively). Once T and p were stabilised, the reactants flow was adjusted to the desired rate (0.07–0.2 mL min^{-1}). The reaction mixture was collected through a Rheodyne® valve (7725i fitted with a 10 µL sample loop) at time intervals of about 30 min, diluted with 1.5 mL of diethyl ether and analysed by GC/FID or GC/MS.

Change of reaction conditions. The oven and the BPR were set to the new desired values of T and p, respectively. Under these conditions, the reactant mixture was flushed for 10 min at 1 mL min^{-1} through the CF-apparatus. Then the flow was adjusted to the chosen rate and a new experiment started.

System cleaning and restart. At the end of each experiment, the oven and the BPR were set to 50 °C and atmospheric pressure, respectively, while a cleaning solution of methanol (50 mL at 1 mL min^{-1}) was allowed to flow through the system. The pump was then stopped and the

oven was allowed to cool at rt. The CF-reactor was then disassembled and the catalytic bed could be replaced by a fresh one.

Reaction of Solketal (1a) and DMC with alkali metal exchanged faujasites (FAUs) as catalysts

The above described procedure was used to tests FAUs as catalysts under a number of conditions by varying the temperature and the pressure from 150–275 °C, and from 5–50 bar, respectively.

Figure 2 reports the most representative results obtained by using NaY, NaX, and CsY, respectively. Before use, each zeolite was dehydrated under vacuum (70 °C, 18 mmHg, overnight): 0.68, 0.54, and 0.86 g of NaY, NaX, and CsY, respectively, were charged into the CF-reactor. In all tests, a 1.83 M solution of solketal in DMC [DMC:solketal molar ratio (*W*)=5] was fed into the reactor at a total volumetric flow rate (*F*) of 0.1 mL min^{-1}. Experiments were performed under a constant pressure of 10 bar, while T was set at 250 and 275 °C, respectively. CF-reactions were followed for 3 h. Two additional runs with both NaY and NaX catalysts were carried out for up to 18 h.

Reaction of Solketal (1a) and DMC with hydrotalcites

As-received hydrotalcites. HTs were dehydrated under vacuum (70 °C, 18 mmHg, overnight): 0.52, 0.73, 0.51, and 0.85 g of KW2000, HT30, HT63, and HT70, respectively, were used for CF-tests. A 1.83 M solution of solketal in DMC [DMC:solketal molar ratio (*W*) = 5] was fed to the reactor at a total volumetric flow rate (*F*) of 0.1 mL min^{-1}. At 275 °C, reactions were performed under a constant pressure of 10 bar, and they were followed for 18 h. In the case of KW2000, additional experiments were carried out under the following conditions: *i*) T = 200 and 250 °C, p = 10 bar, *W* = 5, *F* = 0.1 mL min^{-1}; *ii*) T = 275 °C, p = 5 and 50 bar, *W* = 5, *F* = 0.1 mL min^{-1}; *iii*) T = 275 °C, p = 10 bar, *W* = 1.1, 2, 3.5, *F* = 0.1 mL min^{-1}.

Calcined hydrotalcites. After calcination at 450 °C (see above for details), 0.5 g of each solid (c-KW2000, c-HT30, c-HT63, and c-HT70, respectively) was used for CF-tests. In all cases, a 1.83 M solution of solketal in DMC [DMC:solketal molar ratio *W* = 5] was fed into the reactor at a total volumetric flow rate (*F*) of 0.1 mL min^{-1}. At 10 bar, reactions catalysed by c-KW2000, c-HT30, c-HT63, and c-HT70 were run at 210, 225, and 275 °C, respectively, for 18 h. In the case of c-HT30, experiments were also performed at 210 °C and atmospheric pressure.

Two additional reactions were also conducted by replacing c-HT catalysts by either MgO (0.85 g) or a physical mixture of MgO and basic γ-Al_2O_3 (particle size: 50-200 μm, surface area: 130 m^2/g, pH:9.5±0.3) in 30:70 molar ratio, respectively (0.85 g). The choice of γ-Al_2O_3 was based

on reference 39. Both MgO and the mixture MgO/γ-Al_2O_3 were calcined at 450 °C for 6 h before use. Then, CF-tests were run at 275 °C, 10 bar, *W* = 5, and *F* = 0.01 mL min^{-1}.

The use of different substrates and carbonates

Reaction of Solketal and diethyl carbonate (DEC). According to the above-described general procedure, the reaction of glycerol acetals (**1a** and **2a**/**2a'**) was performed using DEC and c-HT30 (0.5 g) as an alkylating agent and a catalyst, respectively. CF-reactions were carried out at 250 and 275 °C, and ambient pressure. A mixture of DEC and the chosen glycerol acetal in a 5:1 molar ratio was delivered at 0.1 mL min^{-1} to the CF-reactor.

Different substrates. According to the above-described general procedure, the reactions of DMC with glycerol formal (**2a**+**2a'**), glycerol carbonate (**3a**), furfuryl alcohol (**4a**), and tetrahydrofurfuryl alcohol (**5a**) were investigated in the presence of c-HT30 (0.5 g) as a catalyst. Reactions were optimised on a case-by-case basis under the following conditions: *i*) 220 °C, 1 bar, glycerol formal:DMC in a 1:5 molar ratio; *ii*) 210 °C, 1 bar, glycerol carbonate:DMC in 1:20 molar ratio; *iii*) 150 °C, 1 bar, furfuryl alcohol:DMC in 1:10 molar ratio; *iv*) 260 °C, 1 bar, tetrahydrofurfuryl alcohol:DMC in 1:5 molar ratio. The flow rate was 0.1 mL min^{-1} in all cases.

2.5.2.1. Isolation and characterization of products

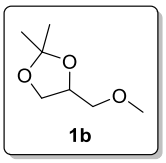

(2,2-Dimethyl-1,3-dioxolan-4-yl)methyl methyl ether (1b). Under the above-described conditions, a CF-reaction was carried out at 210 °C and 1 bar, by using a mixture of solketal:DMC in 1:5 molar ratio (15 h; *F*=0.1 mL min^{-1}) and c-HT30 as the catalyst (0.59 g). The final conversion was >99% with a selectivity >99% towards the desired product **1b**. The mixture collected at the reactor outlet was concentrated by rotary evaporation (40 °C, 40 mbar). Title product was obtained as a colorless liquid in 92% yield (22.04 g, 0.151 mol). Compound **1b** was characterized by ^{1}H NMR, ^{13}C NMR and GC/MS. ^{1}H NMR (400 MHz, $CDCl_3$) δ (ppm) 4.32 – 4.23 (m, 1H), 4.05 (dd, J=8.2, 6.4 Hz, 1H), 3.69 (dd, J = 8.2, 6.5 Hz, 1H), 3.50 – 3.39 (m, 2H), 3.39 (s, 3H), 1.42 (s, 3H), 1.36 (s, 3H). ^{13}C NMR (75 MHz, $CDCl_3$) δ 109.47, 74.61, 73.79, 66.68, 59.41, 26.77, 25.38. GC/MS of **1b** (relative intensity, 70 eV) m/z: 146 ($[M]^+$, 0), 131 (100), 101 (65), 73 (20), 72 (16), 71 (80), 59 (14), 45 (16), 43 (83), 42 (11), 41 (21).

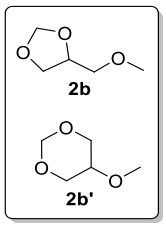

1,3-Dioxan-5-yl methyl ether (2b) and (1,3-dioxolan-4-yl)methyl methyl ether (2b'). Under the above-described conditions, a CF-reaction was carried out 220 °C and 1 bar, by using a mixture of glycerol formal:DMC in 1:5 molar ratio (6 h; *F*=0.1 mL min^{-1}) and c-HT30 as the catalyst (0.59 g). The final conversion was 99% with a selectivity >99% towards the desired product **3b**. The mixture collected at the reactor outlet was concentrated by rotary evaporation (40 °C, 40 mbar). Title product was obtained as a colorless liquid in 81% yield (6.80 g, 0.058 mol). Compound **2b+2b'** was characterized by ^{1}H NMR, ^{13}C NMR and GC/MS. ^{1}H NMR (400 MHz, $CDCl_3$) δ (ppm) 4.32–4.23 (m, 1H), 4.05 (dd, J=8.2, 6.4 Hz, 1H), 3.69 (dd, J=8.2, 6.5 Hz, 1H), 3.50–3.39 (m, 2H), 3.39 (s, 3H), 1.42 (q, J=0.7 Hz, 3H), 1.36 (q, J=0.6 Hz, 3H). ^{13}C NMR (50 MHz, $CDCl_3$) δ (ppm) 95.01, 93.37, 74.02, 72.65, 71.02, 68.64, 66.61, 59.08, 56.55. GC/MS of **2b** (relative intensity, 70 eV) m/z: 118 ($[M]^+$, 0), 88 (26), 86 (11), 73 (32), 72 (21), 59 (16), 58 (10), 57 (12), 45 (100), 44 (15), 43 (15). GC/MS of **2b'** (relative intensity, 70 eV) m/z: 118 ($[M]^+$, 4), 88 (16), 58 (100), 43 (29).

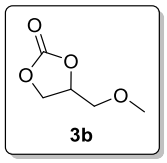

4-(Methoxymethyl)-1,3-dioxolan-2-one (3b). Under the above-described conditions, a CF-reaction was carried out at 210 °C and 1 bar, by using a mixture of **3a**:DMC in 1:20 molar ratio (6 h; *F*=0.1 mL min^{-1}) and c-HT30 as the catalyst (0.59 g). The final conversion was 98% with a 65% selectivity towards the desired product **3b**. The mixture collected at the reactor outlet was concentrated by rotary evaporation (40 °C, 40 mbar) and purified through flash column chromatography. Title product was obtained as a pale yellow liquid in 55% yield (1.49 g, 0.011 mol). Compound **3b** was characterized by ^{1}H NMR, ^{13}C NMR and GC/MS. ^{1}H NMR (300 MHz, $CDCl_3$) δ (ppm) 4.82 (m, J=8.3, 6.1, 3.9 Hz, 1H), 4.55–4.37 (m, 2H), 3.63 (qd, J=10.9, 3.9 Hz, 2H), 3.45 (s, 3H). ^{13}C NMR (75 MHz, $CDCl_3$) δ (ppm) 154.73, 74.80, 71.37, 66.07, 59.56. GC/MS of **3b** (relative intensity, 70 eV) m/z: 132 ($[M]^+$, 0), 100 (40), 90 (59), 87 (23), 77 (49), 59 (100), 58 (33), 57 (16), 56 (19), 45 (75), 43 (89), 42 (16).

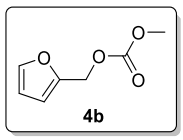

Furan-2-yl methyl methyl carbonate (4b). Under the above-described conditions, a CF-reaction was carried out at 150 °C and 1 bar, by using a mixture of **4a**:DMC in 1:10 molar ratio (6 h; *F*=0.1 mL min^{-1}) and c-HT30 as the catalyst (0.59 g). The final conversion was 88% with a 91% selectivity towards product **4b**. The mixture collected at the reactor outlet was concentrated by rotary evaporation (50 °C, 40

mbar) and purified through flash column chromatography. Title product was obtained as a colorless liquid in 80% yield (4.46 g, 0.029 mol). Compound **4b** was characterized by ^{1}H NMR, ^{13}C NMR and GC/MS. ^{1}H NMR (400 MHz, $CDCl_3$) δ (ppm) 7.45 (dq, J=1.7, 0.8 Hz, 1H), 6.51–6.45 (m, 1H), 6.38 (dt, J=3.2, 1.5 Hz, 1H), 5.14 (d, J=1.2 Hz, 2H), 3.85–3.79 (m, 3H). ^{13}C NMR (101 MHz, $CDCl_3$) δ (ppm) 155.53, 148.77, 143.53, 111.23, 110.58, 61.30, 54.94. GC/MS of **5c** (relative intensity, 70 eV) m/z: 157 ($[M+1]^+$, 3), 156 ($[M]^+$, 39), 97 (20), 81 (100), 80 (26), 53 (32), 52 (34), 39 (11).

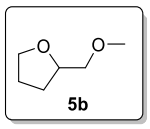

2-(Methoxymethyl)tetrahydrofuran (5b). Under the above-described conditions, a CF-reaction was carried out at 260 °C and 1 bar, by using a mixture of **5a**:DMC in 1:5 molar ratio (6 h; *F*=0.1 mL min^{-1}) and c-HT30 as the catalyst (0.59 g). The final conversion was 99% with a 92% selectivity towards the desired product **5b**. The mixture collected at the reactor outlet was concentrated by rotary evaporation (50 °C, 40 mbar). Title product was obtained as a pale yellow liquid in 82% yield (6.87 g, 0.059 mol). Compound **5b** was characterized by ^{1}H NMR, ^{13}C NMR and GC/MS. ^{1}H NMR (300 MHz, $CDCl_3$) δ (ppm) 4.10–3.96 (m, 1H), 3.95–3.82 (m, 1H), 3.75 (ddd, J=10.0, 7.3, 5.3 Hz, 1H), 3.46–3.29 (m, 5H), 2.01–1.79 (m, 3H), 1.65–1.49 (m, 1H). ^{13}C NMR (101 MHz, $CDCl_3$) δ (ppm) 77.72, 75.34, 68.29, 59.24, 27.97, 25.65. GC/MS of **5b** (relative intensity, 70 eV) m/z: 116 ($[M]^+$, 1), 71 (100), 70 (24), 45 (25), 43 (49), 41 (26), 39 (10).

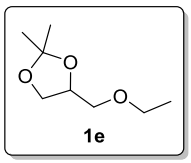

4-(Ethoxymethyl)-2,2-dimethyl-1,3-dioxolane (1e). Under the above-described conditions, a CF-reaction was carried out at 250 °C and 1 bar, by using a mixture of solketal:DEC in 1:5 molar ratio (6 h; *F*=0.1 mL min^{-1}) and c-HT30 as the catalyst (0.59 g). The final conversion was >99% with a 99% selectivity towards the desired product **1e**. The mixture collected at the reactor outlet was concentrated by rotary evaporation (50 °C, 40 mbar). Title product was obtained as a pale yellow liquid in a 92% yield (7.22 g, 0.045 mol). Compound **1e** was characterized by ^{1}H NMR, ^{13}C NMR and GC/MS. ^{1}H NMR (400 MHz, $CDCl_3$) δ (ppm) 4.30–4.20 (m, 1H), 4.04 (ddd, *J*=8.1, 6.3, 1.5 Hz, 1H), 3.73–3.66 (m, 1H), 3.52 (dtt, *J*=10.9, 7.1, 2.5 Hz, 3H), 3.45–3.37 (m, 1H), 1.40 (d, *J*=3.2 Hz, 3H), 1.34 (d, *J*=3.5 Hz, 3H), 1.22–1.14 (m, 3H). ^{13}C NMR (101 MHz, $CDCl_3$) δ (ppm) 109.35, 74.74, 71.63, 66.97, 66.84, 26.73, 25.36, 15.02. GC/MS of **1e** (relative intensity, 70 eV)

m/z: 160 ([M]+, 0), 145 (95), 102 (12), 101 (99), 85 (44), 83 (10), 73 (23), 72 (21), 61 (12), 59 (27), 57 (78), 43 (100), 42 (11), 41 (14).

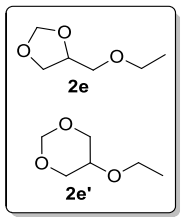

1,3-Dioxan-5-yl ethyl ether (2e) and (1,3-dioxolan-4-yl)methyl ethyl ether (2e'). Under the above-described conditions, a CF-reaction was carried out at 275 °C and 1 bar, by using a mixture of glycerol formal:DEC in 1:5 molar ratio (6 h; *F*=0.1 mL min^{-1}) and c-HT30 as the catalyst (0.59 g). The final conversion was 99% with a 99% selectivity towards the desired isomer products **2e**/**2e'**. The mixture collected at the reactor outlet was concentrated by rotary evaporation (50 °C, 40 mbar). Title product was obtained as a colorless liquid in 84% yield (5.73 g, 0.043 mol). Compound **2e**/**2'e** was characterized by ^{1}H NMR, ^{13}C NMR and GC/MS. ^{13}C NMR (101 MHz, $CDCl_3$) δ (ppm) 95.30, 93.61, 74.48, 70.89, 69.61, 69.52, 67.09, 67.04, 64.84, 15.52, 15.09. GC/MS of **2e** (relative intensity, 70 eV) m/z: 132 ([M]+, 0), 131 (3), 102 (29), 101 (21), 89 (14), 87 (12), 86 (32), 73 (78), 72 (33), 59 (100), 58(45), 57 (43), 45 (88), 44 (40), 43 (27), 41 (11). GC/MS of **2e'** (relative intensity, 70 eV) m/z: 132 ($[M]^+$, 5), 102 (14), 72 (100), 45 (16), 44 (75), 43 (31).

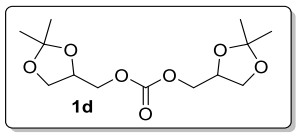

Bis((2,2-dimethyl-1,3-dioxolan-4-yl)methyl) carbonate (1d). Under the above described reaction conditions, a CF-reaction was carried out at 210°C and 1 bar, by using a mixture of solketal methyl carbonate:cyclohexane in 1:5 molar ratio (3 h; *F*=0.1 mL min^{-1}) and c-HT30 as the catalyst (0.59 g). The final conversion was 75% with 80% selectivity towards the desired product **1d**. The mixture collected at the reactor outlet was concentrated by rotary evaporation (50 °C, 40 mbar), and lighter by-products were distilled under high vacuum (70 °C, 3 mmHg). Title product was obtained as a pale yellow liquid in a 60% yield (4.52 g, 0.016 mol). Compound **1d** was characterized by ^{1}H NMR, ^{13}C NMR and GC/MS. ^{1}H NMR (400 MHz, $CDCl_3$) δ 4.39–4.32 (m, 2H), 4.20 (d, J=5.4 Hz, 4H), 4.10 (dd, J=8.5, 6.4 Hz, 2H), 3.80 (dd, J=8.6, 5.8 Hz, 2H), 1.47–1.44 (m, 6H), 1.38 (t, J=0.8 Hz, 6H). ^{13}C NMR (101 MHz, $CDCl_3$) δ 154.83, 109.96, 73.21, 68.12, 66.28, 26.70, 25.32. GC/MS of 1d (relative intensity, 70 eV) m/z: 290 ($[M]^+$, 0), 275 (23), 115 (100), 101 (32), 72 (14), 59 (24), 43 (41).

2.6. Bibliography

[1] P. Tundo, M. Selva, *Acc. Chem. Res.,* 2002, **35**, 706–716.

[2] a) L. Moity, A. Benazzouz, V. Molinier, V. Nardello-Rataj, M. K. Elmkaddem, P. de Caro, S. Thiébaud-Roux, V. Gerbaud, P. Marion and J.-M. Aubry, *Green Chem.,* 2015, **17**, 1779–1792; b) W. K. Teng, G. C. Ngoh, R. Yusoff, M. K. Aroua, *Energy Conv. Manag.,* 2014, **88**, 484–497; c) M. O. Sonnati, S. Amigoni, E. P. Taffin de Givenchy, T. Darmanin, O. Choulet, F. Guittard, *Green Chem*., 2013, **15**, 283–306; d) *Advances in Biorefineries: Biomass and Waste Supply Chain Exploitation*, K. W. Waldron, Ed.; Woodhead Pub. Ltd, 2014.

[3] M. Pagliaro, M. Rossi, *The Future of Glycerol*, 2nd Ed.; 2010, RSC Publishing, Cambridge, UK.

[4] a) M. Balakrishnan, E. R. Sacia, A. T. Bell, *Green Chem*., 2012, **14**, 1626–1634; b) Y. Gu, F. Jerome, *Chem. Soc. Rev.,* 2013, **42**, 9550–9570; c) R. Mariscal, P. Maireles-Torres, M. Ojeda, I. Sadaba, M. Lopez Granados, *Energy Environ. Sci*., 2016, **9**, 1144–1189.

[5] a) W. G. Trindade, W. Hoareau, J. D Megiatto, I. A. T. Razera, A. Castellan, E. Frollini, *Biomacromolecules,* 2005, **6**, 2485–2496; b) W. Chaikittisilp, K. Ariga, Y. Yamauchi, *J. Mater. Chem. A,* 2013, **1**, 14–19; c) L. Pranger, R. Tannenbaum, *Macromolecules,* 2008, **41**, 8682–8687.

[6] M. Chatterjee, H. Kawanami, T. Ishizaka, M. Sato, T. Suzuki, A. Suzuki, *Catal. Sci. Technol.,* 2011, **1**, 1466–1471.

[7] a) M. Sutter, E. D. Silva, N. Duguet, Y. Raoul, E. Metay, M. Lemaire, *Chem. Rev.*, 2015, **115**, 8609–8651; b) A. E. Dıaz-Alvarez, J. Francos, B. Lastra-Barreira, P. Crochet, V. Cadierno, *Chem. Commun*., 2011, **47**, 6208–6227; c) B. J. Nikolau, M. A. Perera, L. Brachova, B. Shanks, *Plant J.*, 2008, **54**, 536–545.

[8] M. Selva, V. Benedet, M. Fabris, *Green Chem.*, 2012, **14**, 188–200.

[9] M. Selva, M. Fabris, A. Perosa, *Green Chem.*, 2011, **13**, 863–872.

[10] A. Bomben, M. Selva, P. Tundo, L. Valli, *Ind. Eng. Chem. Res.*, 1999, **38***,* 2075–2079.

[11] a) A. Y. Platonov, A. N. Evdokimov, A. V. Kurzin, H. D. Maiyorova, *J. Chem. Eng. Data*, 2002, **47**, 1175–1176; b) M. Selva, C. A. Marques, P. Tundo, *J. Chem. Soc., Perkin Trans. I*, 1994, 1323–1328.

[12] a) M. Selva, P. Tundo, A. Perosa, *J. Org. Chem.*, 2001, **66**, 677–680; b) M. Selva, P. Tundo, A. Perosa, *J. Org. Chem.*, 2003, **68**, 7374–7378; c) M. Selva, P. Tundo, *J. Org. Chem.*, 2006, **71**, 1464–1470; d) M. Selva, A. Perosa, M. Fabris, *Green Chem.*, 2008, **10**, 1068–1077; e) J. N. G. Stanley, M. Selva, A. F. Masters, T. Maschmeyer, A. Perosa, *Green Chem.*, 2013, **15**, 3195–3204.

[13] a) A. Takagaki, K. Iwatani, S. Nishimura, K. Ebitani, *Green Chem*., 2010, **12**, 578–581; b) M. G. Álvarez, M. Plísková, A. M. Segarra, F. Medina, F. Figueras, *Appl. Catal. B: Environmental*, 2012, **113–114**, 212–220; c) P. Liu. M. Derchi, E. J.M. Hensen, *Appl. Catal. A: General,* 2013, **467**, 124–131; d) L. Zheng, S. Xia, Z. Hou, M. Zhang, Z. Hou, *Chin. J. Catal.,* 2014, **35**, 310–31.

[14] a) M. B. Talawar, T. M. Jyothi, P. D. Sawant, T. Raja, B. S. Rao*, Green Chem.*, 2000, **2**, 266–268; b) P. Tundo, S. Memoli, D. Hérault, K. Hill, *Green Chem.*, 2004, **6**, 609–612; c) G. Wu, X. Wang, B. Chen, J. Li, N. Zhao, W. Wei, Y. Sun, *Appl. Catal. A: General,* 2007, **329**, 106–111; d) G. D. Yadav, J. Y. Salunke, *Catal. Today,* 2013, **207**, 180–190.

[15] V. Rives, Layered Double Hydroxides: Present and Future, Nova Science Publisher, Inc., New York, 2006.

[16] T. Baskaran, J. Christopher, A. Sakthivel, *RSC Adv.*, 2015, **5**, 98853–98875.

[17] Z. Yong, Mata, A. E. Rodrigues, *Ind. Eng. Chem. Res.*, 2001, **40**, 204–209.

[18] a) M. R. Othman, Z. Helwani, Martunus, W. J. N. Fernando, *Appl. Organometal. Chem.*, 2009, **23**, 335–346; b) T. Lopez, P. Bosch, E. Ramos, R. Gomez, O. Novaro, D. Acosta, F. Figueras, *Langmuir*, 1996, **12**, 189–192.

[19] M. Ogawa, H. Kaiho, *Langmuir*, 2002, **18**, 4240–4242.

[20] W. F. Lee, Y. C. Chen, *Eur. Polym. J.*, 2006, **42**, 1634.

[21] M. Bellotto, B. Rebours, O. Clause, J. Lynch, D. Bazin, E. Elkaïm, *J. Phys. Chem.*, 1996, **100**, 8535-8542.

[22] H. Long, Y. Xu, X. Zhang, S. Hu, S. Shang, Y. Yin, X. Dai, *J. Energy Chem.*, 2013, **22**, 733–739.

[23] a) M. Xu, E. Iglesia, *J. Phys. Chem. B*, 1998, **102**, 961–966; b) Y. Lwin, F. Abdullah, *J. Therm. Anal. Calorim.*, 2009, **97**, 885–889.

[24] P. C. Pavan, E. L. Crepaldi, J. B. Valim, *J. Colloid Interface Sci.*, 2000, **229**, 346–352.

[25] a) M. J. Climent, A. Corma, P. De Frutos, S. Iborra, M. Noy, A. Velty, P. Concepcion, *J. Catal.*, 2010, **269**, 140–149; b) A. Navajas, G. Arzamendi, F. Romero-Sarria, M. A. Centeno, J. A. Odriozola, L. M. Gandìa, *Catal. Commun.*, 2012, **17**, 189–193; c) J. L. Shumaker, C. Crofcheck, S. A. Tackett, E. Santillan-Jimenez, M. Crocker, *Catal. Lett.*, 2007, **115**, 56.

[26] a) L. Smoláková, K. Frolich, J. Kocík, O. Kikhtyanin, L. Čapek, *Ind. Eng. Chem. Res.*, 2017, **56**, 4638–4648; b) T. M. Jyothi, T. Raja, K. Sreekumar, M. B. Talawar, B. S. Rao, *J. Mol. Catal. A*, 2000, **157**, 193–198.

[27] D. K. Dumbre, T. Mozammel, P. Selvakannan, S. B. Hamid, V. R. Choudhary, S. K. Bhargava, *J. Colloid Interface Sci.*, 2015, **441**, 52–58.

[28] T. M. Jyothi, T. Raja, B. S. Rao, *J. Mol. Catal. A: Chem.*, 2001, **168**, 187–191.

[29] a) B. F. Sels, D. E. De Vos, P. A. Jacobs, *Catal. Rev.-Sci. Eng.*, 2001, **43**, 443–488; b) K. Yan, Y. Liu, Y. Lu, J. Chai, L. Sun, *Catal. Sci. Technol.*, 2017, **7**, 1622–1645.

[30] V. Rives, M. Del Arco, C. Martin, *J. Control. Release*, 2013, **169**, 28–39.

[31] In this way, void spaces and preferential pathways of the reactants mixture through the catalytic bed were minimized if not ruled out. (see P. Harriot In Chemical Reactor Design, Dekker, Inc.; 2003)

[32] In the repeated tests carried out under the same conditions, values of conversion and amount of products (determined by GC/MS) differed by less than 5% from one reaction to another.

[33] D. Barthomeuf, *J. Phys. Chem*. 1984, **88**, 42.

[34] Y. Ono, *Cat. Tech*., 1997, **1**, 31.

[35] a) F. Bonino, A. Damin, S. Bordiga, M. Selva, P. Tundo, A. Zecchina, *Angew. Chem. Int. Ed*., 2005, **44**, 4774–4777; b) T. Beutel, M. J. Peltre, B. L. Su, *Colloids Surf., A* 2001, **187–188**, 319–325; c) T. Beutel, *J. Chem. Soc. Faraday Trans.,* 1998, **94**, 985–993.

[36] M. Selva, E. Militello, M. Fabris, *Green Chem*., 2008, **10**, 73–79.

[37] P. Tundo, L. Rossi, A. Loris, *J. Org. Chem.*, 2005, **70**, 2219–2224.

[38] a) M. Selva, S. Guidi, M. Noè, *Green Chem*., 2015, **17**, 1008–1023; b) S. Guidi, A. Perosa, M. Noè, R. Calmanti, M. Selva, *ACS Sus. Chem. Eng*., 2016, **4**, 6144–6151.

[39] a) F. Cavani, F. Trifirò, A. Vaccari, *Catal. Today*, 1991, **11**, 173–301; b) P. Bera, M. Rajamathi, M. S. Hedge, P. Vishnu Kamath, *Bull. Mater. Sci*., 2000, **23**, 141–145; c) P. Kustrowski, D. Sulkowska, L. Chmielarz, A. Rafalska-Lasocha, B. Dudek, R. Dziembaj, *Microporous Mesoporous Mater*., 2005, **78**, 11–22; d) K. J. D. MacKenzie, R. H. Meinhold, B. L. Sherriff, Z. Xu *J. Mater. Chem.*, 1993, **3**, 1263–1269.

[40] M. Hájek, P. Kutálek, L. Smoláková, I. Troppová, L. Capek, D. Kubicka, J. Kocík, D. N. Thanh, *Chem. Eng. J.,* 2015, **263**, 160–167.

[41] a) Y. Ono, H. Hattori (Eds.), Springer Series in Chemical Physics 101: Solid Base Catalysts, Springer, Berlin, 2011; b) S. T. Gadge, A. Mishra, A. L. Gajengi, N. V. Shahi, B. M. Bhanage, *RSC Adv*., 2014, **4**, 50271–50276.

[42] A. J. Parrott, R. A. Bourne, P. N. Gooden, H. S. Bevinakatti, M. Poliakoff, D. J. Irvine, *Org. Process Res. Dev*., 2010, **14**, 1420–1426.

[43] Moity, L.; Benazzouz, A.; Molinier, V.; Nardello-Rataj, V.; Elmkaddem, M. K.; de Caro, P.; Thiébaud-Roux, S.; Gerbaud, V.; Marion, P.; Aubry, J.-M., *Green Chem.,* 2015, **17**, 1779–1792.

[44] During the purification of final reaction mixtures, the more volatile ethers **2b**/**2b'** and **2e**/**2e'** were partly carried away in the first distilled fraction of DMC or DEC.

[45] a) J. S. Choi, F. S. H. Simanjuntaka, J. Y. Oh, K. I. Lee, S. D. Lee, M. Cheong, H. S. Kim, H. Lee, *J. Catal*. 2013, **297**, 248–255; b) D. J. Darensbourg, A. D. Yeung, *Green Chem*., 2014, **16**, 247–252.

[46] F. Leising, Z. Moulongui, Chryso and Tolouse Inst. Nat Polytech. and Agronomique Inst. Nat. Rech., US2015329468 (A1), Nov. 19, 2015.

[47] a) Y. Nakao, S. Ebata, J. Chen, H. Imanaka, T. Hiyama, *Chem. Lett*., 2007, **36**, 606–607; b) I. Franzoni, L. Guénée, C. Mazet, *Org. Biomol. Chem*., 2015, **13**, 6338–6343.

[48] a) Y. Liu, E. Lotero, J. G. Goodwin Jr., X. Mo, *Appl. Catal. A,* 2007, **331**, 138–148; b) H. A. Prescott, Z.-J. Li, E. Kemnitz, A. Trunsche, J. Deutsch, H. Lieske, A. Auroux*, J. Catal*., 2005, **234**, 119–130.

[49] A. Rodrıguez, J. Canosa, A. Domınguez, J. Tojo, *Fluid Phase Equilibria*, 2002, **201**, 187–201.

[50] J. Shen, R. D. Cortright, Y. Chen, J. A. Dumesic, *J. Phys. Chem*., 1994, **98**, 8067–8073.

[51] Y. Fu, H. Zhu, J. Shen, *Thermochim. Acta,* 2005, **434**, 88–92.

[52] P. Tundo, F. Arick, A. E. Rosamilia, S. Memoli, *Green Chem.,* 2008, **10**, 1182–1189.

[53] (a) J. I. Di Cosimo, V. K. Dıez, M. Xu, E. Iglesia, C. R. Apestegua, *J. Catal.,* 1998, **178**, 499–510.

[54] B. Hallstedt, *J. Am. Ceram. Soc.,* 1992, **75**, 1497–1507.

[55] L. Lutterotti, R. Ceccato, R. Dal Maschio, E. Pagani, *Mater. Sci. Forum*, 1998, **278–281**, 87–92. The Rietveld analysis of these samples was performed by the method proposed by Lutterotti et al. for the analysis of amorphous materials. Specifically, the pattern of an amorphous or nanocrystalline phase was fitted by using the structure of a crystalline phase with the same chemical composition. The XRD spectrum of Al_2O_3 with very broad peaks was used to obtain the pattern of the amorphous phase.

[56] S. Vyas, R. W. Grimes, D. J. Binks, F. Rey, *Phys. Chem. Solids,* 1997, **58**, 1619–1624.

[57] M. G. Alvarez, A. M. Segarra, S. Contrera, J. E. Sueiras, F. Medina, F. Figueras, *Chem. Eng. J*., 2010, **161**, 340–345.

[58] a) V. Vàgvolgyi, S. J. Palmer, J. Kristòf, R. L. Frost, E. Horvath, *J. Colloid Interface Sci*., 2008, **318**, 302–308; b) J. C. A. A. Roelofs, J. A. van Bokhoven, A. J. van Dillen, J. W. Geus, K. P. de Jong, *Chem. Eur. J.*, 2002, **8**, 5571–5579.

[59] M. Leon, E. Dìaz, S. Ordonez, *Catal. Today,* 2011, **164**, 436–442.

[60] V. K. Dìez, C. R. Apesteguìa, J. I. Di Cosimo, *J. Catal*., 2003, **215**, 220–233.

[61] M. Bolognini, F. Cavani, D. Scagliarini, C. Flego, C. Perego, M. Saba, *Catal. Today,* 2002, **75**, 103–111.

[62] The basicity data were provided by the supplier of commercial PURAL solids (SASOL). The data referred to c-HT30 and c-HT70 samples calcined at 450 °C.

[63] a) V. Crocellà, G. Cerrato, G. Magnacca, C. Morterra, F. Cavani, L. Maselli, S. Passeri, *Dalton Trans.*, 2010, **39**, 8527 –8537; b) V. Crocellà, G. Cerrato, G. Magnacca, C. Morterra, F. Cavani, S. Cocchi, S. Passeri, D. Scagliarini, C. Flego, C. Perego, *J. Catal*., 2010, **270**, 125–135.

[64] a) S. Abell, F. Medina, D. Tichit, J. Perez-Ramırez, X. Rodriguez, J. E. Sueiras, P. Salagre, Y. Cesteros*, Appl. Catal. A,* 2005, **281**, 191–198; b) J. M. Fraile, N. Garcìa, J. A. Mayoral, E. Pires, L. Roldan, *Appl. Catal. A*, 2009, **364**, 87–94; c) N. N. A. H. Meis, J. H. Bitter, K. P. de Jong, *Ind. Eng. Chem. Res*., 2010, **49**, 8086–8093; d) S. Walspurger, P. D. Cobden, O. V. Safonova, Y. Wu, E. J. Anthony, *Chem. Eur. J*., 2010, **16**, 12694–12700.

[65] M. Selva, P. Tundo, D. Brunelli, A. Perosa, *Green Chem.*, 2007, **9**, 463.

[66] U. Costantino, F. Marmottini, M. Nocchetti, R. Vivani, R. *Eur. J. Inorg. Chem.*, 1998, **10**, 1439–1446.

[67] P. G. Jessop, T. Ikariya, R. Noyori, *J. Am. Chem. Soc*., 1996**, 118**, 344.

3. CF-SYNTHESIS OF SYMMETRICAL DIALKYL ORGANIC CARBONATES

3.1. Introduction

As described in Chapter 1 and 2, dialkyl carbonates (DAlCs) have been widely studied and reported in the literature.[1,2,3] Given their non-toxicity and versatile reactivity, they are extensively used as intermediates in the pharma, lubricant and polymer industries. Additionally, due to their high boiling point and high solvency they also find wide range of applications as aprotic polar solvents in the replacement of conventional noxious media.[4] The carbonate interchange reaction (CIR) of dimethyl carbonate (DMC) and alcohols represents one of the most widespread procedure for the preparation of symmetrical and asymmetrical DAlCs.[5,6,7] This reaction involves two consecutive equilibrium reactions, in which two acyl nucleophilic substitutions take place by formal transesterifications and/or disproportionation mechanisms. However, due to unfavourable equilibrium constants, the use of a large excess of DMC or the co-reacting alcohol is required to shift the equilibrium towards the formation of the desired products.[8]

For example, the synthesis of the diphenyl carbonate was reported using DMC-to-phenol in 1:4 molar ratio respectively: at 90 °C, in the presence of samarium trifluoromethanesulfonate as the catalyst, the selectivity towards the desired product was 80% although, the corresponding isolated yield was only 31%.[9] Better results were obtained through the removal of the MeOH/DMC azeotropic mixture formed over the course of the reaction. In a recent example, the CIR was investigated by using a mixture of DMC and an alcohol (either primary, secondary or tertiary) in a 24:1 molar ratio, respectively, and lanthanum(III) *i*-propoxide [La(i-PrO)$_3$, 3 mol%] as the catalyst:[10] good to excellent isolated yields (55–99%) of both methylalkyl- and dialkyl- carbonates were achieved when the azeotropic mixture MeOH/DMC (bp = 64 °C) was distilled over molecular sieves (MS 5 Å, Scheme 3.1). It was further demonstrated that the reaction also proceeded when La(i-PrO)$_3$ was substituted by the cheaper and less hygroscopic lanthanum(III) nitrate.[11]

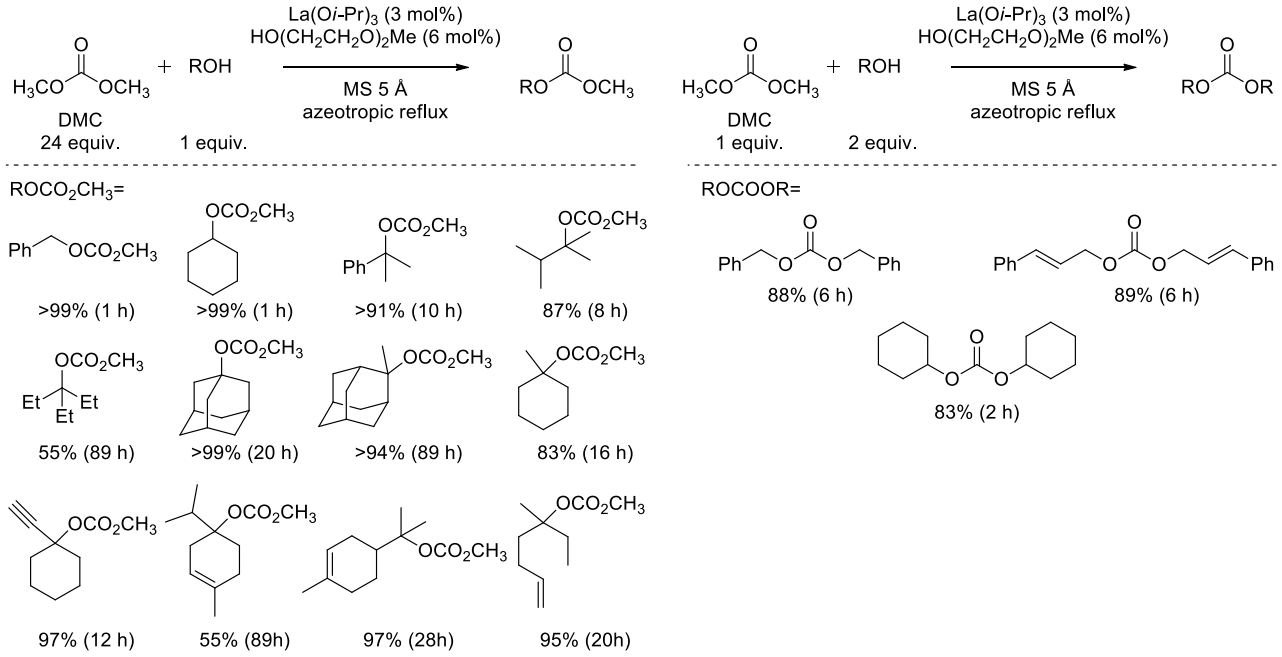

Scheme 3.1. Mono-transesterification of DMC catalysed by a La complex (left); double transesterification of DMC (right).[10]

As described in Chapter 1, the group in which this Thesis work was carried out at Ca' Foscari University also reported some efficient transesterification protocols. In the first instance, dimethyl and diethyl carbonate were set to react with primary and secondary alcohols in the presence of ionic liquid catalysts, namely methyl trioctylphosphonium methylcarbonate, bicarbonate and acetate ([P_{8881}][X]: X=OCO_2CH_3, OCO_2H, and AcO, respectively). Under mild reaction conditions (azeotropic reflux), the reaction proceeded only to mono-transesterification: non-symmetrical dialkyl carbonates ($ROCO_2R'$; R = Me, Et) were obtained with selectivities up to 99% and isolated yields >90% using catalyst loadings as low as 1 mol% (Chapter 1, Scheme 1.10).[12]

A second procedure was based on a thermal catalyst-free protocol in which different DAlCs, including DMC, diethyl carbonate, propylene carbonate and dibenzyl carbonate, underwent transcarbonation reactions with OH-bearing glycerol-derived acetals (solketal and glycerol formal). Under continuous flow (CF) conditions, at 250–300 °C and 20–50 bar, acetals were converted to the corresponding mono-transesterification products with conversions and selectivities of ≥95% and 98%, respectively (Scheme 3.2).[13]

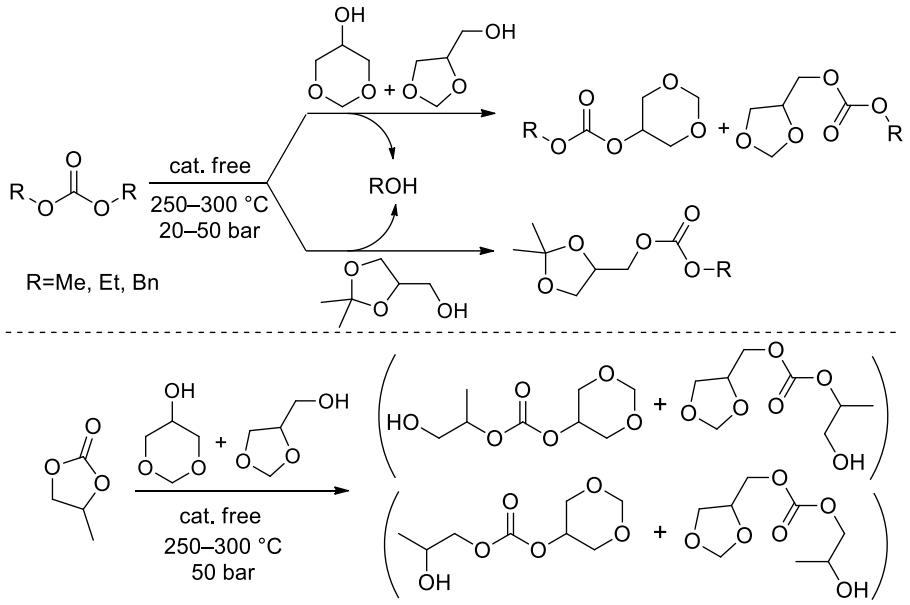

Scheme 3.2. Selective catalyst-free mono-transesterification of dialkyl carbonates with glycerol acetals.[13]

Finally, a third method was developed, still based on a catalyst-free procedure. At 150–260 °C and pressures up to 50 bar, DMC was set to react with both 1,*n*-diols (n=2–4) and glycerol. Of note, both alkylene carbonate and glycerol carbonate were achieved with quantitative conversion and selectivities up to 94%.[14] In this case, the occurrence of multiple transesterifications was plausibly accounted for by the thermodynamic stability of the obtained cyclic products (Scheme 3.3).

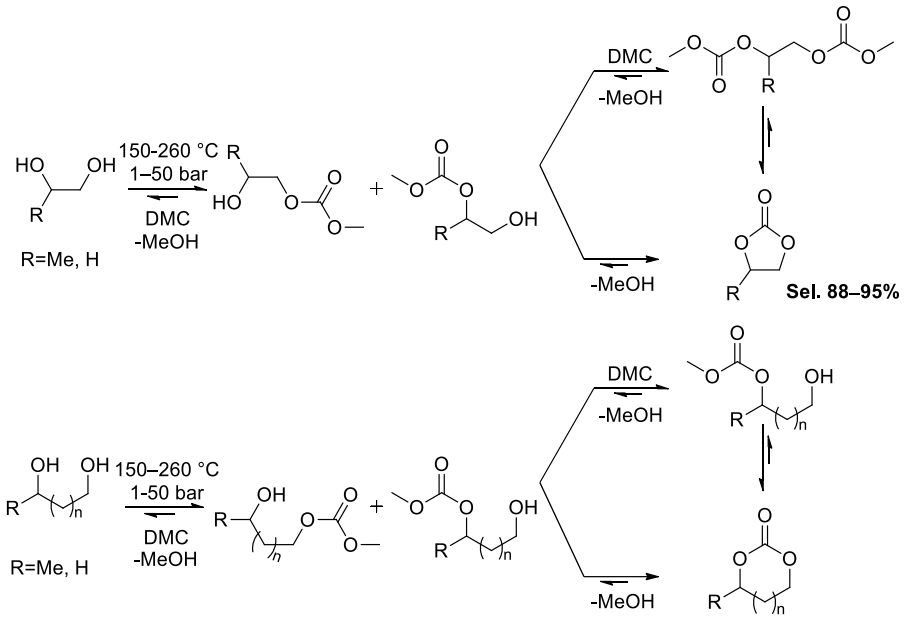

Scheme 3.3. Catalyst-free reactions of 1,*n*-diols with DMC.[14]

The efficiency of the CIR reaction can be favoured by varying the nature of the reacting carbonate. As already mentioned in Chapter 1, the use of catechol carbonate (CC) allowed for transcarbonation processes that were highly selective towards symmetrical carbonates. At 40–80 °C and ambient pressure, these products were obtained in very good yields from the reaction of CC with a variety of model alcohols including primary and secondary substrates such as ethanol, *n*-butanol, allyl alcohol, *i*-propanol and cyclohexanol, and bio-based derivatives such as solketal and glycerol. Both NaOMe and MgO were used as catalysts (Chapter 1, Scheme 1.14).[15] With respect to DMC, these results were due to the better leaving group ability of the catecholate vs methylate anions.

The synthesis of symmetrical DAlCs also became of interest in this Thesis work during the investigation of the alkylation of glycerol acetals described in Chapter 2. The investigation was initially aimed at understanding whether the *O*-alkyl product was achieved *via*: *i*) the direct alkylation reaction with DMC, or *ii*) the transesterification of solketal followed by the decarboxylation of the intermediate carbonate **1c** (Scheme 3.4).

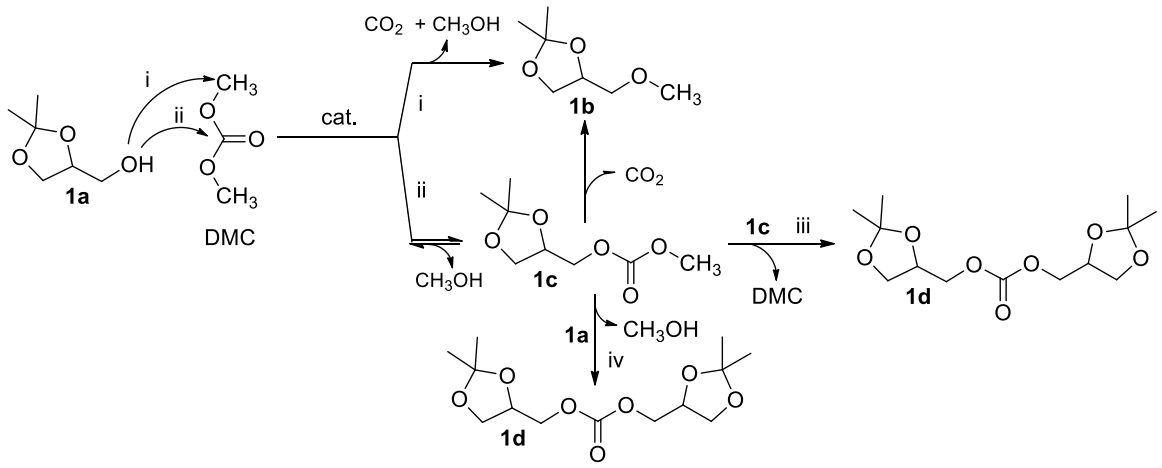

Scheme 3.4. Major products derived from reaction of solketal with DMC.

However, it was noted that if compound **1c** was set to react under conditions similar to those used for solketal (210–275 °C and pressures up to 50 bar), the expected decarboxylation did not occur, rather the reaction proceeded *via* a selective disproportionation reaction producing disolketal carbonate (**1d**) as the major product. This result inspired the work described in the present chapter.

3.2. Results and Discussions

3.2.1. Catalysts used for the synthesis of (non-)symmetrical DAlCs

Three commercially available hydrotalcites (Pural® MG30, Pural® MG63 and Pural® MG70) were used as solid catalysts. The properties of these materials were described in Chapter 2 (Table 2.1). Before use, the samples were all calcined as described in Chapter 2 (450 °C, 14 h, air). Calcined solids were labelled as c-HT30, c-HT63, c-HT70, and c-KW2000.

3.2.2. The synthesis of methyl alkyl carbonate

The initial step of this study was the preparation of four methyl alkyl organic carbonates. These compounds were obtained by catalytic transesterification of DMC with primary renewable alcohols derived from glycerol, such as solketal (**1a**, 1,2-isopropylidene glycerol) and glycerol formal (3.2 mixture of **2a** 5-hydroxy-1,3-dioxane and **2a'** 4-hydroxymethyl-1,3-dioxolane), tetrahydrofurfuryl alcohol (**3a**), and a conventional and less reactive secondary alcohol, such as cyclohexanol (**4a**) (Figure 3.1). Calcined hydrotalcites (HTs) were used as the transesterification catalysts.

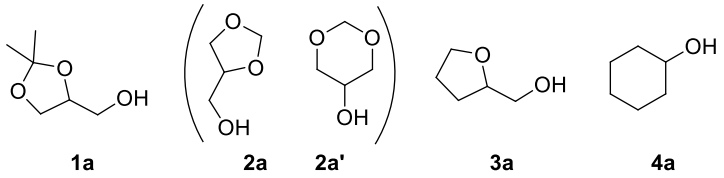

Figure 3.1. Alkyl substrates for the synthesis of methyl alkyl organic carbonates.

The reaction of **1a** with DMC was initially examined. A mixture of **1a** (5.287 g, 0.04 mol), DMC (64.858 g, 0.72 mol) in 1:18 molar ratio and the catalyst (c-HT30 or c-HT63 or c-HT70: 0.159 g each, 3 wt%), was set to react under batch conditions at the reflux temperature (Scheme 3.5). With a view to drive the equilibrium reaction rightwards, the efficient removal of the co-product, MeOH, was implemented by using a condenser that was kept at 70 °C. In this way, MeOH was continuously removed as an azeotropic mixture with DMC (70:30; bp = 64–67 °C) (Figure 3.8).[16]

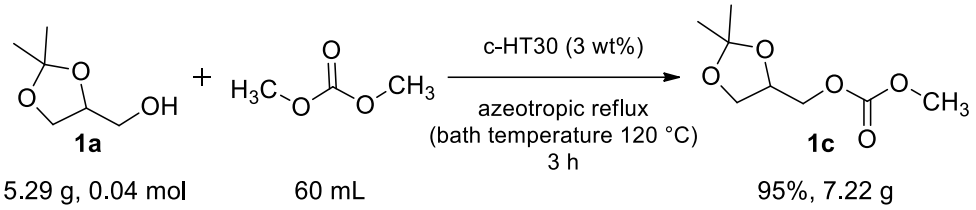

Scheme 3.5. Synthesis of asymmetrical methyl solketal carbonate *via* reactive azeotropic distillation catalysed by c-HT30.

At intervals, samples of the reaction mixtures were collected and analysed by GC/MS. Methyl solketal carbonate (**1c**: 2,2-dimethyl-1,3-dioxolan-4-yl)methyl methyl carbonate) was always achieved with >97% selectivity. The sole by-product, namely the symmetric derivative **1d** (Scheme 3.4), was only detected in trace amounts (<3%). Both compounds **1c** and **1d** were isolated and their structures confirmed by NMR.

The conversion profiles of **1a** for each catalytic test are reported in Figure 3.2.

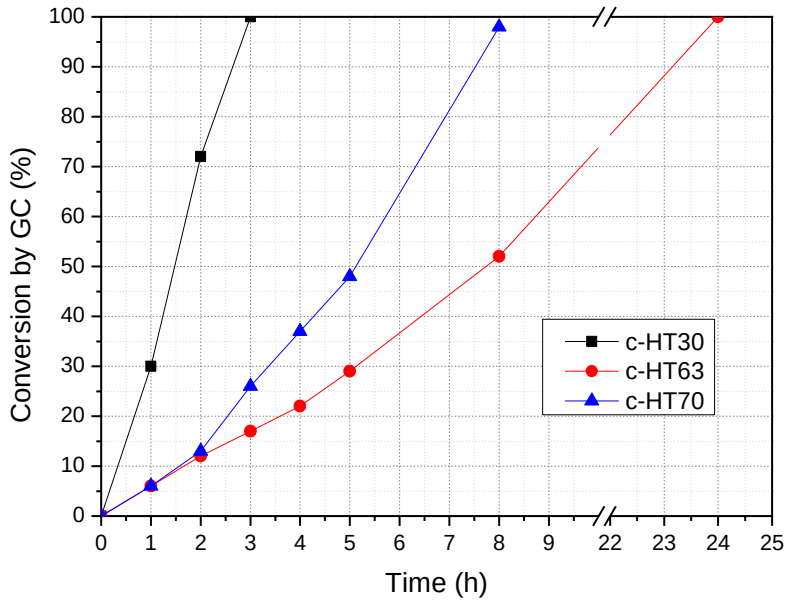

Figure 3.2. The transesterification of **1a** with DMC: conversion profiles achieved over different c-HT catalysts. Reactions were carried out at the reflux temperature. **1a** and DMC were used in 1:18 molar ratio, respectively, while HTs were added in 3 wt% with respect to **1a**. Selectivity towards the desired **1c** was always >97%.

Of the three calcined HTs, c-HT30 was the most active catalyst with a quantitative conversion of **1a** and 97% selectivity towards **1c** were achieved after 3 h. By contrast, in the presence of either c-HT63 or c-HT70 the reactions were complete after 24 and 8 h, respectively. It was noted that the catalytic activity followed the same trend reported for the alkylation reaction of **1a** with DMC, *i.e.* c-HT30 > c-HT70 > c-HT70 (Chapter 2, Table 2.3). One possible explanation

is that the two reactions (CIR and alkylation) were similarly affected by the amphoteric nature of the Mg/Al mixed oxide obtained by the calcination of HTs.

Due to its higher efficiency c-HT30 was chosen as the catalyst for the synthesis of other methyl alkyl carbonates derived from glycerol formal (**2a**/**2a'**), tetrahydrofurfuryl-alcohols (**3a**) and cyclohexanol (**4a**) (Figure 3.1). Accordingly, a mixture of DMC and the corresponding OH-bearing substrate in a 18:1 molar ratio, respectively, was set to react at the reflux temperature in the presence of c-HT30 (3–9 wt%) as the catalyst.

The reaction conditions, substrate conversions, product selectivities and isolated yields for each experiment are listed in Table 3.1, which, for completeness, also includes the above-described results for the transesterification of **1a** with DMC.

Table 3.1. Transesterification reactions of substrates 1a–4a with DMC in the presence of c-HT30.[a]

Entry	Substrate	*W*[b] (wt%)	Time (h)	Conv.[c] (%, GC)	Sel.[d] (%, GC)	Product	
						Structure	Isolated yield (%)
1	**1a**	3	3	100	97	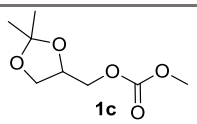 **1c**	95
2	**2a/2a'**	3	24	100	98	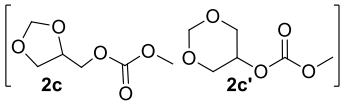 **2c** **2c'**	96
3	**3a**	3	120	98	95	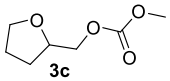 **3c**	93
4	**4a**	3	48	12	100	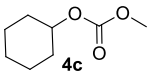 **4c**	-
5	**4a**	9	24	99	98	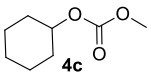 **4c**	95

a) Reactions were carried out at 90 °C. DMC:substrate molar ratio=18. b) *W*=c-HT30:substrate ratio; c) Conversion of the substrate (determined by GC). d) Selectivity towards the shown product (determined by GC).

Results showed that the mono-transesterifications of substrates **2a**–**4a** were always highly selective and high-yield processes, but they required rather longer reaction times than that necessary for **1a**. This trend in reactivity matched the one observed during the alkylation of the same substrates with DMC. In particular: *i*) alike the synthesis of *O*-methyl derivatives of solketal and glycerol formal that took place at 210 and 220 °C, respectively (Chapter 2, Table 2.4), also the preparation of methyl-glycerol formal carbonate (**2c**/**2c'**) was more energy demanding compared to **1c** (Table 3.1, entries 1 and 2). The isomeric methyl carbonates **2c**/**2c'** were obtained in the same (3:2) relative ratio as that of the starting acetals **2a** and **2a'**. *ii*)

Compound **3a** was converted quantitatively after 120 h, *i.e.* a 40-fold increase compared to the time needed for **1a** (3h; Table 3.1, entries 1 and 3). This paralleled the behaviour of *O*-methylation of **1a** and **3a,** which required 210 °C and 260 °C, respectively (Chapter 2, Table 2.4). Finally, the transesterification of DMC with the secondary alcohol **4a** proceeded to a quantitative conversion after 24 h only by tripling the catalyst loading with respect to the reactions of primary substrates (9 wt% instead of 3 wt%; entry 5).

In all cases however, the mono-transesterification selectivity was 95–100% and the products were obtained in excellent isolated yields (93–96%) after vacuum distillation. Compounds **1c-4c** were characterised by NMR spectroscopy and GC/MS chromatography (see Experimental Section and Appendix for details). Moreover, due to the continuous distillation of the MeOH/DMC azeotrope during the reaction, the recovery of the excess DMC (pure by >99%, NMR) was in the range of 75–80 mol% with respect to the starting reactant.

The catalyst was recovered by filtration at the end of each experiment. No tests were carried out to prove the recyclability and stability of c-HT30 for the mono-transesterification protocol. However, since the same system could be reused many times with no variation of activity in the CF-*O*-alkylation reported in Chapter 2 (at 210–275 °C), it is plausible that c-HT30 also had a similar robustness under the less demanding conditions of Table 3.1 (90 °C).

3.2.3. Dialkyl organic carbonates

Once products **1c**–**4c** were synthesised, following the above procedure, they were used as reagents to investigate disproportionation reactions for the synthesis of symmetrical dialkyl carbonates (Scheme 3.5).

Experiments were carried out under CF-conditions, using the same set-up described in Section 2.3.1. of Chapter 2, comprising of: a HPLC pump (P1), a tubular reactor (R) thermostated inside a GC oven (O), a Rheodyne valve and a backpressure regulator (BPR). (Figure 3.3; further details are in the experimental section and Chapter 2).

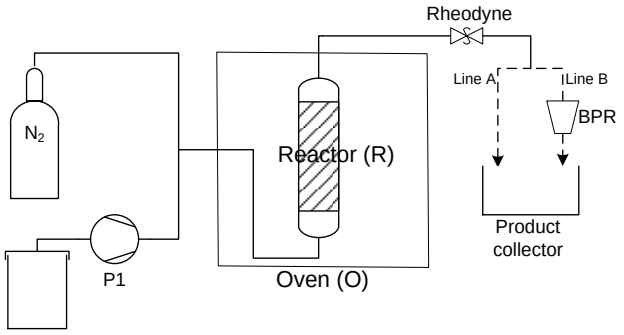

Figure 3.3. Experimental set-up used for the study of continuous-flow disproportionation reactions.

Since starting reactants **1c–4c** were available on relatively moderate amounts (50–100 g), their disproportionation reactions were investigated by using a 1.42 M solution of each methyl alkyl carbonate in cyclohexane. Cyclohexane was initially chosen from among a series of solvents due to its chemical inertness at high temperatures and its mid-range boiling point (80.7 °C), which allowed for easy removal after the reaction. c-HT30 was used as the catalyst for all the experiments and each test was duplicated to check the reproducibility.[17]

The disproportionation of solketal methyl carbonate **1c** was initially investigated as a model reaction (Scheme 3.6).

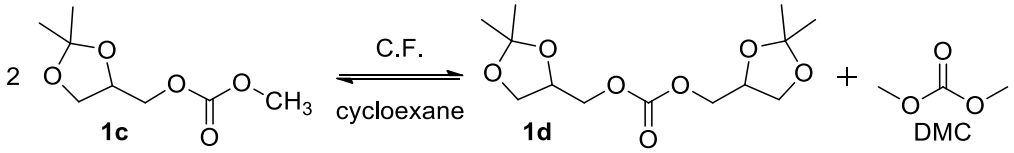

Scheme 3.6. The disproportionation reaction of solketal methyl carbonate to disolketal carbonate.

Effect of temperature. Preliminary tests were aimed at studying the effect of the temperature in the range of 210–275 °C. At ambient pressure (1 bar) a 1.42 M solution of **1c** in cyclohexane was pumped at 0.1 mL min^{-1} through a tubular reactor (L = 12 cm, Ø = 1/4", 1.16 cm^3 inner volume) filled with powdered c-HT30 (0.5 g). The product mixture was collected at time intervals after the BPR, at the outlet of the reactor. GC/MS analyses of such fractions showed that three products formed: the expected disproportionation compound **1d** was the major product along with solketal, **1a**, and solketal methyl ether, **1b,** as side-compounds. The structures of **1a**, **1b** and **1d** were confirmed by NMR and comparison to authentic samples. It was also noted that both the conversion and the selectivity remained substantially steady after 120 min. However, in all cases, reactions were prolonged for up to 5 h. Results are reported in Figure 3.4 and refer to the conversions and selectivities after 5 h.

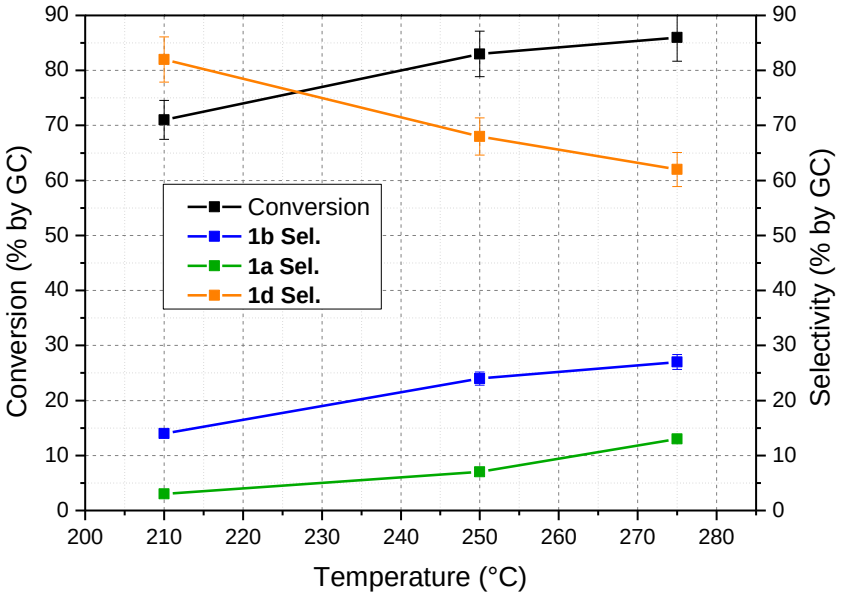

Figure 3.4. Effect of the temperature on the conversion and product distribution for the disproportionation reaction of **1c** in the presence of c-HT30 as the catalyst. Other conditions: 1.42 M solution of **1c** in cyclohexane, F = 0.1 mL min^{-1}, ambient pressure. The selectivities towards the three major products (**1b**, **1a,** and **1d**) are shown by the coloured curves (blue, green, and orange, respectively).

At 210 °C, the conversion of **1c** was 71% and the corresponding disproportionation carbonate **1d** was obtained in 82% selectivity. Increasing the temperature to 250 and 275 °C improved the conversions to 83 and 86%, respectively, but was detrimental to the selectivity towards **1d**: while this still remained the more abundant product, the disproportionation selectivities dropped to 68 and 62%, respectively, in favour of compounds **1b** and **1a** whose selectivities were as high as 27 and 11% respectively.

A mechanistic hypothesis for the disproportionation process was formulated based on the dual (acid/base) nature of calcined hydrotalcites discussed in Chapter 2. Scheme 3.7 illustrates the reaction pathway.

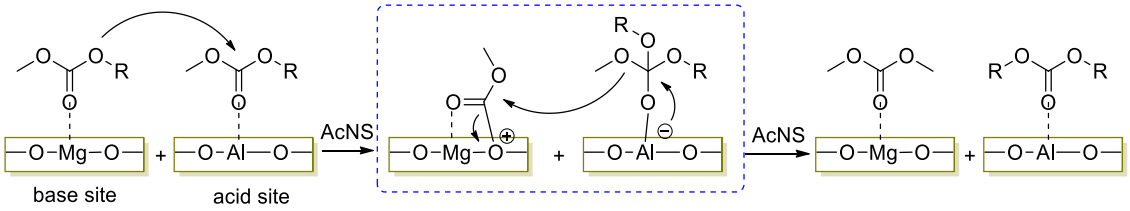

Scheme 3.7. Proposed mechanism for the disproportionation reaction of $ROCO_2Me$.

In this mechanism two molecules of the asymmetrical carbonate are first activated by one of the two types of weak Lewis acidic sites (Mg and Al cations) present on the surface of c-HT30. An acyl nucleophilic substitution (AcNS) then takes place, in which the same molecule acts simultaneously as both an electrophile and a nucleophile. The acceptor and the donor

moieties are stabilised by the acid or the base site of the catalyst, respectively (dashed blue box). These intermediates can then undergo a second AcNS leading to the formation of the asymmetrical dialkyl carbonate and DMC at the surface of c-HT30. The main driving forces behind this disproportionation reaction are probably, both the improved stability of the symmetrical product compared to the asymmetrical reagent and the different leaving group ability of $^{-}OCH_3$ with respect to the ^{-}OR species.

On the other hand, the formation of compounds **1a** and **1b** was ascribed to the onset of the competitive processes of hydrolysis and decarboxylation, respectively. More specifically, hydrolysis took place due to trace amounts of water (up to 0.15 wt%)[18] in the starting reagent **1c**. Under the conditions of Figure 3.4, the reaction of **1c** with water resulted in the formation of solketal and methyl hydrogen carbonate. The latter, due to its instability, further decomposed to CO_2 and MeOH (Scheme 3.8, a). Finally, **1c** underwent transesterification with methanol to produce an additional equivalent of solketal and DMC (Scheme 3.8, b). Trace amount of DMC was confirmed by GC/MS analyses.

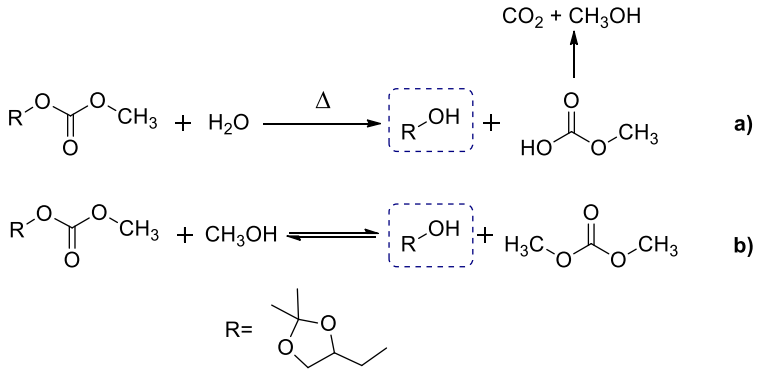

Scheme 3.8. Hydrolysis and transesterification processes of compound **1c**.

The occurrence of the other competitive reaction, *i.e.* the catalytic decarboxylation of dialkyl carbonates, has already discussed in Chapter 2.[19] In that circumstance, it was noted that although calcined HTs such as c-HT30 were far less efficient than other solids (zeolites or alkaline carbonates) at catalysing this (decarboxylation) reaction, the process could not be completely avoided. This offers an explanation for the side-product **1b,** resulting from the loss of CO_2 from the starting carbonate **1c**.

Effect of pressure. The best selectivity towards **1d** was achieved at 210 °C. At this temperature, the effect of the pressure was investigated in the range of 1–50 bar. Other conditions were kept unchanged with respect to those of Figure 3.4 (1.42 M solution of **1c** in cyclohexane; 210 °C, F = 0.1 mL·min^{-1}). Results are summarised in Figure 3.5.

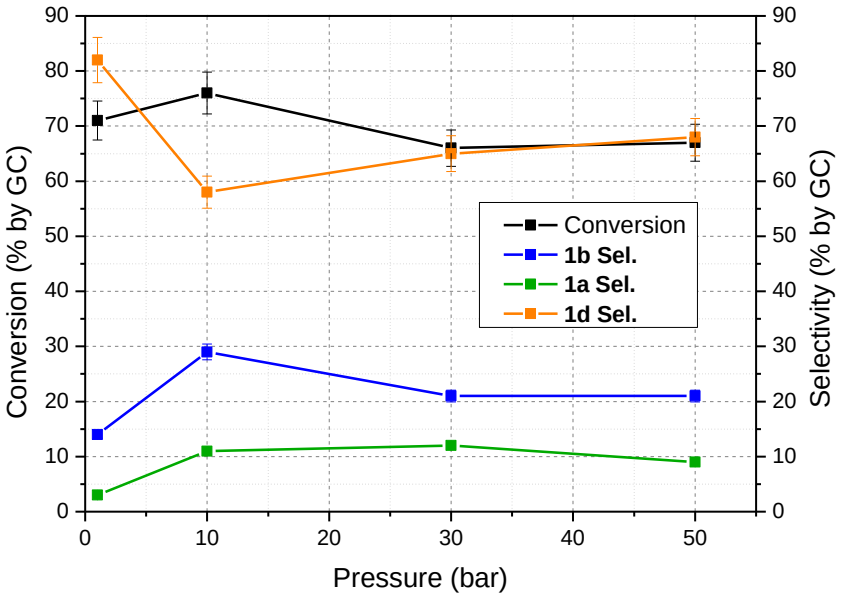

Figure 3.5. Effect of the pressure on the conversion and the product distribution for the disproportionation reaction of **1c** in the presence of c-HT30. Other conditions: 210 °C, 1.42 M solution of **1c** in cyclohexane, *F*=0.1 mL·min^{-1}.

At 210 °C, the increase of the pressure was not beneficial for the disproportionation reaction. In the explored range from ambient to 50 bar: *i*) after a slight increase to 76% at 10 bar, the conversion of **1c** progressively dropped to 66%; *ii*) overall the selectivity towards **1d** decreased from 82 to 68%. On the other hand, the amounts of by-products **1a** (solketal) and **1b** (solketal methyl ether) increased to between 9–12% and 22–29% (by GC), respectively. A hypothesis for this behaviour was based on a reasoning similar to that previously discussed in Chapter 2: if the pressure affected the partition of reactants and products between the liquid and the vapour phases, then it could also influence the contact time, the concentration and the desorption of the different species at the catalyst surface. As a consequence, the product distribution was altered according to the modification induced by the pressure (liquid/vapor partition) on the relative rates of the competitive processes of disproportionation, hydrolysis and decarboxylation of **1c** and the desorption of the corresponding products. An analogous trend was also noticed by us during the *O*-alkylation of solketal with DMC in the presence of KW2000 as the catalyst (Chapter 2, Figure 2.11b). In that circumstance, the best result was achieved at 10 bar, while both conversion and selectivity decreased if the pressure was either decreased to 5 bar or increased to ≥ 20 bar.

Effect of the flow rate. Under the best-found conditions of T and p, resulting from Figures 3.4 and Figure 3.5, respectively, the reaction of **1c** catalysed by c-HT30 was further explored to investigate the effect of the flow rate, which was another key parameter to optimising the

process in the CF-mode. Accordingly, a 1.42 M solution of **1c** in cyclohexane was set to react at 210 °C and 1 bar, progressively increasing the total volumetric flow rate from 0.1 mL·min^{-1} up to 0.4 mL·min^{-1}. The solutions collected from the reactor were analysed by GC/MS to determine both the conversion of **1c** and the product distribution. Results are reported in Figure 3.6. For a more complete comparison, the figure also reports the reaction productivity (*P*) calculated by the mass of desired product **1d** obtained per time unit and per gram of catalyst (*P* = [mg$_{prod}$ (g$_{cat}$·min)$^{-1}$]: dashed aqua profile.

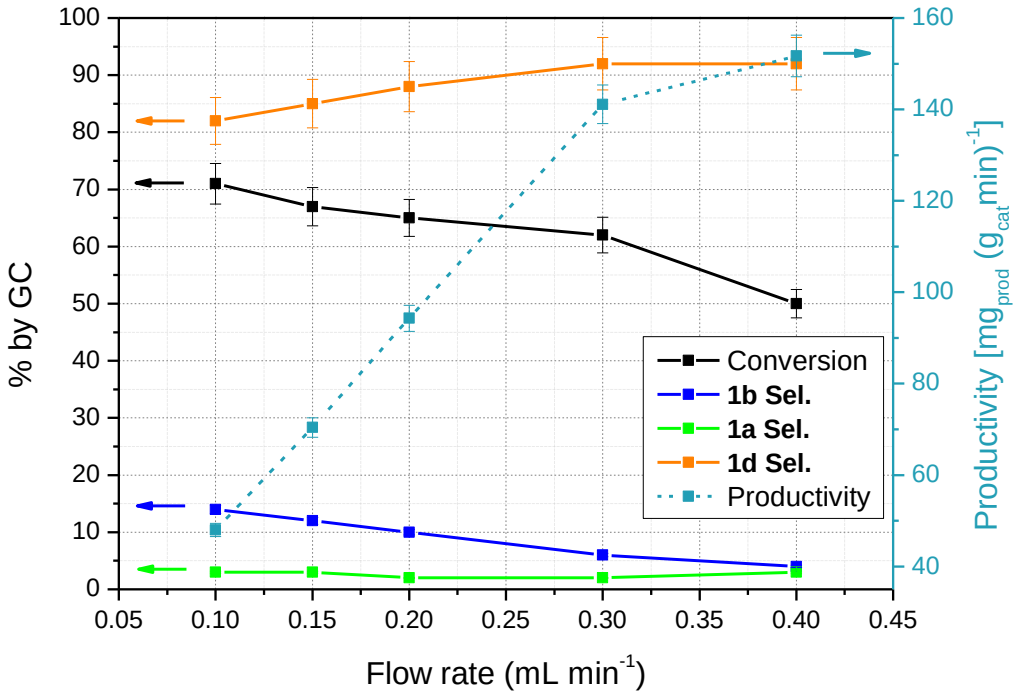

Figure 3.6. Effect of the flow rate (*F*) on the conversion, selectivity and productivity for the disproportionation reaction of **1c** in the presence of c-HT30. Other conditions: 1.42 M solution of **1c** in cyclohexane, p = 1 bar, T=210 °C.

The fourfold increase in the flow rate, from 0.1 to 0.4 mL·min^{-1}, reduced the contact time (τ) of the reagents with the catalyst, which went from approximately 10 min (at 0.1 mL·min^{-1}) to 2.5 min (at 0.4 mL·min^{-1}). As expected, this brought about a remarkable decrease in the reaction conversion from 71 to 50% (black profile).

At the same time, however, a positive effect was noticed in the selectivity of the disproportionation reaction towards **1d,** which increased up to 92% at *F* = 0.3 mL·min^{-1} (orange profile). This result proved to be particularly significant when the reaction productivity (*P*) was plotted against the flow rate: an almost linear rise of *P*, *i.e.* a triplication of *P* from 48.0 to 141.1 mg$_{prod}$ (g$_{cat}$·min)$^{-1}$ was achieved when *F* was changed from 0.1 to 0.3 mL·min^{-1} (dashed aqua profile). A further increment of the flow rate to 0.4 mL·min^{-1} did not improve the reaction

selectivity since the relative amounts of both the desired product **1d** and co-products **1a** and **1b** remained substantially unaltered; though, the productivity was further enhanced from 141.1 to 151.7 mg_{prod} $(g_{cat}\cdot min)^{-1}$.

Overall, the studies described by Figures 3.4–6 proved not only the feasibility of the model disproportionation reaction of solketal methyl carbonate catalysed by c-HT30, but it also offered a strategy to optimise the process in the CF-mode. The best conditions (210 ˚C, 1 bar, 0.3 $mL\cdot min^{-1}$) found for the symmetrical carbonate **1d** had very promising results with excellent selectivity and productivity of 92% and 141.1 mg_{prod} $(g_{cat}\cdot min)^{-1}$ respectively. These results prompted us to continue exploring the potential of this procedure. Additionally, the scope and limitations of this method were explored using the methyl organic carbonates previously prepared as described in Section 3.2.2.

Scope of the reaction: different methyl alkyl organic carbonates. Methyl glycerol formal carbonate (**2c**/**2c'**), methyl tetrahydrofurfuryl carbonate (**3c**) and methyl cyclohexyl carbonate (**4c**), were set to react in the CF-mode under the best conditions found for the model disproportionation reaction of **1c** (Scheme 3.9, path ii). Accordingly, at 180–210 °C and under ambient pressure, a homogeneous 1.42 M solution of each substrate (**2c**–**4c**) in cyclohexane or toluene was pumped at a rate of 0.3 $mL\cdot min^{-1}$, over a catalytic bed of c-HT30 (0.5 g) placed in the above described CF-reactor (L=12 cm, Ø=1/4", 1.16 cm^3 inner volume). Each experiment was carried out for 5 h.

The reaction conversions, selectivities and productivities (*P*: mg_{prod} $(g_{cat}\cdot min)^{-1}$) are listed in Table 3.2, which, for comparison, also includes the results for the disproportionation of **1c**.

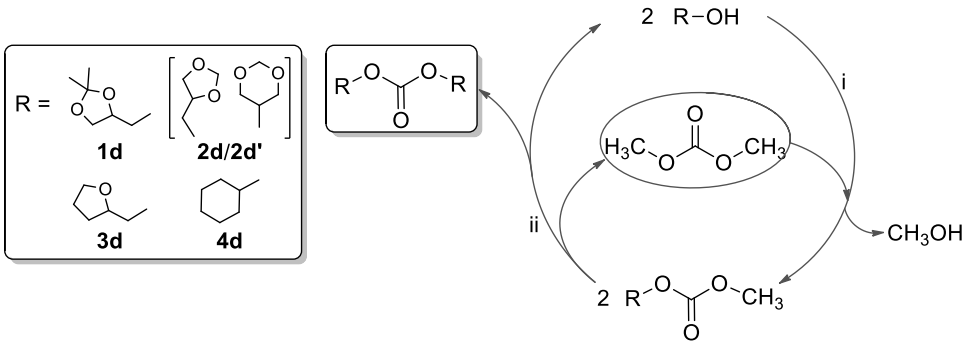

Scheme 3.9. Synthesis of s-DAlCs catalysed by c-HT30: i) batch CIR for the production of methyl alkyl carbonate and ii) CF-disproportionation of methyl alkyl carbonates to the corresponding s-DAlCs.

Table 3.2. Disproportionation reactions of substrates 1c–4c to s-DAlCs 1d–4d in the presence of c-HT30.[a]

Entry	Substrate	Solvent	Conv.'n (%)[c]	Sel. (%)[d]	T (°C)	Product	
							P [mg_{prod}·(g_{cat} min)$^{-1}$]
1	**1c**	cyclohexane	62	92	210	**1d**	141.1
2	**1c**	toluene	76	87	210	**1d**	163.5
3	**2c/2c'**	toluene	22	35	210	**2d**	15.4
4	**2c/2c'**	toluene	30	31	275	**2d**	18.6
5	**3c**	cyclohexane	72	87	210	**3d**	122.9
6	**4c**	toluene	60	71	180	**4d**	82.1
7	**4c**	toluene	90	52	210	**4d**	90.2

a) Reaction conditions: ambient pressure, total flow rate=0.3 mL·min^{-1}, 1.42 M solution of each substrate in cyclohexane or toluene; b) conversion of the substrates was calculated by GC; c) selectivity of the products was determined by GC.

Reaction conditions required a case-by-case optimisation. Except for the case of **2a/2a'**, reaction conditions for substrates **1c**, **3c** and **4c** were changed to achieve comparable conversions (60–76%) of the methyl alkyl carbonates **1c**, **3c** and **4c**. In particular, the temperature needed to be varied in the range of 180–210 °C. From the comparison of data, some facts emerged: *i*) regardless of the starting reactant, the disproportionation reaction was always favoured over the side-processes of hydrolysis and decarboxylation: the bests selectivities towards the symmetrical carbonates **1d**, **3d** and **4d** was between 71%–92%. These results validated the general applicability of this procedure. *ii*) Due to the low solubility of both **2c/2c'** and **4c** in cyclohexane, toluene was used as the solvent for these substrates. For comparison, a reaction was also performed with **1c** in toluene (Table 3.2, entry 2), showing an increase of the conversion from 62 to 76% and a slight decrease in the selectivity of **1d**, from 92 to 87%. Of note, under these reaction conditions, a highest *P* value of 163.5 mg_{prod} (g_{cat} min)$^{-1}$, was achieved. *iii*) The disproportionation of compound **4c** occurred under milder conditions than for **1c** (cfr. entries 2 and 6–7). Since the cyclohexyl rings (in **4c**) are bulky substituents, the result was opposite to what was expected. At present, the reasons for this behavior are still unclear. *iv*) Finally, of the two acetal-derived reagents, the disproportionation was considerably more difficult for **2c/2c'** (entries 1–4). Also at 275 °C it

was not possible to achieve a conversion of **2c**/**2c'** higher than 30% (Table 3.2, entry 4). This behaviour matched already noticed trends, indicating that solketal as such or its derivatives were systematically more reactive than glycerol formal or the corresponding derivatives. In this circumstance however, this difference between solketal methyl carbonate and glycerol formal methyl carbonate was even stronger. A possible explanation for the poor reactivity of **2c**/**2c'** could rely on the formation of strong intramolecular interactions. As shown in Figure 3.7, as opposed to **1c**, the carbonyl moieties of **2c**/**2c'** might H-bond with the two hydrogens of the five members ring. Therefore, the carbonyl moieties might be less available to be activated from the catalyst surface and the disproportionation reaction does not occur.

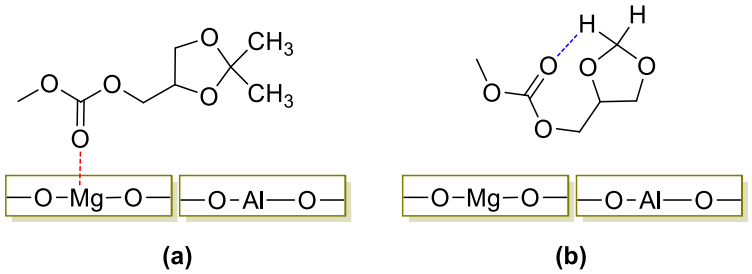

Figure 3.7. Different interaction of **1c** and **2c** with the catalyst surface.

As reported by other Authors, the activation of the carbonyl group by an active center seems to be essential for the disproportionation reaction to occur.[20] Wang and co-workers recently reported a MoO_3/SiO_2 catalysed disproportionation of methyl phenyl carbonate (MPC) to diphenyl carbonate (DPC).[20a] In the proposed reaction mechanism (Scheme 3.10), the reaction between two molecule of MPC occurs only after a previous activation of the carbonyl moieties by the active molybdenum present on the catalyst surface.

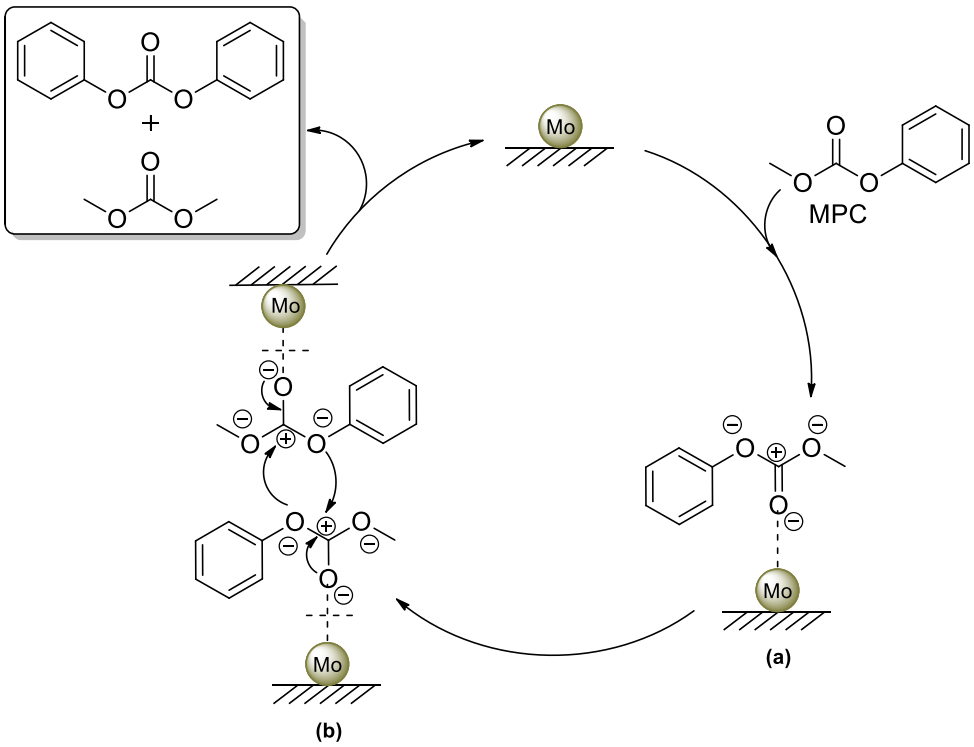

Scheme 3.10. Proposed mechanism for MPC disproportionation over MoO_3/SiO_2 catalyst: a) activation of the carbonyl group by active molybdenum (Mo) and b) subsequent attack by a second methyl phenyl carbonate.[20a]

3.3. Conclusions

This investigation describes two innovative protocols for the carbonate interchange reaction, in which a calcined hydrotalcite, such as c-HT30, is used as the catalyst for both the batch synthesis of asymmetrical methyl alkyl carbonates and the CF-reaction preparation of symmetrical dialkyl carbonates.

Methyl alkyl carbonates are obtained by a reactive azeotropic distillation between DMC and primary or secondary alcohols, the latter being chosen from among bio-based substrates including glycerol acetals and tetrahydrofurfuryl alcohol. Under mild reaction conditions (T=90 °C, atmospheric pressure) quantitative conversions and selectivities were achieved, with products obtained in 93–95% isolated yields.

Subsequently, these methyl alkyl carbonates were employed as the reagents for the synthesis of symmetrical dialkyl carbonates through a disproportionation protocol. The reaction has been optimised under CF-reaction conditions: although a case-by-case adjustment of conditions, especially the temperature, was necessary. Using this method conversions in the range of 60–90% and selectivities of 71–92% towards the disproportionation products were

achieved for all tested substrates. The only exception to this protocol, among the investigated methyl alkyl carbonates, was **2c**/**2c'**. When **2c**/**2c'** was used, also at the higher reaction temperature of 275 °C, it was not possible to achieve a conversion higher than 30%.

The CF-disproportionation not only offers a versatile and productive method for the preparation of symmetrical dialkyl carbonates, but it also discloses interesting perspectives for further investigations on the mechanism of the reaction and the role of calcined hydrotalcites as catalysts.

3.4. Experimental Section

3.4.1. General

Solketal (**1a**), glycerol formal (GlyF, **2a**/**2a'**), tetrahydrofurfuryl alcohol (**4a**) and dimethyl carbonate (DMC) were ACS grade from Aldrich. Unless specified otherwise they were employed without further purification.

GC/MS (EI, 70 eV) analyses were run using a HP5-MS capillary column (L = 30 m, Ø = 0.32 mm, film = 0.25 μm). The following conditions were used: carrier gas: He; flow rate: 1.2 mL·min^{-1}; split ratio: 10:1; initial T: 50 °C (3 min), ramp rate: 10 °C/min; final T: 250 °C (3 min).

CG/FID analyses were run using an Elite-624 capillary column (L = 30 m, Ø=0.32 mm, film = 1.8 μm). The following conditions were used. Carrier gas: N_2; flow rate: 5.0 mL·min^{-1}; split ratio: 1:1; initial T: 100 °C (0 min), ramp rate: 15 °C/min; final T: 220 °C (5 min).

^{1}H NMR were recorded at 400 or 300 MHz, ^{13}C NMR spectra at 100 MHz and chemical shifts were reported in δ values downfield from TMS; $CDCl_3$ was used as the solvent.

3.4.2. Catalysts

Hydrotalcites (HTs) were aluminium magnesium hydroxyl carbonate hydrates of formula $Mg_{2x}Al_2(OH)_{4x+4}(CO_3)\cdot nH_2O$ (x = 0.5–2.3). Three commercial HTs were considered (their Mg/Al molar ratio is given between parentheses): PURAL® MG 30 (0.5), MG 63 (1.9) and MG 70 (2.3). KW2000 was from Kyowa Chemical Industry Co., Ltd., while the PURAL® MG solids were from CONDEA/Sasol Germany GmbH, Inorganic Specialty Chemicals (see Chapter 2 for further details). All HTs were calcined before use. The calcination treatment was carried out according to a procedure already reported for HTs:[21] solid samples (5 g) were heated in a quartz reactor

(in the upright position) under a flow of dry air at 450 °C for 16 h with a heating rate of 30 °C/min.

3.4.3. Batch transesterification of alcohols with hydrotalcites

3.4.3.1. General transesterification procedure

Catalytic tests were carried out in a Pyrex-glass double-necked round-bottom-flask equipped with a magnetic stirrer and a condenser thermostated at 70 °C and capped by a distillation apparatus by which the MeOH/DMC azeotrope, formed during the reaction, was collected (Figure 3.8). In a typical experiment, the flask was charged with a mixture of an alcohol (**1a–4a**; 4.0 to 5.2 g) and DMC in a 1:18 molar ratio, respectively, and a calcined HT (c-HT30 or c-HT63 or c-HT70: 3 to 9 wt% with respect to the alcohol). The suspension was stirred at the reflux temperature (*ca.* 90°C) and atmospheric pressure, for 3–24 h depending on the catalyst used (Figure 3.2). Aliquots (0.2 mL) of the reaction mixture were sampled at set time intervals, filtered over a plug of cotton to remove the HT catalyst, diluted in 5 mL of diethyl ether and analysed *via* GC/MS. The structure of transesterification products **1c–4c** was assigned by GC/MS, ^{1}H NMR and ^{13}C NMR. Details are given below (Section 3.4.5.1).

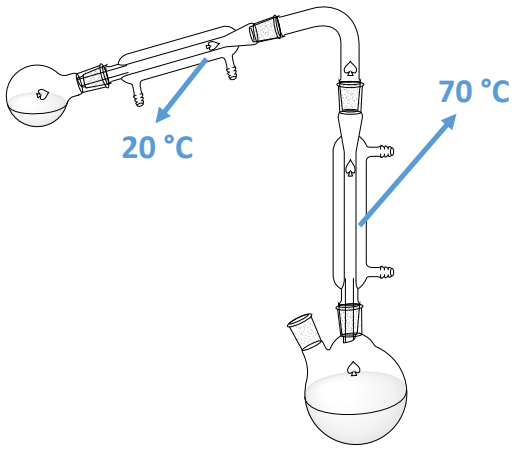

Figure 3.8. Catalytic transesterification of DMC with alcohols: apparatus for the removal of the azeotropic MeOH/DMC mixture (bp=64–67 °C).

3.4.4. CF-dismutation of asymmetrical organic carbonates

3.4.4.1. CF-Apparatus

The apparatus used for the CF-reactions was in-house assembled. It is summarised in Figure 3.3. A HPLC pump (P1) was used to deliver liquid reactants to a stainless-steel tubular reactor

(L=12 cm, Ø=1/4", 1.16 cm^3 inner volume) containing the catalyst. The reactor was placed in the upright position inside a gas chromatographic oven (GC oven), and heated to the desired temperature. A Swagelok back pressure regulator (BPR), placed at the outlet of the reactor, was used to keep the pressure constant throughout the whole system over the course of the reaction (line B). When experiments were carried out under ambient pressure, the BPR was bypassed (line A). A Rheodyne® Model 7725i injector, equipped with a 10 µL sample loop, was placed before the BPR and used for sampling. All components are connected by 1/16", 316 stainless-steel tubing.

SAFETY WARNING. Operators of high pressure equipment should take proper precautions to minimise the risk of personal injury.[22] The individual components that we describe work well, but they are not necessarily the only equipment of this type available.

3.4.4.2. General CF-dismutation procedure

A typical CF-dismutation reaction was carried out according to the following procedure.

The oven was set at a temperature of 150 °C and the CF-apparatus was flushed with N_2 for one hour. A homogeneous 1.42 M solution of the methyl alkyl organic carbonate (**1c**–**4c**) in either cyclohexane or toluene was then allowed to flow for 10 min at 1 $mL \cdot min^{-1}$, while the BPR and the oven were set to the desired operating pressure and temperature (1–50 bar, and 180–275 °C, respectively). Once the T and p stabilised, the flow of reactants was adjusted to the desired rate (0.1–0.4 $mL \cdot min^{-1}$). The reaction mixture was collected through a Rheodyne® valve (7725i fitted with a 10 µL sample loop) at time intervals of about 30 min, diluted with 1.5 mL of cyclohexane and analysed by GC/MS.

Given the low solubility of **2c** and **4c** in cyclohexane, toluene was used as the solvent. As for the previous CF-experiments, a 1.42 M solution of the methyl alkyl carbonate in toluene was used.

System cleaning and restart. At the end of each experiment, the oven and the BPR were set to 50 °C and atmospheric pressure, respectively, while a cleaning solution of methanol (50 mL at 1 $mL \cdot min^{-1}$) was pumped through the system. The pump was then stopped and the oven was allowed to cool to r.t.. The CF-reactor was then disassembled and the catalytic bed could be replaced with a fresh one.

3.4.5. Isolation and characterization of products

3.4.5.1. Methyl alkyl organic carbonates

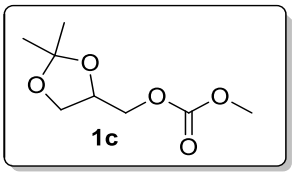

(2,2-Dimethyl-1,3-dioxolan-4-yl)methyl methyl carbonate (1c). Under the above described conditions for the transesterification reaction, solketal (5.29 g, 0.04 mol), DMC (64.86 g, 0.72 mol) and c-HT30 (0.16 g) were reacted under reflux (*ca.* 90 °C) for 3 h. The final conversion was 99% with 97% selectivity towards the desired product **1c**. The mixture collected at the end of the reaction was filtered and concentrated by rotary evaporation (50 °C, 40 mbar). The title product was obtained after vacuum distillation (99 °C, 40 mbar) as a transparent liquid in a 95% yield (7.22 g, 0.04 mol). Compound **1d** was characterised by ^{1}H NMR, ^{13}C NMR and GC/MS. ^{1}H NMR ($CDCl_3$, 400 MHz) δ(ppm): 4.40–4.30 (m, 1H); 4.20–4.15 (m, 2H); 4.05 (dd, *J*=8.6, 6.4 Hz, 1H); 3.80–3.75 (m, 4H); 1.43 (s, 3H); 1.36 (s, 3H). ^{13}C NMR ($CDCl_3$, 100 MHz) δ(ppm): 155.5, 109.8, 73.2, 67.9, 66.2, 54.9, 26.6, 25.5. GC/MS (relative intensity, 70 eV) *m/z*: 190 (M^+, <1%), 175 (50), 101 (17), 73 (10), 72 (11), 71 (19), 59 (31), 57 (14), 43 (100), 42 (12), 41 (19).

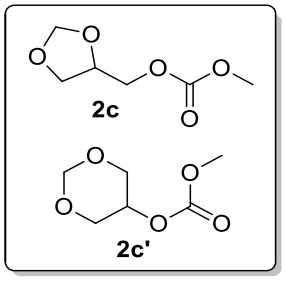

1,3-Dioxan-5-yl methyl carbonate (2c) and (1,3-dioxolan-4-yl)methyl methyl carbonate (2c'). Under the above described conditions for transesterification reactions, glycerol formal (4.16 g, 0.04 mol) DMC (64.86 g, 0.72 mol) and c-HT30 (0.13 g) were reacted under reflux (*ca.* 90 °C) for 24 h. The final conversion was 100% with 98% selectivity towards the desired product **2c**/**2c'**. The mixture collected at the end of the reaction was filtered and concentrated by rotary evaporation (50 °C, 40 mbar). The title product was obtained after vacuum distillation (94 °C, 40 mbar) as a transparent liquid in a 96% yield (4.68 g, 0.04 mol). Compound **2c**/**2c'** was characterised by ^{1}H NMR, ^{13}C NMR and GC/MS. ^{1}H NMR ($CDCl_3$, 400 MHz) δ(ppm): 5.04 (s, 1H), 4.89 (m, 2H), 4.81 (d, *J*=6.2 Hz, 1H), 4.59 (m, 1H), 4.30 (qnt, 1H), 4.25–4.13 (m, 2H), 4.07–3.92 (m, 5H), 3.80 (s, 3H), 3.79 (s, 3H), 3.73 (dd, J=8.5, 5.4 Hz, 1H). ^{13}C NMR ($CDCl_3$, 100 MHz) δ(ppm): 155.5, 155.1, 95.4, 93.5, 72.8, 68.8, 68.1, 67.2, 66.6, 54.9. GC/MS of **2c'** (relative intensity, 70 eV) *m/z*: 162 (M^+, <1%), 161 ($[M-H]^+$, 6), 132 (10), 102 (100), 86 (63), 59 (38), 58 (60), 57 (30), 55 (15), 45 (44), 44 (12), 43

(42). GC/MS of **2c** (relative intensity, 70 eV) *m/z*: 162 (M^+, <1%), 161 ($[M-H]^+$, 8), 103 (32), 86 (61), 77 (25), 73 (100), 59 (38), 58 (23), 57 (40), 45 (92), 44 (35), 43 (23).

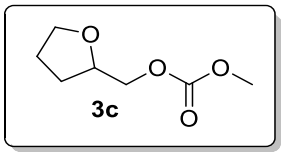

Methyl ((tetrahydrofuran-2-yl)methyl) carbonate (3c). Under the above described conditions for transesterification reactions, tetrahydrofurfuryl alcohol (4.09 g, 0.04 mol) DMC (64.86 g, 0.72 mol) and c-HT30 (0.12 g) were reacted under reflux (*ca.* 90 °C) for 120 h. The final conversion was 98% with 95% selectivity towards the desired product **3c**. The mixture collected at the end of the reaction was filtered and concentrated by rotary evaporation (50 °C, 40 mbar). The title product was obtained after vacuum distillation as a transparent liquid in a 96% yield (4.68 g, 0.04 mol). Compound **3c** was characterised by ^{1}H NMR, ^{13}C NMR and GC/MS. ^{1}H NMR ($CDCl_3$, 400 MHz) δ(ppm): 4.20–4.10 (m, 2H); 3.95–3.85 (m, 1H); 3.80 (s, 3H); 2.10–1.80 (m, 4H); 1.70–1.60 (m, 2H). ^{13}C NMR ($CDCl_3$, 100 MHz) δ(ppm): 155, 76, 70, 69, 55, 28, 25. GC/MS (relative intensity, 70 eV) *m/z*: 84 (24), 71 (100), 43 (47), 41 (23).

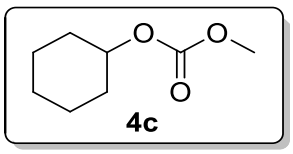

Cyclohexyl methyl carbonate (4c). Under the above described transesterification reaction conditions, glycerol formal (4.01 g, 0.04 mol) DMC (64.86 g, 0.72 mol) and c-HT30 (0.36 g) were reacted under reflux (*ca.* 90 °C) for 24 h. The final conversion was 99% with 98% selectivity towards the desired product **4c**. The mixture collected at the end of the reaction was filtered and concentrated by rotary evaporation (50 °C, 40 mbar). Title product was obtained after vacuum distillation as a transparent liquid in a 95% yield (6.01 g, 0.04 mol). Compound **4c** was characterised by ^{1}H NMR, ^{13}C NMR and GC/MS. ^{1}H NMR ($CDCl_3$, 400 MHz) δ(ppm): 4.65-4.55 (m, 1H); 3.80 (s, 3H); 2.00–1.90 (m, 2H); 1.75 (m, 2H); 1.60–1.20 (m, 6H). ^{13}C NMR ($CDCl_3$, 100 MHz) δ(ppm): 155.2, 76.7, 54.4, 31.5 (2C), 25.1, 23.5 (2C). GC/MS (relative intensity, 70 eV) *m/z*: 99 (21), 82 (89), 77 (56), 71 (39), 67 (100), 55 (48), 41 (44).

3.4.5.2. Symmetrical dialkyl organic carbonates

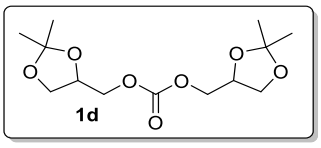

Bis((2,2-dimethyl-1,3-dioxolan-4-yl)methyl) carbonate (1d). Under the above described conditions for the dismutation reaction, a CF-reaction was carried out at 210 °C and 1 bar using a

mixture of solketal methyl carbonate:cyclohexane in 1:5 molar ratio (3 h; *F*=0.1 mL·min^{-1}) and c-HT30 (0.5 g). The final conversion was 62% with 92% selectivity towards the desired product **1d**. The mixture collected at the reactor outlet was first concentrated by rotary evaporation (50 °C, 40 mbar) and then distilled under high vacuum (70 °C, 3 mmHg). The title product was obtained as a pale-yellow liquid in a 57% yield (4.52 g, 0.02 mol). Compound **1d** was characterised by ^{1}H NMR, ^{13}C NMR and GC/MS. ^{1}H NMR (400 MHz, $CDCl_3$) δ(ppm) 4.39–4.32 (m, 2H), 4.20 (d, J=5.4 Hz, 4H), 4.10 (dd, J=8.5, 6.4 Hz, 2H), 3.80 (dd, J=8.6, 5.8 Hz, 2H), 1.47–1.44 (m, 6H), 1.38 (t, J=0.8 Hz, 6H). ^{13}C NMR (100 MHz, $CDCl_3$) δ(ppm) 154.83, 109.96, 73.21, 68.12, 66.28, 26.70, 25.32. GC/MS of **1d** (relative intensity, 70 eV) *m/z*: 290 ([M]$^{+}$, 0), 275 (23), 115 (100), 101 (32), 72 (14), 59 (24), 43 (41).

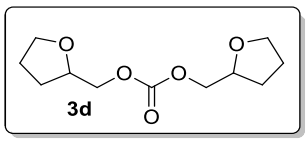

Bis((tetrahydrofuran-2-yl)methyl) carbonate (3d). Under the above described conditions for the dismutation reaction, a CF-reaction was carried out at 210 °C and 1 bar using a mixture of **3c** in cyclohexane in 1:5 molar ratio (3 h; *F*=0.3 mL·min^{-1}) and c-HT30 (0.5 g). The final conversion was 72% with 87% selectivity towards the desired product **3d**. The mixture collected at the reactor outlet was first concentrated by rotary evaporation (50 °C, 40 mbar) and then distilled under high vacuum (70 °C, 3 mmHg). The title product was obtained as a pale yellow liquid. Compound **3d** was characterised by ^{1}H NMR, ^{13}C NMR and GC/MS. ^{1}H NMR ($CDCl_3$, 400 MHz) δ(ppm): 4.25–4.00 (m, 6H); 4.00-3.70 (m, 4H); 2.10–1.80 (m, 6H); 1.70–1.60 (m, 2H). ^{13}C NMR (CDCl3, 100 MHz) δ(ppm): 155, 76, 69, 68, 37, 35. GC/MS of **3d** (relative intensity, 70 eV) *m/z*: 147 (12), 84 (22), 71 (100), 43 (34).

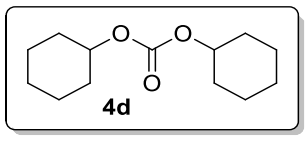

dicyclohexyl carbonate (4d). Under the above described conditions for the dismutation reaction, a CF-reaction was carried out at 210 °C and 1 bar using a mixture of **4c** in toluene in 1:5 molar ratio (3 h; *F*=0.3 mL·min^{-1}) and c-HT30 (0.5 g). The final conversion was 90% with 52% selectivity towards the desired product **4d**. The mixture collected at the reactor outlet was first concentrated by rotary evaporation (50 °C, 40 mbar) and then distilled under high vacuum (70 °C, 3 mmHg). The title product was obtained as a white solid. Compound **3d** was characterised by ^{1}H NMR, ^{13}C NMR and GC/MS. ^{1}H NMR ($CDCl_3$, 400 MHz) δ(ppm): 4.65-4.55 (m, 2H); 2.00-1.90 (m, 4H); 1.80-1.70 (m, 4H); 1.60-1.20 (m, 12H). ^{13}C NMR ($CDCl_3$, 100 MHz)

δ(ppm): 154.1, 76.3 (2C), 31.6 (4C), 25.2 (2C), 23.7 (4C). GC/MS (relative intensity, 70 eV) *m/z*: 145 (9), 83 (100), 67 (19), 55 (37), 41 (16).

3.5. Bibliography

[1] M. Selva, A. Perosa, S. Guidi, L. Cattelan, *Beilstein J. Org. Chem.*, 2016, **12**, 1911–1924.

[2] M. Selva, A. Perosa, S. Guidi, L. Cattelan, Dimethylcarbonate for the Catalytic Upgrading of Amines and Bio-Based Derivatives. In *Encyclopedia of Inorganic and Bioinorganic Chemistry*, John Wiley & Sons, L., Ed. 2016; pp 1–11.

[33] G. Fiorani, A. Perosa, M. Selva, *Green Chem.*, 2017, DOI: 10.1039/c7gc02118f.

[4] J. W. Comerford, I. D. V. Ingram, M. North, X. Wu, *Green Chem*., 2015, **17**, 1966–1987.

[5] A. Xing, M. Zhang, *Chromatographia*, 2005, **61**, 423–426.

[6] J. Haubrock, M. Raspe, G. F. Versteeg, H. A. Kooijman, R. Taylor, J. A. Hogendoorn, *Ind. Eng. Chem. Res.*, 2008, **47**, 9854–9861.

[7] G. Harrison, A. Dennis, M. Sharif, Continuous production process of diarylcarbonates. U.S. Patent 5,426,207, 1995.

[8] H. Lee, S. Joon Kim, B. Sung Ahn, W. Koo Lee, H. Sik Kim, *Catal. Today*, 2003, **87**, 139-–144.

[9] M. Fuming, L. Guangxing, N. Jin, X. Huibi, *J. Mol. Catal. A: Chemical*, 2002, **184**, 465–468.

[10] M. Hatano, Y. Furuya, T. Shimmura, K. Moriyama, S. Kamiya, T. Maki, K. Ishihara, *Org. Lett.*, 2011, **13**, 426–429.

[11] M. Hatano, S. Kamiya, K. Ishihara, *Chem Commun.*, 2012, **48**, 9465–9467.

[12] M. Selva, M. Noe, A. Perosa, M. Gottardo, *Org Biomol Chem*, 2012, **10**, 6569–6578.

[13] M. Selva, S. Guidi, M. Noè, *Green Chem.*, 2015, **17**, 1008–1023.

[14] S. Guidi, R. Calmanti, M. Noe, A. Perosa, M. Selva, *ACS Sustainable Chem. Eng.*, 2016, **4**, 6144–6151.

[15] T. Tabanelli, E. Monti, F. Cavani, M. Selva, *Green Chem.*, 2017, **19**, 1519–1528.

[16] A. Rodrıguez, J. Canosa, A. Domınguez, J. Tojo, *Fluid Phase Equilibria*, 2002, **201**, 187–201.

[17] In the repeated tests performed under the same conditions, the values for the conversion and the amounts of products (determined by GC/MS) differed by less than 5% between reactions.

[18] The presence of water in in **1c** was confirmed *via* Karl Fischer titrations (see Appendix for details). Any attempt to dehydrate **1c** failed due to the highly hydrophilic nature of the compound.

[19] (a) P. Tundo, F. Arick, A. E. Rosamilia, S. Memoli, *Green Chem.,* 2008, **10**, 1182–1189; (b) M. Selva, M. Fabris, A. Perosa, *Green. Chem.* 2011, ***13***, 863–872.

[20] (a) S. Wang, Y. Zhang, T. Chen, G. Wang, *J. Mol. Catal. A: Chem.*, 2015, **398**, 248–254; (b) T. M. Serra, D. R. de Mendonça, J. P. V. da Silva, M. R. Meneghetti, S. M. Plentz Meneghetti, *Fuel*, 2011, **90**, 2203–2206.

[21] Y. Ono, *Cat. Tech*., 1997, **1**, 31.

[22] P. G. Jessop, T. Ikariya, R. Noyori, *J. Am. Chem. Soc*., 1996, **118**, 344.

4. Renewable Aromatics from Kraft Lignin with Molybdenum-Based Catalysts

4.1. Introduction

As a component of lignocellulosic biomass (LCB), lignin is the main source of renewable aromatic compounds in the terrestrial biosphere.[1] Of the many target molecules that can be derived from lignin, phenol(s) and BTX-type arenes (Figure 4.1) are the most attractive due to their huge market volumes.[2] It should be noted that currently worldwide annual production of BTXs, primarily produced from fossil fuels, includes 9–11 million tons of benzene, 13–14 million tons of toluene and 17 million tons of xylenes.[3]

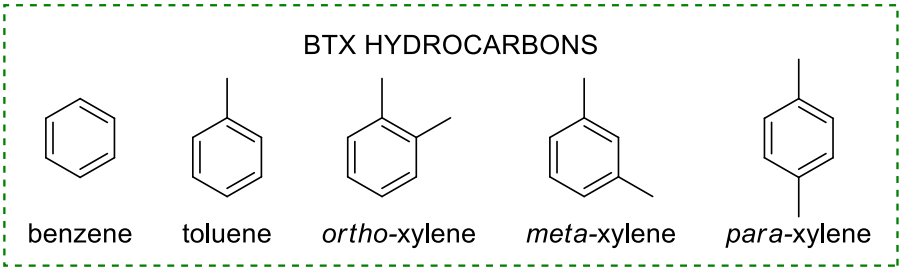

Figure 4.1. The benzene, toluene and xylene (BTX) hydrocarbons.

As described in the introductory Chapter (1) of this Thesis, despite a global estimated production of 130 million tons of lignin annually available by industry,[4] it (lignin) is currently the least valorised fraction of LCB.[5] Difficulties in the processing of woody biomass, particularly the strong propensity of lignin for repolymerisation during thermochemical treatments (*e.g*. pyrolysis and solvothermal liquefaction),[6] still represent a major limitation for the exploitation of lignin for the production of bio-based aromatics. Other promising procedures such as acid- or base- catalysed oxidative or reductive depolymerisation for the breakdown of lignin are currently under investigation.[6] An example is the reductive depolymerisation of lignin, which has been shown to be advantageous over the pyrolysis method. This is because in the presence of hydrogen the radical coupling reactions of the intermediate fragments are hindered, which reduces the amount of char produced compared to the pyrolysis method and hence results in higher yields of the desired products, in this case fuel additives and aromatic chemicals.[7] Similarly, Bai and co-workers demonstrated that

tetralin and isopropanol are suitable solvents for the liquefaction of lignin to short chain alkyl phenols (and vinyl phenols) under flow conditions with rapid heating rates to 300–400 °C in GC-type reactors. In their study the yields of aromatic compounds was reported to be approximately 10 wt% of the lignin input. Conversely, in the absence of hydrogen donating solvents, the extent of repolymerisation is such that high MW species tended to predominate.[8]

It has also been shown that protocols involving the depolymerisation of lignin over supported noble metals (such as bi-metallic Ni-Me, Me = Ru, Rh, Pd) are some of the most efficient approaches to obtain monophenols from lignin.[6,9]

Ford and co-workers[10] investigated the conversion of pine wood flour to a range of aliphatic chemicals (higher alcohols and ethers, HAE and substituted cyclohexyl alcohols and ethers, CAE) in supercritical methanol (at 300–320 °C and 160–220 bar) over a copper-doped porous metal oxide catalyst (Scheme 4.1). Under these conditions methanol is reformed and a water-gas shift reaction occurs generating hydrogen gas, which in turn is consumed for the subsequent cleavage of aromatic ethers and reduction/deoxygenation steps.

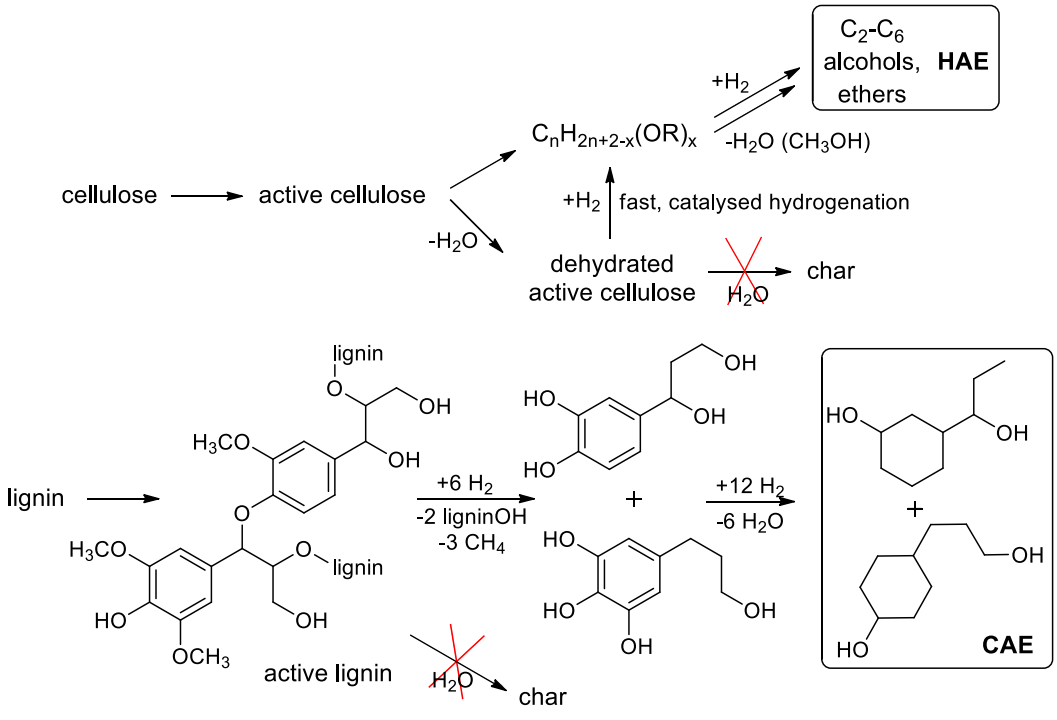

Scheme 4.1. Model reaction steps for the conversion of solid LCB to fluid alcohols in supercritical methanol.[10]

More recently, Hansen and co-workers[11] reported the breakdown of lignin in supercritical methanol and ethanol in the presence of CuMgAlOx as a catalyst. At 300 °C and prolonged reaction times of up to 20 h, this catalyst was found to improve the depolymerisation of lignin.

Additionally, the reaction was found to be more efficient in ethanol, in which a yield of 23 wt% of monomeric aromatic products was achieved, compared to 6 wt% in methanol.

In all the above studies, the presence of hydrogen-donating solvents were found to reduce the formation of char through the stabilisation of reactive phenolic intermediates, which are formed at high temperatures. At its critical point (243 °C, 63 atm), renewable ethanol is especially efficient at suppressing the repolymerisation of lignin because it can act as both an *O*- and a *C*-alkylating agent of phenolic hydroxyl groups and aromatic rings, respectively.[11]

Transition metal-catalysed hydrogenolysis and hydrodeoxygenation reactions are also becoming attractive approaches for lignin valorisation.[12] For example, nickel-based systems were shown to be effective in the reductive depolymerisation of lignin.[13] At 200 °C and autogenous solvent pressure, the Ni-catalysed alcoholysis of native birch wood lignin produced monomeric phenols (*e.g*. propylguaiacol and propylsyringol) in methanol, ethanol and isopropanol, with the best selectivity towards the monomeric phenol products found to be 97% at 50% conversion.[13b] This research showed that the key to the successful production of low molecular weight aromatic compounds is the ability to tune the chemoselectivity of the catalyst towards C–O and C–C bond hydrogenolysis, whilst suppressing hydrogenation of the aromatic rings. In the specific case of Kraft lignin (KL), an additional issue that must be faced is the poisoning effects derived from the sulfur and residual inorganics contained within the substrate. Therefore, any catalyst used to depolymerise KL must be inherently sulfur-tolerant, or conditions must be implemented so that sulfur is continuously removed.

The “sulfophilicity” and sulfur-tolerance of some classes of metal-based catalysts is a well-known subject. For example, in the petrochemical industry, molybdenum-based systems such as $NiMo/Al_2O_3$[14] and MoS_2[15] are standard hydrodesulfurisation catalysts.[16] Such compounds have also been investigated in the hydrodeoxygenation of pre-liquefied lignocellulosic biomass. Recently, Li and co-workers demonstrated that supported molybdenum catalysts were effective for the depolymerisation of lignin.[17] They proved that in the presence of supercritical ethanol (280 °C, autogenous pressure) as the principal hydrogen transfer agent, the breakdown of lignin occurred to produce oligomeric segments of molecular weights in the range of 700–1400 Da. These species were then hydrogenolysed and hydrodeoxygenated into monomeric products including C_6–C_{10} esters, aliphatic alcohols, arenes, phenols and benzyl alcohols. Under these conditions, Kraft lignin was also completely converted. The Authors proposed that the Mo-based catalysts acted as the precursors for a common homogenous

Mo(V)-species (Scheme 4.2, a), which was formed *in situ*. Li *et al.* claimed that the Mo(V) species, specifically ($Mo(OEt)_5$), was the active catalyst. The hypothesis was validated by a separate test in which the direct use of $Mo(OEt)_5$ afforded 690 mg of monomer aromatics per g of reacting lignin.[17b]

Scheme 4.2b-c offers a pictorial description of the reaction pathway: the *in situ* formed Mo species were capable of attacking lignin segments of medium molecular weight, further decomposing them and eventually resulting in the production of a range of low molecular weight aromatic compounds.

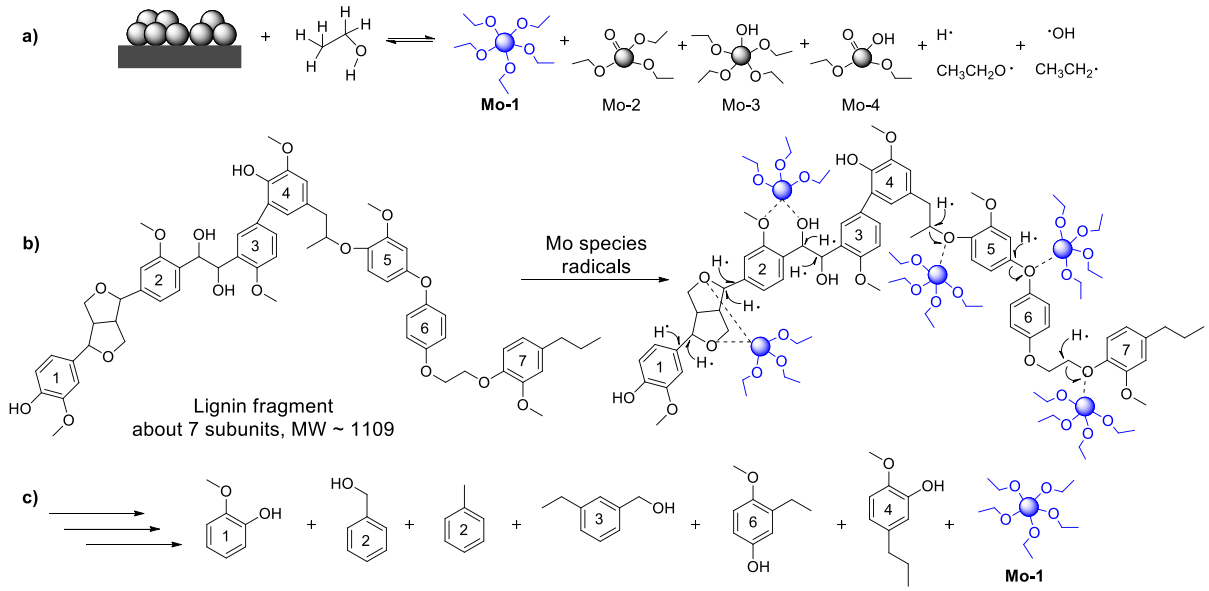

Scheme 4.2. Possible reaction pathways for (a) the formation of active Mo species, and (b, c) the formation of the final products.

Among the investigated catalysts, Mo/Al_2O_3 gave the highest yield of aromatics (330 mg/g lignin), while a molybdenum carbide supported on activated carbon (α-MoC_{1-x}/AC) gave the best overall yield of 1640 mg/g_{lignin} of liquid products (classified as esters, aliphatic alcohols and aromatics). The ethanolysis process could be further improved by using a composite catalyst comprised of α-MoC_{1-x} and Cu-$MgAlO_z$.[17c,11,17a] Both the physical mixture of the components and the composite catalyst were found to afford higher overall yields of products than either MoC_{1-x} or Cu-$MgAlO_z$ alone, with the highest reported yield of aromatics being 575 mg/g lignin when the temperature was pushed to 330 °C.

These results inspired part of this Thesis work carried out at the Laboratory of Advanced Catalysis for Sustainability (LACS) at The University of Sydney, Australia. This section of the project was aimed at the design of new Mo-based catalysts for the hydrogenolysis of Kraft

lignin. The following paragraph outlines some of the properties of MoS_2- and MoC_2-based materials used for this purpose.

4.1.1. MoS_2- and Mo_2C-based catalysts

Sulfides.

Molybdenum sulfide (MoS_2) has been widely studied at LACS (USyd), for catalytic applications in the hydrogen evolution reaction (HER).[18] Bulk MoS_2 is commercially available in its laminated structure, where each molybdenum atom is coordinated to six sulfur atoms oriented in a trigonal prism. Similar to the hydrotalcite materials described in Chapter 2, the MoS_2 layers are stacked one on top of the other, thus forming a sulfur-molybdenum-sulfur "sandwich" that correspond to the basal (0001) plane. In this structure, both the molybdenum and the sulfur atoms are fully saturated and, therefore, chemically inert. The only existing interactions between the layers are weak Van der Waals forces (Figure 4.2).

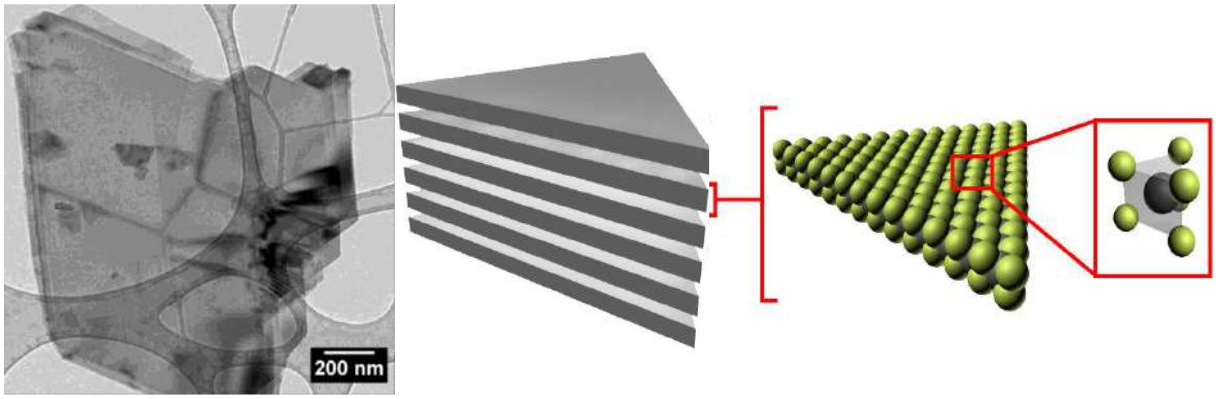

Figure 4.2. TEM image of commercial laminated MoS_2 (left). Representation of the MoS_2 structure, showing the stacking of the individual MoS_2 layer and the co-ordination sphere around an individual molybdenum atom (right). Grey spheres: molybdenum; yellow spheres: sulfur.

On the other hand, structural studies on nanoparticulate MoS_2 have shown that this material is composed almost entirely of flat polygons of S-Mo-S trilayers.[16] These domains can either pack together in a graphite-like structure, or remain as such, in a single trilayer. In the latter case, two different types of surface sites exist: terrace sites are present on the basal (0001) surface, whereas edge sites lie at the edge of the nanoparticles. DFT calculations combined with practical experiments demonstrated how, for the HDS, the active sites are those on the edge. Studies on the effects of the MoS_2 morphology on the catalytic activity have shown that a better performance could be achieved when the catalyst was synthesised with a delaminated structure, which possessed a larger population of accessible catalytically active

edge sites (Figure 4.3).[18b] By contrast, poorer activities were observed for a commercial MoS_2 sample, which was characterised by a well laminated structure, similar to that shown in Figure 4.2, with low accessibility of the catalytic sites to the reaction substrates.

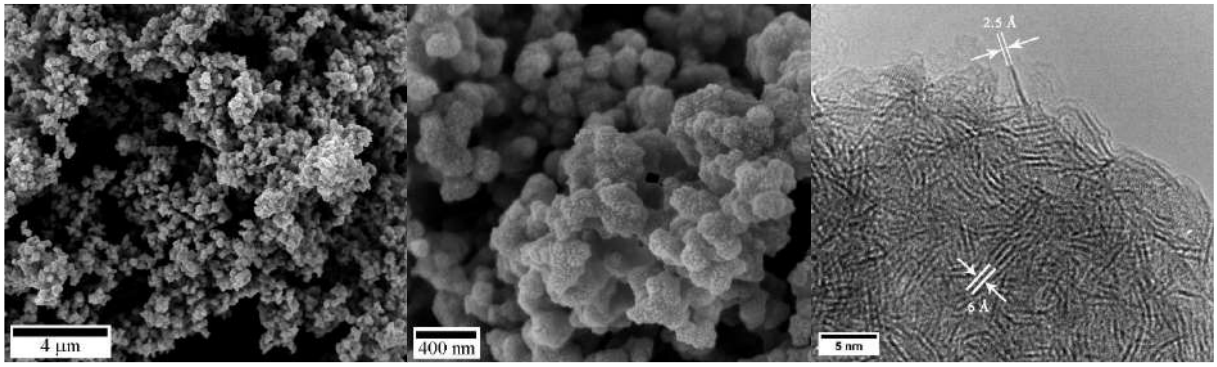

Figure 4.3. SEM of delaminated MoS_2 under low (left) and high (centre) magnification. HRTEM of delaminates MoS_2 (right).

Increasing the population of active edge sites requires a suitable stabilising agent, which has to arrest the crystal growth and, at the same time, selectively stabilise the catalytic surfaces to prevent relaxation. Ionic liquids (ILs) have proven to be perfect compounds to fulfil these requisites; particularly their properties of thermostability and low surface tension were desirable for the synthesis of nano-size materials.[19] For example, 1-butyl-3-methylimidazolium triflate ([C_4Mim][OTf]) was found to be a good model: it was stable at temperatures up to 300 °C under inert atmosphere,[20] and resistant to oxidative and reductive attacks,[21] thereby providing an appropriate environment for synthetic procedures based on thermolysis of solid precursors. One such method was developed by the group of Maschmeyer at LACS, who produced MoS_2 by the thermal decomposition of a sulfido-molybdenum complex as ammonium tetrathiomolybdate ($(NH_4)_2MoS_4$) in the presence of imidazolium-based ILs.[18] It was known that the $(NH_4)_2MoS_4$ precursor afforded MoS_2 when heated at elevated temperatures under an inert or reducing environment (Equation 4.1).[22]

$$2(NH_4)_2MoS_4 \xrightarrow[\text{Inert/Reducing atm}]{>230\ ^\circ C} 2MoS_2 + 4NH_3\uparrow + 2H_2S\uparrow + S_2\uparrow$$

Equation 4.1. Thermal decomposition of $(NH_4)_2MoS_4$ under inert/reducing atmosphere.

This thermal decomposition was improved when imidazolium ILs, such as [C_4Mim][OTf] and [C_{10}Mim][OTf], were used as the reaction media: a delaminated MoS_2 possessing a greater density and accessibility of active edge sites was achieved.[18] These results were consistent

with the hypothesis that ILs can stabilise the highly energetic, reactive surfaces of the catalyst crystals.

Carbides.

Early transition metal carbides started to attract considerable attention after the discovery that they behaved like noble metals in surface catalysis.[23,24] Carbides of transition metals of groups IV-VI combine properties of metal and ceramic materials such as good electrical and thermal conductivity, ultra-hardness (>2000 kg mm^{-2}), high melting points (>3000 °C) and stability. Moreover, depending on the nature of the metal centres, the carbon(C)/metal(M) ratio and the orientation of the carbide surfaces, these solids may act as excellent catalyst for several organic reactions. These include the synthesis and decomposition of ammonia, regioselective hydrogenolysis of inert aryl ether C–O bonds[25] and the deoxygenation of non-edible triglycerides (*i.e.* stearic acid) to alkanes and alkenes.[26,27,23b] Mo_2C in particular, is an effective catalyst for the synthesis of methanol from CO hydrogenation,[28] the water gas shift reaction,[29] steam reforming reactions,[30] the breaking of S–X (X = O, H, C) bonds of SO_2, H_2S, and CH_3SH, respectively, the hydrodesulfurisation (HDS) and the hydrodenitrogenation (HDN) processes.[31] In these processes, Mo_2C displays an activity similar to those of Ru, Pd and other noble metals, with an even higher resistance against impurities.[23b] The performance of Mo_2C is attributed to the permeation of carbon atoms into the lattice of Mo: this phenomenon lengthens the metal-metal distance and increases the electron density of the d-band at the Fermi level of the transition metal.[32] Mo_2C exists in two different stable crystalline forms, *i.e*. α- and β-Mo_2C. These differ in the distribution of interstitial carbon atoms in the Mo matrix. Although the α-Mo_2C phase was historically believed to be a hexagonal close packed (hcp) crystal, it was re-indexed in 1963 when neutron diffraction analyses reported an orthorhombic crystal structure for this compound, with space group P*bcn*. β-Mo_2C instead, possesses a hexagonal close packed (hcp) arrangement.

The literature describes different approaches for the synthesis of Mo_2C, which can be generally grouped into two categories, namely, “outside-in” and “inside-out”, according to the direction of carbon diffusion (Table 4.1). In the former category, the most reported syntheses are based on: *i*) the temperature-programmed reaction of molybdenum trioxide with a mixture of hydrogen and carbon-containing gases,[33] and *ii*) the reduction of molybdenum halides with $LiBEt_3H$.[34] For example, Liang and co-workers described a carbothermal hydrogen

reduction (CHR) method by which supported Mo_2C was prepared starting from ammonium heptamolybdate [$(NH_4)_6Mo_7O_{24}$] and activated carbon (AC), acting as both the support and the carbon source.[35] More recently, microwave heating has been used for an ultra-rapid synthesis of Mo_2C using molybdenum metal or the metal trioxide as the precursor (Table 4.1).[36]

Table 4.1. Different pathways for the synthesis of β-Mo_2C.

Mo-source	C-source	Reduction pathway	T (°C)	Time	Reference
		outside-in synthesis			
$(NH_4)_6Mo_7O_{24}$	AC	pure H_2 (200 cm^3/min)	700–800	1 h	Liang *et al.*[35]
Mo or MoO_3 powder	C powder	MW irradiation	-	90 s (800 W) 20 s (3 kW)	Vallance *et al.*[36]
		inside-out synthesis			
$(NH_4)_6Mo_7O_{24}$	melamine	Ar/H_2 (Ar, 50 mL/min; H_2, 20 mL/min)	650	1 h	Pang *et al.*[37]

A general drawback of these "outside-in" syntheses is that they may lead to the concentration of C species on the surface of the particles higher than in the bulk, with the consequential formation of coke during catalytic processes. "Inside-out" protocols offer a solution to this problem by synthesising the Mo-C precursor prior to the thermal treatment. For example, a β-Mo_2C phase was recently prepared by Pang *et al*. from aqueous solutions of $(NH_4)_6Mo_7O_{24}$ and melamine: after the precipitation of a white Mo(VI)–melamine hybrid solid, heating at 650 °C in either an Ar or Ar/H_2 flow, allowed for the formation of the desired material.[37] A mechanism for the formation of the final solid was proposed using TG/DTG in combination with IR spectra, which indicated that in a reductant-free environment (Ar atmosphere) four pathways took place: first a dehydration reaction of the Mo(VI)–melamine precursor, which occurred between 100–200 °C, followed by a second step (200–380 °C) where hydrogen was removed as either H_2O or NH_3. Then, in the third and fourth steps, C (in the form of CO and CO_2) and N atoms were released above 410 °C and 490 °C, respectively (Table 4.2).[37] XRD analysis also pointed out that the introduction of a small amount of H_2 allowed for the production of a highly crystalline pure phase of β-Mo_2C; otherwise a MoO_x-doped β-Mo_2C was achieved.

Table 4.2. Mo, C, and N Contents; Mo/(C + N) Molar Ratios; and Surface Areas of the Products of the Ar and Ar/H_2 Heat Treatment of the Hybrid at 650 °C for 1 h.[37]

Phase identification[a]	β-Mo_2C	MoO_x-doped β-Mo_2C
Mo content (wt%)	93.3	90.0
C content (wt%)	4.5	7.0
N conten (wt%)	1.1	1.6
Mo/(C + N) (mol mol^{-1})	2.14	1.34
S_{BET} (m^2 g^{-1})[b]	7	10

a) Determined by XRD analysis; b) specific surface area calculated from the Brunauer–Emmett–Teller method.

4.2. Results and Discussions

In this PhD Thesis work, both MoS_2 and Mo_2C were investigated for Kraft lignin depolymerisation and for the conversion of waste lignin to renewable aromatics. Additionally, some apparent anomalies on the identity of Mo_2C were also addressed (see catalyst characterisation section below).

4.2.1. Catalysts: Preparation and Characterisation

Sulfides.

Ammonium tetrathiomolybdate, $(NH_4)_2MoS_4$, a precursor of molybdenum disulfide, was prepared according to the procedures reported by Quagraine and co-workers.[38] As the thermal decomposition of the chosen precursor was reported between 230–360 °C,[22b] all supported catalysts were prepared at 300 °C except for bulk MoS_2, which was used as-purchased. Batches of delaminated MoS_2, either in its supported or unsupported form, were obtained in the presence of an IL, specifically $[C_4Mim][OTf]$, which acted as the decomposition medium under reductive conditions.[18] Reactions were run under a N_2/H_2 flow for 2 h (further details are given in the experimental section).

Catalox® SBa-150 (from Sasol) was used as the alumina support: this solid was chosen due to its well-defined properties and widespread industrial use. As previously described in Chapter 2, hydrotalcites (HTs) exhibit multiple tuneable parameters including the Mg/Al ratio, the interlayer anions and the catalyst preparation method. HTs presenting basic or NO_3^- interlayer anions have been recently reported to catalyse C–C bond cleavage in lignin model dimers.[39]

Table 4.3. Surface area data for the prepared MoS_2 and Mo_2C catalysts.

Entry	Sample	S_{BET} (m^2/g)	v_p (cm^3/g)	Ads. D_{BJH} (nm)
1	MoS_2	8	–	–
2	d-MoS_2[a]	55	0.07	5.6
3	MoS_2/Al_2O_3	113	0.30	12.4
4	d-MoS_2/Al_2O_3[a]	169	0.33	10.8
5	d-MoS_2/KW2000[a]	119	0.50	20.1
6	Mo_2C	6	–	–
7	Mo_2C/Al_2O_3	103	0.32	12.7
8	KW2000	199	1.04	27.8

a) "d-MoS_2" denotes delaminated MoS_2.

In the present study, the Mg/Al hydrotalcite, KW2000 (from Kyowa Industries), was selected for its catalytic performance in alkylation chemistry at high temperatures.[40]

Carbides.

The molybdenum hemicarbide catalysts were synthesised from a single precursor using a previously reported procedure.[37] Accordingly, melamine was dissolved at 80 °C in water, while ammonium heptamolybdate was dissolved separately at 40 °C in water. The two aqueous solutions of melamine and ammonium heptamolybdate were mixed at room temperature to induce the co-precipitation of a melamine–molybdate coordination polymer. The thermal decomposition of the isolated precipitate was then carried out at 650 °C under N_2/H_2 flow for 1 h. The reaction led cleanly to the formation of Mo_2C. Two series of Mo-based carbides were prepared by this protocol (further details are in the experimental section). Both sulfide and carbide materials were characterised by nitrogen sorption at 77 K, transmission electron microscopy (TEM) and powder X-ray diffraction (PXRD).

The results of nitrogen sorption analyses. *i.e.* BET surface areas obtained and BJH pore diameters are shown in Table 4.3. Whilst none of the samples displayed high surface areas or porosities, the surface area of delaminated MoS_2 was significantly higher than the bulk sample (Table 4.3, entries 1 & 2). However, a major increase of S_{BET} was noticed for molybdenum samples supported on both alumina and HT (Table 4.3, entries 3–5).

The very low S_{BET} of unsupported Mo_2C was compatible with the formation of a low-porosity material, largely free from surface defects. This result was comparable to that reported by

Liang and co-workers.[37] As for MoS_2 solids, dispersion of the Mo_2C onto alumina significantly improved the surface area and porosity of the resulting solid. Changes to the morphology and the interaction of the catalysts particles with the support for the MoS_2 series of catalysts were confirmed by TEM (Figure 4.4). The large sheets present in bulk-MoS_2 were not present in the delaminated material as a result of the specific effects of the ionic liquid used during the thermal decomposition of ammonium tetrathiomolybdate. The resulting material consisted of polydisperse MoS_2 nanoparticles containing an increased proportion of edge-sites (Figure 4.4, a and b). For the supported MoS_2 catalysts, an intimate contact was observed between the surface of the supports and the MoS_2 particles (Figure 4.4, d–f). The same (contact) held true also for the Mo_2C catalyst (Figure 4.4, h).

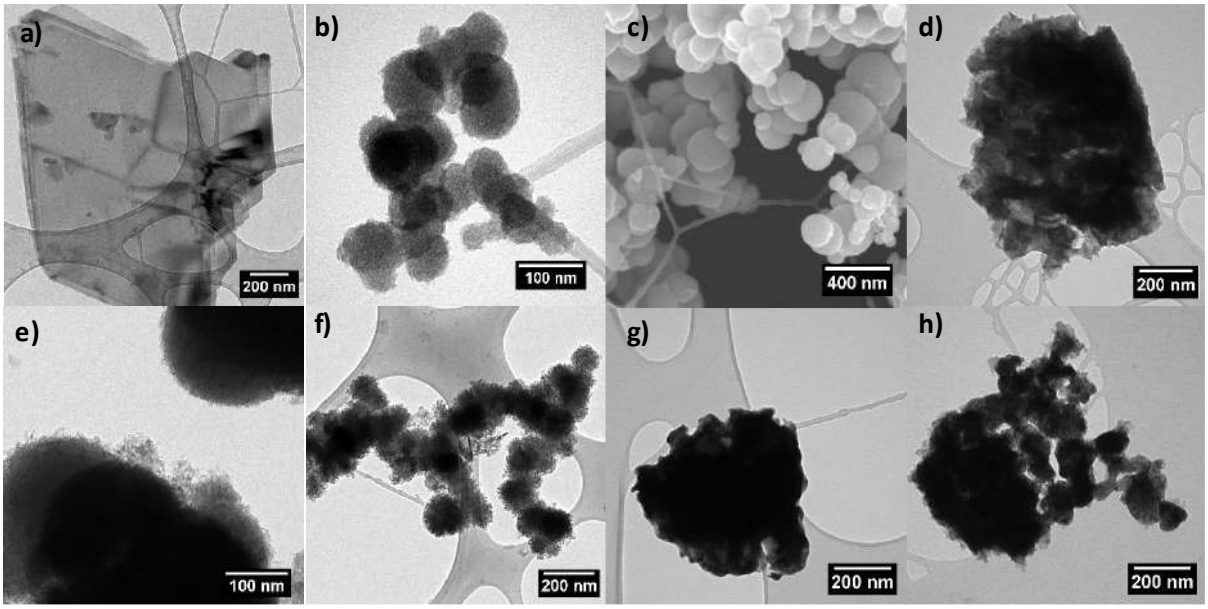

Figure 4.4. TEM (and SEM) images of the catalysts used in this study. Bulk MoS_2 (a); TEM and SEM of delaminated MoS_2 ((b) & (c), respectively); MoS_2/Al_2O_3 (d); delaminated MoS_2/Al_2O_3 (e); delaminated MoS_2/c-KW2000 (f); unsupported Mo_2C (g); Mo_2C/Al_2O_3 (h).

XRD patterns showed a significant line-broadening of the reflections of the molybdenum species upon deposition on high surface area supports, consistent with smaller particle size and therefore higher surface area. The XRD patterns of both the freshly prepared and used (post-reaction) MoS_2-based catalysts are shown in Figure 4.5. Bulk MoS_2 was identified as the 2H polymorph of the *$P6_3/mmc$* hexagonal phase.[41] For the delaminated material the large (002) reflection, corresponding to the 6 Å interlayer spacing, was absent. In addition, the (100) and (110) reflections were significantly broadened and (103) was only just visible as a broad shoulder. For the supported catalysts, the broadening of the reflections in the XRD data generally indicated that the particle size of MoS_2 was smaller than in the bulk. This effect,

combined with delamination, resulted in highly dispersed nanoparticulate MoS_2 phases on both alumina and KW2000 hydrotalcite.

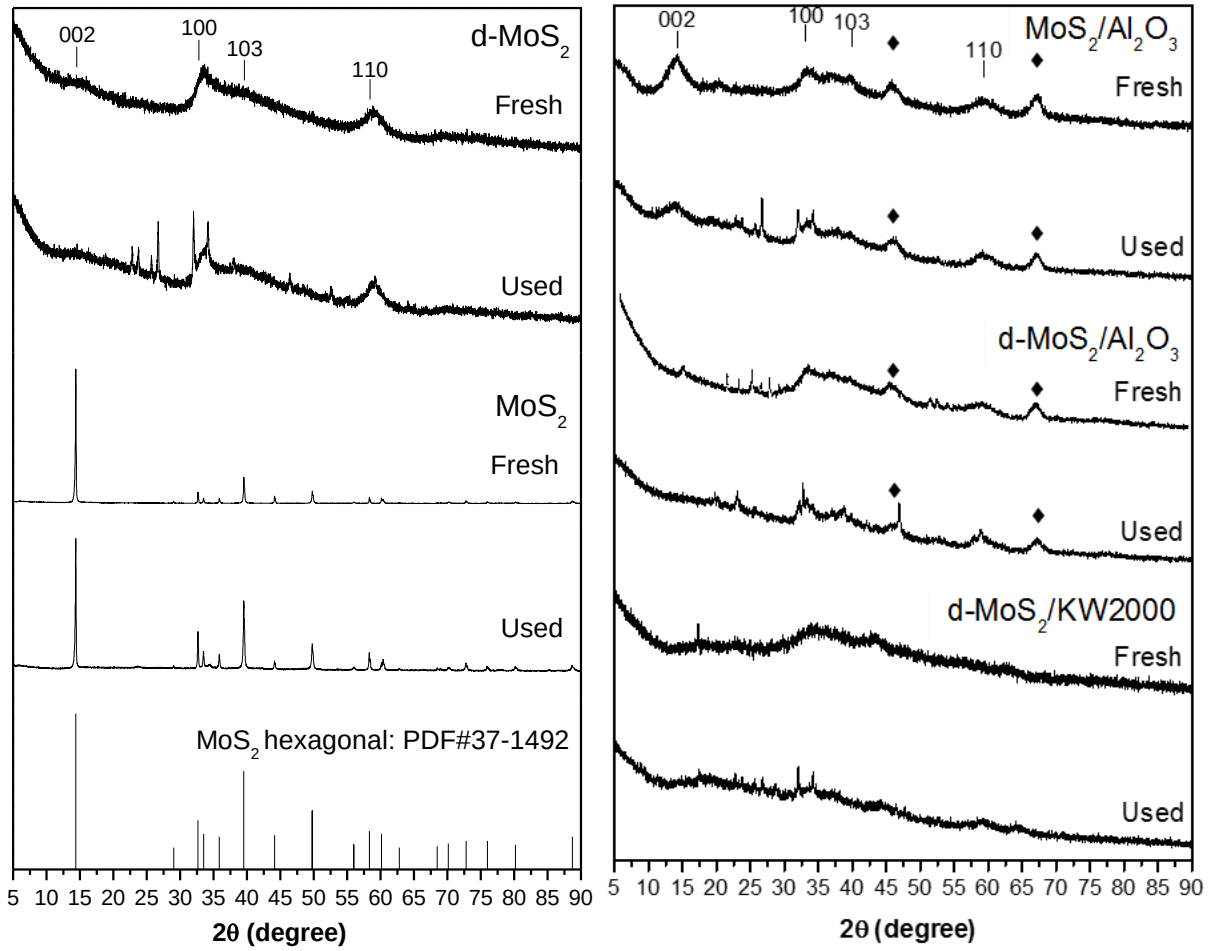

Figure 4.5. Powder XRD patterns of the unsupported MoS_2-based catalysts (left) and supported catalysts (right) before and after catalytic depolymerisation of lignin.
The ♦ symbol marks prominent reflections from the γ-alumina support.

The XRD data for the Mo_2C catalysts are shown in Figure 4.6. The pattern for the unsupported Mo_2C reported here was in close agreement to that published by Liang and co-workers.[37] They referenced their material to PDF# 35-0787:[42] a hexagonal phase with space group *P6₃/mmc*. However, there is a body of literature that suggests that the orthorhombic phase (space group *Pbcn*) is slightly more stable than the hexagonal phase at room temperature.[43] For example, Haines *et al*. have demonstrated that the *Pbcn* phase was 15 meV per formula unit lower in energy than the hexagonal *P6₃/mmc* phase,[44] which corresponded to an energy difference of 1.45 kJ/mol between the two phases. The corresponding reference pattern, PDF# 79-0744,[43b] was included in Figure 4.6 for comparison.

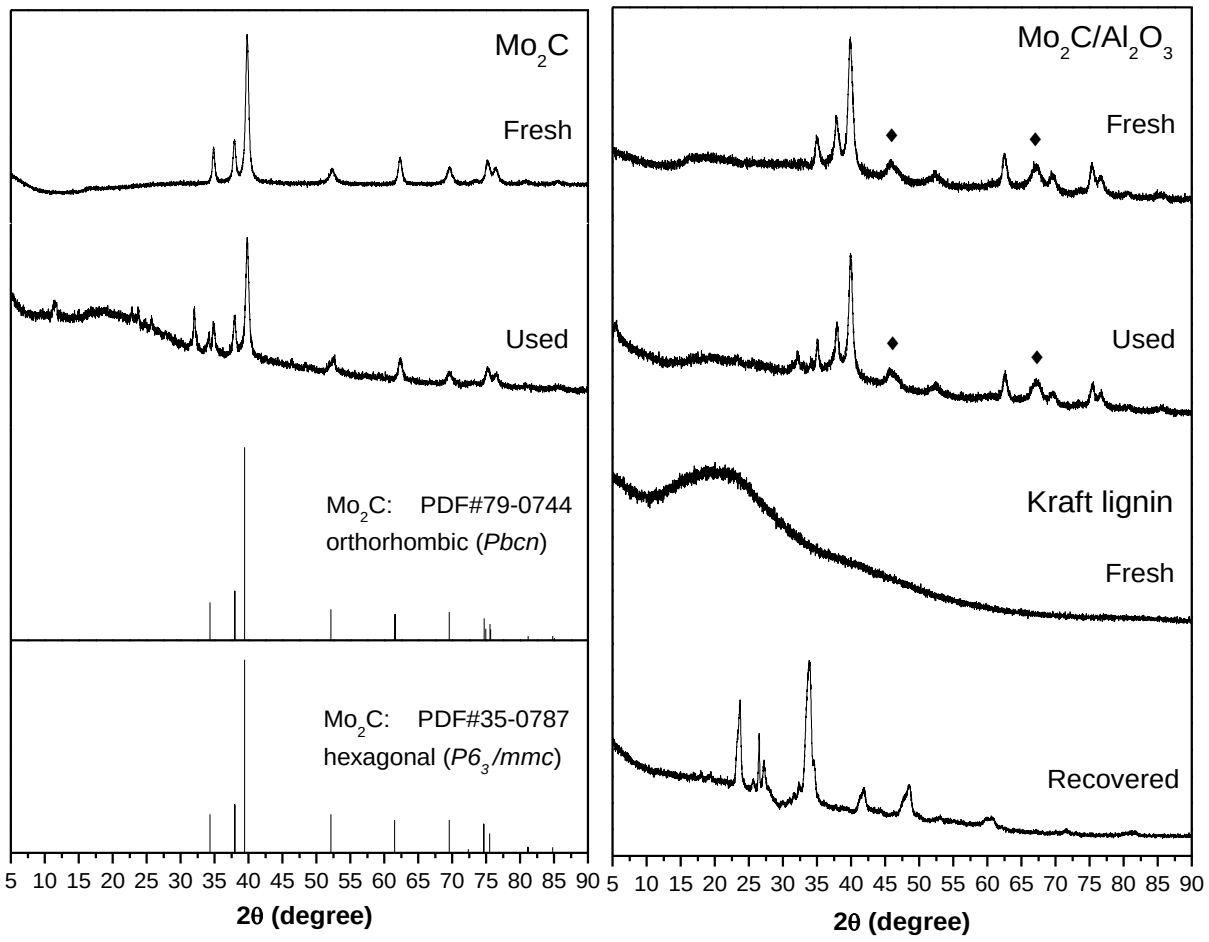

Figure 4.6. Powder XRD patterns of the unsupported Mo_2C-based catalyst and reference patterns (left) and supported catalyst, as well as Kraft lignin (right) before and after catalytic depolymerisation. XRD patterns from fresh and recovered Kraft lignin are also reported for comparison. The ♦ symbol marks prominent reflections from the γ-alumina support.

Given the inevitable broadening of the XRD data for the unsupported Mo_2C, it was difficult to unequivocally assign the synthesised material as either phase. This aspect has also been noted before and the use of neutron diffraction was proposed in order to resolve the structure.[45] In any case, the major reflections for both reference patterns matched those of the experimental pattern. There was also the possibility that the bulk orthorhombic material was overlaid by a disordered hexagonal lattice,[46] which led to the hypothesis that the material used in this study, as well as that prepared by Liang and co-workers,[37] was actually the orthorhombic phase of Mo_2C. That said, the addition of the Mo_2C phase to an alumina support, did not substantially change the Mo_2C crystal structure. Dispersion was increased, based on the sorption data (Table 4.3), however the crystallite size from powder XRD appeared similar to that of the unsupported material.

Finally, the sharp reflections that were present in the XRD patterns of solid residues recovered from depolymerisation reactions were due to changes of the lignin that occurred under the

reaction conditions. This change was clearly shown in Figure 4.6 (RHS). The diffraction data of commercial lignin powder was uninformative, the material being largely amorphous.

Analysis of recovered solid residue after supercritical ethanolysis (reaction conditions are described in the following paragraph, and further detailed later in the experimental section), without a catalyst present, revealed a completely new pattern, containing several prominent reflections (recovered, bottom right of Figure 4.6). Graphitic carbon was ruled out as a candidate (based on the absence of characteristic reflections in the reference patterns in the Highscore Plus, v3.0.5 software package) and, given the heterogeneous nature of lignin, it was unlikely that a single phase was responsible for this pattern.

The certificate of analysis for the batch of lignin used in the current study stated that 3.33 wt% sulfur was present. In addition, calcination of lignin samples at 800 °C for 4 h resulted in 19.5 wt% of pale green, non-volatile inorganic residue. Upon acidification of this residue with 2 mL of 70 %w/v nitric acid, a significant quantity of gas, presumably CO_2, was evolved, indicating that the inorganics were likely primarily carbonates. The residual material was therefore consistent with being derived from the “green liquor” stream of the Kraft pulping process (Chapter 1).

4.2.2. Catalytic conversion of lignin

The catalytic depolymerisation of Kraft lignin was performed in a 250 mL Parr reactor (Hastelloy C), under reaction conditions similar to those reported by Li and co-workers:[17] See Scheme 4.3.

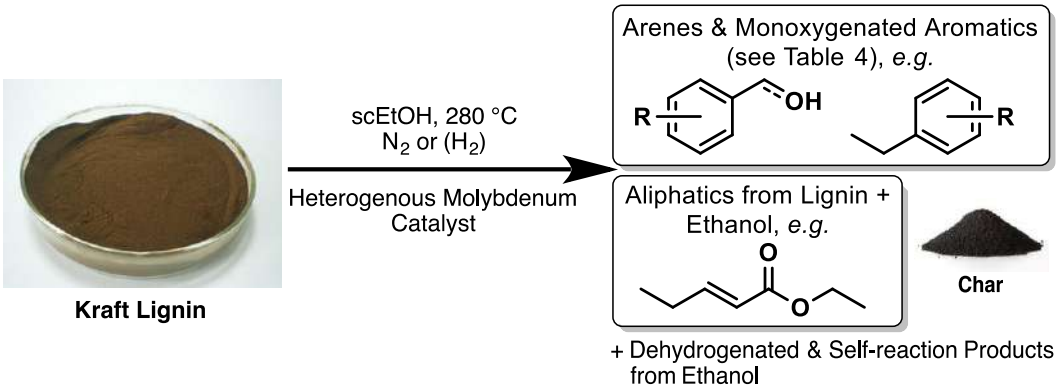

Scheme 4.3. Overview of Kraft lignin depolymerisation under supercritical reaction conditions in the presence of Mo-based heterogeneous catalysts.

Kraft lignin (1.0 g) and an appropriate amount (see below) of catalyst were suspended in 100 mL of ethanol, which was used as the hydrogen-donor solvent. The supported catalysts were nominally 30 wt% molybdenum and 500 mg of catalyst was employed in each case (corresponding to 150 mg of molybdenum). For unsupported catalysts, the mass of catalyst added was calculated to keep the amount of added molybdenum constant across all experiments (corresponding to 160 mg of Mo_2C and 250 mg of MoS_2). Most of the reactions were run for 6 h at 280 °C under an initial N_2 pressure of 1.3 bar; see below for specific details on experiments run at higher temperatures or under hydrogen gas at various pressures. Two parameters were of interest: the substrate conversion, *i.e*. the proportion of lignin converted to soluble products, and the yield of low-molecular weight aromatic compounds in solution (note that the reactor head space was not sampled). More than 1 g of products was observed from the depolymerisation of 1 g of lignin due to the addition of ethyl groups from ethanol to the solubilised species (aromatics, aliphatics) and to the recovered residue. In addition, the self-condensation of ethanol resulted in the detection of a variety of low molecular weight aliphatic products. Hence, conversion was calculated by subtracting the mass of recovered solid from the combined masses of catalyst and substrate lignin.

The recovered solid was presumed to contain the catalyst, inorganic components of lignin and organic material that either failed to depolymerise, or resulted from the repolymerisation of reactive oligomers during the reaction.

4.2.2.1. MoS_2-Series

The overall results from the MoS_2-series of catalysts are shown in Table 4.4 and Figure 4.7. Conversion and yields are the average values of three runs. Ethanolysis of lignin in the absence of catalyst was run as a control experiment and resulted in a conversion of 80%. From this run, a total of 77 mg of aromatic products per g of lignin was quantified. These results were in accordance with similar control reactions reported in the literature.[11,17b]

Table 4.4. Overview of the results from the MoS_2-catalysed depolymerisation of lignin.

Entry	Catalyst	Atm	Solid residue[a] (mg)	Conv.[b] (%)	Aromatic yield (mg/g_{lignin})	Final P[c] (bar)
1	**no catalyst**	N_2	354	80	77	94
2	**MoS_2[d]**	N_2	554[b]	86	178	101
3	**d-MoS_2[d]**	N_2	423[b]	Quantitative	186	131
5	**MoS_2/Al_2O_3**	N_2	939	70	46	163
6	**d-MoS_2/Al_2O_3**	N_2	1059	55	9	153
7		H_2 (20 bar)	924	72	18	171
8	**d-MoS_2/KW2000**	N_2	709	98	72	139
9		H_2 (20 bar)	732	95	56	166
10	**KW2000**	N_2	846	81	57	101

a) The solid residue contained the recovered catalyst and insoluble lignin portion remaining after the reaction; b) conversions took into account the 19.5 wt% of inorganic material (non-depolymerisable) present in the lignin starting material; c) pressure within the reactor after 6 h at 280 °C; d) the amount of catalyst added was 250 mg; "d-MoS_2" denoted delaminated MoS_2.

Overall, the conversion of lignin in the presence of MoS_2-based catalysts was high, with the delaminated material performing better than its bulk counterpart (entries 2 and 3). The presence of the alumina support, however, markedly reduced the efficiency of the catalyst under N_2 (entries 5–7), despite increasing the available surface areas of the catalysis (see Table 4.3). The origin of this inhibitory effect was not well understood and it seemed to affect the delaminated material more severely than it did the bulk material.

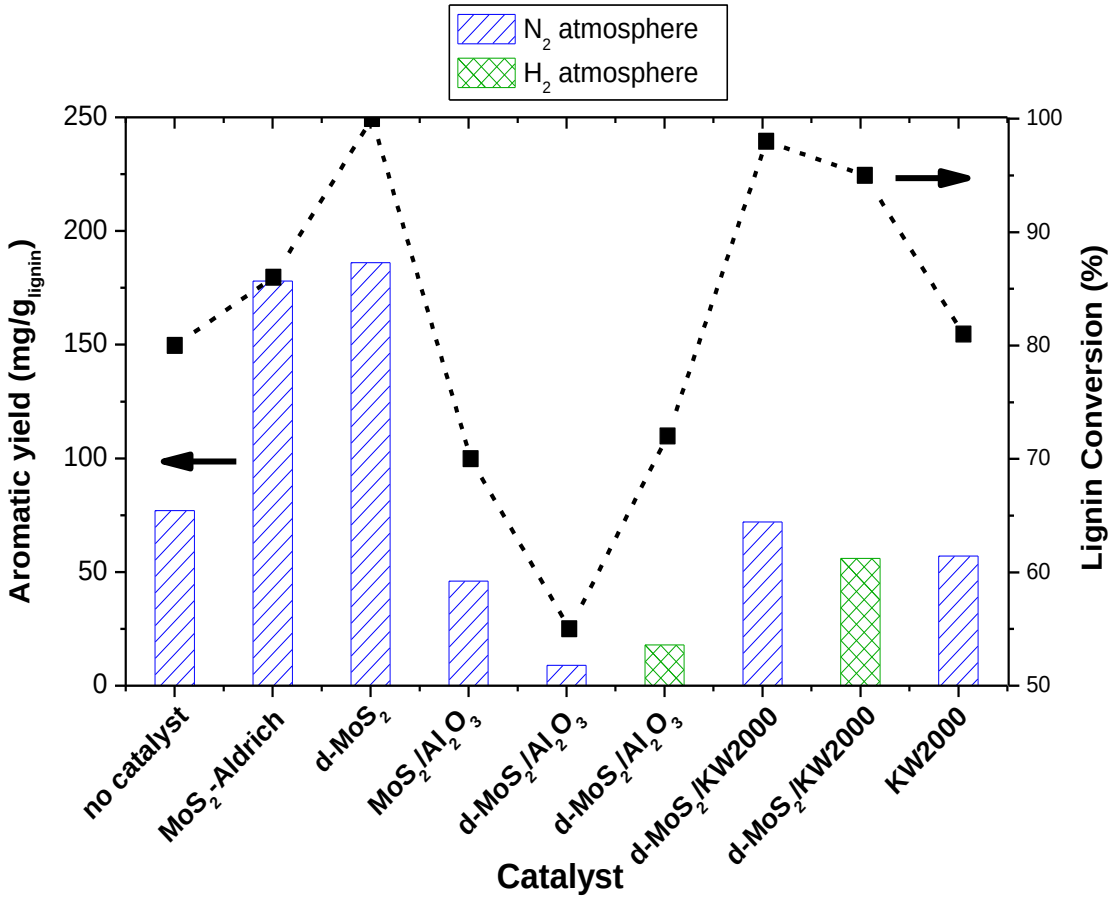

Figure 4.7. Lignin conversion and aromatic yields obtained from ethanolysis of Kraft lignin over different MoS_2-based catalysts. Arrows indicate the y-axis corresponding to the data set.

Running the depolymerisation under H_2 slightly improved the conversion, but it did not make up for the adverse effects of the alumina. Since the presence of a basic hydrotalcite KW2000 support did not result in a reduction of conversion for delaminated MoS_2, the inhibitory effect appeared to be due to the acidity of the alumina support. The KW2000 support was also tested as such in the catalytic depolymerisation of Kraft lignin. Compared to the control reaction, no change in the lignin conversion was observed (entries 1 & 10) while a small decrease in the aromatic yield was detected (from 77 to 57 mg/g_{lignin}). This behaviour was in line with recently reported results in the literature claiming that HT-based catalysts as such were not sufficiently active to cleave C–O and C–C bonds, neither in lignin nor in lignin model compounds. For example, the investigation of β-O-4 bond cleavage of 2-phenoxy-1-phenethanol (PE) proved that after 1 h of reaction at 270 °C, the conversion of the substrate was of only 28 and 23% when a Mg/Al-HT or a 5 wt% Ni/Al_2O_3 were used as catalysts, respectively. However, a 5 wt% Ni-doped HT afforded excellent results, with a quantitative conversion of PE. Similar results

were achieved using NaOH as the catalyst, thereby suggesting that a base-catalysed cleavage of PE was promoted by a synergistic effect between supported nickel and HT.[47]

The highest aromatic yields in the MoS_2 series (Table 4.4), resulted from the unsupported catalysts, with delaminated MoS_2 clearly outperforming its bulk counterpart. Aromatic yields overall were more moderate than those reported by Li and co-workers for other molybdenum-based catalysts.[17b] The final pressure observed at the end of the experiments (6 h at 280 °C), varied between 101 and 163 bar depending on the catalyst employed. Remarkable was the case of d-MoS_2/KW2000 (entry 8), where despite an almost quantitative conversion, only 72 mg of aromatic compounds per gram of lignin were quantified. In conjunction with the high final reaction pressure of 139 bar, these observations suggested that cracking of the solubilised intermediates occurred, as well as de-aromatisation.

These processes, which remove aromatics from the product stream, appear to operate without the need for external H_2 and, hence, the challenge for employing MoS_2-based catalysts is overcoming their inherent chemoselectivity, so as to suppress this unwanted dearomatisation activity whilst maintaining their high conversion ability.

4.2.2.2. Mo_2C-Series

The results of the Mo_2C-series of catalysts are shown in Table 4.5 and Figure 4.8. Compared to most of the MoS_2-based catalysts, Mo_2C and Mo_2C/Al_2O_3 afforded lower lignin conversions (entries 1 and 5). However, the combined yields of the quantified aromatic compounds were much improved over both the control reaction and the MoS_2-series. A slightly higher conversion of 72% was obtained for Mo_2C/KW2000, but it was still lower than that achieved with d-MoS_2/KW2000 (cfr. entries 8 and 7 of Table 4.4 and Table 4.5, respectively). However, the aromatic yield detected with Mo_2C/KW2000 was not satisfactory with respect to the other two Mo_2C-based catalysts. The final reaction pressures for the Mo_2C-series were consistently lower than those observed for the MoS_2-series (114 bar *vs* 130–163 bar). The only noteworthy variation occurred when the reaction was run under 20 bar of H_2, but the final pressure was of only 137 bar compared to 170 bar achieved with MoS_2.

Table 4.5. The amount of solid residue after the reaction at 280 °C, 6 h, over 0.5 g of Mo_2C-based catalysts with initial 1.3 bar of N_2 and 100 mL of ethanol. Lignin conversion, yields of the 11 quantified aromatic products and final reaction pressure at 280 °C.

Entry	Catalyst	Atmosphere	Solid residue[a] (mg)	Conversion[b] (%)	Aromatic yield (mg/g_{lignin})
1	**Mo_2C[c]**	N_2	645	64	425
2		H_2 (1.3 bar)	707	56	427
3		H_2 (3.5 bar)	661	62	339
4		H_2 (20 bar)	572	73	293
5	**Mo_2C/Al_2O_3**	N_2	951	68	419
6		H_2 (20 bar)	860	80	367
7	**Mo_2C/KW2000**	N_2	923	72	204
8	**α-MoC_{1-x}/AC[d]**	N_2 (300 °C)	813	85	232
9	**α-MoC_{1-x}/Cu-$MgAlO_z$[d]**	N_2 (280 °C)	1004	62	82
10	**α-MoC_{1-x}/Cu-$MgAlO_z$[d]**	N_2 (330 °C)	493	quantitative	575

a) The solid residue contains the recovered catalyst and insoluble lignin portion remaining after the reaction; b) conversions take into account the 19.5 wt% of inorganic material (non-depolymerisable) present in the lignin starting material; c) the amount of catalyst added was 160 mg; d) data from Li and co-workers.[17c]

In an attempt to improve the conversion of lignin additional experiments were performed involving the addition of H_2 to the reaction mixture. When unsupported Mo_2C was employed under a H_2 atmosphere (Table 4.5, entries 2–4), a general (slight) increase of the conversion, but also a decrease in the yield of aromatics, was noticed: the result was plausibly due to the onset of undesired hydrogenation pathways.

Results reported in Table 4.5 suggested how the ethanol employed as the solvent in this lignin hydrogenolysis protocol provided a sufficient amount of hydrogen for lignin hydrogenation to take place effectively in the presence of Mo_2C. As previously mentioned, studies reported by Hensen and co-workers demonstrated that ethanol was a suitable H_2-donating solvent in lignin hydrogenolysis protocols, since it decomposed to H_2 and acetaldehyde under these reaction conditions (280–300 °C).[11] The dehydrogenation of ethanol did not only provide H_2 for hydrogenation, but it also helped the selectivity of hydrogenolysis, leading to high aromatic yields, preventing the further hydrogenation to cycloalkanes.

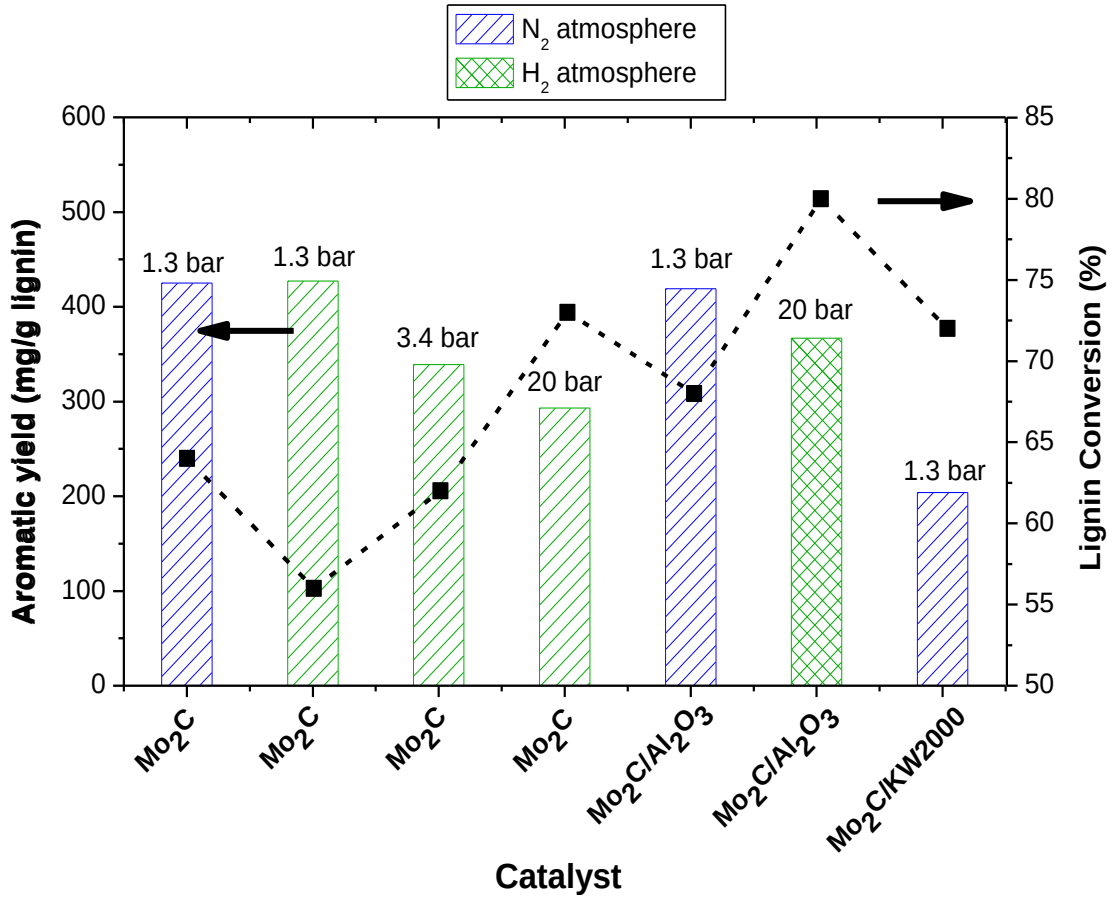

Figure 4.8. Lignin conversion and aromatic yields obtained from ethanolysis of Kraft lignin over Mo_2C-based catalysts. Arrows indicate the y-axis corresponding to the data set.

The use of alumina as a support produced the significant increase in the surface area of the catalyst from 6 to 103 m^2/g. Notwithstanding this, only a moderately positive effect on lignin conversion was observed with no substantial improvement on the yield of aromatics (Table 4.5, entries 1 and 5). When the initial atmosphere in the reactor was replaced with 20 bar of H_2, the aromatic yield dropped as it was observed also for the Mo_2C/Al_2O_3 (Table 4.5, entries 4 and 6).

To the best of our knowledge, these Mo_2C catalysts afford amongst the highest aromatic yields reported for molybdenum-catalysed depolymerisation of Kraft lignin at 280 °C. Table 4.5, entries 8–10 are included for comparison with data published by the Li group.[17b] It is not until their dual α-$MoC_{(1-x)}$/Cu-$MgAlO_z$ catalyst is used at 330 °C, that the yield of aromatics surpasses those produced by the Mo_2C catalysts in the current study.

The catalytic ethanolysis of Kraft lignin was also explored at a higher reaction temperature, under conditions similar to those reported by Li *et al*.[17b] In the presence of Mo_2C and Mo_2C/Al_2O_3, experiments carried out at 330 °C and 1.3 bar N_2 gave the results reported in

Table 4.6. A remarkable increase of both the conversion and the aromatic yield was achieved. The lignin conversion was improved from 64–68% at 280 °C, up to 95–96% at 330 °C (for Mo_2C and Mo_2C/Al_2O_3, respectively). The higher reaction temperature also affected also the aromatic yields, with improvements from 425–419 mg/g_{lignin} at 280 °C up to 446–506 mg/g_{lignin} at 330 °C.

Table 4.6. The amount of solid residue after the reaction at 330 °C, 6 h, over Mo_2C-based catalysts with initial 1.3 bar of N_2 and 100 mL of ethanol. Lignin conversion and yields of the quantified aromatic products.

Entry	Catalyst	Solid residue[a] (mg)	Conversion[b] (%)	Aromatic yield (mg/g_{lignin})
1	**Mo_2C[c]**	396	95	446
2	**Mo_2C /Al_2O_3**	729	96	506

a) The solid residue contained the recovered catalyst and insoluble lignin portion remaining after the reaction; b) conversions took into account the 19.5 wt% of inorganic material (non-depolymerisable) present in the lignin starting material; c) the amount of catalyst added was 160 mg.

4.2.2.3. Product Analysis and leaching of the metal

*Product*s.

GC/MS analyses allowed the identification of eleven aromatics as the major compounds in the product stream (Figure 4.9). These derivatives were quantified by using *o*-cresol as an external standard.

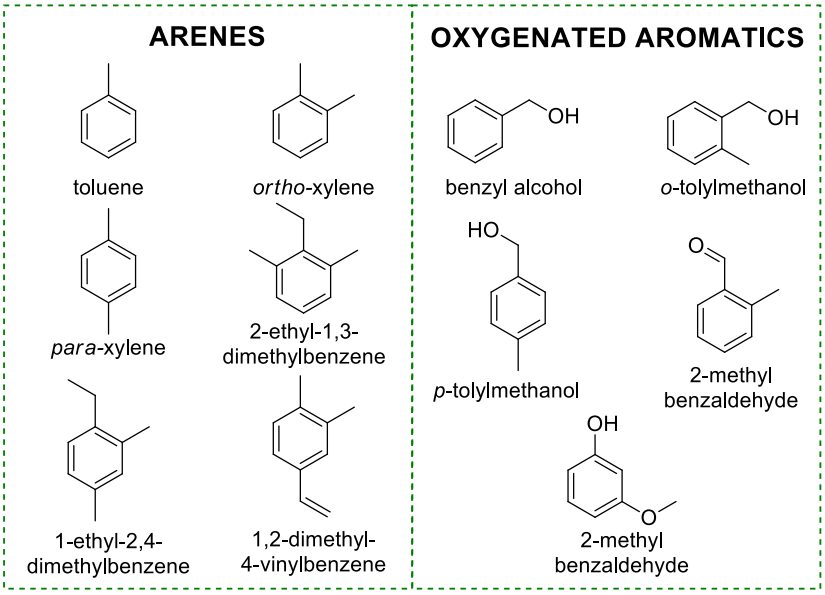

Figure 4.9. List of the 11 quantified aromatic compounds from Kraft lignin hydrogenolysis.

In addition to aromatics, aliphatic alcohols and esters were also present in the reaction mixture. Li and co-workers demonstrated that these products derived from lignin and from other reactions of ethanol under supercritical conditions.[17] These compounds, however, were not of interest for the present study and were not further considered.

The control reaction (without a catalyst) afforded the aromatic compounds used for quantification (Table 4.7, entry 1). These were arenes and mono-oxygenated aromatics, the latter class accounted for 61% of the total. Albeit in a very low yield, a phenolic product was also observed. Guaiacol and its derivatives (*e.g*. 4-methylguaiacol, 4-propylguaiacol, etc.) were instead absent in the product stream. Although this contrasted previously reported results,[17] a clear explanation could not be determined.

The use of unsupported Mo_2C favoured the formation of arene products, which accounted for more than 54% of the total (Table 4.7, entry 3). When Mo_2C/Al_2O_3 was used under N_2, the proportion of arenes decreased to 40% (Table 4.7, entry 7). With both Mo_2C and Mo_2C/Al_2O_3, the selectivity towards arene compounds was slightly improved under a H_2 atmosphere, resulting in an increased proportion of arenes with respect to mono-oxygenated aromatics (from 53% to 57% with Mo_2C and from 40% to 46% with Mo_2C/Al_2O_3). The same held true when MoS_2 was the catalyst, though only low-to-moderate yields of arenes were achieved (Table 4.7, entries 10–16).

Finally, a remarkable change in the product distribution was observed when the reaction was performed at 330 °C, in the presence of Mo_2C-based catalysts (Table 4.8). Aromatics were mostly arene derivatives, which were obtained with selectivities higher than 95% for both Mo_2C and Mo_2C/Al_2O_3. Among oxygenated compounds, 2-methyl benzaldehyde was the major derivative but was only observed in a 5% amount.

Table 4.7. Detailed yields of the quantified aromatic compounds (expressed in mg/g_{lignin}) from the ethanolysis of KL in the presence of Mo-based catalysts at 280 °C.

Entry	Catalyst	Pressure (atm)	ARENES						OXYGENATED AROMATICS				
				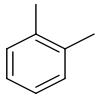	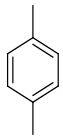	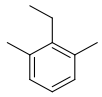	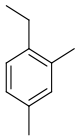	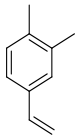	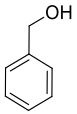	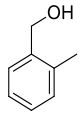	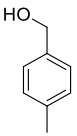		
1	**none**	N_2	2	11	8	2	4	3	8	15	6	13	5
2	**KW2000**	N_2	5	10	-	1	-	3	6	5	23	5	-
3	**Mo_2C**	N_2	47	91	42	10	22	16	35	42	33	87	-
4		1.3 bar H_2	52	98	39	8	20	16	31	34	34	95	-
5		3.4 bar H_2	45	91	34	8	18	15	21	25	10	71	-
6		20 bar H_2	40	67	30	6	14	12	41	27	23	34	-
7	**Mo_2C/Al_2O_3**	N_2	38	39	67	7	15	-	55	63	43	89	-
8		20 bar H_2	39	59	40	7	14	12	55	51	37	54	-
9	**Mo_2C/KW2000**	N_2	46	77	37	7	17	13	-	-	-	2	-
10	**MoS_2**	N_2	13	36	9	3	7	7	14	27	7	54	-
11	**d-MoS_2**	N_2	35	63	35	10	14	10	-	-	-	20	-
12	**MoS_2/Al_2O_3**	N_2	10	16	8	2	3		-	-	-	5	-
13	**d-MoS_2/Al_2O_3**	N_2	-	5	4	-	-	-	-	-	-	-	-
14		20 bar H_2	7	7	5	-	-	-	-	-	-	-	-
15	**d-MoS_2/KW2000**	N_2	18	28	17	3	3	3	-	-	-	-	-
16		20 bar H_2	17	20	14	3	3	-	-	-	-	-	-

Table 4.8. Yields of the quantified arene compounds (expressed in mg/g_{lignin}) from the ethanolysis of KL in the presence of Mo-based catalysts at 330 °C.

Entry	Catalyst	ARENES								
				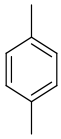		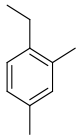	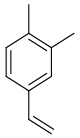	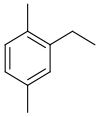	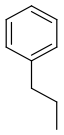	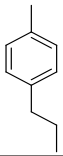
1	**Mo_2C**	128	135	66	15	28	22	7	12	12
2	**Mo_2C/Al_2O_3**	136	154	85	21	36	18	6	11	16

Leaching of the metal.

ICP analyses were performed on the final reaction mixtures to quantify the leaching of molybdenum and the stability of the catalyst (Analytical details are given in the experimental section). The percentage of leached metal varied between 0.04 and 0.38% for the investigated catalysts (Table 4.9). In general, the metal leaching was more conspicuous for the supported catalysts compared to the unsupported ones (cfr. Table 4.9, entries 7, 8, 10 and 11). This result could be partially rationalised by considering that the supported catalysts displayed a higher surface area (see Table 4.3), though the correlation was not strong. ICP analyses were also performed on lignin itself and on the reaction mixtures recovered at the end of both the blank (control) experiment and the reaction catalysed by the support KW2000 (Table 4.9, entries 1–3). It was noticed that the amount of molybdenum leached from the latter reactions (control and catalysed by the hydrotalcite: 27 µg and 31 µg, respectively) was higher than that from Kraft lignin (8 µg per g lignin). This led to the conclusion that molybdenum was plausibly released from the walls of the steel reactor (molybdenum metal in the Hastelloy C is approximately 16 wt%). Moreover, the conversion of lignin reported in Table 4.4 and Table 4.5 and the ICP data in Table 4.9, indicated that there was no correlation between the metal leaching in solution and the extent to which lignin was depolymerised. For example, the release of Mo from Mo_2C/Al_2O_3 was tripled compared to that from unsupported Mo_2C, even though conversions (68% and 60%) and yields of aromatics (425 and 419 mg/g lignin) were comparable between the two catalysts (Table 4.9, entries 10 & 11, and Table 4.7, entry 3 & 7,).

Table 4.9. Molybdenum ICP results from in Kraft lignin and catalysed depolymerisations.

Entry	Catalyst	[Mo] (ppb)	Mo in Reaction Supernatant (µg)	Leached Mo (wt%)
1	Kraft lignin	8[a]	n/a	n/a
2	no catalyst	134	27	0.02[b]
3	KW2000	154	31	0.02[b]
4	MoS_2	312	62	0.04
5	d-MoS_2	364	73	0.05
6	MoS_2/Al_2O_3	560	112	0.07
7	d-MoS_2/Al_2O_3	1232	246	0.16
8	d-MoS_2/KW2000	1944	389	0.26
9	Mo_2C	865	173	0.12
10	Mo_2C/Al_2O_3	2848	739	0.38
11	Mo_2C/KW2000	940	203	0.13

a) Concentration expressed in µg of molybdenum per 1 g of Kraft lignin;
b) Calculated on the same basis as if catalyst were present.

In the case of MoS_2-based systems, bulk and delaminated catalysts were not only robust and rather stable to leaching, but they also allowed for a high conversion (Table 4.4 and Figure 4.7). By contrast, the alumina-supported delaminated MoS_2 showed the highest release of metal and the poorest conversion of lignin among the tested sulfides.

As mentioned above, Li and co-workers proposed that a soluble Mo(V) species, derived from the heterogeneous catalyst, was responsible for catalysis in supercritical ethanol (see Scheme 4.1).[17b,17c] To check if a similar mechanism was also plausible for the catalysts used in this work, an additional experiment was carried out in which 1.0 g of lignin in 100 mL of ethanol was set to react at 280 °C for 6 h over unsupported Mo_2C (160 mg). The reaction took place under a N_2 pressure of 1.3 bar (at r.t.). The final mixture was carefully removed from the solid residue, which was washed several times with ethanol (100 mL). All liquids were combined and the mixture was analysed *via* GC/MS for the quantification of the aromatic monomers, which yielded a total of 425 mg/g_{lignin}. The solution was then concentrated to 100 mL under reduced pressure, resulting in a loss of the lighter aromatic compounds. This solution was therefore analysed to quantify the remaining aromatics (the final yield was 265 mg/g_{lignin}) and then used as the reaction medium, without any additional catalyst, in the presence of fresh Kraft lignin (1.0 g) for a second depolymerisation. The reaction was carried out under the same

reaction conditions (280 °C, 6 h, 1.3 bar N_2) using only the amount of Mo that was leached, as the catalyst. At the end of this second step, the reaction mixture was carefully removed from the solid, which was washed with EtOH (100 mL). Analysis of the combined liquids revealed that a total of 427 mg/g_{lignin} of aromatics was obtained. By comparing the yield of aromatic compounds contained in the initial mixture of this second step, it was possible to calculate the amount of aromatic compounds obtained thanks to the leached Mo in the reaction mixture:

$$A_{HC}=A_{II\text{-}step\text{-}fin}-A_{II\text{-}step\text{-}in} \qquad \text{Eq. (4.2)}$$

where A_{HC} are the aromatics from the "homogeneous catalysis" due to the leached Mo of the first depolymerisation step, $A_{II\text{-}step\text{-}fin}$ are the aromatics quantified at the end of the second depolymerisation step and $A_{II\text{-}step\text{-}in}$ are the amount of aromatics present in the reaction mixture at the beginning of the second depolymerisation step. Given:

$$A_{II\text{-}step\text{-}fin}=427 \text{ mg/g}_{lignin}$$

$$A_{II\text{-}step\text{-}in}=265 \text{ mg/g}_{lignin}$$

by applying the Eq.4.2, a total of 162 mg/g_{lignin} was obtained using the leached Mo. Although this value is higher than the one achieved from the control reaction without a catalyst (77 mg/g_{lignin}, Table 4.4, entry 1), it is still much lower compared to the one obtained in the presence of bulk Mo_2C (425 mg/g_{lignin}, Table 4.5, entry 1). Furthermore, the lignin conversion achieved in the second reaction was markedly lower than that of the first one (25% vs 64%). Although preliminary, these results along with ICP data suggested that MoS_2- and Mo_2C-based catalysts mostly operated as heterogeneous systems, and the postulated homogeneous catalysis probably occurs only to a limited extent.

The high activity of the orthorhombic Mo_2C used in the present work can also be explained in terms of work function. The value of this work function correlates to the energy barrier for electron transfer from the carbide surface to adsorbed substrates or hydrogen. Surfaces with lower work functions result in lower energy barriers and hence more efficient catalysis. In this particular case, a low work function will help facilitate the hydrogenolytic and hydrogenation steps. It has been reported that the orthorhombic Mo_2C is composed of different surfaces including the (100) and (011) surfaces, with work functions of 3.89 and 3.41 eV respectively.[48] In addition, much higher work functions of 5.00 and 5.27 eV were calculated for the (001) surface, depending on the terminal atom (C or Mo, respectively). The presence of the (100) and (011) surfaces, therefore, is expected to contribute the most to the catalytic activity. It

could be expected that increasing the exposed area of the surface with the lowest work function (*i.e.* 011) would enhance the efficiency of the catalyst for the hydrogenolysis of lignin. Furthermore, Liang and co-workers reported that in the hydrogenation of naphthalene to tetralin, Mo_2C performed better with a clean surface than when the surface was covered by excess carbon.[37] Therefore, the choice of the catalyst support for lignin ethanolysis may be crucial for developing a catalyst that is not poisoned by the build-up of organic material on the surface of the Mo_2C. Both of these points could represent interesting directions for future work.

4.3. Conclusions

Two series of sulfur-tolerant molybdenum-based catalysts were prepared and employed for the depolymerisation and upgrading of lignin in supercritical ethanol. The results were consistent with a heterogeneously catalysed path being the major avenue for conversion of solubilised lignin oligomers to low-molecular weight products. MoS_2-based catalysts worked synergistically with supercritical ethanol to efficiently depolymerise Kraft lignin into soluble species. Increasing the proportion of catalyst edge sites was beneficial for the catalytic activity and hence the use of a dopant at these edge sites could possibly overcome the inherent chemoselectivity of MoS_2 for hydrogenation, which led to relatively low yields of aromatic compounds. The use of Mo_2C and Mo_2C/Al_2O_3 as catalysts in the depolymerisation of Kraft lignin at 280 °C in supercritical ethanol as the hydrogen-donor solvent afforded high yields of arene products. Transfer hydrogenation from ethanol was a critical factor in ensuring efficient conversion of the substrate. Despite an increase in the conversion of lignin, the use of additional H_2 proved to be detrimental to the yield of aromatics due to the increased hydrogenation activity of the catalyst. Higher conversions of 95 % and aromatic yields up to 506 mg/g_{lignin} were obtained by performing the ethanolysis of Kraft lignin at 330 °C. Under these conditions, chemoselectivities as high as 95 % towards deoxygenated arene compounds were achieved with both Mo_2C and Mo_2C/Al_2O_3 catalysts. The role of the catalyst support in the depolymerisation process is still not well defined and further investigation on this aspect is certainly required. Also, studies on the interaction of both series of catalysts with the aromatic products under reaction conditions may suggest how to avoid further undesired hydrogenation reactions and which factors may suppress repolymerisation.

4.4. Experimental Section

4.4.1. Materials

Kraft lignin (catalogue number 471003), MoS_2 (catalogue number 234842), 2-methylbenzaldehyde, guaiacol, 4-methyl benzyl alcohol, 2-methyl benzyl alcohol, 1-ethyl-3-methtl benzene were purchased from Sigma Aldrich. Alumina (Catalox® SBa-150) was provided by Sasol. Hydrotalcite KW2000 was supplied from Kyowa Industries. Toluene and benzyl alcohol were purchased from Merck. *o*-Xylene was purchased from Alfa Aesar, *p*-xylene was purchased from Fluka, 2,4-dimethyl styrene was purchased from Enamine, 1-ethyl-2,4-dimethyl benzene was purchased from Fluorochem. All chemicals were used as received.

4.4.2. Synthesis and characterisation of catalysts.

All supported catalysts were prepared in order to reach a nominal molybdenum loading of 30 wt%. Ammonium tetrathiomolybdate was prepared from sodium molybdite hydrate and ammonium sulfide according to the procedure of Reid and co-workers.[38] MoS_2/Al_2O_3 was synthesised by co-grinding $(NH_4)_2MoS_4$ (1.75 g) with Al_2O_3 (1.50 g), followed by heat treatment under H_2/N_2 (1:7; *ca* 80 mL/min): 2 °C/min until 100 °C, held for 1 h, then 10 °C/min until 300 °C, held for 0.5 h. The sample was cooled to room temperature under N_2, affording a grey-black powder.

Delaminated MoS_2 was synthesised following a procedure reported by Maschmeyer and co-workers.[18b] $(NH_4)_2MoS_4$ (0.75 g) was dissolved in 15 g of dried $[C_4C_1im][OTf]$ at 40 °C. This solution was heated at 300 °C under 10 %v/v H_2 in N_2, at a flow rate of 10 mL/min for 2 h, with stirring. The black product was precipitated with 90 mL ethanol and further washed with ethanol (5 × 80 mL), followed by water (2 × 50 mL), acetone (2 × 50 mL) and hexane (2 × 50 mL). The powder was then dried under vacuum at room temperature.

Delaminated MoS_2/Al_2O_3 and delaminated MoS_2/KW2000 were synthesised by dissolving $(NH_4)_2MoS_4$ (0.872 g) in 16 g of dried $[C_4C_1im][OTf]$. Dried alumina (750 mg) or KW2000 (750 mg) were then added to the reaction mixture, and the suspension was heated at 300 °C under 10 %v/v H_2 in N_2, at a flow rate of 10 mL/min for 2 h, with stirring. The resulting black solid was precipitated and washed as described above.

Mo_2C was synthesised according to the procedures described by Liang and co-workers,[37] on a 3.0 g scale. The melamine–[Mo] coordination polymer prepared in the first step was subjected

to heat treatment under flowing H_2 in Ar (70 ml/min; 2:5 ratio) at 650 °C for 1 h, affording 754 mg of catalyst as a hard, blue-grey ceramic.

Mo_2C/Al_2O_3 The dried, isolated melamine–[Mo] coordination polymer (1.52 g) was co-ground with alumina (1.20 g) and heat treated in the same manner as described above, affording 1.76 g of black powder.

PXRD was performed using a PANalytical X'Pert PRO MPD X-ray diffractometer with Cu Kα (λ= 1.5419 Å) as the irradiation source. The scanning was conducted between 2ϑ values of 5 and 90° with a scanning rate of 2°/min. Surface areas of the samples were measured by nitrogen sorption analysis on a Micrometrics Accelerated Surface Area & Porosimetry System (ASAP) 2020 instrument. The powdered sample was outgassed at 90 °C and 13 µbar overnight. Nitrogen adsorption and desorption isotherms were collected at 77 K, and the surface areas were calculated by using the BET model in the framework of the Micrometrics software. High resolution transmission electron microscopy was carried out on a JEOL-TEM-2100 operated at 200 kV. Each sample was prepared by dispersing the powdered sample in ethanol and drop-casting onto a 200 mesh copper grid coated with holey carbon.

4.4.3. Catalysis

Batch reactions were carried out in a 250 mL Parr reactor system (reactor code 4875; Hastelloy C), equipped with a mechanical stirrer, cooling loop and thermowell. The reactor was charged with powdered lignin (1.0 g), catalyst (0.5 g for supported catalysts, 0.25 g for unsupported MoS2, 0.16 g for unsupported Mo2C), and absolute ethanol (100 mL). The reactor was sealed, purged with nitrogen thrice (pressurisation to 50 bar, followed by release) and finally the desired pressure of nitrogen or hydrogen gas was introduced. The reaction was heated to 280 °C over a period of approximately 1.5 h with stirring, held at 280 °C for up to 6 h, then cooled to room temperature. The cooling step was assisted by use of a water bath. The reactor was depressurised, unsealed and the mixture filtered at the pump. The residue was washed with ethanol several times and dried at 80 °C overnight. *o*-Cresol (20 µL) was added and the volume of the filtrate was adjusted to 200 mL volumetrically with ethanol.

4.4.4. Reaction analysis

Compound identification by GC/MS was performed on a Shimadzu GC/MS-QP2010 equipped with Rtx-5MS 0.25 µm × 30 m × 0.25 mm column. The temperature program had an isothermal

period of 3 min at 50 °C, followed by a heating ramp of 10 °C min-1 to 330 °C, followed by an isothermal period of 10 min. Compounds were identified by comparing the EI-MS spectra with those in the system's database (NIST05). Of the prominent aromatic species identified, 12 were quantified using calibration curves of authentic samples. *o*-Cresol was used as an external standard. The calculated yield is reported as mg of analyte per g lignin.

4.4.4.1. ICP analysis

Inductively coupled plasma (ICP) analysis were performed on a Perkin Elmer Nexion 300XX Inductively Coupled Plasma Mass Spectrometer (ICP-MS). The reaction mixture was filtered and centrifuged for the removal of any trace of solid, the residue washed with ethanol several times and made up to 200 mL volumetrically. A 1.0 mL aliquot was digested with 2.0 mL of 70%w/v nitric acid at 80 °C and diluted with Milli-Q H2O to give 100 mL volumetrically. A final five-fold dilution was performed before sample injection. ICP analysis of Kraft lignin was performed by digesting 0.105 g of Kraft lignin with 2.0 mL of 70%w/v nitric acid at 80 °C and diluting with Milli-Q H2O to give 100 mL volumetrically. A final × 100 dilution was performed before sample injection.

4.5. Bibliography

[1] C. O. Tuck, E. Perez, I. T. Horvath, R. A. Sheldon, M. Poliakoff, *Science,* 2012, **337**, 695–699.

[2] R. Rinaldi, R. Jastrzebski, M. T. Clough, J. Ralph, M. Kennema, P. C. A. Bruijnincx, B. M. Weckhuysen, *Angew. Chem. Int. Ed.,* 2016, **55**, 8164–8215.

[3] F. Leusch, M. Bartkow. A short primer on benzene, toluene, ethylbenzene and xylenes (BTEX) in the environment and in hydraulic fracturing fluids. *Smart Water Res Centre*, 2010, **189**, 1-8.

[4] M. Ragnar, G. Henriksson, M. E. Lindström, M. Wimby, J.vBlechschmidt, S. Heinemann, *Ullmann's Encyclopedia of Industrial Chemistry*, Wiley-VCH, Weinheim, 2014.

[5] N. Mahmood, Z. Yuan, J. Schmidt, C. Xu, *Bioresource Technol.,* 2013, **139**, 13–20.

[6] J. Zakzeski, P. C. A. Bruijnincx, A. L. Jongerius, B. M. Weckhuysen, *Chem. Rev.,* 2010, **110**, 3552–3599.

[7] A. Oasmaa, R. Alén, D. Meier, *Bioresource technology*, 1993, **45**, 189–194.

[8] K. H. Kim, R. C. Brown, M. Kieffer, X. Bai, *Energy Fuels,* 2014, **28**, 6429–6437.

[9] C. Li, X. Zhao, A. Wang, G. W. Huber, T. Zhang, *Chem Rev*, 2015, **115**, 11559–11624.

[10] T. D. Matson, K. Barta, A. V. Iretskii, P. C. Ford, *J. Am. Chem. Soc.,* 2011, **133**, 14090–14097.

[11] X. Huang, T. I. Korányi, M. D. Boot, E. J. M. Hensen, *ChemSusChem,* 2014, **7**, 2276–2288.

[12] a) M. P. Pandey, C. S. Kim, *Chem. Eng. Technol.,* 2011, **34**, 29–41; b) A. J. Ragauskas, G. T. Beckham, M. J. Biddy, R. Chandra, F. Chen, M. F. Davis, B. H. Davison, R. A. Dixon, P. Gilna, M. Keller, P. Langan, A. K. Naskar, J. N. Saddler, T. J. Tschaplinski, G. A. Tuskan, C. E. Wyman, *Science,* 2014, **344**, 1246843.

[13] a) Q. Song, F. Wang, J. Xu, *Chem. Commun.,* 2012, **48**, 7019–7022; b) Q. Song, F. Wang, J. Cai, Y. Wang, J. Zhang, W. Yu, J. Xu, *Energy Environ. Sci.,* 2013, **6**, 994–1007; c) P. Ferrini, R. Rinaldi, *Angew. Chem. Int. Ed.,* 2014, **53**, 8634–8639.

[14] M. Grilc, B. Likozar, J. Levec, *Appl. Catal. B,* 2014, **150–151**, 275–287.

[15] G. Veryasov, M. Grilc, B. Likozar, A. Jesih, *Catal. Commun.,* 2014, **46**, 183–186.

[16] H. Topsøe, B. S. Clausen, F. E. Massoth, in *Hydrotreating Catalysis Science and Technology, Vol. 11*, Springer, Berlin, 1996.

[17] a) R. Ma, W. Hao, X. Ma, Y. Tian, Y. Li, *Angew. Chem. Int. Ed.,* 2014, **53**, 7310–7315; b) X. Ma, R. Ma, W. Hao, M. Chen, F. Yan, K. Cui, Y. Tian, Y. Li, *ACS Catal.,* 2015, **5**, 4803–4813; c) F. Yan, R. Ma, X. Ma, K. Cui, M. Chen, Y. Li, *Appl. Catal. B,* 2017, **202**, 305–313.

[18] a) V. W.-h. Lau, A. F. Masters, A. M. Bond, T. Maschmeyer, *ChemCatChem* **2011**, *3*, 1739–1742; b) V. W.-h. Lau, A. F. Masters, A. M. Bond, T. Maschmeyer, *Chem. Eur. J.,* 2012, **18**, 8230–8239.

[19] Z. Ma, J. Yu, S. Dai, *Adv. Mater*. 2010, **22**, 261–285.

[20] C. P. Fredlake, J. M. Crosthwaite, D. G. Hert, S. N. V. K. Aki, J. F. J. Brennecke, *Chem. Eng. Data,* 2004, **49**, 954–964.

[21] S. Sowmiah, V. Srinivasadesikan, M. C. Tseng, Y. H. Chu, *Molecules,* 2009, **14**, 3780–3813.

[22] (a) J. L. Brito, M. Ilija, P. Hernández, *Thermochim. Acta*, 1995, **256**, 325–338; (b) H. W. Wang, P. Skeldon, G. E. Thompson, *J. Mater. Sci*., 1998, **33**, 3079–3083.

[23] (a) R. B. Levy, M. Boudart, *Science,* 1973, **181**, 547−549; (b) S. T. Oyama, *Catal. Today*, 1992, **15**, 179–200.

[24] (a) J. G. Chen, *Chem. Rev*., 1996, **96**, 1447–1498; (b) J. G. Chen, J. Eng, S. P. Kelty, *Catal. Today*, 1998, **43**,147−158.

[25] H. Fang, J. Du, C. Tian, J. Zheng, X. Duan, L. Ye, Y. Yuan, *Chem. Commun.*, 2017, **53**, 10295–10298.

[26] D. R. Stellwagen, J. H. Bitter, *Green Chem.*, 2015, **17**, 582–593.

[27] J. A. Rodriguez, J. Dvorak, T. Jirsak, *J. Phys. Chem. B*., 2000, **104**, 11515–11521.

[28] M.L. Xiang, D.B. Li, H.C. Xiao, J.L. Zhang, W.H. Li, B. Zhong, Y.H. Sun, *Catal. Today*, 2008, **131**, 489–495.

[29] J.A. Schaidle, A.C. Lausche, L.T. Thompson, *J. Catal*., 2010, **272**, 235–245.

[30] R. Barthos, F. Solymosi, *J. Catal*., 2007, **249**, 289–299.

[31] V. Sundaramurthy, A.K. Dalai, J. Adjaye, *Appl. Catal. B*, 2006, **68**, 38–48.

[32] J. S. Choi, G. Bugli, G. D. Mariadassou, *J. Catal*., 2000, **193**, 238–247.

[33] S. Li, W. B. Kim, J. S. Lee, *Chem. Mater*., 1998, **10**, 1853–1862.

[34] J. A. Nelson, M. J. Wagner, *Chem. Mater*., 2002, **14**, 4460–4463.

[35] C. H. Liang, P. L. Ying, C. Li, *Chem.Mater.,* 2002, **14**, 3148–3151.

[36] S. R. Vallance, S. Kingman, D. H. Gregory, *Adv. Mater*., 2007, **19**, 138–142.

[37] M. Pang, X. Wang, W. Xia, M. Muhler, C. Liang, *Ind. Eng. Chem. Res.,* 2013, **52**, 4564–4571.

[38] R. S. Reid, R. J. Clark, E. K. Quagraine, *Can. J. Chem.* 2007, **85**, 1083–1089.

[39] J. S. Kruger, N. S. Cleveland, S. Zhang, R. Katahira, B. A. Black, G. M. Chupka, T. Lammens, P. G. Hamilton, M. J. Biddy, G. T. Beckham, *ACS Catal.*, 2016, **6**, 1316–1328.

[40] L. Cattelan, A. Perosa, P. Riello, T. Maschmeyer, M. Selva, *ChemSusChem,* 2017, **10**, 1571–1583.

[41] H. McMurdie, M. Morris, E. Evans, B. Paretzkin, W. Wong-Ng, C. Hubbard, *Powder Diffraction,* 1986, **1**, 269.

[42] H. Lux, A. Ignatowicz, *Chemische Berichte,* 1968, **101**, 809–814.

[43] a) J. Dubois, T. Epicier, C. Esnouf, G. FantozziG, P.Convert, *Acta Metall.,* 1988, **36**, 1891–1901; b) T. Epicier, J. Dubois, C. Esnouf, G. Fantozzi, P. Convert, *Acta Metall.,* 1988, **36**, 1903–1921.

[44] J. Haines, J. M. Léger, C. Chateau, J. E. Lowther, *J. Phys.: Condens. Matter,* 2001, **13**, 2447–2454.

[45] E. Parthe, V. Sadagopan, *Acta Cryst.,* 1963, **16**, 202–205.

[46] T. P. St.Clair, S. T. Oyama, D. F. Cox, S. Otani, Y. Ishizawa, R.-L. Lo, K. Fukui, Y. Iwasawa, *Surf. Sci.,* 1999, **426**, 187–198.

[47] M. R. Sturgeon, M. H. O'Brien, P. N. Ciesielski, R. Katahira, J. S. Kruger, S. C. Chmely, J. Hamlin, K. Lawrence, G. B. Hunsinger, T. D. Foust, R. M. Baldwin, M. J. Biddy, G. T. Beckham, *Green Chem*., 2014, **16**, 824–835.

[48] J. R. d. S. Politi, F. Viñes, J. A. Rodriguez, F. Illas, *Phys. Chem. Chem. Phys.,* 2013, **15**, 12617–12625.

5. Extractive Denitrogenation of Fuel Oils with Ionic Liquids: A Systematic Study

5.1. Introduction

As mentioned in Chapter 1, the use of biofuels is included among the priorities of government policies aimed at limiting climate change through the decarbonisation of the global energy system.[1] Specifically, measures for the "carbon abandonment" are focussed on zero-carbon energy sources and fuels, such as renewables and biofuels. The latter, by itself, is expected to reduce CO_2 emissions by at least 35% over the next 20 years.[2]

In this respect, lignocellulosic biomass has emerged as a sustainable energy source for both second-generation biofuels and, more recently, third-generation biofuels from algae, with bio-ethanol, bio-methane, bio-oil and bio-hydrogen attracting a great deal of attention.

Natural feedstocks, however, contain components that may cause major issues for the utilisation of the desired bio-derivatives. Among them, proteins are recognised because they break down into various nitrogen-bearing organics. Specifically, the nitrogenated aromatics (N-bearing compounds) commonly found in (bio-)fuel oils can be divided into two groups: neutral (*e.g.* pyrroles, indoles, carbazoles) or basic (*e.g.* pyridines, quinolones, acridines). A selection of these is shown in Table 5.1.[3]

For example, the bio-crude from HTL of lignocellulosic materials usually has nitrogen levels of roughly 2%, which is derived from the deamination of amino acids from proteins.[4] Higher levels of nitrogen, up to 10%, have been reported for bio-crudes produced from garbage, wastewater sludge and algae, due to the protein content of these feedstocks.[5,6] Such a high nitrogen content results in a bio-crude that is unsuitable for refining, from neither an economical nor a technical point of view, due to the high energy demand required to convert this bio-crude to a high specification liquid fuel.

Therefore, several strategies have been devised and implemented to reduce nitrogen, sulfur and ash content in a series of biomass feedstocks. As a recent example, Cole *et al*. optimised a protocol to produce a high quality renewable biofuel from macroalgae, which included

growing macroalgae using a nutrient starvation method, a continuous co-solvent hydrothermal liquefaction producing a non-polar bio-crude containing <1 wt% N and a final hydrogenation step to obtain a paraffinic mixture with only 227 ppm of nitrogen.[7,8,9]

Table 5.1. Common nitrogenated aromatics found in fuel oils.[10]

Basic nitrogen compounds		Non-basic nitrogen compounds	
Structure	**Name/Properties**	**Structure**	**Name/Properties**
	Pyridine MW: 79.10 g mol^{-1} Density: 0.98 g mL^{-1} Boiling point: 115 °C	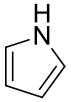	Pyrrole MW: 67.09 g mol^{-1} Density: 0.97 g mL^{-1} Boiling point: 129 °C
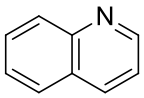	Quinoline MW: 129.16 g mol^{-1} Density: 1.09 g mL^{-1} Boiling point: 237 °C	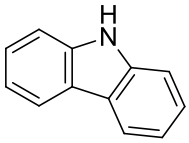	Carbazole MW: 167.21 g mol^{-1} Density: 1.30 g mL^{-1} Boiling point: 354 °C
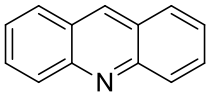	Acridine MW: 179.22 g mol^{-1}	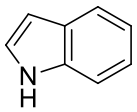	Indole MW: 117.15 g mol^{-1} Density: 1.17 g mL^{-1} Boiling point: 253 °C
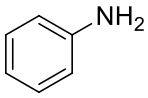	Aniline MW: 93.13 g mol^{-1} Density: 1.02 g mL^{-1} Boiling point: 184 °C	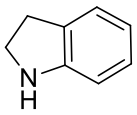	Indoline MW: 119.17 g mol^{-1} Density: 1.06 g mL^{-1} Boiling point: 220 °C

Despite the impressive improvement in the composition of the feedstocks for the production of bio-crude, the removal of nitrogen-containing compounds (N-compounds) - *for all type of fuel oils* - should be maximised, since these hinder the hydrodesulfurisation (HDS) process[11,12] and are partially responsible for the pollution resulting from the production of NO_x gases during the combustion process.[11,13] This is why recent legislation by numerous governments, in both developed and developing countries, is focussed on the introduction of corrective measures to lower the N-content in fuel oils. To cite the model case, in the USA the allowed threshold for the N-content present in diesel fuels has been significantly reduced from <70 ppm to <1 ppm over only seven years, from 2003 to 2010.[14]

The conventional method for eliminating nitrogenated derivatives in fuel oils is the hydrodenitrogenation (HDN) process,[15,16] which is based on the conversion of organonitrogen compounds into ammonia (Equation 5.1).[17] This reaction is usually completed in the presence of a sulfided Co(Ni)/Mo(W)-Al_2O_3 catalyst.

$$C_aH_bN + c\ H_2 \rightarrow NH_3 + C_aH_d \qquad \text{Eq. (5.1)}$$

Cyclic and non-cyclic alkyl amines undergo HDN under milder reaction temperatures (260–350 °C), while N-containing ring of unsaturated heterocycles (*e.g.* pyridines, quinolones, pyrroles and indoles) need to be saturated before C-N bond cleavage to occur, as shown for indole in Scheme 5.1. Therefore, these molecules require harsher conditions and larger quantities of H_2 (340–380°C and 80–120 bar H_2) than the saturated compounds.[18]

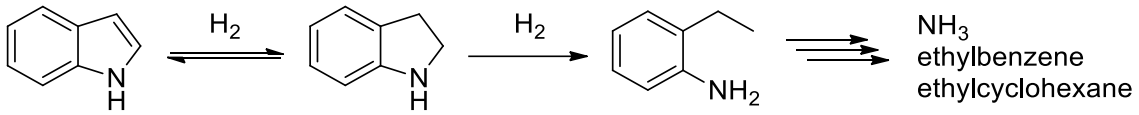

Scheme 5.1. HDN pathway for indole.[17]

Overall, the process is not only energy intensive, but it also generates large amounts of CO_2 and it is hardly applicable to the (recalcitrant) heterocycles seen above, which negatively impact on the catalyst performance.[19]

Unfortunately, as for fossil fuels, in bio-crude oils most N atoms generally form part of aromatic rings. Therefore, in order to meet the stringent government fuel specifications, (bio-)crude oils with higher N content will require either improved reactors (so as to operate at higher H_2 pressures or longer contact times), higher performing catalysts and/or the application of new and alternative technologies.[20]

To overcome some of the shortcomings of the HDN technology other techniques for the removal of N-compounds have been studies. These techniques include adsorptive denitrogenation (ADN),[21] extraction denitrogenation (EDN), oxidation denitrogenation (ODN) and biodenitrogenation (BDN).[22] Of these, EDN is one of the more attractive methods and, due to the specific interest for this Thesis work, conditions for EDN are described in this section. EDN does not require the use of either a catalyst or hydrogen pressures, and it can be performed at ambient temperature. In this method, the fuel is purified by either a batch or continuous flow extraction in which a solvent, which is immiscible with the fuel, allows for the selective removal of the undesired nitrogenated compounds.[23] Under such conditions, the structure composition of both the fuel and the separated nitrogenated compounds does not change. Solvents for EDN are usually chosen for their reusability and recyclability, with non-volatile green solvents preferred over conventional liquids (*i.e*. pyrimidinone, polyalkylene glycol, imidazolidinone, etc.).[24]

In this respect, ionic liquids (ILs) have also been conceived as suitable candidates for EDN because of their low vapour pressure and their capability to provide a non-aqueous alternative

for polar/non-polar two-phase systems.[25] Moreover, they can be efficiently grafted to solid supports, forming heterogeneous supported ionic liquids (SILPs) that can be confined in a reactor and used in continuous-flow systems.[23]

It has been demonstrated that several ILs were efficient extractants of N-compounds:[22] specifically, the dicyanamide-based IL $[C_4C_1im][N(CN)_2]$ proved a good solvent to extract pyridine from a model oil, consisting of a mixture of toluene and hexane,[26] to the extent that the nitrogen content could be reduced from about 500 ppm to 130-205 ppm in a single extraction at ambient temperature. An analogous dicyanamide-exchanged ionic liquid, 1-butyl-3,5-dimethyl-2-pentylpyridinium dicyanamide $[C_4{}^3C_1{}^5C_1{}^2C_5py][N(CN)_2]$, was also found to be an efficient extractant of pyrrole and pyridine.[27] Yu and co-workers reported the use of both Lewis acidic ILs (*e.g.* $[C_4C_1im]Cl/ZnCl_2$) and Brønsted acidic ILs ($[C_4C_1im]HSO_4$) to remove pyridine and carbazole from a mixture of octane and toluene.[19] Significantly, all of the ILs studied achieved N-extraction efficiencies for pyridine of >90% with only a single extraction.[19] However, notwithstanding the several investigations on this subject, a systematic study on the influence of structural and functional properties of different cations and anions of ILs is still lacking. This observation inspired part of this Thesis work in which room-temperature (r.t.) ionic liquids based on common cations, *i.e.* imidazolium, pyrrolidinium and pyridinium, and common anions, such as bis(trifluoromethane)sulfonimide (NTf_2^-) and trifluoromethanesulfonate (OTf^-), were investigated for their extraction capability of two archetypical N-compounds, *i.e.* pyridine and indole, from a model fuel oil consisting of *n*-decane and toluene.[28] The structures of the typical ILs used in this study are shown in Figure 5.1.

Particularly, the effect of chain length of the 1-alkyl-3-methylimidazolium cation on the extraction efficiency was explored. It was noticed that a careful manipulation of the identity and the size of ions allowed for the IL-solute interactions to be enhanced, while at the same time decreased the undesirable solubility of the hydrocarbon mixture, mimicking the fuel oil, in the IL phase.

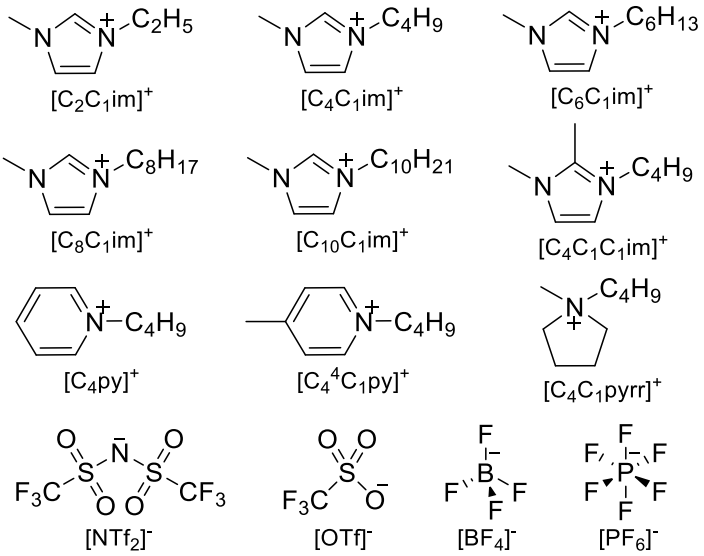

Figure 5.1. Cations and anions of the ionic liquids employed in this study.

5.2. Results and Discussion

Fuel oils, such as diesel, consist of mixtures of aliphatic and aromatic hydrocarbons. Saturated hydrocarbons (*i.e.* linear, branched and cyclic alkanes) are the predominant species in the mixtures and comprise approximately 80–90% of total fuel oils.[29] On the other hand, aromatic hydrocarbons, mostly alkylbenzenes, constitute about 10–20 % of fuel oils.[29] In this investigation a model oil, consisting of a binary mixture of *n*-decane (85 wt%, representative of saturated hydrocarbons) and toluene (15 wt%, representative of aromatic hydrocarbons), was employed. Pyridine and indole (Table 5.1 and Figure 5.2) were selected as the representative Lewis basic and neutral N-compounds, respectively.

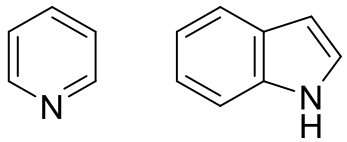

Figure 5.2. N-compounds used in this study: pyridine (left) and indole (right).

5.2.1. Extraction efficiency with [NTf_2] exchanged ILs: the dependence on the cation structure

In the preliminary extraction experiments, a mixture of IL (3.43 mmol) and solution of pyridine or indole ($5.00 \cdot 10^{-3}$ mol·L^{-1}) in the model oil (*n*-decane and toluene, 2 mL in total) was stirred at 25 °C for different time intervals of 10, 20 and 30 min. Four commercially available ILs exchanged with bistriflimide anion were used: specifically, 1-butyl-3-methylimidazolium bis(trifluoromethane)sulfonimide ([C_4C_1im][NTf_2]), 1-butyl-1-methylpyrrolidinium bis(trifluoromethane)sulfonimide ([C_4C_1pyrr][NTf_2]), 1-butylpyridinium bis(trifluoromethane)sulfonimide ([C_4py][NTf_2]) and 1-butyl-2,3-dimethylimidazolium bis(trifluoromethane)sulfonimide ([$C_4C_1C_1$im][NTf_2]). These ILs were selected because not only were they widely studied model compounds, but they also bore similar sized cations with butyl chains. (Table 5.2).[30]

Table 5.2. Ionic volumes for ions employed in this study.[31]

Ion	Ionic volume/nm^3	Ion	Ionic volume/nm^3	Ion	Ionic volume/nm^3
$[C_2C_1im]^+$	0.156	$[C_4C_1C_1im]^+$	0.229	$[NTf_2]^-$	0.232
$[C_4C_1im]^+$	0.196	$[C_4py]^+$	0.198	$[OTf]^-$	0.131
$[C_6C_1im]^+$	0.242	$[C_4{}^4C_1py]^+$	0.240[a]	$[PF_6]^-$	0.109
$[C_8C_1im]^+$	0.288	$[C_4C_1pyrr]^+$	0.221	$[BF_4]^-$	0.073
$[C_{10}C_1im]^+$	0.346[a]				

[a] Literature values were unavailable. The shown ionic volume was derived by extrapolation from published values with the addition of $–CH_2$ and $–CH_3$ groups, each of which occupy 0.029 nm^3 and 0.042 nm^3, respectively.[32]

Most of the available data in the literature reported the results of denitrogenation extractions by using a weight ratio of IL/oil. In this study, however, in order to investigate the intrinsic capabilities of ILs for the extraction of N-compounds, data were compared by considering not the weight but the molar amount of each of the tested ILs instead. The N-extraction efficiencies were therefore reported in terms of mol%, and were calculated by equation (5.2).

$$\text{N-extraction efficiency (mol\%)} = \left(1 - \frac{\text{N-compound in oil phase}_{\text{final}}\ \text{(mol)}}{\text{N-compound in oil phase}_{\text{initial}}\ \text{(mol)}}\right) \times 100\ \% \qquad \text{(Eq. 5.2)}$$

The molar amount of any N-compound in the oil phase after each extraction experiment (final) was calculated with equation (5.3), in which the concentrations of N-compounds were determined by HPLC measurements.

$$\text{Ncompound in oil phase}_{\text{final}}\ (\text{mol}) = [\text{N-compound in oil phase}]\ (\text{mol.dm}^{-3}) \times \text{volume of oil phase}_{\text{final}}\ (\text{dm}^3) \qquad \text{(Eq. 5.3)}$$

The final volume of oil phase was calculated by equation (5.4), in which the oil content in IL phases was determined by quantitative ^{1}H NMR.

$$\text{Volume of oil phase}_{\text{final}}\ (\text{dm}^3) = 0.002 - \text{oil content in IL phase} \qquad \text{(Eq. 5.4)}$$

Where 0.002 is the initial volume (in dm^3) of the oil phase (*n*-decane, 85 wt%, and toluene, 15 wt%). Equation (5.4) gives a good estimation of the final volume of oil phase since the investigated ILs have negligible solubility in the oil phase, as confirmed by HPLC and ^{1}H NMR measurements.

Extraction results are reported in Table 5.3 and Table 5.4 for pyridine and indole, respectively.

Table 5.3. Decrease in pyridine concentration of oil phase *vs* time (temperature: 25 °C; 3.43 mmol of IL/2 mL model oil).

	Decrease in pyridine concentration of oil phase (M/M %)		
	10 minutes	**20 minutes**	**30 minutes**
[C_4C_1im][NTf_2]	75.1	75.8	75.9
[C_4C_1pyrr][NTf_2]	71.1	70.7	71.4
[C_4py][NTf_2]	71.8	72.7	71.0
[$C_4C_1C_1$im][NTf_2]	73.9	73.6	72.7

Table 5.4. Decrease in indole concentration of oil phase *vs* time (temperature: 25 °C; 3.43 mmol of IL/2 mL model oil).

	Decrease in indole concentration of oil phase (M/M %)		
	10 minutes	**20 minutes**	**30 minutes**
[C_4C_1im][NTf_2]	97.5	97.5	97.5
[C_4C_1pyrr][NTf_2]	97.9	98.0	98.0
[C_4py][NTf_2]	98.3	98.3	98.3
[$C_4C_1C_1$im][NTf_2]	98.0	98.1	97.8

It was noticed that extraction equilibria for both pyridine and indole could be reached within 10 min of stirring. However, for a more accurate evaluation of the extraction performance of

the different ILs, experiments carried out at 20 min were duplicated. In the repeat runs, values of the decrease of the extract concentration in the oil phase differed by less than 1% for pyridine and less than 0.4% for indole from one test to another.

The N-extraction efficiencies were then calculated by eq. 5.2. Results are plotted in Figure 5.3. A relatively small variation of the extraction efficiency was observed for pyridine: values ranged from 71.8 to 76.8 mol%, with $[C_4C_1im][NTf_2]$ showing the best extraction efficiency.

An even smaller difference was observed for indole with almost quantitative extraction efficiencies varying in the narrow interval of 97.5–98.3 mol%. In this case, all the tested ILs proved excellent extractants.

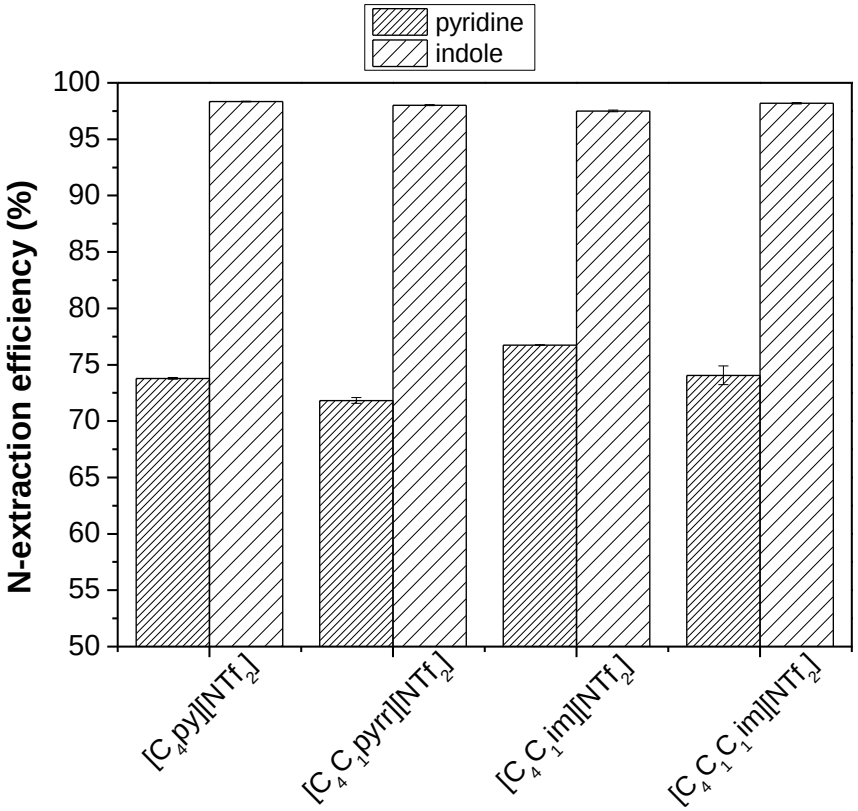

Figure 5.3. N-extraction efficiencies of pyridine and indole with $[NTf_2]^-$ ionic liquids of different classes of cations (temperature: 25 °C; 3.43 mmol of IL/2 mL model oil; extraction time: 20 min).

To further investigate the effect of cation size of ILs on the N-extraction efficiency, a series of ILs with the formula $[C_nC_1im][NTf_2]$ (n = 2, 6, 8, 10), $[C_4C_1C_1im][NTf_2]$, and $[C_4C_1py][NTf_2]$ were synthesised and their extraction capacities measured.

Extraction experiments were carried out under the same conditions previously described for Table 5.3 and Table 5.4, and Figure 5.3. Also in this case, the extraction equilibria for both pyridine and indole were reached within 10 min of stirring, but for a more accurate evaluation,

tests were prolonged up to 20 min (details are shown in Tables 7.3 and 7.4 reported in the Appendix section of this Thesis).

Results on the N-extraction efficiency are illustrated in Table 5.5. For the sake of completeness, the table also includes the data reported in Figure 5.3 for $[C_4C_1pyrr][NTf_2]$, $[C_4py][NTf_2]$, $[C_4C_1C_1im][NTf_2]$ and $[C_4C_1im][NTf_2]$.

Table 5.5. N-extraction efficiencies of pyridine and indole with different $[NTf_2]^-$ ILs (temperature: 25 °C; 3.43 mmol of IL/2 mL model oil; extraction time: 20 min).

Ionic liquid	Pyridine-extraction efficiency (mol/mol %)	Decrease in pyridine concentration of oil phase (M/M %)	Indole-extraction efficiency (mol/mol %)	Decrease in indole concentration of oil phase (M/M %)
$[C_2C_1im][NTf_2]$	70.7 ± 0.3	69.6 ± 0.4	97.2 ± 0.1	97.2 ± 0.1
$[C_4C_1im][NTf_2]$	76.8 ± 0.01	75.8 ± 0.02	97.5 ± 0.09	97.5 ± 0.03
$[C_6C_1im][NTf_2]$	78.7 ± 0.1	77.0 ± 0.2	97.9 ± 0.08	97.8 ± 0.09
$[C_8C_1im][NTf_2]$	80.6 ± 0.08	78.1 ± 0.1	98.2 ± 0.2	98.1 ± 0.1
$[C_{10}C_1im][NTf_2]$	84.7 ± 0.3	81.4 ± 0.3	98.1 ± 0.02	97.7 ± 0.03
$[C_4C_1C_1im][NTf_2]$	74.1 ± 0.8	73.6 ± 0.4	98.2 ± 0.06	98.1 ± 0.06
$[C_4py][NTf_2]$	73.8 ± 0.08	72.7 ± 0.06	98.3 ± 0.03	98.3 ± 0.03
$[C_4{}^4C_1py][NTf_2]$	79.6 ± 0.2	78.4 ± 0.2	98.8 ± 0.001	98.8 ± 0.003
$[C_4C_1pyrr][NTf_2]$	71.8 ± 0.3	70.7 ± 0.2	98.0 ± 0.06	98.0 ± 0.06

For the $[C_nC_1im][NTf_2]$ series, the pyridine-extraction efficiency increased with respect to the cation volume. Figure 5.4 (top) clearly highlights this result.

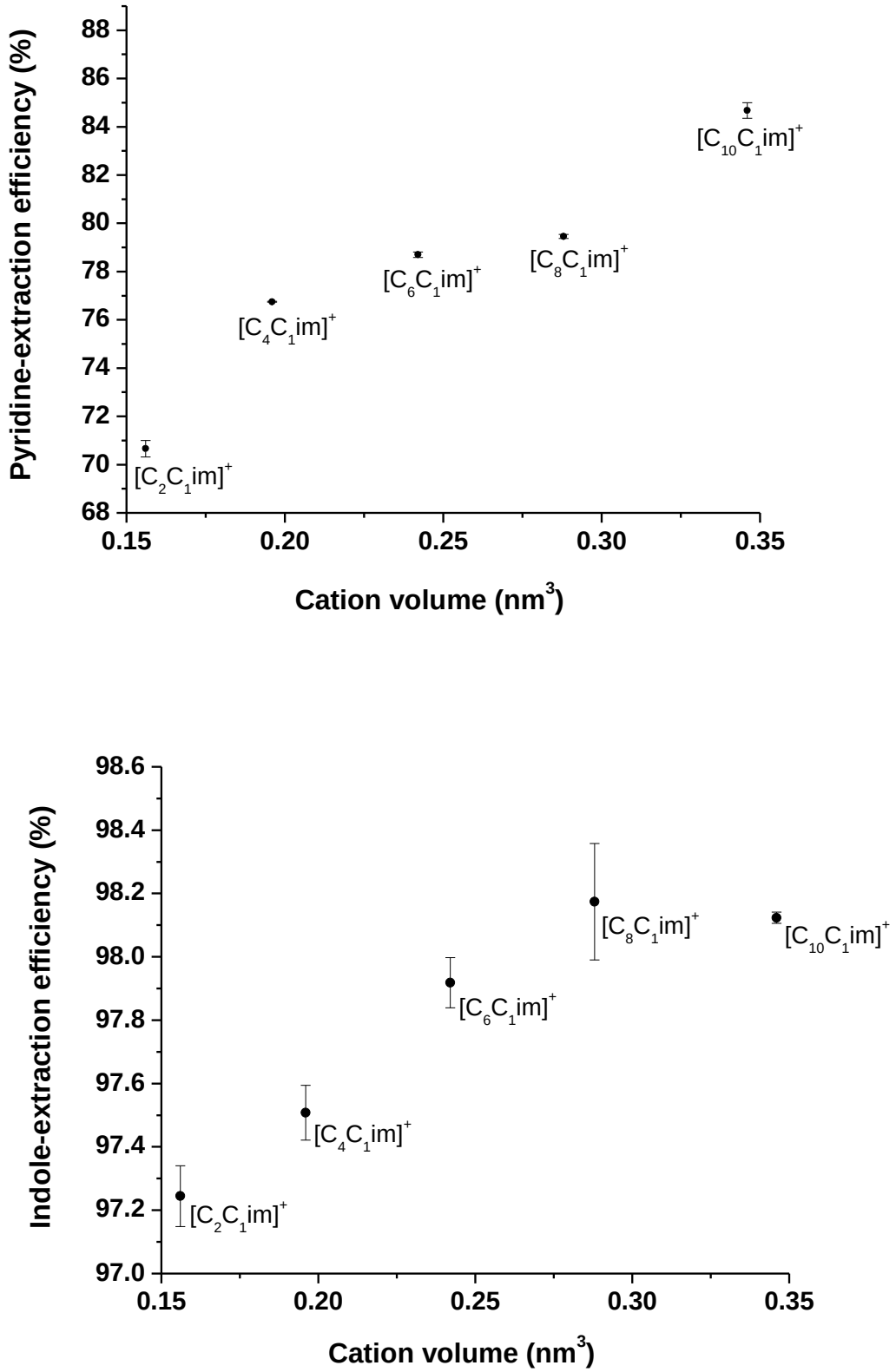

Figure 5.4. Pyridine (above) and indole (below)-extraction efficiencies with respect to cation volume of different $[C_nC_1im][NTf_2]$ ionic liquids (temperature: 25 °C; 3.43 mmol of ionic liquid/2 mL model oil; extraction time: 20 min).

Extraction of pyridine was also carried out with 1-butyl-2,3-dimethylimidazolium bis(trifluoromethane)sulfonimide [$C_4C_1C_1$im][NTf_2], in which the C2-position was methylated. In this case, the extraction efficiency was slightly lower (74.1 mol%) than that achieved with [C_4C_1im][NTf_2] (76.8 mol%), even though [$C_4C_1C_1$im]$^+$ was larger in volume (Table 5.2). This result suggests that the C2-proton of the imidazolium ring could possibly play a role in the extraction of the basic pyridine through hydrogen bonding interactions.

In line with this consideration, the Kamlet-Taft α values for the cations of the investigated ILs were examined. The (α) parameter is a measure of the hydrogen bond donation capability of cations of each salt. It was noticed that the H-bond donor strengths of [C_4py][NTf_2] and [C_4C_1pyrr][NTf_2] (α=0.54 and 0.43, respectively[33,34]) were lower than that of [C_4C_1im][NTf_2] (α=0.64[33], 0.61[34]), thereby indicating that the C4- and C5-protons on the imidazolium ring could also participate in hydrogen bonding, but that they were not as "acidic" as the C2-proton of C_4C_1im$^+$.[35] This was further confirmed by [$C_4C_1C_1$im][NTf_2] that displayed an even lower α of 0.38:[34] this salt was clearly a considerably weaker hydrogen bond donor than was [C_4C_1im][NTf_2].

The behaviour of pyridinium-based ILs was also affected by the size of cations. For example, the slightly larger [$C_4{}^4C_1$py][NTf_2] was a better extractant of pyridine than [C_4py][NTf_2] (see Table 5.5): the corresponding extraction efficiencies were 79.6 and 73.8 mol%, respectively. A similar tendency was already observed in the case of desulfurisation, where the extraction of tiophene from heptane was improved by increasing the number of alkyl groups, as substituents on the pyridinium ring, of the ILs used as extractants.[36]

The extraction capability for indole also increased with respect to the cation volume for the [$C_nC_1$im][NTf_2] series, until a plateau was reached for n=8–10 (Figure 5.4, bottom). This trend was noted also for the pyridinium series: [$C_4{}^4C_1$py][NTf_2] was a slightly better extractant of indole than the smaller [C_4py][NTf_2] (98.8 and 98.3 mol%, respectively). However, contrary to the case of pyridine, the efficiency for the extraction of indole was slightly higher in the presence of [$C_4C_1C_1$im][NTf_2] than with [C_4C_1im][NTf_2] (98.2 and 97.5 mol %, respectively).

Overall, bis(trifluoromethane)sulfonamide ILs based on common cations were good extractants of N-compounds from the model oil, and, within the same class of cations, the extraction efficiencies generally increased with the cation volume. The results were consistent with the fact that bulky cations offered a larger surface area for absorption through van der Waals' interactions.

5.2.2. Anion dependence with common cation ($[C_4C_1im]^+$)

The effect of different anions on the N-extraction capability was investigated by using $[C_4C_1im]$-based salts exchanged with four different anions: specifically, the performance of 1-butyl-3-methylimidazolium trifluoromethanesulfonate ($[C_4C_1im][OTf]$), 1-butyl-3-methylimidazolium hexafluorophosphate ($[C_4C_1im][PF_6]$) and 1-butyl-3-methylimidazolium tetrafluoroborate ($[C_4C_1im][BF_4]$) were compared to that of ($[C_4C_1im][NTf_2]$).

Extraction experiments were carried out according to the same conditions previously reported for Table 5.5. Significant differences were observed for the extraction of pyridine by the different salts. Results are described in Figure 5.5.

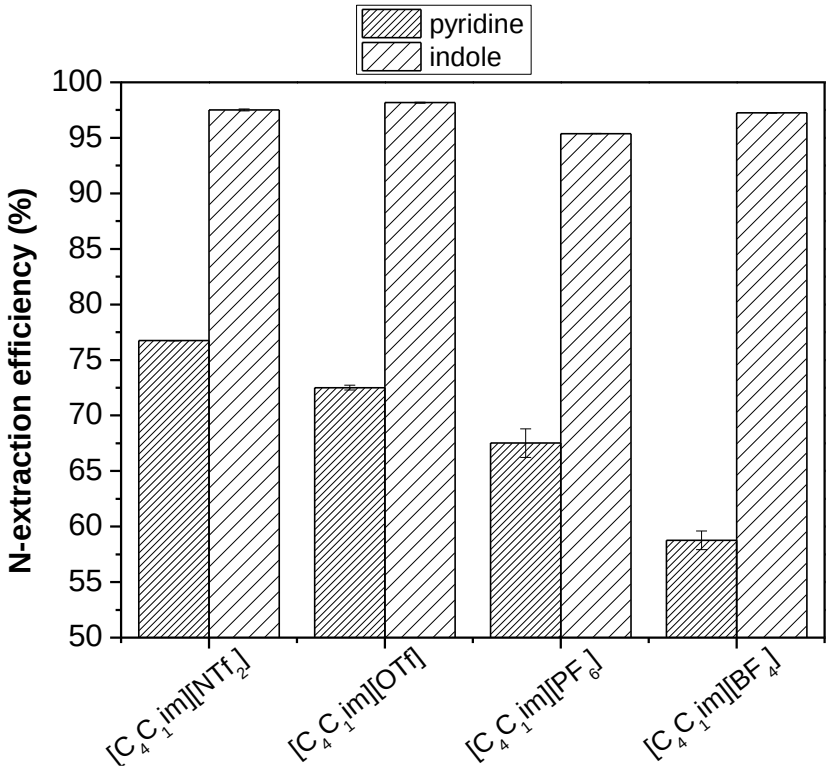

Figure 5.5. N-extraction efficiencies of pyridine and indole with $[C_4C_1im]^+$ IL of different anions (temperature: 25 °C; 3.43 mmol of IL/2 mL model oil; extraction time: 20 min).

The efficiency in the extraction of pyridine clearly followed the order $[C_4C_1im][NTf_2]$ > $[C_4C_1im][OTf]$ > $[C_4C_1im][PF_6]$ > $[C_4C_1im][BF_4]$: the corresponding values were 76.8, 72.5, 67.5 and 58.8 mol%, respectively. Contrary to the previously described effects of the cations, the analysis of Kamlet-Taft parameters did not show any relationship between the extraction capability (of pyridine) and the hydrogen bonding ability of the different anions. Nor could the results be explained by the difference in the calculated interaction energies between the imidazolium ring and the anions, which followed the order $[BF_4]^-$ > $[OTf]^-$ > $[NTf_2]^-$ ~ $[PF_6]^-$.[37]

However, the pyridine extraction efficiency for these ILs correlated with the ionic volume of the anions (Table 5.2), $[NTf_2]^-$ being the largest and $[BF_4]^-$ being the smallest. Therefore, as for cations, the size of the anions strongly affected the extraction power.

Again, the results were consistent with the fact that bulky anions offered a large surface area for absorption through van der Waals' interactions.

The extraction efficiency for the case of indole followed the order $[C_4C_1im][OTf]$ > $[C_4C_1im][NTf_2]$ > $[C_4C_1im][BF_4]$ > $[C_4C_1im][PF_6]$. The corresponding values were 98.2, 97.5, 97.2 and 95.4 mol%, respectively, with a trend that could not be rationalised by the size effect alone. The unexpectedly high efficiency of $[C_4C_1im][OTf]$ and $[C_4C_1im][BF_4]$ might perhaps be explained by the ability of the anions to undergo relatively strong hydrogen bonding with the NH group of indole, which is known to be a hydrogen bond donor.[38,39] This was consistent with the fact that the Kamlet Taft values of both $[C_4C_1im][OTf]$ and $[C_4C_1im][BF_4]$ (β=0.49 and 0.37, respectively) are higher than those of $[C_4C_1im][NTf_2]$ and $[C_4C_1im][PF_6]$ (β = 0.24 and 0.19, respectively).[34] Overall, the indole extraction efficiency was plausibly dependent on both the size and hydrogen bond basicity of the anions.

5.2.3. Mutual solubility

The investigation of the mutual solubility of ILs and the model oil was an important aspect because if ILs were (even sparingly) soluble in fuel oils, both a loss of extractants and a contamination of the fuel oil occurred. This would clearly impact on process costs.

Many denitrogenation and desulfurisation studies reported that pure ILs were generally insoluble in either model oils or actual fuels at ambient temperature.[19,40,41,42,43] As mentioned before, this behaviour was confirmed by all the ILs investigated in this work, which were not soluble in the model oil comprised of *n*-decane and toluene. However, a problem could arise from the partial dissolution of the oil in the IL phase during the extractions.[19,40-45]

Albeit that previous (denitrogenation or desulfurisation) studies described the use of gravimetric methods[26,44,45] and GC analyses[46] to evaluate the solubility of oil in ILs, in this work, the same parameter (oil-in-IL solubility) was determined by ^{1}H NMR (Figure 5.6). The advantage of using NMR quantification over other methods (mostly gravimetry) was that the solubility of individual components (*i.e. n*-decane and toluene) of the oil in the IL could be determined directly.

Results are summarised in Table 5.6. It was noted that the solubility of oil components in ILs was largely dependent on the volume of the cation and the anion: in general, an ionic liquid with a larger cation/anion dissolved a larger amount of oil due to the larger surface area for absorption through van der Waals' interactions. Moreover, toluene was extracted to a significantly larger extent than *n*-decane. This was in line with previous investigations on denitrogenation and desulfurisation processes, which reported ILs as far more selective extractants of aromatics than aliphatic hydrocarbons. ILs could separate even simple aromatics such as benzene from alkanes.[47] Both cation-π and CH-π interactions were invoked to explain the behaviour.[48,49]

It should be finally noted that less than 1% of *n*-decane was dissolved by $[C_6C_1im][NTf_2]$, $[C_8C_1im][NTf_2]$ and $[C_{10}C_1im][NTf_2]$ (Table 5.6). However, the solubility of *n*-decane in $[C_nC_1im][NTf_2]$ dramatically increased from n = 4 (0.5 mol%) to 10 (14 mol%). This result confirmed the prediction of Chen and co-workers,[50] who pointed out how for ILs, the shorter the length of alkyl chains of cations, the weaker the van der Waals' energies, which lowers the solvent ability.

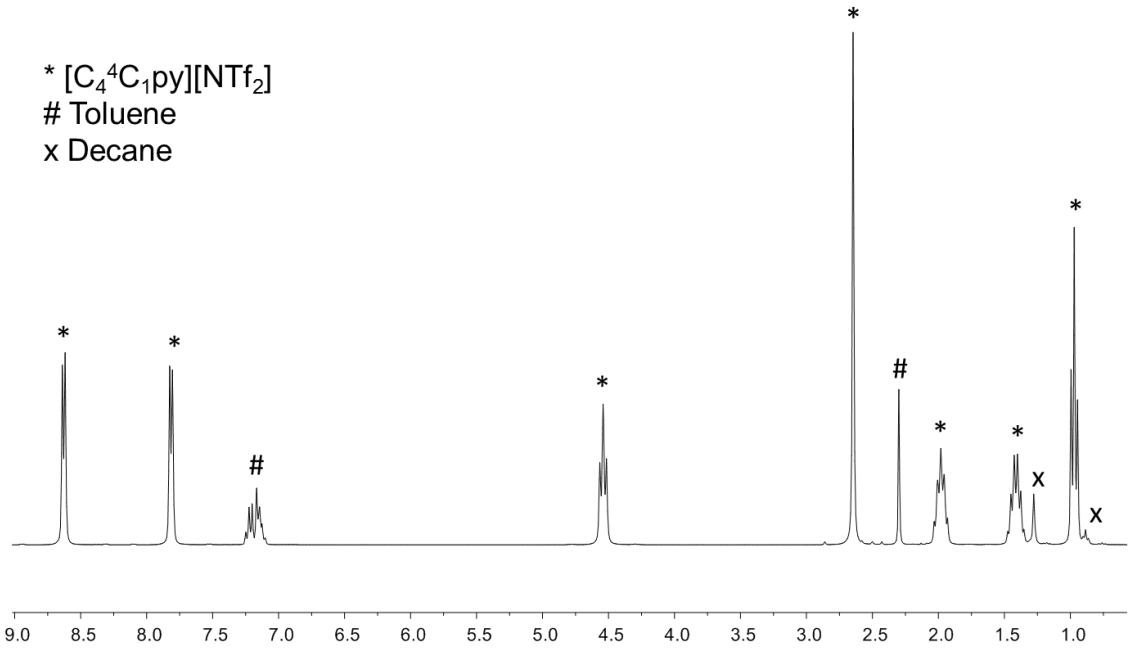

Figure 5.6. ^{1}H NMR of IL phase after N-extraction.

Table 5.6. Solubility of oil contents in different ILs after N-extractions, quantified by ^{1}H-NMR. (temperature: 25 °C; 3.43 mmol of IL/2 mL model oil; extraction time: 20 min).

Ionic liquid	Toluene in IL phase (mmol)	*n*-decane in IL phase (mmol)
$[C_4C_1im][NTf_2]$	0.58 ± 0.04	0.046 ± 0.002
$[C_4C_1im][OTf]$	0.35 ± 0.02	0.017 ± 0.001
$[C_4C_1im][PF_6]$	0.26 ± 0.02	0.010 ± 0.001
$[C_4C_1im][BF_4]$	0.20 ± 0.03	0.008 ± 0.001
$[C_4C_1C_1im][NTf_2]$	0.57 ± 0.02	0.043 ± 0.002
$[C_2C_1im][NTf_2]$	0.47 ± 0.00	0.022 ± 0.001
$[C_6C_1im][NTf_2]$	0.81 ± 0.01	0.26 ± 0.01
$[C_8C_1im][NTf_2]$	0.95 ± 0.04	0.61 ± 0.03
$[C_{10}C_1im][NTf_2]$	0.93 ± 0.01	1.23 ± 0.02
$[C_4C_1pyrr][NTf_2]$	0.49 ± 0.02	0.047 ± 0.002
$[C_4py][NTf_2]$	0.57 ± 0.01	0.027 ± 0.001
$[C_4{}^4C_1py][NTf_2]$	0.77 ± 0.02	0.071 ± 0.003

5.3. Conclusions

This investigation was aimed at determining whether a correlation existed between the structure of common room-temperature ionic liquids, including imidazolium-, pyrrolium- and pyridinium-based compounds, and the ability of such compounds in the extraction of pyridine and indole from model oils. In this respect, it was noticed that a pivotal role was played by the size of both the cation and the anion of the ILs. Extraction efficiencies for pyridine were found to correlate positively with the ionic volume of the cations (within the same class) and the anions. The same held true for the extraction of toluene, which was one of the components of the model oil used in this study.

However, under comparable conditions, it was also observed that the extraction of indole was consistently better than that of pyridine. This result could plausibly be ascribed to the different acid-base properties of the two compounds; though, this aspect is still controversial. For example, Dupont and co-workers noted that the efficiency for the extraction of nitrogenated aromatics (from oils) by $[C_4C_1im][NTf_2]$, was improved by an increase in the pK_a of N-heterocycles.[49] They argued that this was due to a strong hydrogen bonding between

N(heteroaromatic) and H(imidazolium) atoms. Such a trend, however, was opposite to that observed in the present study, since indole (pK_a -3.6) has a lower pK_a than pyridine (pK_a 5.2).[51] Reasons for these discrepancies are not clear, but one hypothesis is that the extra aromatic ring of indole (with respect to pyridine) might provide a larger volume for the contact between the extractants (ILs) and the solute, thereby favouring cation-π and CH-π interactions.
Moreover, the use of an extractant with strong hydrogen bond donor capacity was favoured in the case of basic pyridine, while for indole, a good hydrogen bond acceptor was a better choice.

5.4. Experimental Section

5.4.1. Materials

n-Decane (Fluka), toluene (Merck), 1-methylimidazole (Aldrich), 1-methylpyrrolidine (Aldrich), pyridine (Ajax), 1,2-dimethylimidazole (Aldrich), 4-picoline (Aldrich), 1-bromoethane (BDH), 1-bromobutane (Merck), 1-bromohexane (Merck), 1-bromooctane (Merck), 1-bromodecane (Merck), lithium bis(trifluoromethane)sulfonimide (IoLiTec), sodium hexafluorophosphate (Aldrich), sodium tetrafluoroborate (Sigma-Aldrich), 1-butyl-3-methylimidazolium trifluoromethanesulfonate (Aldrich), indole (Alfa Aesar) were used as obtained.

5.4.2. Synthesis of Ionic Liquids

Quaternary ammonium bromide salts [$C_nC_1$im]Br (n= 2, 4, 6, 8, 10), [C_4C_1pyrr]Br, [C_4py]Br, [$C_4C_1C_1$im]Br and [$C_4{}^4C_1$py]Br were synthesised by adapting a method already reported by Burrell *et al*..[52] Bromoalkane (0.16 mol) was heated at 30 °C with the desired amine (0.16 mol) under nitrogen for 24 h. The products were then washed with diethyl ether (3 x 10 mL). Subsequently, solid products were recrystallised from a minimum amount of acetonitrile and filtered. The solid was then dried *in vacuo* to yield the desired quaternary ammonium bromide salts.
[$C_nC_1$im][NTf_2], [C_4C_1pyrr][NTf_2], [C_4py][NTf_2], [$C_4C_1C_1$im][NTf_2] and [$C_4{}^4C_1$py][NTf_2] were synthesised with the corresponding quaternary ammonium bromide salts using a procedure similar to that reported by Weber *et al.*.[32] The relevant ammonium bromide salt (91 mmol) and lithium bis(trifluoromethane)sulfonimide (96 mmol) were separately dissolved in distilled water (200 mL total) and then combined, resulting in the formation of a separate liquid phase.

To this solution was added dichloromethane (200 mL) and the organic phase collected and washed successively with water until no halide could be detected by concentrated aqueous silver nitrate. Removal of solvent *in vacuo* afforded the bis(trifluoromethane)sulfonamide IL product.

The synthesis of $[C_4C_1im][BF_4]$ and $[C_4C_1im][PF_6]$ was carried out by adapting a procedure reported by Zhao *et al.*[53] $[C_4C_1im]Br$ (69 mmol) and sodium tetrafluoroborate or sodium hexafluorophosphate (76 mmol) were stirred in acetone (500 mL) for 24 h at room temperature. The resulting white solid was separated by filtration and the solvent removed *in vacuo*. Then the mixture was redissolved in dichloromethane and purified through neutral alumina. The dichloromethane solution was washed successively with water until no bromide could be detected (assay by aqueous silver nitrate). Removal of solvent *in vacuo* afforded the $[C_4C_1im][BF_4]$ or $[C_4C_1im][PF_6]$ IL product. All of the ILs were analysed with ^{1}H and ^{19}F NMR before use and found to be >99 % pure. Spectra are reported in the Appendix of this Thesis work.

5.4.3. Extractive Denitrogenation

The model oil used in this study was a mixture comprised of *n*-decane (85 wt%) and toluene (15 wt%). To this mixture, pyridine and indole were added in order to achieve a concentration of $5.00 \cdot 10^{-3}$ mol·L^{-1} for both the nitrogenated aromatics. In a typical experiment, 3.43 mmol of IL (pre-dried *in vacuo*) and 2 mL of the model oil were placed in a 20 mL test tube and magnetically stirred at 1000 rpm at 25 °C for a determined time, followed by equilibration for 5 min without stirring. The oil phase was removed by a pipette, taking care to not disturb the phase boundary. A sample (1 mL) of the oil phase was placed in a vial with 0.1 mL of external standard (anisole, $1.66 \cdot 10^{-2}$ mol·L^{-1} for the quantification of pyridine; guaiacol, $1.66 \cdot 10^{-2}$ mol·L^{-1} for the quantification of indole) and filtered on a PTFE cartridge.

5.4.4. Analysis of the N-content

Analyses were performed on a LC-CTO-20A (Shimadzu) liquid chromatograph equipped with a reversed phase Luna C18 column (150 x 2.00 mm; 5 µm) and a UV detector. The external standard condition for pyridine and indole were set at 225 nm. The mobile phase for quantification of both N-compounds was 60 % acetonitrile in water (v/v) with a flow rate of 0.8 mL·min^{-1}. Triplicate injections were performed for each sample.

5.4.5. Mutual solubility analysis

The solubility of toluene and *n*-decane in ILs were quantified by ^{1}H NMR analysis. NMR spectra were collected using a Bruker 300 MHz instrument at 300 K after 4 scans. ^{1}H NMR spectra were obtained using a 90° flip angle with a recycle delay (D1) of 20 seconds externally locked to DMSO-d_6. The ILs signals were employed as standards. As examples, the 1H NMR of $[C_4{}^4C_1py][NTf_2]$ after N-extraction is reported in Figure 5.6.

5.5. Bibliography

[1] C. A. Green. 'Fair and ambitious' climate agreement is not nearly enough: Paris 2015 take heed!. Environ. Res. Lett., 2015, 10.

[2] Y.C. Sharma, V. Singh, *Renew. Sustain. Energy. Rev*., 2017, **67**, 72–88.

[3] M. Hosseinpour, A. Golzary, M. Saber, K. Yoshikawa, *Fuel*, 2017, **206**, 628–637.

[4] A. A. Peterson, F. Vogel, R. P. Lachance, M. Fröling, M. J. Antal, J. W. Tester, J.W., *Energy Environ. Sci.,* 2008, **1**, 32–65.

[5] T. Minowa, M. Murakami, Y. Dote, T. Ogi, S. Y. Yokoyama, *Biomass Bioenergy*, 1995, **8**, 117–120.

[6] J. Ramirez, R. Brown, T. Rainey, *Energies*, 2015, **8**, 6765–6794.

[7] N. Neveux, A. K. Yuen, C. Jazrawi, M. Magnusson, B. S. Haynes, A. F. Masters, A. Montoya, N. A. Paul, T. Maschmeyer, R. de Nys, *Bioresource technology*, 2014, **155**, 334–341.

[8] N. Neveux, A. K. L. Yuen, C. Jazrawi, Y. He, M. Magnusson, B. S. Haynes, A. F. Masters, A. Montoya, N. A. Paul, T. Maschmeyer, *Algal Res*., 2014, **6**, 22–31.

[9] A. Cole, Y. Dinburg, B. S. Haynes, Y. He, M. Herskowitz, C. Jazrawi, M. Landau, X. Liang, M. Magnusson, T. Maschmeyer, A. F. Masters, N. Meiri, N. Neveux, R. de Nys, N. Paul, M. Rabaev, R. Vidruk-Nehemya, A. K. L. Yuen, *Energy Environ. Sci.*, 2016, **9**, 1828–1840.

[10] M. Hosseinpour, A. Golzary, M. Saber, K. Yoshikawa, *Fuel*, 2017, **206**, 628–637.

[11] P. Wiwel, K. Knudsen, P. Zeuthen, D. D. Whitehurst, *Ind. Eng. Chem. Res.,* 2000, **39**, 533–540.

[12] H. Yang, J. Chen, Y. Briker, R. Szynkarczuk, Z. Ring, *Catal. Today,* 2005, **109**, 16–23.

[13] P. Zeuthen, K. Knudsen, D. D. Whitehurst, *Catal. Today,* 2001, **65**, 307–314.

[14] A. Jayaraman, F. H. Yang, R. T. Yang, *Energy Fuels*, 2006, **20**, 909–914.

[15] M. J. Girgis, B. C. Gates, *Ind. Eng. Chem. Res.,* 1991, **30**, 2021–2058.

[16] J. R. Katzer, Sivasubramanian, *Catal. Rev.-Sci. Eng.,* 1979, **20**, 155–208.

[17] R. J. Angelici, *Polyhedron*, 1997, **16**, 3073–3088.

[18] Stoimenov, P. K.; Klinger, R. L.; Marchin, G. L.; Klabunde, K. J., Langmuir 2002, **18**, 6679–6686.

[19] X. Chen, S. Yuan, A. A. Abdeltawab, S. S. Al-Deyab, J. Zhang, L. Yu, G. Yu, *Sep. Purif. Technol.,* 2014, **133**, 187–193.

[20] M. Bachrach, T. J. Marks, J. M. Notestein, *Acs Catal*, 2016, **6**, 1455–1476.

[21] A. Jayaraman, F. H. Yang, R. T. Yang, *Energy Fuels,* 2006, **20**, 909–914.

[22] R. Abro, M. Abro, S. Gao, A. W. Bhutto, Z. M. Ali, A. Shah, X. Chen, G. Yu, *RSC Adv.*, 2016, **6**, 93932–93946.

[23] P. Forte, A. Sachse, M. Maes, A. Galarneau, D. De Vos, *RSC Adv.*, 2014, **4**, 1045–1054.

[24] Q. Zhou, J. W. Yang, A. K. Du, Y. Z. Wang, J.M. N. Van Kasteren, *AIChE journal*, 2009, **55**, 3294–3297.

[25] T. Welton, *Chem. Rev.,* 1999, **99**, 2071–2083.

[26] C. Asumana, G. Yu, Y. Guan, S. Yang, S. Zhou, X. Chen, *Green Chem.,* 2011, **13**, 3300–3305.

[27] M. Vilas, E. J. González, E. Tojo, E. *Fluid Phase Equilib.*, 2015, **396**, 66–73.

[28] M. Y. Lui, L. Cattelan, L. C. Player, A. F. Masters, A. Perosa, M. Selva, T. Maschmeyer, *Energ Fuel*, 2016, **31**, 2183–2189.

[29] Toxicological Profile for Fuel Oils, Agency for Toxic Substances and Disease Registry (ATSDR), June 1995.

[30] Y. Shimizu,Y. Ohte, Y. Yamamura, S. Tsuzuki, K. Saito, *J. Phys. Chem. B,* 2012, **116**, 5406–5413.

[31] J. M. Slattery, C. Daguenet, P. J. Dyson, T. J. S. Schubert, I. Krossing, *Angew. Chem. Int. Ed.,* 2007, **46**, 5384–5388.

[32] C. C. Weber, A. F. Masters, T. Maschmeyer, *Angew. Chem. Int. Ed.,* 2012, **51**, 11483–11486.

[33] C. Chiappe, D. J. Pieraccini, *J. Phys. Chem. A.,* 2006, **110**, 4937–4941.

[34] M. A. Ab Rani, A. Brant, L. Crowhurst, A. Dolan, M. Lui, N. H. Hassan, J. P. Hallett, P. A. Hunt, H. Niedermeyer, J. M. Perez-Arlandis, M. Schrems, T. Welton, R. Wilding R. *Phys. Chem. Chem. Phys.,* 2011, **13**, 16831–16840.

[35] A. G. Avent, P. A. Chaloner, M. P. Day, K. R. Seddon, T. Welton, *J. Chem. Soc. Dalton Trans.,* 1994, 3405–3413.

[36] P. Verdía, E. J. González, B. Rodríguez-Cabo, E. Tojo, *Green Chem.*, 2011, **13**, 2768–2776.

[37] S. Tsuzuki, H. Tokuda, K. Hayamizu, M. Watanabe, *J. Phys. Chem. B,* 2005, **109**, 16474–16481.

[38] J.E. Braun, Th. L. Grebner, H. J. Neusser, *J. Phys. Chem. A,* 1998, **102**, 3273–3278.

[39] J. R. Carney, F. C. Hagemeister, T. S. Zwier, *J. Chem. Phys*., 1998, **108**, 3379–3382.

[40] Y. Nie, C. Li, Z. Wang, *Ind. Eng. Chem. Res.,* 2007, **46**, 5108–5112.

[41] H. Gao, M. Luo, J. Xing, Y. Wu, Y. Li, W. Li, W. Q. Liu, H. Liu, *Ind. Eng. Chem. Res.,* 2008, **47**, 8383–8388.

[42] H. Gao, S. Zeng, X. Liu, Y. Nie, X. Zhang, S. Zhang, *RSC Adv.,* 2015, **5**, 30234.

[43] C. Asumana, G. Yu, X. Li, J. J. Zhao, G. Liu, X. C. Chen, *Green Chem.,* 2010, **12**, 2030–2037.

[44] Y. Nie, C. Li, H. Meng, Z. Wang, *Fuel Process. Technol.,* 2008, **89**, 978–983.

[45] Y. Nie, C. Li, A. Sun, H. Meng, Z. Wang, *Energy Fuels,* 2006, **20**, 2083–2087.

[46] M. Safa, B. Mokhtarani, H. R. Mortaheb, *Chem. Eng. Res. Des.,* 2016, **111**, 323–331.

[47] T. M. Letcher, N. Deenadayalu, *J. Chem. Thermodyn.,* 2003, **35**, 67–76.

[48] T. Shimomura, T. Takamuku, T. Yamaguchi, *J. Phys. Chem. B,* 2011, **115**, 8518–8527.

[49] C. C. Cassol, A. P. Umpierre, G. Ebeling, B. Ferrera, S. S. X. Chiaro, J. Dupont, *Int. J. Mol. Sci.,* 2007, **8**, 593–605.

[50] S. Gao, G. Yu, R. Abro, A. A. Abdeltawab, S. S. Al-Deyab, X. Chen, *Fuel*, 2016, **173**, 164–171.

[51] A. R. Katritzky, C. A. Ramsden, J. A. Joule, V. V. Zhdankin, Handbook of Heterocyclic Chemistry (3rd Edition), Elsevier, 2010.

[52] A. K. Burrell, R. E.D. Sesto, S. N. Baker, T. M. McCleskey, G. A. Baker, *Green Chem.,* 2007, **9**, 449–454.

[53] Y. Zhao, J. Long, F. Deng, X. Liu, Z. Li, C. Xia, J. Peng, *Catal. Commun.,* 2009, **10**, 732–736.

6. CONCLUDING REMARKS

This PhD project was developed as part of a cotutelle agreement between the Green Organic Synthesis Team (GOST; Università Ca' Foscari, Venice) and the Laboratory of Advanced Catalysis for Sustainability (The University of Sydney). As it was presented in the introduction, the aim of this PhD work was mainly focused on the development of new eco-friendly technologies for the upgrading of platform molecules obtainable from renewable feedstocks. The starting compounds were chosen from among those considered to be the most promising for the development of a modern biorefinery.

The experimental work was divided into three main areas, which were all commonly aimed at combining green technologies and biobased compounds for the development of sustainable protocols.

1. Development of new methodologies for the upgrading of glycerol and furan bio-based derivatives.

In Chapter 2, the optimisation of a new CF-protocol for the alkylation of biobased derivatives was reported. In particular, the CF-alkylation protocol allowed for the synthesis of a series of alkyl ethers from OH-bearing biobased derivatives. The produced ethers have a range of applications in the synthesis of added-value products, including intermediates, solvents and biologically active molecules, such as glycerol ethers and carbonates; in addition, they can be used as additives for biodiesel blends based on furanyl ethers.

The CF-alkylation protocol was implemented with green and safe dialkyl carbonates (*i.e.* dimethyl carbonate and diethyl carbonate), which avoided the use of common toxic and poorly atom economic alkylating agents, such as alkyl halides and dialkyl sulfates. Moreover, no additional solvents were required since DAlCs acted as both the alkylating agents and as the solvents. Two classes of heterogeneous catalysts were compared: Na-exchanged Y- and X-faujasites and Mg-Al hydrotalcites. Calcined hydrotalcites, particularly c-HT30 (Mg:Al ratio=30), proved to be the most effective systems for highly chemoselective transformations: functionalised bio-based alcohols and dialkyl carbonates were activated towards *O*-alkylations

over the competitive transesterifications and other side-reactions. *O*-alkylation selectivities as high as 99% were achieved at complete conversions. Interestingly, characterisation studies proved that the hydrotalcites acted as catalyst precursors: during the thermal activation pre-treatments of such solids, the lamellar structure typical of hydrotalcites was broken down gradually into a magnesia-alumina solid solution, which was the genuine catalytic phase.

A new CF-protocol for the synthesis of symmetrical dialkyl organic carbonates was reported in Chapter 3.

Two carbonate interchange reactions were analysed. In the first step, conducted under batch conditions, methyl alkyl organic carbonates were obtained in quantitative conversions and high yields from a hydrotalcite catalysed reaction of OH-bearing bio-based derivatives (including solketal, glycerol formal, tetrahydro furfuryl alcohol and cyclohexanol) with the non-toxic DMC. The equilibrium of the reaction was efficiently driven towards completion by continuously removing the by-produced MeOH as an azeotropic mixture with DMC.

Subsequently, a CF-protocol was optimised for the synthesis of symmetrical DAlCs *via* catalytic disproportionation reactions of the starting methyl alkyl carbonates. The hydrotalcite c-HT30 proved to be the most active heterogeneous catalyst among those investigated and it allowed for the achievement of high conversions, selectivities and productivities.

1. *Catalytic depolymerisation of Kraft lignin into renewable aromatic compounds.*

Lignocellulosic biomass has been proposed as one renewable feedstock to supplement dwindling fossil reserves, and lignin, which is present in the LCB in roughly 25% amount, is the most abundant source of renewable aromatic compounds. In Chapter 4 it is reported the catalytic depolymerisation of Kraft lignin in supercritical ethanol. The protocol was explored in the presence of eight different Mo_2C- and MoS_2-based catalysts, which were synthesised and characterised according to reported procedures. Ethanol, which is produced industrially using renewable protocols, acted as both the solvent and the H-donor. Aromatic yields as high as 506 mg/g lignin were achieved, which are amongst the highest yields reported to date. Studies on the leached molybdenum from the catalyst were also performed in order to better understand the nature of the catalysis, whether it was heterogeneous or homogeneous. While

this is a contentious issue, ICP analysis and supplementary experiments showed that, in our system, the bulk of the catalysis was heterogeneous. The interesting results obtained from these studies pave the way for future work.

2. *Cleaning up fuels: removing pollutants from renewable feedstock with ionic liquids.*

In Chapter 5, twelve ionic liquids based on common cations and anions were synthesised and used for the selective extraction of two archetypical N-compounds, pyridine and indole, from a model oil, consisting of *n*-decane and toluene. The performance of these ionic liquids as extractants of N-compounds was compared and rationalised, demonstrating that the cation and anion sizes and the hydrogen bond donor/acceptor abilities are the major factors that determine the effectiveness of N-compound extraction. The mutual solubility of ILs and the model oil was also investigated. This represent an important aspect to avoid the loss of the extractants and the contamination of the fuel oil.

ACKNOWLEDGEMENTS

I would like to express my special appreciation and thanks to my supervisors and advisors Professor Maurizio Selva and Professor Thomas Maschmeyer, for encouraging my research and for allowing me to mature as a research scientist. All my gratitude to A/Professor Alvise Perosa and A/Professor Tony Masters, for their useful advice, contributions and guidance.

This project would not have been as successful without the instrumental assistance of professors and staff from both Ca' Foscari University of Venice and the University of Sydney. From Ca' Foscari, I would like to thank Professor Piero Riello, for his support for the XRD analyses and interpretation advise. From the University of Sydney, I would like to thank the Australian Centre for Microscopy & Microanalysis for the use of their electron microscopes. In particular, I would like to thank Ms Ellen Hemming and Ms Grace Rui Zhang for assistance with microscopy analysis. From the School of Geoscience, I would like to thank Dr. Tom Savage for assistance with ICP analysis.

A special thanks to Dr. Marco Noè for valuable discussion particularly regarding the *O*-alkylation of solketal, to Dr. Matthew Lui and Ms Lisa Player, who assisted me in the synthesis of ionic liquids to be used in the extractive denitrogenation of fuel oils and to Dr. Alex Yuen for his important contribution in the synthesis of renewable aromatics from Kraft lignin.

I would also like to thank Dr. Francesca Guidi, Dr. Thommy Gatling and everyone involved in the writing of the Cotutelle agreement, which allowed me to live and study in Australia for one year at the University of Sydney.

I would like to thank the MIUR (Ministry of Education, Universities and Research, Italy) for the three years PhD scholarship, the Erasmus+ for the 6 months scholarship KA1-ICM and the Postgraduate Research Support Scheme (University of Sydney).

I would also like to express all my gratitude to the two wonderful teams that I had the immense pleasure to work with: GOST (Ca' Foscari) and the MM group (USyd). You all, present and past members, made my three and a half years of PhD unforgettable: I had a really great time with you guys, thank you!

To all my friends outside the university, thank you for helping me strike a balance between my PhD studies and my social life, especially during the toughest months of intense writing.

Thank you for being always there, even 16000 km apart! And to Jordan, thank you because your faith in me makes everything possible.
Finally, I would like to dedicate this thesis to my family. To them my deepest gratitude for their support, patience and encouragements.

Lisa Cattelan

7. APPENDIX

7.1. C-F O-alkylation of BBDs with DAlCs in the presence of Mg–Al HTs as Catalyst Precursors (Chapter 2)

7.1.1. Continuous-flow reactions

General Information. Unless otherwise stated, all solvents and reagents were used as obtained from commercial sources without further purification. GC/MS (EI, 70 eV) analyses were run using a HP5-MS capillary column (L=30 m, Ø=0.32 mm, film=0.25 µm) and CG/FID analyses were run using an Elite-624 capillary column (L=30 m, Ø=0.32 mm, film=1.8 µm). ^{1}H NMR were recorded at 400 or 300 MHz, ^{13}C NMR spectra at 100 MHz, and chemical shifts were reported in δ values downfield from TMS; $CDCl_3$ was used as the solvent.

CF-Apparatus. The continuous-flow (CF) apparatus used in this investigation is depicted in Figure 7.1. Major components were an HPLC pump (P1) for the delivery of liquid reactants, a thermostat oven (O) equipped with additional thermocouples, a tubular reactor (R) made of an 1/4" steel tube (L = 12 cm; V = 1.16 mL) filled with the catalyst and placed in the upright position, a 7725i-Rheodyne injector fitted with a 10 µL sample loop for the withdrawal of samples, and a back-pressure regulator (BPR, Swagelok K-series) for pressure control.

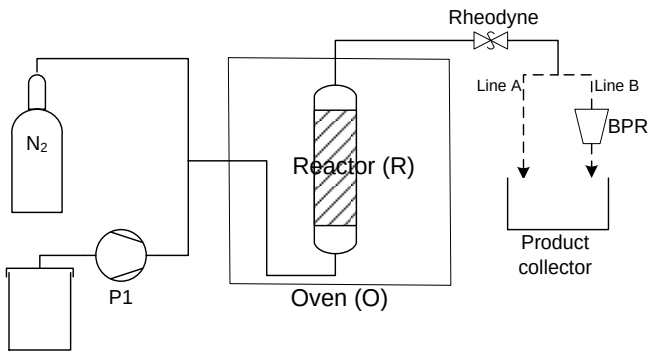

Figure 7.1. Experimental set-up used for the continuous-flow reactions.

7.1.1.1. CF-reactions of compounds 1a, (2a+2a'), 3a, 4a, 5a with DMC

Procedure. CF-reactions was carried out by using the continuous-flow (CF) apparatus above described. Catalyst loadings were chosen according to the apparent density of the solids used (Hydrotalcites and Faujasites): typical amounts were in the range of 0.5-0.85 g.

The following procedure was used. The CF-system was initially set at a temperature of 150 °C, while N_2 was flushed for one hour. Then, the reacting mixture (dialkyl carbonate and the bio-based alcohol) was allowed to flow through the catalytic bed for 10 minutes at 1 mL/min. At the same time, the BPR and the oven were set at the operating pressure and temperature (5-60 bar, and 150-300 °C, respectively). Once T and p were stabilised, the reactants flow was adjusted at the desired rate (0.07-0.2 mL/min). The reaction mixture was collected through a Rheodyne® valve (7725i fitted with a 10 µL sample loop) at time intervals of about 30 minutes, diluted with 1.5 mL of diethyl ether and analysed by GC/FID or GC/MS.

7.1.2. Karl-Fisher titrations

Titrations of solketal (**1a**) and solketal methyl carbonate (**1c**) were carried out by using HYDRANAL®-composite one from Sigma-Aldrich. The titration procedure is described in detail elsewhere.[1] Each titration was repeated three times.

The water content of each compound is calculated with equations 7.1, 7.2 and 7.3 from the volume consumed and the water equivalent (WE) of the HYDRANAL®-reagent (**HR**):

$$mg\ (H_2O, \boldsymbol{substrate}) = a \cdot WE \qquad \text{Eq. 7.1}$$

$$wt\%(H_2O, \boldsymbol{substrate}) = \frac{a \cdot WE}{10 \cdot e} \qquad \text{Eq. 7.2}$$

$$mol\%(H_2O, \boldsymbol{substrate}) = \frac{mol\ (H_2O, substrate)}{mol\ (substrate)} \cdot 100 \qquad \text{Eq. 7.3}$$

Where:

a= consumption of reagent **HR** in mL

WE= water equivalent of the reagent **HR** in mg H_2O/mL = 0.8-1.2 mg/mL

e= weight of the sample in g

	1a	**1c**
e (g, **substrate**)	2.13	2.00
a (mL, **HR**)	3.10	2.70
mg (H_2O, **substrate**)	3.10	2.70
STD. DEV mg (H_2O, **substrate**)	0.43	0.85
wt% (H_2O, **substrate**)	0.15	0.13
STD. DEV wt% (H_2O, **substrate**)	0.03	0.03
mol% (H_2O, **substrate**)	1.07	1.43
STD. DEV mol% (H_2O, **substrate**)	0.15	0.45

7.1.3. NMR and mass analysis

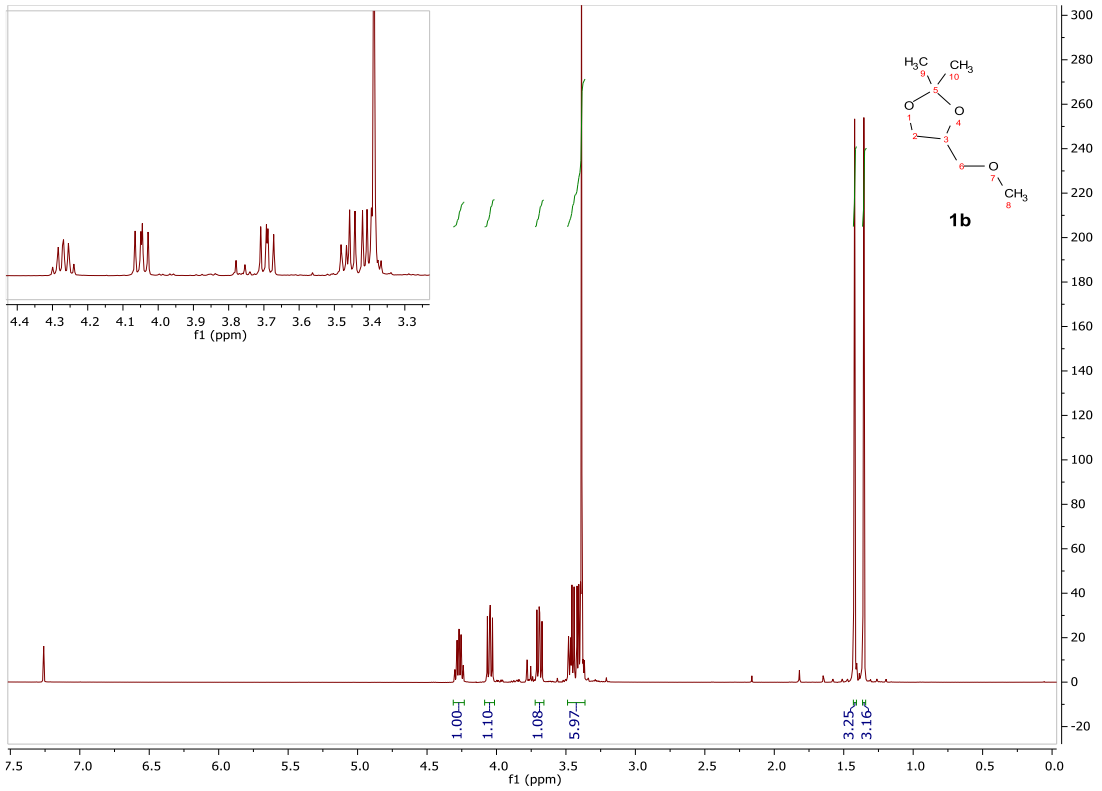

Figure 7.2. ^{1}H NMR of (2,2-Dimethyl-1,3-dioxolan-4-yl)methyl methyl ether (**1b**).

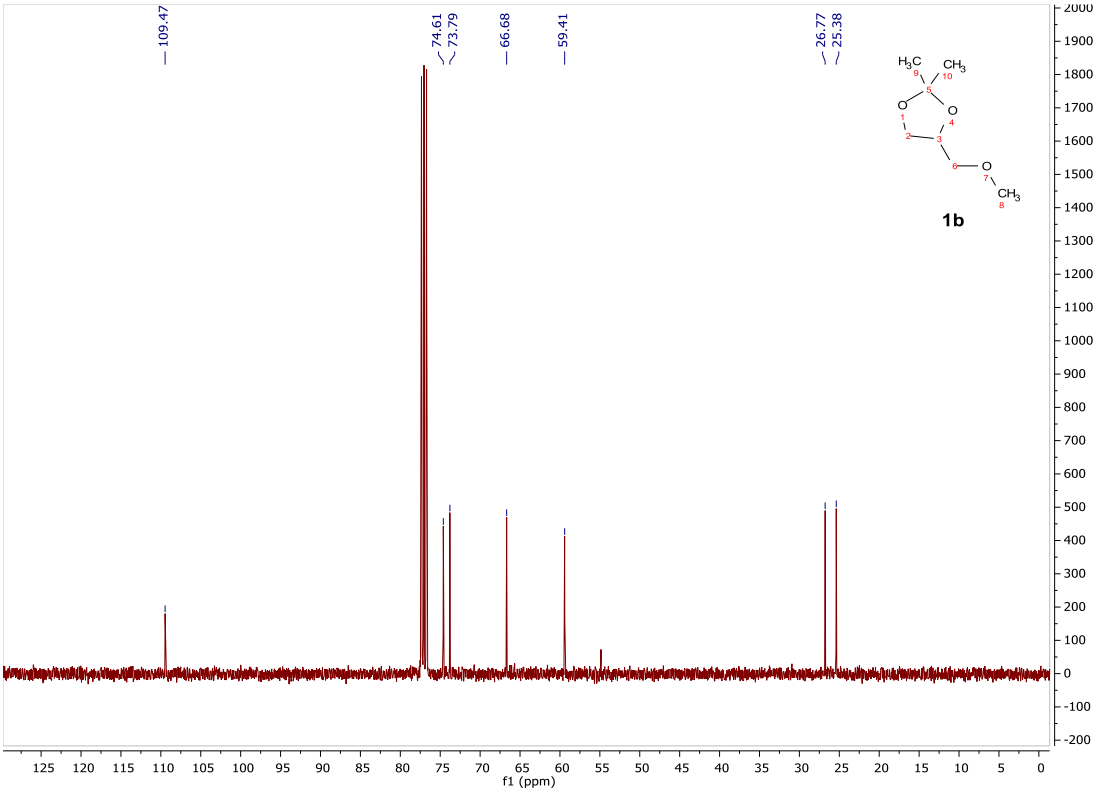

Figure 7.3. ^{13}C NMR of (2,2-Dimethyl-1,3-dioxolan-4-yl)methyl methyl ether (**1b**).

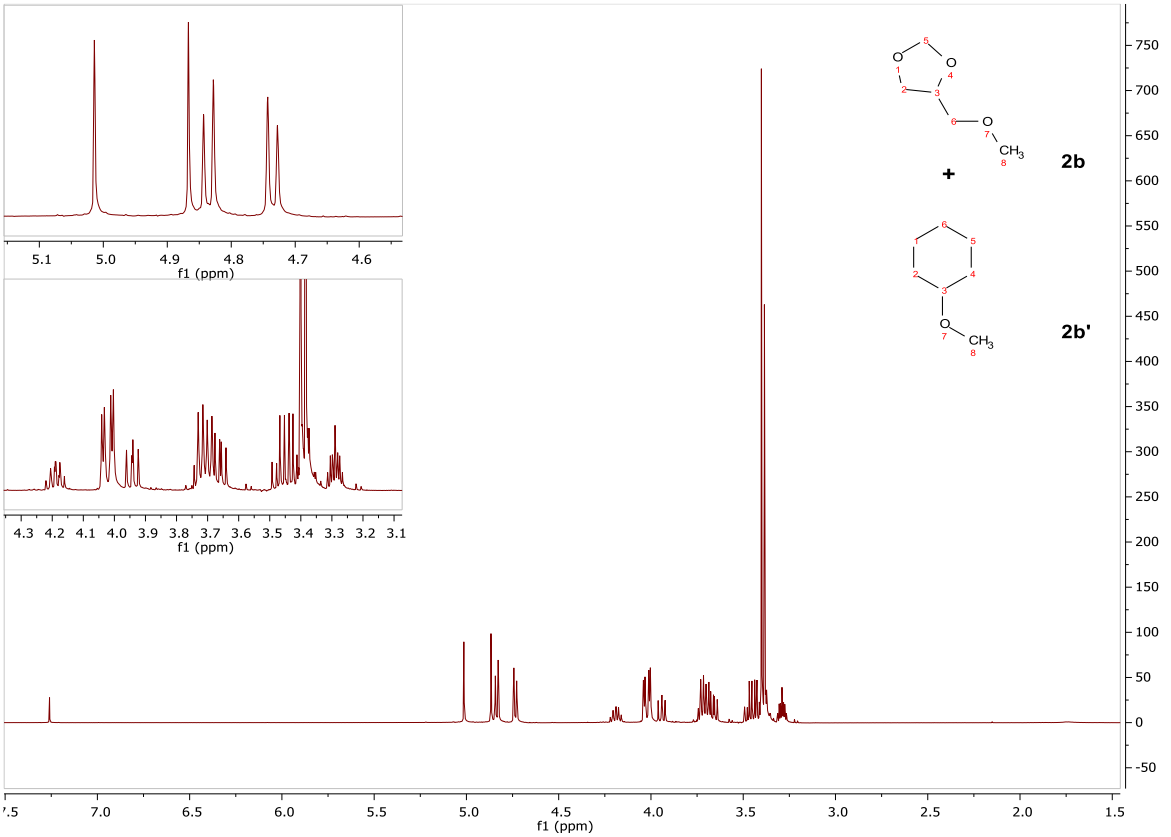

Figure 7.4. ^{1}H NMR of 1,3-Dioxan-5-yl methyl ether (**2b**) and (1,3-dioxolan-4-yl)methyl methyl ether (**2b'**).

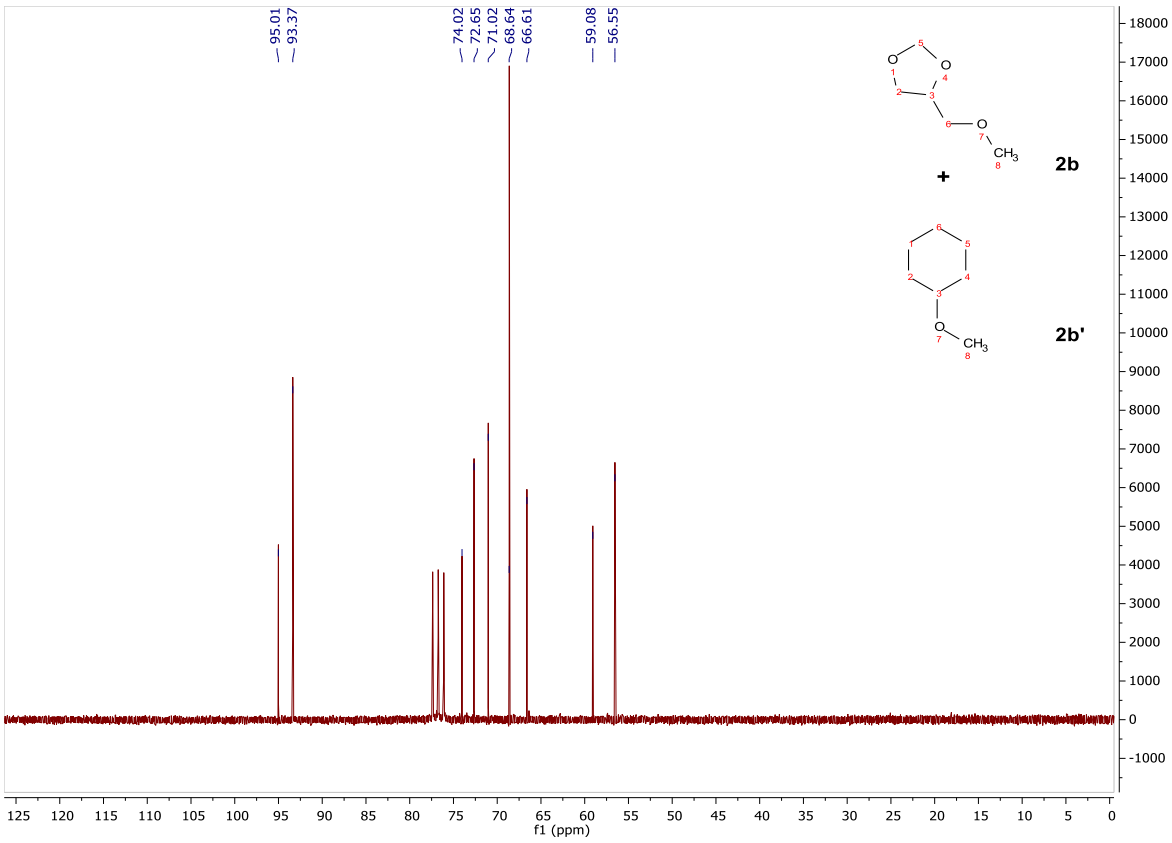

Figure 7.5. ^{13}C NMR of 1,3-Dioxan-5-yl methyl ether (**2b**) and (1,3-dioxolan-4-yl)methyl methyl ether (**2b'**).

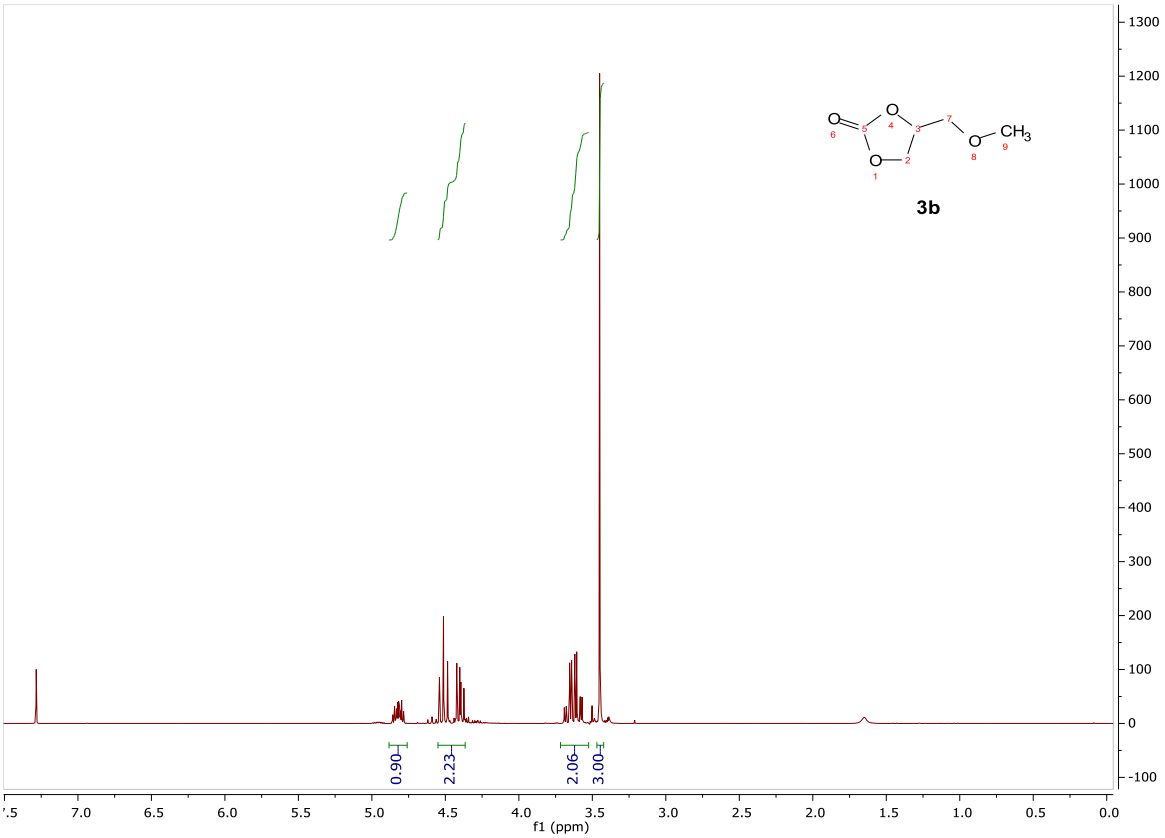

Figure 7.6. ^{1}H NMR of 4-(methoxymethyl)-1,3-dioxolan-2-one (**3b**).

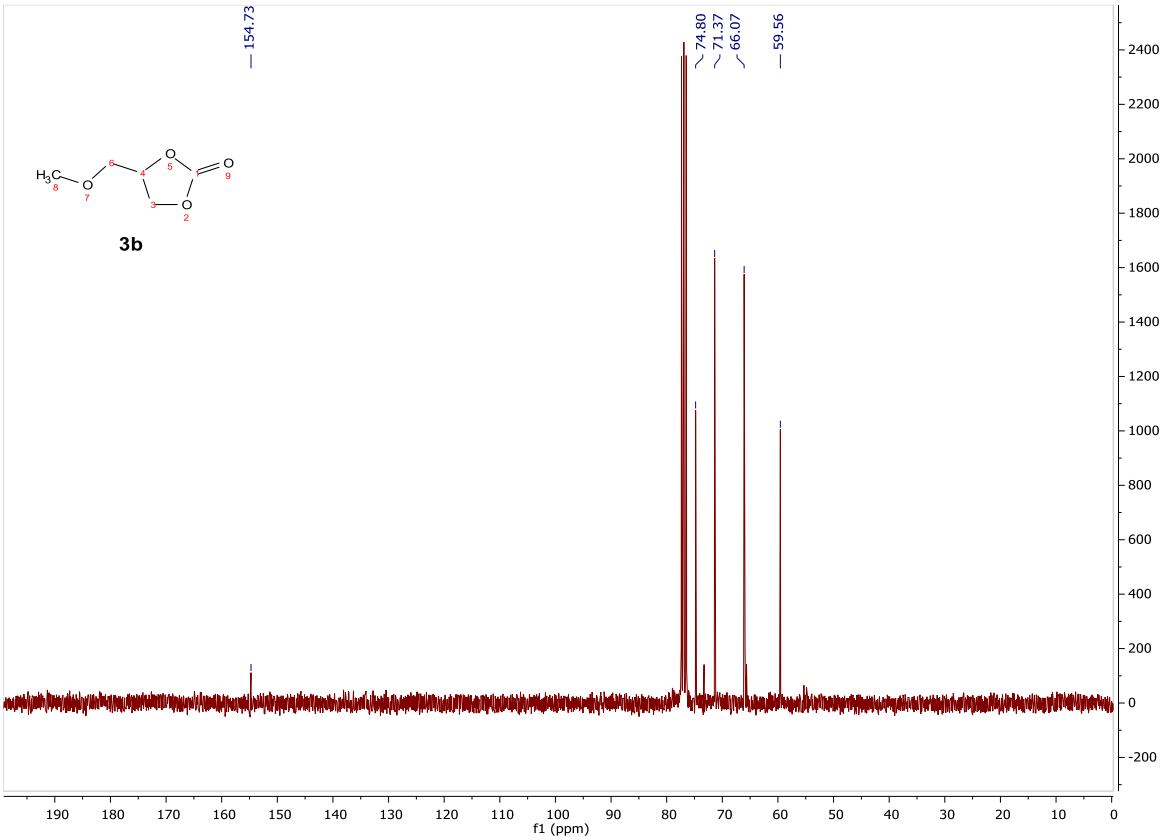

Figure 7.7. ^{13}C NMR of 4-(methoxymethyl)-1,3-dioxolan-2-one (**3b**).

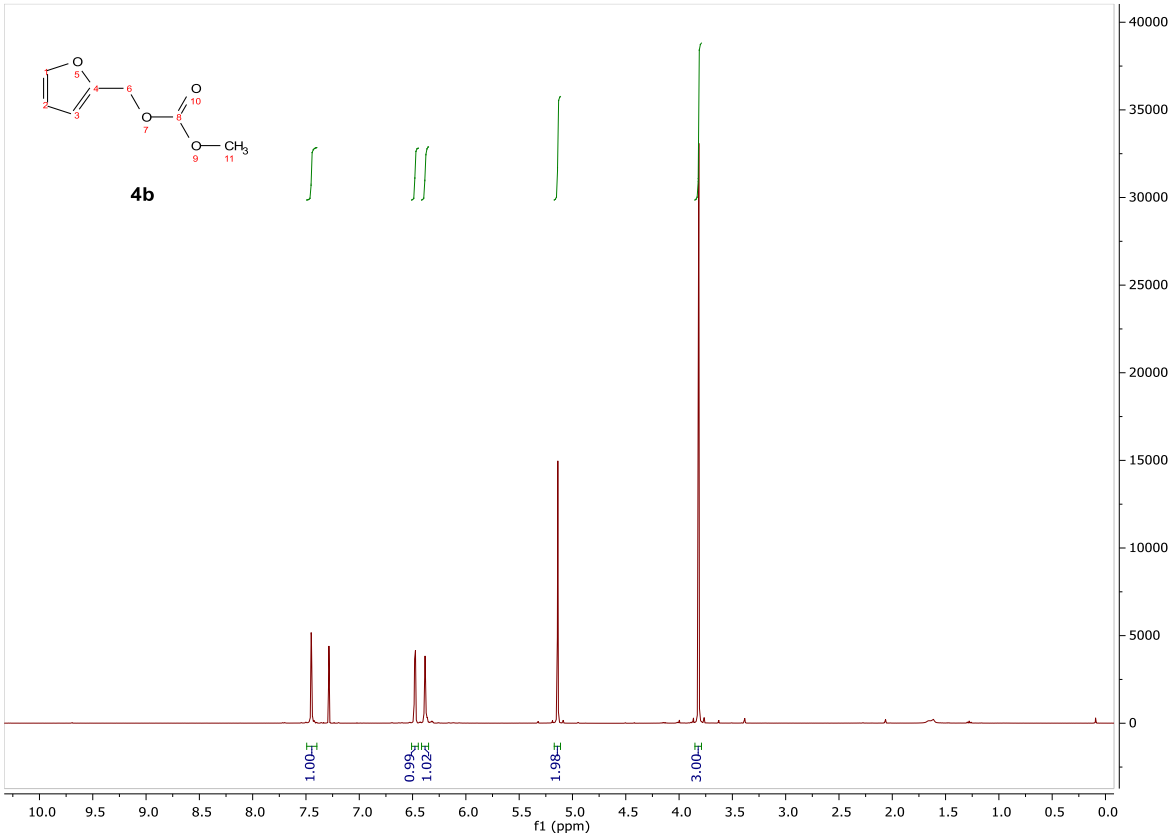

Figure 7.8. ^{1}H NMR of furan-2-ylmethyl methyl carbonate (**4b**).

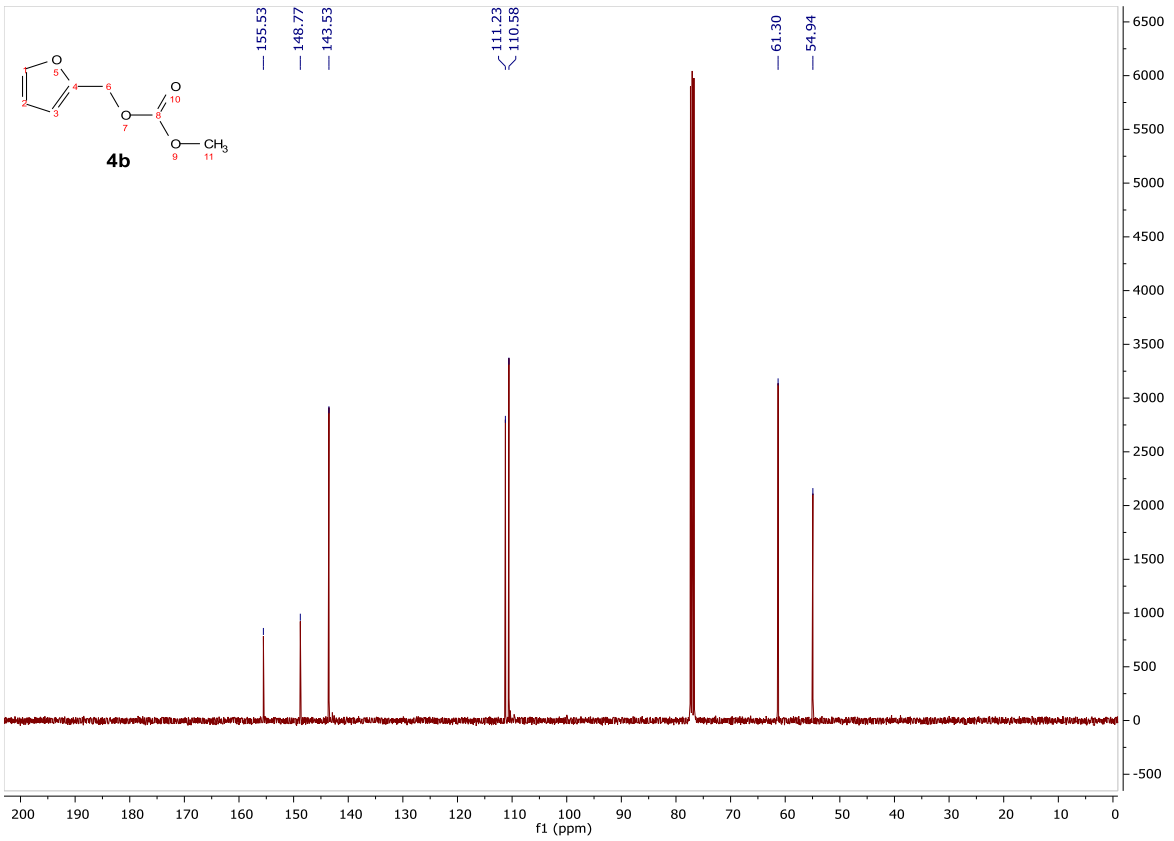

Figure 7.9. ^{13}C NMR of furan-2-ylmethyl methyl carbonate (**4b**).

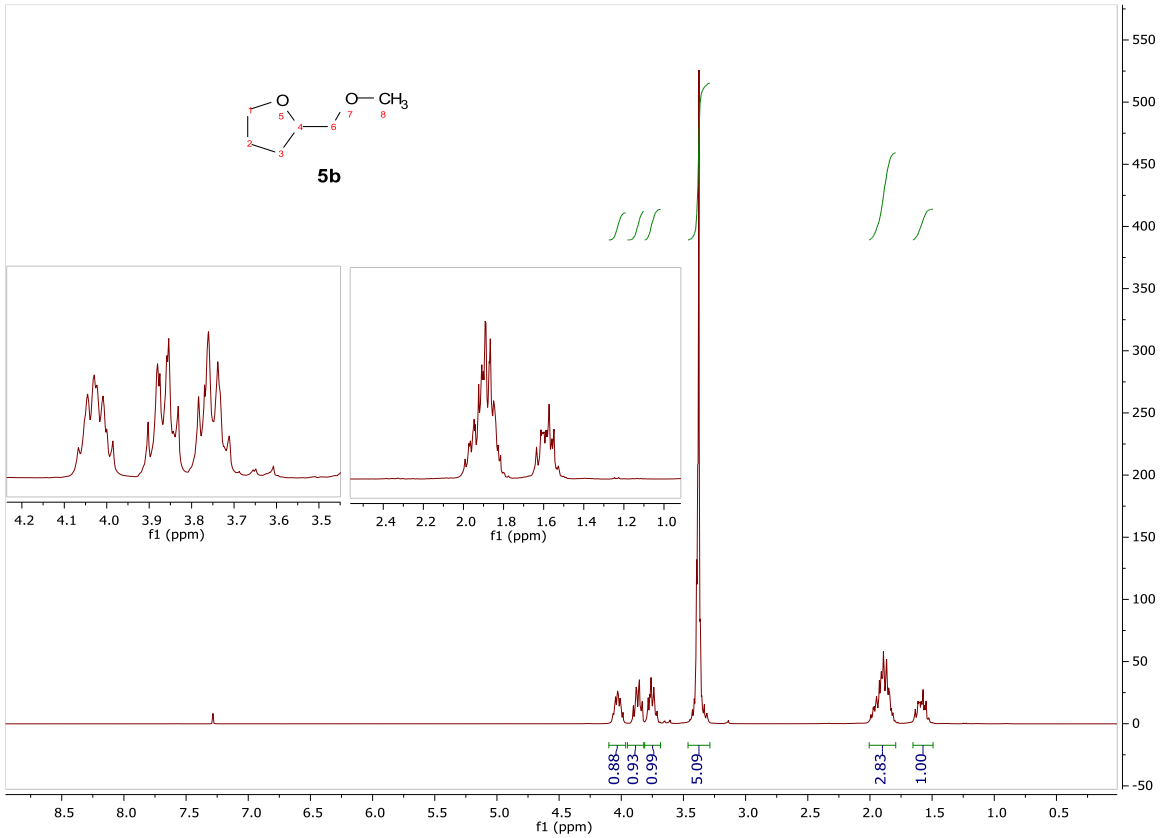

Figure 7.10. ^{1}H NMR of 2-(methoxymethyl)tetrahydrofuran (**5b**).

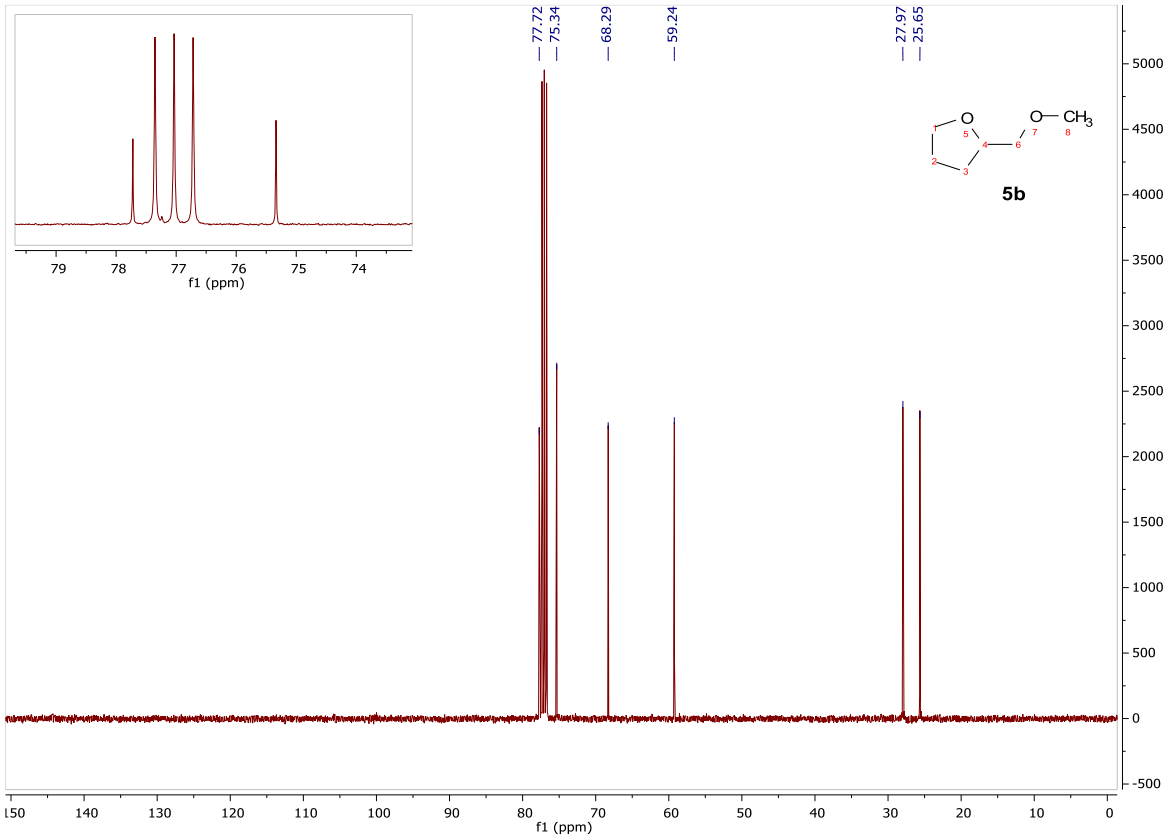

Figure 7.11. ^{13}C NMR of 2-(methoxymethyl)tetrahydrofuran (**5b**).

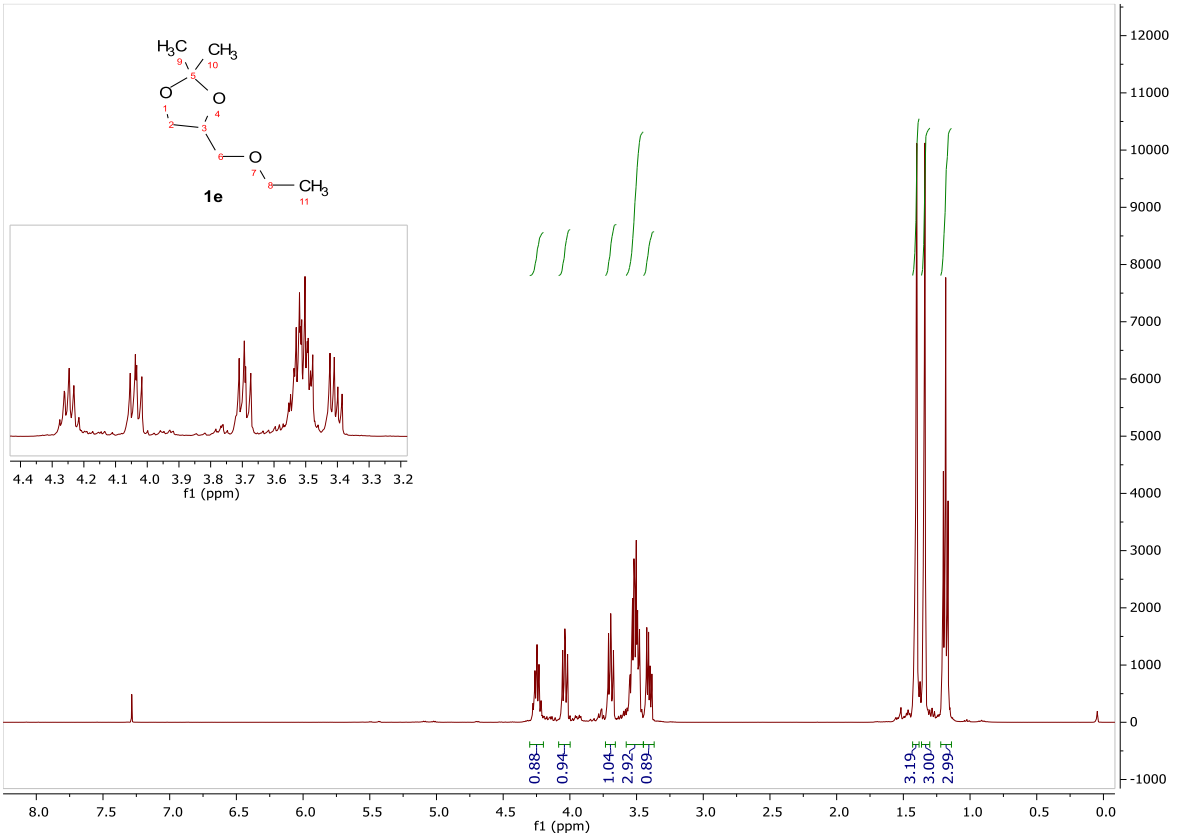

Figure 7.12. ^{1}H NMR of 4-(ethoxymethyl)-2,2-dimethyl-1,3-dioxolane (**1e**).

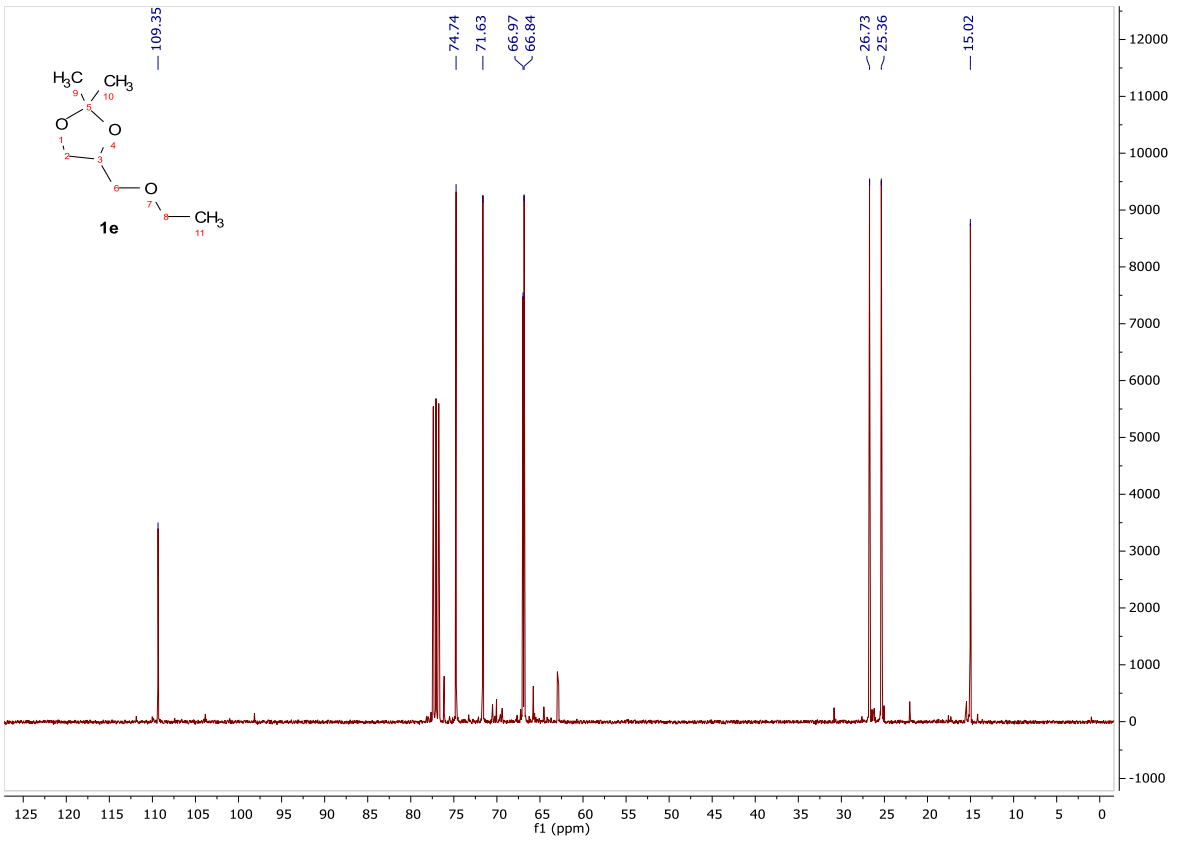

Figure 7.13. ^{13}C NMR of 4-(ethoxymethyl)-2,2-dimethyl-1,3-dioxolane (**1e**).

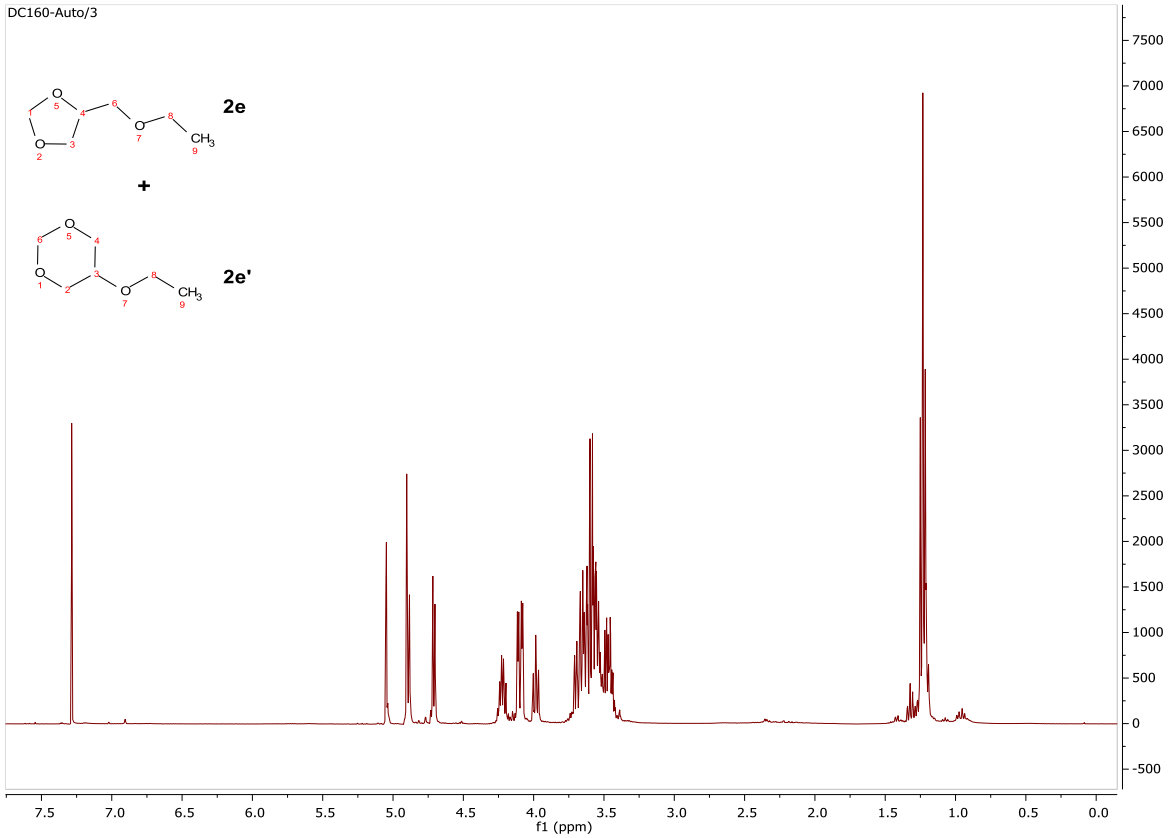

Figure 7.14. ^{1}H NMR of 1,3-Dioxan-5-yl ethyl ether (**2e**) and (1,3-dioxolan-4-yl)methyl ethyl ether (**2e'**).

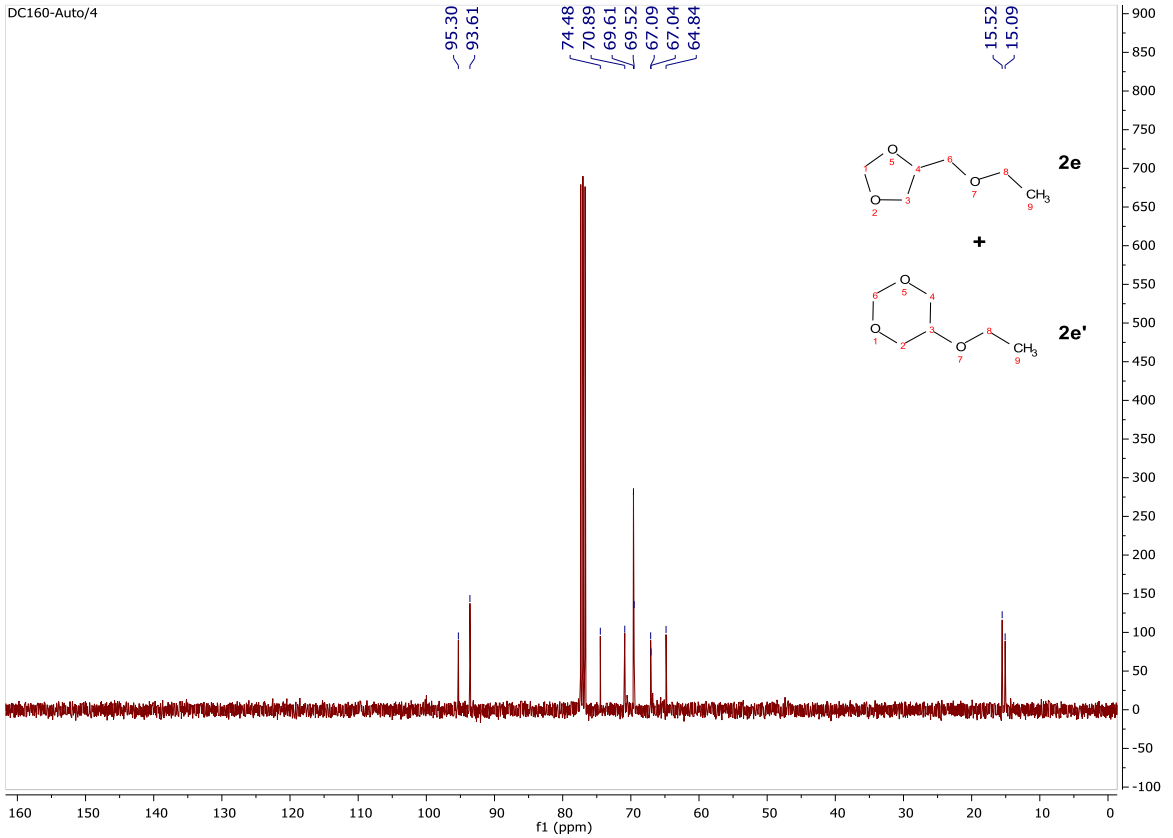

Figure 7.15. ^{13}C NMR of 1,3-Dioxan-5-yl ethyl ether (**2e**) and (1,3-dioxolan-4-yl)methyl ethyl ether (**2e'**).

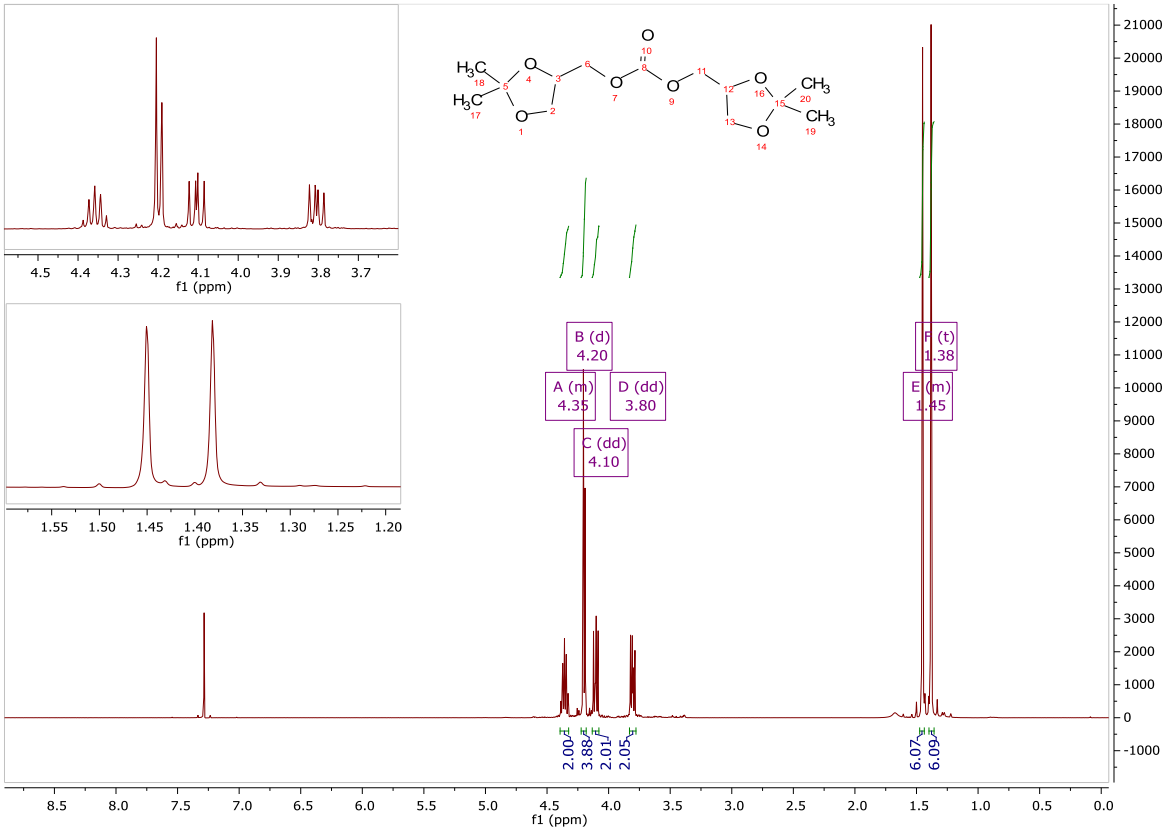

Figure 7.16. ^{1}H NMR of bis((2,2-dimethyl-1,3-dioxolan-4-yl)methyl) carbonate (**1d**).

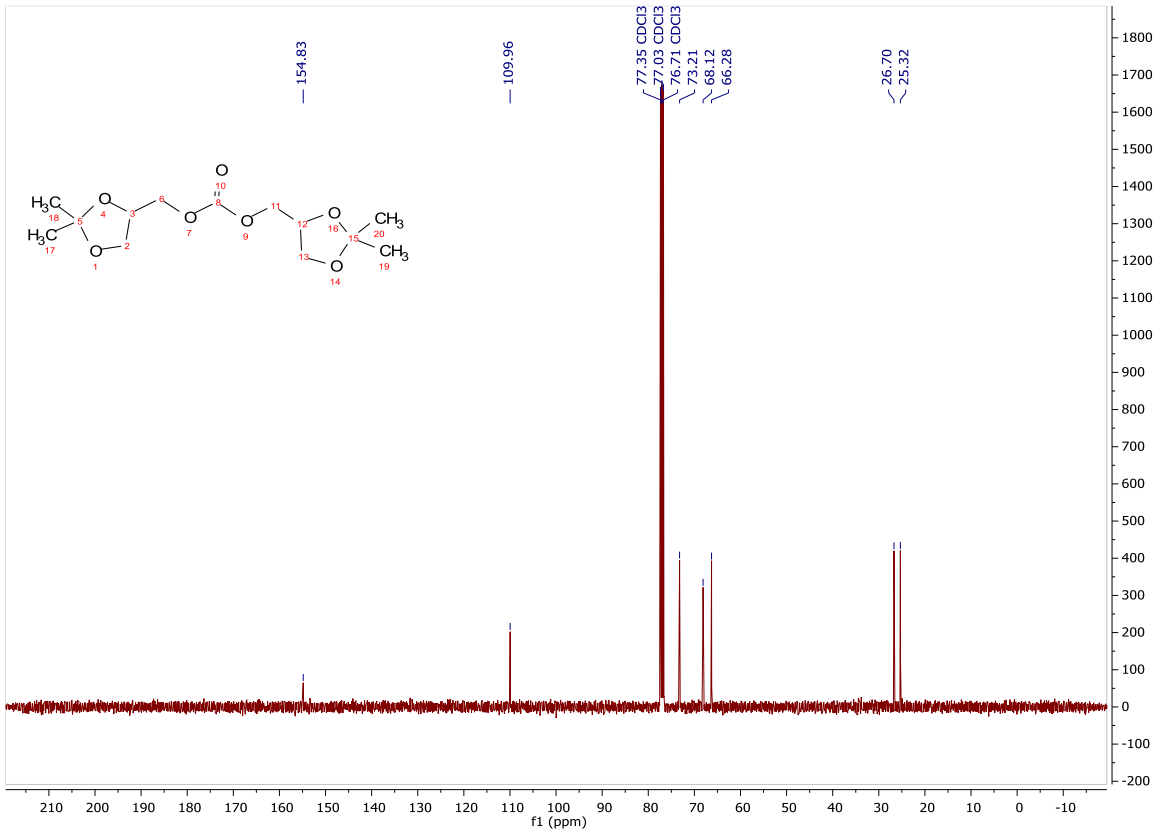

Figure 7.17. ^{13}C NMR of bis((2,2-dimethyl-1,3-dioxolan-4-yl)methyl) carbonate (**1d**).

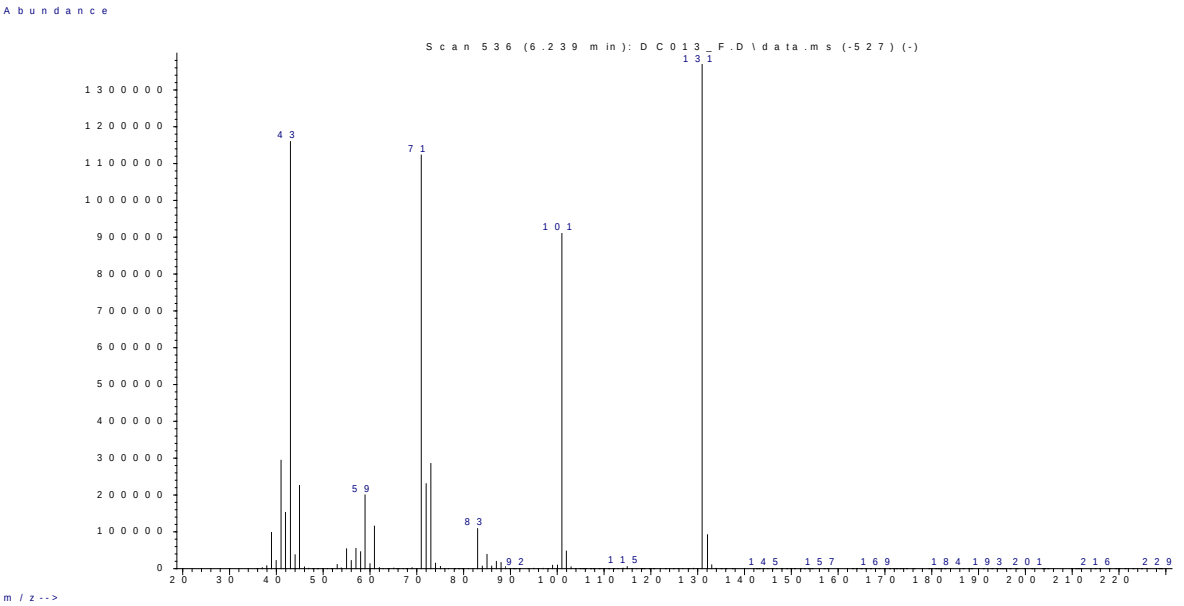

Figure 7.18. MS spectrum of compound **1b.**

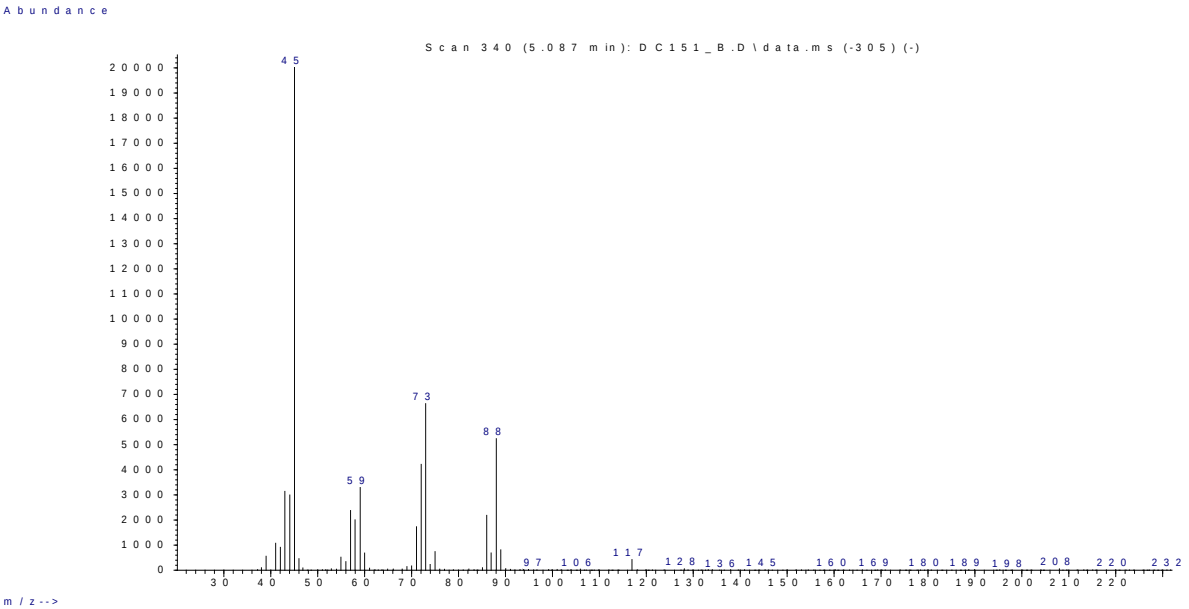

Figure 7.19. MS spectrum of compound **2b.**

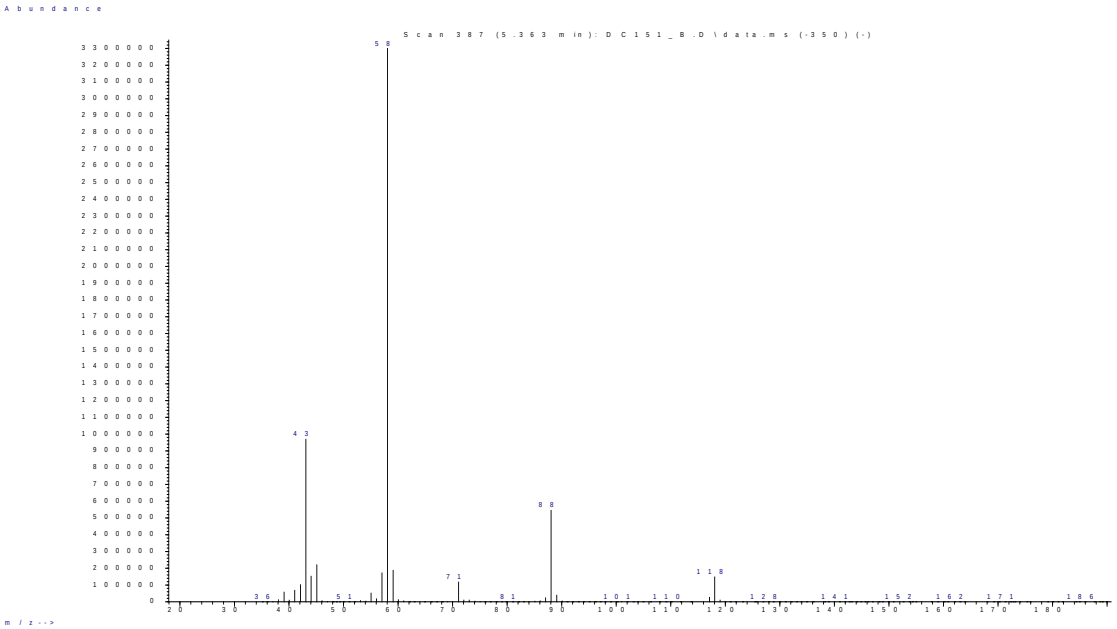

Figure 7.20. MS spectrum of compound **2b'.**

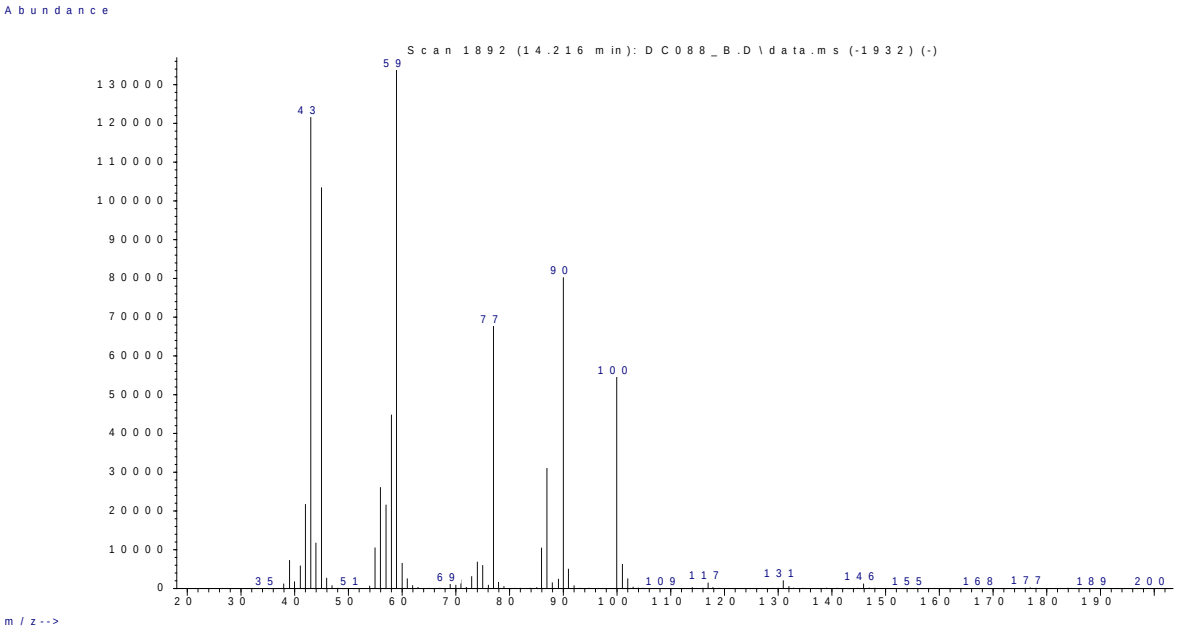

Figure 7.21. MS spectrum of compound **3b.**

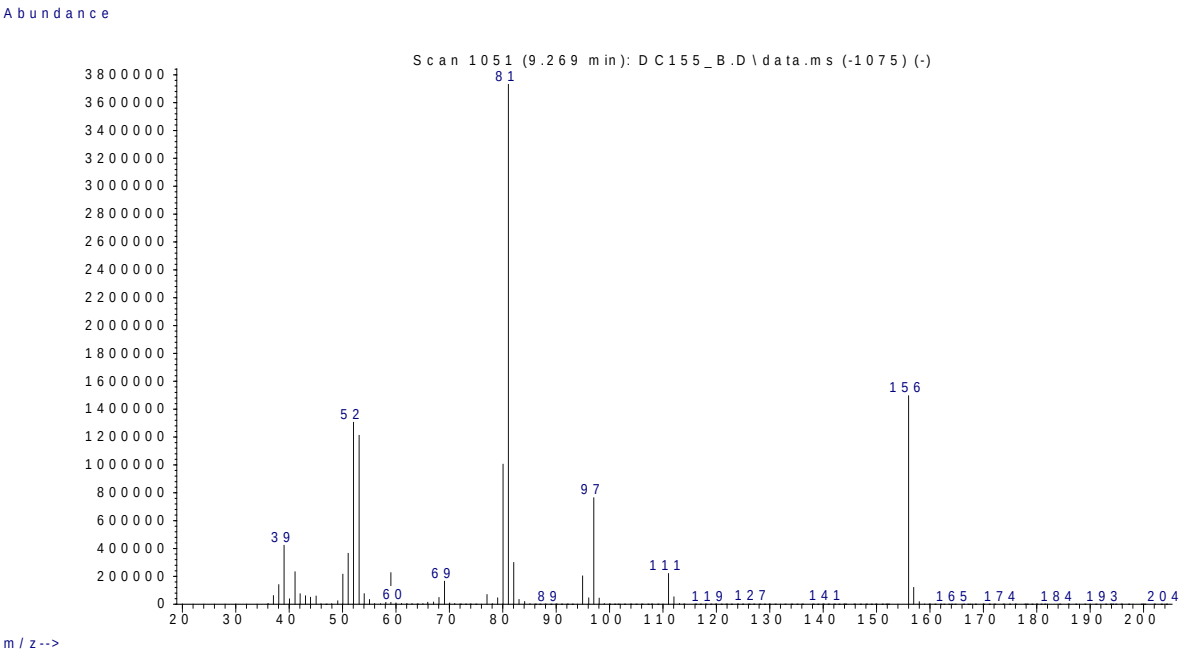

Figure 7.22. MS spectrum of compound **4b.**

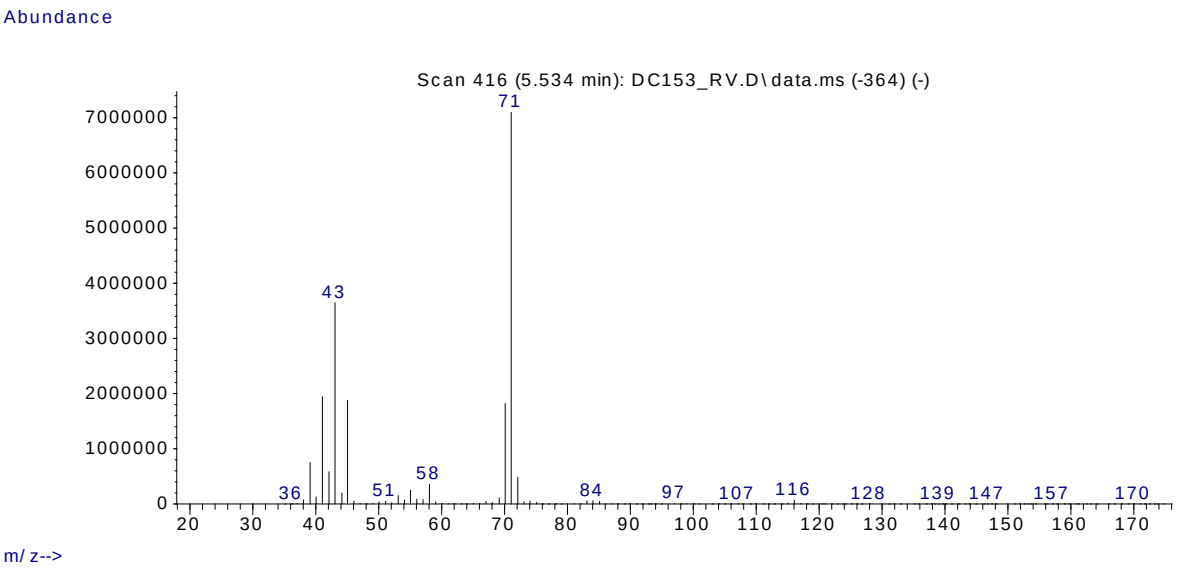

Figure 7.23. MS spectrum of compound **5b.**

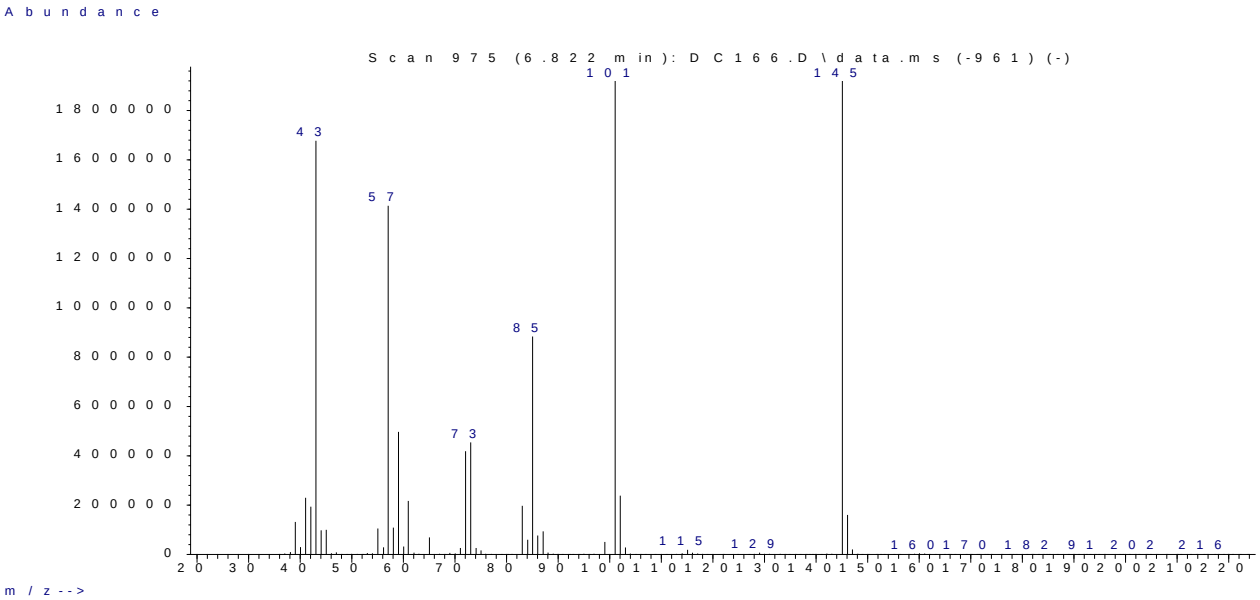

Figure 7.24. MS spectrum of compound **1e.**

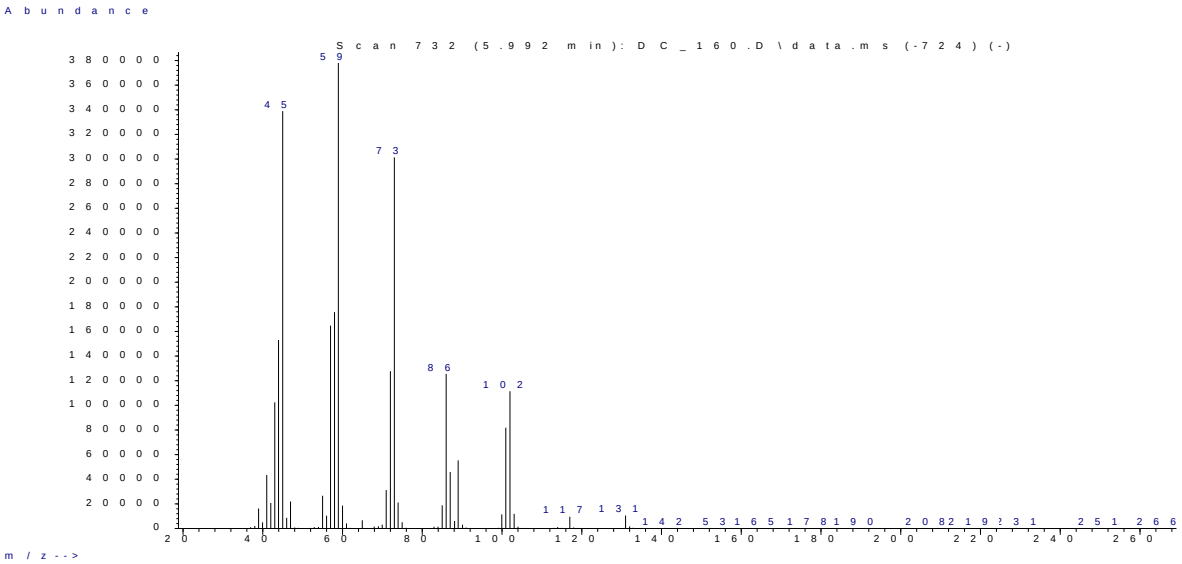

Figure 7.25. MS spectrum of compound **2e.**

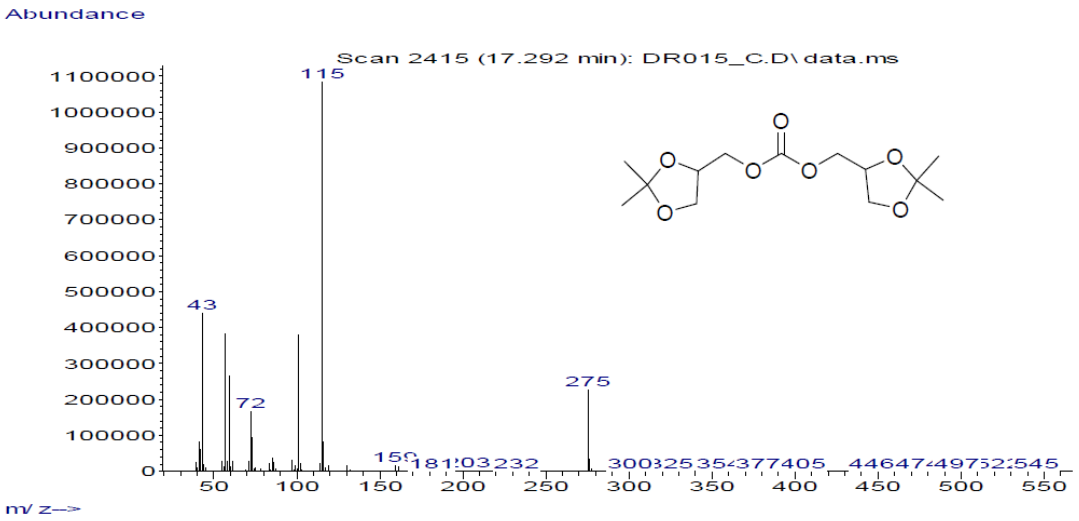

Figure 7.26. MS spectrum of compound **1d.**

.

7.1.4. XRD characterisation of catalysts

Table 7.1. Samples of KW2000 and HT30 for XRD analyses. All samples were stored at 70 °C, 18 mmHg, overnight before any measure.

Entry	Label	Calcination (450 °C, air, 16 h)	Surface area (m^2/g)	Pore Volume (cm^3/g)[a]	Conditions of use
1	f-KW2000	none	108	0.79	None[b]
2	c-KW2000	yes	199	0.72	18 h at 210 °C, 10 bar[c]
3	f-HT30	none	138	0.33	None[b]
4	c-HT30	yes	247	0.48	18 h at 210 °C, 10 bar[c]

Surface area and pore volume were determined by BET analyses. a) Determined from the nitrogen adsorbed volume at p/p0 = 0.977; b) The fresh (f-) solids were not used for catalytic tests; c) Calcined (c-) samples were used for catalytic tests under the conditions of Table 2. BET analyses were carried out before the use of c-solids as catalysts.

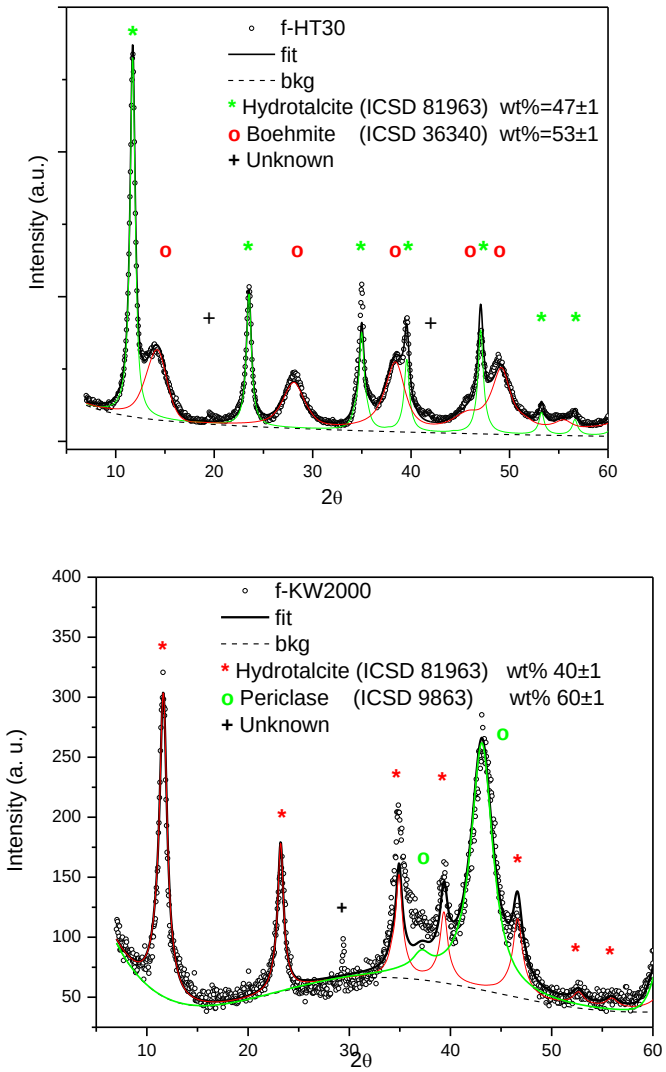

Figure 7.27. Further details (in color) of the Rietveld analysis of samples f-HT30 and f-KW2000.

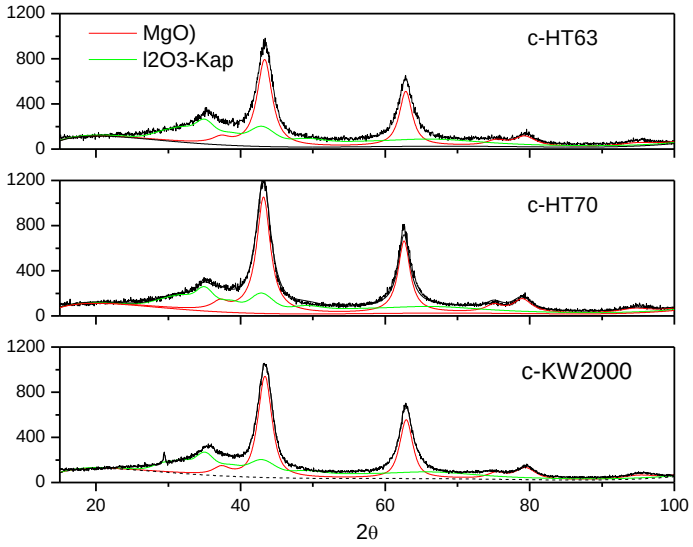

Figure 7.28. XRD patterns of samples c-HT-63 and c-HT-70.

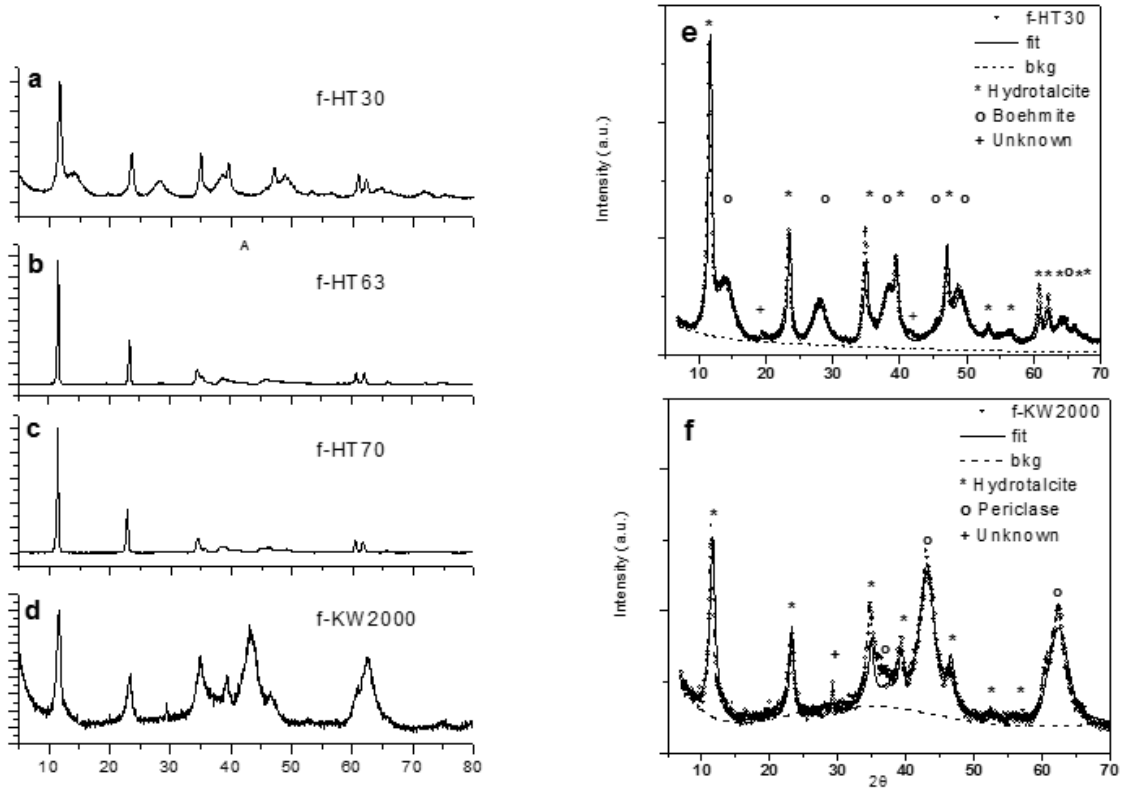

Figure 7.29. Left: XRD patterns of samples f-HT30, f-HT63, f-HT70 and f-KW2000. Right: Rietveld fit of f-HT30 and f-KW2000.

7.1.5. ICP analysis

ICP analyses were carried out to evaluate both the composition of the KW2000 including the Mg:Al ratio and the post-synthesis amounts of Na and K, and the leaching of Mg and Al from the catalytic bed of c-HT30 used in this investigation. Analyses were run on a Perkin Elmer Nexion 300XX Inductively Coupled Plasma Mass Spectrometer (ICP-MS). Calibration curves were obtained by using three aqueous solutions containing 50, 100 and 200 ppb of Na, K, Al and Mg respectively.

These solutions were all prepared by dilutions of a 200 mg/L multi element commercially prepared standard solution.

Mg:Al ratio and post-synthesis amounts of Na and K in KW2000

KW2000 (0.1 g) was dissolved in concentrated HCl and subsequently diluted with Milli-Q H_2O in a 100 mL volumetric flask.[2] Analyses were performed twice.

Leaching of Mg and Al from the catalytic bed of c-HT30

Once the CF-reaction of solketal with DMC was carried out under the conditions of Figure 2 (20 hours), the mixture sampled at the reactor outlet was rotary evaporated (50 °C, 5 mbar). The residual was digested with concentrated HNO_3, and diluted with Milli-Q H_2O in a 10 mL volumetric flask.

Table 7.2 reports the results.

Table 7.2. ICP analyses of the Na, K, Mg and Al contents.

Entry	**Sample**	**Metal content (µg/L)**			
		Na	**K**	**Mg**	**Al**
1	f-KW2000 (0.1 g/100 mL)	265	117	246842	130660
2	Effluent from c-HT30[a]	-	-	40	85

a) Liquid solution recovered after the reaction of solketal with DMC: conditions of Figure 2.12 (20 hours).

7.2. Symmetrical carbonates (Chapter 3)

7.2.1. NMR and mass analysis

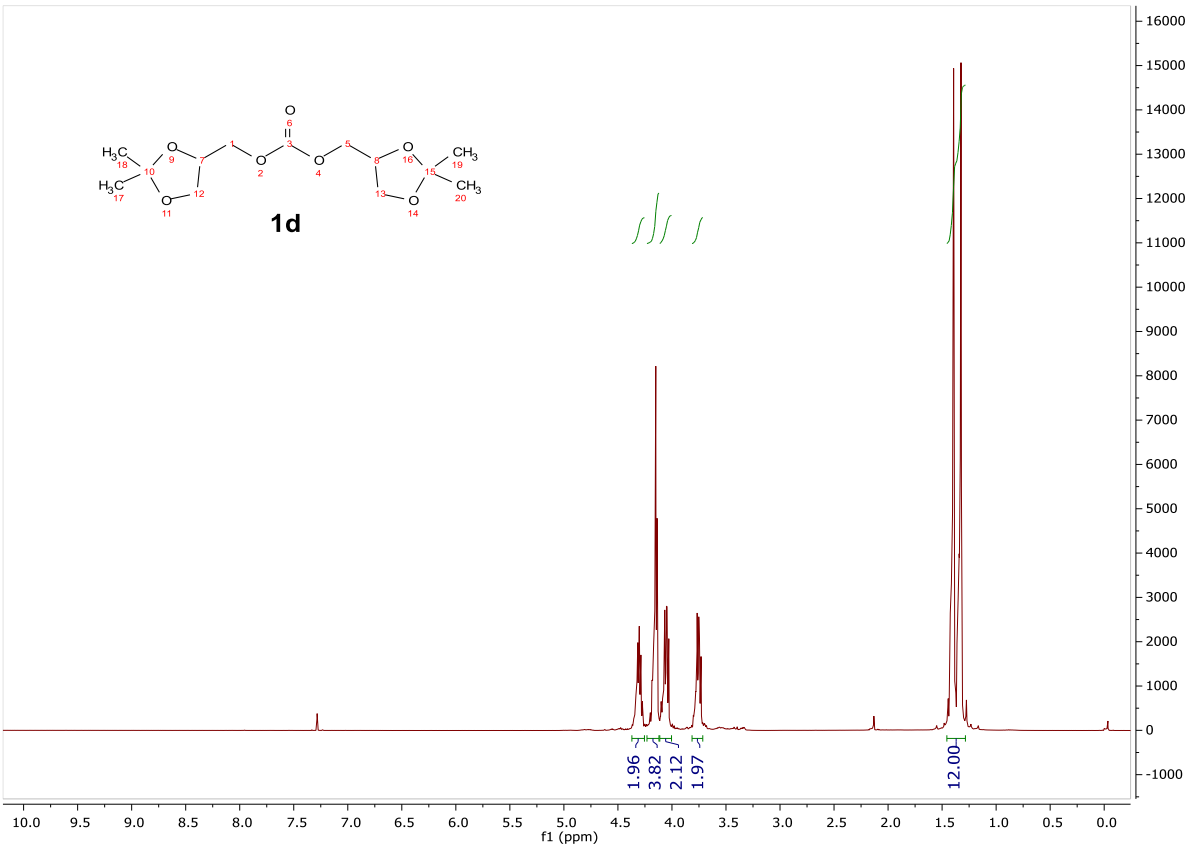

Figure 7.30. ^{1}H NMR of bis((2,2-dimethyl-1,3-dioxolan-4-yl)methyl) carbonate (**1d**).

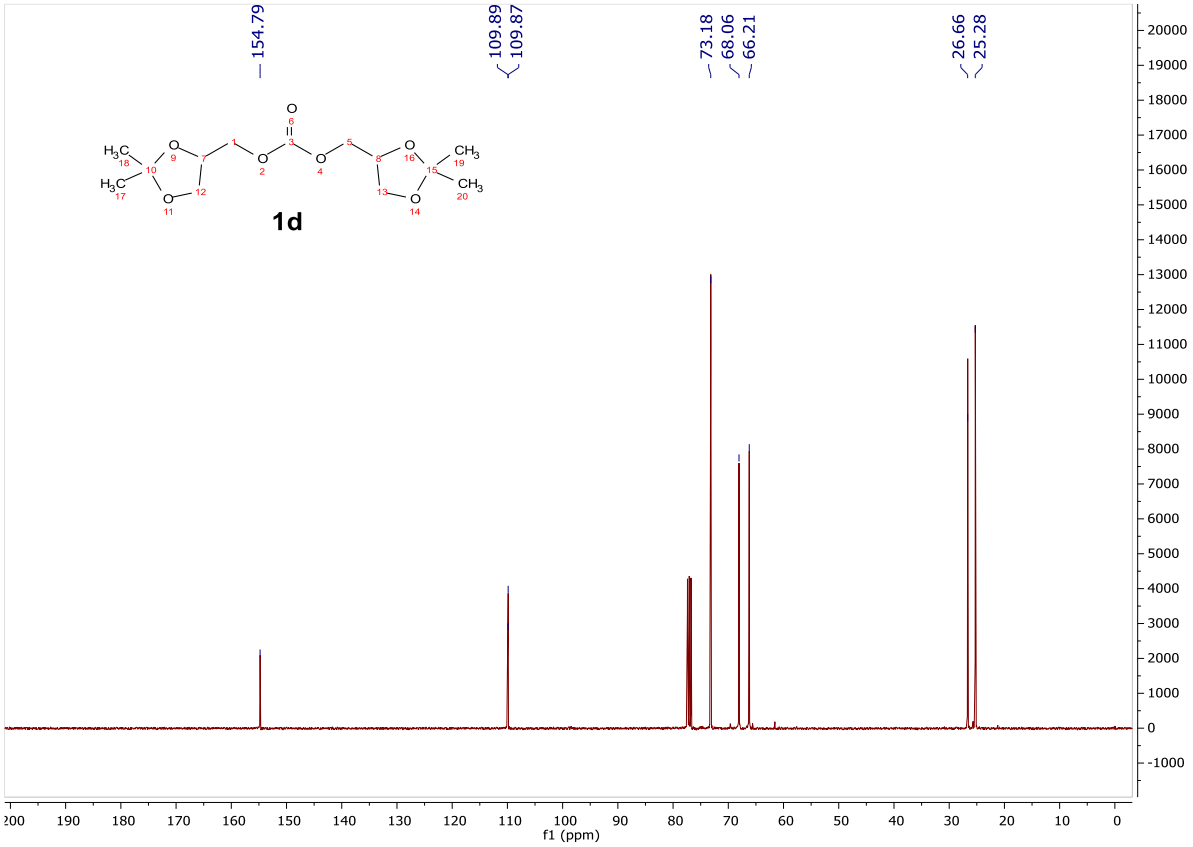

Figure 7.31. ^{13}C NMR of bis((2,2-dimethyl-1,3-dioxolan-4-yl)methyl) carbonate (**1d**).

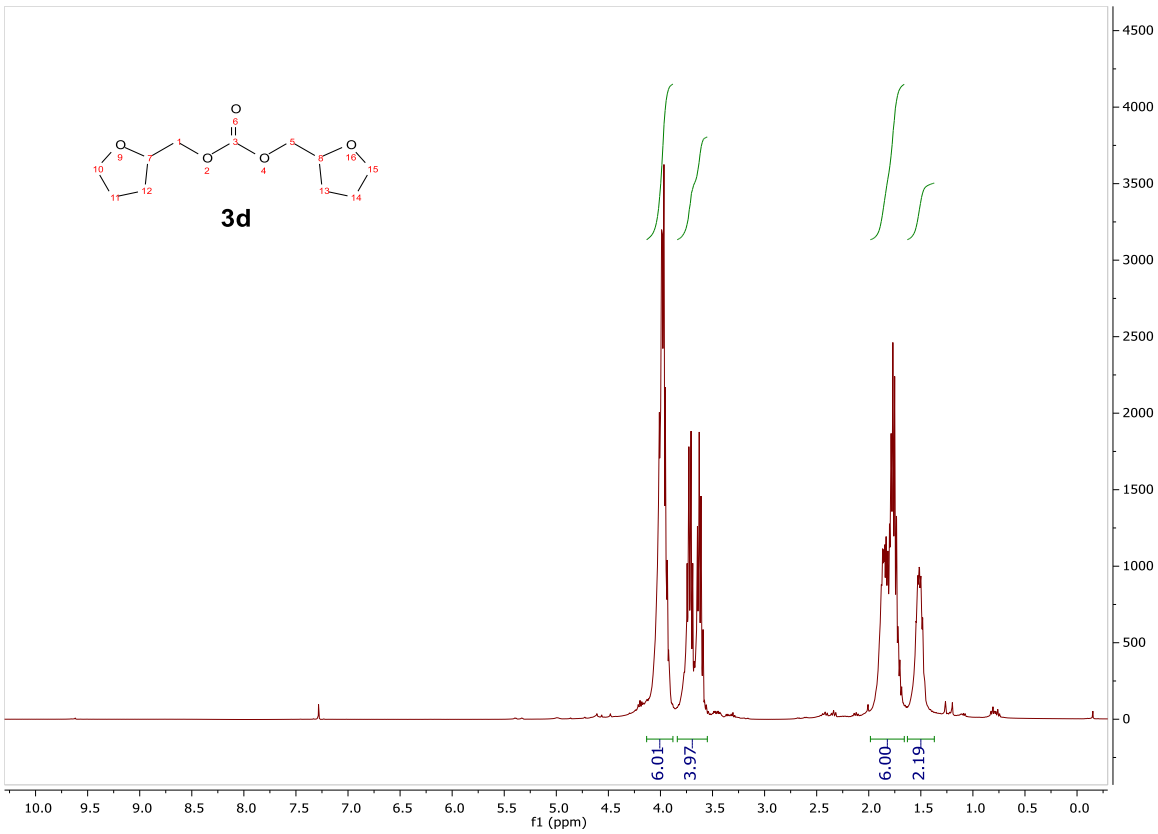

Figure 7.32. ^{1}H NMR of bis((tetrahydrofuran-2-yl)methyl) carbonate (**3d**).

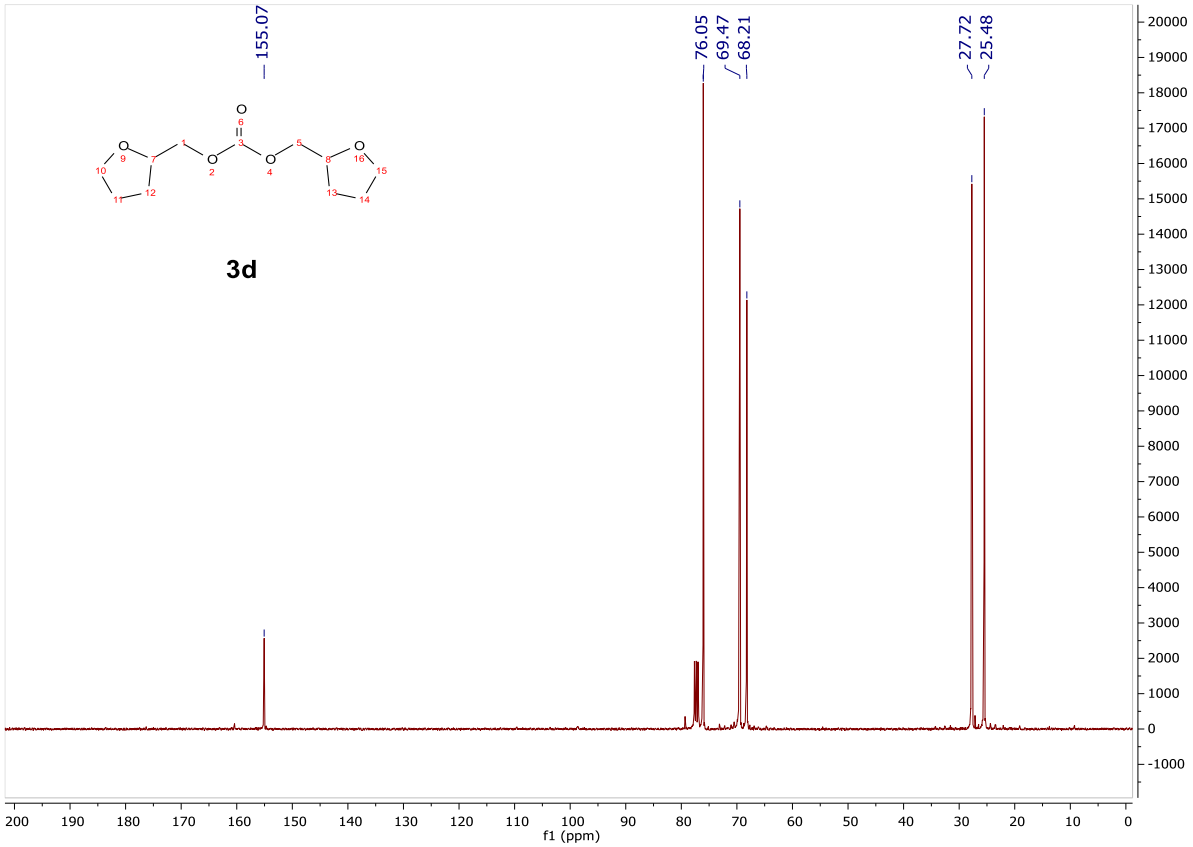

Figure 7.33. ^{13}C NMR of bis((tetrahydrofuran-2-yl)methyl) carbonate (**3d**).

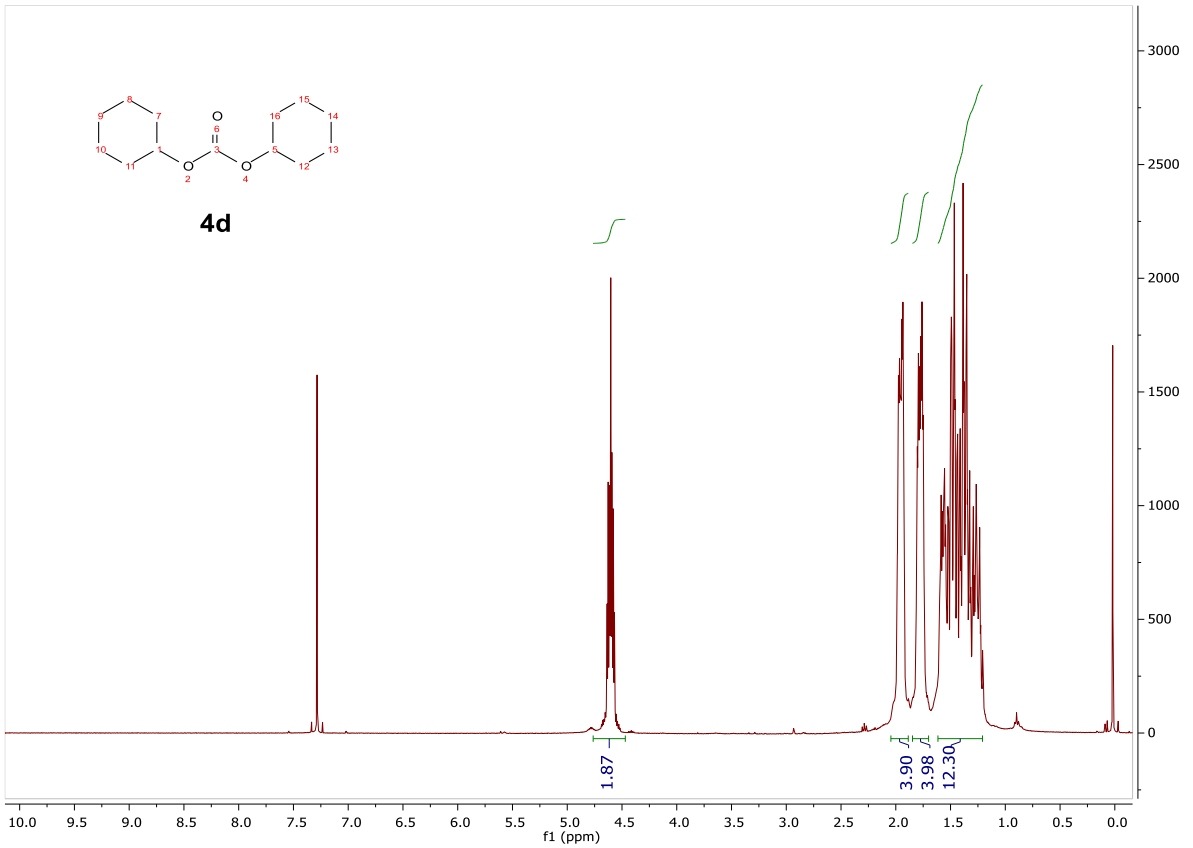

Figure 7.34. ^{1}H NMR of dicyclohexyl carbonate (**4d**).

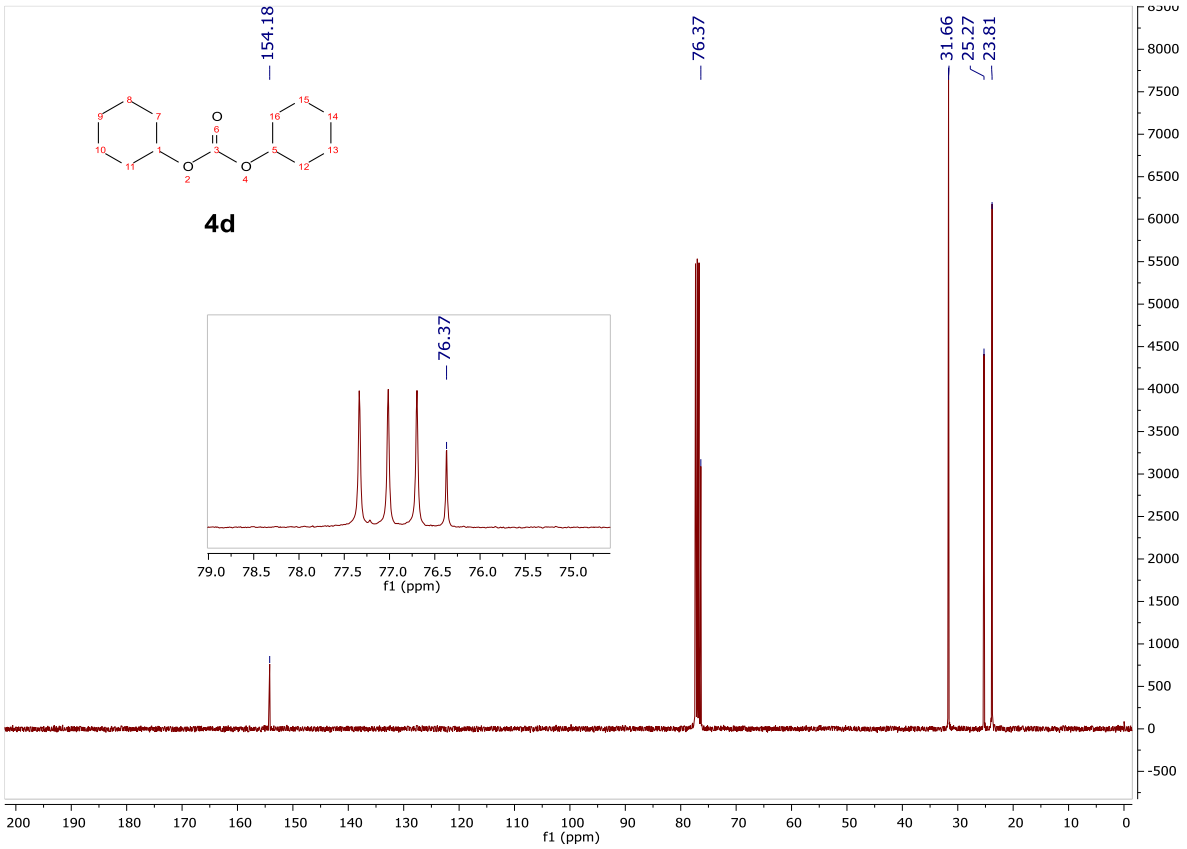

Figure 7.35. ^{13}C NMR of dicyclohexyl carbonate (**4d**).

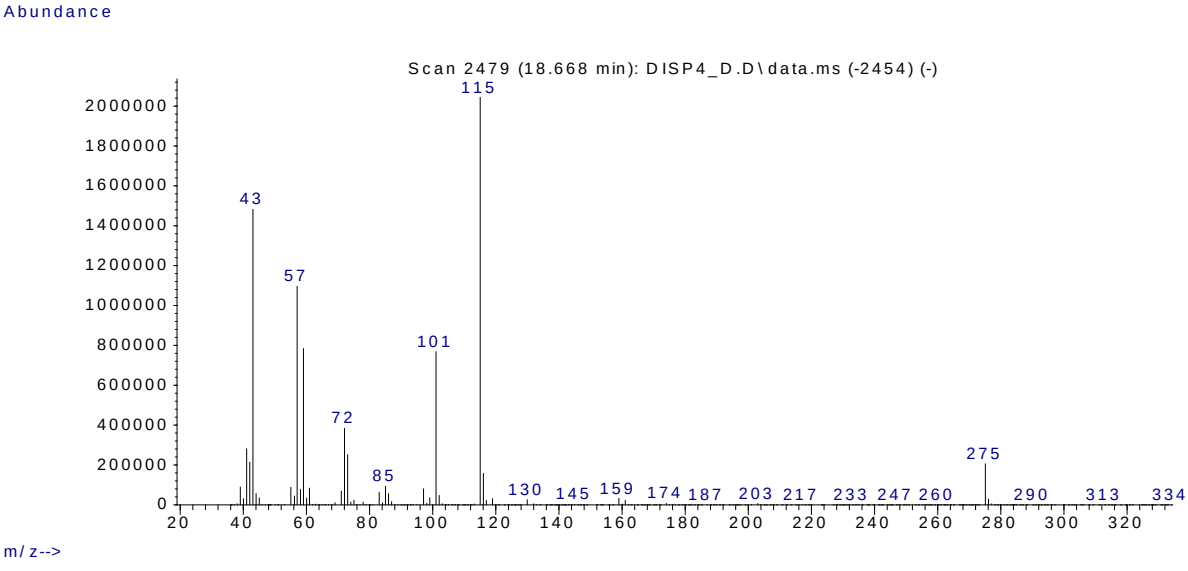

Figure 7.36. MS spectrum of compound **1d.**

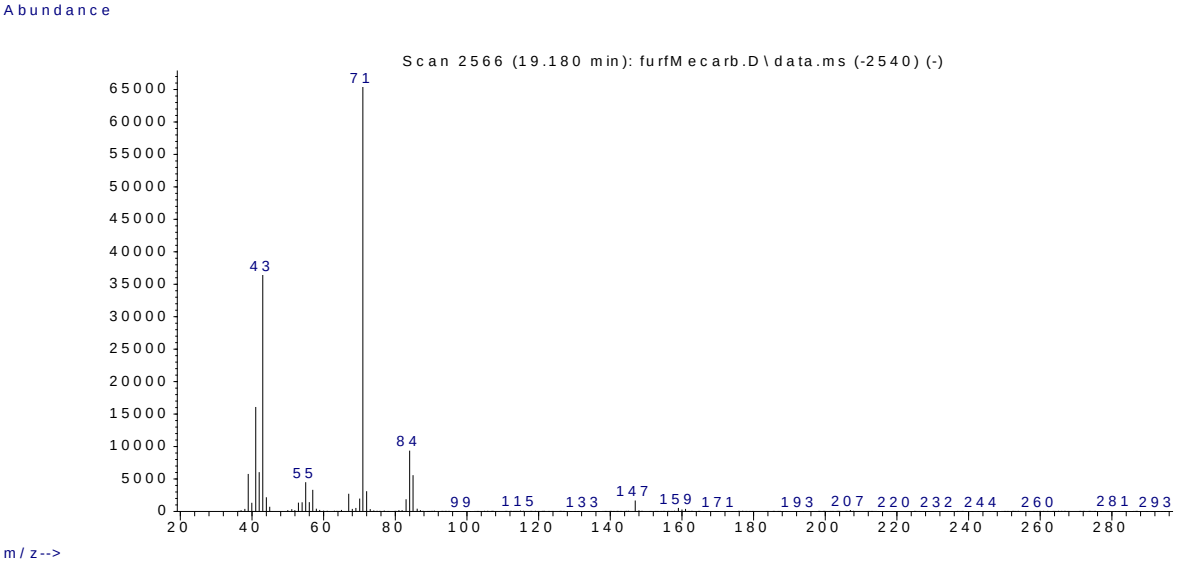

Figure 7.37. MS spectrum of compound **3d.**

7.3. Renewable Aromatics from Kraft Lignin with Molybdenum-Based Catalysts (Chapter 4)

7.3.1. GC calibration curves

The GC calibration curve for the quantification of toluene, o-xylene, p-xylene, benzyl alcohol, o-tolylmethanol, p-tolylmethanol, 2-methyl benzaldehyde, 3-methoxyphenol, 1,2-dimethyl-4-vinylbenzene, propylbenzene and 1-ethyl-2,4-dimethylbenzene were obtained using *o*-cresol as the internal standard. Five different solutions of the commercial anisole, previously distilled under vacuum, were prepared in a mixture comprised of *n*-decane (85 wt%) and toluene (15 wt%). Specifically, the solution were prepared at $5.0 \cdot 10^{-3}$ M, $1.7 \cdot 10^{-3}$ M, $8.73 \cdot 10^{-4}$ M, $4.1 \cdot 10^{-4}$ M and $2.1 \cdot 10^{-4}$ M concentration. To each solution, the same quantity of anisole was added.

Figure 7.46 shows the results of the calibration test.

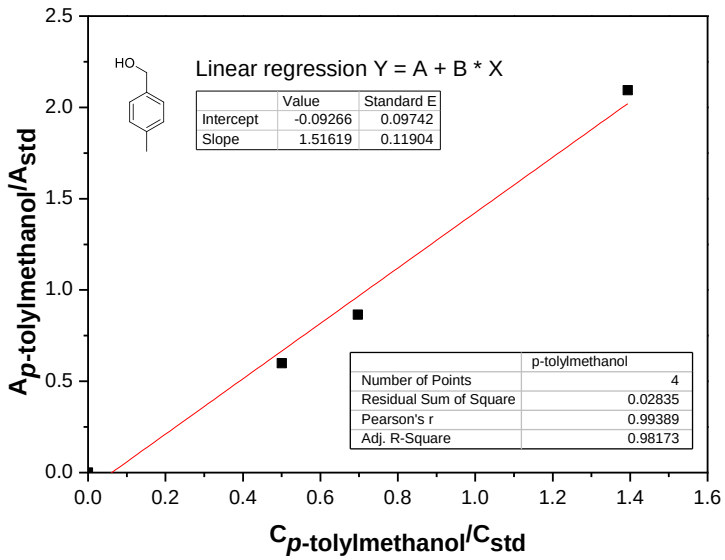

Figure 7.38. Calibration curve for *p*-tolylmethanol. $A_{p\text{-tolylmethanol}}/A_{std}$ was the ratio of the HPLC area responses of *p*-tolylmethanol and *o*-cresol.

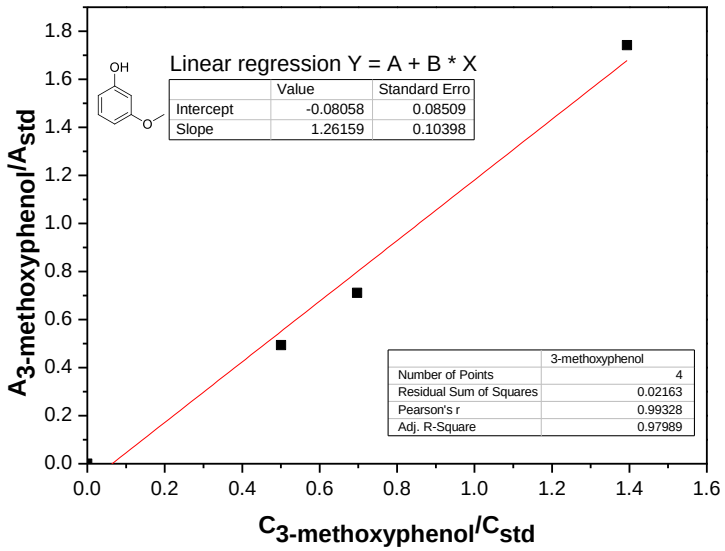

Figure 7.39. Calibration curve for 3-methoxyphenol. $A_{3\text{-methoxyphenol}}/A_{std}$ was the ratio of the HPLC area responses of 3-methoxyphenol and *o*-cresol.

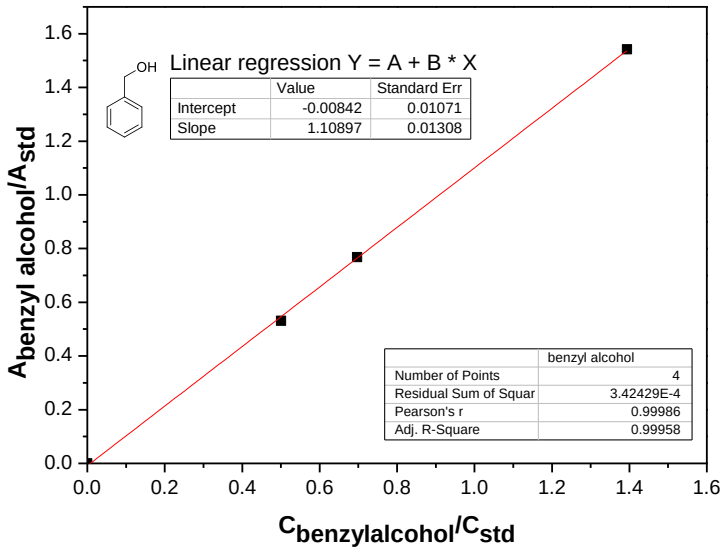

Figure 7.40. Calibration curve for 3-methoxyphenol. $A_{3\text{-methoxyphenol}}/A_{std}$ was the ratio of the HPLC area responses of 3-methoxyphenol and *o*-cresol.

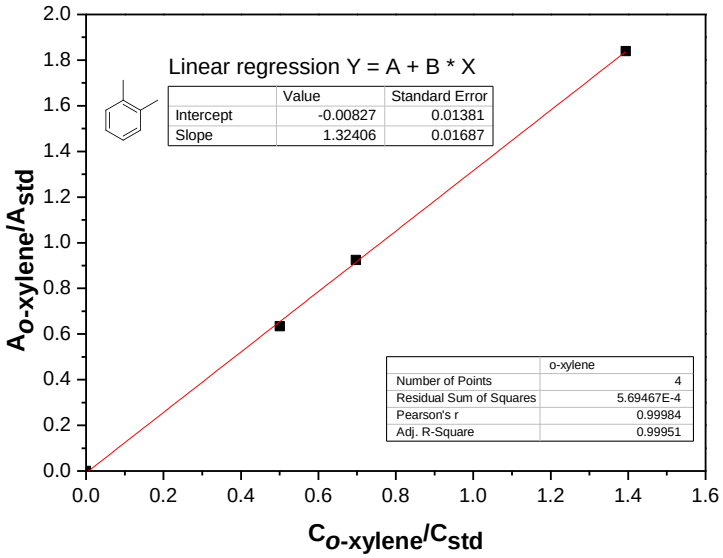

Figure 7.41. Calibration curve for *o*-xylene. $A_{o\text{-xylene}}/A_{std}$ was the ratio of the HPLC area responses of *o*-xylene and *o*-cresol.

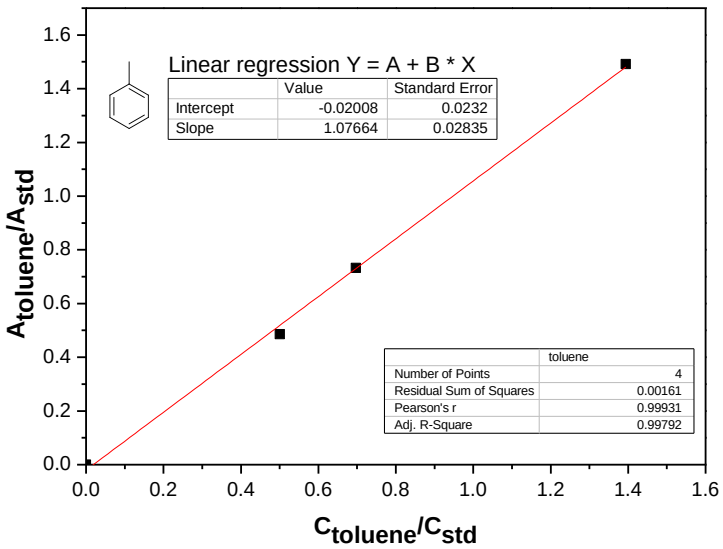

Figure 7.42. Calibration curve for toluene. $A_{toluene}/A_{std}$ was the ratio of the HPLC area responses of toluene and *o*-cresol.

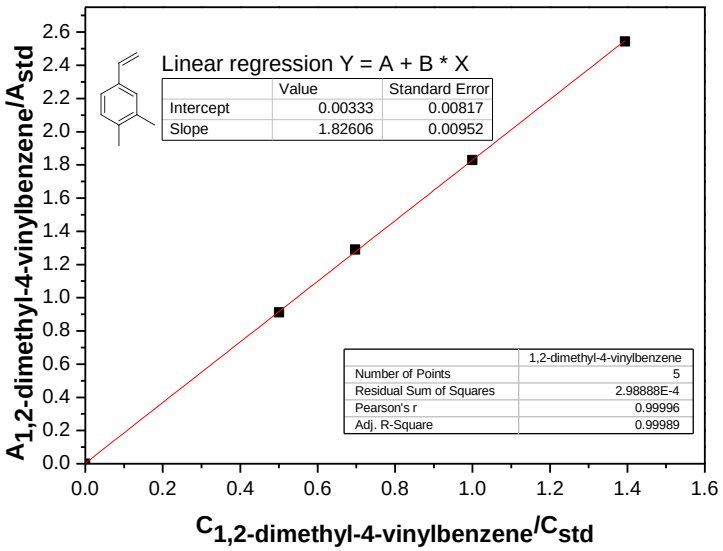

Figure 7.43. Calibration curve for 1,2-dimethyl-4-vinylbenzene. $A_{1,2\text{-dimethyl-4-vinylbenzene}}/A_{std}$ was the ratio of the HPLC area responses of 1,2-dimethyl-4-vinylbenzene and *o*-cresol.

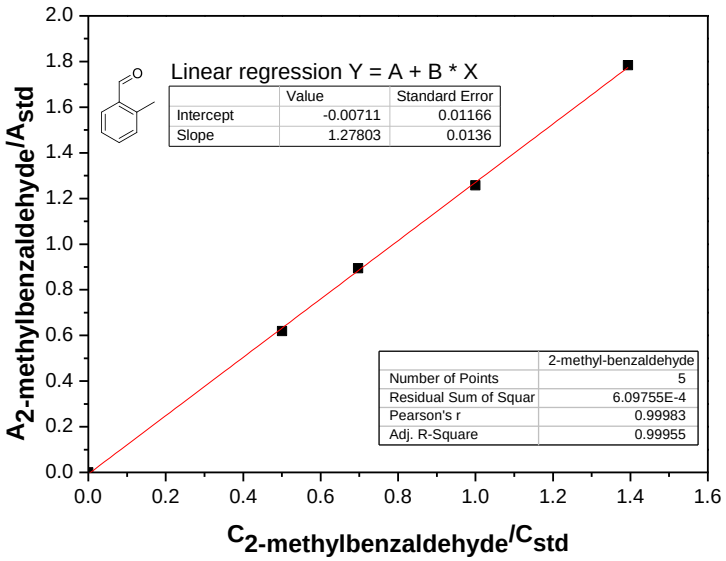

Figure 7.44. Calibration curve for 2-methylbenzaldehyde. $A_{2\text{-methylbenzaldehyde}}/A_{std}$ was the ratio of the HPLC area responses of 2-methylbenzaldehyde and *o*-cresol.

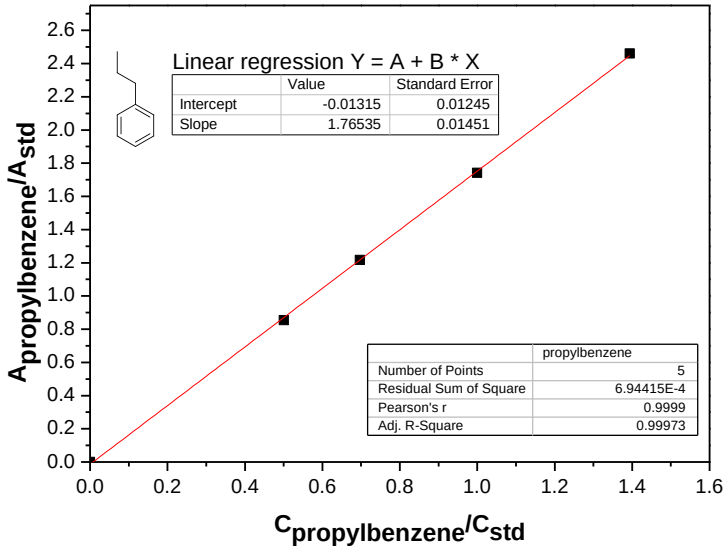

Figure 7.45. Calibration curve for propylbenzene. $A_{propylbenzene}/A_{std}$ was the ratio of the HPLC area responses of propylbenzene and *o*-cresol.

7.4. Extractive Denitrogenation of Fuel Oils with Ionic Liquids: A Systematic Study (Chapter 5)

7.4.1. HPLC calibration curves

The HPLC calibration curve for the quantification of pyridine was obtained using anisole as the external standard. Five different solutions of the commercial anisole, previously distilled under vacuum, were prepared in a mixture comprised of *n*-decane (85 wt%) and toluene (15 wt%). Specifically, the solution were prepared at $5.0 \cdot 10^{-3}$ M, $1.7 \cdot 10^{-3}$ M, $8.73 \cdot 10^{-4}$ M, $4.1 \cdot 10^{-4}$ M and $2.1 \cdot 10^{-4}$ M concentration. To each solution, the same quantity of anisole was added.

Figure 7.46 shows the results of the calibration test.

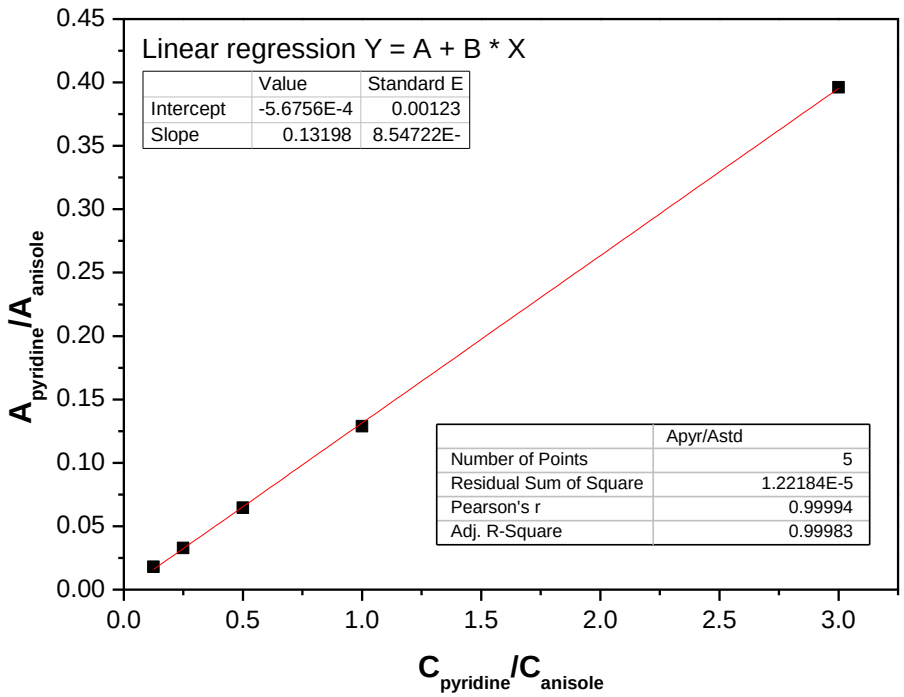

Figure 7.46. Calibration curve for pyridine. Anisole was used as the standard, $A_{pyridine}/A_{anisole}$ was the ratio of the HPLC area responses of pyridine and anisole.

The HPLC calibration curve for the quantification of indole was obtained using guaiacole as the external standard. Four different solutions of the commercial indole, previously distilled under vacuum, were prepared in a mixture comprised of *n*-decane (85 wt%) and toluene (15 wt%). Specifically, the solution were prepared at $5.0 \cdot 10^{-3}$ M, $1.6 \cdot 10^{-3}$ M, $5.0 \cdot 10^{-4}$ M and $2.1 \cdot 10^{-4}$ M concentration. To each solution, the same quantity of guaiacole was added.

Figure 7.47 shows the results of the calibration test.

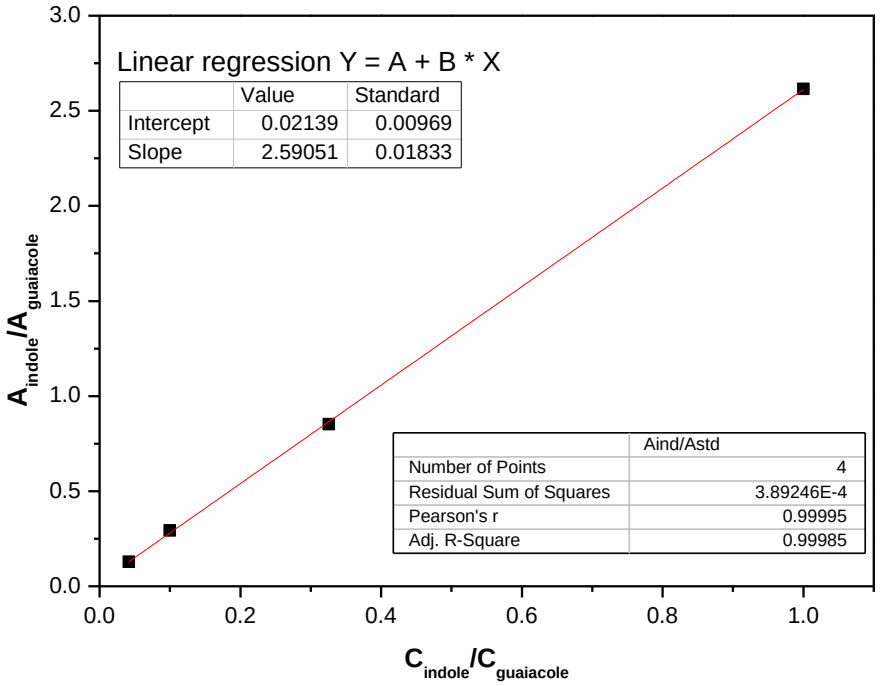

Figure 7.47. Calibration curve for indole. Guaiacole was used as the standard, $A_{indole}/A_{guaiacole}$ was the ratio of the HPLC area responses of pyridine and anisole.

Table 7.3. Decrease in pyridine concentration of oil phase versus time (temperature: 25 ºC; 3.43 mmol of ionic liquids/2 mL model oil).

	Decrease in pyridine concentration of oil phase (M/M %)		
	10 minutes	**20 minutes**	**30 minutes**
$[C_2C_1im][NTf_2]$	69.5	69.6	69.9
$[C_4C_1im][NTf_2]$	75.1	75.8	75.9
$[C_6C_1im][NTf_2]$	76.7	77.0	77.4
$[C_8C_1im][NTf_2]$	78.4	78.1	78.4
$[C_{10}C_1im][NTf_2]$	81.5	81.4	81.6
$[C_4C_1pyrr][NTf_2]$	71.1	70.7	71.4
$[C_4py][NTf_2]$	71.8	72.7	71.0
$[C_4{}^4C_1py][NTf_2]$	78.1	78.4	77.4
$[C_4C_1C_1im][NTf_2]$	73.9	73.6	72.7
$[C_4C_1im][OTf]$	71.9	71.8	71.5
$[C_4C_1im][PF_6]$	66.1	66.2	67.4
$[C_4C_1im][BF_4]$	57.8	57.3	58.4

Table 7.4. Decrease in indole concentration of oil phase versus time (temperature: 25 ºC; 3.43 mmol of ionic liquids/2 mL model oil).

	Decrease in indole concentration of oil phase (M/M %)		
	10 minutes	**20 minutes**	**30 minutes**
$[C_2C_1im][NTf_2]$	97.1	97.2	97.1
$[C_4C_1im][NTf_2]$	97.5	97.5	97.5
$[C_6C_1im][NTf_2]$	97.9	97.8	97.8
$[C_8C_1im][NTf_2]$	98.1	98.1	98.0
$[C_{10}C_1im][NTf_2]$	98.0	97.7	97.9
$[C_4C_1pyrr][NTf_2]$	97.9	98.0	98.0
$[C_4py][NTf_2]$	98.3	98.3	98.3
$[C_4{}^4C_1py][NTf_2]$	98.7	98.8	98.8
$[C_4C_1C_1im][NTf_2]$	98.0	98.1	97.8
$[C_4C_1im][OTf]$	98.0	98.1	98.0
$[C_4C_1im][PF_6]$	95.1	95.3	94.8
$[C_4C_1im][BF_4]$	97.1	97.2	97.2

7.4.2. NMR analysis of ILs

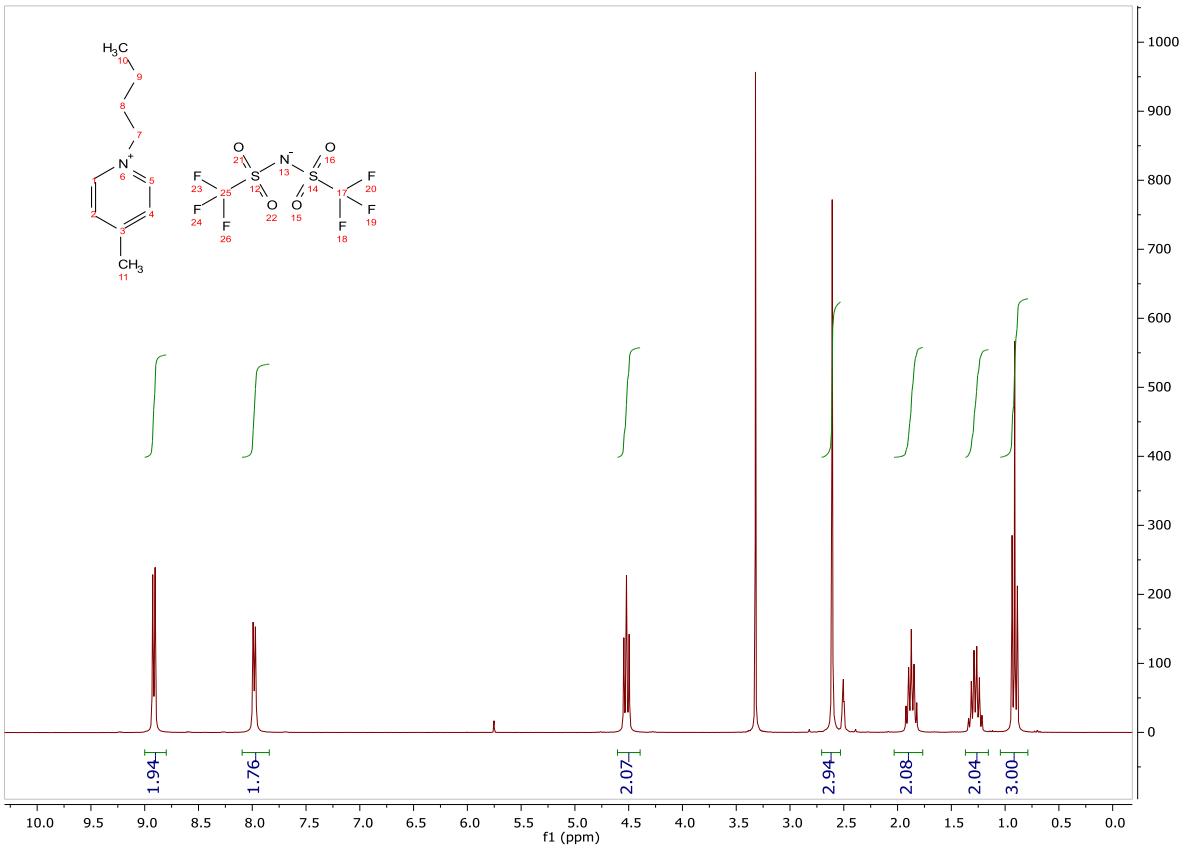

Figure 7.48. ^{1}H NMR of $[C_4{}^4C_1py][NTf_2]$.

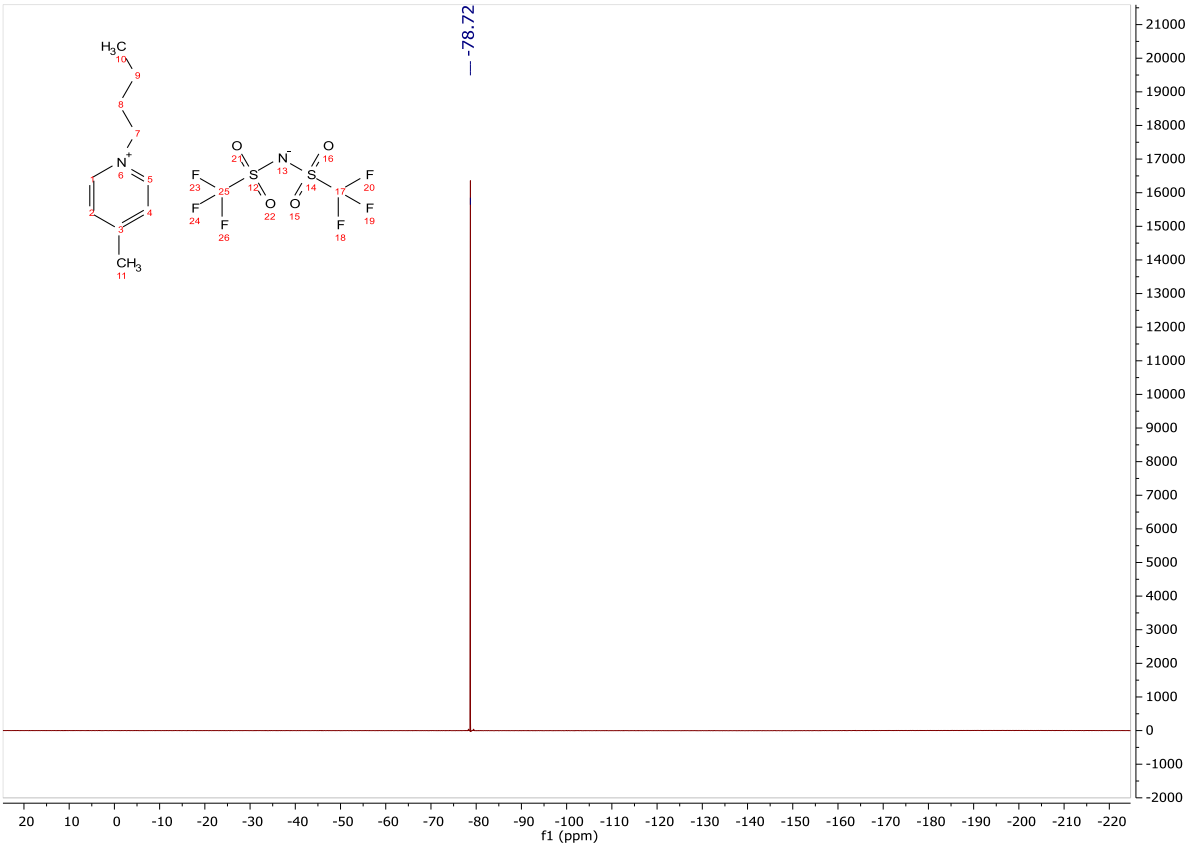

Figure 7.49. ^{19}F NMR of $[C_4{}^4C_1py][NTf_2]$.

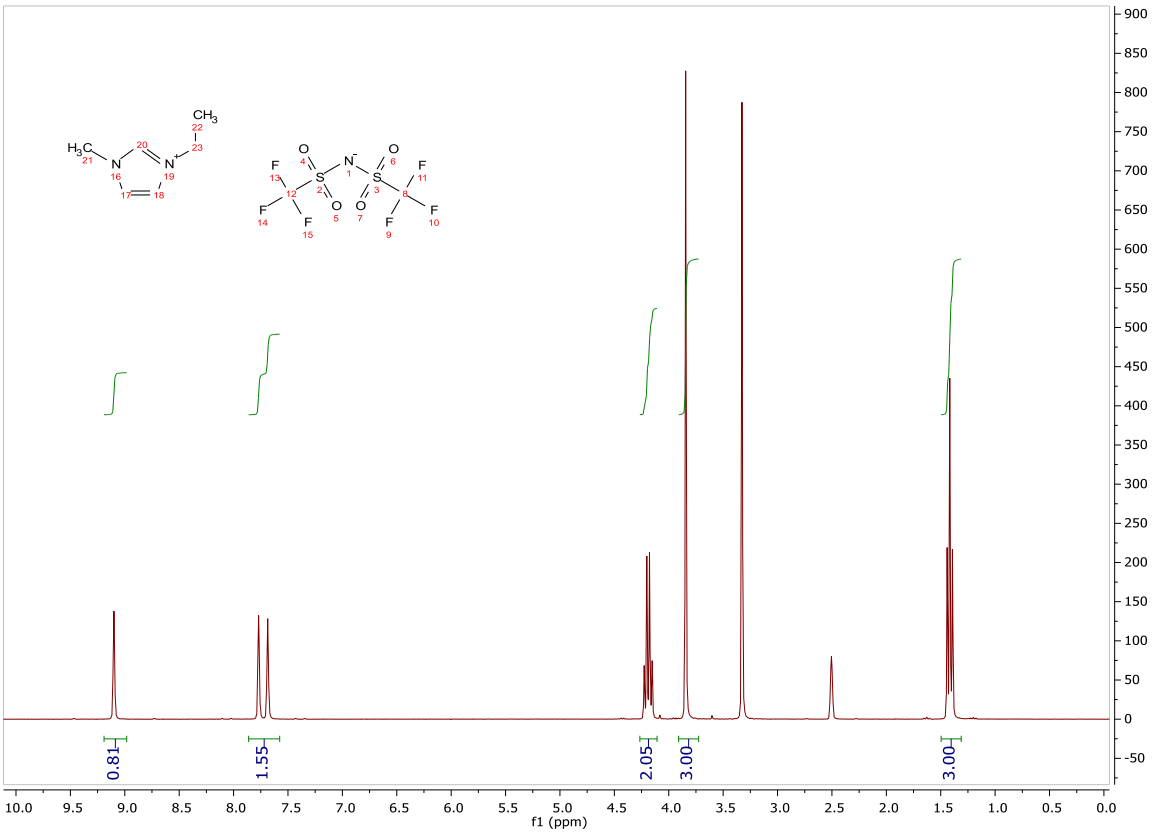

Figure 7.50. ^1H NMR of $[C_2C_1im][NTf_2]$.

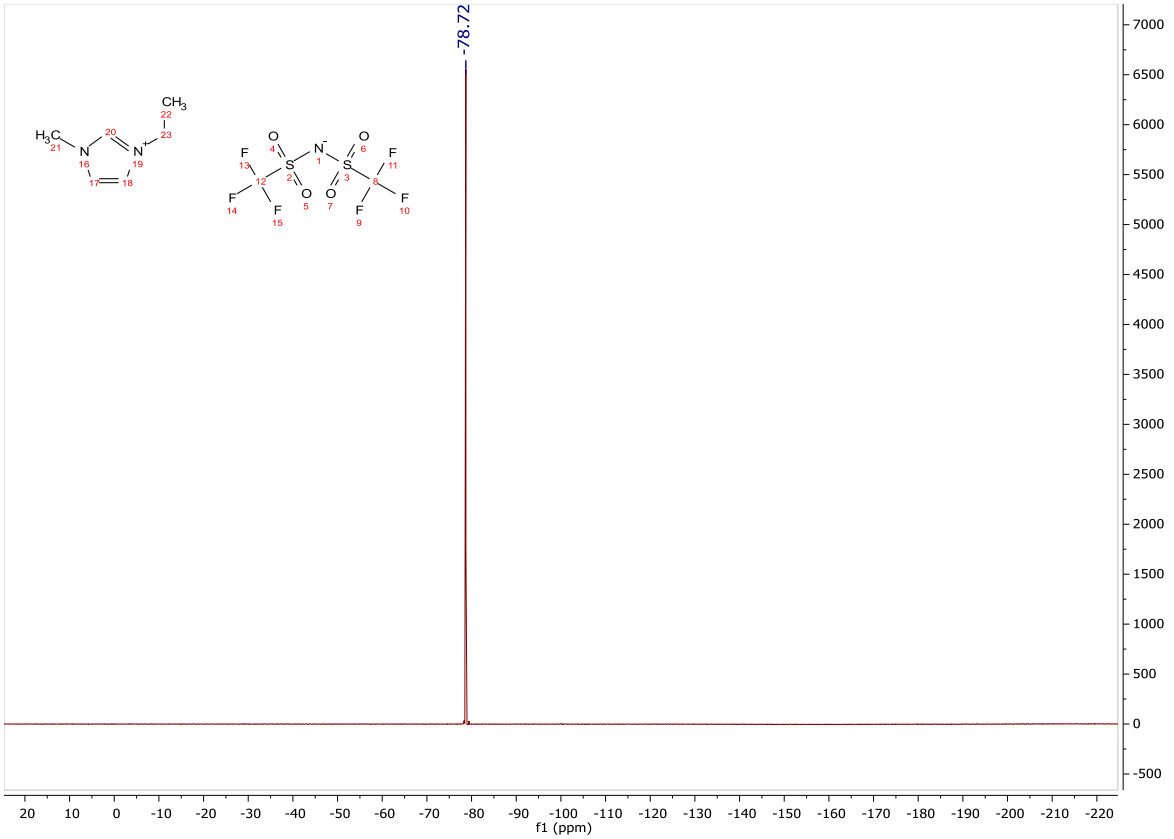

Figure 7.51. ^{19}F NMR of $[C_2C_1im][NTf_2]$.

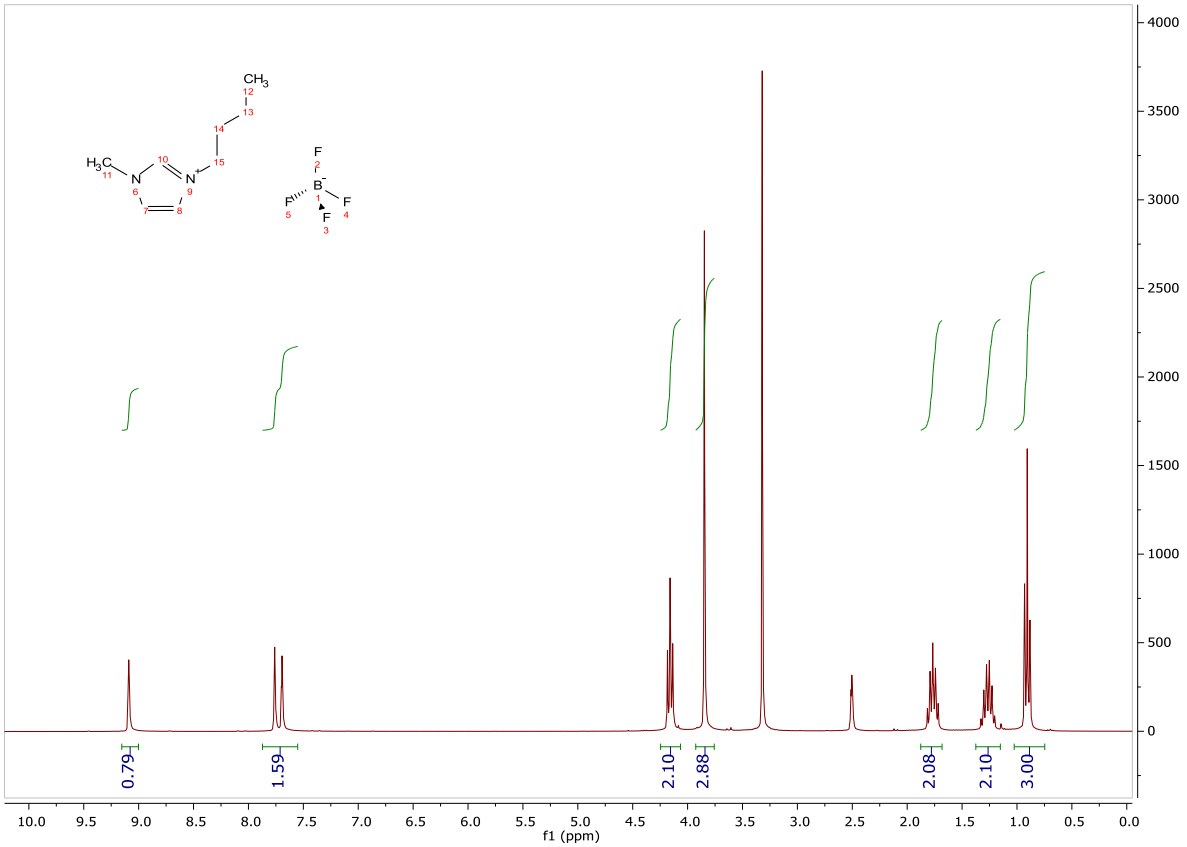

Figure 7.52. ^{1}H NMR of $[C_4C_1im][BF_4]$.

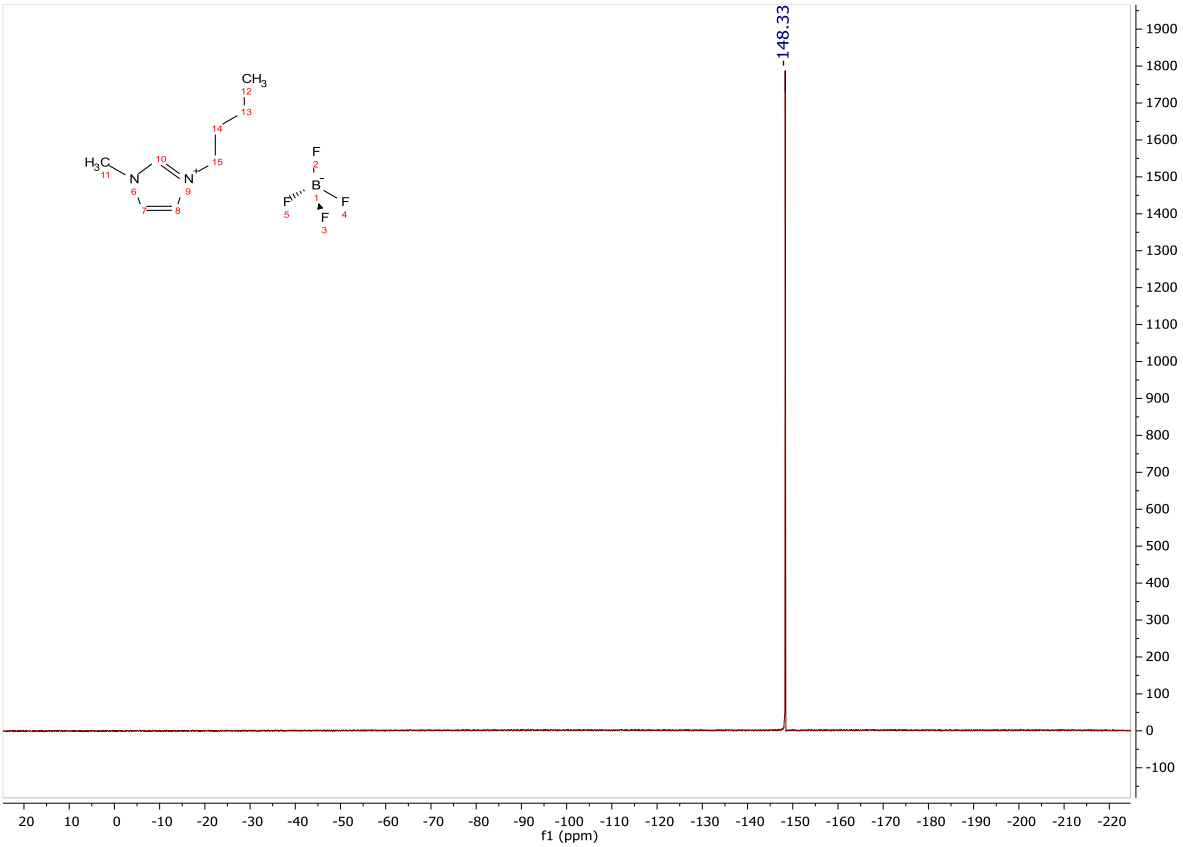

Figure 7.53. ^{19}F NMR of $[C_4C_1im][BF_4]$.

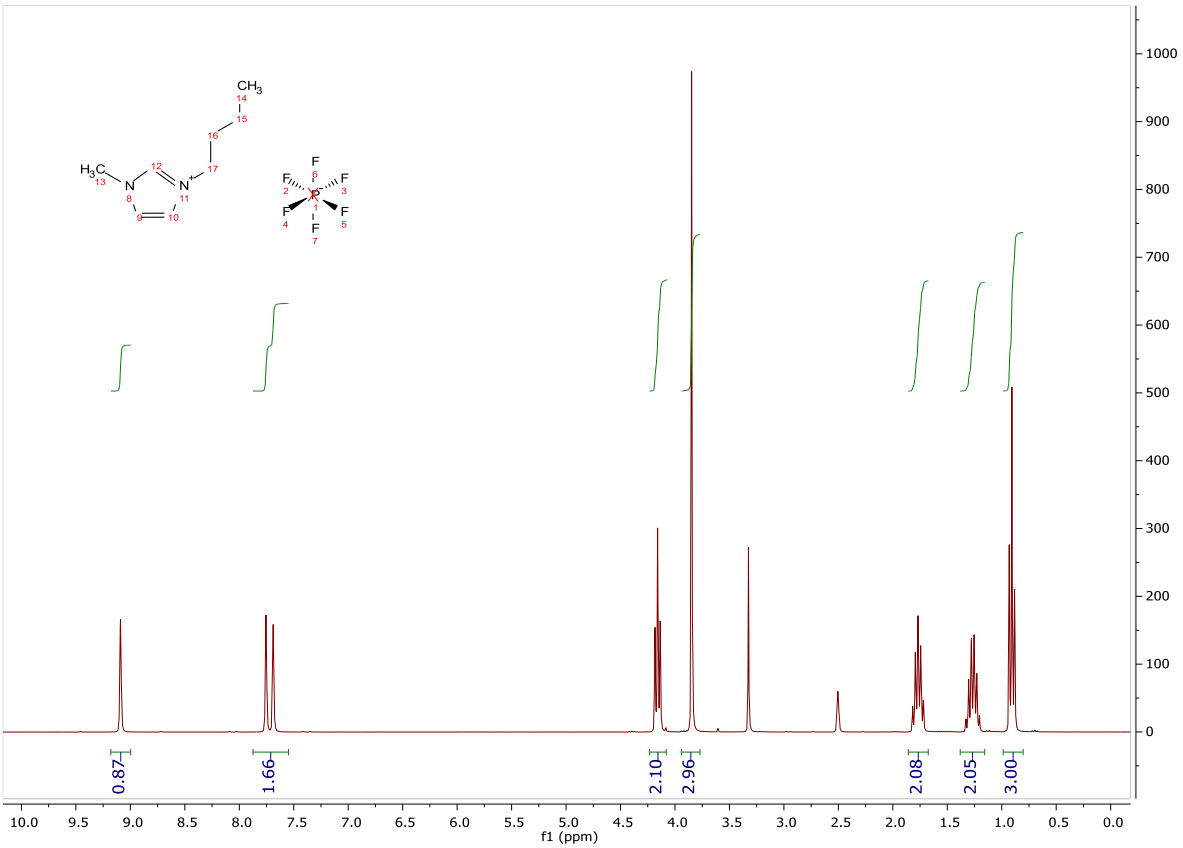

Figure 7.54. ^{1}H NMR of $[C_4C_1im][PF_6]$.

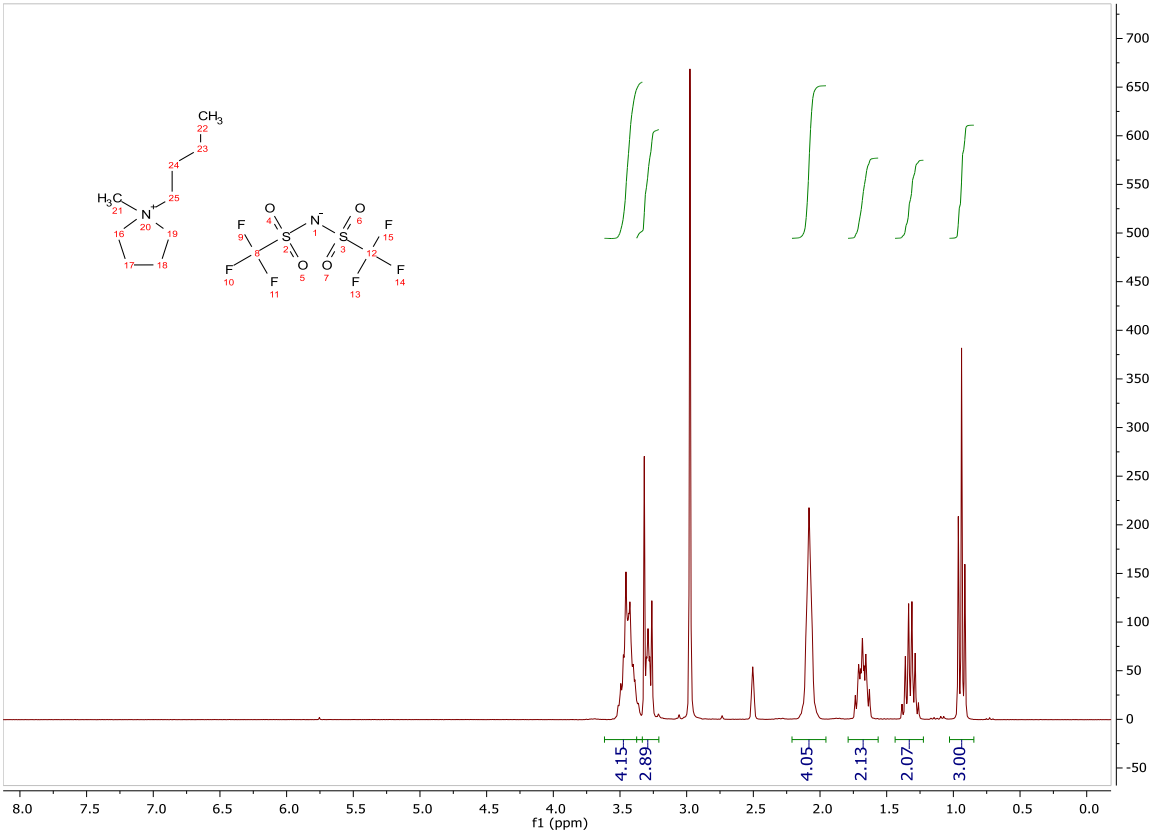

Figure 7.55. ^{1}H NMR of [C_4C_1pyrr][NTf_2].

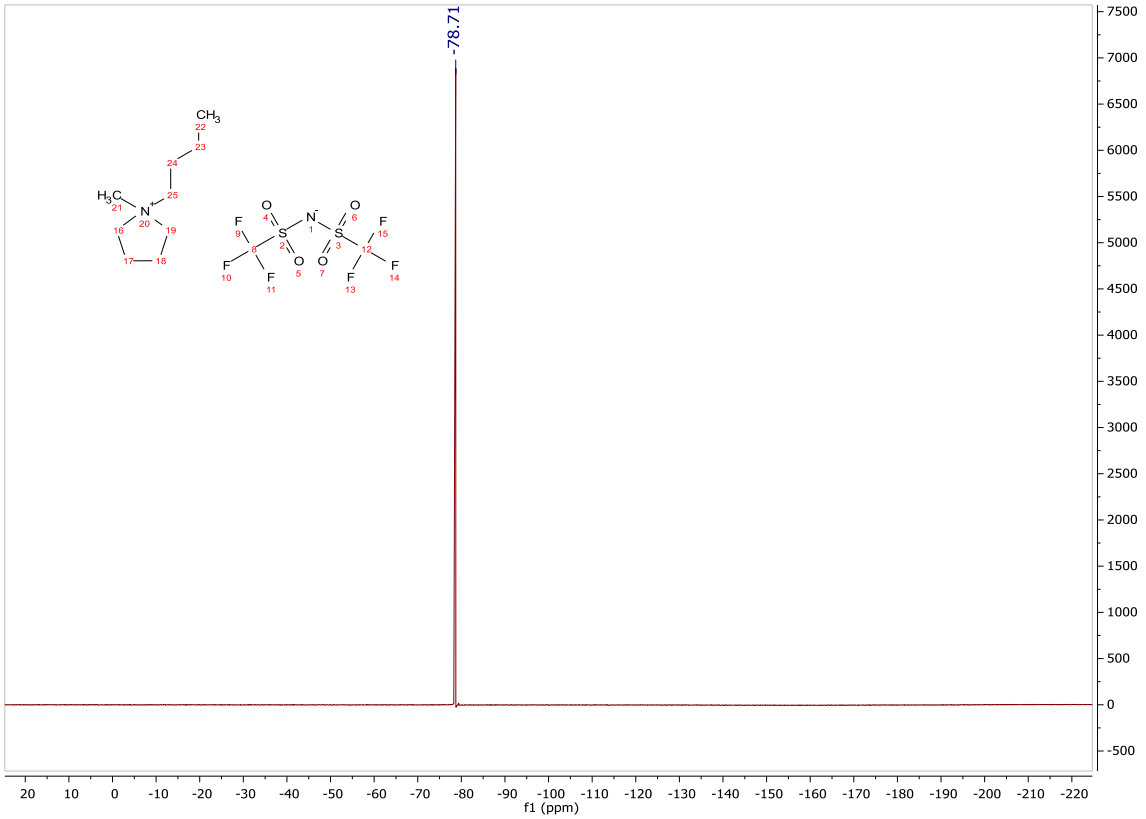

Figure 7.56. ^{19}F NMR of [C_4C_1pyrr][NTf_2].

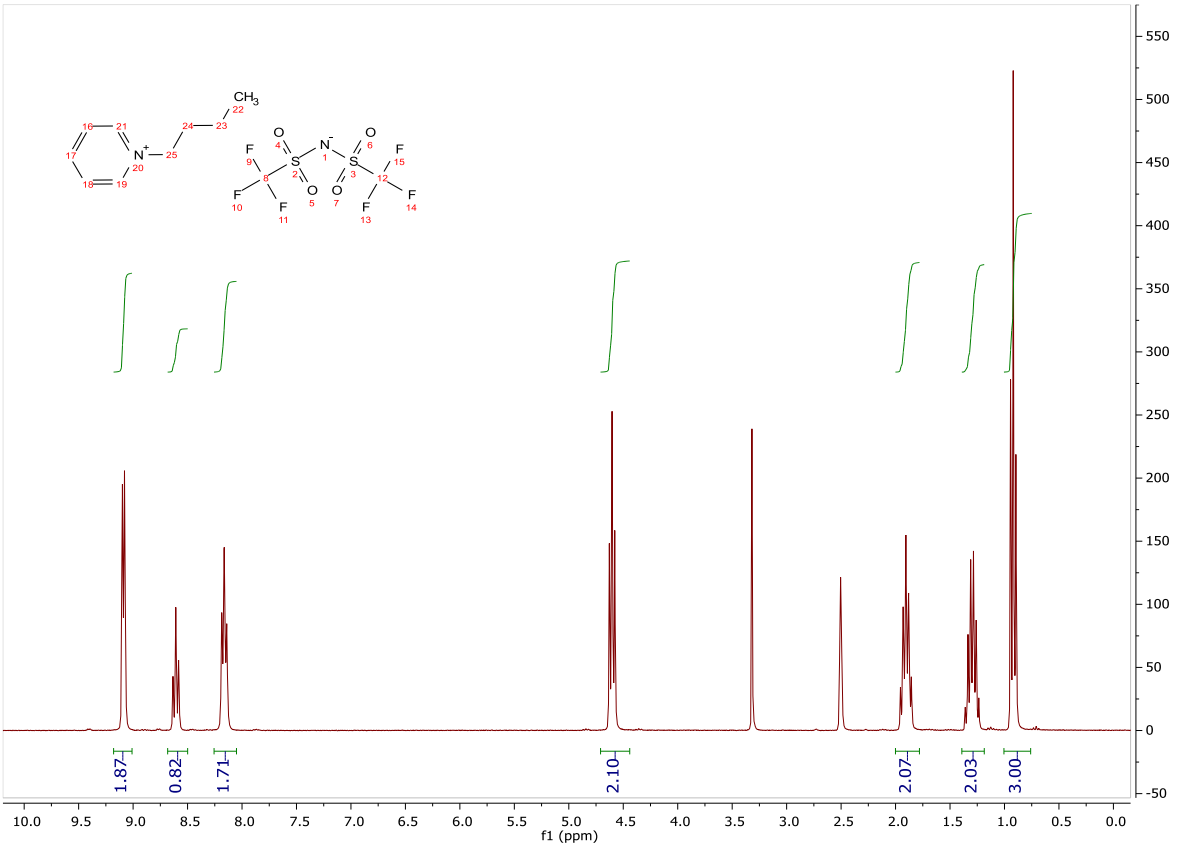

Figure 7.57. ^{1}H NMR of [C_4py][NTf_2].

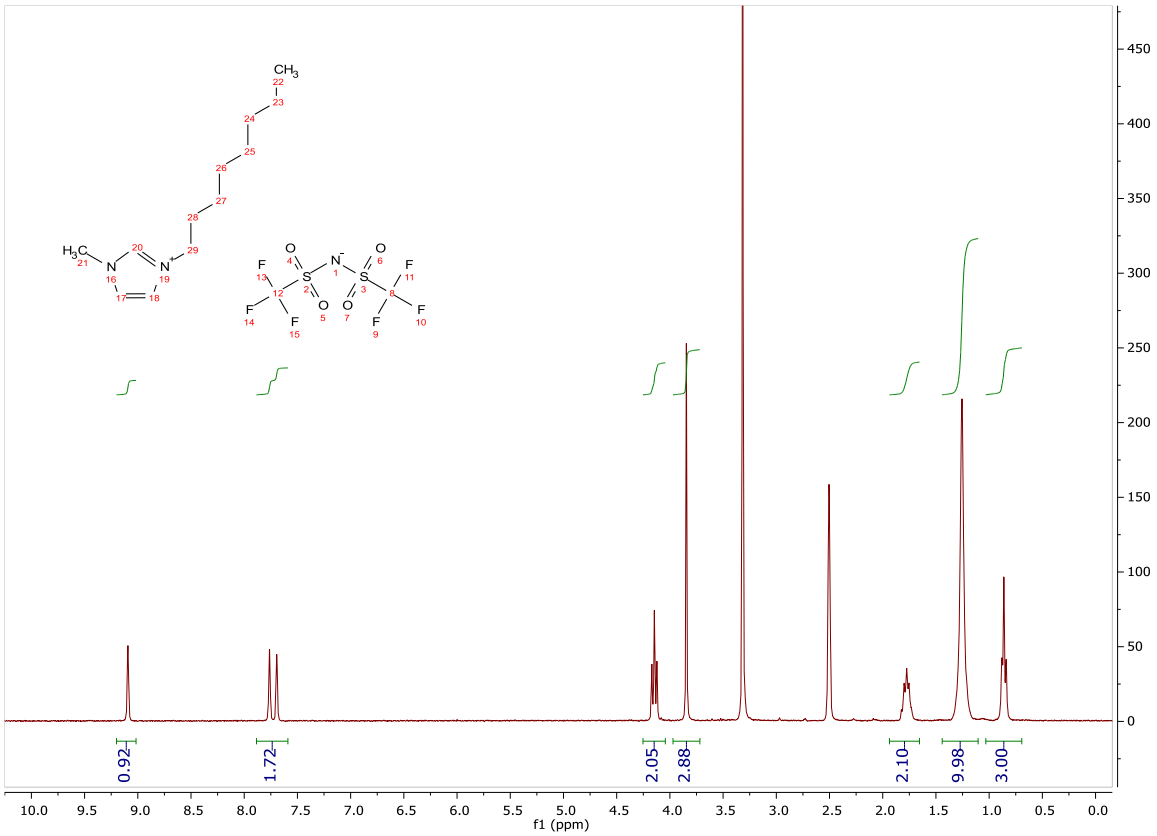

Figure 7.58. ^{1}H NMR of [C_8C_1][NTf_2].

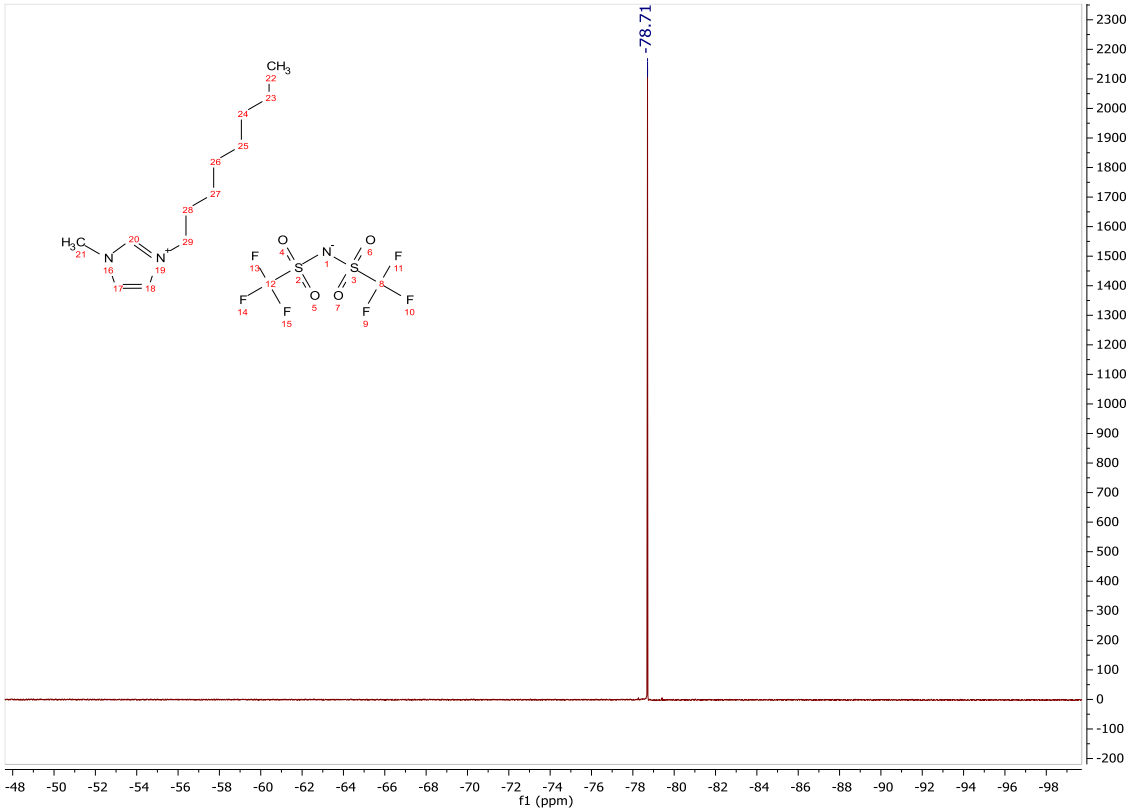

Figure 7.59. ^{19}F NMR of $[C_8C_1][NTf_2]$.

7.5. Bibliography

[1] Scholz, E.; HYDRANAL®-manual, 2012, Sigma-Aldrich Laborchemikalien GmbH, Seelze, Germany;
[2] U. Costantino, F. Marmottini, M. Nocchetti, R. Vivani, R. *European Journal of Inorganic Chemistry*, 1998, **10**, 1439-1446.

BEILSTEIN JOURNAL OF ORGANIC CHEMISTRY

Ionic liquids as transesterification catalysts: applications for the synthesis of linear and cyclic organic carbonates

Maurizio Selva*, Alvise Perosa, Sandro Guidi and Lisa Cattelan

Review

Open Access

Address:
Dipartimento di Scienze Molecolari e Nanosistemi, Università Ca' Foscari Venezia, Via Torino, 155 – Venezia Mestre, Italy

Email:
Maurizio Selva* - selva@unive.it

* Corresponding author

Keywords:
ionic liquids; transesterification; organocatalysts; organic carbonates

Beilstein J. Org. Chem. **2016,** *12,* 1911–1924.
doi:10.3762/bjoc.12.181

Received: 04 April 2016
Accepted: 10 August 2016
Published: 26 August 2016

This article is part of the Thematic Series "Green chemistry".

Guest Editor: L. Vaccaro

Abstract

The use of ionic liquids (ILs) as organocatalysts is reviewed for transesterification reactions, specifically for the conversion of nontoxic compounds such as dialkyl carbonates to both linear mono-transesterification products or alkylene carbonates. An introductory survey compares pros and cons of classic catalysts based on both acidic and basic systems, to ionic liquids. Then, innovative green syntheses of task-specific ILs and their representative applications are introduced to detail the efficiency and highly selective outcome of ILs-catalyzed transesterification reactions. A mechanistic hypothesis is discussed by the concept of cooperative catalysis based on the dual (electrophilic/nucleophilic) activation of reactants.

Review

Introduction

Transesterification catalysts

The transesterification is one of the classical organic reactions that has found numerous applications in laboratory practice as well as in the synthesis of a variety of intermediates in the pharmaceutical, cosmetic, fragrance, fuel and polymers industries [1]. Transesterification reactions are catalyzed under acidic, basic or even neutral conditions [2]. An excellent review by Otera et al. has detailed many applications of the most popular catalytic systems [3]. These include both acids such as sulfuric, sulfonic, phosphoric, and hydrochloric, and bases such as metal alkoxides, acetates, oxides, and carbonates. It is worth mentioning, that transesterification reactions are frequently carried out over solid (heterogeneous) catalysts to facilitate work-up, recycling, and purification of products, especially for large-scale preparations. These heterogeneous systems include supported metal oxides and binary oxide mixtures. For example, MoO_3/SiO_2 and sol–gel MoO_3/TiO_2 is used for the preparation of diphenyl oxalate monomer (DPO, Scheme 1) in polycarbonate chemistry [4,5], and TiO_2/SiO_2 and similar binary combina-

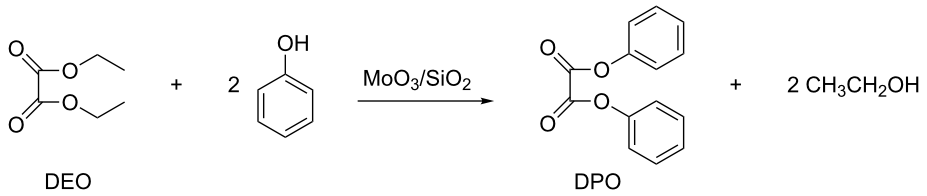

Scheme 1: The transesterification of diethyl oxalate (DEO) with phenol catalyzed by MoO_3/SiO_2.

tions are applied in the transesterification of β-ketoesters [6], and in the synthesis of unsymmetrical carbonates $R^1OC(O)OR^2$ [7].

Superacidic solids have also been described as transesterification catalysts and a remarkable example is the recently patented synthesis of sucrose-6-ester – a food sweetener – carried out over a mixture of sulfated oxides of various metals [8]. In addition, acidic ion exchange resins are worth mentioning in this context. Van de Steene et al. have proved the performance of such systems in an elegant investigation on the model transesterification of ethyl acetate with methanol [9].

The production of biodiesel blends is another sector in which the catalytic transesterification is extensively used. In particular, heterogeneous catalysts including calcium, manganese and zinc oxides as such or as mixtures are widely used to convert natural triglycerides into FAMEs or FAEEs (fatty acid methyl or ethyl esters) with methanol or ethanol, respectively [10]. The most commonly used system is CaO, which is obtained by calcination of readily available and cheap resources including waste products such as shells and even livestock bones [11-14]. However, traditional catalysts such as alkali hydroxides or alkaline methoxides are still encountered even for novel syntheses of biofuels. An example is the transesterification of oils by dimethyl carbonate (DMC) in the presence of KOH (Scheme 2) [15,16].

The reaction allows obtaining FAMEs and fatty acid glycerol carbonate monoesters (FAGCs), without the concurrent formation of glycerol, a frequently formed highly undesirable byproduct.

Enzyme catalysts: A major driving force for the choice of enzymes is their high efficiency, which allows reactions to be performed under very mild conditions and with a variety of raw materials. However, the high cost and relatively short lifetime of enzymes partly offset their advantages and an implementation of biocatalytic processes makes sense almost exclusively for the preparation of high added-value chemicals. This holds true also for enzyme-catalyzed transesterification reactions. To cite a few examples, the literature claims the use of lipase as a biocatalyst for i) the reaction of glycerol with DMC for the synthesis of glycerol carbonate (GlyC) under solvent-free conditions. A 60% yield was achieved along with an effective recycle of the catalyst [17], ii) the formation of six-membered cyclic carbonates by the transesterification of dialkyl carbonates with trimethylolpropane. The products were achieved in high yields (85%) and used as monomers for polyurethanes and polycarbonates [18], and iii) the conversion of oils for which lipase was identified as the most suitable enzyme for an innovative and green production of biodiesel [19].

Other catalytic systems: In addition to the above-described catalysts, amines and organometallic derivatives also find applications in the field of homogeneous catalytic systems for transesterification reactions. Remarkable examples are those of triethylamine (TEA) and Fe–Zn double-metal cyanide complexes [20,21]. Among other applications, these compounds successfully catalyzed the reaction of DMC and other organic carbon-

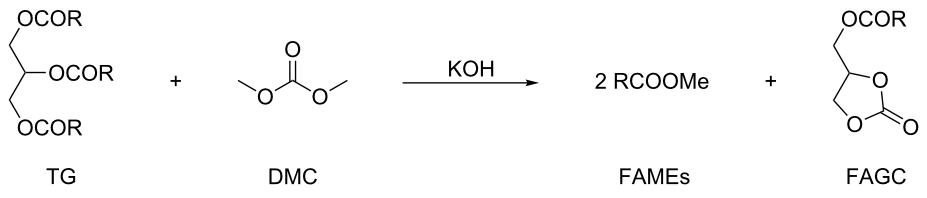

Scheme 2: Transesterification of a triglyceride (TG) with DMC for biodiesel production using KOH as the base catalyst.

ates with polyols (e.g., glycerol) to produce the expected transesterification products with total conversion and selectivity.

Ionic liquid-based organocatalysts

Conventional acid or base liquid catalysts for transesterification processes often entail several synthetic and environmental concerns including equipment corrosion, separation and purification drawbacks, and production of waste. As already mentioned in the previous paragraph, practical solutions to such problems are offered by using solid acids, although these systems may suffer from mass-transfer limitations causing low activity, and consequently, extended reaction times and deactivation from coking [22,23]. Valuable alternatives are biocatalysts, which are very active but costly. Economic issues usually restrict the use of enzymes to highly specialized productions rather than to large commercial applications [24].

In this scenario, the implementation of transesterification procedures based on innovative and possibly green catalysts remains still a highly desirable target. A strategy can be conceived by the use of task-specific ionic liquids (ILs). These compounds have shown to catalyze a number of different reactions. Only to cite a few: nitrations, Michael reactions, Friedel–Crafts alkylations and acylations are successfully promoted by ILs [25,26]. The key to such a flourishing research lies in the unique physical properties (negligible vapor pressure, wide liquid range, and non-flammability) of ILs, but mostly on the virtually infinite number of different chemical structures for liquid organic salts. These properties are often referred to as “tunable catalysts”, “task-specific ionic liquids”, and “designer solvents”, which involve the concept of optimizing the use of ILs by tailoring their chemical features for a specific transformation or for classes of similar processes [27,28]. Notably, the screening of the reaction variables includes not only the required reaction steps, but also the associated operations including separation and purification of products, recycling of solvents and catalysts, and waste treatments as well. All these additional steps contribute to the impact of the chemical process as the whole from an environmental and sustainability standpoint. For example, the isolation and purification of the desired product and reuse of the IL-based catalyst may require additional solvents for extraction and/or complex and energy-intensive separation and purification technologies. Therefore, when designing a catalytic IL-based process, one should factor-in all the reagents and solvents as well as all the downstream operations, in order to evaluate the advantages of the proposed process correctly. In this context, green metrics can provide a screening guide.

IL-based catalysts for transesterification reactions

Synthesis of IL-catalysts: IL-based catalysts for transesterification reactions mostly comprise imidazolium, phosphonium, ammonium, sulfonium and pyridinium salts. The conventional syntheses of such compounds usually start from the protonation or quaternization of neutral precursors (imidazoles, amines, phosphines, pyridine or sulfides) with Brønsted acids or haloalkanes/dialkylsulfates, respectively. In the next step, a variety of ionic liquids are obtainable by anion exchange, either through direct treatments with Lewis acids or by anion metathesis [29]. There are several reviews detailing these synthetic procedures [30,31].

More sustainable methods that avoid the use of noxious and undesirable halogens have also been recently designed [32,33]. An example is the preparation of methyl carbonate onium salts ([Q_{1nnn}][$MeOCO_2$]; Q = N, P; n = 4, 6, 8, Ph), obtained by the methylation of trialkylphosphines or -amines with nontoxic DMC (Scheme 3, top) [34,35]. Such methyl carbonate onium salts are versatile platforms as they allow access to a number of ionic liquids via anion-metathesis reactions, which produce only CH_3OH and CO_2 as byproducts (Scheme 3, bottom).

Seedon et al. reported another green protocol for the preparation of ILs. The authors described the synthesis of aqueous hydroxide solutions of organic cations, subsequently neutralized by simple acid–base reactions, giving access to ionic liquids that are difficult to prepare by any other route. This protocol avoids the use of halides, and generates water as the only byproduct [33].

Synthesis of supported ionic liquids (SILs): Ionic liquids are far more expensive than classical solvents, with costs higher by

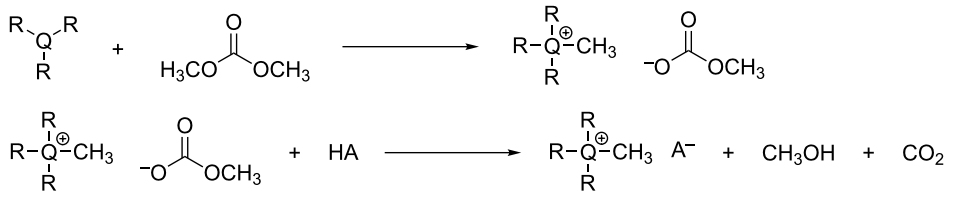

Scheme 3: Top: Green methylation of phosphines and amines by dimethyl carbonate (Q = N, P). Bottom: anion metathesis of methyl carbonate onium salts.

a factor of 10-to-50. The recycling of the ILs is therefore imperative not only to limit their release to the environment, but also for economic reasons. One strategy to cope with the recycling issue is based on the immobilization of ionic liquids onto solid supports. In the specific field of transesterification reactions, supported ionic liquid (SILs) catalysts are achieved by the dispersion of liquid organic salts on highly porous materials, amongst which montmorillonite clays, modified silica, and polystyrene-based solids are the most frequently used [36,37]. Some very recent examples described the production of biodiesel via the transesterification of glycerol trioleate with methanol: both, acidic ionic liquids (e.g., 1-allyl-3-(butyl-4-sulfonyl)imidazolium trifluoromethanesulfonate [BsAIm][OTf]) supported onto sulfhydryl-group-modified SiO_2 (MPS-SiO_2) [38], and imidazolium salts (e.g., 1-allyl-dodecylimidazolium hydroxide ([ADIm][OH]) dispersed on magnetic mesoporous $SiO_2/CoFe_2O_4$ and $CoFe_2O_4$ nanoparticles [39,40] have been reported as catalysts. In addition, the reaction of ethylene carbonate with methanol for the synthesis of DMC was described in the presence of a mesocellular silica foam (MCF) material [41]. These catalysts are easy to recover and recycled by physical separation, washing and drying.

A similar approach has been implemented through the design of polymeric ionic liquid (PILs) based systems, such as poly(*N*-heterocyclic carbene)s and ordered mesoporous resol (OMR) polymers (OMR based on hexamethylenetetramine, [C_4HMTA][SO_4H]). They have been employed to catalyze different transesterification reactions, including also the conversion of brown grease into biodiesel [42,43]. Recycling tests of polymeric ionic liquids proved their robustness for prolonged use (Figure 1).

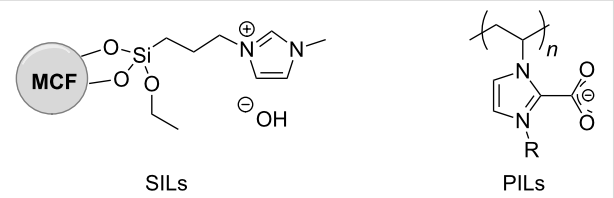

Figure 1: Structures of some representative SILs and PILs systems. MCF is a silica-based mesostructured material with ultra-large mesopores of 20–50 nm [42,43].

Recently, Zhan et al. synthesized a new acidic polyionic liquid by the copolymerization of a zwitterionic liquid based on vinylpyridinium, styrene and ethyleneglycol dimethacrylate (Scheme 4) [44]. The resulting PIL with particle sizes of about 0.5–3 mm, was an efficient catalyst for a series of esterification reactions of different acids including acetic, succinic, benzoic, and methacrylic acid and alcohols such as linear, branched and cyclic C_1–C_6 compounds. The PIL could be reused up to five times without any loss of catalytic activity and yields of various esters were always nearly quantitative.

Applications of ILs: Organocatalysts find uses in place of the common homogeneous or heterogeneous catalysts for the transesterification of natural triglycerides in the production of biodiesel. A recent example has reported that a methylimidazolium salt with an alkyl chain mimicking the glycerol structure, promotes the almost quantitative conversion of rapeseed oils into FAMEs products [45].

A series of Brønsted acidic imidazolium ILs has been investigated for the catalytic synthesis of *sec*-butanol by transesterification of *sec*-butyl acetate with methanol (Scheme 5) [46].

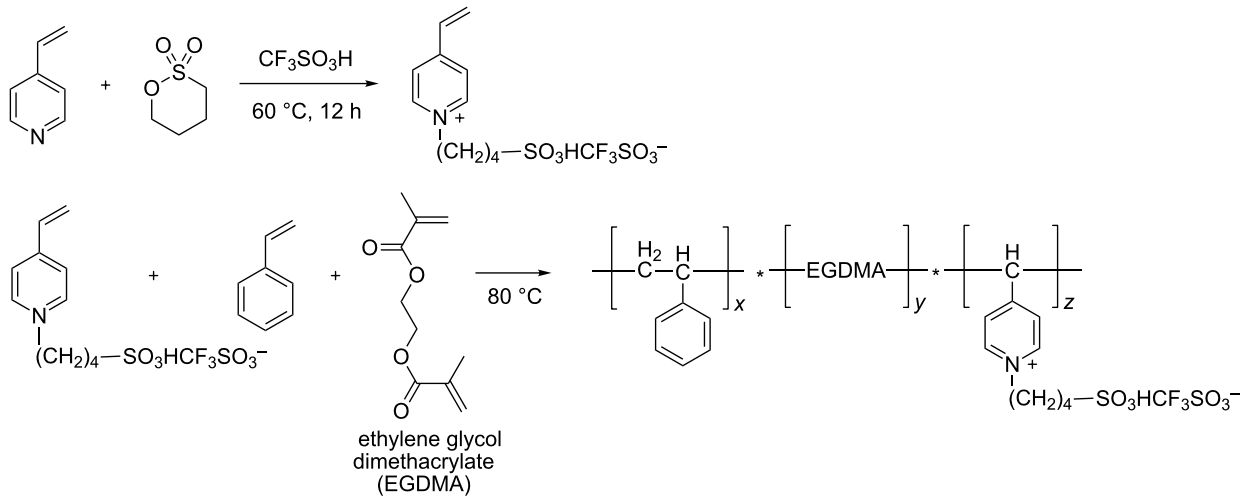

Scheme 4: Synthesis of the acid polymeric IL. EGDMA: ethylene glycol dimethacrylate.

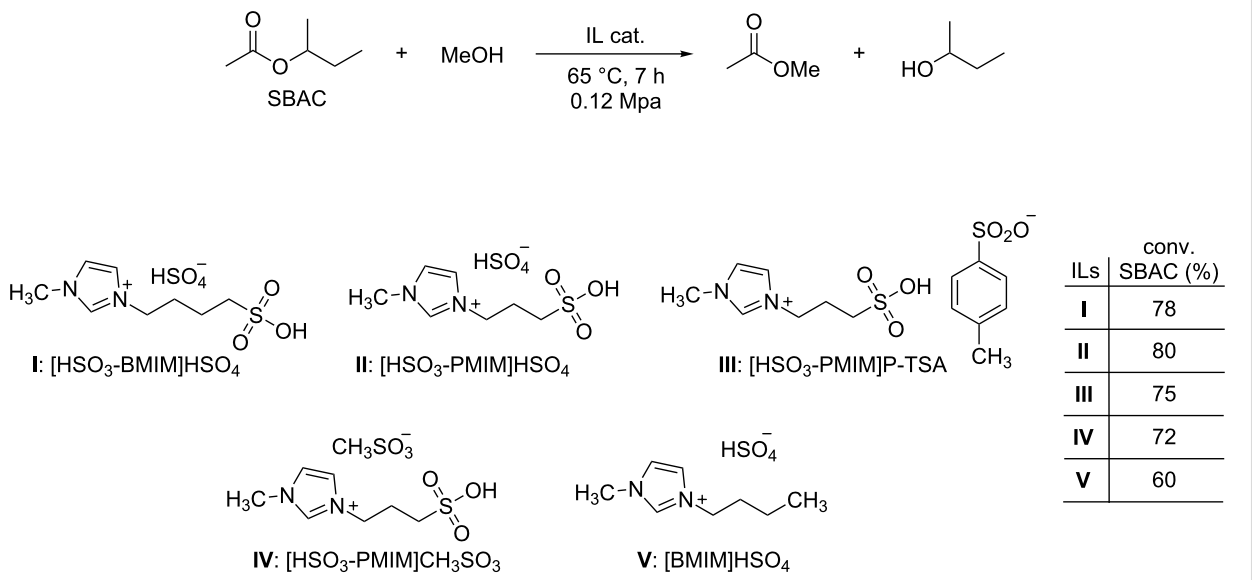

ILs	conv. SBAC (%)
I	78
II	80
III	75
IV	72
V	60

Scheme 5: The transesterification of sec-butyl acetate with MeOH catalyzed by some acidic imidazolium ILs.

The reaction is of interest for the preparation of less toxic oxygenated derivatives, such as *sec*-butanol, in place of compounds like MTBE (methyl *tert*-butyl ether) for the formulation of gasoline blends. Tests with the imidazolium salts collected in Scheme 5 have demonstrated that they are not only competitive with conventional acid catalysts, but that they also can be recovered and reused to allow quantitative conversions even after several recycles. Moreover, the study highlighted that the catalytic activity increased with increasing acidity of the ILs and particularly with cations bearing SO_3H anions (Scheme 5: ILs **I**, **II**, **III**, and **IV**). The same imidazolium salts (**I** and **II**, respectively) have been used also by Cui et al. for the transesterification of methyl acetate and *n*-butanol [47]. The authors observed that the presence of two acidic sites in both the cation and the anion of ILs improved the performance of the catalyst, in analogy to previously reported results for the synthesis of esters from the reaction of nitriles and alcohols [48].

4-(3-Methyl-1-imidazolium)-1-butanesulfonic acid triflate ([HSO_3-BMIM][CF_3SO_3]) has been chosen as a model organocatalyst to explore the kinetics of the transesterification of methyl acetate with ethanol [49,50]. Again, in this case, the investigation proved that the activity of the organic salt was higher than that of sulfuric acid.

The use of ionic liquids for the catalytic production of biodiesel was recently reviewed by Fauzi and Amin [51], who focused on the improvements made possible by organocatalysts with respect to traditional homogenous systems in terms of milder reaction conditions and easier separation and recycle workups. Two representative examples of ionic liquids employed for the synthesis of FAMEs are the pyridinium and oxazolidinone-based compounds shown in Figure 2 [52,53].

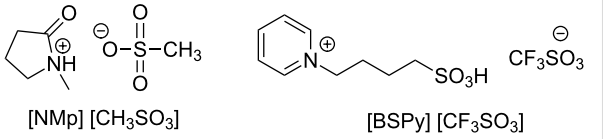

Figure 2: Representative examples of ionic liquids for biodiesel production.

It should be noted that for such reactions, acidic IL-based catalysts are preferred over basic ones due to the presence of significant amounts of free fatty acids in the bio-oils used as feedstocks for biodiesel. Li et al. for example designed an innovative combination of imidazolium ILs and metal sulfates acting as Brønsted and Lewis acids, respectively [54]. A model case is [HSO_3-BMIM]HSO_4–$Fe_2(SO_4)_3$ that offered an excellent catalytic performance in the transesterification of *Camptotheca acuminata* seed oil with methanol, with substantially quantitative conversions achieved in only 60 minutes at 60 °C.

The transesterification reaction for the synthesis of organic carbonates

Organic carbonates (OCs) are promising candidates as *green* replacements of conventional noxious solvents and fuel additives as well as for the development of innovative intermediates in the pharma, lubricant and polymer industries [55,56]. Before the 1980's, the industrial synthesis of the simplest representative of the series, dimethyl carbonate (DMC), was based on the

phosgenation of methanol, which used a lethal chemical reagent such as phosgene (Scheme 6, top). Since then, the processes for the production of DMC have progressively evolved in terms of environmental impact, safety and economics.

Thus, by the end of the 1990's, two main phosgene-free large-capacity processes were operative, both based on the incorporation of carbon monoxide (CO) and methanol by transition metal catalysis: one developed by EniChem [57,58], and the other by Ube Industries [59]. The EniChem process involved an oxidative carbonylation of methanol, i.e., the reaction of methanol with carbon monoxide and oxygen catalyzed by cuprous chloride, while the Ube process used an oxidative carbonylation of methanol via methyl nitrite using NO*x* as oxidant, instead of oxygen and a palladium catalyst (Scheme 6, middle). Though safer than the phosgenation of methanol, these synthetic routes still involved poisonous carbon monoxide and methyl nitrite, and chlorine-based catalysts.

Carbon dioxide is the natural green alternative carbonyl source to these undesirable feedstocks, in particular to CO, except that its thermodynamic stability poses severe challenges. This potential limitation was overcome by the Asahi Kasei Corp. that recently industrialized a catalytic polycarbonate production process based on the use of carbon dioxide (CO_2) for the synthesis of DMC as an intermediate towards the diphenyl carbonate monomer. The first step is the insertion of CO_2 into ethylene oxide to give ethylene carbonate, which is catalyzed by onium salts. The second step involves the transesterification of ethylene carbonate with methanol. The reaction is carried out in a continuous distillation reactor loaded with quaternary ammonium strongly basic anion exchange resin and alkali hydroxides: dimethyl carbonate (DMC) is achieved in practically quantitative yields (Scheme 6, bottom). The third and final step is the transesterification of DMC with phenol by a catalytic reactive distillation in the presence of a homogeneous Ti, Bu–Sn, or Pb catalyst. This reaction provides the desired diphenyl carbonate (yield up to 99%) in a high purity [60].

The catalytic transesterification appears therefore as a crucial reaction, not only for the preparation of the simplest homologue, dimethyl carbonate (DMC), but also for the synthesis of higher organic carbonates as well (Scheme 7).

Notwithstanding the excellent results with respect to previous methods, it should be pointed out, that ethylene oxide still represents a concern for its carcinogenic and mutagenic properties. Future procedures should therefore implement greener reactions, such as the direct carboxylation of diols by CO_2, for which however, effective catalysts are currently not available.

The Asahi Kasei process also highlights that the synthesis of DMC by transesterification of ethylene carbonate with methanol does not necessarily require transition metal catalysis as did the EniChem and Ube processes. Instead, the reaction can be effectively catalyzed by a combination of supported basic ammonium resins and homogeneous alkaline bases [60], thereby

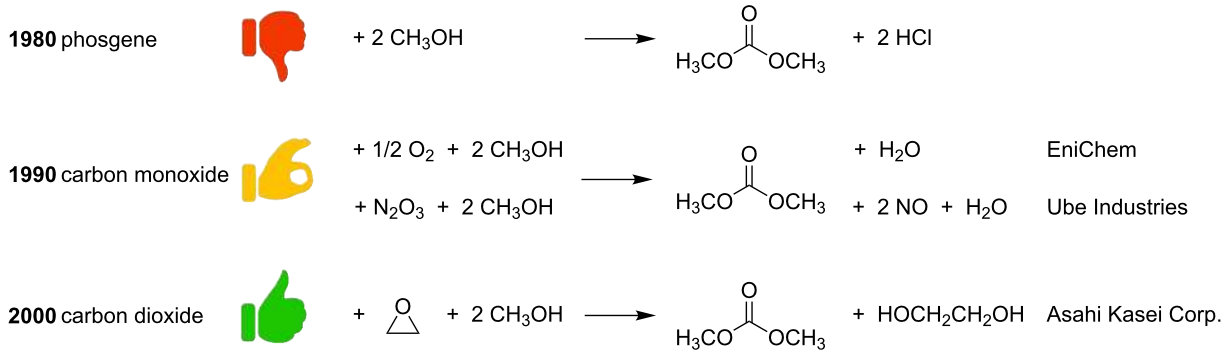

Scheme 6: Top: phosgenation of methanol; middle: EniChem and Ube processes; bottom: Asahi process for the production of DMC.

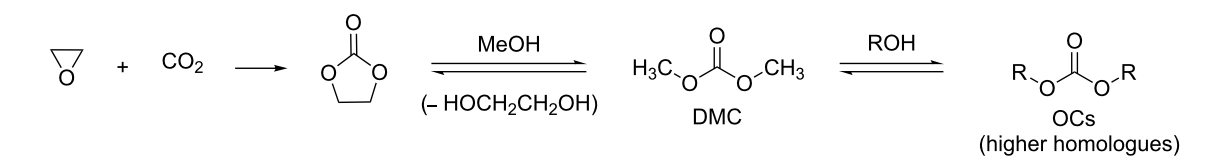

Scheme 7: The transesterification in the synthesis of organic carbonates.

demonstrating the potential of transition metal-free catalytic systems for the synthesis and the further transformation of organic carbonates. These transesterification catalysts can include both acidic and basic ionic liquids, which will be a topic of the further discussion.

Applications of ionic liquids for the synthesis of organic carbonates

The commonly used method to synthesize organic carbonates consists in the acid or base-catalyzed transesterification of dimethyl carbonate (DMC), the simplest organic carbonate, with alcohols R–OH or diols to yield either acyclic organic carbonates or cyclic carbonates, respectively (Scheme 8).

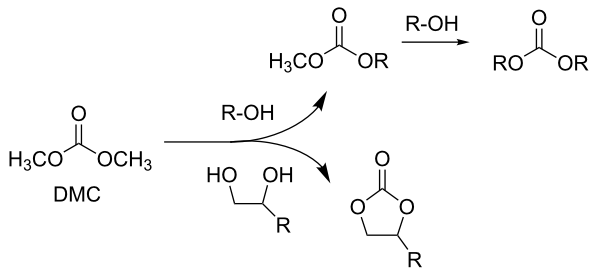

Scheme 8: The transesterification of DMC with alcohols and diols.

A literature survey on the synthesis of organic carbonates by ionic-liquid catalysis goes back approximately five years. Both acidic and basic ionic liquids were employed as catalysts for the pursuit of this scope. The following section is divided into two topics: the first focuses on basic catalysis, and the second on acid catalysis.

Basic catalysis: In a communication published in 2009, Naik P. U. et al. reported an expeditious protocol towards the formation of glycerol carbonate through the transesterification of glycerol with DMC (Scheme 9) [61]. They employed the ionic liquid 1-*n*-butyl-3-methylimidazolium-2-carboxylate (BMIM-2-CO_2) in a concentration of only 1–5 mol %, and the target molecule was quantitatively obtained in 30 min at 74 °C, by using 3.2 equivalents of DMC with respect to glycerol.

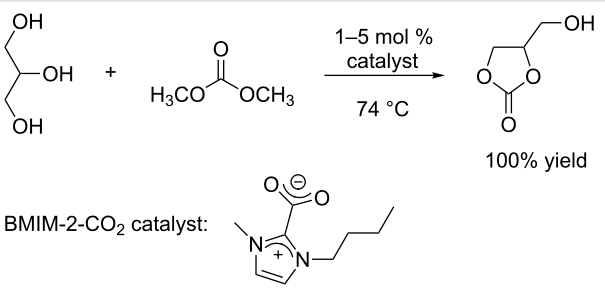

Scheme 9: Transesterification of glycerol with DMC in the presence of 1-*n*-butyl-3-methylimidazolium-2-carboxylate (BMIM-2-CO_2).

As the BMIM-2-CO_2 catalyst is synthesized starting from butylimidazole and DMC (Scheme 10), the authors also attempted to combine the in situ formation of the catalyst with the transesterification of glycerol. The process however, became much slower due to an induction time required to obtain BMIM-2-CO_2.

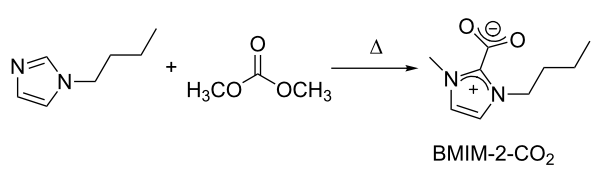

Scheme 10: Synthesis of the BMIM-2-CO_2 catalyst from butylimidazole and DMC.

The study proved that even starting from crude glycerol (which contained 41 mol % water and alkaline salts) and 5 mol % BMIM-2-CO_2, glycerol carbonate was achieved with a 93% yield after 5 h.

More recently, Yuxuan Yi et al. described the transesterification of glycerol with DMC in the presence of four catalytic ionic liquids such as 1-methyl-3-butylimidazolium imidazolium ([BMIM]Im), 1-methyl-3-allylimidazolium imidazolium ([AMIM]Im), 1-methyl-3-butylimidazolium hydroxide ([BMIM]OH), and 1-methyl-3-allylimidazolium hydroxide ([AMIM]OH) [62]. The highest activity was achieved with [BMIM][Im]: after screening of reaction conditions, using 10 mol % of catalyst, 98.4% glycerol conversion and up to 100% selectivity towards glycerol carbonate were reached at 70 °C and ambient pressure. An easy recovery of the catalyst allowed the reuse of the IL up to three times without significant reduction of its activity.

According to the authors, the result was due to a higher basicity of the imidazolium anion with respect to the hydroxy group, and to the poorer steric hindrance of the AMIM cation with respect to the BMIM cation, the latter exerting less effective interactions with the corresponding (imidazolium) anion. Regardless of its nature, the cation might also activate DMC towards nucleophilic addition: a cooperative nucleophilic–electrophilic mechanism could therefore operate (Scheme 11) [63].

Munshi et al. also recently investigated the reaction of glycerol and DMC by proposing a novel ionic liquid catalyst based on the reaction of diazabicyclo[5.4.0]undec-7-ene (DBU) with an alcohol ROH and CO_2 (Scheme 12) [64].

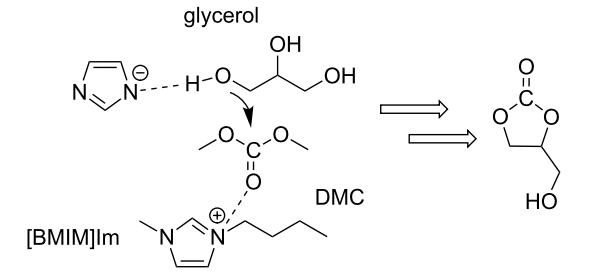

Scheme 11: Plausible cooperative (nucleophilic–electrophilic) mechanism for the transesterification of glycerol with DMC in the presence of [BMIM]Im.

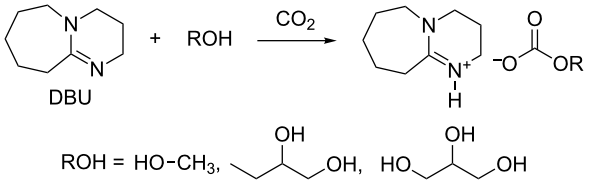

Scheme 12: Synthesis of diazabicyclo[5.4.0]undec-7-ene-based ionic liquids.

As best found reaction conditions (only 0.22 mol % IL loading, glycerol to DMC molar ratio 1:3, 100 °C), conversion and selectivity (towards glycerol carbonate) were 96% and 82%, respectively, after 30 min reaction time. Glycidol (GD, 18%) was the major byproduct. In a further study by the same group, the formation of glycidol from glycerol carbonate was examined in the presence of the ionic liquid DABCO–DMC obtained in situ by reacting DABCO and DMC (Scheme 13) [65].

DABCO by itself is more basic than the DABCO–DMC IL as indicated by its pH in aqueous solution. Nonetheless the DABCO–DMC IL promoted higher glycerol conversion (77% vs 19% after 10 minutes), and, most importantly, higher GD selectivity (63% compared to 45% after 30 minutes) under the same reaction conditions. In order to explain such a behavior, a cooperative mechanism for the ionic liquid catalysis was invoked, whereby the electrophilic nitrogen atom aids in activating the carbonyl moiety (Scheme 14).

It must be noted that in these two examples the selectivity of the reaction could be tuned just by changing the catalyst precursor: by switching from the DBU-based IL to the DABCO–DMC IL, the selectivity changed from 82% for glycerol carbonate, to 83% for glycidol.

In another publication, Gade et al. also achieved a high selectivity toward GD in a one-pot reaction starting from glycerol and DMC [66]. Using tetramethylammonium hydroxide ([TMA][OH]) as basic catalyst, a high selectivity (78%) for GD was reached under mild operating conditions (80 °C, 90 min). The results suggested that the decarboxylation of glycerol carbonate increased with increasing catalyst concentration in solution and thus, the high basicity of the catalyst was not the sole reason for the high activity.

This implied that both, the presence of a basic (anionic) center and an electrophilic (cationic) center in the ionic liquid were involved in the reaction. It was therefore proposed that an interaction of the quaternary ammonium center with the carbonyl oxygen of glycerol carbonate (GlyC) could weaken the C=O bond (Scheme 15).

It is worth mentioning that glycidol was previously obtained at much higher temperatures (170–200 °C).

An acyclic organic carbonate that has recently received attention from the synthetic lubricant market is dipentyl carbonate (DPC). An environmentally friendly process for its synthesis has been recently proposed by the transesterification of DMC with 1-pentanol in the presence of 2 mol % of 1-butyl-3-methylimidazolium hydroxide ([BMIM]OH) as a basic ionic liquid catalyst [67]. At the best found reaction conditions (110 °C, DMC:1-pentanol in 1:4 ratio), DPC was obtained in 76% yield after 4 h reaction time. The catalyst proved to be very stable and active even after five reaction cycles where the DPC yield still exceeded 70%. The proposed reaction mechanism consisted in the activation of the carbonyl group of DMC by the hydrogen-bond interaction with the cation of the IL catalyst followed by a nucleophilic attack of 1-pentanol (Scheme 16).

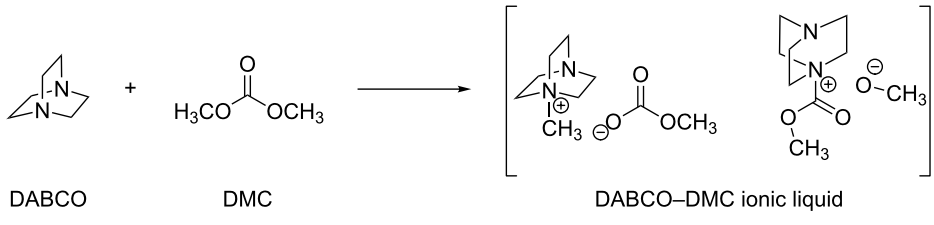

Scheme 13: Synthesis of the DABCO–DMC ionic liquid.

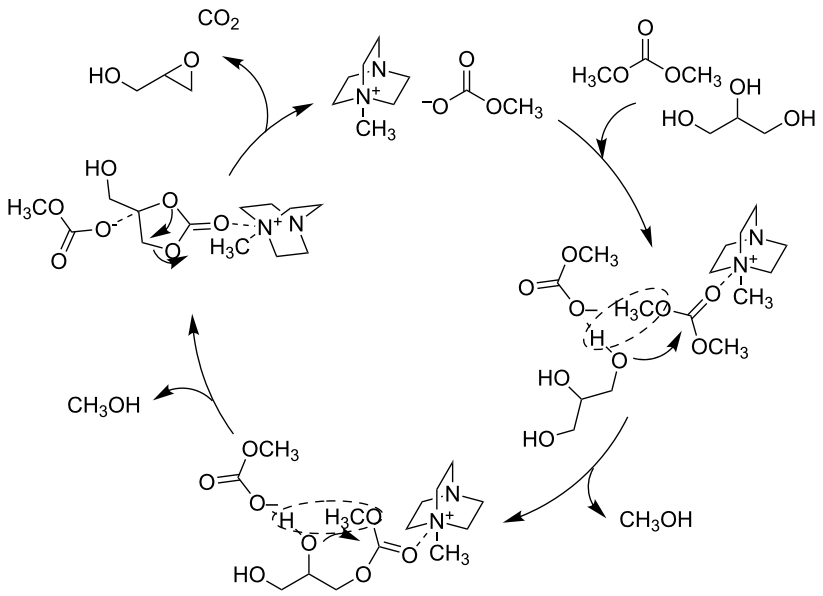

Scheme 14: Cooperative mechanism of ionic liquid-catalyzed glycidol production.

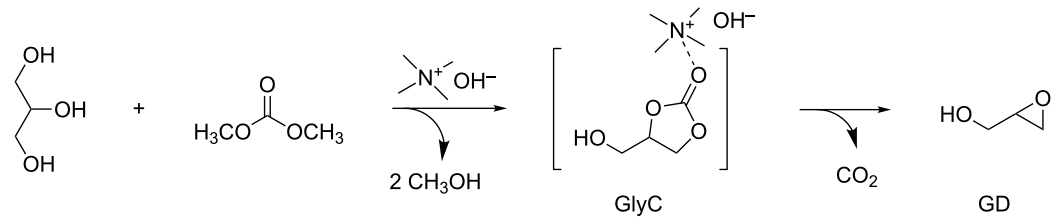

Scheme 15: [TMA][OH]-catalyzed synthesis of glycidol (GD) from glycerol and dimethyl carbonate [46].

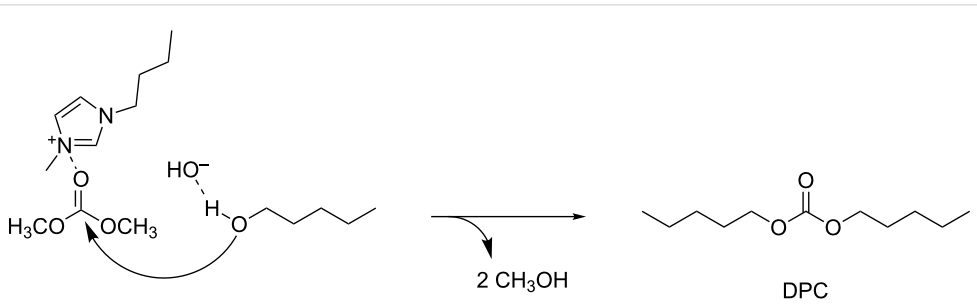

Scheme 16: [BMIM]OH-catalyzed synthesis of DPC from DMC and 1-pentanol.

A similar transesterification reaction of dimethyl carbonate with *n*-butanol has been accomplished using tetraethylammonium-based amino acid ionic liquids ([N_{2222}][AA]) as homogeneous catalysts (Figure 3) [68]. [N_{2222}][Pro] exhibited the best catalytic activity yielding an overall 72% yield of the dibutyl carbonate (DBC) product. Quantum-mechanical calculations indicated that the catalyst synergistically activated both BuOH and DMC.

A wide variety of acyclic non-symmetrical organic carbonates of general formula ROC(O)OCH_3 were prepared by Kumar et al. through the transesterification of DMC using the ionic liquid 1-(trimethoxysilyl)propyl-3-methylimidazolium chloride as the catalyst (Figure 4). With a 10 mol % ionic liquid loading, the transesterification reaction of DMC with eighteen different alcohols ROH yielded the desired unsymmetrical carbonates

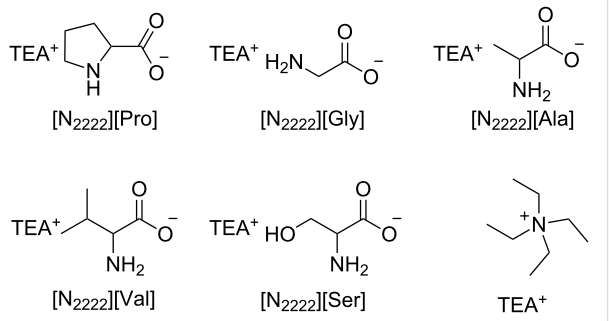

Figure 3: Representative examples of ionic liquids for biodiesel production.

(Figure 4) under mild reaction conditions (80 °C, DMC:ROH in 1:1 ratio) [69].

Acid catalysis: In the transesterification reaction of dimethyl carbonate with phenol to methyl phenyl carbonate (MPC) and diphenyl carbonate (DPhC), Deshmukh et al. studied dibutyltin oxide as a catalyst in conjunction with Brønsted and Lewis acidic ionic liquids [70]. The authors investigated the relative Lewis and Brønsted acidity of the ionic liquids by monitoring the IR bands in the presence of pyridine as a probe molecule. The highest conversions (30–39%) of phenol and the best selectivity toward DPhC were achieved using *N*-methyl-2-pyrrolidone hydrogen sulfate [NMP][HSO_4] and choline chloride zinc chloride ([ChCl][$ZnCl_2$]). The ionic liquid increases the catalytic activity of dibutyltin oxide fourfold probably by forming a highly active tin species where the anion of the ionic liquid acts as a ligand. The developed protocol was further studied for various substituted phenols, proving that electron-donating groups (EDG) at the para position enhance the substrate conversion, while electron-withdrawing groups (EWG) provide the aryl methyl carbonate with a very low conversion. Any substituents in the ortho position led to lower conversions due to an increase of the steric hindrance.

Ionic liquid catalyzed transesterification for dimethyl carbonate production: Ionic liquid-based catalysts brought about a number of improvements for the synthesis of DMC. As mentioned above, the synthesis of DMC through CO_2 insertion into an epoxide and the subsequent transesterification of the formed cyclic carbonate with methanol represent a valid alternative for the industrial production of DMC [59]. Although ionic liquids can catalyze both reactions, this review will only briefly discuss the second transesterification step. Yang et al. tested many basic ILs derived from DABCO for the synthesis of DMC starting from ethylene carbonate (EC) and methanol [71]. In their study, the best performing one was 1-butyl-4-azo-1-azoniabicyclo[2.2.2]octane hydroxide ([C_4DABCO]OH), that achieved 90% conversion, 81% DMC yield and 82% EC yield under optimized conditions (EC:methanol in a 1:10 molar ratio, 1 mol % catalyst loading with respect to EC; 4 h, 70 °C). The catalyst reusability was tested in four successive runs, in which the conversion decreased from 90 to 88% and the DMC yield from 81 to 79%, thereby proving the high stability of the investigated IL and the greenness of the process.

A one-step synthesis of DMC from ethylene oxide (EO), CO_2 and methanol was proposed by Li et al., using a series of quaternary ammonium ILs in reactions carried out in an autoclave at 150 °C, and under CO_2 pressure (2 MPa) [72]. Even though conversions were good after 8 h, the selectivity toward the desired product was still subject to improvement. Up to 99% EO conversion and 74% DMC selectivity were the best performances, obtained using 6-(*N',N'*-dimethylamino)-1-(*N,N,N*-trimethylammonium)hexane iodide [$N_{111,6}N_{11}$]I as the catalyst. The reusability of the catalyst was further studied in eight subsequent reactions. Wang et al. investigated the dependence of the catalytic activity on the structure of IL cations and anions for the synthesis of DMC through the transesterification of EC with methanol [73]. They achieved the best results using a halogen and metal-free IL such as 1,3-dimethylimidazolium-2-carboxylate (DMIM-2-CO_2), which was easily prepared by the

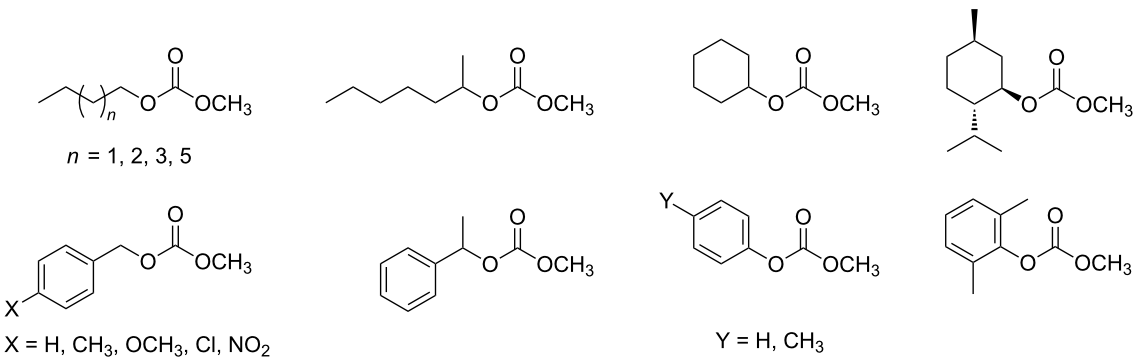

Figure 4: Acyclic non-symmetrical organic carbonates synthetized with 1-(trimethoxysilyl)propyl-3-methylimidazolium chloride as the catalyst.

reaction methylimidazole and DMC. Under the best found reaction conditions (1 mol % catalyst loading with respect to EC, EC:MeOH in 1:10 molar ratio, 110 °C, 80 min) the IL catalyst demonstrated high activity, as it gave 82% and 99% yield and selectivity, respectively, on DMC. Scheme 17 summarizes the reaction mechanism proposed for the synthesis of DMC. The same paper described also the results obtained by supporting the imidazolium salt onto a polystyrene resin (PS). This catalytic system proved to be highly stable and no loss of activity was detected after 200 h of reaction performed in a fixed bed reactor at 110 °C. The authors indicated the perspective of full industrial application for such a system.

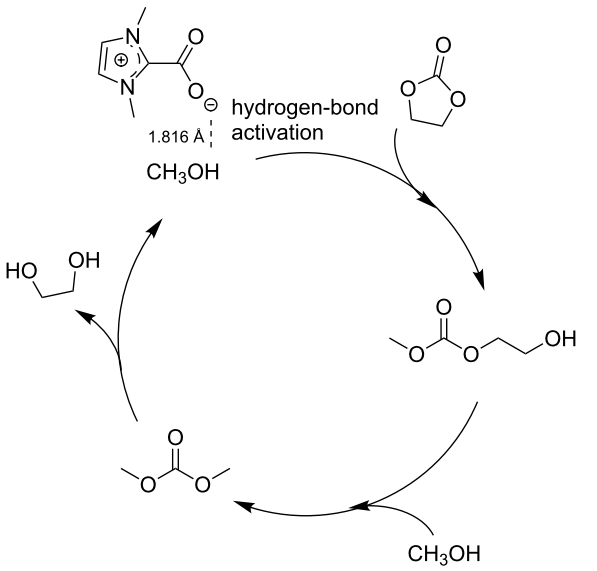

Scheme 17: A simplified reaction mechanism for DMC production.

Phosphonium salts as catalysts for the selective transesterification of carbonates

As mentioned above, the transesterification reaction between organic carbonates and alcohols or diols can be carried out in the presence of basic (e.g., tertiary phosphines and amines, alkali metal hydroxides, alkoxides, halides, carbonates, alkali metal exchanged faujasites and hydrotalcites) or acidic catalysts or co-catalysts, and under thermal (non-catalytic) conditions. All applicable catalysts show common issues: the reactions (i) often proceed beyond the mono-transesterification products to yield the symmetrical higher organic carbonate, (ii) with polyols, primary and secondary OH groups are not discriminated leading to mixtures of different carbonates.

An effective strategy to improve the mono-transesterification selectivity of such reactions is through the design of new ionic liquid catalysts, such as the recently developed methyl trioctylphosphonium methyl carbonate ($[P_{8881}][MeOCO_2]$) and its anion metathesis analogues (Scheme 3) [34]. Of note, the preparation of these organocatalysts offers several practical advantages: (i) the synthesis of $[P_{8881}][CH_3OCO_2]$ involves a halide-free methylation of a trialkyl phosphine with nontoxic DMC, (ii) acetate and phenolate salt derivatives could be obtained from $[P_{8881}][CH_3OCO_2]$ through a chlorine-free metathesis with acetic acid and phenol (Scheme 18), and (iii) all the ILs are produced in very high purity, they are stable for months and usable straight from the reaction vessel.

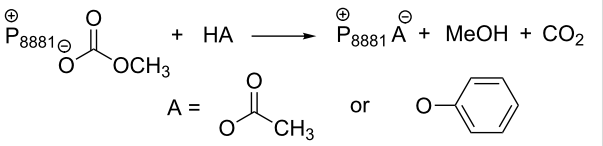

Scheme 18: $[P_{8881}][MeOCO_2]$ metathesis with acetic acid and phenol.

Carbonate, acetate and phenolate phosphonium catalysts were shown to be effective for the mono-transesterification reaction of DMC and DEC with a number of alcohols such as benzyl alcohol, cyclopentanol and menthol [74]. Figure 5 shows some examples of the carbonates obtained in the study. The desired products were achieved at temperatures between 90 and 220 °C.

These results highlight the excellent activity and selectivity of these catalytic systems (conversion >99% and yield >90%) with respect to conventional organic and inorganic bases. In addition, the reactions proceed without decarboxylation even at high temperatures (T > 150 °C), as opposed to the outcome using both solid bases and zeolites, that generate large amounts of CO_2.

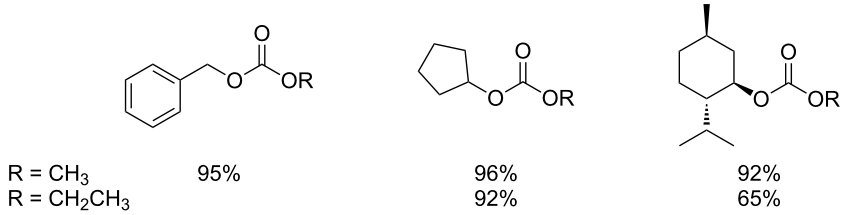

Figure 5: Examples of carbonates obtained through transesterification using phosphonium salts as catalysts.

The transesterification activity of $[P_{8881}][CH_3OCO_2]$-based ionic liquids was also tested on bio-based diols possessing primary and secondary hydroxy groups. Although a number of different products is expectable, the organocatalysts allowed highly selective reactions. For example, 1,2-diols afforded exclusively the corresponding cyclic carbonates, while 1,3-diols, depending on their structures, could yield both, cyclic or acyclic carbonates, such as the ones shown in Scheme 19 [75].

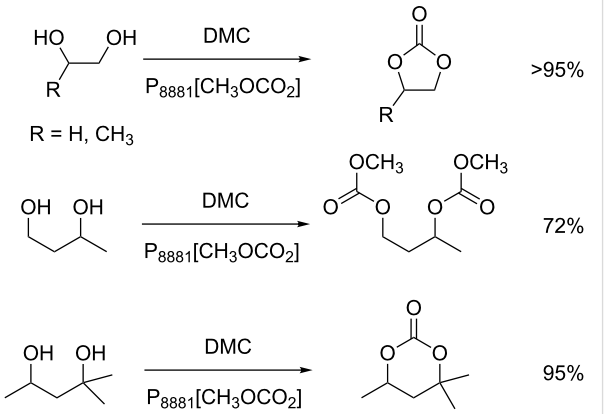

Scheme 19: Examples of carbonates obtained from different bio-based diols using $[P_{8881}][CH_3OCO_2]$ as catalyst.

There is no direct relation of the performance of these IL-catalysts to their basicity. Curiously, it should be noted that the activity of such systems was found to be higher than that of strong bases including DBU or DABCO. This phenomenon was observed by several authors [64,76] and explained by a cooperative ambiphilic (nucleophilic–electrophilic) activation effect in which the IL anion and cation may activate respectively the nucleophile and the electrophile. Scheme 20 shows the proposed mechanisms for the exemplar transesterification of a generic alcohol ROH with DMC using $[P_{8881}][MeOCO_2]$ as catalyst.

The catalytic cooperative activation also explains the selective formation of cyclic or linear products of Scheme 20, without the concurrent production of polycarbonate byproducts. In fact, the selectivity is plausibly due to the steric hindrance of the products, which are much less prone to electrophilic activation (by the catalyst) than the starting DMC or DEC.

Recently, phosphonium salts have been reported as transesterification catalysts of light organic carbonates (dimethyl and diethyl carbonate) with complex polyalcohols, such as cellulose. In particular, trioctylphosphonium acetate ($[P_{8881}][OAc]$) was active for the synthesis of cellulose dialkyl carbonates which find applications as intermediates, supports for the delivery of therapeutics, imaging agents and packaging films and coatings [77].

Conclusion

The literature survey illustrated in this review highlights three main facts. Firstly, organocatalysis by ionic liquids can be an efficient tool for base and even acid-catalyzed transesterification reactions in place of traditional inorganic or solid acids and bases. Advantages in this case are mainly the recovery and recyclability of the catalyst system and the improved selectivity that is often achievable. Secondly, the here presented reactions have a common mechanistic feature based on the cooperative nucleophilic–electrophilic catalysis by the ionic liquid. This type of ambiphilic catalysis is characterized by the nucleophile and the electrophile both being activated respectively by the

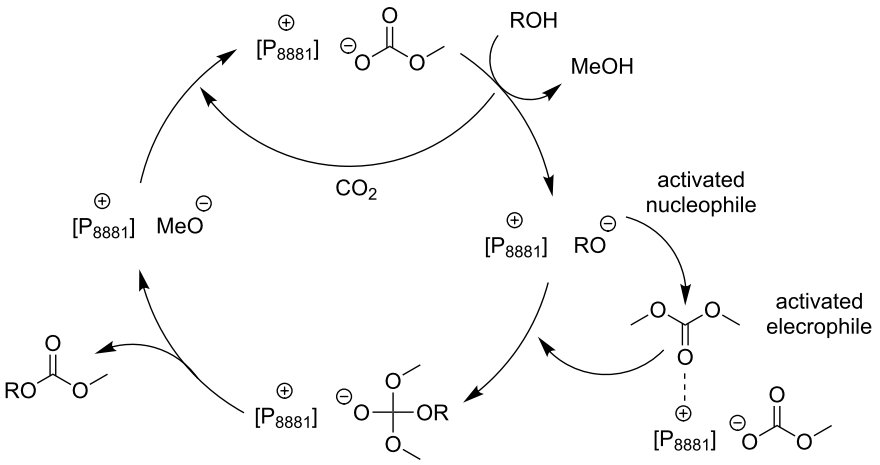

Scheme 20: Ambiphilic catalysis for transesterification reactions in the presence of carbonate phosphonium salts, the model case of methyltrioctylphosphonium methyl carbonate $[P_{8881}][MeOCO_2]$.

anion and by the cation of the ionic liquid. Thirdly, organic carbonates – used as feedstocks or produced by transesterification – are valuable synthetic targets in view of the development of new greener solvents, additives, reagents, and in general of chemical products with improved safety and chemical properties.

References

1. Riemenschneider, W.; Bolt, H. M. *Esters, Organic;* Wiley-VCH Verlag GmbH & Co. KGaA: Weinheim, Germany, 2000.
2. Smith, M. B.; March, J. Addition to Carbon–Hetero Multiple Bonds. *March's Advanced Organic Chemistry: Reactions, Mechanisms, and Structure,* 6th ed.; John Wiley & Sons: Hoboken, NJ, U.S.A., 2006. doi:10.1002/9780470084960.ch16
3. Otera, J. *Chem. Rev.* **1993,** *93,* 1449–1470. doi:10.1021/cr00020a004
4. Biradar, A. V.; Umbarkar, S. B.; Dongare, M. K. *Appl. Catal., A* **2005,** *285,* 190–195. doi:10.1016/j.apcata.2005.02.028
5. Kotbagi, T.; Nguyen, D. L.; Lancelot, C.; Lamonier, C.; Thavornprasert, K.-A.; Wenli, Z.; Capron, M.; Jalowiecki-Duhamel, L.; Umbarkar, S.; Dongare, M.; Dumeignil, F. *ChemSusChem* **2012,** *5,* 1467–1473. doi:10.1002/cssc.201100802
6. Srinivas, D.; Srivastava, R.; Ratnasamy, P. *Catal. Today* **2004,** *96,* 127–133. doi:10.1016/j.cattod.2004.06.113
7. Yanmin, D.; Xingquan, C.; Chunxiang, Z.; Tiansheng, Z. *J. Mol. Catal. A: Chem.* **2010,** *331,* 125–129. doi:10.1016/j.molcata.2010.08.015
8. Ho, D. L.; Zhenghao, W. Process for the preparation of sucrose-6-ester by esterification in the presence of solid superacid catalyst. U.S. Patent 0,103,295 A1, May 1, 2008.
9. Van de Steene, E.; De Clercq, J.; Thybaut, J. W. *Chem. Eng. J.* **2014,** *242,* 170–179. doi:10.1016/j.cej.2013.12.025
10. Limmanee, S.; Naree, T.; Bunyakiat, K.; Ngamcharussrivichai, C. *Chem. Eng. J.* **2013,** *225,* 616–624. doi:10.1016/j.cej.2013.03.093
11. Boro, J.; Deka, D.; Thakur, A. J. *Renewable Sustainable Energy Rev.* **2012,** *16,* 904–910. doi:10.1016/j.rser.2011.09.011
12. Suryaputra, W.; Winata, I.; Indraswati, N.; Ismadji, S. *Renewable Energy* **2013,** *50,* 795–799. doi:10.1016/j.renene.2012.08.060
13. Smith, S. M.; Oopathum, C.; Weeramongkhonlert, V.; Smith, C. B.; Chaveanghong, S.; Ketwong, P.; Boonyuen, S. *Bioresour. Technol.* **2013,** *143,* 686–690. doi:10.1016/j.biortech.2013.06.087
14. Rezaei, R.; Mohadesi, M.; Moradi, G. R. *Fuel* **2013,** *109,* 534–541. doi:10.1016/j.fuel.2013.03.004
15. Kai, T.; Mak, G. L.; Wada, S.; Nakazato, T.; Takanashi, H.; Uemura, Y. *Bioresour. Technol.* **2014,** *163,* 360–363. doi:10.1016/j.biortech.2014.04.030
16. Zhang, L.; Sheng, B.; Xin, Z.; Liu, Q.; Sun, S. *Bioresour. Technol.* **2010,** *101,* 8144–8150. doi:10.1016/j.biortech.2010.05.069
17. Tudorache, M.; Protesescu, L.; Coman, S.; Parvulescu, V. I. *Green Chem.* **2012,** *14,* 478–482. doi:10.1039/c2gc16294f
18. Pyo, S.-H.; Persson, P.; Lundmark, S.; Hatti-Kaul, R. *Green Chem.* **2011,** *13,* 976–982. doi:10.1039/c0gc00783h
19. Guldhe, A.; Singh, B.; Mutanda, T.; Permaul, K.; Bux, F. *Renewable Sustainable Energy Rev.* **2015,** *41,* 1447–1464. doi:10.1016/j.rser.2014.09.035
20. Ochoa-Gómez, J. R.; Gómez-Jiménez-Aberasturi, O.; Ramírez-López, C.; Maestro-Madurga, B. *Green Chem.* **2012,** *14,* 3368–3376. doi:10.1039/c2gc35992h
21. Srivastava, R.; Srinivas, D.; Ratnasamy, P. *J. Catal.* **2006,** *241,* 34–44. doi:10.1016/j.jcat.2006.04.002
22. Tanabe, K.; Hölderich, W. F. *Appl. Catal., A* **1999,** *181,* 399–434. doi:10.1016/S0926-860X(98)00397-4
23. Clark, J. H. *Green Chem.* **1999,** *1,* 1–8. doi:10.1039/a807961g
24. Parawira, W. *Crit. Rev. Biotechnol.* **2009,** *29,* 82–93. doi:10.1080/07388550902823674
25. Olivier-Bourbigou, H.; Magna, L.; Morvan, D. *Appl. Catal., A* **2010,** *373,* 1–56. doi:10.1016/j.apcata.2009.10.008
26. Zhang, Q.; Zhang, S.; Deng, Y. *Green Chem.* **2011,** *13,* 2619–2637. doi:10.1039/c1gc15334j
27. Giernoth, R. *Angew. Chem., Int. Ed.* **2010,** *49,* 2834–2839. doi:10.1002/anie.200905981
28. Chatel, G.; Pereira, J. F. B.; Debbeti, V.; Wang, H.; Rogers, R. D. *Green Chem.* **2014,** *16,* 2051–2083. doi:10.1039/c3gc41389f
29. Wasserscheid, P.; Welton, T. *Ionic Liquids In Synthesis;* Wiley-VCH: Weinheim, Germany, 2002.
30. Weber, C. C.; Masters, A. F.; Maschmeyer, T. *Green Chem.* **2013,** *15,* 2655–2679. doi:10.1039/c3gc41313f
31. Hallett, J. P.; Welton, T. *Chem. Rev.* **2011,** *111,* 3508–3576. doi:10.1021/cr1003248
32. Holbrey, J. D.; Reichert, W. M.; Swatloski, R. P.; Broker, G. A.; Pitner, W. R.; Seddon, K. R.; Rogers, R. D. *Green Chem.* **2002,** *4,* 407–413. doi:10.1039/b204469b
33. Ferguson, J. L.; Holbrey, J. D.; Ng, S.; Plechkova, N. V.; Seddon, K. R.; Tomaszowska, A. A.; Wassell, D. F. *Pure Appl. Chem.* **2012,** *84,* 723–744. doi:10.1351/PAC-CON-11-07-21
34. Fabris, M.; Lucchini, V.; Noè, M.; Perosa, A.; Selva, M. *Chem. – Eur. J.* **2009,** *15,* 12273–12282. doi:10.1002/chem.200901891
35. Cattelan, L.; Noè, M.; Demitri, N.; Selva, M.; Perosa, A. *ChemSusChem* **2015,** *8,* 3963–3966. doi:10.1002/cssc.201500935
36. Selvam, T.; Machoke, A.; Schwieger, W. *Appl. Catal., A* **2012,** *445–446,* 92–101. doi:10.1016/j.apcata.2012.08.007
37. Ratti, R.; Kaur, S.; Vaultier, M.; Singh, V. *Catal. Commun.* **2010,** *11,* 503–507. doi:10.1016/j.catcom.2009.11.015
38. Zhen, B.; Jiao, Q.; Wu, Q.; Li, H. *J. Energy Chem.* **2014,** *23,* 97–104. doi:10.1016/S2095-4956(14)60122-4
39. Zhang, Y.; Jiao, Q.; Zhen, B.; Wu, Q.; Li, H. *Appl. Catal., A* **2013,** *453,* 327–333. doi:10.1016/j.apcata.2012.12.029
40. Mrówczyński, R.; Nan, A.; Liebscher, J. *RSC Adv.* **2014,** *4,* 5927–5952. doi:10.1039/c3ra46984k
41. Xu, J.; Wu, H.-T.; Ma, C.-M.; Xue, B.; Li, Y.-X.; Cao, Y. *Appl. Catal., A* **2013,** *464–465,* 357–363. doi:10.1016/j.apcata.2013.06.016
42. Pinaud, J.; Vignolle, J.; Gnanou, Y.; Taton, D. *Macromolecules* **2011,** *44,* 1900–1908. doi:10.1021/ma1024285
43. Coupillaud, P.; Pinaud, J.; Guidolin, N.; Vignolle, J.; Fèvre, M.; Veaudecrenne, E.; Mecerreyes, D.; Taton, D. *J. Polym. Sci., Part A: Polym. Chem.* **2013,** *51,* 4530–4540. doi:10.1002/pola.26869
44. Zhang, J.; Zhang, S.; Han, J.; Hu, Y.; Yan, R. *Chem. Eng. J.* **2015,** *271,* 269–275. doi:10.1016/j.cej.2015.02.093
45. Nowicki, J.; Nosal, H.; Muszyński, M. *ChemPlusChem* **2015,** *80,* 648–651. doi:10.1002/cplu.201402366
46. Wang, H.; Wu, C.; Bu, X.; Tang, W.; Li, L.; Qiu, T. *Chem. Eng. J.* **2014,** *246,* 366–372. doi:10.1016/j.cej.2014.02.081
47. Cui, X.; Cai, J.; Zhang, Y.; Li, R.; Feng, T. *Ind. Eng. Chem. Res.* **2011,** *50,* 11521–11527. doi:10.1021/ie2000715
48. Jiang, D.; Wang, Y. Y.; Tu, M.; Dai, L. Y. *React. Kinet. Catal. Lett.* **2008,** *95,* 265–271. doi:10.1007/s11144-008-5345-8

49. Peng, Y.; Cui, X.; Zhang, Y.; Feng, T.; Tian, Z.; Xue, L. *Appl. Catal., A* **2013,** *466,* 131–136. doi:10.1016/j.apcata.2013.06.048
50. Peng, Y.; Cui, X.; Zhang, Y.; Feng, T.; Tian, Z.; Xue, L. *Int. J. Chem. Kinet.* **2014,** *46,* 116–125. doi:10.1002/kin.20835
51. Fauzi, A. H. M.; Amin, N. A. S. *Renewable Sustainable Energy Rev.* **2012,** *16,* 5770–5786. doi:10.1016/j.rser.2012.06.022
52. Li, K.-X.; Chen, L.; Yan, Z.-C.; Wang, H.-L. *Catal. Lett.* **2010,** *139,* 151–156. doi:10.1007/s10562-010-0409-x
53. Zhang, L.; Xian, M.; He, Y.; Li, L.; Yang, J.; Yu, S.; Xu, X. *Bioresour. Technol.* **2009,** *100,* 4368–4373. doi:10.1016/j.biortech.2009.04.012
54. Li, J.; Peng, X.; Luo, M.; Zhao, C.-J.; Gu, C.-B.; Zu, Y.-G.; Fu, Y.-J. *Appl. Energy* **2014,** *115,* 438–444. doi:10.1016/j.apenergy.2013.10.025
55. Santos, B. A. V.; Silva, V. M. T. M.; Loureiro, J. M.; Rodrigues, A. E. *ChemBioEng Rev.* **2014,** *1,* 214–229. doi:10.1002/cben.201400020
56. Martín, C.; Fiorani, G.; Kleij, A. W. *ACS Catal.* **2015,** *5,* 1353–1370. doi:10.1021/cs5018997
57. Romano, U.; Tesei, R.; Cipriani, G.; Micucci, L. Method for the preparation of esters of carbonic acid. U.S. Patent 4,218,391, Aug 19, 1980.
58. Romano, U.; Tesel, R.; Mauri, M. M.; Rebora, P. *Ind. Eng. Chem. Prod. Res. Dev.* **1980,** *19,* 396–403. doi:10.1021/i360075a021
59. Nishihira, K.; Yoshida, S.; Tanaka, S. Process for purifying dimethyl carbonate. U.S. Patent 5,292,917, March 8, 1994.
60. Fukuoka, S.; Fukawa, I.; Tojo, M.; Oonishi, K.; Hachiya, H.; Aminaka, M.; Hasegawa, K.; Komiya, K. *Catal. Surv. Asia* **2010,** *14,* 146–163. doi:10.1007/s10563-010-9093-5
61. Naik, P. U.; Petitjean, L.; Refes, K.; Picquet, M.; Plasseraud, L. *Adv. Synth. Catal.* **2009,** *351,* 1753–1756. doi:10.1002/adsc.200900280
62. Yi, Y.; Shen, Y.; Sun, J.; Wang, B.; Xu, F.; Sun, R. *Chin. J. Catal.* **2014,** *35,* 757–762. doi:10.1016/S1872-2067(14)60036-X
63. Lucchini, V.; Noè, M.; Selva, M.; Fabris, M.; Perosa, A. *Chem. Commun.* **2012,** *48,* 5178–5180. doi:10.1039/c2cc31099f
64. Munshi, M. K.; Biradar, P. S.; Gade, S. M.; Rane, V. H.; Kelkar, A. A. *RSC Adv.* **2014,** *4,* 17124–17128. doi:10.1039/c3ra47433j
65. Munshi, M. K.; Gade, S. M.; Rane, V. H.; Kelkar, A. A. *RSC Adv.* **2014,** *4,* 32127–32133. doi:10.1039/C4RA04290E
66. Gade, S. M.; Munshi, M. K.; Chherawalla, B. M.; Rane, V. H.; Kelkar, A. A. *Catal. Commun.* **2012,** *27,* 184–188. doi:10.1016/j.catcom.2012.07.003
67. Han, S.; Luo, M.; Zhou, X.; He, Z.; Xiong, L. *Ind. Eng. Chem. Res.* **2012,** *51,* 5433–5437. doi:10.1021/ie202628m
68. Ouyang, F.; Wang, Z.-Z.; Zhou, Y.; Cheng, Z.; Lu, Z.-H.; Yang, Z.; Tao, D.-J. *Appl. Catal., A* **2015,** *492,* 177–183. doi:10.1016/j.apcata.2014.12.037
69. Kumar, S.; Jain, S. L. *New J. Chem.* **2013,** *37,* 3057–3061. doi:10.1039/c3nj00640a
70. Deshmukh, K. M.; Qureshi, Z. S.; Dhake, K. P.; Bhanage, B. M. *Catal. Commun.* **2010,** *12,* 207–211. doi:10.1016/j.catcom.2010.09.017
71. Yang, Z.-Z.; He, L.-N.; Dou, X.-Y.; Chanfreau, S. *Tetrahedron Lett.* **2010,** *51,* 2931–2934. doi:10.1016/j.tetlet.2010.03.114
72. Li, J.; Wang, L.; Shi, F.; Liu, S.; He, Y.; Lu, L.; Ma, X.; Deng, Y. *Catal. Lett.* **2011,** *141,* 339–346. doi:10.1007/s10562-010-0498-6
73. Wang, J.-Q.; Sun, J.; Cheng, W.-G.; Shi, C.-Y.; Dong, K.; Zhang, X.-P.; Zhang, S.-J. *Catal. Sci. Technol.* **2012,** *2,* 600–605. doi:10.1039/C1CY00342A
74. Selva, M.; Noè, M.; Perosa, A.; Gottardo, M. *Org. Biomol. Chem.* **2012,** *10,* 6569–6578. doi:10.1039/c2ob25447f
75. Selva, M.; Caretto, A.; Noè, M.; Perosa, A. *Org. Biomol. Chem.* **2014,** *12,* 4143–4155. doi:10.1039/c4ob00655k
76. Chakraborti, A. K.; Roy, S. R. *J. Am. Chem. Soc.* **2009,** *131,* 6902–6903. doi:10.1021/ja900076a
77. Labafzadeh, S. R.; Helminen, K. J.; Kilpeläinen, I.; King, A. W. T. *ChemSusChem* **2015,** *8,* 77–81. doi:10.1002/cssc.201402794

License and Terms

Dimethyl carbonate for amine upgrading

Maurizio Selva*, Alvise Perosa, Sandro Guidi & Lisa Cattelan
Ca' Foscari University Venezia, Venezia Mestre, Italy

1 OVERVIEW

This chapter describes the use of dimethylcarbonate (DMC) as a nontoxic reagent for catalytic alkylation and carboxyalkylation/transesterification processes. First, an introductory survey on synthetic methods and general electrophilic reactivity of DMC is presented. In the second part, model reactions are detailed for the upgrading of primary amines and some bio-based derivatives of glycerol, lignin, and lactones with DMC in the presence of solid catalysts, including alkaline carbonates, faujasites, and hydrotalcites. The sustainability of such protocols is discussed by placing emphasis on the green features of DMC, the nature of the catalytic systems, and on the high reaction selectivity that reduces by-products and minimizes work-up and disposal issues.

2 INTRODUCTION

2.1 Dimethyl Carbonate

2.1.1 Synthesis

In the past three decades, the evolution of the methods for the chemical synthesis of dialkyl carbonates (DAlCs) has fueled a growing interest for this class of compounds. DAlCs, in fact, are the most promising *greener* candidates for the replacement of conventional noxious solvents and fuel additives as well as for the development of innovative intermediates in the pharma, lubricant, and polymer industries.[1,2] The simplest term of the series, DMC, well exemplifies the situation. Before the 1980s, the industrial synthesis of DMC was based on a reaction involving a lethal chemical: the phosgenation of methanol (Scheme 1, path a). Since then, however, the processes for the production of DMC have been remarkably improved in terms of environmental impact, safety, and economics. Two main phosgene-free large-capacity processes were operative by the end of the 1990s: they were developed by EniChem[3] and UBE industries,[4] respectively, both based on catalytic reactions of carbon monoxide with methanol. In particular, the EniChem process involved oxidative carbonylation of methanol with air catalyzed by cuprous chloride (Scheme 1, path b), while the Ube process used methyl nitrite, NO_x as an oxidant, and a palladium catalyst (Scheme 1, path c). The choice of reagents, catalysts, and conditions not only improved safety with respect to the phosgenation of methanol but also allowed the industrial synthesis of DMC as a nontoxic chemical. Both routes, however, still involved poisonous reagents (carbon monoxide and methyl nitrite) and chlorine-based catalysts. A breakthrough in this field occurred 15 years later when carbon dioxide was reported as a building block for DMC. Carbon dioxide is the natural green alternative carbonyl source, although its thermodynamic stability often poses severe challenges for applications. This limitation was overcome by Asahi Kasei Corporation, which industrialized a multistep integrated process for the catalytic production of polycarbonate:[5] in this sequence, the first reaction is the insertion of CO_2 into ethylene oxide to give ethylene carbonate and is catalyzed by onium salts (Scheme 1, path d: cat. 1). The second step yields pure dimethylcarbonate through the transesterification of ethylene carbonate with methanol carried out in a continuous mode over quaternary ammonium, strongly basic anion exchange resin, and in the presence of alkali hydroxides (Scheme 1, path d: cat. 2).

Thereafter, in the same plant, DMC undergoes a catalytic transesterification with phenol to prepare diphenylcarbonate as a monomer for the final polymerization step with bis-phenol A. The overall transformation represents one of the best examples of green and sustainable chemical processes available today for industrial productions.

2.1.2 Reactivity

DMC is an ambident electrophile that exhibits a flexible reactivity at both the carbonyl and methyl carbon atoms (Scheme 2, a and b).[6] In the presence of a generic nucleophile (NuH), two reactions take place: (a) an addition/elimination at the carbonyl group to produce a carboxymethylated product ($NuCO_2CH_3$), or

*corresponding author

Encyclopedia of Inorganic and Bioinorganic Chemistry, Online © 2011–2016 John Wiley & Sons, Ltd.

This article was published in the *Encyclopedia of Inorganic and Bioinorganic Chemistry* in 2016 by John Wiley & Sons, Ltd.
DOI: 10.1002/9781119951438.eibc2428

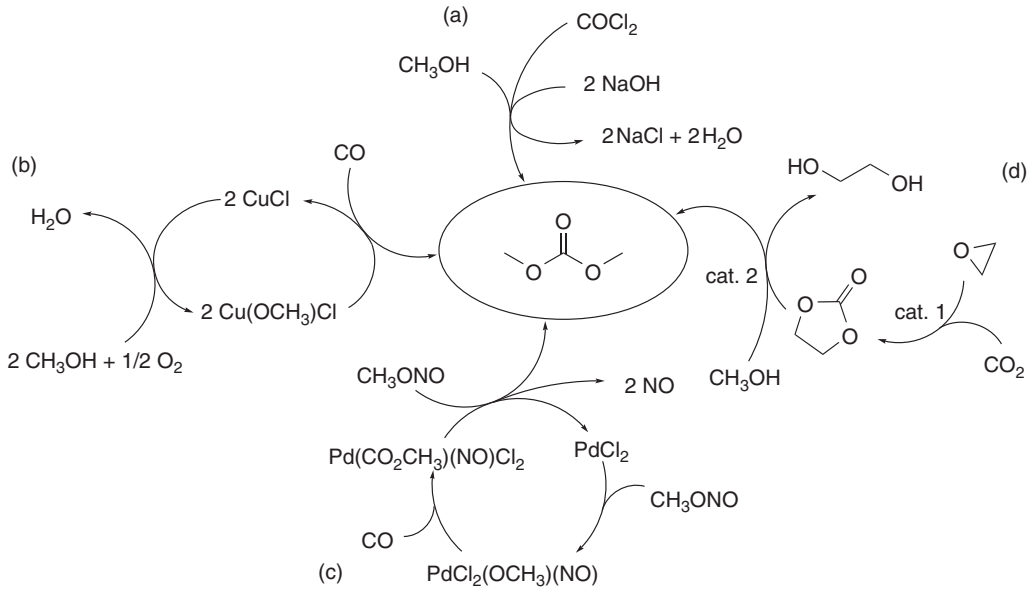

Scheme 1 The methods of synthesis of dimethyl carbonate

(b) an S_N2 methylation reaction via the attack at the methyl carbon, originating a methyl derivative ($NuCH_3$). Both transformations are catalytic with no-by products, except for methanol (recyclable to the synthesis of DMC), and CO_2. Although a clear cut-off between such pathways cannot be drawn, the nature of the catalyst and the temperature can be used to tune the reactivity of DMC. Basic catalysts favor the addition/elimination mechanism in refluxing DMC (90 °C), while they allow predominant methylation reactions above 120 °C. This change of reactivity is also plausibly accounted for by solvation phenomena.[7] Neutral or weak acidic catalysts (e.g., zeolites) preferably induce the formation of methyl derivatives.

Therefore, depending on the conditions, DMC may act as a safe replacement of phosgene or methyl halides and dimethyl sulfate for carboxymethylation or methylation reactions, respectively.

It should finally be noted that the base-catalyzed transesterification of DMC with alcohols affords higher DAlCs homologs. These compounds show a dual reactivity similar to that of Scheme 2, although for steric reasons they are usually poorer electrophiles compared to DMC.

The following paragraphs focus on two topics: (i) synthetic and mechanistic investigations of selective methylation of anilines with dimethyl carbonate and asymmetric methyl alkyl carbonates, and (ii) applications of DMC as both a methylating and carboxymethylating agent of bio-based substrates including glycerol acetals, *p*-coumaryl-type alcohols, and lactones.

3 SELECTIVE REACTIONS OF DIMETHYL CARBONATE WITH AMINES

3.1 Mono-N-Methylations of Primary Aromatic Amines

3.1.1 Alkali Metal-Exchanged Faujasites Catalysts

Mono-*N*-alkyl anilines are building blocks for the synthesis of a variety of pharmaceuticals and dyes.[8] Their preparation is however not trivial since the reaction with common alkylating agents such as alkyl halides and dialkyl sulfates often generates undesired over-alkylated by-products (tertiary amines and ammonium salts). This is especially true in the case of highly reactive methyl halides and sulfates, for which mono-methyl selectivity is elusive even at low substrate conversion.[9] Therefore, multistep protection and de-protection sequences must be adopted.

An alternative method for the straightforward synthesis of mono-*N*-methyl anilines involves dimethyl carbonate (DMC, $MeOCO_2Me$). Results reported by us and by others[10–16] have demonstrated that the alkylation of different primary aromatic amines with DMC proceeds with a mono-N-methylation selectivity up to 98% at complete conversion, at temperatures above 120 °C, and in the presence of zeolite catalysts belonging to the class of alkali metal exchanged Y- or X-faujasites (FAU) (Scheme 3).

For example, at 130 °C, the model reaction of aniline and DMC takes place quantitatively in 195 min over KY zeolite, and the corresponding mono-*N*-methyl aniline is obtained with 97% selectivity. It should be highlighted that conventional bases used to catalyze most of DMC-mediated O-, C-, and S-methylation reactions[6,11]

Encyclopedia of Inorganic and Bioinorganic Chemistry, Online © 2011–2016 John Wiley & Sons, Ltd.

This article was published in the *Encyclopedia of Inorganic and Bioinorganic Chemistry* in 2016 by John Wiley & Sons, Ltd.
DOI: 10.1002/9781119951438.eibc2428

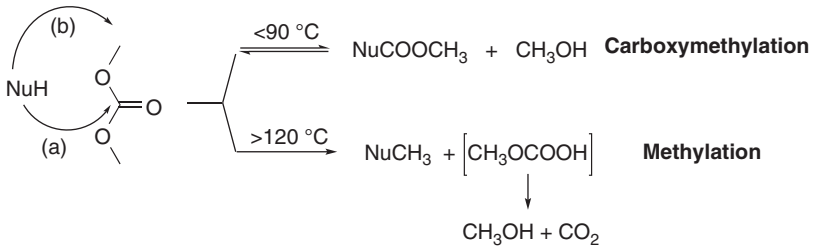

Scheme 2 The general reactivity of DMC

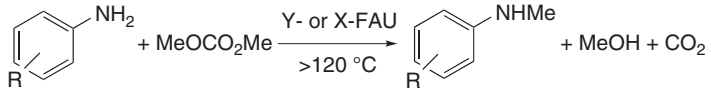

Scheme 3 Mono-*N*-methylation of anilines with DMC

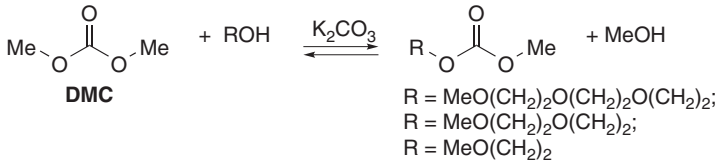

Scheme 4 The synthesis of unsymmetrical alkyl methyl carbonates (MACs)

are ineffective for anilines. In fact, when alkaline carbonates (M_2CO_3: M = Li, Na, K) are used in place of FAU, alkylation reactions are significantly slower and they are no longer selective because of the formation of sizeable amounts (up to ∼30%) of methyl *N*-methyl-*N*-arylcarbamates [ArNH(Me)CO_2Me]. On the contrary, the reaction in Scheme 3 is of very general scope: a variety of amines, even deactivated by electronic or steric effects such as *p*-$O_2NC_6H_4NH_2$, *p*-$NCC_6H_4NH_2$, *o*-$CH_3O_2CC_6H_4NH_2$, and 2,6-$(CH_3)_2C_6H_4NH_2$, are successfully converted into their mono-*N*-methyl derivatives with a selectivity of 92–97%, at conversions from 72% to 93%, respectively. In a typical batch procedure, DMC serves not only as a methylating agent but also as a solvent, and FAU is used in excess with respect to the reactant amine (1.2 up to 6 weight excess for less active substrates). The reaction takes place in a stainless steel autoclave under an autogenic pressure of 3–6 bar (bp of DMC: 90 °C), and the desired product is isolated with minimal work-up including filtration of solid catalyst and distillation of the residual solution. The recovered DMC and FAU can be recycled and reused without additional treatments.

The activity of DMC and the efficiency of the overall N-alkylation procedure have been also assessed in terms of green metrics (atom economy and mass index) and compared to results obtained with other methylation reagents, including methanol, dimethyl sulfate, and methyl iodide. Analysis of the metrics has indicated that the reactions with DMC have more favorable mass indexes (in the range 3–6), with a significant decrease in the overall flow of materials (reagents, catalysts, solvents, *etc.*), thereby providing sustainable catalytic reactions with no waste.[17]

The experimental setup of DMC-mediated methylations may be further simplified and made even safer by using unsymmetrical methyl alkyl carbonates (MACs: $MeOCO_2R$), obtained by base-catalyzed transesterification of DMC with commercial derivatives of ethylene glycol monomethyl ethers (Scheme 4).[12,18]

Such carbonates have two remarkable features: (i) they are high boiling and can be used at atmospheric pressure at temperatures over 150 °C; (ii) they promote chemoselective alkylation reactions only at the methyl group because steric bulk hinders the electrophilic reactivity of the R terminus. Accordingly, in the presence of NaY catalyst, MACs act as excellent surrogates of DMC to carry out methylation reactions of a plethora of primary aromatic amines: at 130–160 °C, conversions and mono-*N*-methyl selectivities up to 100% and 97%, respectively, are achieved operating

Encyclopedia of Inorganic and Bioinorganic Chemistry, Online © 2011–2016 John Wiley & Sons, Ltd.

This article was published in the *Encyclopedia of Inorganic and Bioinorganic Chemistry* in 2016 by John Wiley & Sons, Ltd.
DOI: 10.1002/9781119951438.eibc2428

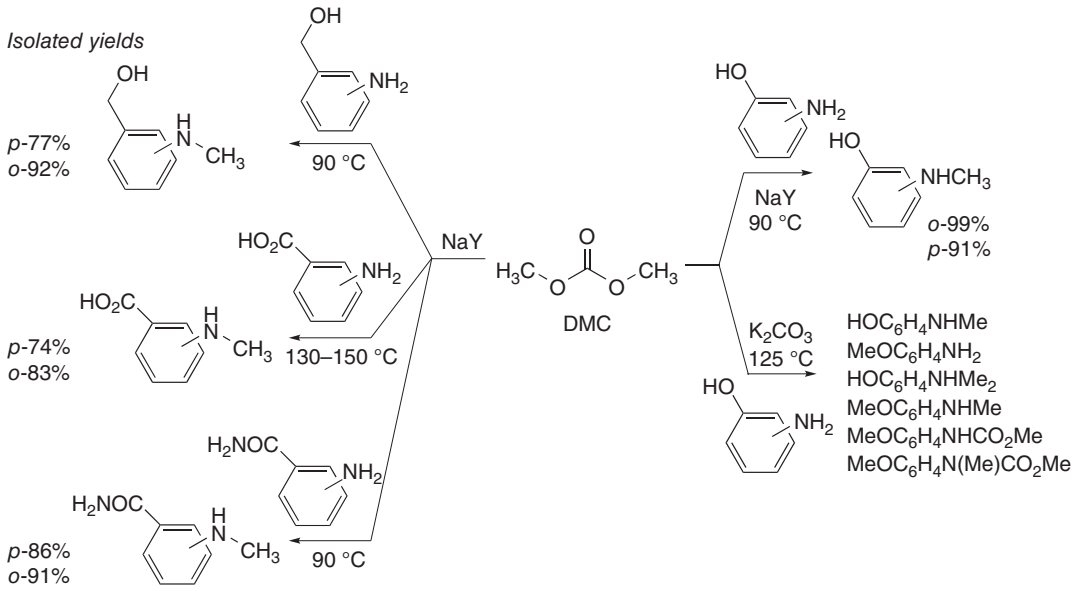

Scheme 5 The selective mono-*N*-methylation of functionalized anilines with DMC

in conventional laboratory glassware at ambient pressure.[12] Since pressure reactors are unnecessary, the use of MACs allows to easily perform kinetic and mechanistic investigations (see Section 3.1.3).

3.1.2 Functionalized Anilines as Ambident Nucleophiles

The combined use of DMC and sodium-exchanged Y-zeolite (NaY) allows the N-methylation of ambident nucleophiles, including aminophenols, aminobenzyl alcohols, aminobenzoic acids, and aminobenzamides. Although such anilines bear aromatic substituents (OH, CH_2OH, CO_2H, and $CONH_2$) that could be reactive toward DMC, they undergo only a very selective (up to 99%) mono-N-methylation of the amino group, while the other functionalities are fully preserved from alkylation and/or transesterification side-processes (Scheme 5, right and left).[14] These results highlight the role of the FAU catalyst on both chemo- and mono-*N*-methyl- selectivity. For example, the model reaction of DMC with aminophenol catalyzed by NaY yields 99% and 91% of the corresponding *ortho*- and *para*-*N*-methyl isomers, respectively (Scheme 5, top, right). On the contrary, by replacing the zeolite with K_2CO_3, a variety of products including derivatives of mono- and bis-N-methylation, O-methylation, and N-carboxylation are observed (Scheme 5, bottom, right).

A high N-methylation selectivity can also be achieved by the reaction of ambident anilines with MACs (Scheme 5) in the presence of NaY.[15]

3.1.3 Zeolite-Catalyzed Methylation of DMC: The Reaction Mechanism and the Selectivity

The FAU-catalyzed methylation of amines by DMC and MACs has been the object of a kinetic analysis.[13,15] This investigation has demonstrated that: (i) the disappearance of the substrates (either alkyl- and alkoxy-substituted primary aromatic amines or ambident anilines) occurs under diffusion-free conditions following a pseudo first order rate law; (ii) the reaction rate is affected by the solvent polarity as well as by the steric and electronic effects of ring substituents; (iii) the amphoteric acid–base properties of the catalyst and the steric requisites of cavities in the FAU-framework improve the kinetics and, importantly, they tune the methylation selectivity; (iv) for bifunctional anilines (Scheme 5), the observed reactivity scale is aminophenols > amino benzyl alcohols > aminobenzamides > aminobenzoic acids. Such results, along with the modes of adsorption of reagents over the catalyst, have all been taken into account in order to formulate a reaction mechanism. The model case of aniline and DMC is considered as an example. Experimental evidence indicates that aniline may diffuse into the supercavities of Y- or X-faujasites and adsorb therein *via* H-bonding to the basic oxygens of the catalyst structure and *via* the formation of a π complex between the aryl ring and Lewis-acid cations (e.g., Na^+ in NaY).[19] On the other hand, IR and Raman investigations demonstrate that faujasites induce an electrophilic activation of DMC owing to the formation of acid–base complexes between the organic carbonate and the Lewis acidic cations of the catalysts.[15,20] Once the amine and DMC migrate into the pores, they come together based on

Encyclopedia of Inorganic and Bioinorganic Chemistry, Online © 2011–2016 John Wiley & Sons, Ltd.

This article was published in the *Encyclopedia of Inorganic and Bioinorganic Chemistry* in 2016 by John Wiley & Sons, Ltd.
DOI: 10.1002/9781119951438.eibc2428

the steric requisites of their adsorption patterns. A pictorial description is offered in Scheme 6 where, for simplicity, only one adsorption mode is considered for both reagents.

The reaction then proceeds via a $B_{Al}2$ displacement of aniline on DMC. The product, mono-*N*-methyl aniline (PhNHMe), adsorbs into the zeolite differently with respect to aniline: the NHMe group forces the molecule farther from the surface in a way that is less suitable to meet DMC and react with it. Accordingly, mono-*N*-methyl selectivity is accounted for by a combined effect of its dual acid–base properties and the size of its cavities. This also explains why anilines bearing bulky substituents (e.g., *t*-butyl) are not only poorly reactive, but also form a mixture of mono- and bis-*N*-methyl derivatives. In this case, the diffusion of reagents and products through the catalytic pores is hampered by steric effects and the shape selectivity effect cannot operate.

As for bifunctional anilines, steric/electronic effects of substituents and the occurrence of weak (H-bonding) substrate–catalyst interactions are plausibly responsible for the observed reactivity scale. For example, the small size and acidity ($pK_a \sim 10$) of OH in aminophenols help the reaction by favoring the migration of reagents into the faujasite pores and stabilizing them through H-bonding over the catalytic surface (ArO-H•••O-zeolite). However, stronger acid–base interactions expected between carboxylic functions of aminobenzoic acids and oxygen atoms of the zeolite block the reagents on the catalyst and slow down the process. These considerations are further supported by the kinetic results gathered for *o*- and *p*-anisidines whose substituents (OMe), unable to H-bond with the catalyst, make these amines remarkably less reactive than aminophenols. It should be noted that molecular simulations have proved that all these bifunctional substrates can be hosted by the zeolite supercavities, thereby confirming the role of the catalyst morphology and H-bonding to address both activity and selectivity of the reaction. Finally, the hard–soft acids and bases principle may offer an explanation for the chemoselectivity of the reaction: in an S_N2-type reaction, a soft electrophilic center (i.e., a carbon atom) is preferably attacked by the less electronegative atom (N with respect to O) of an ambident nucleophile. In addition, zeolites may also act as solid solvents with "solvation effects" due to noncovalent (van der Waals type) host–guest interactions able to confine preferably some molecules versus others, within the intracrystalline volume.[21]

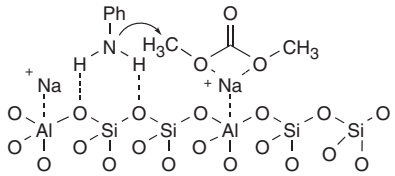

Scheme 6 The selective mono-*N*-methylation of aniline with DMC in a faujasite supercavity

4 SELECTIVE REACTIONS OF DIMETHYL CARBONATE WITH BIO-BASED DERIVATIVES

4.1 Upgrading of Glycerol Derivatives: Alkylation and Carboxyalkylation of Glycerol Acetals

The chemical relevance of glycerol as a nontoxic biodegradable compound is recognized worldwide in a number of sectors, including pharma, polymer, and food. Not by chance, in 2004, the National Laboratories of the US Department of Energy have classified glycerol among the 12 most attractive platform chemicals that can be produced from biological or chemical conversions of biomass. The ranking was confirmed in 2010 by a further analysis on the sustainability of modern biorefineries.[22] This evidence, along with the market surplus of glycerol generated by the biodiesel production, has stimulated an intensive research activity aimed at the conversion of glycerol and its derivatives into energy and chemicals. In this context, glycerol acetals (GAs), and in particular light derivatives such as glycerol formal (GlyF) and solketal, are promising candidates (Scheme 7).

Not only are these compounds attractive nontoxic solvents for injectable preparations, paints, plastifying agents, insecticide delivery systems, and flavors,[23–25] but they also possess a short OH-capped hydroxymethylene tether, which provides synthetic access to a number of other functionalities. In particular, innovative eco-friendly protocols for the upgrading of such GAs to the corresponding *O*-methyl and carboxymethyl derivatives can be devised with dimethyl carbonate.

4.1.1 O-Methylation of Glycerol Acetals with DMC

Results recently reported by us have demonstrated that a highly selective etherification of both glycerol formal and solketal is achieved under batch conditions (autoclave) in the presence of K_2CO_3 as a catalyst.[26] The reaction is best carried out at temperatures of 200–220 °C and the mechanistic investigation is consistent with the sequence outlined in Scheme 8.

In the first step, the base (B) converts the acetal/ketal (ROH: GlyF or solketal) into the corresponding alcoholate anion [RO^-] that reacts with both electrophilic centers of DMC [paths a and b, $B_{Ac}2$ and $B_{Al}2$ mechanisms]. However, the onset of the methylation process makes the reversible transesterification backtrack: after an initial formation of the carboxymethyl product ($ROCO_2Me$, path a), the concentration of this derivative falls to zero,

Encyclopedia of Inorganic and Bioinorganic Chemistry, Online © 2011–2016 John Wiley & Sons, Ltd.

This article was published in the *Encyclopedia of Inorganic and Bioinorganic Chemistry* in 2016 by John Wiley & Sons, Ltd.
DOI: 10.1002/9781119951438.eibc2428

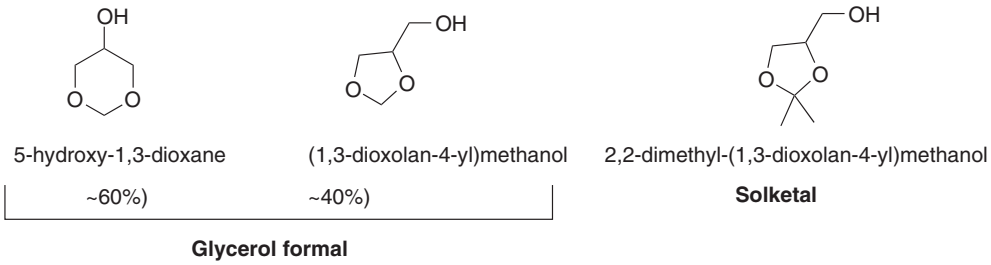

Scheme 7 Most common glycerol acetals

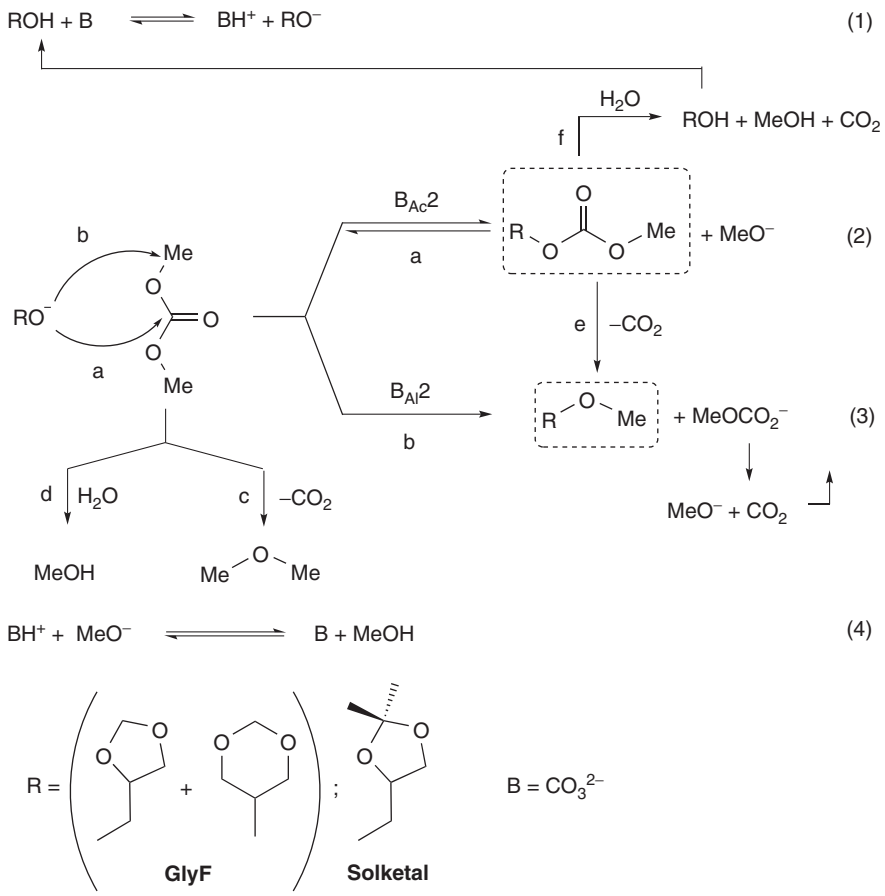

Scheme 8 The mechanism of etherification of glycerol acetals with DMC in the presence of a catalytic base ($B = K_2CO_3$)

while ROMe becomes the final product (path b). A further contribution to the disappearance of the carboxymethyl compound is given by competitive decarboxylation and hydrolysis reactions,[27] shown in paths (e) and (f), respectively. In addition, DMC undergoes the same decarboxylation/hydrolysis transformations [paths c–d] that become relevant for long reaction times. Overall, several concurrent processes take place, but if the temperature is high enough and sufficient time is allowed, the system equilibrates to thermodynamically favored products: the result is the formation of *O*-methyl derivatives of both GlyF and solketal with selectivity and yields up to 99% and 86%, respectively, at complete conversion. The procedure shows other remarkable features: (i) it can be scaled up for multigram preparation without loss of selectivity; (ii) the catalyst may be recycled indefinitely; (iii) no additional solvents are required and major by-products are methanol and CO_2; (iv) the use of innocuous renewables (glycerol acetals) is

Encyclopedia of Inorganic and Bioinorganic Chemistry, Online © 2011–2016 John Wiley & Sons, Ltd.

This article was published in the *Encyclopedia of Inorganic and Bioinorganic Chemistry* in 2016 by John Wiley & Sons, Ltd.
DOI: 10.1002/9781119951438.eibc2428

coupled to the nontoxic alkylating agent in a genuine green archetype process; (v) the scope may be extended to higher homologs of DMC, including diethyl and dibenzyl carbonate. A limitation, however, is the decomposition of the alkylating agents (dialkyl carbonates) due to decarboxylation and hydrolysis processes taking place over K_2CO_3. Studies are in progress to minimize this drawback by changing both the nature of the base catalyst and the reaction conditions, possibly by considering continuous-flow systems.[28]

4.1.2 Thermal Transesterification of Glycerol Acetals with DMC

A challenging objective of the reaction of GAs with DMC is to switch from the synthesis of ethers described in Scheme 8 to the selective formation of mono-transesterification derivatives (Scheme 9).

Among the possibilities to envisage such a reaction, we have very recently discovered the potential of thermal (catalyst-free) processes.[29] Under such conditions, an excellent procedure has been implemented for the continuous-flow (CF) conversion of GAs into the corresponding mono-transesterification products (Scheme 9) with a selectivity up to 98% even at a substantially quantitative conversion. The result has been achieved by the combined effect of temperature, pressure, and flow rate. For example, at 275–300 °C, the reaction of DMC with glycerol formal shows a sharp increase of the substrate conversion (from 1–2% to ~85%) for small increments in the pressure in the range of 20–50 bar (Figure 1).

At $T \geq 200$ °C and ambient pressure, reactants are in the vapor state (bp of DMC and GlyF: 90 and 193 °C, respectively), even though dynamic flow conditions may allow some mixing of gases. As the pressure is increased, the contact of reactants is more and more favored since GlyF rapidly turns liquid, while DMC is progressively partitioned between the gas and the liquid phases. The sigmoid-like curves of Figure 1 indicate that intimate interactions between GlyF and DMC allow the transesterification reaction to take place at an optimal pressure (and density of the reacting mixture) that corresponds to an abrupt improvement of the conversion. The hypothesis for this behavior rests on the occurrence of near-critical or supercritical solutions able to favor the process kinetics. It should be noted that T and P used for the thermal transesterification of Figure 1 (275–300 °C and 20–50 bar, respectively) are not far from the supercritical state of DMC ($T_c = 284$ °C; $P_c = 48$ bar[30]), which shows a density four times higher than in its liquid state.

The continuous-flow thermal procedure has proved successful also for the selective mono-transesterification of other liquid carbonates including diethyl and propylene carbonate, with glycerol formal and solketal. In all cases, conversions and selectivity can be raised up to 85% and 98%, respectively, with a productivity of ~70 mg min^{-1} based on the design and the capacity of the CF-apparatus. Overall, not only a clean synthetic route but also a potentially valuable strategy for large scale preparations has been identified, taking advantages of typical benefits of the CF-mode such as the optimization of the process parameters, product separation, and minimization of reaction volumes (process intensification). Moreover, modern technologies for heat and energy recovery may considerably mitigate the issue of energy consumption for thermal reactions: effective engineering solutions have already been reported for the supercritical transesterification of oils, proving that supercritical processes may be even economically advantageous over conventional base-catalyzed transesterification methods.[31]

4.2 Upgrading of *p*-Coumaryl-Like Alcohols as Models for Lignin Derivatives

Lignin is an amorphous, highly substituted, aromatic polymer that constitutes the major bio-based source of aromatics. A plethora of products may derive from the disruption of lignin linkages, all based on the structure of the three units constituting lignin: *p*-coumaryl, coniferyl, and sinapyl alcohol.[32] Such structures indicate that simple alcohols including, for example, cinnamyl alcohol and 4-(3-hydroxy propyl)phenol, are good model compounds to devise strategies for chemical upgrading of aromatics derived from lignin. In one such recent study of our group, reactions of these compounds with dimethylcarbonate have been analyzed in the presence of heterogeneous catalysts.[33] The investigation has proved that the reactivity of aromatic and aliphatic OH groups of reactants is tuned by the nature of the catalyst and the temperature: at 70–90 °C, weak bases (K_2CO_3 and CsF/αAl_2O_3) favor transesterification processes, while at 165–180 °C, alkali metal exchanged faujasites (NaX and NaY) promote the irreversible formation of methyl ethers. This behavior is exemplified in Scheme 10.

Results are consistent with the general reactivity trend shown in Scheme 2. It is worth noting that despite 4-(3-hydroxypropyl)phenol possessing both an aromatic and an aliphatic hydroxyl nucleophilic group, the first one remains inert relatively with weak bases, while it undergoes a selective methylation only at a high temperature and with a zeolite catalyst (Scheme 10, bottom). Overall, a straightforward catalytic upgrading of *p*-coumaryl-type alcohols is possible with DMC as a solvent/reagent and derivatives with largely different chemical properties compared to the starting molecules (e.g., polarity, hydrogen-bonding ability, etc.) can be obtained, making them potentially interesting in their own right.

4.3 Upgrading of Renewable Lactones

Current advances of research on biorefinery derived chemicals have demonstrated that useful lactones can be

Encyclopedia of Inorganic and Bioinorganic Chemistry, Online © 2011–2016 John Wiley & Sons, Ltd.

This article was published in the *Encyclopedia of Inorganic and Bioinorganic Chemistry* in 2016 by John Wiley & Sons, Ltd.
DOI: 10.1002/9781119951438.eibc2428

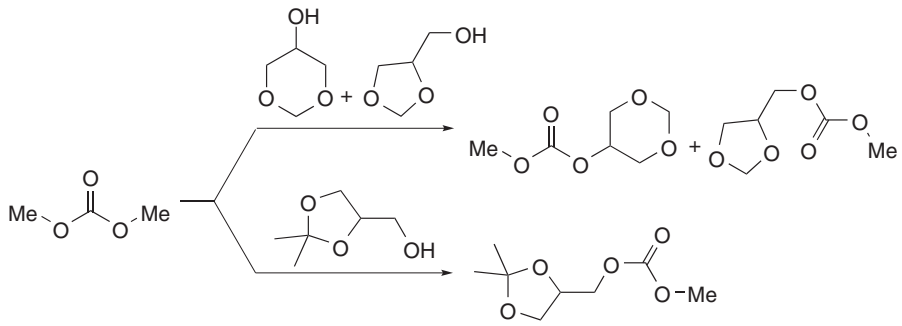

Scheme 9 The transesterification of DMC with glycerol formal (top) and solketal (bottom)

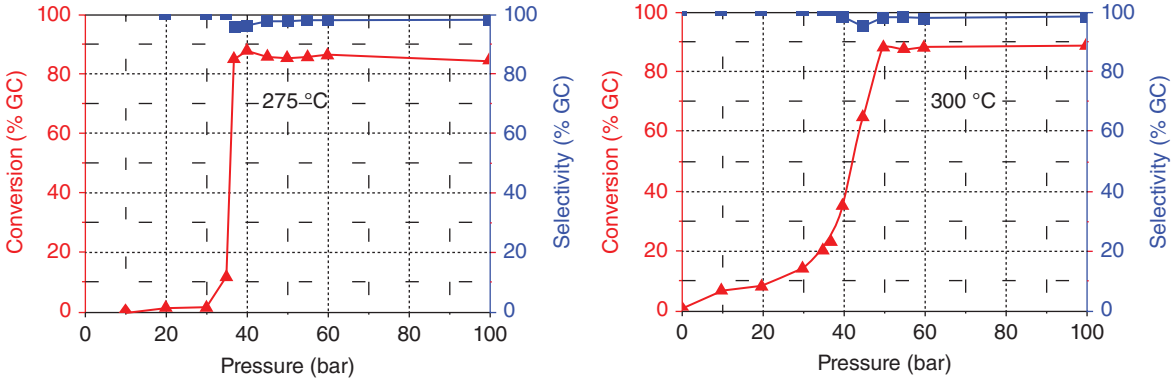

Figure 1 Effects of temperature and pressure on the non-catalytic (thermal) continuous-flow transesterification of DMC with glycerol formal. (Reproduced from Ref. 29 with permission from the Royal Society of Chemistry)

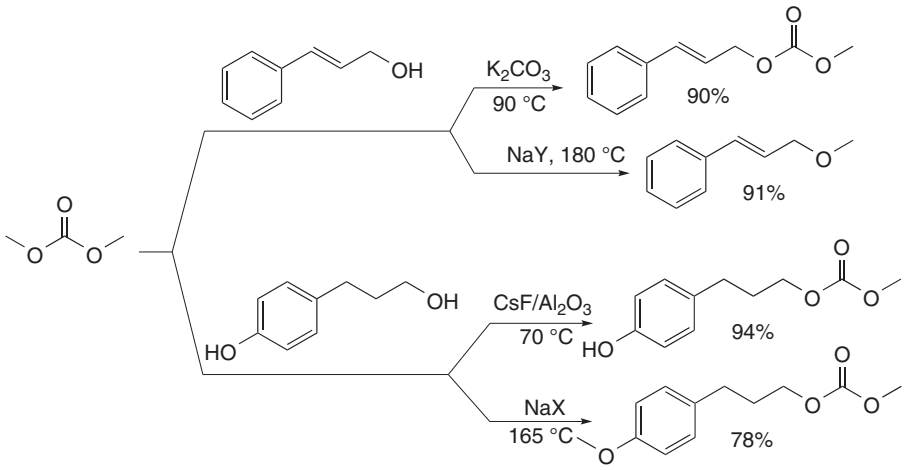

Scheme 10 The tunable selectivity of reaction of cinnamyl alcohol (top) and 4-(3-hydroxypropyl)phenol (bottom) with DMC

obtained by processing vegetable biomass. Examples are γ-butyrolactone (GBL) and γ-valerolactone (GVL) that can originate from succinic acid and levulinic acid (LA), respectively, both acids being platform chemicals of the fermentation of glucose and the chemical transformation (acidic digestion) of cellulose and hemicelluloses.[34,35] Promising routes starting from bio-furfural and hydroxymethylfurfural (HMF) are also available for the

Encyclopedia of Inorganic and Bioinorganic Chemistry, Online © 2011–2016 John Wiley & Sons, Ltd.

This article was published in the *Encyclopedia of Inorganic and Bioinorganic Chemistry* in 2016 by John Wiley & Sons, Ltd.
DOI: 10.1002/9781119951438.eibc2428

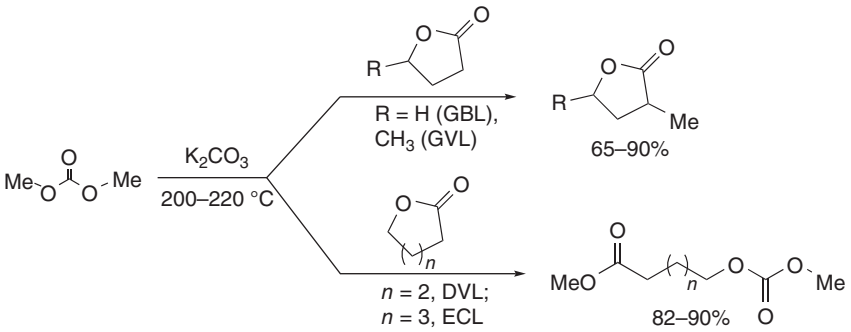

Scheme 11 Reactions between lactones and dimethyl carbonate with K_2CO_3 as a catalyst

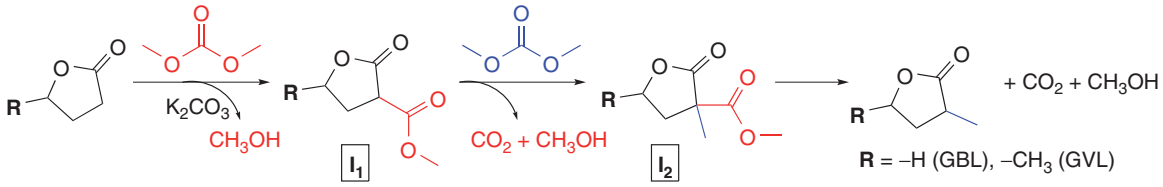

Scheme 12 Base-catalyzed alkylation of 5-membered ring Lactones with DMC

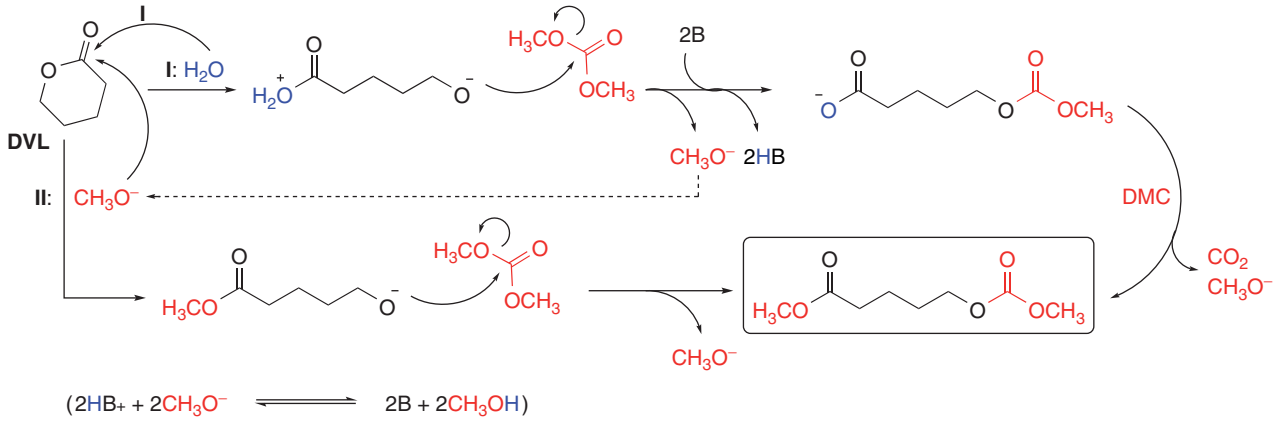

Scheme 13 The ring-opening reaction of DVL by DMC in the presence of catalytic base (B: K_2CO_3)

production of δ-valerolactone (DVL) and ε-caprolactone (ECL), respectively.[36,37] The derivatization of such lactones, particularly their alpha-alkylation, is an important strategy for the broadening of the possible uses of such compounds. In this respect, the achievement of a catalytic alkylation method is a desirable goal since available procedures make use of stoichiometric reactions with harmful alkyl halides and sulfates, generating polluted salts to be disposed of.[38,39] An alternative green method was devised by the use of dimethyl carbonate as a methylation agent. Although the reaction of γ-butyrolactone with DMC has been known since early 1990s,[40] no substantial studies or extension of such a protocol have been reported until it has been reviewed by us in 2014.[41] Results have demonstrated that in the presence of K_2CO_3 as a basic catalyst, either the α-alkyl derivatives of the five-membered ring GBL and GVL or the highly oxygenated acyclic derivatives of six- and seven-membered rings DVL and ECL, can be obtained (Scheme 11).

Experiments have proved that the methylation pathway (top) is consistent with a mechanism similar to that reported for base-catalyzed alkylations of CH_2-active compounds by DMC[42] outlined in Scheme 12. This involves a three-step sequence, including (i) a $B_{AC}2$ attack of the

Encyclopedia of Inorganic and Bioinorganic Chemistry, Online © 2011–2016 John Wiley & Sons, Ltd.

This article was published in the *Encyclopedia of Inorganic and Bioinorganic Chemistry* in 2016 by John Wiley & Sons, Ltd.
DOI: 10.1002/9781119951438.eibc2428

nucleophilic α-carbon of the lactone to DMC to form a carboxyalkyl derivative (**I1**); (ii) a $B_{AL}2$ methylation reaction to produce an alkyl-carboxyalkyl derivative (**I2**) as a second intermediate; (iii) a final decarboxylation process originating the α-alkylated lactone.

Rather than giving alpha-alkylated lactones, six- and seven-membered ring DVL and ECL undergo a ring-opening reaction that yields acyclic products bearing an ester and a carbonate group at each end (Scheme 11, bottom). In this case, DMC formally acts as an oxidant.[43] It seems plausible that the ring-opening is triggered by traces of water according to Scheme 13 (path I).

Next, the open intermediate reacts twice with DMC, releasing methoxide, which continues the process via pathway (II). This behavior is due to the higher reactivity of DVL and ECL with respect to the five-membered analogs. It should be noted that DVL polymerizes spontaneously to give linear polyesters at room temperature. Therefore, whatever is the mechanism, a procedure able to trap such a lactone (and ECL as well) in a monomeric form provides a useful synthetic perspective, particularly in view of the high oxygen content of the products obtained.

5 RELATED ARTICLES

Renewable Plant-Based Raw Materials for Industry; Methylethers from Alcohols and Dimethyl Carbonate; Catalytic Cyclic Carbonate Synthesis with Sustainable Metals.

6 ABBREVIATIONS AND ACRONYMS

CF = continuous flow; DAlC = dialkylcarbonate; DMC = dimethylcarbonate; DVL = delta-valerolactone; ECL = epsilon-caprolactone; FAU = faujasites; GA = glycerol acetal; GBL = gamma-butyrolactone; GlyF = glycerol formal; HMF = hydroxymethylfurfural; LA = levulinic acid; MAC = methyl alkyl carbonate; NaY = sodium exchanged Y-zeolite; PhNHMe = mono-*N*-methyl aniline.

7 REFERENCES

1. B. A. V. Santos, V. M. T. M. Silva, J. M. Loureiro and A. E. Rodrigues, *ChemBioEng Rev.*, 2014, **1**, 214.
2. C. Martín, G. Fiorani and A. W. Kleij, *ACS Catal.*, 2015, **5**, 1353.
3. U. Romano, R. Tesel, M. M. Mauri and P. Rebora, *Ind. Eng. Chem. Prod. Res. Dev.*, 1980, **19**, 396.
4. K. Nishihira, S. Yoshida and S. Tanaka, US5292917, 1994.
5. S. Fukuoka, I. Fukawa, M. Tojo, K. Oonishi, H. Hachiya, M. Aminaka, K. Hasegawa and K. Komiya, *Catal. Surv. Asia*, 2010, **14**, 146.
6. P. Tundo and M. Selva, *Acc. Chem. Res.*, 2002, **35**, 706.
7. E. K. Fukuda and R. T. McIver, *J. Am. Chem. Soc.*, 1979, **101**, 2498.
8. D. MacWilliams, 'Kirk-Othmer: Encyclopedia of Chemical Technology', 3rd edition, John Wiley & Sons, Inc., New York, 1978.
9. J. March, 'Advanced Organic Chemistry', 4th edition, John Wiley & Sons, Inc., New York, 1991.
10. Z.-H. Fu and Y. Ono, *Catal. Lett.*, 1993, **22**, 277.
11. M. Selva, A. Bomben and P. Tundo, *J. Chem. Soc., Perkin Trans.*, 1997, **1**, 1041.
12. M. Selva, P. Tundo and A. Perosa, *J. Org. Chem.*, 2001, **66**, 677.
13. M. Selva, P. Tundo and A. Perosa, *J. Org. Chem.*, 2002, **67**, 9238.
14. M. Selva, P. Tundo and A. Perosa, *J. Org. Chem.*, 2003, **68**, 7374.
15. M. Selva, P. Tundo and T. Foccardi, *J. Org. Chem.*, 2005, **70**, 2476.
16. A. Dhakshinamoorthy, M. Alvaro and H. Garcia, *Appl. Catal. A-Gen.*, 2010, **378**, 19.
17. M. Selva and A. Perosa, *Green Chem.*, 2008, **10**, 457.
18. A. Perosa, M. Selva, P. Tundo and F. Zordan, *Synlett*, 2000, **1**, 272.
19. M. Czjzek, H. Fuess and T. Vogt, *J. Phys. Chem.*, 1991, **95**, 5255.
20. F. Bonino, A. Damin, S. Bordiga, M. Selva, P. Tundo and A. Zecchina, *Angew. Chem. Int. Ed.*, 2005, **44**, 4774.
21. E. G. Derouane, *J. Mol. Catal. A-Chem.*, 1998, **134**, 29.
22. J. J. Bozell and G. R. Petersen, *Green Chem.*, 2010, **12**, 539.
23. A. E. Diaz-Alvarez, J. Francos, B. Lastra-Barreira, P. Crochet and V. Cadierno, *Chem. Commun.*, 2011, **47**, 6208.
24. L. Moity, A. Benazzouz, V. Molinier, V. Nardello-Rataj, M. K. Elmkaddem, P. de Caro, S. Thiébaud-Roux, V. Gerbaud, P. Marion and J.-M. Aubry, *Green Chem.*, 2015, **17**, 1779.
25. V. R. Ruiz, A. Velty, L. L. Santos, A. Leyva-Pérez, M. J. Sabater, S. Iborra and A. Corma, *J. Catal.*, 2010, **271**, 351.
26. M. Selva, V. Benedet and M. Fabris, *Green Chem.*, 2012, **14**, 188.
27. J. S. Moya, E. Criado and S. De Aza, *J. Mater. Sci.*, 1982, **17**, 2213.
28. L. Cattelan, PhD program under progress at Ca' Foscari University of Venice, Italy (2014–).
29. M. Selva, S. Guidi and M. Noè, *Green Chem.*, 2015, **17**, 1008.
30. W. V. Steele, R. D. Chirico, S. E. Knipmeyer, A. Nguyen and N. K. Smith, *J. Chem. Eng. Data*, 1997, **42**, 1037.

Encyclopedia of Inorganic and Bioinorganic Chemistry, Online © 2011–2016 John Wiley & Sons, Ltd.

This article was published in the *Encyclopedia of Inorganic and Bioinorganic Chemistry* in 2016 by John Wiley & Sons, Ltd.
DOI: 10.1002/9781119951438.eibc2428

31. V. F. Marulanda, *J. Clean. Prod.*, 2012, **33**, 109.
32. J. Zakzeski, P. C. Bruijnincx, A. L. Jongerius and B. M. Weckhuysen, *Chem. Rev.*, 2010, **110**, 3552.
33. J. N. G. Stanley, M. Selva, A. F. Masters, T. Maschmeyer and A. Perosa, *Green Chem.*, 2013, **15**, 3195.
34. B. Litsanov, A. Kabus, M. Brocker and M. Bott, *Microb. Biotechnol.*, 2012, **5**, 116.
35. A. Corma, S. Iborra and A. Velty, *Chem. Rev.*, 2007, **107**, 2411.
36. L. Wang, K. Thai and M. Gravel, *Org. Lett.*, 2009, **11**, 891.
37. T. Buntara, S. Noel, P. H. Phua, I. Melian-Cabrera, J. G. de Vries and H. J. Heeres, *Angew. Chem. Int. Ed.*, 2011, **50**, 7083.
38. J. L. Herrmann and R. H. Schlessinger, *J. Chem. Soc., Chem. Commun.*, 1973, 711.
39. M. Kowalczuk, P. Kurcok, W. Glowkowski and Z. Jedlinski, *J. Org. Chem.*, 1992, **57**, 389.
40. M. Selva, F. Trotta and P. Tundo, *Chim. Ind.*, 1991, **12**, 919.
41. A. Caretto, M. Noè, M. Selva and A. Perosa, *ACS Sustain. Chem. Eng.*, 2014, **2**, 2131.
42. M. Selva, C. A. Marques and P. Tundo, *J. Chem. Soc., Perkin Trans. 1*, 1994, 1323.
43. M. Selva, C. A. Marques and P. Tundo, *Gazz. Chim. Ital.*, 1993, **123**, 515.

Encyclopedia of Inorganic and Bioinorganic Chemistry, Online © 2011–2016 John Wiley & Sons, Ltd.

This article was published in the *Encyclopedia of Inorganic and Bioinorganic Chemistry* in 2016 by John Wiley & Sons, Ltd.
DOI: 10.1002/9781119951438.eibc2428

ChemPubSoc Europe

DOI: 10.1002/cssc.201601765

CHEMSUSCHEM Full Papers

Continuous-Flow *O*-Alkylation of Biobased Derivatives with Dialkyl Carbonates in the Presence of Magnesium–Aluminium Hydrotalcites as Catalyst Precursors

Lisa Cattelan,[a, b] Alvise Perosa,[a] Piero Riello,[a] Thomas Maschmeyer,[b] and Maurizio Selva*[a]

The base-catalysed reactions of OH-bearing biobased derivatives (BBDs) including glycerol formal, solketal, glycerol carbonate, furfuryl alcohol and tetrahydrofurfuryl alcohol with non-toxic dialkyl carbonates (dimethyl and diethyl carbonate) were explored under continuous-flow (CF) conditions in the presence of three Na-exchanged Y- and X-faujasites (FAUs) and four Mg–Al hydrotalcites (HTs). Compared to previous etherification protocols mediated by dialkyl carbonates, the reported procedure offers substantial improvements not only in terms of (chemo)selectivity but also for the recyclability of the catalysts, workup, ease of product purification and, importantly, process intensification. Characterisation studies proved that both HT30 and KW2000 hydrotalcites acted as catalyst precursors: during the thermal activation pre-treatments, the typical lamellar structure of the hydrotalcite was broken down gradually into a MgO-like phase (periclase) or rather a magnesia–alumina solid solution, which was the genuine catalytic phase.

Introduction

In the past 15 years, an enormous effort has been devoted to the identification of the most promising biomass-derived compounds. Among the available analyses, extensive work performed by the US Department of Energy in 2004 and its revisitation in 2010 still represent cornerstones in this field. For the first time, they offered rational criteria for the selection of the so-called "top 10" platform chemicals, that is, a small group of biobased derivatives (BBDs) that could be utilised as building blocks for higher-value products and materials.[1] Although this approach has been refined further over the years,[2] current top 10 lists of biomass-derived platform compounds still include most of the originally identified compounds, particularly mono- and dicarboxylic-functionalised acids, 3-hydroxybutyrolactone, several bio-hydrocarbons derived from isoprene, glycerol and derivatives as well as several other sugars such as sorbitol and xylitol. These considerations have inspired us to try to integrate green protocols mediated by dialkyl carbonates ($ROCO_2R$, DAICs)[3] with the chemical valorisation of biobased platform molecules. Such an activity requires a multidisciplinary approach to combine aspects of organic and physical chemistry as well as chemical engineering and materials science.

Within this context, our attention has been focused on five model OH-bearing BBDs (Scheme 1) including solketal (**1a**), glycerol formal (**2a**/**2a**′) and glycerol carbonate (**3a**), which are among the most celebrated derivatives of glycerol. The applications of these compounds span multiple sectors from fine chemicals, cosmetics and pharmaceuticals to biofuels and lubricants, biobased solvents and polymers.[4] The availability of glycerol is mostly fuelled by plant-oil-based biodiesel manufacture, which generates large amounts of glycerol as a co-product.[5] The other two compounds shown in Scheme 1, that is, furfuryl alcohol (**4a**) and its hydrogenated homologue tetrahydrofurfuryl alcohol (**5a**), are derived from furfural, which, in turn, is generated through the dehydration of the sugar components (glucose and xylose) that constitute a large portion of lignocellulosic biomass.[6] Compounds **4a** and **5a** find uses as modifiers and templates for polymers, as fibers and nanocomposites[7] and as sources of polyols.[8]

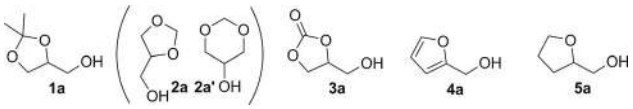

Scheme 1. Model OH-bearing BBDs.

In addition, the presence of an OH-capped tether (hydroxymethylene group) enables an avenue for the derivatisation of all five compounds (**1a**–**5a**): of particular note, esterification and alkylation protocols allow for the expansion of the potential of OH-BBDs through the synthesis of substantially value-added products, including intermediates, solvents and biologically active molecules such as glycerol ethers, esters and carbo-

[a] L. Cattelan, Prof. A. Perosa, Prof. P. Riello, Prof. M. Selva
Department of Molecular Sciences and Nanosystems
Università Ca' Foscari Venezia
Via Torino, 155, Venezia Mestre (Italy)
E-mail: selva@unive.it

[b] L. Cattelan, Prof. T. Maschmeyer
Laboratory of Advanced Catalysis for Sustainability
School of Chemistry F11
University of Sydney
Sydney, 2006 (Australia)

Supporting Information and the ORCID identification number(s) for the author(s) of this article can be found under http://dx.doi.org/10.1002/cssc.201601765.

nates[9] as well as additives for biodiesel blends based on furanyl ether derivatives.[6a]

The combined effect of a high reaction temperature (200–220 °C) and a base catalyst (K_2CO_3) allowed an almost exclusive *O*-alkylation of glycerol acetals (GAs). The reaction showed excellent features from both synthetic and environmental standpoints because it not only proceeded with etherification selectivities and yields as high as 99 and >80%, respectively but also coupled the use of renewable and non-toxic reactants such as glycerol acetals and DAlCs in a catalytic process with no byproducts other than CO_2 (which did not present a disposal problem) and alcohols, which were recyclable for the synthesis of dialkyl carbonates. Only trace amounts of byproducts from competitive transesterification processes were detected. However, under the explored batch conditions, the sequence suffered from two major drawbacks: 1) slow alkylation kinetics, that is, the reactions could require up to 80 h for completion, and 2) extensive competitive decarboxylations of dialkyl carbonates to form the corresponding dialkyl ethers (Scheme 2, dashed path).[10]

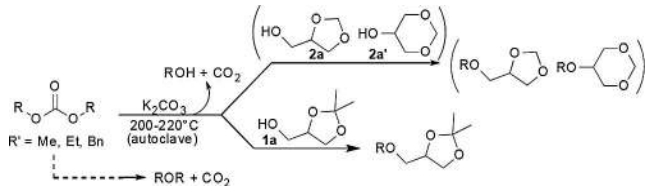

Scheme 2. The etherification of glycerol acetals with dialkyl carbonates in the presence of K_2CO_3 catalyst (top). The dashed path shows the concurrent decarboxylation reaction of dialkyl carbonates.

This necessitates the use of a large excess of the alkylating agent and, importantly, involves the co-generation of an autogenous pressure of ≥60 bar; both of these aspects hindered the scale-up of the process. However, the benefits and disadvantages stimulated us to devise a new broad-based protocol to expand the alkylating capabilities of dialkyl carbonates to different OH-bearing BBDs and, at the same time, minimise the limitations described above. The implementation of a continuous-flow (CF) procedure was an attractive option to reach the conversion target because it offered the best possible control of the reaction parameters (*T*, *p* and reactant molar ratio) to improve the process kinetics, productivity and safety. However, under CF conditions, alkaline carbonates needed anion activators (polyethylene glycols), specifically shaped reactors (e.g., continuous-stirred-tank-reactors, CSTRs) or both to perform as catalysts,[11] because the basicities of the alkaline carbonates were too low and they were partially soluble in the reactant DAlCs and the co-produced alcohols (Scheme 2).[12] Therefore, alternative solid systems had to be considered. Candidates were chosen from the families of faujasite (FAU) and Mg–Al hydrotalcite (HT) solids. We have reported both Y- and X-type FAUs extensively as catalysts for DAlC-promoted *N*-, *O*- and *S*-alkylations of a large variety of nucleophiles, including anilines, benzyl alcohols, aminophenols, aminobenzyl alcohols, mercaptophenols, mercaptobenzoic acids, hydroxybenzoic acids and functionalised phenols of the lignin scaffold.[13] However, HTs have been investigated almost exclusively as catalysts for transesterifications with dialkyl carbonates,[14] whereas only a few reports have described the methylation of some phenols and benzyl alcohol with dimethyl carbonate over Mg–Al hydrotalcites or modified HT systems.[15] The role of the catalyst is still under debate.

The present work demonstrates that the use of HTs allows for the setup of a particularly robust catalytic CF method for the etherification of OH-bearing BBDs with DAlCs. For example, at 210 °C and ambient pressure, the model reaction of solketal (**1a**) with dimethyl carbonate shows the formation of the corresponding methyl ether with quantitative conversion and >99% selectivity in the presence of calcined HT Pural® MG30 (cHT30; Mg/Al = 0.5) as a catalyst.

The CF protocol can be extended to the reactions of the substrates shown in Scheme 1 with both dimethyl and diethyl carbonate. Quantitative conversions and *O*-alkylation selectivity comparable to those of solketal were achieved over calcined HT catalysts, except for furfuryl alcohol (**4a**) for which only the transesterification derivative [(furan-2-yl)methyl methyl carbonate] was obtained. Overall, the CF procedure not only exemplifies an original approach to the upgrade of OH-bearing bio-based substrates but can also overcome the safety and scale-up limitations of batchwise reactions as it operates at atmospheric pressure and with a productivity [≈2 $g/(g_{cat}\,h)$] for ether derivatives that is up to 200-fold higher than those of batch methods.

Results and Discussion

The apparatus used for the CF reactions comprised an HPLC pump, an oven containing a tubular reactor filled with the catalyst, a Rheodyne sampling valve and a back-pressure regulator (the details are reported in the Supporting Information). The dialkyl carbonates including dimethyl and diethyl carbonate as well as **1a**–**5a** were commercially available ACS-grade compounds.

Catalyst

Three alkali-metal-exchanged X- and Y-type FAUs including two commercially available NaX and NaY solids and a CsY zeolite were used. The latter was prepared as described in the Experimental Section. Four HTs were also used. Three of them were obtained from Sasol, Italy and labelled as HT30, HT63 and HT70. A fourth sample from Kyowa Kagaku Kogyo Company Limited was labelled as KW2000. Some features of these HT solids are summarised in Table 1. For KW2000, inductively coupled plasma mass spectrometry (ICP-MS) analysis was used to determine the post-synthesis Na and K residues (see Experimental Section). MgO and a 30:70 physical mixture of MgO (Aldrich, particle size 325 mesh, surface area 114 $m^2\,g^{-1}$, average pore diameter 9.4 nm) and basic γ-Al_2O_3 (Macherey–Nagel, pH 9.5±0.3, particle size 50–200 μm, surface area 130 $m^2\,g^{-1}$) were also used as additional catalysts for two comparative tests. The reaction of solketal with dimethyl carbonate (DMC)

Table 1. Hydrotalcites used in this work.

Entry	Sample label	MgO/Al_2O_3 [%]	Surface area[a] [$m^2 g^{-1}$]	Source	Post-synthesis residues [%]
1	HT30	30:70[b]	250	Pural® MG30, Sasol	Na: 1.5×10^{-3}[a]
2	HT63	63:37[b]	230	Pural® MG63, Sasol	K: 1.7×10^{-3}[a]
3	HT70	70:30[b]	180	Pural® MG70, Sasol	
4	KW2000	64:36[b] (65:35)[c]	190	Kyowa Kagaku Kogyo Co. Ltd.	Na: 2.5×10^{-2}[c] K: 1.1×10^{-2}[c]

[a] Data specified by the supplier. [b] Ratio [wt%] specified by the supplier. [c] Determined by ICP-MS measurement.

was chosen as a model to investigate the activities of the different catalysts and the effects of four major reaction parameters, that is, temperature, pressure, time and reactant molar ratio.

CF tests over different catalysts

The performances of the FAU and HT catalysts in the above-described CF apparatus were compared. The temperature and pressure for the initial tests were selected according to our previous results obtained for the batch alkylation and CF transesterification reactions of glycerol acetals with dialkyl carbonates.[10,16] In particular, the experiments were performed in the ranges $T=200$–$275\,^{\circ}C$ and $p=5$–50 bar. Each of the investigated catalysts was used to fill the inner volume of the CF reactor as uniformly and completely as possible.[17] Therefore, the amount of each solid sample was adjusted according to its apparent density: NaY, NaX, CsY, KW2000, HT30, HT63 and HT70 were used as such in slightly different quantities of 0.68, 0.54, 0.86, 0.52, 0.73, 0.51 and 0.85 g, respectively. Each catalyst was dehydrated under vacuum (70 °C, 18 mm, overnight) before use. In all of the tests, the same 1.83 M solution of solketal in DMC [DMC/solketal molar ratio (W) = 5] was fed to the reactor at a total volumetric flow rate (F) of 0.1 mL min^{-1}, which corresponds to a contact time of approximately 10 min. The excess DMC served both as a reagent and a carrier/solvent. During the CF experiments, samples of the mixtures were collected periodically at the reactor outlet for GC–MS analysis, which allowed for the evaluation of both the reaction conversion (measured with respect to solketal as the limiting reagent) and the product distribution. Each test was duplicated to check the reproducibility; in each reaction, a fresh sample from the same batch of catalyst was used.[18]

Several reactions occurred under the conditions explored; the double electrophilic reactivity of dimethyl carbonate accounted for the formation of *O*-methyl and transesterification derivatives, **1b** and **1c**, respectively (Scheme 3: paths i and ii). Subsequently, compound **1c** could plausibly undergo a further transesterification with solketal or a dismutation reaction to afford the symmetric carbonate product **1d** (Scheme 3: paths iii and iv). The structures of **1b**, **1c** and **1d** were assigned by GC–MS and NMR spectroscopy analyses and by comparison to previously synthesised authentic samples. Moreover, some unidentified side-products were also observed. These compounds are referred to as "others", and their GC–MS data are consistent with a ring-opening reaction of the acetal ring followed by methylation and transesterification of the corresponding (linear) derivative.

At 250–275 °C and 10 bar, FAUs were unsuitable catalysts for the reaction investigated. At best, the conversion of solketal was moderate (60–70%). The more basic NaX and CsY systems were slightly more active than NaY but favoured the transesterification product **1c** with a selectivity of 60–70%.[19] NaY improved the formation of the *O*-methyl derivative **1b** (up to 40%) but also induced side-reactions to afford a sizeable amount of unidentified byproducts. In all cases, the conversion and selectivity were steady after 180 min and did not vary substantially if the CF tests were prolonged to 18 h (Supporting Information, Figures S2 a–b and Table S1).

This behaviour neatly contrasted with our previously reported results for the reaction of benzyl-type alcohols with DMC, through which the corresponding *O*-methyl ethers were achieved quantitatively and selectively in the presence of NaX and NaY catalysts.[20] Unlike aromatic or benzyl substrates,[14,21,22] solketal has a cycloaliphatic structure, which could be more weakly coordinated to the FAU surface and, thereby, alter the reaction outcome. On the basis of the hard and soft acids and bases (HSAB) principle, other authors have also proposed that hard nucleophiles such as aliphatic alcohols prefer the hard electrophilic site of DMC (i.e., the carboxyl carbon atom) rather than the softer methyl group.[23]

The scenario changed completely in the presence of HTs. In particular, the use of KW2000 improved the conversion and, even more remarkably, the methylation selectivity. The reactions were performed under the same conditions as those for Figure 2b (275 °C, 10 bar, $W=5$, $F=0.1$ mL min^{-1}), but the reactions were performed for a longer time (18–20 h). The performances of the HT catalysts are summarised in Figure 1a and b with emphasis on KW2000.

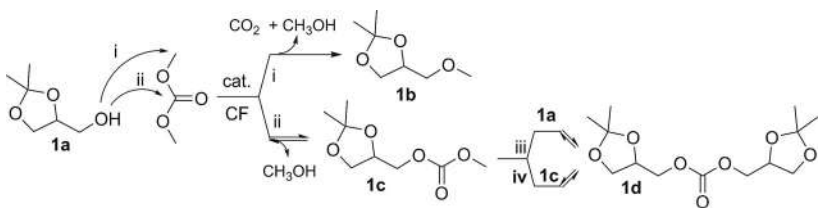

Scheme 3. Major products of the CF catalytic reaction of solketal with DMC.

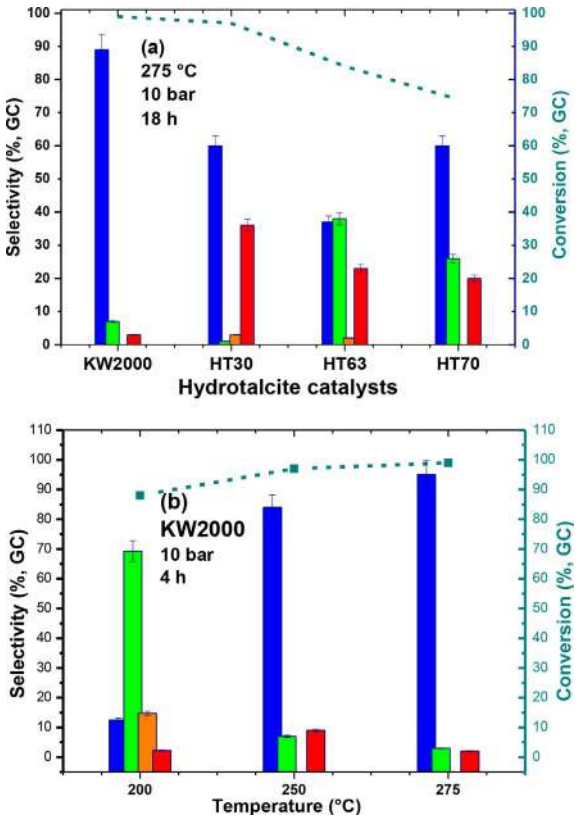

Figure 1. Trends for the conversion and product distribution for the CF reaction of solketal with DMC: (a) comparison of different HT catalysts at 275 °C and 10 bar; (b) effect of the temperature during catalysis by KW2000 at different temperatures. The coloured bars (from left to right) show the selectivity towards the *O*-methyl product (**1 b**, ●), the transesterification or dismutation derivatives (**1 c**, ● and **1 d**, ●, respectively) and unidentified compounds (others, ●). The dashed line (from right to left) shows the trend of solketal conversion. DMC and solketal were used in a 5:1 molar ratio (*W*), and the total flow rate was 0.1 mL min^{-1}.

All hydrotalcites investigated were better catalysts than the FAUs, but KW2000 offered a performance far superior to those of the other HTs (HT30, HT63 and HT70; Figure 1 a). The KW2000-catalysed reaction proceeded with a very good conversion and *O*-methylation selectivity of 99 and 89 %, respectively (dashed green line and blue bar, Figure 1 a). The ring of the reactant acetal was substantially preserved, and further transformations were avoided; only traces of the transesterification product **1 c** were observed. The second best hydrotalcite, that is, HT30, still allowed an almost quantitative process (conversion 96 %), although the methyl derivative **1 b** did not exceed 60 % of the total of the observed products (Figure 1 a).

The reactions catalysed by KW2000 and HT30 were explored in greater depth through the analysis of samples of the mixture collected at the CF reactor every 60 min for 20 h (Figures S3 a–b). In the presence of KW2000, a steady and almost complete conversion was obtained after just 1 h, whereas the *O*-methylation selectivity reached a maximum of 95 % in 4 h and only decreased slightly to 87–89 % at the end of the test (18–20 h; Figure S3a). For the HT-30-catalysed process, the conversion was below 80 % in the first 4 h, and the transesterification compound, **1 c**, was the dominant product (Figure S3 b). After 18–20 h, the residual solketal was present in trace amounts (2–5 %), and a steady formation of both **1 b** and unidentified products was observed (≈60 and 40 %, respectively). Although their product distributions were different, both reactions displayed an initial (induction) period during which mixtures of products formed. Thereafter, the conversion and selectivity stabilised, and the almost exclusive formation of ether **1 b** was observed for KW2000. For this catalyst, three additional short experiments (4 h each) were performed to examine the effect of the temperature in the range 200–275 °C with the other conditions unaltered (10 bar, $W=5$, $F=0.1$ mL min^{-1}; Figure 1 b). For KW2000 at 200 °C, the transesterification and disproportion reactions were the major transformations (green and ochre bars, Figure 1 b). However, the *O*-methylation process was triggered by a temperature increase and was favoured progressively above 250 °C.

For KW2000, further tests were also devised to investigate the effects of the pressure and the DMC/solketal molar ratio *W* (see Figures S4 a and b). At 275 °C ($W=5$, $F=0.1$ mL min^{-1}, 4 h), if the pressure was decreased or increased to 5 or 50 bar, the conversion diminished slightly (from 99 to ≈95 %), but the methylation selectivity dropped from 95 to 75–80 % because of the onset of transesterification and unidentified side-reactions. It is plausible that the pressure influenced the partition of the reactants between the liquid and the vapour phases and, consequently, the contact of solketal and DMC with the catalyst surface. We previously observed a similar behaviour during an investigation of the thermal (catalyst-free) transesterification of glycerol acetals and glycerol with DMC.[24] However, at 275 °C and 10 bar ($F=0.1$ mL min^{-1}, 4 h), if *W* decreased from 5 to 1.1, both the conversion and the *O*-methylation selectivity decreased to 58 and 62 %, respectively, and there was a significant formation of products **1 c**, **1 d** and "others".

Two effects might plausibly account for this result at a constant *F*: (1) If more DMC is present ($W=5$), the rates (and conversion) of the DMC-mediated reactions are higher. Under these conditions, even though (reversible) transesterifications occurred, the corresponding products (**1 c** and **1 d**) were observed in only minor amounts, because these compounds were consumed by the onset of the parallel irreversible *O*-alkylation reaction, which proceeded almost to completion (Scheme 3 and Figures 1 a, S3 and S4). However, for $W<5$ and particularly at $W=1.1$, lower-energy-demanding reaction pathways, that is, transesterification processes, became more evident; therefore, the quantities of derivatives **1 c** and **1 d** increased. (2) A low DMC/solketal molar ratio ($W=1.1$–2) not only disfavoured the solvation of the acetal by DMC and the mutual interactions between reactants but also facilitated the occurrence of intramolecular side-processes including, for example, the ring opening of solketal ("others" as byproducts) adsorbed over the catalyst surface.

CF tests with calcined HTs

If hydrotalcites are heated to approximately 200 °C, they release water; however, at approximately 300 °C (near the tem-

perature used in Figure 1) and above, a collapse of the typical layered structure of HTs occurs, and Mg/Al mixed oxides form.[25] These facts prompted us to explore the catalytic activities of calcined hydrotalcites (c-HTs) in the reaction of solketal with DMC. The c-HTs were prepared by heating the Pural® (HT30, HT63 and HT70) and KW2000 solids at 450 °C in a dried air flow for 16 h.[26] The c-HTs showed quite similar apparent densities, and the same amounts (0.5 g each) were used for the catalytic tests. In all cases, a 1.83 M solution of solketal in DMC ($W=5$) was fed to the reactor at $F=0.1$ mL min^{-1}. The experiments proved that the calcined hydrotalcites, particularly c-HT30, improved the reaction outcome dramatically. The solketal conversion and the *O*-methylation selectivity increased, and the c-HT30 catalyst was also active at temperatures and pressures remarkably lower than those used previously. With the other conditions unaltered ($W=5$, $F=0.1$ mL min^{-1}), the reactions could be run at temperatures and pressures as low as only 210 °C and 1 bar.

The performance of c-HT30 over 20 h on-stream is detailed in Figure 2, and the activities and *O*-methylation selectivities of

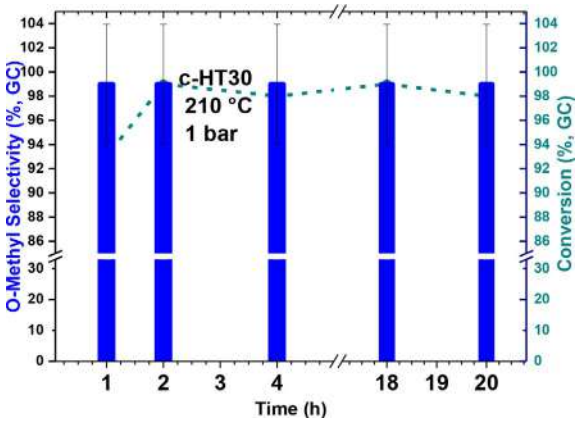

Figure 2. CF reaction of solketal with DMC in the presence of c-HT30 catalyst at 210 °C and ambient pressure. Trends of *O*-methylation selectivity and conversion of solketal with time (blue bars and dashed green profile). Other conditions: $W=5$, $F=0.1$ mL min^{-1}.

different c-HTs are compared in Table 2. Each test was duplicated to check the reproducibility of the results.[18] The outcome of the reaction catalysed by c-HT30 exemplifies one of the best reported *O*-methylation reactions of an alcohol-like function mediated by DMC. The solketal was transformed quantitatively to the methyl ether **1 b**, and a steady efficiency was ensured for at least 20 h. The comparison of Figures 2, 1 and S2 a and b also indicated that the catalytic properties of both HT30 and KW2000 were modified considerably not only by the calcination of the HTs but also by the thermal treatment during high-temperature (275 °C) reactions. At the same reaction temperature (210 °C) used for c-HT30, the other c-HT catalysts resulted in conversions and *O*-methylation selectivities not exceeding 88 and 27%, respectively, even at 10 bar (Table 2: compare c-HT70, c-KW2000 and c-HT63 in entries 2–4, columns 4–7). Minor improvements were achieved at 225 °C (entries 2–4, columns 8–11). The reaction proceeded with the complete conversion of solketal to the methyl derivative **1 b** over all c-HTs catalysts only at 275 °C (10 bar, $W=5$, $F=0.01$ mL min^{-1}).

The ability of calcined hydrotalcites to promote the investigated reaction was contrasted with other CF experiments in which the c-HTs were replaced by either MgO (0.85 g of a mixture of 60 wt% MgO with ground-glass Raschig rings) or a physical mixture of MgO and basic γ-Al_2O_3 in a 30:70 molar ratio (0.85 g), both of which mimicked the formal composition of HT30. Both of these solids were calcined at 450 °C for 6 h before use. Under the conditions described above (275 °C, 10 bar, $W=5$, $F=0.01$ mL min^{-1}), the two catalysts gave modest results: the best one was MgO, for which the reaction proceeded with a conversion and *O*-methyl selectivity of only 80 and 48%, respectively. Although MgO and γ-Al_2O_3 were reported recently to catalyse both *O*- and *N*-alkylations mediated by DMC,[27,28] these solids were clearly inadequate for the reaction investigated.

The study so far demonstrated that KW2000 and HT30 were the most promising catalysts. To continue our exploration of the potential of such materials, in particular the calcined system c-HT30, we focused the investigation on the scope and limitations of the CF-etherification of other OH-bearing bio-based derivatives with both dimethyl and diethyl carbonate.

Scope of the reaction: different reactants, mass balance and productivity

The substrates shown in Scheme 1, including glycerol formal (**2 a**+**2 a**′), glycerol carbonate (**3 a**), and furfuryl and tetrahydrofurfuryl alcohols (**4 a** and **5 a**), were reacted with DMC or diethyl carbonate (DEC) under CF conditions. Accordingly, a homo-

Table 2. Comparison of c-HTs catalysts for the reaction of solketal with DMC.

Entry	Catalyst	p/t [bar h^{-1}]	Reaction temperature 210 °C Conversion[a] [%]	Selectivity[a] [%]			225 °C Conversion[a] [%]	Selectivity[a] [%]		
				1 b	**1 c**	others		**1 b**	**1 c**	others
1	c-HT30	10/18	99	99	–	–	99	99	–	–
2	c-HT70	10/18	88	27	49	24	95	40	42	18
3	c-KW2000	10/18	85	15	61	24	93	20	68	12
4	c-HT63	10/18	78	2	68	30	87	8	61	31

[a] Conversion of solketal and selectivity towards the *O*-methyl derivative **1 b**, the transesterification compound **1 c** and other products (including the disproportionation derivative **1 d** and unidentified byproducts), respectively. Other conditions: $W=5$, $F=0.1$ mL min^{-1}.

Table 3. The CF reactions of substrates **1a**–**5a** with DMC and DEC in the presence of c-HT30 catalyst.[a]

Entry	Substrate	Dialkyl carbonate	W[b]	T [°C]	Conversion [%][c]	Selectivity [%][d]	Product Structure	Y[e] [%]	P[f] [$g_{prod}\,g_{cat}^{-1}\,h^{-1}$]
1	**1a**	DMC	5	210	99	99	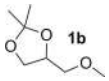 **1b**	92	2.64
2	**2a**/**2a**′	DMC	5	220	99	99	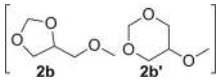 **2b** **2b'**	81	1.92
3	**3a**	DMC	20	210	98	65	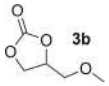 **3b**	55	0.42
4	**4a**	DMC	10	150	88	91	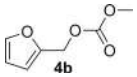 **4b**	80	1.26
5	**5a**	DMC	5	260	99	92	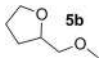 **5b**	82	1.94
6	**1a**	DEC	5	250	99	99	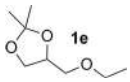 **1e**	92	2.04
7	**2a**/**2a**′	DEC	5	275	99	99	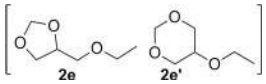 **2e** **2e'**	84	1.62

[a] Reactions were performed for 6 h (20 h for **1a**, entry 1) at ambient pressure and at $F = 0.1\ mL\,min^{-1}$. [b] Dialkyl carbonate/substrate molar ratio. [c] Conversion of the substrate (determined by GC). [d] Selectivity towards the shown product (determined by GC). [e] The isolated yield was evaluated by the workup of a mixture collected at the reactor outlet after 6 h (15 h for **1a**, entry 1). [f] The reaction productivities were calculated for isolated yields.

geneous solution of dialkyl carbonate and the substrate was delivered to the CF reactor filled with c-HT30 (0.5 g) as a catalyst for 6 h. The total flow rate was of 0.1 $mL\,min^{-1}$, and all of the CF tests were repeated twice to check their reproducibility. The reaction conditions, isolated yields (Y) and productivities (P: g products obtained in 1 h per g catalyst) for each of the studied processes are listed in Table 3, and the reactions and the structures of the products are summarised in Scheme 4. For completeness, the above-described results for the reaction of solketal with DMC are included in Table 3. The reactions could be performed at atmospheric pressure, but the operating temperature and the molar ratio of the reactants had to be optimised on a case-by-case basis in the ranges 210–275 °C and 5–20, respectively. Except for **4a**, quantitative conversions were reached for all of the substrates, and the *O*-alkylation selectivities were 65–99%. All of the products were isolated and characterised by NMR spectroscopy and GC–MS (the details are provided in the Supporting Information).

Solketal and glycerol formal (**1a** and **2a**/**2a**′) could be converted quantitatively into the corresponding methyl and ethyl ethers (**1b** and **2b**/**2b**′) by using DMC and DEC as *O*-alkylating agents. From the results, two facts emerged: (1) Regardless of the dialkyl carbonate, the etherification of glycerol formal was more energy-demanding than that of solketal. Methyl and ethyl ethers **2b**/**2b**′ and **2e**/**2e**′ were obtained at 220 and 275 °C, respectively, whereas **1b** and **1e** formed at the lower temperatures of 210 and 250 °C (compare Table 3, entries 1 and 2 with 6 and 7). A similar difference was observed for the transesterification of glycerol acetals with DAICs.[24] The higher density of glycerol formal (1.21 $g\,mL^{-1}$) with respect to that of solketal (1.07 $g\,mL^{-1}$) might play a role. (2) The syntheses of ethyl ethers required considerably higher temperatures (250–

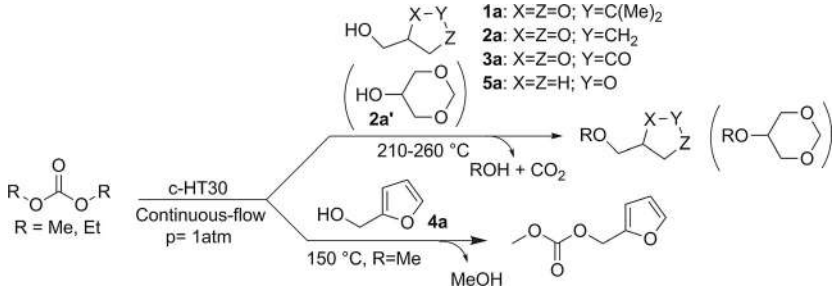

Scheme 4. The etherification of OH-bearing BBDs **1a**–**3a** and **5a** (top). The transesterification of furfuryl alcohol with DMC (bottom).

275 °C) than those for methyl ethers (210–220 °C; Table 3, compare entries 1 and 6 with 2 and 7). This result was in line with the trend noticed for several processes mediated by DAICs, including transesterifications, decarboxylations, etherifications and alkylations.[10] Steric reasons probably account for the lower electrophilic reactivity of DEC compared with that of DMC. The products were recovered in good-to-excellent isolated yields (81–92%); however, the more volatile derivatives of glycerol formal gave slightly poorer results because of some technical difficulties with their separation from DMC or DEC (**2b**/**2b**′: 81%; **2e**/**2e**′: 84%; Table 3, entries 2 and 7).[29] The isomeric ethers **2b**/**2b**′ and **2e**/**2e**′ were obtained in the same (3:2) relative ratio as that of the starting acetals **2a** and **2a**′.

The reaction productivity, calculated from the isolated yield, allowed further remarkable considerations: compared with the *P* values of 0.01–0.02 $g_{prod}\,g_{cat}^{-1}\,h^{-1}$) for the syntheses of compounds **1b** and **2b**/**2b**′ by our previously reported batchwise (autoclave) method,[16] the CF procedure boosted the productivity by a factor of 100–200 [to ≈2 $g_{prod}\,g_{cat}^{-1}\,h^{-1}$); Table 3, entries 1 and 2] and, thereby, substantiated the synthetic potential of such a protocol. The overall mass balance for the alkylation of glycerol acetals was also validated by NMR spectroscopy of crude mixtures collected at the reactor outlet and gravimetric analyses of the catalytic bed before and after the CF tests; both of these checks indicated that neither heavy products nor noticeable coke formation (on the catalyst) occurred even after prolonged experiments (up to 20 h, Table 3, entry 1). A similar outcome was also observed for the CF reaction of tetrahydrofurfuryl alcohol (**5a**) with DMC, in which we obtained the corresponding *O*-methyl ether (**5b**) with 92 and 80% selectivity and isolated yield, respectively (Table 3, entry 5). However, a higher operating temperature of 250 °C was necessary.

The control of the chemoselectivity was significantly more difficult for the reactions of glycerol carbonate (**3a**) and furfuryl alcohol (**4a**). Glycerol carbonate was sensitive to competitive transesterification[24b] and decarboxylation[30,31] reactions to produce higher carbonate homologues and glycidol, respectively. In this case, 65% *O*-methylation selectivity was achieved at 210 °C in the presence of a large excess of the alkylating agent (Table 3, entry 3 and Scheme 5). Owing to dilution or solvation effects, these conditions contribute to minimise the contact between the glycerol carbonate and the catalytic surface and, thereby, limit undesired decarboxylation reactions. Of note, the methylation productivity (0.42) of the process was twice as much as the best value reported previously (0.21) for a batch reaction of glycerol carbonate with DMC catalysed by Al_2O_3.[32]

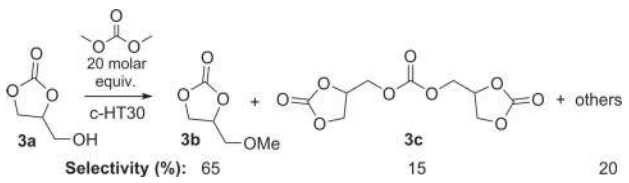

Scheme 5. The CF reaction of glycerol carbonate with DMC in the presence of c-HT30 (the structure of **3c** was assigned by GC–MS; the others were unidentified byproducts).

Furfuryl alcohol (**4a**) was too reactive to allow the formation of the corresponding alkyl ether. At $T \geq 180$ °C, the reaction of **4a** with DMC gave polymeric byproducts, which blocked the catalytic bed rapidly. However, at a lower temperature (150 °C), a highly selective transesterification provided (furan-2-yl)methyl methyl carbonate (**4b**) in 80% isolated yield (Table 3, entry 4). This equilibrium reaction was also favoured by a large excess of DMC (10 equiv. with respect to **4a**). Of note, all of the previously reported syntheses of **4b** were based on the reaction of furfuryl alcohol with a harmful phosgene derivative such as methyl chloroformate;[33] the process described here is the first successful example of the same preparation with DMC as a non-toxic reagent.

The results listed in Table 3 proved that c-HT30 was an efficient catalyst and that it could be recycled without loss of performance. For example, once the CF alkylation of solketal was run for 20 h (entry 1), a simple cleaning cycle of the catalytic bed with methanol (50 mL at 1 mL min^{-1}, 50 °C, atmospheric pressure) restored the system to its initial conditions, and the same reactions or a new reaction (e.g., the alkylation of glycerol formal) could be performed. No activity differences were observed if a used c-HT30 catalyst was compared to a freshly calcined HT30 sample; therefore, the CF procedure is robust. This was further substantiated by the very low metal leaching from the catalyst: after the test of entry 1 (Table 3), ICP-MS measurements demonstrated that the Al and Mg concentrations in the stream recovered at the outlet of the reactor were 40 and 85 ppb, respectively (see Experimental Section and Supporting Information for details). The estimated mass loss of the catalytic bed corresponded to 38 μg per 20 working hours. Very low levels of metal leaching were observed previously for others reactions catalysed by HT-derived Mg/Al mixed oxides: two examples are the transesterifications of natural fats and liquid-phase Michael additions.[34] After the vacuum distillation of the mixtures collected at the reactor outlet, it was also estimated that up to 80% of the unreacted DMC (and its azeotrope with MeOH)[35] and DEC could be recovered and recycled with minimal waste generation.

Overall, the CF procedure was versatile and suitable for both carbonates and alcohols. In particular, c-HT30 provided a rational long-term stability and selectivity (with no appreciable leaching or poisoning) as well as a productivity that could be orders of magnitude higher than that achieved by batch alkylation methods. To the best of our knowledge, a result comparable to that of c-HT30 was reported only for the continuous-flow *O*-methylation of primary alcohols with DMC catalysed by γ-Al_2O_3.[28] However, this protocol could hardly be extended: *sec* alcohols gave substantial side-reactions through eliminations to afford alkenes promoted by the acidity of the catalyst;[36] moreover, even at 150 °C, DMC underwent an extensive decarboxylation reaction to afford dimethyl ether.[37] For the functionalised alcohols used in this study, γ-Al_2O_3 would have posed a chemoselectivity concern; glycerol acetals (solketal and glycerol formal) and furfuryl alcohol are extremely sensitive to ring aperture and polymerisation reactions catalysed by acids, whereas glycerol carbonate would release CO_2 rapidly.

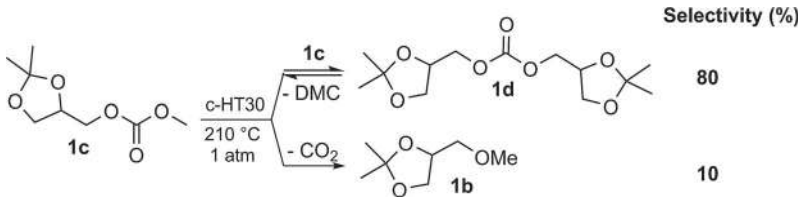

Scheme 6. The CF reaction of **1 c** over c-HT30 at 210 °C and ambient pressure. Cyclohexane was used as a solvent (5 equiv. with respect to **1 c**). Total flow rate: 0.1 mL min^{-1}.

It should be noted that the decarboxylation of dialkyl carbonates may be catalysed by FAUs[10] or by hydrotalcites as such.[38] However, under the CF conditions explored here, we observed that calcined HTs were far less efficient for the same process. This was corroborated by an additional test in which solketal methyl carbonate (**1 c**) was reacted at 210 °C and ambient pressure over a catalytic bed of c-HT30. At a conversion of 75%, **1 c** underwent a predominant disproportion reaction towards bis[(2,2-dimethyl-1,3-dioxolan-4-yl)methyl] carbonate (**1 d**, 80%) rather than the decarboxylation to derivative **1 b** (10%, Scheme 6). Product **1 d** was isolated in a 58% yield and characterised by GC–MS and NMR spectroscopy (see Supporting Information). Albeit indirectly, this test confirmed that c-HT30 could also improve the efficiency of the alkylation reactions desired here.

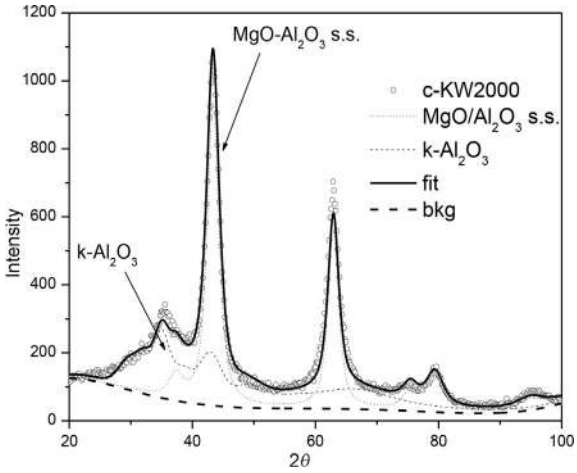

Figure 4. XRD pattern and Rietveld fit of c-KW2000 (R_{wp} = 9.5%).

Characterisation and role of the catalyst

The performance of the investigated catalysts was consistent with structural modifications induced by calcination and, potentially, during the reaction itself. Therefore, the two most active systems, KW2000 and HT30, were subjected to a more in-depth analysis and characterisation. A total of four samples were examined for XRD analyses. Two of them (f-KW2000 and f-HT30) were fresh solids that had never been used for catalytic tests, and the other two specimens (c-KW2000 and c-HT30) were calcined catalysts used for reactions under the conditions for Table 2 (for details, see Table S2). The XRD patterns for the fresh materials are shown in Figure 3, and those of the calcined solids are shown in Figures 4 and 5.

The fresh solids contained at least two phases. The hydrotalcite structure (ICSD 81963) was present along with large fractions of periclase [MgO, ICSD 9863; (60 ± 1) wt%] in f- KW2000

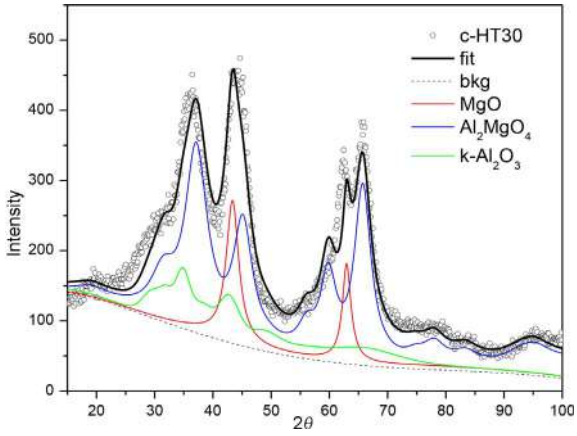

Figure 5. XRD pattern and Rietveld fit of c-HT30 (R_{wp} = 11.6%).

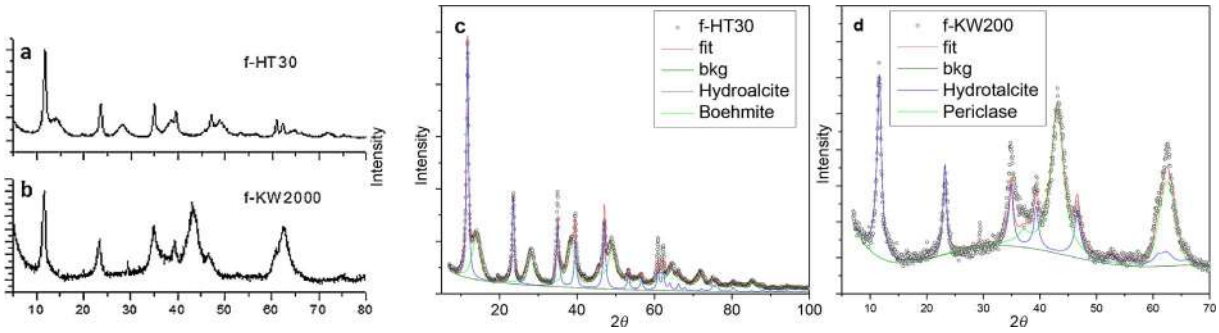

Figure 3. XRD patterns (left) and Rietveld fits (right) for f-HT30 and f-KW2000 samples.

and boehmite [aluminum oxide hydroxide, ICSD 36340; (53±1) wt%] in f-HT30. The quantitative relationships between the constituent phases were obtained by the Rietveld analysis shown in Figure 3c and d. For comparison, XRD patterns were also acquired for fresh solid samples of HT63 and HT70, and these materials were single-phase hydrotalcites (for further details, see Figure S31).

The XRD pattern of c-KW2000 showed the presence of cubic MgO (periclase) along with an extremely dispersed or amorphous phase responsible for a broad peak at $2\theta = 35^\circ$ (Figure 4). The XRD pattern was typical of c-HT systems characterised by an Al/(Al+Mg) molar fraction of up to approximately 50% (≈55 wt% of Al_2O_3).[39,40] A Rietveld analysis was then performed with the following considerations: (1) In addition to MgO, both Al_2O_3 and the spinel Al_2MgO_4 would be the other most probable components of the c-KW2000 system.[41] (2) If the thermal degradation of a hydrotalcite occurred at 300–500 °C, metastable phases of MgO and finely dispersed Al_2O_3 or solid solutions of Al_2MgO_4/Al_2O_3, MgO/Al_2O_3 or both could form.[42] Among the aluminas, k-Al_2O_3 (ICSD 94485) gave the best fit of the XRD pattern (Figure 4). It was also noticed that the refined cell for MgO was smaller [(4.190±0.001) Å] than that of pure MgO (4.2112 Å) and, thereby, indicated the formation of a solid solution (ss) of alumina in magnesia in which the Al atoms occupied 15% of the cationic sites.[42] By assuming that the ss dissolved the Al_2O_3 phase, the quantitative Rietveld analysis of Figure 4 allowed us to estimate proportions of Al_2O_3 (39 wt%) and MgO (61 wt%) that were very close to the nominal composition of the sample. This indirectly supported the presence of almost pure Al_2O_3 as the amorphous phase. Finally, the ss was totally absent in the fresh sample of KW2000 (Figure 3b), in which periclase showed a unit-cell parameter of (4.213±0.002) Å. The XRD patterns of the c-HT63 and c-HT70 solids were very similar to that of c-KW2000 (see Figure S32).

By contrast, the diffraction pattern of c-HT30, which contains a higher fraction of Al, was totally different (Figure 5). Rietveld analyses were performed as mentioned above and allowed us to identify the presence of a MgO/Al_2O_3 ss, the spinel Al_2MgO_4 and k-Al_2O_3, and the corresponding amounts of these three phases were estimated to be 15, 63 and 22 wt%, respectively. Although the obtained fit was not as good as the previous one (cf. the R_{wp} indices of Figures 4 and 5), the calculated proportions of Al_2O_3 (69 wt%) and MgO (31 wt%) were very close to those of the nominal composition of the sample.

The BET results were in substantial agreement with the surface-area trend that is usually observed for fresh and calcined HTs.[25a,43] Although the fresh samples of KW2000 and HT30 were not pure hydrotalcite phases, an increase of S_{BET} was noticed once both solids were calcined at 450 °C (Table S2: 108 and 199 $m^2 g^{-1}$ for f- and c-KW2000 and 136 and 247 $m^2 g^{-1}$ for f- and c-HT30, respectively).

Overall, the comparative bulk characterisation indicated that fresh f-KW2000 and f-HT30 acted as precursors of active catalysts for the *O*-alkylation reactions investigated here. Such active phases were composed of solid solutions of Mg/Al oxides along with amorphous alumina and formed during the thermal treatment of the hydrotalcites investigated.[27,39,40] This matched the behaviour described previously, as is summarised in Scheme 7.[25]

Above 250 °C, HTs decompose because of the release of water and extensive dehydroxylation and decarbonation reac-

$$Mg_{1-x}Al_x(OH)_2(CO_3)_{x/2}\cdot mH_2O \xrightarrow{25\text{-}200\ ^\circ C} Mg_{1-x}Al_x(OH)_2(CO_3)_{x/2}$$
$$x/2\ MgAl_2O_4 + (1\text{-}3x/2)\ MgO \xleftarrow{250\text{-}500\ ^\circ C}$$

Scheme 7. The decomposition of Mg–Al hydrotalcite.

tions of the intralayer OH^- and CO_3^{2-} anions. However, as the produced phases ($MgAl_2O_4$, Al_2O_3 or Al-doped MgO) often have small nuclei, they are hardly distinguishable from each other;[44,45] therefore, the outcome of the thermal process and the precise nature of the mixed oxides is still not resolved completely. These considerations allowed us to formulate a hypothesis to explain why KW2000 could be used as such in the investigated *O*-alkylation reactions (Figure 1: f-KW2000), whereas HT30 was active only upon calcination (Figure 2 and Table 3). As the two solids showed quite different chemical compositions in which the layered HT structure coexisted with large proportions of periclase in f-KW2000 or boehmite in f-HT30 (Figure 3a and b, respectively), it was plausible that the breakdown shown in Scheme 7 occurred under different conditions. For f-KW2000, the process could be completed during the CF alkylation reactions at 275 °C, whereas the collapse of f-HT30 required a more energy-demanding transformation, which was achieved only during a high-temperature calcination at 450 °C.

Another question was the different performances of the investigated c-HT systems. Mixed Mg/Al oxides obtained through the calcination of HTs are often defined as amphoteric solids.[27,40,46] This dual (acid/base) activity has been invoked to account for the nucleophilic and electrophilic activation of organic substrates promoted by c-HTs in several model reactions including transfer hydrogenations and aldol condensations of ketones,[27,47] transesterification and carbonylation processes[48] as well as eliminations and condensations of alcohols.[43,49]

The basicity of c-HT systems has been the subject of many fundamental investigations, and it is generally agreed that basic sites of different strength can be defined including OH groups (weak), Mg–O or Al–O pairs (medium) and low-coordinate O^{2-} anions (strong).[25,39,50] In this respect, the densities of total basic sites determined from the CO_2 temperature-programmed desorption (TPD) profiles of HT30 and HT70 solids after calcination at 450 °C were 1.35 and 3.00 μmol m^{-2}, respectively.[51] This finding was consistent with the Mg/Al ratios of the samples: the higher the Al content (the more electronegative metal cation), the higher the nucleation of Al-rich phases and the lower the average basicity of the solid.[27,40,47] In particular, the segregation of a large amount of a spinel phase observed through the XRD analysis of c-HT30 (Al_2MgO_4: 63 wt%; Figure 5) probably indicated a partial coverage of the sites at the surface of MgO; therefore, the basicity would be lower than that of c-HT70 solid (the latter was composed mostly of a solid solution of alumina in magnesia: Figure S32). An exten-

sive analysis of these aspects was performed by Cavani et al.,[25,50,52] who concluded that the Al/Mg ratio of the c-HTs induced a variability to the surface properties. However, in the range $2.0 < Mg/Al < 3.5$, all materials possessed basic sites mostly of medium strength, whereas Lewis-acid sites were manifest at low Mg/Al ratios in the form of coordinatively unsaturated Al^{3+} species. Moreover, the c-HTs were less basic than MgO. The same authors then proposed that a cooperative mechanism trough a synergetic effect of the basic and Lewis-acidic sites could explain the selective *O*-methylation of phenol with methanol in the gas phase in the presence of c-HTs of $Mg/Al = 2$ as catalysts.[52]

A similar formulation appeared consistent with the behaviour of the c-HTs shown in Figure 2 and Tables 2 and 3. Clearly, the results could not be attributed to a purely basic mechanism, as the best-performing catalyst c-HT30 was less basic than c-HT70 and far less basic than pure MgO. On the other hand, among the tested c-HTs, c-HT30 had not only a different bulk structure (Figure 5) but also a lower Mg/Al ratio, which could plausibly favour the occurrence of Lewis-acid sites. c-HT30 apparently displayed the best compromise of acid–base properties for the hypothesised mechanism shown in Scheme 8.

Both nucleophilic and electrophilic partners were activated by the catalyst. After the adsorption of an OH-bearing BBD (ROH: Scheme 1) at a Brønsted-basic site (e.g., Mg–O pairs), a deprotonation reaction followed to form the alkoxide intermediate RO_{ads}. The dialkyl carbonate (DMC in Scheme 8) was activated by the Lewis-acid sites (Al^{3+} cations) in the HT framework. Previously, we observed an electrophilic activation of DAlCs by metal cations for FAU catalysts.[22] Then, RO_{ads} undergoes a $B_{Al}2$-type reaction with the adsorbed DMC to produce the desired methyl ether (ROMe) and methyl hydrogen carbonate ($MeOCO_2H$). The latter is an unstable derivative and decomposes spontaneously into MeOH and CO_2. RO_{ads} could also attack the carboxyl carbon atom of DMC to form the corresponding transesterification product ($ROCO_2Me$; $B_{Ac}2$ mechanism, see Scheme 3). However, the equilibrium of the transesterification process is shifted by the irreversible *O*-methylation reaction. The product distribution is also directed by the temperature. In line with previously reported results,[3,16,10,14,33] alkylation and transesterification processes involving DAlCs are discriminated between on the basis of their different energy demands, and methylations occur only at relatively high temperatures, usually above 150 °C.

A different situation was manifest for the four fresh HT solids investigated here, of which f-KW2000 was the best catalytic system (Figure 1). As mentioned above, the composition of f-KW2000 with a large excess of periclase (Figure 3b) could facilitate the decomposition of the solid towards a catalytically active phase (MgO/Al_2O_3 ss) even at the temperature of 275 °C used for the CF tests. However, KW2000 showed remarkable similarities to the HT63 and HT70 samples with comparable Mg/Al ratios (Table 1) and the bulk structure obtained by calcination (see Figures 4 and S32). This was further substantiated by the similar catalytic performances of the three calcined solids (c-KW2000, c-HT63 and c-HT70) in the *O*-methylation of solketal (Table 2). Therefore, although f-KW2000 could be converted into a catalyst at 275 °C (and 10 bar), the corresponding Mg/Al oxide active phase had to be more basic; consequently it was less efficient than c-HT30.

The effect of post-synthetic alkaline impurities on the catalytic activities of c-HTs was finally considered. Although doping with alkali-metal carbonates and hydroxides increases the basicity and the activity of HT systems, the necessary quantity of alkaline dopants must corresponded to an alkali-metal (Na, K) content of 0.5–10 wt%.[53] These values were at least 250- and 20-fold higher than those of HT30 and KW2000, respectively (Table 1). Reasonably, the alkalinity from the residual Na or K salts in the investigated catalysts had a negligible role in the catalysis of the *O*-alkylation reactions with DAlCs.

Conclusions

The investigation integrates an archetypical green reaction involving non-toxic and renewable reactants with an efficient continuous-flow (CF) procedure for the synthesis of alkyl ethers of a class of biobased derivatives. Calcined hydrotalcites (HTs), particularly c-HT30, are effective for highly chemoselective transformations: functionalised biobased alcohols and dialkyl carbonates are activated towards *O*-alkylations with respect to the competitive transesterifications and other side-reactions including the ring opening of acetal functions, decarboxylations of dialkyl carbonates and oligo- or polymerisations. An *O*-alkylation selectivity as high as 99% at complete conversion was achieved. To the best of our knowledge, this result has no precedent in the class of biomass-derived compounds investigated. The analyses of the bulk structures of the fresh and calcined hydrotalcites investigated here are consistent with the formation of catalytically active phases constituted by

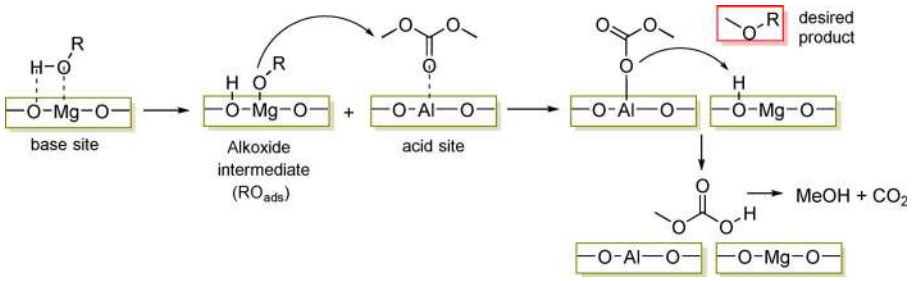

Scheme 8. Proposed mechanism for the reaction of OH-bearing BBDs (ROH) and DMC at the HT surface.

mixed Al/Mg oxides. These originate either upon calcination or simply through heating to the reaction temperature, and their composition varies between the different HTs. The activity of the best catalyst (c-HT30) is consistent with both a lower density of basic sites and a more pronounced acid character than those of the other solids of the family. Overall, the CF protocol provides multiple advantages, of which the most relevant ones include the high process safety, the recyclability of the solvents and unconverted reagents, the reuse of the catalysts and the simplification of downstream operations for the isolation and purification of products to improve the productivity (greater by orders of magnitude) with respect to those of batch methods.

Experimental Section

General

Solketal (**1 a**), glycerol formal (GlyF, **2 a**+**2 a′**), tetrahydrofurfuryl alcohol (**4 a**), furfuryl alcohol (**5 a**), dimethyl carbonate (DMC), diethyl carbonate (DEC) and MgO were ACS-grade from Aldrich. If not otherwise specified, they were employed without further purification. Glycerol carbonate (**3 a**) was from JEFFSOL® and used as received. Solketal methyl carbonate (**1 c**) was prepared through the transesterification reaction of Solketal with DMC by a modification of a method developed by us.[16]

GC–MS (EI, 70 eV) analyses were performed with an HP5-MS capillary column ($L = 30$ m, $\varnothing = 0.32$ mm, film = 0.25 μm), and GC analyses with a flame ionisation detector (CG/FID) were performed with an Elite-624 capillary column ($L = 30$ m, $\varnothing = 0.32$ mm, film = 1.8 μm). The ^{1}H NMR spectra were recorded at 400 or 300 MHz, and the ^{13}C NMR spectra were recorded at 100 MHz; the chemical shifts are reported downfield from tetramethylsilane (TMS), and $CDCl_3$ was used as the solvent.

Catalysts

Faujasites of formula $M_z[(AlO_2)_z(SiO_2)_w]\cdot m H_2O$ (M = Na, Cs; X- and Y-type: $z = 86$ and 56, $w = 104$ and 136, $m = 264$ and 250, respectively) included NaX and NaY faujasites from Aldrich and a CsY zeolite synthesised by a conventional ion-exchange reaction of NaY with aq CsCl.[18] The percentage of ion exchange ($Na^+ \rightarrow Cs^+$) was 58%, as evaluated through atomic emission according to a procedure that we reported previously.[54] Before use, they were dehydrated under vacuum (70 °C, 18 mm, overnight).

According to the specifications provided by the manufacturers, the HTs were aluminium magnesium hydroxy carbonate hydrates of formula $Mg_{2x}Al_2(OH)_{4x+4}(CO_3)\cdot n H_2O$ ($x = 0.5$–2.3). Four commercial HTs were considered (their Mg/Al molar ratios are given in parentheses), namely, KW2000 (1.8), PURAL® MG 30 (0.5), MG 63 (1.9) and MG 70 (2.3). KW2000 was from Kyowa Chemical Industry Co., Ltd., whereas the PURAL® MG solids were from CONDEA/Sasol Germany GmbH, Inorganic Specialty Chemicals. The carbonate contents were approximately 10 wt%, and the maximum losses on ignition (3 h, 1000 °C) were in the 40–45% range. All HTs were used both as received and after calcination. If used as received, the solids were dehydrated under vacuum (70 °C, 18 mm, overnight) before they were loaded into the CF reactor. Otherwise, the calcination treatment was performed according to a procedure for HTs that we reported previously:[21] solid samples (5 g) were heated in a quartz reactor (in the upright position) under a flow of dry air at 450 °C for 16 h. The heating rate was 30 °C min^{-1}.

Catalyst characterisation

Nitrogen adsorption–desorption isotherms were obtained at the liquid nitrogen temperature with a Micromeritics ASAP 2010 system. Each sample was degassed at 130 °C overnight before the measurement of the N_2 physisorption isotherm. From the data, the BET equation was used to calculate the specific surface areas.

The X-ray powder diffraction (XRPD) patterns were recorded with a Philips X'Pert powder diffractometer (Bragg–Brentano parafocusing geometry). Nickel-filtered CuKα1 radiation ($\lambda = 0.15406$ nm) and a voltage of 40 kV were employed. The XRD patterns were collected for all fresh (as-received) hydrotalcites and the corresponding calcined solids.

The ICP-MS analyses were performed with a PerkinElmer Nexion 300XX instrument.

CF Apparatus

The apparatus used for the investigation was assembled in-house, as shown in Figure S1. An HPLC pump was used to deliver the liquid reactants to a stainless-steel tubular reactor ($L = 12$ cm, $\varnothing =$ 1/4", 1.16 cm^3 inner volume) containing the catalyst, the amount of which was chosen on the basis of the apparent densities of the hydrotalcites and faujasites. Typical catalyst loadings were in the range 0.5–0.85 g (see Figures 1 and 2 and Tables 2 and 3). The reactor was placed in the upright position in a thermostatted oven and heated to the desired temperature. A Swagelok back-pressure regulator (BPR) at the outlet of the reactor was used to keep the pressure constant over the whole system throughout the reaction. For experiments at ambient pressure, the BPR was bypassed. A Rheodyne Model 7725i injector equipped with a 10 μL sample loop was placed before the BPR and used for sampling.

SAFETY WARNING: Operators of high pressure equipment should take proper precautions to minimise the risk of personal injury.[55] The individual components that we describe work well, but they are not necessarily the only equipment of this type available.

General procedure for the CF reactions of 1 a, 2 a+2 a′, 3 a, 4 a, 5 a with DMC

A typical reaction with the CF apparatus described above was performed through the following procedure. The oven was set at a temperature of 150 °C, and N_2 was flushed through the system for 1 h. Then, the reaction mixture (dialkyl carbonate and the bio-based alcohol) was flowed for 10 min at 1 mL min^{-1}, and the BPR and oven were set to the operating pressure and temperature (5–60 bar and 150–300 °C, respectively). Once T and p were stable, the reactant flow was adjusted to the desired rate (0.07–0.2 mL min^{-1}). The reaction mixture was collected through a Rheodyne® valve (7725i fitted with a 10 μL sample loop) at time intervals of approximately 30 min, diluted with diethyl ether (1.5 mL) and analysed by GC/FID or GC–MS.

Change of reaction conditions: The oven and the BPR were set to the new desired T and p values, respectively. Under these conditions, the reactant mixture was flushed for 10 min at 1 mL min^{-1}. Then, the flow was adjusted to the chosen rate, and a new experiment was started.

System cleaning and restart: At the end of each experiment, the oven and the BPR were set to 50 °C and atmospheric pressure, respectively, and a cleaning solution of methanol (50 mL at 1 mL min^{-1}) was flowed through the system. The pump was then stopped, and the oven was allowed to cool to RT. The CF reactor

was then disassembled, and the catalytic bed could be replaced by a fresh one.

Reaction of Solketal (1 a) and DMC with alkali-metal-exchanged faujasites as catalysts

The above-described procedure was used to tests Faujasites as catalysts. Before use, each zeolite was dehydrated under vacuum (70 °C, 18 mm, overnight): NaY, NaX and CsY (0.68, 0.54 and 0.86 g, respectively) were charged in the CF reactor. In all tests, a 1.83 M solution of solketal in DMC [DMC/solketal molar ratio (W) = 5] was fed to the reactor at F = 0.1 mL min^{-1}. The CF reactions were performed under a constant pressure of 10 bar, and T was set to 250 or 275 °C. The experiments were followed for 3 h. Two additional runs with the NaY and NaX catalysts were performed for 18 h.

Reaction of Solketal (1 a) and DMC with hydrotalcites

As-received hydrotalcites: The HTs were dehydrated under vacuum (70 °C, 18 mm, overnight): KW2000, HT30, HT63 and HT70 (0.52, 0.73, 0.51 and 0.85 g, respectively) were used for the CF tests. A 1.83 M solution of solketal in DMC (W = 5) was fed to the reactor at F = 0.1 mL min^{-1}. At 275 °C, reactions were performed under a constant pressure of 10 bar and followed for 18 h (Figure 3 a). For KW2000, additional experiments were performed under the following conditions: 1) T = 200 and 250 °C, p = 10 bar, W = 5, F = 0.1 mL min^{-1}; 2) T = 275 °C, p = 5 and 50 bar, W = 5, F = 0.1 mL min^{-1}; 3) T = 275 °C, p = 10 bar, W = 1.1, 2, 3.5, F = 0.1 mL min^{-1}.

Calcined hydrotalcites: After calcination at 450 °C (see above for details), each solid (c-KW2000, c-HT30, c-HT63, and c-HT70; 0.5 g) was used for the CF tests. In all cases, a 1.83 M solution of solketal in DMC (W = 5) was fed to the reactor at F of 0.1 mL min^{-1}. At 10 bar, the reactions catalysed by c-KW2000, c-HT30, c-HT63 and c-HT70 were run at 210, 225, and 275 °C for 18 h. For c-HT30, experiments were also performed at 210 °C and atmospheric pressure.

Two additional reactions were also conducted in which the c-HT catalysts were replaced by MgO (0.85 g) or a physical mixture of MgO and basic γ-Al_2O_3 (particle size: 50–200 μm, surface area: 130 m^2 g^{-1}, pH 9.5 ± 0.3) in a 30:70 molar ratio (0.85 g). Both MgO and the MgO/γ-Al_2O_3 mixture were calcined at 450 °C for 6 h before use. Then, the CF tests were run at 275 °C, 10 bar, W = 5, and F = 0.01 mL min^{-1}.

Different substrates and carbonates

Reaction of Solketal and diethyl carbonate

According to the above-described general procedure, the reactions of glycerol acetals (**1 a** and **2 a+2 a′**) were performed with DEC and c-HT30 (0.5 g) as the alkylating agent and catalyst, respectively. The CF reactions were performed at 250 and 275 °C and ambient pressure. A mixture of DEC and the chosen glycerol acetal in a 5:1 molar ratio was delivered at 0.1 mL min^{-1} to the CF reactor.

Different substrates

According to the above-described general procedure, the reactions of DMC with glycerol formal (**2 a+2 a′**), glycerol carbonate (**3 a**), furfuryl alcohol (**4 a**) and tetrahydrofurfuryl alcohol (**5 a**) were investigated in the presence of c-HT30 (0.5 g) as a catalyst. The reactions were optimised case-by-case under the following conditions: 1) 220 °C, 1 bar, glycerol formal/DMC in a 1:5 molar ratio; 2) 210 °C, 1 bar, glycerol carbonate/DMC in a 1:20 molar ratio; 3) 150 °C, 1 bar, furfuryl alcohol/DMC in a 1:10 molar ratio; 4) 260 °C, 1 bar, tetrahydrofurfuryl alcohol/DMC in a 1:5 molar ratio. The flow rate was set to 0.1 mL min^{-1} in all cases.

The isolation and characterisation of all of the products (**1 b**, **2 b+2 b′**, **3 b**, **4 b**, **5 b**, **1 e**, and **2 e+2 e′**) by NMR spectroscopy and GC–MS is reported in the Supporting Information.

Acknowledgements

MIUR (Italian Ministry of University and Research) is acknowledged for funding the PhD program of L.C. through "Borse aggiuntive di dottorato, fondo giovani". Dr. Roberto Clerici from Sasol Italy SpA is gratefully acknowledged for his generous supply of Pural® hydrotalcites and the discussion of the properties of these solids. Dr. Alexander Malyschew from Sasol Germany GmbH is also acknowledged. Finally, Mr. Tom Savage (University of Sydney) is acknowledged for his support with the ICP analyses.

Keywords: alkylation · aluminium · biomass · continuous flow · hydrotalcites

[1] a) T. Werpy, G. Petersen, A. Aden, J. Bozell, J. Holladay, J. White, A. Manheim, D. Eliot, L. Lasure, S. Jones in *Top Value Added Chemicals from Biomass: Volume 1 – Results of Screening for Potential Candidates from Sugars and Synthesis Gas*, US DOE (DOE/GO-102004-1992), Washington, DC, **2004**; b) J. Bozell, G. R. Petersen, *Green Chem.* **2010**, *12*, 539 – 554.

[2] T. J. Farmer, M. Mascal in *Introduction to Chemicals from Biomass*, 2nd ed. (Eds.: J. Clark, F. Deswarte), Wiley, Chichester, **2015** .

[3] P. Tundo, M. Selva, *Acc. Chem. Res.* **2002**, *35*, 706 – 716.

[4] a) L. Moity, A. Benazzouz, V. Molinier, V. Nardello-Rataj, M. K. Elmkaddem, P. de Caro, S. Thiébaud-Roux, V. Gerbaud, P. Marion, J.-M. Aubry, *Green Chem.* **2015**, *17*, 1779 – 1792; b) W. K. Teng, G. C. Ngoh, R. Yusoff, M. K. Aroua, *Energy Convers. Manage.* **2014**, *88*, 484 – 497; c) M. O. Sonnati, S. Amigoni, E. P. Taffin de Givenchy, T. Darmanin, O. Choulet, F. Guittard, *Green Chem.* **2013**, *15*, 283 – 306; d) *Advances in Biorefineries: Biomass and Waste Supply Chain Exploitation* (Ed.: K. W. Waldron), Woodhead Publishing, Cambridge, **2014**.

[5] M. Pagliaro, M. Rossi, *The Future of Glycerol*, 2nd ed., RSC Publishing, Cambridge, **2010**.

[6] a) M. Balakrishnan, E. R. Sacia, A. T. Bell, *Green Chem.* **2012**, *14*, 1626 – 1634; b) Y. Gu, F. Jerome, *Chem. Soc. Rev.* **2013**, *42*, 9550 – 9570; c) R. Mariscal, P. Maireles-Torres, M. Ojeda, I. Sádaba, M. López Granados, *Energy Environ. Sci.* **2016**, *9*, 1144 – 1189.

[7] a) W. G. Trindade, W. Hoareau, J. D. Megiatto, I. A. T. Razera, A. Castellan, E. Frollini, *Biomacromolecules* **2005**, *6*, 2485 – 2496; b) W. Chaikittisilp, K. Ariga, Y. Yamauchi, *J. Mater. Chem. A* **2013**, *1*, 14 – 19; c) L. Pranger, R. Tannenbaum, *Macromolecules* **2008**, *41*, 8682 – 8687.

[8] M. Chatterjee, H. Kawanami, T. Ishizaka, M. Sato, T. Suzuki, A. Suzuki, *Catal. Sci. Technol.* **2011**, *1*, 1466 – 1471.

[9] a) M. Sutter, E. D. Silva, N. Duguet, Y. Raoul, E. Metay, M. Lemaire, *Chem. Rev.* **2015**, *115*, 8609 – 8651; b) A. E. Díaz-Álvarez, J. Francos, B. Lastra-Barreira, P. Crochet, V. Cadierno, *Chem. Commun.* **2011**, *47*, 6208 – 6227; c) B. J. Nikolau, M. A. Perera, L. Brachova, B. Shanks, *Plant J.* **2008**, *54*, 536 – 545.

[10] M. Selva, M. Fabris, A. Perosa, *Green Chem.* **2011**, *13*, 863 – 872.

[11] A. Bomben, M. Selva, P. Tundo, L. Valli, *Ind. Eng. Chem. Res.* **1999**, *38*, 2075 – 2079.

[12] a) A. Y. Platonov, A. N. Evdokimov, A. V. Kurzin, H. D. Maiyorova, *J. Chem. Eng. Data* **2002**, *47*, 1175 – 1176; b) M. Selva, C. A. Marques, P. Tundo, *J. Chem. Soc. Perkin Trans. 1* **1994**, 1323 – 1328.

[13] a) M. Selva, P. Tundo, A. Perosa, *J. Org. Chem.* **2001**, *66*, 677 – 680; b) M. Selva, P. Tundo, A. Perosa, *J. Org. Chem.* **2003**, *68*, 7374 – 7378; c) M.

Selva, P. Tundo, *J. Org. Chem.* **2006**, *71*, 1464 – 1470; d) M. Selva, A. Perosa, M. Fabris, *Green Chem.* **2008**, *10*, 1068; e) J. N. G. Stanley, M. Selva, A. F. Masters, T. Maschmeyer, A. Perosa, *Green Chem.* **2013**, *15*, 3195.

[14] a) A. Takagaki, K. Iwatani, S. Nishimura, K. Ebitani, *Green Chem.* **2010**, *12*, 578 – 581; b) M. G. Álvarez, M. Plísková, A. M. Segarra, F. Medina, F. Figueras, *Appl. Catal. B* **2012**, *113 – 114*, 212 – 220; c) P. Liu, M. Derchi, E. J. M. Hensen, *Appl. Catal. A* **2013**, *467*, 124 – 131; d) L. Zheng, S. Xia, Z. Hou, M. Zhang, Z. Hou, *Chin. J. Catal.* **2014**, *35*, 310 – 331.

[15] a) M. B. Talawar, T. M. Jyothi, P. D. Sawant, T. Raja, B. S. Rao, *Green Chem.* **2000**, *2*, 266 – 268; b) P. Tundo, S. Memoli, D. Hérault, K. Hill, *Green Chem.* **2004**, *6*, 609; c) G. Wu, X. Wang, B. Chen, J. Li, N. Zhao, W. Wei, Y. Sun, *Appl. Catal. A* **2007**, *329*, 106 – 111; d) G. D. Yadav, J. Y. Salunke, *Catal. Today* **2013**, *207*, 180 – 190.

[16] M. Selva, V. Benedet, M. Fabris, *Green Chem.* **2012**, *14*, 188 – 200.

[17] In this way, void spaces and preferential pathways of the reactant mixture through the catalytic bed were minimised if not ruled out; see: P. Harriot, *Chemical Reactor Design*, Marcel Dekker, New York, **2003**.

[18] In the repeated tests performed under the same conditions, the values for the conversion and the amounts of products (determined by GC–MS) differed by less than 5% from one reaction to another.

[19] D. Barthomeuf, *J. Phys. Chem.* **1984**, *88*, 42.

[20] M. Selva, E. Militello, M. Fabris, *Green Chem.* **2008**, *10*, 73 – 79.

[21] Y. Ono, *Cattech* **1997**, *1*, 31.

[22] a) F. Bonino, A. Damin, S. Bordiga, M. Selva, P. Tundo, A. Zecchina, *Angew. Chem. Int. Ed.* **2005**, *44*, 4774 – 4777; *Angew. Chem.* **2005**, *117*, 4852 – 4855; b) T. Beutel, M. J. Peltre, B. L. Su, *Colloids Surf. A* **2001**, *187 – 188*, 319 – 325; c) T. Beutel, *J. Chem. Soc. Faraday Trans.* **1998**, *94*, 985 – 993.

[23] P. Tundo, L. Rossi, A. Loris, *J. Org. Chem.* **2005**, *70*, 2219 – 2224.

[24] a) M. Selva, S. Guidi, M. Noè, *Green Chem.* **2015**, *17*, 1008 – 1023; b) S. Guidi, A. Perosa, M. Noè, R. Calmanti, M. Selva, *ACS Sustainable Chem. Eng.* **2016**, *4*, 6144 – 6151.

[25] a) F. Cavani, F. Trifirò, A. Vaccari, *Catal. Today* **1991**, *11*, 173 – 301; b) P. Bera, M. Rajamathi, M. S. Hedge, P. Vishnu Kamath, *Bull. Mater. Sci.* **2000**, *23*, 141 – 145; c) P. Kuśtrowski, D. Sulkowska, L. Chmielarz, A. Rafalska-Lasocha, B. Dudek, R. Dziembaj, *Microporous Mesoporous Mater.* **2005**, *78*, 11 – 22; d) K. J. D. MacKenzie, R. H. Meinhold, B. L. Sherriff, Z. Xu, *J. Mater. Chem.* **1993**, *3*, 1263 – 1269.

[26] M. Hájek, P. Kutálek, L. Smoláková, I. Troppová, L. Capek, D. Kubicka, J. Kocík, D. N. Thanh, *Chem. Eng. J.* **2015**, *263*, 160 – 167.

[27] a) Y. Ono, H. Hattori (Eds.), *Springer Series in Chemical Physics 101: Solid Base Catalysts*, Springer, Berlin, **2011**; b) S. T. Gadge, A. Mishra, A. L. Gajengi, N. V. Shahi, B. M. Bhanage, *RSC Adv.* **2014**, *4*, 50271 – 50276.

[28] A. J. Parrott, R. A. Bourne, P. N. Gooden, H. S. Bevinakatti, M. Poliakoff, D. J. Irvine, *Org. Process Res. Dev.* **2010**, *14*, 1420 – 1426.

[29] During the purification of the final reaction mixtures, the more volatile ethers **2b**/**2b**′ and **2e**/**2e**′ were partly removed in the first distilled fraction of DMC or DEC.

[30] J. S. Choi, F. S. H. Simanjuntaka, J. Y. Oh, K. I. Lee, S. D. Lee, M. Cheong, H. S. Kim, H. Lee, *J. Catal.* **2013**, *297*, 248 – 255.

[31] D. J. Darensbourg, A. D. Yeung, *Green Chem.* **2014**, *16*, 247 – 252.

[32] F. Leising, Z. Moulongui, (Chryso, Institut National Polytechique de Tolouse and Institut National de la Recherche Agronomique), US2015329468 (A1), **2015**.

[33] a) Y. Nakao, S. Ebata, J. Chen, H. Imanaka, T. Hiyama, *Chem. Lett.* **2007**, *36*, 606 – 607; b) I. Franzoni, L. Guénée, C. Mazet, *Org. Biomol. Chem.* **2015**, *13*, 6338 – 6343.

[34] a) Y. Liu, E. Lotero, J. G. Goodwin Jr., X. Mo, *Appl. Catal. A* **2007**, *331*, 138 – 148; b) H. A. Prescott, Z.-J. Li, E. Kemnitz, A. Trunsche, J. Deutsch, H. Lieske, A. Auroux, *J. Catal.* **2005**, *234*, 119 – 130.

[35] A. Rodríguez, J. Canosa, A. Domínguez, J. Tojo, *Fluid Phase Equilib.* **2002**, *201*, 187 – 201.

[36] J. Shen, R. D. Cortright, Y. Chen, J. A. Dumesic, *J. Phys. Chem.* **1994**, *98*, 8067 – 8073.

[37] Y. Fu, H. Zhu, J. Shen, *Thermochim. Acta* **2005**, *434*, 88 – 92.

[38] P. Tundo, F. Aricò, A. E. Rosamilia, S. Memoli, *Green Chem.* **2008**, *10*, 1182 – 1189.

[39] J. I. Di Cosimo, V. K. Dıez, M. Xu, E. Iglesia, C. R. Apesteguía, *J. Catal.* **1998**, *178*, 499 – 510.

[40] B. Hallstedt, *J. Am. Ceram. Soc.* **1992**, *75*, 1497 – 1507.

[41] L. Lutterotti, R. Ceccato, R. Dal Maschio, E. Pagani, *Mater. Sci. Forum* **1998**, *278 – 281*, 87 – 92. The Rietveld analysis of these samples was performed by the method proposed by Lutterotti et al. for the analysis of amorphous materials. Specifically, the pattern of an amorphous or nanocrystalline phase was fitted by using the structure of a crystalline phase with the same chemical composition. The XRD spectrum of Al_2O_3 with very broad peaks was used to obtain the pattern of the amorphous phase.

[42] S. Vyas, R. W. Grimes, D. J. Binks, F. Rey, *Phys. Chem. Solids* **1997**, *58*, 1619 – 1624.

[43] M. G. Alvarez, A. M. Segarra, S. Contrera, J. E. Sueiras, F. Medina, F. Figueras, *Chem. Eng. J.* **2010**, *161*, 340 – 345.

[44] V. Vágvölgyi, S. J. Palmer, J. Kristóf, R. L. Frost, E. Horváth, *J. Colloid Interface Sci.* **2008**, *318*, 302 – 308.

[45] J. C. A. A. Roelofs, J. A. van Bokhoven, A. J. van Dillen, J. W. Geus, K. P. de Jong, *Chem. Eur. J.* **2002**, *8*, 5571 – 5579.

[46] a) M. León, E. Díaz, S. Ordónez, *Catal. Today* **2011**, *164*, 436 – 442.

[47] T. M. Jyothi, T. Raja, K. Sreekumar, M. B. Talawar, B. S. Rao, *J. Mol. Catal. A* **2000**, *157*, 193 – 198.

[48] a) M. J. Climent, A. Corma, P. De Frutos, S. Iborra, M. Noy, A. Velty, P. Concepción, *J. Catal.* **2010**, *269*, 140 – 149; b) A. Navajas, G. Arzamendi, F. Romero-Sarria, M. A. Centeno, J. A. Odriozola, L. M. Gandía, *Catal. Commun.* **2012**, *17*, 189 – 193.

[49] V. K. Díez, C. R. Apesteguía, J. I. Di Cosimo, *J. Catal.* **2003**, *215*, 220 – 233.

[50] M. Bolognini, F. Cavani, D. Scagliarini, C. Flego, C. Perego, M. Saba, *Catal. Today* **2002**, *75*, 103 – 111.

[51] The basicity data were provided by the supplier of commercial PURAL solids (SASOL). The data referred to c-HT30 and c-HT70 samples calcined at 450 °C.

[52] a) V. Crocellà, G. Cerrato, G. Magnacca, C. Morterra, F. Cavani, L. Maselli, S. Passeri, *Dalton Trans.* **2010**, *39*, 8527 – 8537; b) V. Crocellà, G. Cerrato, G. Magnacca, C. Morterra, F. Cavani, S. Cocchi, S. Passeri, D. Scagliarini, C. Flego, C. Perego, *J. Catal.* **2010**, *270*, 125 – 135.

[53] a) S. Abelló, F. Medina, D. Tichit, J. Perez-Ramırez, X. Rodriguez, J. E. Sueiras, P. Salagre, Y. Cesteros, *Appl. Catal. A* **2005**, *281*, 191 – 198; b) J. M. Fraile, N. Garcıa, J. A. Mayoral, E. Pires, L. Roldan, *Appl. Catal. A* **2009**, *364*, 87 – 94; c) N. N. A. H. Meis, J. H. Bitter, K. P. de Jong, *Ind. Eng. Chem. Res.* **2010**, *49*, 8086 – 8093; d) S. Walspurger, P. D. Cobden, O. V. Safonova, Y. Wu, E. J. Anthony, *Chem. Eur. J.* **2010**, *16*, 12694 – 12700.

[54] M. Selva, P. Tundo, D. Brunelli, A. Perosa, *Green Chem.* **2007**, *9*, 463.

[55] P. G. Jessop, T. Ikariya, R. Noyori, *J. Am. Chem. Soc.* **1996**, *118*, 344.

Manuscript received: December 1, 2016
Revised: January 20, 2017
Accepted Article published: January 31, 2017
Final Article published: March 7, 2017

ChemPubSoc Europe

DOI: 10.1002/cctc.201700374

CHEMCATCHEM Full Papers

Renewable Aromatics from Kraft Lignin with Molybdenum-Based Catalysts

Lisa Cattelan,[a, b] Alexander K. L. Yuen,[a] Matthew Y. Lui,[a] Anthony F. Masters,[a] Maurizio Selva,[b] Alvise Perosa,[b] and Thomas Maschmeyer*[a]

The catalytic depolymerization of Kraft lignin in supercritical ethanol was explored in the presence of Mo_2C- and MoS_2-based catalysts. At 280 °C, Mo_2C and Mo_2C/Al_2O_3 afforded aromatic yields of 425 and 419 mg g^{-1} lignin, respectively: amongst the highest yields reported to date. Ionic–liquid–assisted delamination of MoS_2 resulted in highly active catalysts, capable of quantitative conversion of lignin at the expense of aromatic yield (approximately 186 mg g^{-1} lignin). Across all the catalysts studied, between 0.04 wt% and 0.38 wt% of molybdenum leached into the solution under supercritical conditions, according to inductively coupled plasma (ICP) analyses (corresponding to 27–570 μg of molybdenum in the reaction supernatant). A small contribution to the molybdenum in solution comes from the reactor itself (Hastelloy C contains 16 wt% Mo). Analysis of a depolymerization performed with fresh Kraft lignin and the soluble portion of the reaction mixture from a previous reactor run indicated that the leached species were neither active enough to afford the high conversions observed, nor selective enough to give high yields of aromatic products. In conjunction with the ICP data and differential chemoselectivities of the Mo_2C- and MoS_2-based catalysts, these results suggest that the bulk of the catalysis is heterogeneous.

Introduction

The depletion of fossil fuel resources, coupled with the growing concern over climate change, has prompted global efforts to explore more sustainable routes to generate fuels and chemicals. Lignocellulosic biomass has been proposed as one renewable feedstock to supplement dwindling fossil reserves, particularly if the biomass use can be integrated into existing supply chains to avoid detrimental land use changes or if combined with waste treatment and recycling. Despite an estimated 130 million tons of lignin that is generated annually by industry,[1] lignin is currently the least valorized fraction of woody biomass. The vast majority of lignin is recovered from spent black liquor by the pulp and paper industry and used as boiler fuel for energy recovery, rather than upgrading it to higher value platform chemicals.[2]

The main technical difficulties for processing lignin are attributed to its complex, irregular structure and its propensity for repolymerization during thermochemical depolymerization (e.g., pyrolysis and solvothermal liquefaction).[3] Nevertheless, it is an attractive feedstock as it is the most abundant source of renewable aromatic compounds in the terrestrial biosphere.[4] Of the many target products that can be produced from the successful conversion of lignin, phenol(s) and BTX-type arenes are particularly attractive economically owing to their market volumes.[5]

The solvolysis of lignin has several advantages over the pyrolysis method. For example, solvolysis in hydrogen-donating solvents was found to produce smaller quantities of char than did pyrolysis. Bai and co-workers demonstrated that tetralin and isopropanol are suitable solvents for the liquefaction of lignin to short chain alkyl phenols (and vinyl phenols) under flow conditions with rapid heating rates to 300–400 °C in GC-type reactors. In their study, the yield of aromatics was reported to be approximately 10 wt% of the lignin input. Conversely, in the absence of hydrogen-donating solvents, the extent of repolymerization is such that high-molecular-weight species tended to predominate.[6]

Ford and co-workers[7] have investigated the conversion of pine wood flour to a range of aliphatic chemicals in supercritical methanol over a copper-doped porous metal oxide catalyst. The catalyst reforms methanol and catalyzes the water–gas shift reaction to generate hydrogen gas, which is consumed in the subsequent cleavage of aromatic ethers and reduction/deoxygenation steps. More recently, Hansen and co-workers[8] reported the methanolysis and ethanolysis of lignin under

[a] L. Cattelan, Dr. A. K. L. Yuen, Dr. M. Y. Lui, Prof. A. F. Masters, Prof. T. Maschmeyer
Laboratory of Advanced Catalysis for Sustainability,
School of Chemistry
The University of Sydney
Sydney, 2006 (Australia)
E-mail: thomas.maschmeyer@sydney.edu.au

[b] L. Cattelan, Prof. M. Selva, Prof. A. Perosa
Department of Molecular Sciences and Nanosystems
Università Ca" Foscari Venezia
Via Torino, 155-Venezia Mestre (Italy)

Supporting information and the ORCID identification number(s) for the author(s) of this article can be found under https://doi.org/10.1002/cctc.201700374.

This manuscript is part of a Special Issue on the "Catalytic Conversion of Biomass".

supercritical conditions with a $CuMgAlO_x$ catalyst. In this work, prolonged reaction times were found to enhance lignin depolymerization and reduce the amount of repolymerized products. Ethanol was found to be more effective than methanol as ethanolysis gave a yield of up to 23 wt% of monomeric aromatic products.

In all the above studies, hydrogen-donating solvents reduced char formation by stabilization of reactive phenolic intermediates produced at high temperatures. Ethanol is especially useful in suppressing repolymerization by O-alkylating phenolic hydroxyl groups and by C-alkylating reactive positions on aromatic rings.[8] Hence, supercritical ethanol (renewable itself; critical point 243 °C, 63 atm) is particularly advantageous as a medium for depolymerization and conversion of lignin if used in conjunction with a catalyst.

Transition-metal-catalyzed hydrogenolysis and hydrodeoxygenation have established themselves as attractive approaches for lignin valorization.[9] For example, nickel-based catalysts were effective in the reductive depolymerization of lignin.[10] Xu and co-workers[10b] reported the Ni-catalyzed alcoholysis of native birch wood lignin into monomeric phenols (e.g., propylguaiacol and propylsyringol) in methanol, ethanol, and isopropanol. The alcoholic solvents dehydrogenated over nickel, providing active hydrogen species, in which monomers are generated by means of a fragmentation–hydrogenolysis mechanism. In general, the key to successful production of low-molecular-weight aromatic compounds is the ability to tune the chemoselectivity of the catalyst towards C–O and C–C bond hydrogenolysis, whilst suppressing hydrogenation of the aromatic rings. For the upgrading of Kraft lignin, there is the additional consideration of poisoning from the sulfur and residual inorganics within the substrate. Therefore, the catalyst must be inherently sulfur tolerant, or conditions contrived so that sulfur is continuously removed.

The "sulfophilicity" and sulfur-tolerance of molybdenum and its availability at moderate cost has meant that alumina-supported nickel- and cobalt-promoted molybdenum sulfides are standard hydrodesulfurization catalysts for the petrochemical industry.[11] Such molybdenum-based catalysts ($NiMo/Al_2O_3$)[12] and urchin-like MoS_2[13] have found use in studies for the hydrodeoxygenation of pre-liquefied lignocellulosic biomass. Recently, Li and co-workers demonstrated that several supported molybdenum-based catalysts were effective for the depolymerization of lignin.[14] Supercritical ethanol (280 °C, autogenous pressure) was used as the solvent and principal hydrogen transfer agent, with hydrogen gas shown to be detrimental to the yield of aromatic products. It was revealed that supercritical ethanol on its own could break lignin down into oligomeric segments with molecular weights in the range of about 700–1400 Da. Under catalytic conditions, these fragments were then hydrogenolyzed and hydrodeoxygenated into the observed monomeric products: C_6–C_{10} esters, aliphatic alcohols, arenes, phenols, and benzyl alcohols. In addition, the self-condensation products of supercritical ethanol were identified and quantified. Kraft lignin was reported to be completely converted regardless of which catalyst was employed, leading the authors to propose that the heterogeneous catalysts were precursors to a common homogenous Mo species that formed in situ under the reaction conditions. EPR studies of the reaction mixture confirmed the presence of a Mo^V species in solution.[14b] At 280 °C, Mo/Al_2O_3 gave the highest yield of aromatics (330 mg g^{-1} lignin), however, α-MoC_{1-x}/activated carbon (AC) gave the best overall yield of liquid products (classified as esters, aliphatic alcohols, and aromatics). To improve the process even further, Li and co-workers reported the ethanolysis with an α-MoC_{1-x}/Cu-$MgAlO_z$ composite catalyst,[14c] which combines the virtues of both the catalysts previously reported by the Li and Hensen groups.[8,14a] Both the physical mixture of the components and the composite catalyst afforded higher overall yields of products than either MoC_{1-x} or Cu-$MgAlO_z$ alone, in which the highest reported yield of aromatics is 575 mg g^{-1} lignin if the temperature was pushed to 330 °C.

Based on our recent success in tailoring the morphology of MoS_2 to improve its catalytic activity for the hydrogen evolution reaction (HER),[15] we were interested in using delaminated MoS_2 for Kraft lignin depolymerization. In addition, the rich history of metal carbide catalysts,[16] specifically molybdenum carbide phases as alternatives to noble metals,[17] prompted us to evaluate Mo_2C for its potential for the conversion of waste lignin to renewable aromatics in supercritical ethanol and to compare the different catalysts. Additionally, we wished to resolve some apparent anomalies in the literature regarding the identity of Mo_2C (see catalyst characterization section below).

Results and Discussion

Catalyst preparation and characterization

Ammonium tetrathiomolybdate, a precursor to molybdenum disulfide, was prepared according to the procedures reported by Quagraine and co-workers.[18] The thermal decomposition of this precursor to MoS_2 through Mo_2S_5 was reported by Thompson and co-workers to occur between 230–360 °C.[19] Accordingly, a decomposition temperature of 300 °C was chosen for all catalyst preparations other than unsupported, bulk MoS_2, which was used as-purchased. Batches of supported and unsupported, delaminated MoS_2 were prepared in a straightforward manner by employing the ionic liquid 1-butyl-3-methylimidazolium triflate as the decomposition medium under reductive conditions.[15]

The choice of Catalox SBa-150 (Sasol) as the alumina support was based on its well-defined properties and widespread industrial use. The magnesium–aluminium hydrotalcite, KW2000 (Kyowa Industries), was chosen on the basis of its previously reported performance for alkylation chemistry at high temperatures.[20]

The molybdenum hemicarbide catalysts were synthesized by using a reported procedure, which made use of a single precursor: a melamine–molybdate coordination polymer that co-precipitated when aqueous solutions of melamine and ammonium heptamolybdate were mixed.[21]

Thermal decomposition of the isolated precipitate, under hydrogen, led cleanly to the formation of Mo_2C, avoiding the need for carburization protocols and thus allowing for control

over the molybdenum to carbon stoichiometry. The two series of Mo-based catalysts were characterized by nitrogen sorption, transmission electron microscopy (TEM), and powder X-ray diffraction (PXRD).

The results of nitrogen sorption analyses are shown in Table 1. Brunauer–Emmett–Teller (BET) surface areas obtained at 77 K, and the Barrett–Joyner–Halenda (BJH) pore diameters were calculated from the adsorption branch of the isotherms.

Table 1. Surface area data for the prepared MoS_2 and Mo_2C catalysts.

Entry	Sample	S_{BET} [$m^2 g^{-1}$]	V_P [$cm^3 g^{-1}$]	Ads. D_{BJH} [nm]
1	MoS_2	8	–	–
2	d-MoS_2[a]	55	0.07	5.6
3	MoS_2/Al_2O_3	113	0.30	12.4
4	d-MoS_2/Al_2O_3[a]	169	0.33	10.8
5	d-MoS_2/KW2000[a]	119	0.50	20.1
6	Mo_2C	6	–	–
7	Mo_2C/Al_2O_3	103	0.32	12.7

[a] "d-MoS_2" denotes delaminated MoS_2.

Whilst none of the samples displayed particularly high surface areas or porosities, the surface area of delaminated MoS_2 was significantly higher than the bulk sample (entries 1 and 2). However, the major factor that increased the molybdenum catalyst surface area was the use of the alumina and hydrotalcite supports (entries 3–5). What can be seen in the associated XRD patterns is that there is significant line-broadening of the reflections of the molybdenum species upon deposition on high surface area supports, consistent with smaller particle size and therefore higher surface area. The surface area of unsupported Mo_2C was comparable to the value reported by Liang and co-workers, the result of the formation of a low-porosity material, largely free from surface defects.[21] As was the case for MoS_2-derived catalysts, dispersion of the Mo_2C onto alumina significantly improved the surface area and porosity of the resulting catalyst. Changes to the morphology and interaction of the catalyst particles with the support for the MoS_2 series of catalysts were confirmed by TEM (Figure 1). The large sheets present in bulk molybdenum disulfide are not present in the delaminated material, as a result of the specific effects of the ionic liquid during the thermal decomposition of ammonium tetrathiomolybdate. The resulting material consists of polydisperse MoS_2 nanoparticles containing a greatly increased proportion of edge sites (Figure 1 a,b). For the supported MoS_2 catalysts, there appears to be intimate contact between the surface of the supports and the MoS_2 particles (Figure 1 d–f), and similar contact for the Mo_2C catalyst (Figure 1 h).

The powder XRD patterns of the catalysts freshly prepared and post-reaction are given in Figure 2. Bulk MoS_2 was identified as the 2H polymorph of the $P6_3/mmc$ hexagonal phase.[22] For the delaminated material, the large (0 0 2) reflection, corresponding to the 6 Å interlayer spacing, is absent. In addition, the (1 0 0) and (1 1 0) reflections are broadened significantly and (1 0 3) is only just visible as a broad shoulder. For the supported catalysts, the broadening of the reflections in the XRD data generally indicates that the particle size of MoS_2 is smaller than in the bulk. This effect, combined with delamination, results in highly dispersed nanoparticulate MoS_2 phases on both alumina and KW2000 hydrotalcite. The sharp reflections that are present in the XRD patterns of solid residues recovered from depolymerization reactions are owing to changes to the lignin under the reaction conditions. This change is clearly observable in Figure 3 (right). The diffraction data of commercial lignin powder is uninformative as the material is largely amorphous. However, analysis of the recovered solid residue after

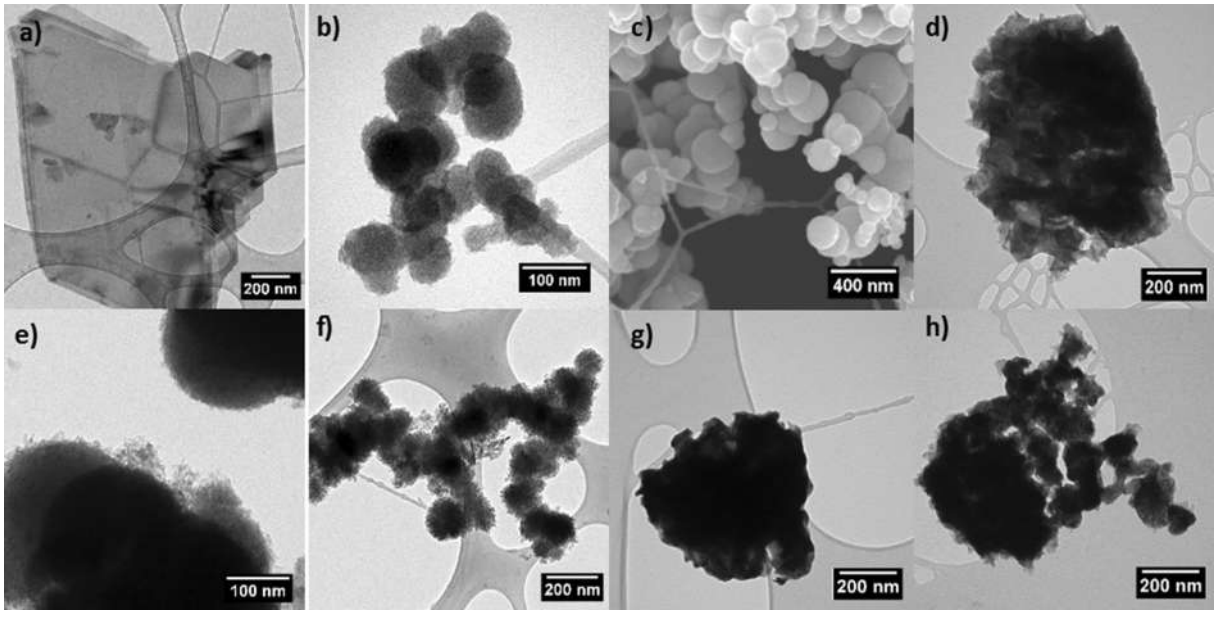

Figure 1. TEM (and SEM) images of the catalysts used in this study. Bulk MoS_2 (a); TEM and SEM of delaminated MoS_2 ((b) and (c), respectively); MoS_2/Al_2O_3 (d); delaminated MoS_2/Al_2O_3 (e); delaminated MoS_2/KW2000 (f); unsupported Mo_2C (g); Mo_2C/Al_2O_3 (h).

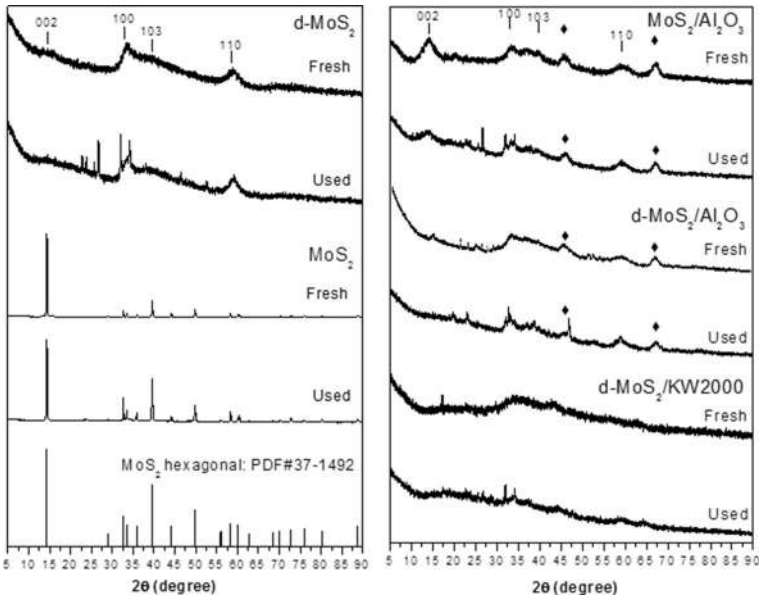

Figure 2. Powder XRD patterns of the unsupported MoS_2-based catalysts (left) and supported catalysts (right) before and after catalytic depolymerization of lignin. The ◆ symbol marks prominent reflections from the γ-alumina support.

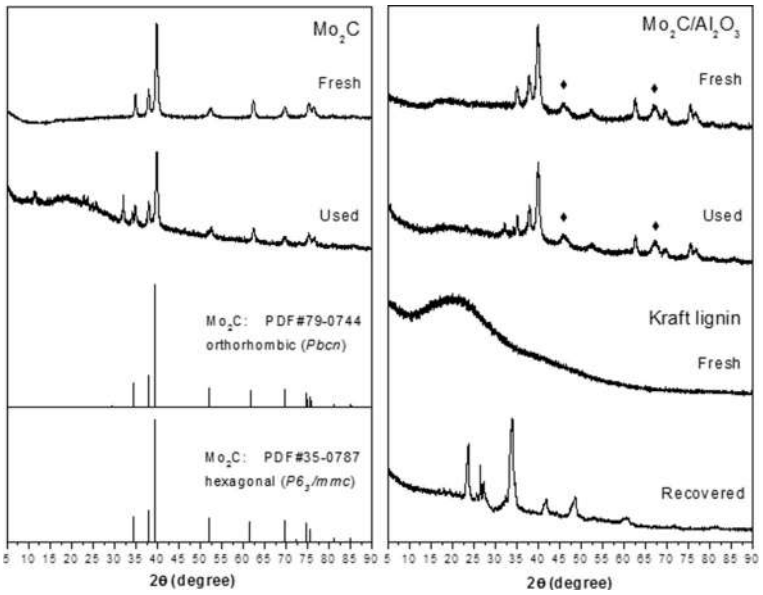

Figure 3. Powder XRD patterns of the unsupported Mo_2C-based catalyst and reference patterns (left) and supported catalyst, as well as Kraft lignin (right) before and after catalytic depolymerization. XRD patterns from fresh and recovered Kraft lignin are also reported for comparison as well as reference patterns. The ◆ symbol marks prominent reflections from the γ-alumina support.

supercritical ethanolysis, without a catalyst present, revealed a completely new pattern, containing several prominent reflections. Graphitic carbon was ruled out as a candidate (based on the absence of characteristic reflections in the reference patterns in the Highscore Plus, v3.0.5 software package) and given the heterogeneous nature of lignin, it is unlikely that a single phase is responsible for this pattern. The certificate of analysis for the batch of lignin used in the current study stated that 3.33 wt% sulfur was present. In addition, calcination of lignin samples at 800 °C for 4 h resulted in 19.5 wt% of pale green, non-volatile inorganic residue. Upon acidification of this residue with 2 mL of 70% w/v nitric acid, a significant quantity of presumably CO_2 gas was evolved, indicating that the inorganics were likely primarily carbonates. The material is consistent as coming from the "green liquor" stream of the Kraft pulping process. The data for the Mo_2C catalysts are also shown in Figure 3. The pattern for the unsupported Mo_2C reported here is in close agreement to that published by Liang and co-workers.[21] They referenced their material to PDF# 35-0787:[23] a hexagonal phase with space group $P6_3/mmc$. There is a body of literature, however, that suggests that the orthorhombic phase (space group *Pbcn*) is very slightly more stable than the hexagonal phase at room temperature.[24] For example, Haines et al. have demonstrated that the *Pbcn* phase is 15 meV per formula unit lower in energy than the hexagonal $P6_3/mmc$ phase,[25] which corresponds to an energy difference of just 1.45 kJ mol^{-1} between the two. Accordingly, the corresponding reference pattern, PDF# 79-0744,[24b] is included here for comparison. Given the inevitable broadening of the XRD data for the unsupported Mo_2C, it is difficult to unequivocally assign the synthesized material as either phase. The major reflections for both reference patterns agree with those of the experimental pattern. The specific difficulty of phase assignment from powder XRD data for Mo_2C has been noted before, requiring neutron diffraction to resolve the issue[26] and there is also the possibility that the bulk orthorhombic material is overlaid by a disordered hexagonal lattice.[27] We therefore strongly suspect that the material in the current study and that prepared by Liang and co-workers[21] is actually the orthorhombic phase of Mo_2C. That aside, the addition of the Mo_2C phase to an alumina support does not substantially change the Mo_2C crystal structure. Dispersion is increased, based on the sorption data, however, the crystallite size appears similar to that of the unsupported material according to powder XRD.

Catalytic conversion of lignin

The catalytic depolymerization of Kraft lignin was performed in a Parr reactor (Hastelloy C), under similar reaction conditions to those reported by Li and co-workers:[14] see Scheme 1.

Kraft lignin (1.0 g) and an appropriate amount (see below) of catalyst were suspended in ethanol. The supported catalysts were nominally 30 wt% molybdenum, and 500 mg of catalyst was employed in each case (corresponding to 150 mg of molybdenum). For unsupported catalysts, the mass of catalyst added was calculated to keep the amount of added molybdenum constant across all experiments (corresponding to

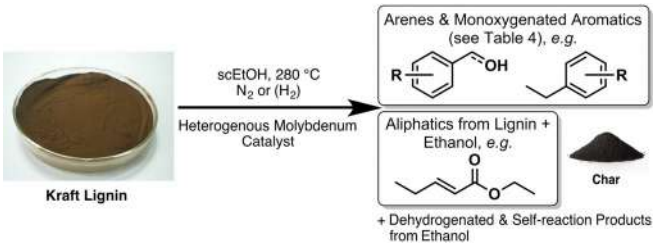

Scheme 1. Overview of Kraft lignin depolymerization under supercritical reaction conditions in the presence of Mo-based heterogeneous catalysts.

160 mg of Mo_2C and 250 mg of MoS_2). The majority of the reactions were run for 6 h under an initial 1.3 bar of nitrogen gas; see below for specific details on experiments run under hydrogen gas at various pressures. Two parameters were of particular interest: the substrate conversion, that is, the proportion of lignin converted to soluble products, and the yield of low-molecular-weight aromatic compounds in solution (notably the reactor head space was not sampled). More than 1 g of products are observed from the depolymerization of 1 g of lignin owing to the addition of ethyl groups from ethanol to the solubilized species (aromatics, aliphatics) and to the recovered residue. In addition, the self-condensation of ethanol results in the detection of a variety of low-molecular-weight aliphatic products. Hence, conversion was calculated by subtracting the mass of recovered solid from the combined masses of catalyst and substrate lignin. The recovered solid was presumed to contain the catalyst, inorganic components of lignin, and organic material that either failed to depolymerize, or resulted from the repolymerization of reactive oligomers during the reaction.

MoS_2 series

The overall results from the MoS_2 series of catalysts are shown in Table 2 and Figure 4. Ethanolysis of lignin in the absence of catalyst was run as a control experiment and resulted in a conversion of 85%. From this run, a total of 102 mg g^{-1} lignin of aromatic products were quantified. These results are in accord with similar control reactions reported in the literature, for example, references [8, 14b]. Overall, the conversion of lignin in the presence of MoS_2-based catalysts was high, with the delaminated material performing better than its bulk counterpart (entries 2 and 3).

Table 2. Overview of the results from the MoS_2-catalyzed depolymerization of lignin.

Entry	Catalyst	Atmosphere	Solid residue[a] [mg]	Conversion[b] [%]	Aromatic yield [mg g^{-1} lignin]	Final pressure[c] [bar]
1	no catalyst	N_2	318	85	102	94
2	MoS_2[d]	N_2	554[b]	86	178	101
3	d-MoS_2[d]	N_2	423[b]	quant.	186	131
5	MoS_2/Al_2O_3	N_2	939	70	46	163
6	d-MoS_2/Al_2O_3	N_2	1059	55	9	153
7		H_2 (20 bar)	924	72	18	171
8	d-MoS_2/	N_2	709	98	72	139
9	KW2000	H_2 (20 bar)	732	95	56	166

[a] The solid residue contains the recovered catalyst and insoluble lignin portion remaining after the reaction. [b] Conversions take into account the 19.5 wt% of inorganic material (non-depolymerizable) present in the lignin starting material. [c] Pressure within the reactor after 6 h at 280 °C. [d] The amount of catalyst added was 250 mg; "d-MoS_2" denotes delaminated MoS_2.

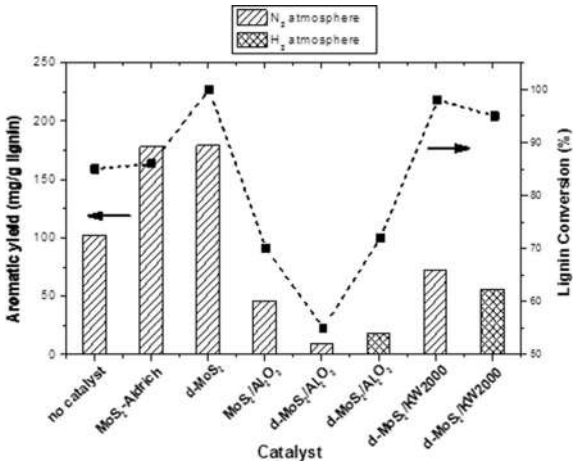

Figure 4. Lignin conversion and aromatic yields obtained from ethanolysis of Kraft lignin over different MoS_2-based catalysts. Arrows indicate the *y*-axis corresponding to the data set.

The presence of the alumina support, however, markedly reduced the efficiency of the catalyst under nitrogen (entries 5–7), despite increasing the available surface areas of the catalysis (See Table 1). The origin of this inhibitory effect is not well-understood and seemed to affect the delaminated material more severely that it did the bulk material. Running the depolymerization under hydrogen improved the conversion somewhat, but did not make up for the adverse effects of the alumina. As the presence of a basic hydrotalcite KW2000 support did not result in a reduction of conversion for delaminated MoS_2, the inhibitory effect appeared to be owing to the acidity of the alumina support. The highest aromatic yields in this series resulted from the unsupported catalysts, with delaminated MoS_2 clearly outperforming its bulk counterpart. Aromatic yields overall were more moderate than those reported by Li and co-workers for other molybdenum-based catalysts.[14b] The final pressure observed at the end of 6 h at 280 °C, varied between 101 and 163 bar depending on the catalyst employed. Particularly interesting was the case of d-MoS_2/KW2000 (entry 8), in which despite almost quantitative conversion, only 72 mg of aromatic compounds per gram of lignin were quantified. In conjunction with the high final reaction pressure of 139 bar, these observations suggested that cracking of the solubilized intermediates occurred, as well as de-aromatization.

These processes which remove aromatics from the product stream appear to operate without the need for external hydrogen gas and, hence, the challenge for employing MoS_2-based catalysts is overcoming their inherent chemoselectivity, so as to suppress this

unwanted dearomatization activity, whilst maintaining their high conversion ability.

Mo_2C series

The overall results from the Mo_2C series of catalysts are shown in Table 3 and Figure 5. Compared with the majority of the MoS_2-based catalysts, Mo_2C and Mo_2C/Al_2O_3 afforded lower lignin conversions; lower than those obtained under the control conditions (entries 1 and 5). The combined yields of the quantified aromatic compounds, however, were much improved over both the control and MoS_2 series. The final reaction pressures for the Mo_2C series were consistently lower than those observed for the MoS_2 series (114 bar vs. 130–163 bar). The only noteworthy variation in pressure arose if the reaction was run with an initial pressure of 20 bar of hydrogen. However, this was still significantly lower than if similar conditions were employed with MoS_2 (137 bar vs. 170 bar).

In an attempt to improve the conversion of lignin through increased hydrogenolysis, unsupported Mo_2C was employed in the presence of a hydrogen atmosphere (entries 2–4). Despite the unexpected decrease in the conversion if 1.3 bar of hydrogen was introduced, the general trend is towards increasing conversion with increased hydrogen pressure. Unfortunately, it seems that the hydrogenation pathways are favored as this increased conversion was accompanied by a decrease in the yield of aromatics. These results suggest that dehydrogenation of ethanol not only provides a sufficient amount of hydrogen for hydrogenation to take place effectively in the presence of Mo_2C, but also balances the hydrogen requirements for selective hydrogenolysis, leading to high aromatic yields.

Generally, the alumina support had a moderately positive effect on lignin conversion, but almost no effect on the yield of aromatics, despite the significant increase in the surface area of the catalyst from 6 to 103 $m^2 g^{-1}$ (cf. entries 1 and 5). If the initial atmosphere in the reactor was replaced with 20 bar of hydrogen, a comparable drop in the aromatic yield was observed for the Mo_2C/Al_2O_3 catalyst compared with that observed with the unsupported catalyst (cf. entries 4 and 6).

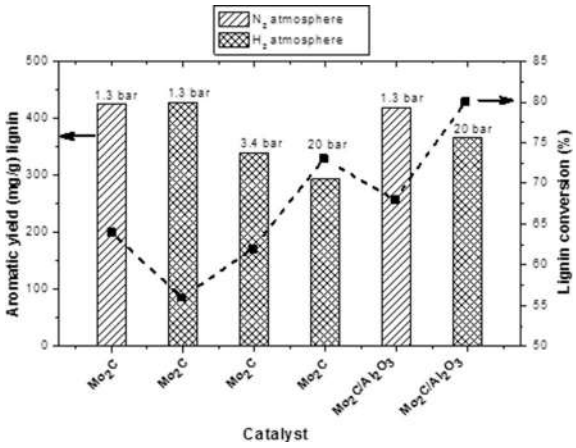

Figure 5. Lignin conversion and aromatic yields obtained from ethanolysis of Kraft lignin over Mo_2C-based catalysts. Arrows indicate the *y*-axis corresponding to the data set.

To the best of our knowledge, these Mo_2C catalysts afford amongst the highest aromatic yields reported for molybdenum-catalyzed depolymerization of Kraft lignin at 280 °C. Table 3, entries 7–9 are included for comparison with data published by the Li group.[14b] It is not until their dual α-$MoC_{(1-x)}$/Cu-$MgAlO_z$ catalyst is used at 330 °C, that the yield of aromatics surpasses those produced by the Mo_2C catalysts in the current study.

Product analysis

The 11 major aromatic compounds identified by GC-MS in the product stream were quantified, by using *o*-cresol as the external standard, and are listed in Table 4. In addition to aromatic compounds, the reaction mixture also contained aliphatic alcohols and esters. These were derived from both lignin, and from ethanol reacting with itself under supercritical conditions. Overall, the distribution of products was similar to that reported previously.[14] One noteworthy difference between the current study and previous reports was the absence of guaiacol derivatives (e.g., guaiacol, 4-methylguaiacol, 4-propylguaiacol) in the product stream. Apart from the noticeable absence of toluene, the control reaction afforded the other ten aromatic compounds used for quantification (Table 4, entry 1). This reaction was also the only one in which a phenolic product was observed, albeit in very low yield. The other products of interest are categorized as arenes and mono-oxygenated aromatics. On performing the reaction without a catalyst (i.e., the "control"), the latter category accounted for 75% of the total. If Mo_2C/Al_2O_3 was used under nitrogen, the proportion of mono-oxygenates decreased to 60% (entry 6) and if unsupported Mo_2C was employed, the arene prod-

Table 3. Amount of solid residue after the reaction at 280 °C for 6 h over 0.5 g of Mo_2C-based catalysts with initial 1.3 bar of N_2 and 100 mL of ethanol. Lignin conversion, yields of the 11 quantified aromatic products, and final reaction pressure at 280 °C.

Entry	Catalyst	Atmosphere	Solid residue[a] [mg]	Conversion[b] [%]	Aromatic yield [mg g^{-1} lignin]
1	Mo_2C[c]	N_2	645	64	425
2		H_2 (1.3 bar)	707	56	427
3		H_2 (3.5 bar)	661	62	339
4		H_2 (20 bar)	572	73	293
5	Mo_2C/Al_2O_3	N_2	951	68	419
6		H_2 (20 bar)	860	80	367
7	α-MoC_{1-x}/AC[d]	N_2 (300 °C)	813	85	232
8	α-MoC_{1-x}/Cu-$MgAlO_z$[d]	N_2 (280 °C)	1004	62	82
9	α-MoC_{1-x}/Cu-$MgAlO_z$[d]	N_2 (330 °C)	493	quantitative	575

[a] The solid residue contains the recovered catalyst and insoluble lignin portion remaining after the reaction. [b] Conversions take into account the 19.5 wt% of inorganic material (non-depolymerizable) present in the lignin starting material. [c] The amount of catalyst added was 160 mg. [d] Data from Li and co-workers.[14c]

Table 4. Detailed yields of the quantified aromatic compounds from the ethanolysis of Kraft lignin in the presence of Mo-based catalysts at 280 °C.

Entry	Catalyst	Atm	Arenes						Oxygenated aromatics				
						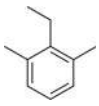	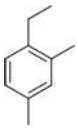	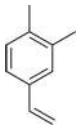	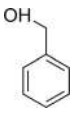	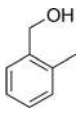	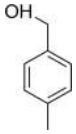	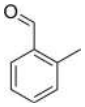	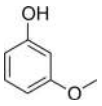
1	none	N_2	–	7	9	2	5	2	11	23	8	33	2
2	Mo_2C	N_2	47	91	42	10	22	16	35	42	33	89	–
3		H_2 (1.3 bar)	52	98	39	8	20	16	31	34	34	95	–
4		H_2 (3.4 bar)	45	91	34	8	18	15	21	25	10	71	–
5		H_2 (20 bar)	40	67	30	6	14	12	41	27	23	34	–
6	Mo_2C/	N_2	38	39	67	7	15	-	55	63	43	89	–
7	Al_2O_3	H_2 (20 bar)	39	59	40	7	14	12	55	51	37	54	–
8	MoS_2	N_2	13	36	9	3	7	7	14	27	7	54	–
9	d-MoS_2	N_2	35	63	35	10	14	10	–	–	–	20	–
10	MoS_2/ Al_2O_3	N_2	10	16	8	2	3		–	–	–	5	–
11	d-MoS_2/	N_2	-	5	4	–	–	–	–	–	–	–	–
12	Al_2O_3	H_2 (20 bar)	7	7	5	–	–	–	–	–	–	–	–
13	d-MoS_2/	N_2	18	28	17	3	3	3	–	–	–	–	–
14	KW2000	H_2 (20 bar)	17	20	14	3	3	-	–	–	–	–	–

ucts tended to dominate, accounting for more than 50% of the total (entries 2–5). The latter result contrasts with those reported by Li and co-workers in which arenes account for less than 50% of the total aromatic products.[14a,b] There was also a general trend towards increased hydrodeoxygenation with increasing hydrogen pressure, resulting in an increased proportion of arenes with respect to mono-oxygenated aromatics (from 55% to 63%). In the presence of MoS_2, despite the moderate to low yields of aromatic products, arenes were still favored over mono-oxygenated species (entries 8–14).

To quantify the leached molybdenum and the stability of the catalyst, inductively coupled plasma (ICP) analyses were performed on the recovered reaction mixtures. For the different Mo-based catalysts, the percentage of leached molybdenum varies between 0.04 and 0.38% (Table 5). For a given material, a greater proportion of molybdenum leaches from the supported catalyst compared with the unsupported one. This result can be partially rationalized on the basis of increased surface area for the supported catalysts (see Table 1), although the correlation is not strong.

Table 5. Molybdenum ICP results of Kraft lignin and catalyzed depolymerizations.

Catalyst	[Mo] [ppb]	Mo in reaction supernatant [μg]	Leached Mo [wt%]
Kraft lignin	8[a]	n/a	n/a
no catalyst	134	27	0.02[b]
MoS_2	312	62	0.04
d-MoS_2	364	73	0.05
MoS_2/Al_2O_3	560	112	0.07
d-MoS_2/Al_2O_3	1232	246	0.16
d-MoS_2/KW2000	1944	389	0.26
Mo_2C	865	173	0.12
Mo_2C/Al_2O_3	2848	739	0.38

[a] Concentration expressed in μg of molybdenum per 1 g of Kraft lignin. [b] Calculated on the same basis as if catalyst were present.

ICP analyses were also performed on lignin itself and on the reaction mixture of the control reaction. The amount of leached molybdenum in the control reaction (27 μg) is higher than the inherent amount of molybdenum present in Kraft lignin (8 μg g^{-1} lignin). Therefore, it is highly likely that this increase is owing to the leaching of molybdenum from the wall of the reactor itself (the proportion of molybdenum metal in the Hastelloy C used for the reactor is approximately 16 wt%). Importantly, from the lignin conversion data shown in Table 2 and Table 3 and the ICP data in Table 5, it appears that there is no correlation between the amount of molybdenum leached into solution and the extent to which lignin is depolymerized. For example, three times more molybdenum is leached from Mo_2C/Al_2O_3 than from unsupported Mo_2C, however, their conversions are 68% and 60%, respectively, and the yield of aromatic products was comparable (425 and 419 mg g^{-1} lignin). Similar observations were made for bulk and delaminated MoS_2: these catalysts were the most robust of those tested, leaching the least molybdenum, and yet the conversion was high. By contrast, the alumina-supported delaminated MoS_2 was the least stable, resulting in the greatest amount of leaching and displaying the lowest conversion of lignin overall.

Li and co-workers have published the results of experiments that support the idea that a soluble molybdenum(V) species, derived from the heterogeneous catalyst, is responsible for a large part of the observed catalysis in supercritical ethanol.[14b,c]

To examine this idea with our catalysts, 1.0 g of lignin in 100 mL of ethanol was reacted at 280 °C for 6 h over 160 mg of unsupported Mo_2C, with an initial N_2 pressure at room temperature of 1.3 bar. The reaction mixture was carefully removed from the solid residue, which was then washed several times with ethanol. All liquids were combined and then concentrated

to 100 mL at reduced pressure. This solution was analyzed to quantify the aromatics and then used as the reaction medium for a second lignin depolymerization without any added catalyst. Analysis of this second reaction that relied only on the leached molybdenum as the catalyst revealed that only 162 mg g^{-1} of aromatics were obtained (compared with 425 mg g^{-1} for the first run and 102 mg g^{-1} in a control reaction without catalyst). Furthermore, the lignin conversion was markedly lower than what was observed initially (25% vs. 64%). These initial results and the above ICP data suggest that although homogeneous catalysis may operate to a limited extent, for MoS_2 and Mo_2C the majority of the catalysis is heterogeneous in these lignin depolymerizations. The behavior of Mo_2C is demonstrably different from that of the α-MoC_{1-x}-based catalysts reported by Li and co-workers.

Although there has been a wealth of experimental evidence for the practical utility of Mo_2C as a catalyst, recent DFT studies by Illas and co-workers have confirmed that the orthorhombic *Pbcn* phase of Mo_2C has electronic and structural properties that make it particularly suitable for use as a catalyst in reductive processes.[28] The (0 1 1) surface was calculated to be particularly stable (low cleavage energy) and have the lowest work function (3.64 eV) of the Mo_2C and MoC phases studied. The value of this work function implies that there is a low energy barrier for electron transfer from the carbide surface to adsorbed substrate or hydrogen, which thus facilitates hydrogenolytic (and hydrogenation) steps. With a work function of 3.89 eV, the (1 0 0) surface was also determined to be suited to this task and both these surfaces had lower work functions than any of the corresponding surfaces in cubic δ-MoC and hexagonal α-MoC phases. Of relevance to the discussion here is that the (0 0 1) surface in the hexagonal $P6_3/mmc$ phase corresponds to the (1 0 0) orthorhombic *Pbcn* phase[26] and hence the catalytic activity of hexagonal Mo_2C present may also be rationalized on the basis of low values for cleavage energy and work function.

Furthermore, Liang and co-workers reported that in the hydrogenation of naphthalene to tetralin, Mo_2C performed better with a clean surface than if the surface was covered by excess carbon.[21] Therefore, the choice of the catalyst support for lignin ethanolysis may be crucial for developing a catalyst that is not poisoned by the build-up of organic material on the surface of the Mo_2C.

Conclusions

Two series of sulfur-tolerant molybdenum-based catalysts were prepared and employed for the depolymerization and upgrading of lignin in supercritical ethanol. The results presented here are consistent with a heterogeneously catalyzed path as the major avenue for conversion of solubilized lignin oligomers to low–molecular–weight products. MoS_2-based catalysts worked synergistically with supercritical ethanol to efficiently depolymerize Kraft lignin into soluble species. Increasing the proportion of catalyst edge sites was beneficial for the catalytic activity and hence the use of a dopant at these edge sites may possibly overcome the inherent chemoselectivity of MoS_2 for hydrogenation, which currently leads to relatively low yields of aromatic compounds. The use of Mo_2C and Mo_2C/Al_2O_3 as catalysts in the depolymerization of Kraft lignin at 280 °C in supercritical ethanol afforded high yields of aromatic compounds favoring arenes. Transfer hydrogenation from ethanol was a critical factor in ensuring efficient conversion of the substrate. Despite an increase in the conversion of lignin, the use of additional hydrogen proved to be deleterious to the yield of aromatics owing to the increased hydrogenation activity of the catalyst. Further work to increase the conversion ability of Mo_2C catalysts, without sacrificing their attractive chemoselectivity, is required to improve them. Based on the results reported here, optimization would involve examining catalyst behavior at higher temperatures and determining whether a catalyst support was really necessary. It is clear from this study that the precise role the catalyst support plays in the depolymerization process is unclear and the key design features that make for a beneficial support require further investigation. Directed studies to determine the interaction of both series of catalysts with the aromatic products under the reaction conditions may also reveal how to avoid their loss, once formed, owing to hydrogenation, and which factors suppress repolymerization.

Experimental Section

Materials

Kraft lignin (catalogue number 471003), MoS_2 (catalogue number 234842), 2-methylbenzaldehyde, guaiacol, 4-methyl benzyl alcohol, 2-methyl benzyl alcohol, and 1-ethyl-3-methyl benzene were purchased from Sigma–Aldrich. Alumina (Catalox SBa-150) was provided by Sasol. Hydrotalcite KW2000 was supplied from Kyowa Industries. Toluene and benzyl alcohol were purchased from Merck. *o*-Xylene was purchased from Alfa Aesar, *p*-xylene was purchased from Fluka, 2,4-dimethyl styrene was purchased from Enamine, 1-ethyl-2,4-dimethyl benzene was purchased from Fluorochem. All chemicals were used as received.

Synthesis and characterization of catalysts

All supported catalysts were prepared such that the nominal molybdenum loading was 30 wt%.

Ammonium tetrathiomolybdate was prepared from sodium molybdate hydrate and ammonium sulfide according to the procedure of Reid and co-workers.[18]

MoS_2/Al_2O_3 was synthesized by co-grinding $(NH_4)_2MoS_4$ (1.75 g) with Al_2O_3 (1.50 g), followed by heat treatment under H_2/N_2 (1:7; ca. 80 mL min^{-1}): 2 °C min^{-1} until 100 °C, held for 1 h, then 10 °C min^{-1} until 300 °C, held for 0.5 h. The sample was cooled to room temperature under N_2, affording a grey-black powder.

Delaminated MoS_2 was synthesized by following a procedure reported by Maschmeyer and co-workers.[15b] $(NH_4)_2MoS_4$ (0.75 g) was dissolved in 15 g of dried $[C_4C_1im][OTf]$ at 40 °C. This solution was heated at 300 °C under 10% v/v H_2 in N_2, at a flow rate of 10 mL min^{-1} for 2 h, with stirring. The black product was precipitated with 90 mL ethanol and further washed with ethanol (5× 80 mL), followed by water (2×50 mL), acetone (2×50 mL), and

hexane (2×50 mL). The powder was then dried under vacuum at room temperature.

Delaminated MoS_2/Al_2O_3 and delaminated MoS_2/KW2000 were synthesized by dissolving $(NH_4)_2MoS_4$ (0.872 g) in 16 g of dried $[C_4C_1im][OTf]$. Dried alumina (750 mg) or KW2000 (750 mg) were then added to the reaction mixture, and the suspension was heated at 300 °C under 10% v/v H_2 in N_2, at a flow rate of 10 mL min^{-1} for 2 h, with stirring. The resulting black solid was precipitated and washed as described above.

Mo_2C was synthesized according to the procedures described by Liang and co-workers,[21] on a 3.0 g scale. The melamine–[Mo] coordination polymer prepared in the first step was subjected to heat treatment under flowing H_2 in Ar (70 mL min^{-1}; 2:5 ratio) at 650 °C for 1 h, affording 754 mg of catalyst as a hard, blue-grey ceramic.

For Mo_2C/Al_2O_3, the dried, isolated melamine–[Mo] coordination polymer (1.52 g) was co-ground with alumina (1.20 g) and heat treated in the same manner as described above, affording 1.76 g of black powder.

PXRD was performed by using a PANalytical X'Pert PRO MPD X-ray diffractometer with CuK_α ($\lambda = 1.5419$ Å) as the irradiation source. The scanning was conducted between 2θ values of 5 and 90° with a scanning rate of 2° min^{-1}. Surface areas of the samples were measured by nitrogen sorption analysis with a Micrometrics Accelerated Surface Area and Porosimetry System (ASAP) 2020 instrument. The powdered sample was outgassed at 90 °C and 13 μbar overnight. Nitrogen adsorption and desorption isotherms were collected at 77 K, and the surface areas were calculated by using the BET model in the framework of the Micrometrics software. High-resolution transmission electron microscopy was performed with a JEOL-TEM-2100 operated at 200 kV. Each sample was prepared by dispersing the powdered sample in ethanol and drop-casting onto a 200 mesh copper grid coated with holey carbon.

Catalysis

Batch reactions were performed in a 250 mL Parr reactor system (reactor code 4875; Hastelloy C), equipped with a mechanical stirrer, cooling loop, and thermowell. The reactor was charged with powdered lignin (1.0 g), catalyst (0.5 g for supported catalysts, 0.25 g for unsupported MoS_2, 0.16 g for unsupported Mo_2C), and absolute ethanol (100 mL). The reactor was sealed, purged with nitrogen thrice (pressurization to 50 bar, followed by release), and finally the desired pressure of nitrogen or hydrogen gas was introduced. The reaction was heated to 280 °C over a period of approximately 1.5 h with stirring, held at 280 °C for up to 6 h, then cooled to room temperature. The cooling step was assisted by use of a water bath. The reactor was depressurized, unsealed, and the mixture filtered at the pump. The residue was washed with ethanol several times and dried at 80 °C overnight. *o*-Cresol (20 μL) was added and the volume of the filtrate was adjusted to 200 mL volumetrically with ethanol.

Reaction analysis

Compound identification by GC-MS was performed with a Shimadzu GCMS-QP2010 equipped with Rtx-5MS 0.25 μm×30 m×0.25 mm column. The temperature program had an isothermal period of 3 min at 50 °C, followed by a heating ramp of 10 °C min^{-1} to 330 °C, followed by an isothermal period of 10 min. Compounds were identified by comparing the EI-MS spectra with those in the system's database (NIST05). Of the prominent aromatic species identified, 12 were quantified by using calibration curves of authentic samples. *o*-Cresol was used as an external standard. The calculated yield is reported as mg of analyte per g lignin.

ICP analysis

Inductively coupled plasma (ICP) analysis was performed with a PerkinElmer Nexion 300XX Inductively Coupled Plasma Mass Spectrometer (ICP-MS). The reaction mixture was filtered, the residue washed with ethanol several times, and made up to 200 mL volumetrically. A 1.0 mL aliquot was digested with 2.0 mL of 70% w/v nitric acid at 80 °C and diluted with Milli-Q H_2O to give 100 mL volumetrically. A final five-fold dilution was performed before sample injection. ICP analysis of Kraft lignin was performed by digesting 0.105 g of Kraft lignin with 2.0 mL of 70% w/v nitric acid at 80 °C and diluting with Milli-Q H_2O to give 100 mL volumetrically. A final ×100 dilution was performed before sample injection.

Acknowledgments

The authors thank the Australian Centre for Microscopy & Microanalysis for the use of their electron microscopes; Ms. Ellen Hemming and Ms. Rui Zhang for assistance with microscopy analysis; Dr. Tom Savage at the School of Geoscience for assistance with ICP analysis. This work was supported by the Erasmus+ Scholarship (L. Cattelan) and the Australian Research Council (M. Y. Lui).

Conflict of interest

The authors declare no conflict of interest.

Keywords: Kraft lignin · molybdenum carbide · molybdenum disulfide · renewable chemicals · supercritical ethanol

[1] M. Ragnar, G. Henriksson, M. E. Lindström, M. Wimby, J. Blechschmidt, S. Heinemann, in *Ullmann's Encyclopedia of Industrial Chemistry*, Wiley-VCH, Weinheim, **2014**.
[2] N. Mahmood, Z. Yuan, J. Schmidt, C. Xu, *Bioresour. Technol.* **2013**, *139*, 13–20.
[3] J. Zakzeski, P. C. A. Bruijnincx, A. L. Jongerius, B. M. Weckhuysen, *Chem. Rev.* **2010**, *110*, 3552–3599.
[4] C. O. Tuck, E. Perez, I. T. Horvath, R. A. Sheldon, M. Poliakoff, *Science* **2012**, *337*, 695–699.
[5] R. Rinaldi, R. Jastrzebski, M. T. Clough, J. Ralph, M. Kennema, P. C. A. Bruijnincx, B. M. Weckhuysen, *Angew. Chem. Int. Ed.* **2016**, *55*, 8164–8215; *Angew. Chem.* **2016**, *128*, 8296–8354.
[6] K. H. Kim, R. C. Brown, M. Kieffer, X. Bai, *Energy Fuels* **2014**, *28*, 6429–6437.
[7] T. D. Matson, K. Barta, A. V. Iretskii, P. C. Ford, *J. Am. Chem. Soc.* **2011**, *133*, 14090–14097.
[8] X. Huang, T. I. Korányi, M. D. Boot, E. J. M. Hensen, *ChemSusChem* **2014**, *7*, 2276–2288.
[9] a) M. P. Pandey, C. S. Kim, *Chem. Eng. Technol.* **2011**, *34*, 29–41; b) A. J. Ragauskas, G. T. Beckham, M. J. Biddy, R. Chandra, F. Chen, M. F. Davis, B. H. Davison, R. A. Dixon, P. Gilna, M. Keller, P. Langan, A. K. Naskar, J. N. Saddler, T. J. Tschaplinski, G. A. Tuskan, C. E. Wyman, *Science* **2014**, *344*, 1246843.
[10] a) Q. Song, F. Wang, J. Xu, *Chem. Commun.* **2012**, *48*, 7019–7022; b) Q. Song, F. Wang, J. Cai, Y. Wang, J. Zhang, W. Yu, J. Xu, *Energy Environ. Sci.* **2013**, *6*, 994–1007; c) P. Ferrini, R. Rinaldi, *Angew. Chem. Int. Ed.* **2014**, *53*, 8634–8639; *Angew. Chem.* **2014**, *126*, 8778–8783.
[11] H. Topsøe, B. S. Clausen, F. E. Massoth, in *Hydrotreating Catalysis Science and Technology, Vol. 11*, Springer, Berlin, **1996**.

[12] M. Grilc, B. Likozar, J. Levec, *Appl. Catal. B* **2014**, *150 – 151*, 275 – 287.
[13] G. Veryasov, M. Grilc, B. Likozar, A. Jesih, *Catal. Commun.* **2014**, *46*, 183 – 186.
[14] a) R. Ma, W. Hao, X. Ma, Y. Tian, Y. Li, *Angew. Chem. Int. Ed.* **2014**, *53*, 7310 – 7315; *Angew. Chem.* **2014**, *126*, 7438 – 7443; b) X. Ma, R. Ma, W. Hao, M. Chen, F. Yan, K. Cui, Y. Tian, Y. Li, *ACS Catal.* **2015**, *5*, 4803 – 4813; c) F. Yan, R. Ma, X. Ma, K. Cui, M. Chen, Y. Li, *Appl. Catal. B* **2017**, *202*, 305 – 313.
[15] a) V. W.-h. Lau, A. F. Masters, A. M. Bond, T. Maschmeyer, *ChemCatChem* **2011**, *3*, 1739 – 1742; b) V. W.-h. Lau, A. F. Masters, A. M. Bond, T. Maschmeyer, *Chem. Eur. J.* **2012**, *18*, 8230 – 8239.
[16] R. B. Levy, M. Boudart, *Science* **1973**, *181*, 547 – 549.
[17] a) S. K. Gade, S. J. Chmelka, S. Parks, J. D. Way, C. A. Wolden, *Adv. Mater.* **2011**, *23*, 3585 – 3589; b) J. Han, J. Duan, P. Chen, H. Lou, X. Zheng, H. Hong, *Green Chem.* **2011**, *13*, 2561 – 2568; c) A. P. E. York, J. B. Claridge, A. J. Brungs, S. C. Tsang, M. L. H. Green, *Chem. Commun.* **1997**, 39 – 40; d) A. L. Jongerius, R. W. Gosselink, J. Dijkstra, J. H. Bitter, P. C. A. Bruijnincx, B. M. Weckhuysen, *ChemCatChem* **2013**, *5*, 2964 – 2972.
[18] R. S. Reid, R. J. Clark, E. K. Quagraine, *Can. J. Chem.* **2007**, *85*, 1083 – 1089.
[19] H. W. Wang, P. Skeldon, G. E. Thompson, *J. Mater. Sci.* **1998**, *33*, 3079 – 3083.
[20] L. Cattelan, A. Perosa, P. Riello, T. Maschmeyer, M. Selva, *ChemSusChem* **2017**, *10*, 1571 – 1583.
[21] M. Pang, X. Wang, W. Xia, M. Muhler, C. Liang, *Ind. Eng. Chem. Res.* **2013**, *52*, 4564 – 4571.
[22] H. F. McMurdie, M. C. Morris, E. H. Evans, B. Paretzkin, W. Wong-Ng, C. R. Hubbard, *Powder Diffr.* **1986**, *1*, 269 – 275.
[23] H. Lux, A. Ignatowicz, *Chem. Ber.* **1968**, *101*, 809 – 814.
[24] a) J. Dubois, T. Epicier, C. Esnouf, G. Fantozzi, P. Convert, *Acta Metall.* **1988**, *36*, 1891 – 1901; b) T. Epicier, J. Dubois, C. Esnouf, G. Fantozzi, P. Convert, *Acta Metall.* **1988**, *36*, 1903 – 1921.
[25] J. Haines, J. M. Léger, C. Chateau, J. E. Lowther, *J. Phys. Condens. Matter* **2001**, *13*, 2447 – 2454.
[26] E. Parthé, V. Sadagopan, *Acta Crystallogr.* **1963**, *16*, 202 – 205.
[27] T. P. St. Clair, S. T. Oyama, D. F. Cox, S. Otani, Y. Ishizawa, R.-L. Lo, K. Fukui, Y. Iwasawa, *Surf. Sci.* **1999**, *426*, 187 – 198.
[28] J. R. D. S. Politi, F. Viñes, J. A. Rodriguez, F. Illas, *Phys. Chem. Chem. Phys.* **2013**, *15*, 12617 – 12625.

Manuscript received: February 27, 2017
Revised manuscript received: March 29, 2017
Accepted manuscript online: March 30, 2017
Version of record online: June 26, 2017

energy&fuels

Article

pubs.acs.org/EF

Extractive Denitrogenation of Fuel Oils with Ionic Liquids: A Systematic Study

Matthew Y. Lui,[†] Lisa Cattelan,[†,‡] Lisa C. Player,[†] Anthony F. Masters,[†] Alvise Perosa,[‡] Maurizio Selva,[‡] and Thomas Maschmeyer*[,†]

[†]Laboratory of Advanced Catalysis for Sustainability, School of Chemistry F11, The University of Sydney, Sydney, New South Wales 2006, Australia

[‡]Department of Molecular Sciences and Nanosystems, Ca' Foscari University of Venice, Via Torino 155, 30170 Venezia Mestre, Italy

Supporting Information

ABSTRACT: Ionic liquids (ILs) have been suggested as useful extractants of aromatic nitrogen-containing compounds (N compounds) from fuel oils. In this systematic study, ILs based on common cations and anions are employed as extractants of the archetypical N compounds pyridine and indole from a model oil consisting of decane and toluene. The performance of these ILs as extractants of N compounds is compared and rationalized. It is demonstrated that the cation and anion sizes (offering more surface area for extractants to interact) are the major factors determining the effectiveness of N compound extraction, although hydrogen bond donor/acceptor abilities of ILs can also play a role in the removal of these N compounds. In this study, some ILs are found to dissolve a considerable amount of oil contents. This undesired property can be controlled by the size of IL ions.

INTRODUCTION

The removal of nitrogen-containing compounds (N compounds) from fuel oils, such as diesel, is important for the reduction of exhaust emissions during combustion.[1,2] In addition, their inhibiting effect on the hydrodesulfurization process is severe.[1,3] These aromatic N compounds are commonly divided into two groups: neutral (e.g., indoles and carbazoles) and basic (e.g., pyridines and quinolines). The conventional method of eliminating these N compounds in fuel oils is hydrodenitrogenation (HDN),[4,5] which is an energy-intensive, expensive process that also generates a large amount of CO_2.[6] To overcome the shortcomings of HDN technology, other techniques, such as adsorption[7] and extraction, for removal of N compounds have been studied.

Common ionic liquids (ILs) are composed of large asymmetric organic cations (e.g., 1-alkyl-3-methylimidazolium) and inorganic (e.g., Cl^-) or organic (e.g., trifluoromethanesulfonate) anions (Figure 1). They have been extensively employed for the extraction of N compounds of fuel oils and are often described as "green solvents" for their nonvolatility, nonflammability, and good recyclability. Many also possess high chemical and thermal stability. ILs are ideal extractants of N compounds, providing a non-aqueous alternative for polar/nonpolar two-phase systems.[8] Furthermore, their physical and chemical properties can be "designed" to tailor specific needs.[9] In the case of extraction, careful manipulation of the identity of cations and anions in ILs can enhance the interaction with the solute as well as diminish undesired solubility of fuel oil in the IL phase.

Several ILs have been described as efficient extractants of N compounds. Chen and co-workers have demonstrated that some dicyanamide-based ILs, such as $[C_4C_1im][N(CN)_2]$, are reasonable extractants of pyridine from a model oil consisting of a mixture of toluene and hexane.[10] In their study, it was shown that the nitrogen contents could be reduced from about 500 to 130−205 ppm in a single extraction at ambient temperature. In the work of Tojo and co-workers, the IL 1-butyl-3,5-dimethyl-2-pentylpyridinium dicyanamide was shown to be an efficient extractant of pyrrole and pyridine.[11] Yu and co-workers demonstrated the use of both Lewis acidic ILs (e.g., $[C_4C_1im]Cl/ZnCl_2$) and Brønsted acidic ILs ($[C_4C_1im]HSO_4$) as very efficient extractants of pyridine and carbazole from the mixture of octane and toluene.[6] In particular, all of the ILs studied could achieve >90% N extraction efficiency of Lewis basic pyridine in a single extraction.

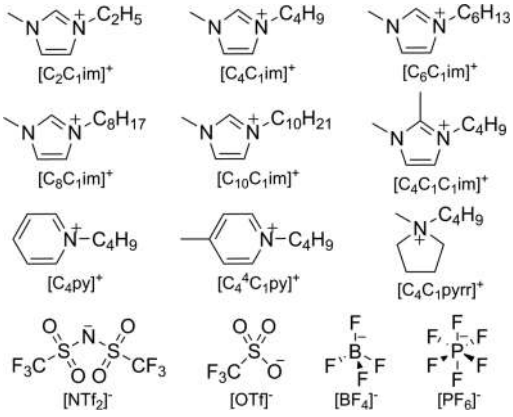

Figure 1. Cations and anions of ILs employed in this study.

Special Issue: In Honor of Professor Brian Haynes on the Occasion of His 65th Birthday

Received: August 26, 2016
Revised: November 17, 2016
Published: November 21, 2016

DOI: 10.1021/acs.energyfuels.6b02157
Energy Fuels 2017, 31, 2183−2189

Although there have already been a number of notable studies on the extraction of N compounds with ILs, a general study on the influence of structural and functional properties of different cations and anions of ILs is lacking. In the present work, room-temperature ILs containing common cations, i.e., imidazolium, pyrrolidinium, and pyridinium, and common anions, such as bis(trifluoromethane)sulfonimide and trifluoromethanesulfonate, were investigated for their extraction ability of N compounds from a model fuel oil. Furthermore, the effect of the chain length of the 1-alkyl-3-methylimidazolium cation on the extraction efficiency was also studied.

EXPERIMENTAL SECTION

Materials. *n*-Decane (Fluka), toluene (Merck), 1-methylimidazole (Aldrich), 1-methylpyrrolidine (Aldrich), pyridine (Ajax), 1,2-dimethylimidazole (Aldrich), 4-picoline (Aldrich), 1-bromoethane (BDH), 1-bromobutane (Merck), 1-bromohexane (Merck), 1-bromooctane (Merck), 1-bromodecane (Merck), lithium bis(trifluoromethane)sulfonimide (IoLiTec), sodium hexafluorophosphate (Aldrich), sodium tetrafluoroborate (Sigma-Aldrich), 1-butyl-3-methylimidazolium trifluoromethanesulfonate (Aldrich), and indole (Alfa Aesar) were used as obtained.

Synthesis of ILs. Quaternary ammonium bromide salts $[C_nC_1im]Br$ (n = 2, 4, 6, 8, and 10), $[C_4C_1pyrr]Br$, $[C_4py]Br$, $[C_4C_1C_1im]Br$, and $[C_4{}^4C_1py]Br$ were synthesized using a modified method from Burrell et al.[12] Bromoalkane (0.16 mol) was heated at 30 °C with the desired amine (0.16 mol) under nitrogen for 24 h. The products were then washed with diethyl ether (3 × 10 mL). Subsequently, solid products were recrystallized from a minimum amount of acetonitrile and filtered. The solid was then dried *in vacuo* to yield the desired quaternary ammonium bromide salts.

$[C_nC_1im][NTf_2]$, $[C_4C_1pyrr][NTf_2]$, $[C_4py][NTf_2]$, $[C_4C_1C_1im][NTf_2]$, and $[C_4{}^4C_1py][NTf_2]$ were synthesized with the corresponding quaternary ammonium bromide salts using a method similar to that of Weber et al.[13] The relevant ammonium bromide salt (91 mmol) and lithium bis(trifluoromethane)sulfonimide (96 mmol) were separately dissolved in distilled water (200 mL total) and then combined, resulting in the formation of a separate liquid phase. To this solution was added dichloromethane (200 mL), and the organic phase was collected and washed successively with water until no halide could be detected by concentrated aqueous silver nitrate. Removal of solvent *in vacuo* afforded the bis(trifluoromethane)sulfonamide IL product.

For the synthesis of $[C_4C_1im][BF_4]$ and $[C_4C_1im][PF_6]$, a modified procedure to that of Zhao et al.[14] was used. $[C_4C_1im]Br$ (69 mmol) and sodium tetrafluoroborate or sodium hexafluorophosphate (76 mmol) were stirred in acetone (500 mL) for 24 h at room temperature. The resultant white solid was separated by filtration, and the solvent was removed *in vacuo*. Then, the mixture was redissolved in dichloromethane and passed through neutral alumina. The dichloromethane solution was washed successively with water until no bromide could be detected by concentrated aqueous silver nitrate. Removal of solvent *in vacuo* afforded the $[C_4C_1im][BF_4]$ or $[C_4C_1im][PF_6]$ IL product. All of the ILs were analyzed with ^1H and ^{19}F nuclear magnetic resonance (NMR) and electrospray ionization mass spectrometry (ESI−MS) before use and found to be >99% pure.

Extractive Denitrogenation. The model oil containing the basic N compound comprises *n*-decane (85 wt %), toluene (15 wt %), and pyridine (5.00×10^{-3} mol L^{-1}), while the model oil containing the neutral N compound comprises *n*-decane (85 wt %), toluene (15 wt %), and indole (5.00×10^{-3} mol L^{-1}). Extractive experiments were performed under standardized conditions. In a typical experiment, 3.43 mmol of IL (predried *in vacuo*) and 2 mL of the model oil are placed in a 20 mL test tube and are magnetically stirred at 1000 rpm at 25 °C for a determined time, followed by equilibration for 5 min without stirring. The oil phase is removed with a pipet, taking care to not disturb the phase boundary. A sample (1 mL) of the oil phase is placed in a vial with 0.1 mL of external standard (anisole, 1.66×10^{-2} mol L^{-1} for the quantification of pyridine; guaiacol, 1.66×10^{-2} mol L^{-1} for the quantification of indole) and filtered on a polytetrafluoroethylene (PTFE) cartridge.

N Content Analysis. Analyses were performed on a LC-CTO-20A (Shimadzu) liquid chromatograph equipped with a reversed-phase Luna C18 column (150 × 2.00 mm, 5 μm) and an ultraviolet (UV) detector. The external standard condition for pyridine and indole is set at 225 nm. The mobile phase for quantification of both N compounds is 60% acetonitrile in water (v/v, %), with a flow rate of 0.8 mL min^{-1}. Triplicate injections are performed for each sample.

Mutual Solubility Analysis. The solubility of toluene and *n*-decane in ILs was quantified by ^1H NMR analysis. NMR spectra were collected using a Bruker 300 MHz instrument at 300 K after four scans. ^1H NMR spectra were obtained using a 90° flip angle with a recycle delay (D1) of 20 s externally locked to dimethyl sulfoxide (DMSO)-d_6. The IL signals were employed as standards.

RESULTS AND DISCUSSION

Fuel oils, such as diesel, consist of mixtures of aliphatic and aromatic hydrocarbons. Saturated hydrocarbons, i.e., linear, branched, and cyclic alkanes, are the predominant species in the mixtures and comprise approximately 80−90% of total fuel oils.[15] On the other hand, aromatic hydrocarbons, mostly alkylbenzenes, comprise about 10−20% of fuel oils.[15] In this investigation, a model oil consisting of a binary mixture of *n*-decane (85 wt %, representative of saturated hydrocarbons) and toluene (15 wt %, representative of aromatic hydrocarbons) was employed. Pyridine and indole (Figure 2) were selected as the representative Lewis basic and neutral N compounds, respectively.

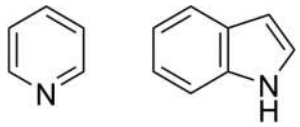

Figure 2. N compounds pyridine (left) and indole (right).

Almost all of the denitrogenation results reported in the literature are reported with respect to the weight (IL)/weight (oil) ratio. We believe, however, that to investigate and compare the "intrinsic" capabilities of ILs for the extraction of N compounds, results should be compared and reported with respect to a constant amount (mole) of ILs. The N extraction efficiencies are also reported in terms of mol % and were calculated by eq 1.

$$\text{N extraction efficiency (mol \%)} = \left(1 - \frac{\text{N compound in oil phase}_{\text{final}}\ \text{(mol)}}{\text{N compound in oil phase}_{\text{initial}}\ \text{(mol)}}\right) \times 100\% \quad (1)$$

The final mole of N compound in the oil phase of each measurement was calculated with eq 2, for which the concentrations of N compounds were determined by high-performance liquid chromatography (HPLC) measurements.

$$\text{N compound in oil phase}_{\text{final}}\ \text{(mol)} = [\text{N compound in oil phase}]\ (\text{mol dm}^{-3}) \times \text{volume of oil phase}_{\text{final}}\ (\text{dm}^{-3}) \quad (2)$$

The final volume of oil phase was measured with eq 3, for which the oil contents in IL phases were determined by quantitative ^1H NMR.

DOI: 10.1021/acs.energyfuels.6b02157
Energy Fuels 2017, 31, 2183−2189

$$\text{volume of oil phase}_{\text{final}}\ (\text{dm}^{-3}) = 0.002 - \text{oil content in IL phase} \quad (3)$$

Equation 3 is a good estimation of the final volume of the oil phase because the ILs investigated have negligible solubility in the oil phase, as determined by HPLC and ^{1}H NMR measurements.

In the preliminary extraction experiments, 3.43 mmol of IL and 2 mL of solution of pyridine or indole (5.00×10^{-3} mol L^{-1}) in the model oil were stirred for periods of 10, 20, and 30 min at 25 °C. For both pyridine and indole, extraction equilibria could be achieved within 10 min of stirring for all of the ILs, as shown in Tables S1 and S2 of the Supporting Information. To realize the extraction performance of different ILs, the extraction experiments (20 min) were duplicated and the N extraction efficiency values were compared.

Cation Dependence with Common Anion ($[NTf_2]^-$). The N extraction efficiencies of 1-butyl-3-methylimidazolium bis(trifluoromethane)sulfonimide ($[C_4C_1im][NTf_2]$), 1-butyl-1-methylpyrrolidinium bis(trifluoromethane)sulfonimide ($[C_4C_1pyrr][NTf_2]$), and 1-butylpyridinium bis(trifluoromethane)sulfonimide ($[C_4py][NTf_2]$) for pyridine and indole were investigated. These widely studied ILs contain similar sized cations with butyl chains (Table 1).[16] A relatively small variation of the extraction efficiency for pyridine was observed (Figure 3 and Table 2), with values in the range of 71.8–76.8 mol %. The extraction efficiencies of $[C_4C_1pyrr][NTf_2]$ and $[C_4py][NTf_2]$ are 71.8 and 73.8 mol %, respectively, while $[C_4C_1im][NTf_2]$ demonstrated the highest capacity of the three, with an efficiency of 76.8 mol %.

Table 1. Ionic Volumes for Ions Employed in This Study[17]

ion	ionic volume (nm^3)	ion	ionic volume (nm^3)	ion	ionic volume (nm^3)
$[C_2C_1im]^+$	0.156	$[C_4C_1C_1im]^+$	0.229	$[NTf_2]^-$	0.232
$[C_4C_1im]^+$	0.196	$[C_4py]^+$	0.198	$[OTf]^-$	0.131
$[C_6C_1im]^+$	0.242	$[C_4{}^4C_1py]^+$	0.240[a]	$[PF_6]^-$	0.109
$[C_8C_1im]^+$	0.288	$[C_4C_1pyrr]^+$	0.221	$[BF_4]^-$	0.073
$[C_{10}C_1im]^+$	0.346[a]				

[a]Literature values were unavailable and derived by extrapolation from published values with the addition of each incremental $-CH_2$ group occupying 0.029 nm^3 and each $-CH_3$ group occupying 0.042 nm.[13]

For indole, an even smaller difference was observed in the extraction efficiencies with $[C_4C_1im][NTf_2]$, $[C_4C_1pyrr][NTf_2]$, and $[C_4py][NTf_2]$ as extractants. All of these ILs are excellent extractants of indole, with almost quantitative extraction efficiencies (97.5–98.3 mol %).

To investigate the effect of cation size of ILs on the N extraction efficiency, a series of ILs with the formula of $[C_nC_1im][NTf_2]$ (n = 2, 4, 6, 8, and 10) as well as $[C_4C_1C_1im][NTf_2]$ and $[C_4{}^4C_1py][NTf_2]$ were synthesized and their extraction capacities were measured (Table 2 and Figure 4). For the $[C_nC_1im][NTf_2]$ series, the pyridine extraction efficiency increased with respect to the cation volume (Figure 4). Extraction of pyridine was also carried out with 1-butyl-2,3-dimethylimidazolium bis(trifluoromethane)sulfonimide $[C_4C_1C_1im][NTf_2]$, in which the C2 position was methylated. The pyridine extraction efficiency of $[C_4C_1C_1im][NTf_2]$ was 74.1 mol %, which was slightly lower than that of $[C_4C_1im][NTf_2]$ (76.8 mol %), even though

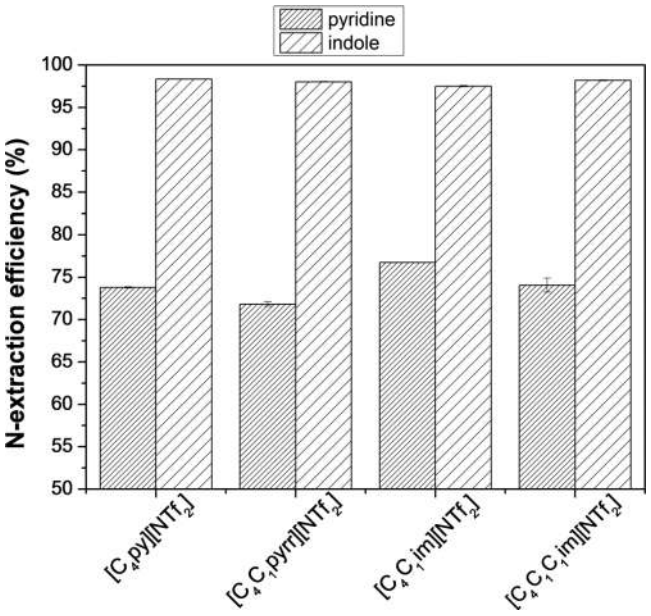

Figure 3. N extraction efficiencies of pyridine and indole with $[NTf_2]^-$ ILs of different classes of cations (temperature, 25 °C; 3.43 mmol of ILs/2 mL of model oil; and extraction time, 20 min).

$[C_4C_1C_1im]^+$ is larger in volume (Table 1). This result demonstrated that the C2 proton of the imidazolium ring could play a role in the extraction of pyridine, possibly through hydrogen bonding interaction between this proton and the basic pyridine. Although both $[C_4py]^+$ ($[C_4py][NTf_2]$: α = 0.54[18]) and $[C_4C_1pyrr]^+$ ($[C_4C_1pyrr][NTf_2]$: α = 0.43[19]) have hydrogen bond donation capabilities, their donor strengths are lower than that of $[C_4C_1im]^+$ ($[C_4C_1im][NTf_2]$: α = 0.64[18] and 0.61[19]), as reflected by their Kamlet–Taft α values. C4 and C5 protons on the imidazolium ring can also participate in hydrogen bonding, but they are not as "acidic" as the C2 proton;[20] hence, $[C_4C_1C_1im]^+$ is a considerably weaker hydrogen bond donor ($[C_4C_1C_1im][NTf_2]$: α = 0.38[19]) than the $[C_4C_1im]^+$ cation. In the case of pyridinium-based ILs, the slightly larger $[C_4{}^4C_1py][NTf_2]$ (79.6 mol %) was able to extract noticeably more pyridine than $[C_4py][NTf_2]$ (73.8 mol %). This tendency was also observed in the case of desulfurization, where the extraction efficiency increased with respect to the number of alkyl groups on the pyridnium ring.[21] For the extraction of indole, the N extraction efficiency also increased with respect to the cation volume for the $[C_nC_1im][NTf_2]$ series, until the value reached a plateau between n = 8 and 10 (Figure 4).

Contrary to the extraction of pyridine, the indole extraction efficiency of $[C_4C_1C_1im][NTf_2]$ (98.2 mol %) is slightly higher than that of $[C_4C_1im][NTf_2]$ (97.5 mol %). For pyridinium-based ILs, $[C_4{}^4C_1py][NTf_2]$ (98.8 mol %) also has a higher indole extraction efficiency than $[C_4py][NTf_2]$ (98.3 mol %). Overall, within the same class of cations, the N extraction efficiencies generally increased with cation volume and bis(trifluoromethane)sulfonamide ILs based on common cations are good extractants of N compounds from the model oil. Our results are consistent with larger cations offering more surface area for absorption through van der Waals interactions.

Anion Dependence with Common Cation ($[C_4C_1im]^+$). With the cation dependence for N extractions established, the effect of different anions on the N extraction capacities was

DOI: 10.1021/acs.energyfuels.6b02157
Energy Fuels 2017, 31, 2183–2189

Table 2. N Extraction Efficiencies of Pyridine and Indole with Different $[NTf_2]^-$ ILs (Temperature, 25 °C; 3.43 mmol of IL/2 mL of Model Oil; and Extraction Time, 20 min)

IL	pyridine extraction efficiency (mol/mol %)	decrease in pyridine concentration of the oil phase (M/M %)	indole extraction efficiency (mol/mol %)	decrease in indole concentration of the oil phase (M/M %)
$[C_2C_1im][NTf_2]$	70.7 ± 0.3	69.6 ± 0.4	97.2 ± 0.1	97.2 ± 0.1
$[C_4C_1im][NTf_2]$	76.8 ± 0.01	75.8 ± 0.02	97.5 ± 0.09	97.5 ± 0.03
$[C_6C_1im][NTf_2]$	78.7 ± 0.1	77.0 ± 0.2	97.9 ± 0.08	97.8 ± 0.09
$[C_8C_1im][NTf_2]$	80.6 ± 0.08	78.1 ± 0.1	98.2 ± 0.2	98.1 ± 0.1
$[C_{10}C_1im][NTf_2]$	84.7 ± 0.3	81.4 ± 0.3	98.1 ± 0.02	97.7 ± 0.03
$[C_4C_1C_1im][NTf_2]$	74.1 ± 0.8	73.6 ± 0.4	98.2 ± 0.06	98.1 ± 0.06
$[C_4py][NTf_2]$	73.8 ± 0.08	72.7 ± 0.06	98.3 ± 0.03	98.3 ± 0.03
$[C_4{}^4C_1py][NTf_2]$	79.6 ± 0.2	78.4 ± 0.2	98.8 ± 0.001	98.8 ± 0.003
$[C_4C_1pyrr][NTf_2]$	71.8 ± 0.3	70.7 ± 0.2	98.0 ± 0.06	98.0 ± 0.06

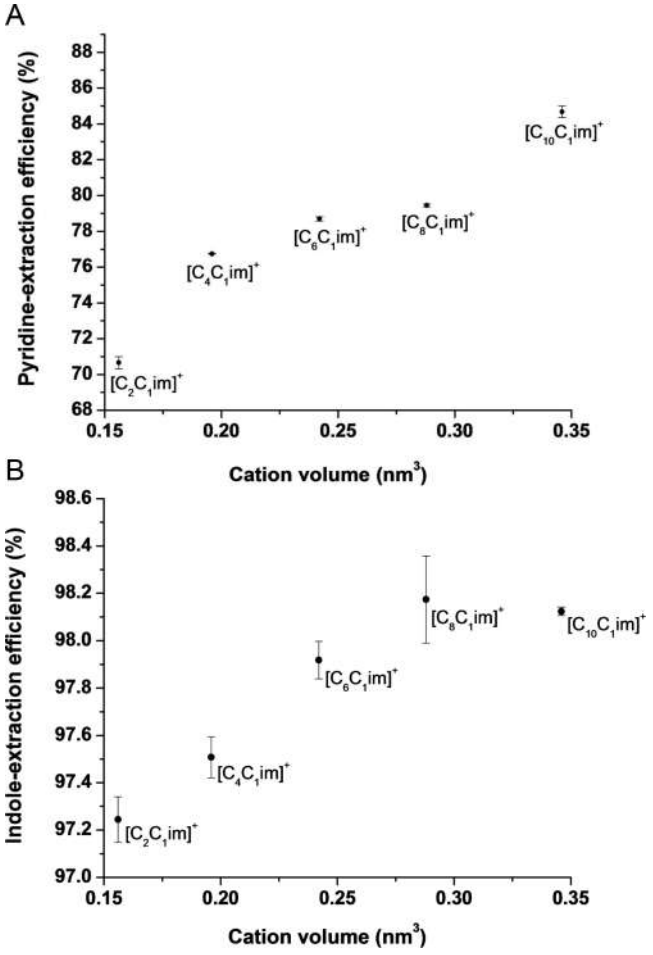

Figure 4. Pyridine (above) and indole (below) extraction efficiencies with respect to the cation volume of different $[C_nC_1im][NTf_2]$ ILs (temperature, 25 °C; 3.43 mmol of IL/2 mL of model oil; and extraction time, 20 min).

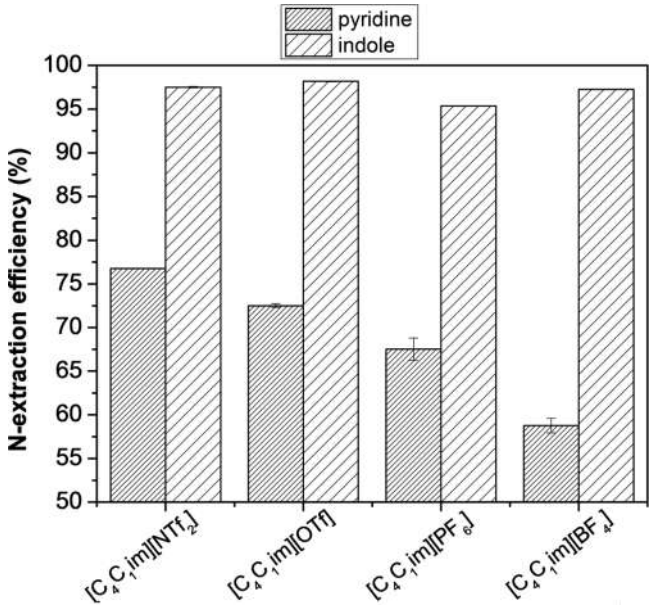

Figure 5. N extraction efficiencies of pyridine and indole with $[C_4C_1im]^+$ ILs of different anions (temperature, 25 °C; 3.43 mmol of ILs/2 mL of model oil; and extraction time, 20 min).

investigated. The N extraction efficiencies with 1-butyl-3-methylimidazolium trifluoromethanesulfonate $[C_4C_1im][OTf]$, 1-butyl-3-methylimidazolium hexafluorophosphate $[C_4C_1im][PF_6]$, and 1-butyl-3-methylimidazolium tetrafluoroborate $[C_4C_1im][BF_4]$ were measured and compared to that with $[C_4C_1im][NTf_2]$, and considerable differences could be observed for the extraction of pyridine (Figure 5 and Table 3). The pyridine extraction efficiency follows the order $[C_4C_1im][NTf_2]$ (76.8 mol %) > $[C_4C_1im][OTf]$ (72.5 mol %) > $[C_4C_1im][PF_6]$ (67.5 mol %) > $[C_4C_1im][BF_4]$ (58.8 mol %). In contrast to the case of cation dependence, i.e., $[C_4C_1im]^+$ and $[C_4C_1C_1im]^+$, an influence of hydrogen bonding on pyridine extraction with different anions was not noticeable after consideration of their respective Kamlet–Taft parameters nor could the results be explained by the difference in the calculated interaction energies between the imidazolium ring and the anions, which follow the order $[BF_4]^-$ > $[OTf]^-$ > $[NTf_2]^-$ ~ $[PF_6]^-$.[22] The pyridine extraction efficiency values for these ILs, however, correlate with the ionic volume of the anions (Table 1), with $[NTf_2]^-$ being the largest and $[BF_4]^-$ being the smallest. Therefore, as in the case of cations, the size of the anions strongly affects the extraction power for pyridine. Again, these results are consistent with, in this case, a larger anion having more surface area for absorption through van der Waals interactions.

However, the indole extraction efficiency follows the order $[C_4C_1im][OTf]$ (98.2 mol %) > $[C_4C_1im][NTf_2]$ (97.5 mol %) > $[C_4C_1im][BF_4]$ (97.2 mol %) > $[C_4C_1im][PF_6]$ (95.4 mol %), and this trend could not be rationalized by the size effect only. The unexpectedly high indole extraction efficiency for $[C_4C_1im][OTf]$ and $[C_4C_1im][BF_4]$ might be best rationalized as a result of the ability of their anions to form relatively strong hydrogen bonds with the NH group of indole, which is known to be a hydrogen bond donor.[23,24] This is

DOI: 10.1021/acs.energyfuels.6b02157
Energy Fuels 2017, 31, 2183–2189

Table 3. N Extraction Efficiencies of Pyridine and Indole with Different $[C_4C_1im]^+$ ILs (Temperature, 25 °C; 3.43 mmol of ILs/2 mL of Model Oil; and Extraction Time, 20 min)

IL	pyridine extraction efficiency (mol/mol %)	decrease in pyridine concentration of the oil phase (M/M %)	indole extraction efficiency (mol/mol %)	decrease in indole concentration of the oil phase (M/M %)
$[C_4C_1im][NTf_2]$	76.8 ± 0.01	75.8 ± 0.02	97.5 ± 0.09	97.5 ± 0.03
$[C_4C_1im][OTf]$	72.5 ± 0.2	71.8 ± 0.2	98.2 ± 0.05	98.1 ± 0.05
$[C_4C_1im][PF_6]$	67.5 ± 1.3	66.2 ± 0.8	95.4 ± 0.01	95.3 ± 0.003
$[C_4C_1im][BF_4]$	58.8 ± 0.8	57.3 ± 0.3	97.2 ± 0.03	97.2 ± 0.03

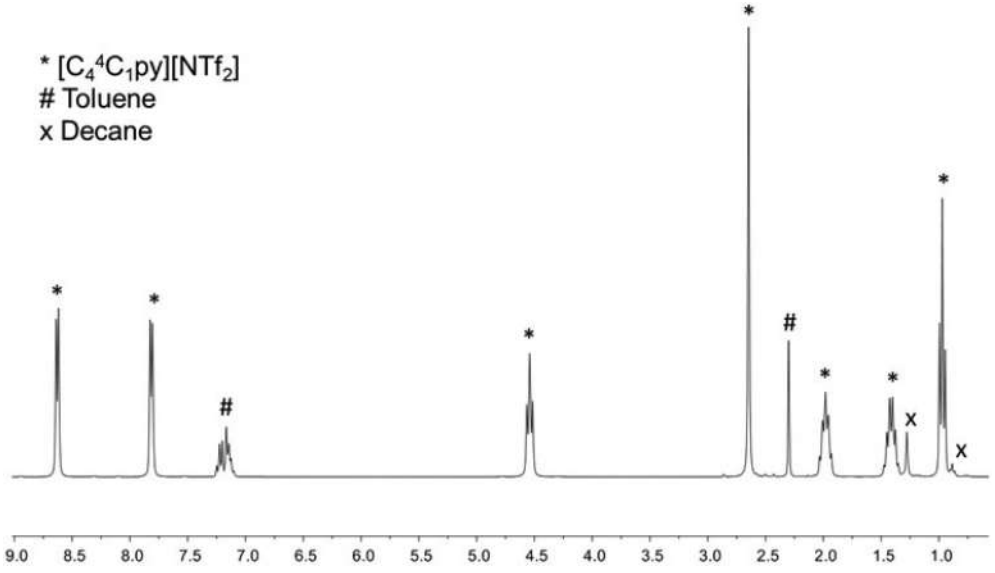

Figure 6. ^{1}H NMR of the IL phase after N extraction.

consistent with the fact that these ILs have higher Kamlet−Taft β values ($[C_4C_1im][OTf]$, β = 0.49; $[C_4C_1im][BF_4]$, β = 0.37) than those of $[C_4C_1im][NTf_2]$ (β = 0.24) and $[C_4C_1im][PF_6]$ (β = 0.19).[19] Overall, the indole extraction efficiency is dependent upon both the size and hydrogen bond basicity of the anions.

Mutual Solubility. The study of mutual solubility of IL and model oil is important because the solubility of ILs in fuel oils may give rise to the loss of extractants and contamination of the fuel oil. Furthermore, significant solubility of oils in ILs would result in the loss of fuel oil and increase in process costs. It had been reported in many denitrogenation and desulfurization studies that pure ILs are generally insoluble in model oil or actual fuel oils at ambient temperature.[6,25−30] Indeed, all ILs investigated in this study were not soluble in the model oil, as mentioned earlier. However, it has been shown that some oil contents can dissolve in the IL phase during the extractions.[6,25−30] In previous denitrogenation or desulfurization studies, the solubility of oil in ILs was mostly determined by gravimetric methods,[10,28,29] with some gas chromatography (GC) methods also being used.[31] Because it had been observed by us and others that ILs are completely insoluble in the oil at ambient temperature, quantitative ^{1}H NMR was used to determine the solubility of model oil in ILs (Figure 6). The advantage of using this method over gravimetry is that the solubility of individual components (i.e., decane and toluene) of the oil can be determined directly, as summarized in Table 4. For the cases shown, the solubility of oil contents in ILs is largely dependent upon the volume of the cation and anion. In general, an IL with a larger cation/anion dissolved more oil contents as a result of the larger surface area for absorption

Table 4. Solubility of Oil Contents in Different ILs after N Extractions, Quantified by ^{1}H NMR (Temperature, 25 °C; 3.43 mmol of ILs/2 mL of Model Oil; and Extraction Time, 20 min)

IL	toluene in the IL phase (mmol)	decane in the IL phase (mmol)
$[C_4C_1im][NTf_2]$	0.58 ± 0.04	0.046 ± 0.002
$[C_4C_1im][OTf]$	0.35 ± 0.02	0.017 ± 0.001
$[C_4C_1im][PF_6]$	0.26 ± 0.02	0.010 ± 0.001
$[C_4C_1im][BF_4]$	0.20 ± 0.03	0.008 ± 0.001
$[C_4C_1C_1im][NTf_2]$	0.57 ± 0.02	0.043 ± 0.002
$[C_2C_1im][NTf_2]$	0.47 ± 0.00	0.022 ± 0.001
$[C_6C_1im][NTf_2]$	0.81 ± 0.01	0.26 ± 0.01
$[C_8C_1im][NTf_2]$	0.95 ± 0.04	0.61 ± 0.03
$[C_{10}C_1im][NTf_2]$	0.93 ± 0.01	1.23 ± 0.02
$[C_4C_1pyrr][NTf_2]$	0.49 ± 0.02	0.047 ± 0.002
$[C_4py][NTf_2]$	0.57 ± 0.01	0.027 ± 0.001
$[C_4{}^4C_1py][NTf_2]$	0.77 ± 0.02	0.071 ± 0.003

through van der Waals interactions. Besides all of the denitrogenation and desulfurization studies described in the literature, it is well-established that ILs are good extractants of aromatic compounds from aliphatic hydrocarbons. It was shown that ILs could separate even the simplest aromatic compound, benzene, from alkanes,[32] likely through cation−π[33] and CH−π[34] interactions. Hence, there should be no surprise that these ILs could extract substantial amounts of both the N compounds and the alkylbenzene, i.e., toluene, from the oil phase. However, the solubility of decane in ILs is very low. Besides $[C_6C_1im][NTf_2]$, $[C_8C_1im][NTf_2]$, and $[C_{10}C_1im][NTf_2]$, less than 1% of decane dissolved in the IL phases

DOI: 10.1021/acs.energyfuels.6b02157
Energy Fuels 2017, 31, 2183−2189

during extractions in this study. However, the solubility of *n*-decane in $[C_nC_1im][NTf_2]$ dramatically increased from $n = 4$ (0.5 mol %) to $n = 10$ (14 mol %). Overall, these results confirmed the prediction by Chen and co-workers,[35] who pointed out that cations with a shorter alkyl chain length and less symmetry tend to have weaker van der Waals energies and smaller mutual solubility.

General Consideration. The results of this investigation showed that, besides hydrogen bonding effects, the sizes of IL cations and anions play a pivotal role in determining the extraction efficiencies of the ILs for pyridine and toluene. In general, the extraction efficiencies of the ILs for pyridine and toluene correlated positively with the size of cations (within the same class) and anions. However, these efficiencies for indole extraction were consistently higher than those for pyridine in the same IL. It was suggested by Dupont and co-workers[34] that, for $[C_4C_1im][NTf_2]$, the effectiveness of extraction of N compounds is largely governed by the nitrogen heterocycle pK_a, with the quantity of N compounds in the IL phase increasing with the pK_a. They argued that it was due to the stronger N (heteroaromatic)−H (imidazolium) hydrogen bond. However, the opposite effect was observed in the present study, because indole ($pK_a = -3.6$) has a lower pK_a than pyridine ($pK_a = 5.2$).[36] This might be due to the extra aromatic ring on indole providing more space for interactions, e.g., cation−π and CH−π, between the extractants and solute.

CONCLUSION

In this investigation, a number of common room-temperature ILs were evaluated regarding their extraction power of N compounds from model fuel oil. It was found that the extraction efficiencies of either pyridine or indole were largely dependent upon the size of cations and anions of the ILs. Additionally, hydrogen bonding interactions could also be important in the extraction of N compounds. In the case of the Lewis basic pyridine, the use of an extractant with strong hydrogen bond donor capacity is favored. Conversely, for extraction of indole, a good hydrogen bond acceptor should be employed.

The effect of different cations and anions on the mutual solubility of ILs and the model oil was also investigated. As reported elsewhere, it was shown that the solubility of all of these ILs in the model oil is negligible. On the other hand, the solubility of the oil in the ILs is also largely dependent upon the size of individual ions of the ILs.

ASSOCIATED CONTENT

Supporting Information

The Supporting Information is available free of charge on the ACS Publications website at DOI: 10.1021/acs.energyfuels.6b02157.

Decrease in the pyridine concentration of the oil phase versus time (temperature, 25 °C; and 3.43 mmol of ILs/2 mL of model oil) (Table S1), decrease in the indole concentration of the oil phase versus time (temperature, 25 °C; and 3.43 mmol of ILs/2 mL of model oil) (Table S2), and N extraction efficiencies of pyridine and indole with respect to 0.1 g of different ILs (temperature, 25 °C; 3.43 mmol of ILs/2 mL of model oil; and extraction time, 20 min) (Table S3) (PDF)

AUTHOR INFORMATION

Corresponding Author

*Telephone: +61-2-93512581. E-mail: thomas.maschmeyer@sydney.edu.au.

ORCID

Matthew Y. Lui: 0000-0003-2201-3956
Lisa Cattelan: 0000-0002-3217-422X
Alvise Perosa: 0000-0003-4544-8709
Maurizio Selva: 0000-0002-9986-2393
Thomas Maschmeyer: 0000-0001-8494-9907

Notes

The authors declare no competing financial interest.

ACKNOWLEDGMENTS

The authors thank the Science and Industry Endowment Fund (SIEF, Grant RP03-028) (to Matthew Y. Lui), the Erasmus+ Scholarship (to Lisa Cattelan), and the Henry Bertie and Florence Mabel Gritton Research Scholarship (to Lisa C. Player) for financial support for this research. The authors also acknowledge Dr. Ian Luck for assistance in NMR analysis and Dr. Alex Yuen for valuable discussions.

REFERENCES

(1) Wiwel, P.; Knudsen, K.; Zeuthen, P.; Whitehurst, D. D. *Ind. Eng. Chem. Res.* **2000**, *39*, 533−540.
(2) Zeuthen, P.; Knudsen, K.; Whitehurst, D. D. *Catal. Today* **2001**, *65*, 307−314.
(3) Yang, H.; Chen, J.; Briker, Y.; Szynkarczuk, R.; Ring, Z. *Catal. Today* **2005**, *109*, 16−23.
(4) Girgis, M. J.; Gates, B. C. *Ind. Eng. Chem. Res.* **1991**, *30*, 2021−2058.
(5) Katzer, J. R.; Sivasubramanian. *Catal. Rev.: Sci. Eng.* **1979**, *20*, 155−208.
(6) Chen, X.; Yuan, S.; Abdeltawab, A. A.; Al-Deyab, S. S.; Zhang, J.; Yu, L.; Yu, G. *Sep. Purif. Technol.* **2014**, *133*, 187−193.
(7) Jayaraman, A.; Yang, F. H.; Yang, R. T. *Energy Fuels* **2006**, *20*, 909−914.
(8) Welton, T. *Chem. Rev.* **1999**, *99*, 2071−2083.
(9) Visser, A. E.; Swatloski, R. P.; Reichert, W. M.; Mayton, R.; Sheff, S.; Wierzbicki, A.; Davis, J. H., Jr.; Rogers, R. D. *Chem. Commun.* **2001**, 135−136.
(10) Asumana, C.; Yu, G.; Guan, Y.; Yang, S.; Zhou, S.; Chen, X. *Green Chem.* **2011**, *13*, 3300−3305.
(11) Vilas, M.; González, E. J.; Tojo, E. *Fluid Phase Equilib.* **2015**, *396*, 66−73.
(12) Burrell, A. K.; Sesto, R. E. D.; Baker, S. N.; McCleskey, T. M.; Baker, G. A. *Green Chem.* **2007**, *9*, 449−454.
(13) Weber, C. C.; Masters, A. F.; Maschmeyer, T. *Angew. Chem., Int. Ed.* **2012**, *51*, 11483−11486.
(14) Zhao, Y.; Long, J.; Deng, F.; Liu, X.; Li, Z.; Xia, C.; Peng, J. *Catal. Commun.* **2009**, *10*, 732−736.
(15) Agency for Toxic Substances and Disease Registry (ATSDR). *Toxicological Profile for Fuel Oils*; ATSDR: Atlanta, GA, June 1995.
(16) Shimizu, Y.; Ohte, Y.; Yamamura, Y.; Tsuzuki, S.; Saito, K. *J. Phys. Chem. B* **2012**, *116*, 5406−5413.
(17) Slattery, J. M.; Daguenet, C.; Dyson, P. J.; Schubert, T. J. S.; Krossing, I. *Angew. Chem., Int. Ed.* **2007**, *46*, 5384−5388.
(18) Chiappe, C.; Pieraccini, D. *J. Phys. Chem. A* **2006**, *110*, 4937−4941.
(19) Ab Rani, M. A.; Brant, A.; Crowhurst, L.; Dolan, A.; Lui, M.; Hassan, N. H.; Hallett, J. P.; Hunt, P. A.; Niedermeyer, H.; Perez-Arlandis, J. M.; Schrems, M.; Welton, T.; Wilding, R. *Phys. Chem. Chem. Phys.* **2011**, *13*, 16831−16840.
(20) Avent, A. G.; Chaloner, P. A.; Day, M. P.; Seddon, K. R.; Welton, T. *J. Chem. Soc., Dalton Trans.* **1994**, 3405−3413.

DOI: 10.1021/acs.energyfuels.6b02157
Energy Fuels 2017, 31, 2183−2189

(21) Verdía, P.; González, E. J.; Rodríguez-Cabo, B.; Tojo, E. *Green Chem.* **2011**, *13*, 2768−2776.
(22) Tsuzuki, S.; Tokuda, H.; Hayamizu, K.; Watanabe, M. *J. Phys. Chem. B* **2005**, *109*, 16474−16481.
(23) Braun, J. E.; Grebner, Th. L.; Neusser, H. J. *J. Phys. Chem. A* **1998**, *102*, 3273−3278.
(24) Carney, J. R.; Hagemeister, F. C.; Zwier, T. S. *J. Chem. Phys.* **1998**, *108*, 3379−3382.
(25) Nie, Y.; Li, C.-X.; Wang, Z.-H. *Ind. Eng. Chem. Res.* **2007**, *46*, 5108−5112.
(26) Gao, H.; Luo, M.; Xing, J.; Wu, Y.; Li, Y.; Li, W.; Liu, Q.; Liu, H. *Ind. Eng. Chem. Res.* **2008**, *47*, 8384−8388.
(27) Gao, H.; Zeng, S.; Liu, X.; Nie, Y.; Zhang, X.; Zhang, S. *RSC Adv.* **2015**, *5*, 30234.
(28) Nie, Y.; Li, C.; Meng, H.; Wang, Z. *Fuel Process. Technol.* **2008**, *89*, 978−983.
(29) Nie, Y.; Li, C.; Sun, A.; Meng, H.; Wang, Z. *Energy Fuels* **2006**, *20*, 2083−2087.
(30) Asumana, C.; Yu, G.; Li, X.; Zhao, J. J.; Liu, G.; Chen, X. C. *Green Chem.* **2010**, *12*, 2030−2037.
(31) Safa, M.; Mokhtarani, B.; Mortaheb, H. R. *Chem. Eng. Res. Des.* **2016**, *111*, 323−331.
(32) Letcher, T. M.; Deenadayalu, N. *J. Chem. Thermodyn.* **2003**, *35*, 67−76.
(33) Shimomura, T.; Takamuku, T.; Yamaguchi, T. *J. Phys. Chem. B* **2011**, *115*, 8518−8527.
(34) Cassol, C. C.; Umpierre, A. P.; Ebeling, G.; Ferrera, B.; Chiaro, S. S. X.; Dupont, J. *Int. J. Mol. Sci.* **2007**, *8*, 593−605.
(35) Gao, S.; Yu, G.; Abro, R.; Abdeltawab, A. A.; Al-Deyab, S. S.; Chen, X. *Fuel* **2016**, *173*, 164−171.
(36) Katritzky, A. R.; Ramsden, C. A.; Joule, J. A.; Zhdankin, V. V. *Handbook of Heterocyclic Chemistry*, 3rd ed.; Elsevier: Amsterdam, Netherlands, 2010.

DOI: 10.1021/acs.energyfuels.6b02157
Energy Fuels 2017, 31, 2183−2189